NUCLEAR REACTOR ANALYSIS

Volume II

James J. Duderstadt

Louis J. Hamilton

Department of Nuclear Engineering

The University of Michigan

Ann Arbor, Michigan

A Note of Caution to the Discerning Reader:

These lecture notes represent a first crack at the second half of a text on nuclear reactor analysis. It should be noted that Chapter 10 on lattice calculations actually was intended as the final chapter in Volume I since it is certainly more involved with the study of reactor calculational methods than applications. Unfortunately, the author's despondence over the decision to send Ohio State to the 1974 Rose Bowl delayed the preparation of this chapter until this time.

The second volume is primarily intended to illustrate the application of the concepts and methods developed earlier to problems which will almost certainly be encountered by the practicing nuclear engineer. We have attempted to present a reasonably condensed exposure to the subjects of nuclear reactor core design and nuclear power plant analysis suitable for seniors or first year graduate students in nuclear engineering. While it is our hope that most of the topics relevant to these subjects have surfaced somewhere in Volume II, we wish to stress that this is only a preliminary draft, and considerable modifications and rearrangement are no doubt necessary.

And, as is characteristic of any set of lecture notes frantically prepared to keep pace with an ongoing lecture course, numerous errors appear throughout. Yet another casualty of the hot breath of impending lectures breathing down the back of the author's neck has been adequate acknowledgement to the many sources from which this material has been pirated. Although these acknowledgements will be included in later versions, we would particularly like to acknowledge here our substantial use of course material prepared by Harvey Graves, Jr., while a

Visiting Professor at The University of Michigan. (This material will hopefully be published in its entirety elsewhere.) The lecture notes of Paul J. Turinsky of R.P.I. were also of immeasurable assistance.

And, finally, yet one more apology to those readers of taste. Once again, these notes have been contaminated with numerous, shall we say, "diversions" intended not so much to relieve the boredom of the reader, but rather to preserve the sanity of the author (although, perhaps somewhat belatedly).

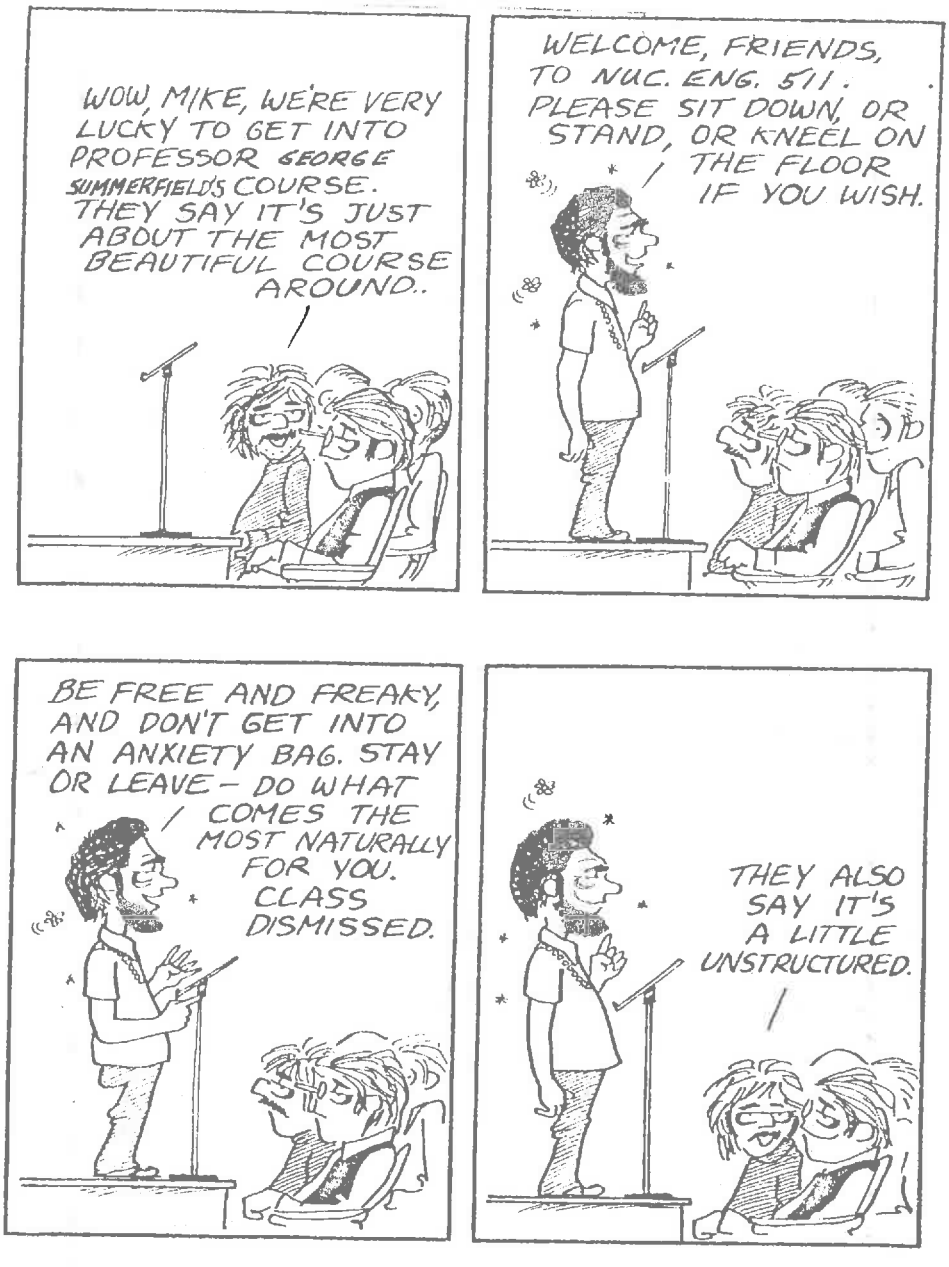

JJD
1/17/74

TABLE OF CONTENTS (Vol. II)

CHAPTER 10: HETEROGENEOUS EFFECTS IN CORE LATTICES

I. A QUALITATIVE DISCUSSION OF HETEROGENEOUS EFFECTS ON CORE MULTIPLICATION

A. Introduction

Thus far we have been concerned with homogeneous reactor cores in which fuel, moderator, coolant, and structural materials are intimately mixed. But of course nuclear reactor cores are constructed in a highly heterogeneous configuration to facilitate thermal design (coolant channels, heat transfer surfaces), mechanical design (structural integrity, fuel handling), and reactivity control (control rods, burnable poisons). For example, a cross section of a typical PWR core is shown in Figure 10-1, while that of a fuel subassembly is shown in Figure 10-2. Such heterogenieties in the reactor fuel array or lattice must be taken into account in nuclear design to some degree, since they influence core multiplication. In fact, we will find that lumping the fuel into a heterogeneous lattice actually tends to enhance core multiplication, thereby reducing the fuel inventory or enrichment required for reactor criticality.

The degree to which heterogenieties must be accounted for in reactor design depend upon the characteristic dimensions of the nonuniformities in the core lattice, e.g., the diameter of a fuel pin or the spacing between fuel elements, compared to the mean free paths of neutrons in the core. For example, in light water reactors, the thermal neutron mean free path is typically on the order of centimeters which is comparable to the fuel pin diameter. Hence the flux distribution in the fuel

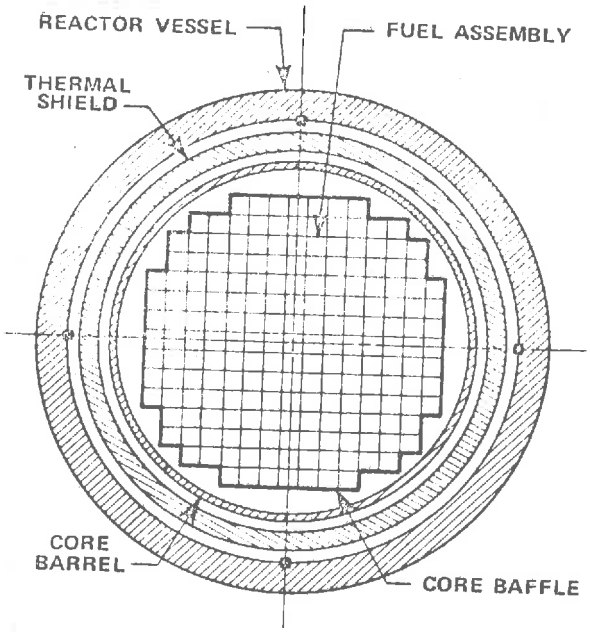
REACTOR VESSEL
FUEL ASSEMBLY
THERMAL SHIELD
CORE BARREL
CORE BAFFLE

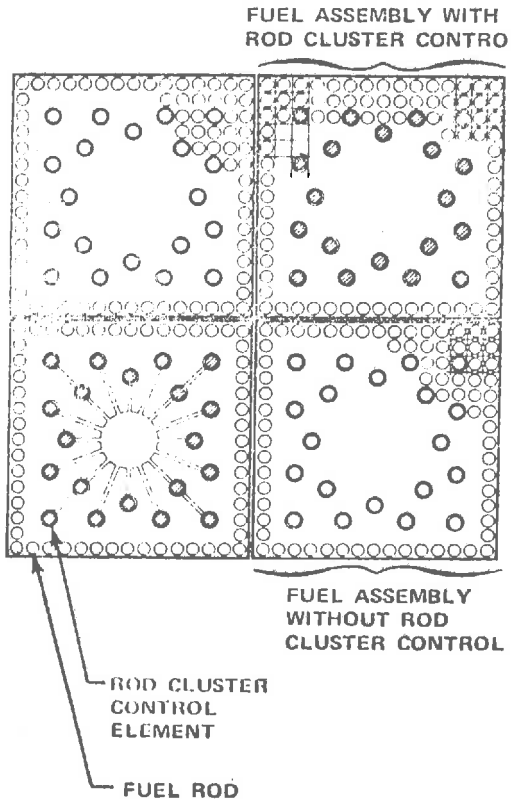
FUEL ASSEMBLY WITH ROD CLUSTER CONTROL
FUEL ASSEMBLY WITHOUT ROD CLUSTER CONTROL
ROD CLUSTER CONTROL ELEMENT
FUEL ROD

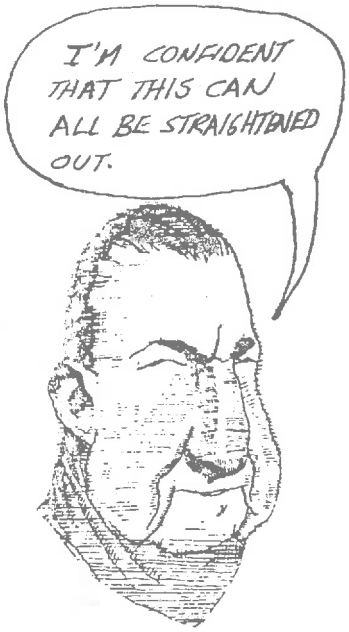
I'M CONFIDENT THAT THIS CAN ALL BE STRAIGHTENED OUT.

might be expected to be quite different from that in the moderator or coolant channel, thereby necessitating a detailed treatment of the heterogeniety. By way of contrast, the much longer mean free path lattice characteristic of the neutrons in a fast reactor (typically tens of centimeters) allows a much grosser treatment of lattice effects.

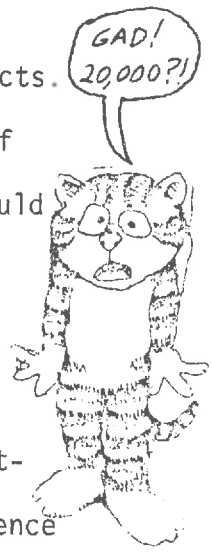

Of course a detailed treatment of the core lattice on a scale of a neutron mean free path is clearly out of the question, since it would require an unmanagebly large array of mesh points in a multigroup diffusion calculation (typical light water reactors have over 20,000 fuel elements). Indeed, the strongly absorbing nature of fuel and control elements in the core frequently require a more accurate treatment of neutron transport than that provided by diffusion theory. Hence one must adopt a more piecemeal approach by seeking to selectively "homogenize" the analysis of the core--that is, by providing prescriptions for including lattice effects into existing infinite medium neutron energy spectrum calculations or by calculating few group constants which have been spatially averaged over the finer details of the flux distribution.

Of course the type of treatment one chooses will depend upon the purpose of the calculation. For example one can contrast a hand calculation based upon the 6-factor formula suitable for a crude survey estimate with an extremely detailed transport calculation which might be used in a comparison with a critical experiment or perhaps as a benchmark for the testing of other calculational schemes. Our concern in this chapter is with more routine design calculations which must be performed very frequently and hence place a premium on calculational ease. For such schemes to yield adequate accuracy, one is forced to rely upon

frequent cross calibration with experiment--that is, to accept a certain amount of empiricism (fudging) in the technique. And, of course, as in any fast yet accurate method, one relies heavily upon a cancellation of errors. For example, in a LWR core study, one might attempt to generate group constants for a few group diffusion analysis using a SOFOCATE-MUFT description similar to that discussed in Chapters 8 and 9. But of course these schemes perform calculations for a homogeneous, infinite medium. Hence our objective here is to provide a prescription for modifying these homogeneous results to account for heterogeneous lattice effects. In practice, these modifications most significantly enter into the calculation of the thermal utilization, the resonance absorption, and the fast fission factor.

For more detailed calculations, one is frequently forced to utilize a transport theory description, based either upon so-called collision probability methods or a direct solution of the transport equation itself (or perhaps a Monte Carlo calculation). Since the trend in recent years has been toward more detailed treatments of the heterogeneous effects and more precise transport descriptions, we will include as well some discussion of these latter techniques.

B. Core Homogenization

To be more specific, let us outline one possible approach to the treatment of core lattice effects. We begin by noting that reactor cores have a regular or periodic lattice structure in which one subelement or so-called "unit cell" is repeated throughout the core. For example, a fuel subassembly or group of fuel subassemblies could be regarded as a unit cell.

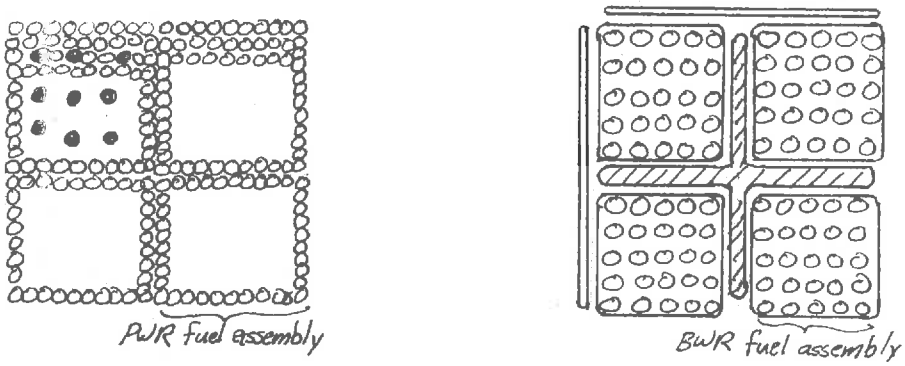

On a more detailed scale, a given fuel element and adjacent coolant channel might be chosen as the unit cell:

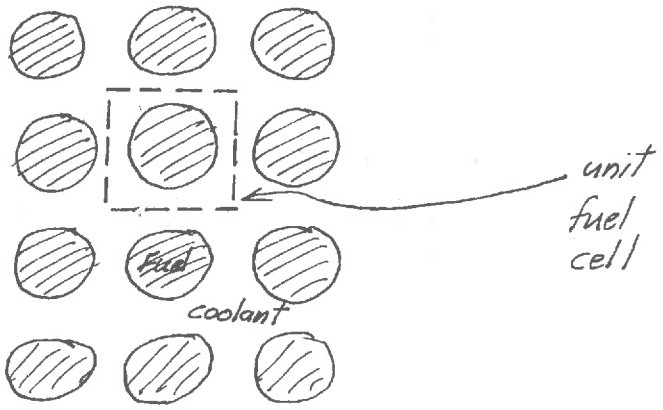

The essential scheme then is to perform a detailed calculation of the flux distribution in a given unit cell of the lattice--usually assuming that there is zero net neutron current across the boundary of the cell (using arguments based upon the symmetry of the lattice). The various multigroup cross sections characterizing materials in the cell are then spatially averaged over the cell, using the flux distribution as a weighting function. In this way one can characterize the cell by effective group constants which take account of the inhomogeneous flux distribution in the cell. This scheme essentially replaces the actual unit cell by an equivalent homogeneous unit cell characterized by these effective cross sections.

For example, one usually begins by considering a typical fuel cell--i.e., fuel plus clad plus coolant. The fuel cell is first reduced to an equivalent cell of simpler geometry to expedite calculations:

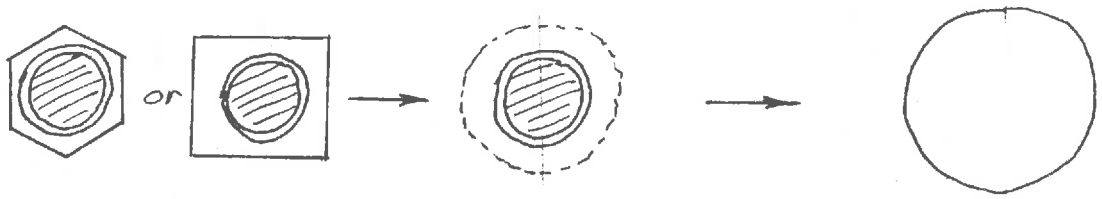

fuel cell equivalent cell homogeneous cell

Fuel Cell Homogenization (0.3 to 0.8 inches)

Our primary interest is usually concerned with the generation of fast and thermal group constants for such a cell. In the fast range, the heterogeneities enter primarily as modifications to the resonance escape probability, for reasons which will become apparent in Section 10-3. Hence it is usually sufficient to simply perform the usual infinite medium fast spectrum calculation, taking care however to account for heterogeneous effects in resonance absorption via techniques which will be discussed later in this chapter.

The much shorter mean free path characterizing thermal neutrons necessitates a somewhat more detailed treatment of heterogeneities in determining the thermal flux spectrum in a fuel cell. For less detailed corecalculations, one can frequently get by with simply modifying the results of an infinite medium thermal spectrum calculation (e.g., SOFOCATE) to account for the variations in average flux in the fuel, $\overline{\phi}_F$, and the moderator, $\overline{\phi}_M$. Of primary concern here is the calculation of the so-called thermal disadvantage factors, $\overline{\phi}_M / \overline{\phi}_F$,

which enter into modifying the infinite medium spectrum results. More detailed calculations of thermal spectra usually involve a direct solution of the neutron transport equation characterizing the cell. Both schemes will be discussed in section 10-2.

Such fuel cell calculations are customarily performed under the assumption of zero net neutron leakage between cells (which decouples the fuel cells from one another). Actually, such single fuel rod spectrum calculations are of questionable validity when rod neighbors include water holes, poison shims, control rods, or Pu-loaded fuel pins, since then one needs to account for cell-to-cell leakage.

The next step in the analysis of the core is to consider a typical fuel assembly or grouping of fuel assemblies, including control or shim elements. The few group constants calculated for the fuel cell can be used to describe most of the assembly, with the exception of control material which requires rather specialized techniques. Usually a detailed multigroup 2-D diffusion or transport code is used to determine the flux in such an assembly, and then once again these fluxes are used to generate assembly averaged group constants.

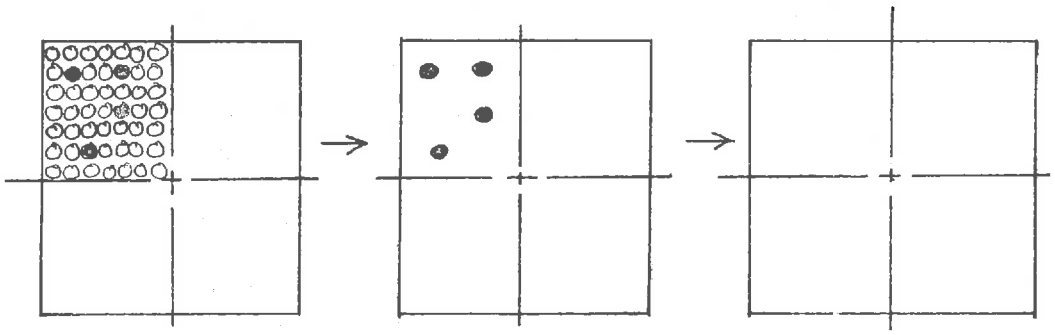

Fuel Assembly Homogenization (5 to 8 inches)

The final step is to use either these assembly averaged group constants (or, in very detailed calculations, the original fuel cell group

constants) to determine the flux and power distribution over the entire core. The symmetry of the core will frequently allow one to consider only a quadrant in detail. It may occasionally be desirable to homogenize the core still further to facilitate gross survey calculations:

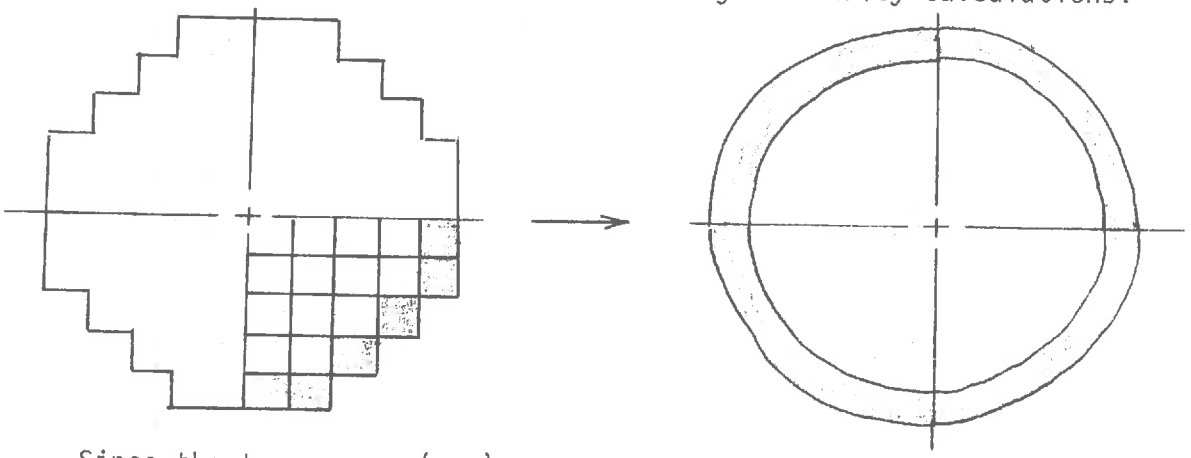

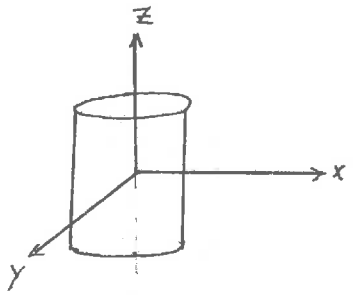

Since the transverse (x-y) power distribution in many reactor cores is to first order independent of the axial (z) power distribution, one can frequently iterate back and forth between a 2-D transverse and a 1-D axial multigroup diffusion calculation of the flux (hence avoiding a 3-D calculation). However for certain classes of problems (detailed power distribution studies or safety analyses), a full 3-D calculation cannot be avoided. It has been found that accurate multigroup calculations usually require between 4 (LWR) and 6 (HTGR) energy groups for thermal reactor analysis.

In fast reactor cores, the neutron mean free path is quite large. Hence fast reactors aremore susceptible to a homogeneous analysis (except for a small fraction of neutrons with energies less than several keV). On the other hand, it is much more important to treat the energy dependence accurately in fast reactor analysis. Hence one usually relies

on many groups (~20) in a diffusion calculation for a few region model of the core in fast reactor analysis.

C. A Qualitative Discussion of Heterogeneous Effects in Thermal Reactors

It is possible to obtain a very useful qualitative understanding of the influence of fuel lumping on core multiplication in thermal reactors by simply examining how the various terms in the 6-factor formula

$$k = \eta f p \epsilon P_{NFL} P_{NTL} \qquad (10\text{-}1)$$

are modified in passing from a homogeneous reactor core, in which the fuel and moderator are intimately mixed, to a heterogeneous lattice in which the fuel is lumped. This discussion actually has a rather interesting historical significance, since without fuel lumping, it would have been impossible to achieve a critical assembly using natural uranium and graphite in Fermi's "pile" at the University of Chicago in 1942. More specifically, for a natural uranium system, η = 1.33 while ϵ = 1.05. If one studies f and p for various homogeneous mixtures of natural uranium and graphite, then, at best, one finds

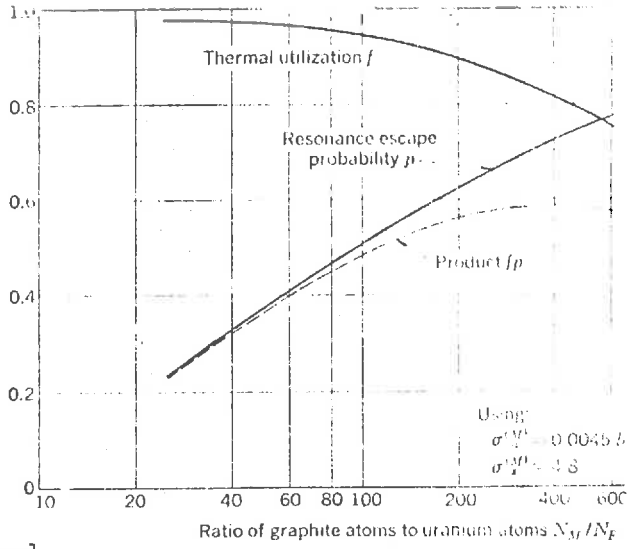

$$fp = 0.59$$

Hence for a homogeneous system,

$$k_\infty < (1.33)(1.05)(.59) = 0.85$$

Thus such a system could never be made critical.

There are several ways in which this situation can be alleviated. One approach would be to choose an alternative moderator. Unfortunately, the only moderator which would yield $k_\infty > 1$ in a homogeneous natural uranium fueled assembly is heavy water (D_2O). Since this material was available in only microscopic quantities at Fermi's time, one was forced to explore other schemes. Of course, one could attempt to enrich the amount of U^{235} in natural uranium, but at that time the enrichment facilities at Oak Ridge were still only in the planning stage.

Hence Fermi and Szilard chose the only feasible approach by noting that by lumping the fuel into a heterogeneous lattice, one could greatly increase k_∞ by increasing the resonance escape probability p. This occurs because neutrons which are slowed down to resonance energies in the moderator are primarily absorbed in the outer regions of the fuel element--hence leading to a depression in the neutron flux within the fuel at the resonance energy. That is, the outer layers of the fuel tend to shield its interior from resonance energy neutrons, thereby decreasing the net resonance absorption and hence increasing the resonance escape probability p. This "self-shielding" effect is sufficiently strong, that k_∞ increases to a value of 1.08 in a graphite-natural uranium lattice.

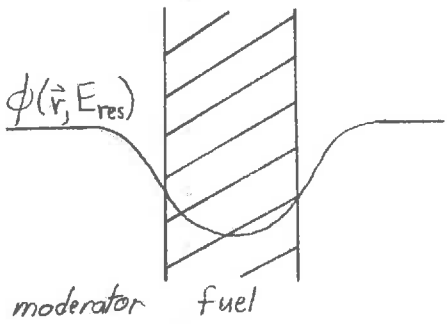

There are other effects due to fuel lumping, however. On the positive side, the fast fission factor ϵ also increases slightly in a heterogeneous assembly because the probability of a fast neutron

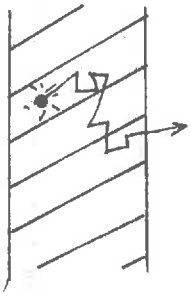

suffering a collision with a fuel nucleus while its energy is still above the fast fission threshold will increase. On the negative side, the thermal utilization f will decrease somewhat because the thermal flux tends to be depressed in the fuel, hence yielding less absorption in the fuel at thermal energies (again due to self-shielding). Since thermal absorption (in contrast to resonance absorption) can lead to fission, the net result is a decrease in core multiplication due to f. Fortunately, this decrease is far outweighed by the increase in p.

To examine these effects in somewhat more detail, we will now consider the influence of fuel lumping on each term in the 6-factor formula. Then in later sections of this chapter, we will turn to the more practical problem of just how such effects are included in core neutronics analysis.

η : First recall that η depends only upon the macroscopic cross sections characterizing the fuel

$$\eta = \frac{\nu \sigma_f^F}{\sigma_a^F} \longrightarrow \frac{\sum_j \nu_j \Sigma_f^{(j)}}{\sum_j \Sigma_a^{(j)}} \qquad (10\text{-}2)$$

(where the latter expression holds for a mixture of fuel isotopes). Hence one would not expect fuel lumping to appreciably affect this ratio. In actuality, however, the cross sections which appear in η are group constants characterizing the thermal energy group. These are dependent, of course, upon the thermal neutron energy spectrum, and this spectrum depends, in turn, upon the fuel-moderator lattice configuration. Hence there will be a slight modification in η when going

to a heterogeneous lattice. This change is usually ignored in less sophisticated thermal spectrum codes which include heterogenieties via thermal disadvantage factors. More elaborate cell calculations which account for space-energy effects whithin the cell will include this correction automatically.

f: In our earlier treatment of homogeneous systems we defined the thermal utilization f as the ratio of the rate of thermal neutron absorption in the fuel to the total rate of thermal neutron absorption in all materials. This definition can be applied as well to a heterogeneous core by writing

$$f = \frac{\int d^3r\, \Sigma_a^F(\vec{r})\, \Phi(\vec{r})}{\int d^3r\, \Sigma_a^F(\vec{r})\, \Phi(\vec{r}) + \int d^3r\, \Sigma_a^M(\vec{r})\, \Phi(\vec{r})} \qquad (10\text{-}3)$$

Here we are considering the core to be made up of only two types of material, fuel, denoted by the superscript F, and moderator, denoted by M. (The extension to more than two regions will be given later.) Since the core is made up of a number of identical fuel cells, we can consider the average in (10-3) as being taken only over the volume, V_{cell}, of one such cell. Now if we recognize that the macroscopic cross sections $\Sigma_a^F(\vec{r})$ and $\Sigma_a^M(\vec{r})$ are actually constant over the volume V_F of the fuel and V_M of the moderator respectively, and vanish elsewhere, then we can limit the range of integration and pull the cross sections out of the integrals to write

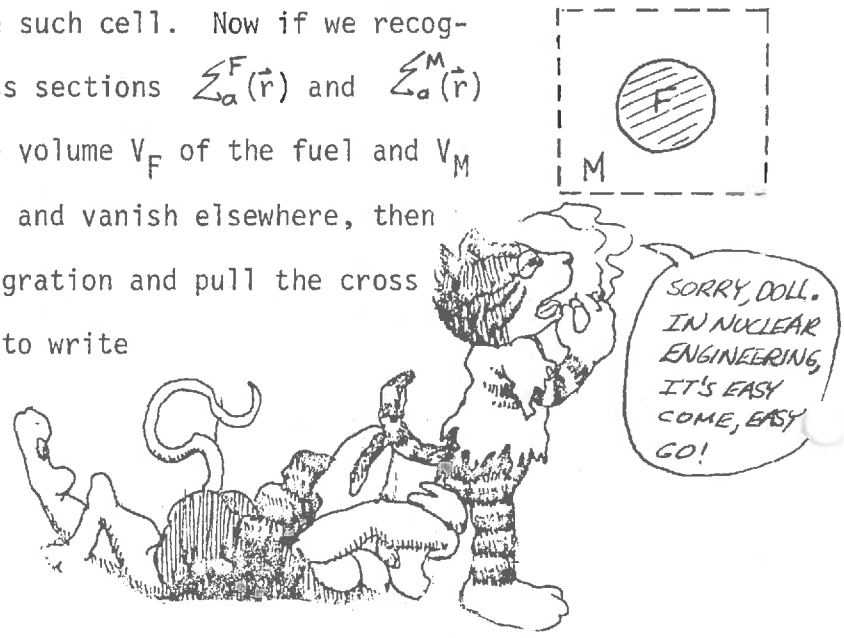

$$f = \frac{\Sigma_a^F \int_{V_F} d^3r\, \Phi(\vec{r})}{\Sigma_a^F \int_{V_F} d^3r\, \Phi(\vec{r}) + \Sigma_a^M \int_{V_M} d^3r\, \Phi(\vec{r})} \quad . \tag{10-4}$$

Next, suppose we define the spatially averaged flux in each region as

$$\bar{\phi}_F \equiv \frac{1}{V_F} \int_{V_F} d^3r\, \Phi(\vec{r})$$

$$\bar{\phi}_M \equiv \frac{1}{V_M} \int_{V_M} d^3r\, \Phi(\vec{r}) \quad . \tag{10-5}$$

Then we can rewrite the thermal utilization f in terms of these averages as

$$f = \frac{\Sigma_a^F V_F \bar{\phi}_F}{\Sigma_a^F V_F \bar{\phi}_F + \Sigma_a^M V_M \bar{\phi}_M} \tag{10-6}$$

or, dividing both numerator and denominator by $\bar{\phi}_F V_F$,

$$f = \frac{\Sigma_a^F}{\Sigma_a^F + \Sigma_a^M \left(\frac{V_M}{V_F}\right) \xi} \quad , \tag{10-7}$$

where we have defined the "thermal disadvantage factor" ξ as the ratio of the average flux in the moderator to that in the fuel

$$\xi \equiv \bar{\phi}_M / \bar{\phi}_F \quad . \tag{10-8}$$

This terminology arises because the thermal flux tends to be depressed in the highly absorbing fuel region, leading to a value of $\xi > 1$. Hence, since the average flux is somewhat higher in the moderator than in the fuel, the fuel nuclei are at a relative disadvantage in competing with moderator nuclei for the capture of thermal neutrons.

The depression of the thermal flux in the fuel is again a consequence of the self-shielding effect. That is, neutrons which are born in fission events in the fuel will tend to thermalize in the moderator and then must eventually diffuse back into the fuel to induce a further fission. However, the highly absorbing nuclei near the surface of the fuel pin tend to absorb the thermal neutrons diffusing back in from the moderator and hence in effect shield the fuel nuclei in the interior of the pin. This leads to the observed flux depression.

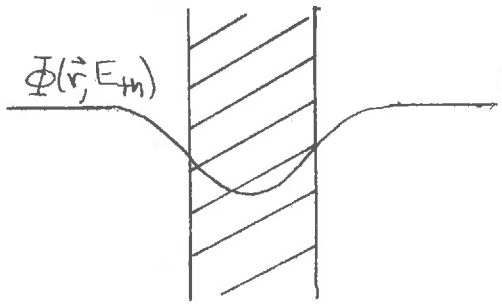

We can compare this more general definition of thermal utilization f with our earlier expression for a homogeneous system

$$f^{hom} = \frac{\Sigma_a^{F\,hom}}{\Sigma_a^{F\,hom} + \Sigma_a^{M\,hom}} \qquad (10\text{-}9)$$

if we consider the homogeneous system to consist of unit cells of the same volume $V_{cell} = V_F + V_M$ as our heterogeneous cell, but with the fuel and moderator now spread uniformly over the cell. Hence we would now find the fuel and moderator number densities in the homogeneous cell as

$$N_F^{hom} = \frac{N_F V_F}{V_{cell}} \quad , \quad N_M^{hom} = \frac{N_M V_M}{V_{cell}} \tag{10-10}$$

If we now note that the macroscopic cross sections for the homogeneous cell are $\Sigma_a^{F\,hom} = N_F^{hom} \sigma_a^F$, $\Sigma_a^{M\,hom} = N_M^{hom} \sigma_a^M$, we find from Eq. (10-9)

$$f^{hom} = \frac{\Sigma_a^F}{\Sigma_a^F + \Sigma_a^M \left(\frac{V_M}{V_F}\right)} \tag{10-11}$$

Comparing this with our more general definition for a heterogeneous system in Eq. (10-8), which we will now refer to as f^{het}, we note that in general

$$f^{het} \leq f^{hom} \quad , \tag{10-12}$$

since $\xi \geq 1$ (as the flux depression in the fuel would imply). Therefore, lumping the fuel into a heterogeneous lattice will actually lower thermal utilization, thereby decreasing core multiplication.

One can generalize the concept of thermal utilization even further to account for a multiregion fuel cell. Consider, for example, a three region fuel cell composed of fuel, clad, and moderator material. Then, in analogy with our two region example, we would write

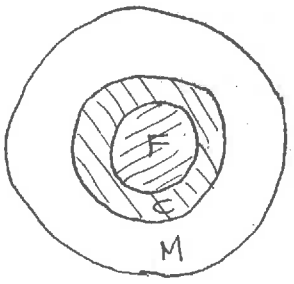

$$f = \frac{\Sigma_a^F V_F \bar{\phi}_F}{\Sigma_a^F V_F \bar{\phi}_F + \Sigma_a^M V_M \bar{\phi}_M + \Sigma_a^C V_C \bar{\phi}_C} \qquad (10\text{-}13)$$

If we now divide through by the average flux in the fuel, we find that the thermal utilization f involves two thermal disadvantage factors, one for the fuel to moderator, $\bar{\phi}_M / \bar{\phi}_F$, and one for the fuel to clad, $\bar{\phi}_C / \bar{\phi}_F$.

As yet we have said nothing concerning just how one calculates these thermal disadvantage factors. Of course it might be argued that the concept of thermal utilization within the context of the 6-factor formula has very limited utility aside from crude survey estimates. We will see later, however, that the disadvantage factor ζ can be used to spatially average thermal group constants over unit fuel cells, and hence plays an extremely important role in reactor design. For this reason, we will devote a considerable amount of attention towards its calculation in the next section. We will examine both approximate ("quick-and-dirty") ways to estimate ζ as well as more elaborate schemes based upon transport theory and collision probability methods.

P_{NFL}, P_{NTL}: Since most heterogeneous effects enter into thermal neutron diffusion, we will consider only the thermal nonleakage probability

$$P_{NTL} = \left(1 + L^2 B^2\right)^{-1} \qquad (10\text{-}14)$$

Here B^2 characterizes the overall geometry of the system, and hence will not be affected by heterogeneous effects. We will confine our immediate attention to a study of the effects of heterogeneities upon the diffusion length L.

If we recall $L^2 = D/\Sigma_a$ and define the average cross section over a unit cell as

$$\Sigma \equiv \frac{\Sigma^F V_F \bar{\phi}_F + \Sigma^M V_M \bar{\phi}_M}{\bar{\phi}_M V_M + \bar{\phi}_F V_F} , \qquad (10\text{-}15)$$

then we find

$$L^2 = \frac{(\bar{\phi}_M V_M + \bar{\phi}_F V_F)^2}{3(\Sigma_{tr}^M V_M \bar{\phi}_M + \Sigma_{tr}^F V_F \bar{\phi}_F)(\Sigma_a^F V_F \bar{\phi}_F + \Sigma_a^M V_M \bar{\phi}_M)}$$

$$= \left(\frac{\bar{\phi}_M V_M + \bar{\phi}_F V_F}{\bar{\phi}_M V_M}\right)^2 \frac{(1-f) L_M^2}{1 + (\Sigma_{tr}^F V_F / \Sigma_{tr}^M V_M \xi)} \qquad (10\text{-}16)$$

In particular, notice that for small fuel pins, $V_F << V_M$, we find that $\bar{\phi} \sim \bar{\phi}_M$ and

$$\frac{\Sigma_{tr}^F V_F}{\Sigma_{tr}^M V_M \xi} << 1$$

such that

$$L^2 \cong \frac{(1-f) L_M^2}{1 + \left(\frac{\Sigma_{tr}^F V_F}{\Sigma_{tr}^M V_M \xi}\right)} \cong L_M^2 (1-f) . \qquad (10\text{-}17)$$

Hence the diffusion length tends to be decreased from its value in a purely moderating medium by an amount dependent upon the fuel absorption. Thus the nonleakage probability $P_{NTL} = (1 + L^2B^2)^{-1}$ is increased.

p: Perhaps the most significant effect due to heterogeneous arrangement of fuel in a thermal reactor is a significant increase in the resonance escape probability. This modification occurs as a consequence of two phenomena: First, there is a geometrical effect arising because the physical separation of the fuel and the moderator will allow some neutrons to slow down without ever encountering the fuel. This effect is of secondary importance to the phenomenon of self-shielding, however.

To understand this second effect more clearly, consider a sketch of the spatial dependence of the neutron flux at several different energies characterizing a resonance:

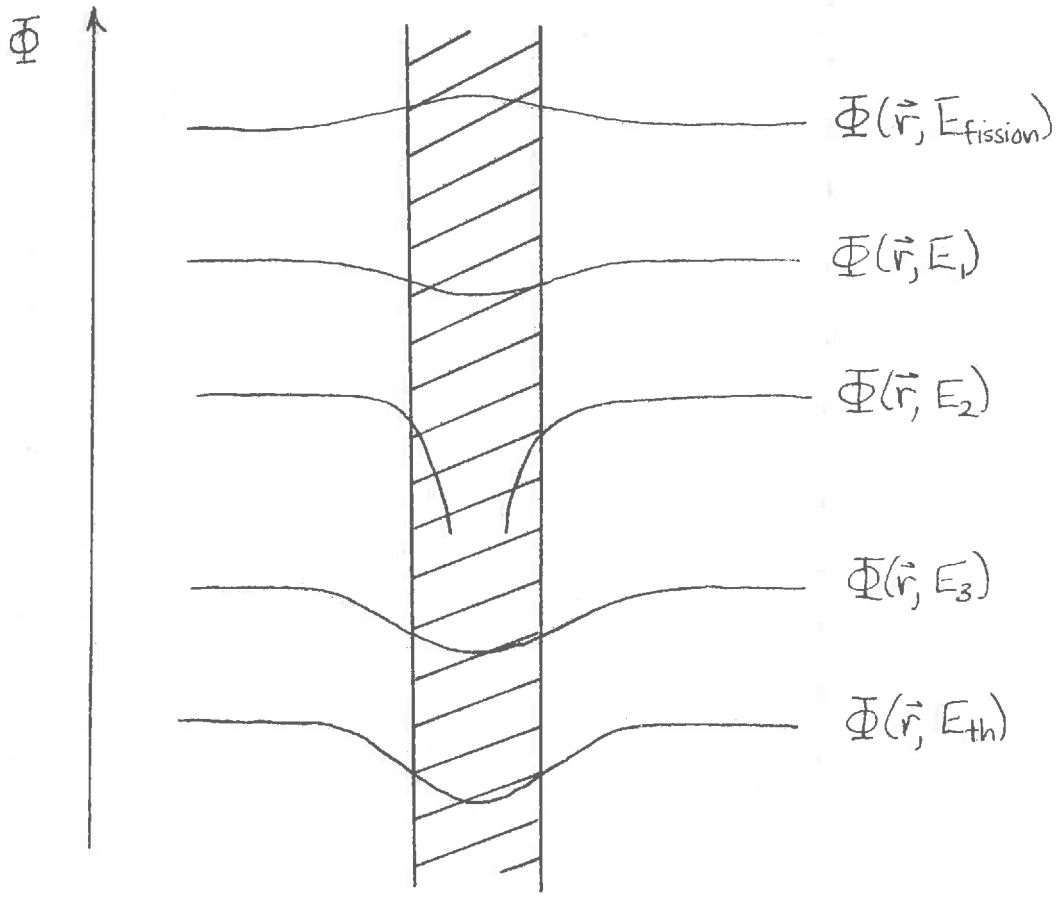

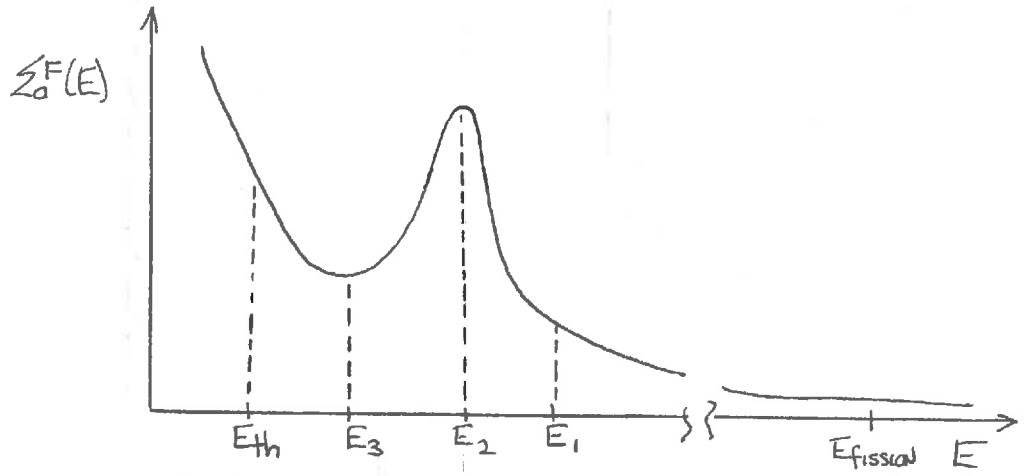

Of course at fission energies, we might expect the flux to peak in the fuel since the fission sources are confined to the fuel. However once we have dropped in energy much below the fission energy, we will begin to see a flux depression in the fuel. This arises because the fission neutrons must escape the fuel pin into the moderator in order to be appreciably moderated. [Nuclear inelastic scattering from fuel isotopes as well as elastic scattering from light isotopes such as oxygen admixed into the fuel cause some moderation, but this is a secondary effect in thermal reactors.] Hence the moderator presents effectively a volumetric source of neutrons appearing at the lower energies. These neutrons must then either downscatter to even lower energies, or diffuse into the fuel where they are absorbed.

The fuel presents a very highly absorbing medium to the neutrons diffusing in from the moderator. This absorption is sufficiently strong, that many of the neutrons incident upon the fuel are absorbed in the outer layers of the fuel pin. Hence the fuel nuclei in the pin interior see a somewhat depressed flux due to the effective shielding presented by the fuel nuclei near the fuel pin surface. Such self-shielding is present to a certain degree at all energies below fission energies.

However it becomes much more pronounced when the fuel absorption cross section is large--such as at a resonance in the absorption cross section or in the thermal energy range.

This effect is quite pronounced. For example, the resonance integral characteristic of natural uranium uniformly mixed with moderating material is about 280 barns, lumping the uranium, we can reduce the resonance integral to a value of 9 barns--a reduction of 30-fold. We will see later than one can usually write the effective resonance integral in the form

$$I = C_1 + C_2\left(\frac{A_F}{M_F}\right) \quad , \tag{10-18}$$

where A_F is the surface area of the fuel lump, and M_F is its mass (proportional to its volume). As (A_F/M_F) decreases--corresponding to more highly heterogeneous lattice configurations -- the resonance integral decreases.

To treat the effects of heterogeneities in resonance absorption requires the use of several concepts from transport theory. Since this subject is of considerable importance in thermal reactor design, we will discuss it in some detail in Section 10-3.

ϵ : The fast fission factor is also increased somewhat by going to a heterogeneous lattice. To understand why, one need only recall that a neutron's energy must be above a certain threshold in order to induce a fast fission reaction in a fissionable isotope such as U^{238}. By lumping the fuel, one effectively increases the probability that a high

energy fission neutron will encounter a fuel nucleus before it is slowed down below the fast fission energy threshold, either by elastic scattering collisions with moderator nuclei or inelastic scattering from fuel nuclei.

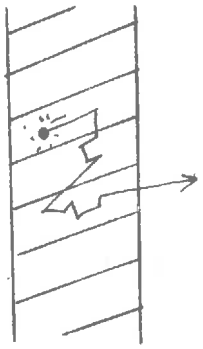

In summary, then, lumping the fuel into a heterogeneous lattice can significantly increase k_∞ for natural and slightly enriched ($\lesssim 5\%$) uranium cores. The dominant effect is contained in the behavior of f and p. By way of example, for a natural uranium-graphite lattice with cylindrical fuel rods of 1.25 cm radius, the values of f and p for several different pitches is given below:

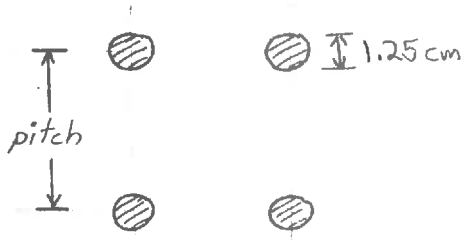

cell pitch (cm)	f	p	k_∞
10	.907	.866	1.073
11	.888	.890	1.082
12	.867	.908	1.076
13	.846	.923	1.066

We will now proceed to discuss the various techniques used to account for lattice effects in nuclear reactor analysis. Our primary concern will be a consideration of just how heterogeneous effects are included in reactor design methods. To this end, we first will study how lattice effects enter into the generation of thermal group constants, with primary attention devoted to the calculation and use of

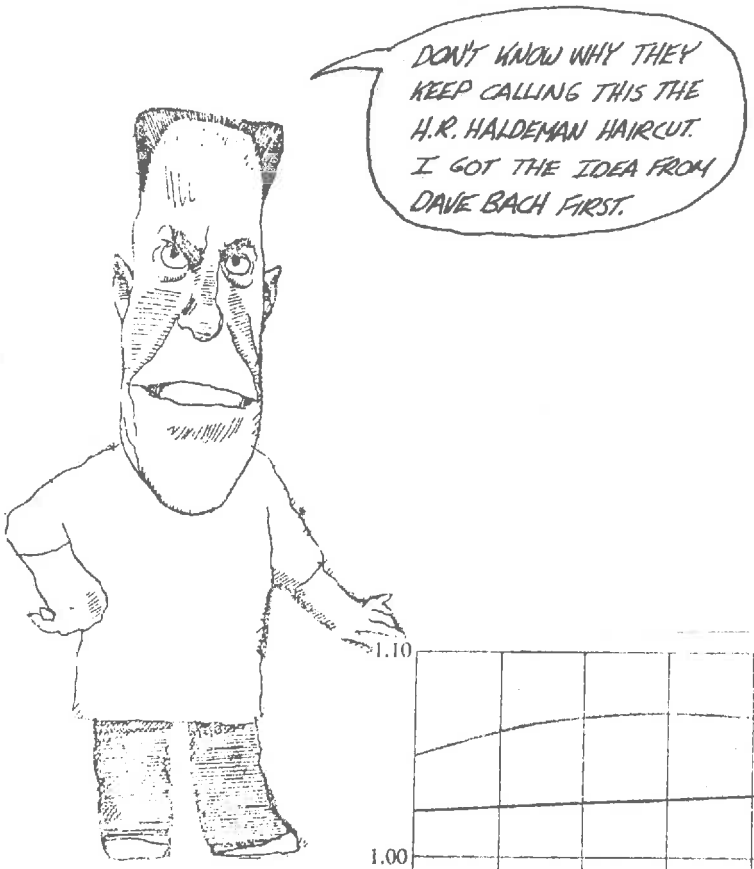

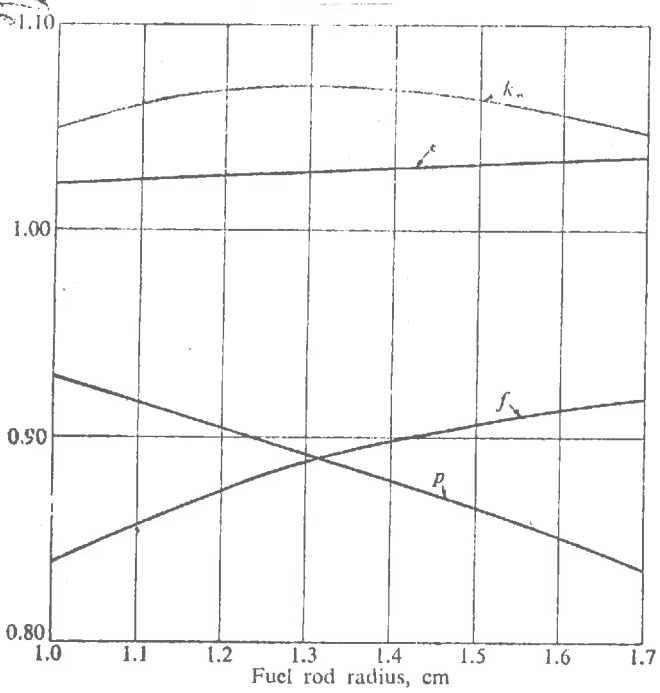

Reactor parameters for the Brookhaven Research Reactor. [Based on I. Kaplan and J. Chernick, "The Brookhaven Nuclear Reactor: Theory and Nuclear Design Calculations," BNL-152 (January 1952).]

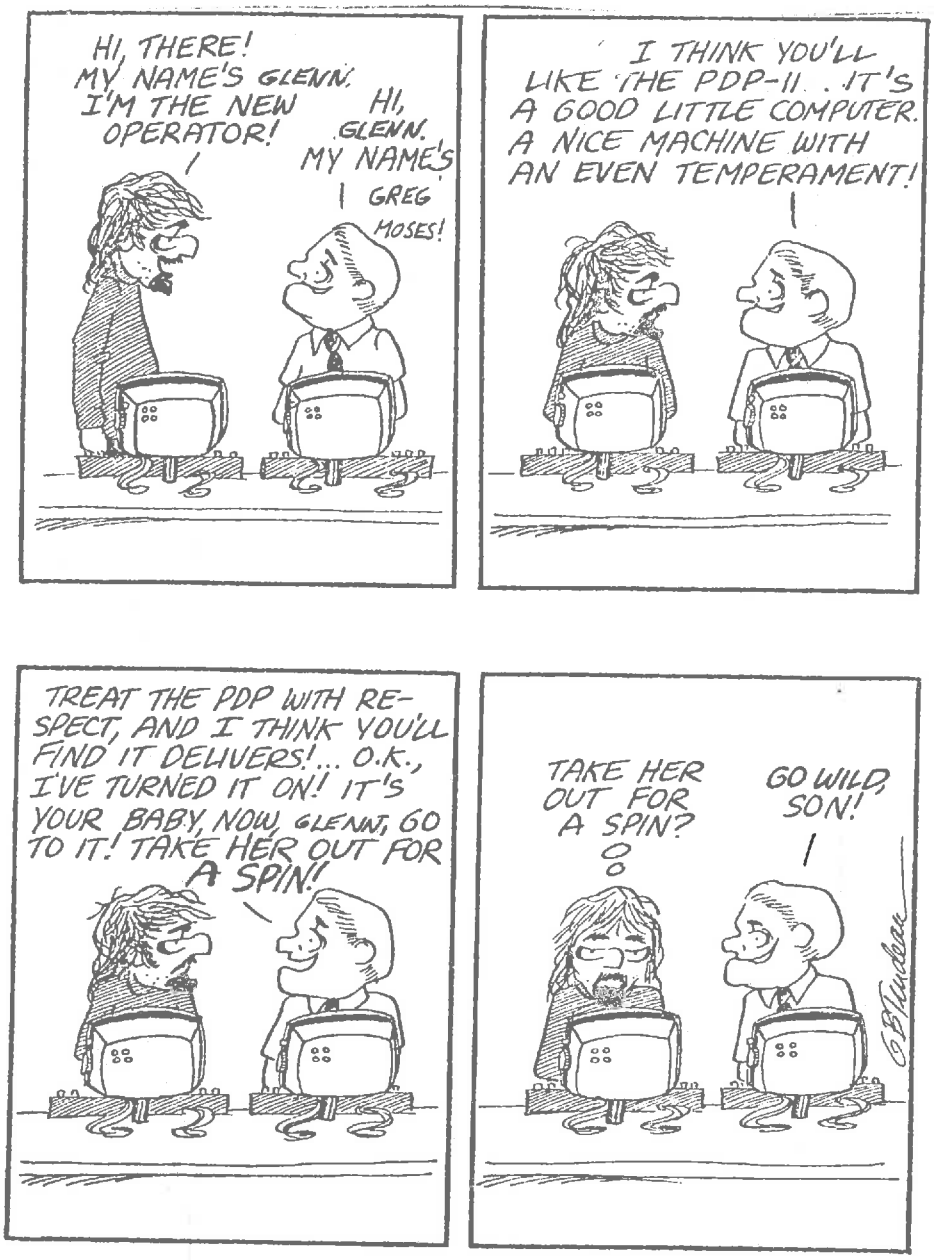
HI, THERE! MY NAME'S GLENN. I'M THE NEW OPERATOR!
HI, GLENN. MY NAME'S GREG MOSES!
I THINK YOU'LL LIKE THE PDP-11. IT'S A GOOD LITTLE COMPUTER. A NICE MACHINE WITH AN EVEN TEMPERAMENT!
TREAT THE PDP WITH RESPECT, AND I THINK YOU'LL FIND IT DELIVERS!... O.K., I'VE TURNED IT ON! IT'S YOUR BABY, NOW, GLENN, GO TO IT! TAKE HER OUT FOR A SPIN!
TAKE HER OUT FOR A SPIN?
GO WILD, SON!
©B Hudson

thermal disadvantage factors. We then will discuss heterogeneous effects in fast spectrum calculations--both in resonance absorption and fast fission.

It should be admitted that our principal orientation in this chapter is with thermal reactor analysis, since for these systems the treatment of heterogeneities is of paramount importance. However many of the techniques we will develop can be (and are) used as well in the analysis of fast reactors (particularly those schemes used in the treatment of resonance absorption).

II. HETEROGENEOUS EFFECTS IN THERMAL NEUTRON PHYSICS

A. Thermal Utilization, Disadvantage Factors, and Cell-Averaged Thermal Group Constants

As we have seen, the core of a nuclear reactor is made up of thousands of individual fuel cells, each characterized by the fuel element itself, usually some cladding material (separated from the fuel element by a gap), and an adjacent moderator which may also serve as a coolant:

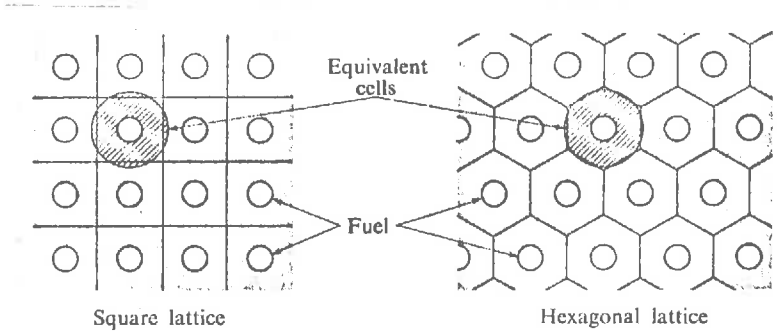

Two typical heterogeneous lattices and equivalent cells for each.

We have also noted that it would be prohibitively expensive to perform a detailed few group diffusion calculation taking into account the detailed configuration and composition of each fuel cell--indeed, the very high absorption present in the fuel element makes the use of the diffusion approximation highly questionable.

Instead the approach is to perform a detailed calculation of the flux in only one typical fuel cell, and then to use this flux to spatially average the thermal group constants over the cell. Let us illustrate this by an example: Consider a typical square lattice fuel cell with a cylindrical fuel pin. One first replaces this geometry by an equivalent unit cell to simplify the calculations, taking care to preserve the same volume of fuel, V_F, and moderator, V_M. Now suppose that somehow we can calculate the average thermal flux in the fuel, $\bar{\phi}_F$, and in the moderator, $\bar{\phi}_M$. Suppose that we have also obtained the few group constants characterizing a homogeneous mixture of fuel and moderator--that is, suppose we have performed a thermal spectrum calculation (e.g., using SOFOCATE) for an infinite medium of identical composition, however with the number densities of fuel and moderator being uniformly distributed over the cell volume. We then use this spectrum to determine the group constants characterizing the fuel and moderator, e.g.,

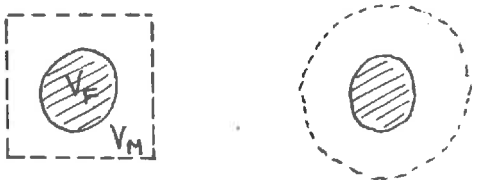

$$\Sigma_a^F = \frac{\int_0^{E_{th}} dE\, \Sigma_a^F(E)\, \phi(E)}{\int_0^{E_{th}} dE\, \phi(E)} \qquad (10\text{-}19)$$

where $\Sigma_a^F(E) = N_F \sigma_a^F(E)$ is the macroscopic cross section in the fuel region alone (although the spectrum $\phi(E)$ has been calculated for a homogeneous mixture of fuel and moderator). Similar definitions could be given for group constants characterizing the moderator.

One can now define cell-averaged group constants as follows:

$$\langle \Sigma_a \rangle_{cell} = \frac{\int_{V_{cell}} d^3r \, \Sigma_a(\vec{r}) \Phi(\vec{r})}{\int_{V_{cell}} d^3r \, \Phi(\vec{r})}$$

$$= \frac{\Sigma_a^F \int_{V_F} d^3r \, \Phi(\vec{r}) + \Sigma_a^M \int_{V_M} d^3r \, \Phi(\vec{r})}{\int_{V_F} d^3r \, \Phi(\vec{r}) + \int_{V_M} d^3r \, \Phi(\vec{r})} , \qquad (10\text{-}20)$$

or using our earlier definitions of region averaged fluxes, i.e.,

$$\bar{\phi}_F \equiv \frac{1}{V_F} \int_{V_F} d^3r \, \Phi(\vec{r}) , \quad \bar{\phi}_M \equiv \frac{1}{V_M} \int_{V_M} d^3r \, \Phi(\vec{r}) , \qquad (10\text{-}21)$$

we find

$$\langle \Sigma_a \rangle_{cell} = \frac{\Sigma_a^F V_F \bar{\phi}_F + \Sigma_a^M V_M \bar{\phi}_M}{V_F \bar{\phi}_F + V_M \bar{\phi}_M} , \qquad (10\text{-}22)$$

or

$$\langle \Sigma_a \rangle_{cell} = \frac{\Sigma_a^F + \Sigma_a^M \left(\frac{V_M}{V_F}\right) \xi}{1 + \left(\frac{V_M}{V_F}\right) \xi} . \qquad (10\text{-}23)$$

Hence, provided we can determine the ratio of the average thermal fluxes in each region, i.e., the thermal disadvantage factor

$$\xi \equiv \bar{\phi}_M / \bar{\phi}_F \,, \tag{10-24}$$

then we can immediately calculate cell-averaged group constants which effectively replace the equivalent heterogeneous cell by an effective homogeneous cell:

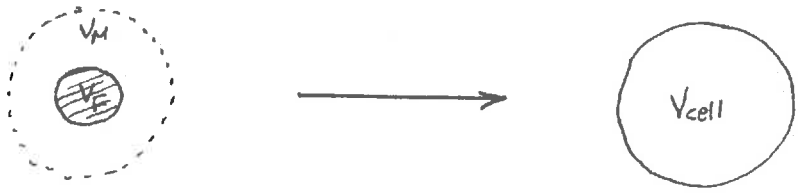

We can perform similar cell averages of the other thermal group constants. For example, the transport cross section is defined by

$$\langle \Sigma_{tr} \rangle_{cell} = \frac{\Sigma_{tr}^F + \Sigma_{tr}^M \left(\frac{V_M}{V_F}\right) \xi}{1 + \left(V_M/V_F\right) \xi} \,. \tag{10-25}$$

Now since $\langle D \rangle = 1/3 \langle \Sigma_{tr} \rangle$, we find

$$\left\langle \frac{1}{D} \right\rangle_{cell} = \frac{\frac{1}{D_F} + \frac{1}{D_M}\left(\frac{V_M}{V_F}\right) \xi}{1 + \left(V_M/V_F\right) \xi} \,. \tag{10-26}$$

Finally, noting that $L^2 = D/\Sigma_a$,

$$\langle L^2 \rangle_{cell} = \frac{\left[1 + \left(\frac{V_M}{V_F}\right) \xi\right]^2}{\left[\frac{1}{D_F} + \frac{1}{D_M}\left(\frac{V_M}{V_F}\right) \xi\right]\left[\Sigma_a^F + \Sigma_a^M \left(\frac{V_M}{V_F}\right) \xi\right]} \,. \tag{10-27}$$

It should be noted here that we have merely performed a formal spatial average of these quantities over the thermal flux shape, just as we did when we expressed the thermal utilization in terms of the thermal disadvantage factor

$$f = \frac{\Sigma_a^F}{\Sigma_a^F + \Sigma_a^M \left(\frac{V_M}{V_F}\right) \xi} \qquad (10\text{-}27)$$

Thus we once again find that the key to including heterogeneities in the generation of thermal group constants rests on our ability to estimate the spatial dependence of the thermal flux in the cell--that is, to determine the thermal disadvantage factor ξ .

[We might remark here that we have only presented one of several possible schemes to perform cell averaging using disadvantage factors. Later in the next section we will present an alternative scheme which utilizes an energy-dependent disadvantage factor $\xi(E)$.]

For the large natural uranium-graphite moderated reactors of interest during the early years of the nuclear energy program, one could actually utilize one-speed diffusion theory to calculate ξ . However in the more highly enriched and tightly packed core lattices utilized in today's modern power reactors, diffusion theory estimates are quite poor. Hence we will describe two alternative schemes useful for determining the thermal disadvantage factor, both of which are based upon transport theory. The first method is an analytic scheme first proposed by Amouyal, Benoist, and Horowitz, the so-called ABH method. It relies upon concepts very closely related to the method of collision probabilities we will introduce in more detail when we discuss resonance

absorption. The second scheme we shall discuss actually solves the energy-dependent neutron transport equation for the equivalent cell of interest to generate the thermal flux and perform spatial averaging over the cell. This scheme, known as THERMOS, discretizes the integral form of the transport equation, thereby reducing it to a system of algebraic equations which can be solved on a computer.

There are still other methods for calculating spatially dependent thermal neutron spectra, ranging all the way from the assumption of a fundamental spatial mode (such as was used in the B_N or P_N methods discussed in Chapter 8) to direct S_N solutions of the transport equation or Monte Carlo calculations. The choice of the method will depend both upon the detail required in the design as well as upon computer capability (and allowable expense). In recent years, the trend has been towards more careful treatment of the spatial detail of the lattice, and towards more precise transport descriptions, with increasing use of Monte Carlo techniques.

B. The ABH Method

The ABH method combines aspects of transport theory, collision probability methods, and diffusion theory to calculate the thermal disadvantage factor characteristic of a unit fuel cell. More specifically, diffusion theory is used to describe the flux in the moderator, although a transport correction is introduced into the boundary condition at the moderator-fuel interface. Neutron transport in the fuel is described by multiple collision probabilities. All of these calculations are performed in the one-speed approximation and yield ξ in terms of the one-group constants characterizing materials in the cell.


AIEE!
AIEE!!
AIEE!!
I TAKE IT YOU WANT OUT.
©Hindman

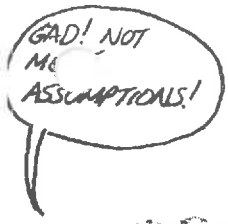

Before we begin our description of the method, let us be a bit more precise in our definition of a unit fuel cell. We will make four assumptions concerning the treatment of the cell:

(i) There are no neutrons slowing to thermal energies in the fuel region. This assumption is quite reasonable in thermal power reactor lattices, since moderation in the fuel occurs only via inelastic scattering or elastic scattering with admixed materials such as oxygen or carbon, both of which yield inconsequential moderation when compared to the surrounding moderating region.

(ii) We can treat the spatial distribution of neutrons slowing down within the moderator region as uniform. To motivate this assumption, notice that in most cases, the distance required to slow a fission neutron to thermal energies ($\sqrt{\langle r^2 \rangle} = \sqrt{6\tau}$) is quite large compared to the lattice spacing or pitch. For example, in a LWR, the rms distance to slow down is roughly 12 cm, compared to a typical pitch of 2-3 cm. Hence the neutrons slowing down within any moderating region come from a large number of the surrounding fuel pins. This tends to yield a more uniformly distributed slowing down source, as the simple sketch below indicates:

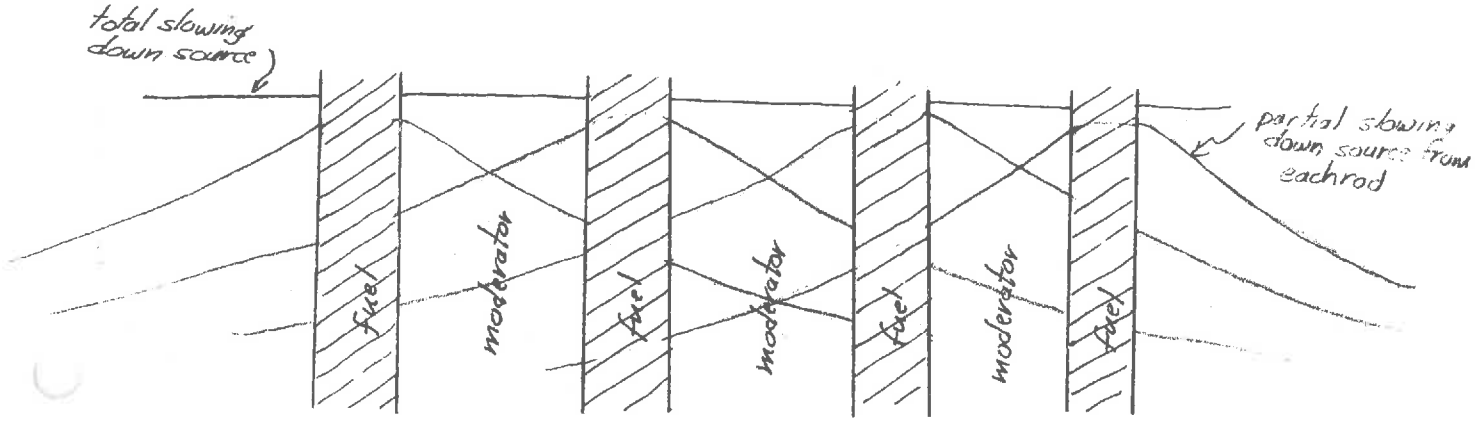

(iii) We will finally assume that there is no net flow of neutrons between the cells. Surely this requirement would be true for an infinite lattice of identical fuel cells. It would be expected to break down only near the core boundaries or near to control elements or fuel pins of nonuniform enrichment or composition (e.g., Pu loaded fuel pins which are characterized by strong absorption resonances in the ~.5 eV range).

(iv) We will assume that a one-speed treatment of the neutron flux in the cell is sufficient. Actually, a one-speed calculation ignores the fact that the flux in the cell is frequently inseparable in space and energy, but provided the proper thermal group constants are used in the one-speed treatment, this latter correction can frequently be ignored.

Hence our task now is to determine the neutron flux in a cell resulting from a uniformly distributed source in the moderator region, subject to the condition of zero neutron current on the boundaries of the cell.

To proceed, suppose we can determine the flux at a point $\vec{r}$ in the fuel due to a unit point source at $\vec{r}'$--that is, suppose that by hook or by crook we have obtained the point source kernel or Green's function for this geometry, call it $G(\vec{r},\vec{r}')$. Now the effective source in the moderator is just the slowing down density at thermal energies, $q(\vec{r},E_{th})$.

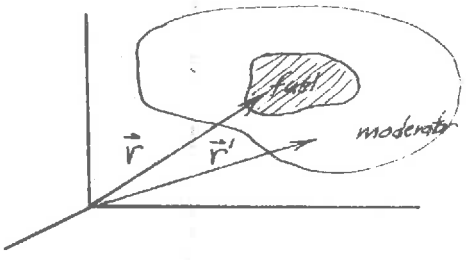

Hence we can use the point source kernel to write the flux at any point $\vec{r}$ as

$$\Phi(\vec{r}) = \int_{V_{cell}} d^3r' \; G(\vec{r}, \vec{r}') \, q(\vec{r}', E_{th})$$

$$= q_0 \int_{V_M} d^3r' \; G(\vec{r}, \vec{r}') \qquad (10\text{-}28)$$

where we have noted that the slowing down source is presumed to be zero in the fuel, and to be constant, say $q(\vec{r}, E_{th}) = q_0$, for $\vec{r}$ in the moderator.

Let's now calculate the rate at which neutrons are absorbed in the fuel

$$\text{rate of absorption in fuel} = \int_{V_F} d^3r \, \Sigma_a^F \Phi(\vec{r}) = \Sigma_a^F q_0 \int_{V_F} d^3r \int_{V_M} d^3r' \, G(\vec{r}, \vec{r}') \qquad (10\text{-}29)$$

The total number of neutrons slowing down per second in the cell is just $q_0 V_M$. In a steady state situation, all of these neutrons must be absorbed. Hence the total rate at which absorption is occurring in the cell is just $q_0 V_M$. We can use this to calculate the thermal utilization for the cell as

$$f = \frac{\text{rate of absorption in fuel}}{\text{total rate of absorption in cell}} = \frac{\Sigma_a^F}{V_M} \int_{V_F} d^3r \int_{V_M} d^3r' \, G(\vec{r}, \vec{r}') \qquad (10\text{-}30)$$

We will turn this problem around a bit by using a rather interesting property of the one-speed point source kernel known as the "reciprocity theorem":

$$G(\vec{r},\vec{r}') = G(\vec{r}',\vec{r}) \tag{10-31}$$

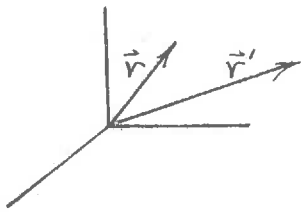

Notice that this theorem says that the flux at a point $\vec{r}$ due to a unit point source at $\vec{r}'$ is the same as when the source and detector positions are switched. A quick inspection of the explicit forms we obtained for $G(\vec{r},\vec{r}')$ in Chapter 5 using one-speed diffusion theory indicates that at least in this approximation, $G(\vec{r},\vec{r}')$ does indeed exhibit this symmetry. However, the reciprocity theorem is much more general, and indeed one can show that it holds even when $G(\vec{r},\vec{r}')$ is obtained from the one-speed transport equation (see Appendix J for details).

We will now use Eq. (10-31) to rewrite f as

$$f = \frac{\Sigma_a^F}{V_M}\int_{V_F} d^3r \int_{V_M} d^3r' \, G(\vec{r}',\vec{r}) = \frac{\Sigma_a^F}{V_M}\int_{V_M} d^3r' \int_{V_F} d^3r \, G(\vec{r}',\vec{r}) \tag{10-32}$$

Notice that $\int_{V_F} d^3r \, G(\vec{r}',\vec{r})$ is just the flux produced at a point $\vec{r}'$ in the moderator due to a uniformly distributed source in the fuel. Furthermore we can identify

$$\frac{\Sigma_a^M}{V_F}\int_{V_M} d^3r' \int_{V_F} d^3r \, G(\vec{r}',\vec{r}) \equiv P \tag{10-33}$$

as the probability that a neutron produced by a uniformly distributed source in the fuel will be absorbed in the moderator. In this sense,

we have used the reciprocity theorem to formally switch our problem around.

It is useful to formally break this probability into two components:

$$P = P_F \, P'$$

where

P_F = probability that a neutron born uniformly in the fuel escapes from the fuel without being absorbed

P' = conditional probability that the neutron, having escaped from the fuel will be absorbed in the moderator

Hence we can now rewrite the thermal utilization in terms of these probabilities as

$$f = \left(\frac{\Sigma_a^F}{\Sigma_a^M}\right)\left(\frac{V_F}{V_M}\right) P_F \, P' \quad . \tag{10-34}$$

We are usually not interested in the thermal utilization f, but rather in the thermal disadvantage factor ξ which can be used directly in the generation of cell-averaged group constants. But if we use Eq. (10-27), we can express ξ in terms of f as

$$\xi = \left(\frac{\Sigma_a^F}{\Sigma_a^M}\right)\left(\frac{V_F}{V_M}\right)\left(\frac{1}{f} - 1\right) \quad . \tag{10-35}$$

After some manipulation, we can rewrite

$$\left(\frac{1}{f} - 1\right) = \left(\frac{\Sigma_a^M}{\Sigma_a^F}\right)\left(\frac{V_M}{V_F}\right)\frac{1}{P_F} + \frac{1 - f - P'}{f} \quad . \tag{10-36}$$

This rearrangement proves useful because the second term on the RHS is usually much smaller than the preceding term. Hence rather crude estimates for f and P' can be used to evaluate this term.

In fact, one can usually just assume for this calculation that the fuel lump is "black"--that is, it absorbs all incident neutrons. For such a cell, obviously

$f = P_M$ = probability that a neutron born uniformly and isotropically in the moderator passes into the fuel

Furthermore, the escape probability in a black fuel lump will later be shown to be

$$P_F\Big|_{\substack{\text{black}\\ \text{lump}}} = \frac{S_F}{4V_F \Sigma_a^F}, \tag{10-37}$$

where S_F is the surface area of the fuel lump. If we recall

$$f = \left(\frac{\Sigma_a^F}{\Sigma_a^M}\right)\left(\frac{V_F}{V_M}\right) P_F P', \tag{10-38}$$

we can solve for

$$P' = \frac{4 \Sigma_a^M V_M P_M}{S_F}. \tag{10-39}$$

Hence, using these results for P' and f in the second term of Eq. (10-36), we find

$$\left(\frac{1}{f} - 1\right) = \left(\frac{\Sigma_a^M}{\Sigma_a^F}\right)\left(\frac{V_M}{V_F}\right)\frac{1}{P_F} + \frac{1-P_M}{P_M} - \frac{4\Sigma_a^M V_M}{S_F}. \tag{10-40}$$

We now turn to a more precise estimate of the escape probability for a "grey" fuel lump--that is, for a fuel lump in which scattering may occur--which is necessary in order to adequately calculate the first term. Suppose we first write

$$P_F = P_{F_0} + P_{F_1} + P_{F_2} + \cdots = \sum_{n=0}^{\infty} P_{Fn} \qquad (10\text{-}41)$$

where P_{Fn} is the probability that a neutron escapes from the fuel lump after scattering n times within the fuel.

Let's begin by considering

P_{Fo} = probability that a neutron escapes from fuel without scattering

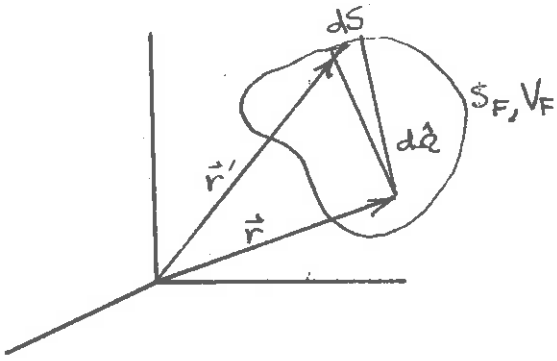

Let there be S_0 neutrons emitted uniformly and isotropically in the fuel per cm^3-sec. Then the number of neutrons from d^3r passing through a differential surface area is

$$\frac{S_0}{4\pi} d^3r\, d\hat{\Omega}\, e^{-\Sigma_t^F |\vec{r}-\vec{r}'|}$$

Hence the total escape rate is obtained by integrating over all angles and all the surface

$$\text{escape rate} = \frac{S_0}{4\pi} \int_{V_F} d^3r \int_{4\pi} d\hat{\Omega}\, e^{-\Sigma_t^F |\vec{r}-\vec{r}'|} \qquad (10\text{-}42)$$

But

$$P_{F_o} = \frac{\text{escape rate}}{V_F S_o} = \frac{1}{4\pi V_F} \int_{V_F} d^3r \int_{4\pi} d\hat{\Omega}\, e^{-\Sigma_t^F |\vec{r}-\vec{r}'|} \qquad (10\text{-}43)$$

[Of course, for a purely absorbing or black fuel lump, $P_F = P_o$.]

Now it is useful to introduce a variable transformation:

$$d^3r = \hat{\Omega}\cdot\hat{n}_s\, dS\, dR$$

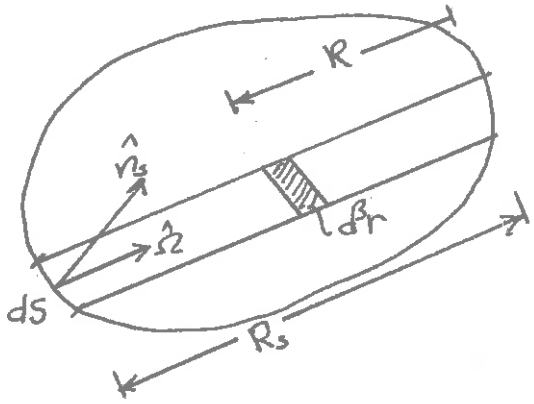

Thus

$$P_{F_o} = \frac{1}{4\pi V_F} \int_{S_F} dS \int_0^{R_s} dR \int_{4\pi} d\hat{\Omega}\, e^{-\Sigma_t^F R}\, \hat{\Omega}\cdot\hat{n}_s \qquad (10\text{-}44)$$

$$= \frac{1}{4\pi V_F \Sigma_t^F} \int_{S_F} dS \int_{4\pi} d\hat{\Omega}\, (\hat{\Omega}\cdot\hat{n}_s)\left(1 - e^{-\Sigma_t^F R_s}\right).$$

To proceed further, we will utilize the so-called "chord method" developed by Dirac. First note that the number of chords which are drawn in a given direction are proportional to $\hat{\Omega}\cdot\hat{n}_s$, the cosine of the angle between the normal to the surface, $\hat{n}_s$, and the chord direction $\hat{\Omega}$. Define the chord length distribution function $\phi(R)$ as

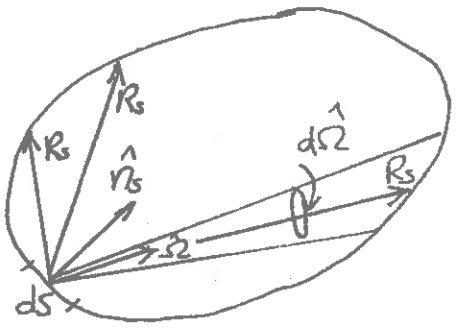

$\varphi(R)dR$ = probability that a chord is of length between R and R + dR

Then we see

$$\varphi(R)dR = \frac{\int ds \int_{R_s \in (R,dR)} d\hat{\Omega}\ \hat{\Omega}\cdot\hat{n}_s}{\int ds \int_{\hat{\Omega}\cdot\hat{n}_s>0} d\hat{\Omega}\ \hat{\Omega}\cdot\hat{n}_s} \tag{10-45}$$

But

$$\int ds \int_{\hat{\Omega}\cdot\hat{n}_s>0} d\hat{\Omega}\ \hat{\Omega}\cdot\hat{n}_s = \int_0^{2\pi} d\phi \int_S ds \int_0^1 \mu\, d\mu = \pi S \tag{10-46}$$

so that

$$\varphi(R)dR = \frac{1}{\pi S}\int ds \int_{R_s\in(R,dR)} d\hat{\Omega}\ \hat{\Omega}\cdot\hat{n}_s \tag{10-47}$$

Thus the average chord length is

$$\langle R\rangle = \int R\varphi(R)dR = \frac{1}{\pi S}\int dR \int ds \int_{R_s\in(R,dR)} d\hat{\Omega}\ R(\hat{\Omega}\cdot\hat{n}_s) \tag{10-48}$$

$$= \frac{1}{\pi S} V \int d\hat{\Omega} = \frac{4V}{S}$$

Thus we can write

$$\int ds \int_{R_s\in(R,dR)} d\hat{\Omega}\ \hat{\Omega}\cdot\hat{n}_s = \pi S \varphi(R)\, dR \tag{10-49}$$

and

$$\int_{R_s \in (R, dR)} ds \int d\hat{\Omega}\ \hat{\Omega}\cdot\hat{n}_s = \frac{4\pi V}{\langle R\rangle}\,\varphi(R)\,dR \qquad (10\text{-}50)$$

Hence, from Eq. (10-44), we find

$$P_{F_o} = \frac{1}{\Sigma_t^F \langle R\rangle_F} \int_{R_{min}}^{R_{max}} dR\,(1-e^{-\Sigma_t^F R})\,\varphi(R). \qquad (10\text{-}51)$$

Therefore, the calculation of P_{F_o} is reduced to the purely geometrical problem of calculating the chord length distribution function $\varphi(R)$.

Example: Calculate P_{F_o} for a sphere

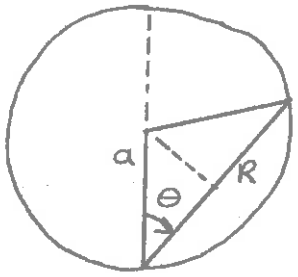

$$\varphi(R)dR = \frac{1}{\pi S}\int_{R_s\in(R,dR)} ds \int d\hat{\Omega}\ \hat{\Omega}\cdot\hat{n}_s$$

$$= \frac{1}{\pi S}\int_{R_s\in(R,dR)} ds \int \sin\theta\, d\theta\, d\phi\, \cos\theta$$

$$= \frac{1}{\pi S}\, S\, 2\pi\mu\, d\mu = 2\mu\, d\mu$$

where

$$\mu = \cos\theta = R/2a$$

$$d\mu = dR/2a$$

Hence

$$\varphi(R)dR = \frac{R}{2a^2}\,dR$$

$$\langle R\rangle = \frac{4V}{S} = 4\,\frac{\left(\frac{4}{3}\pi a^3\right)}{(4\pi a^2)} = \frac{4}{3}a$$

and

$$P_{F_0} = \frac{3}{4\Sigma_t a}\int_0^{2a} dR\,(1-e^{-\Sigma_t R})\,\frac{R}{2a^2}$$

$$= \frac{3}{8(\Sigma_t a)^3}\left[2(\Sigma_t a)^2 - 1 + (1+2\Sigma_t a)e^{-2\Sigma_t a}\right]$$

We have plotted P_{F0} vs. $\Sigma_t a$ below for several typical fuel geometries:

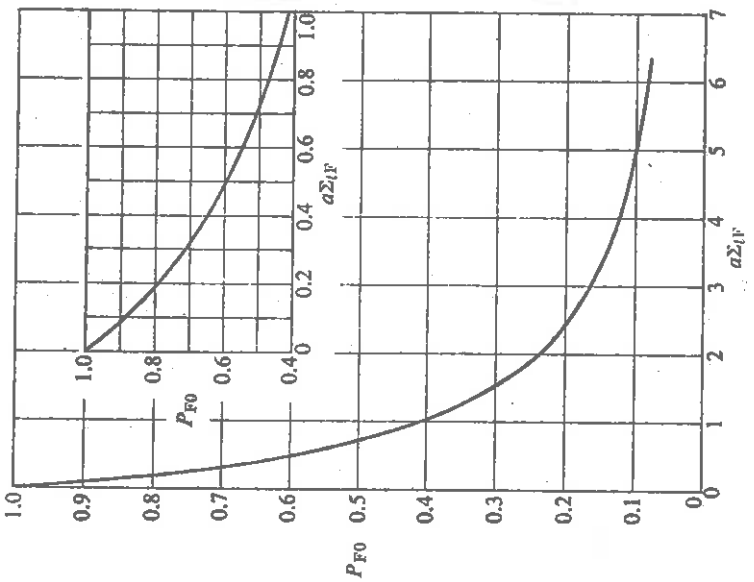

These functions have been calculated and tabulated in detail by Case, de Hoffman, and Placzek.

We next turn to the calculation of P_{F1}, the probability of escape after making one scattering collision. If we assume that the distribution of first collisions is uniform, then we can write

$$P_{F_1} = (1-P_{F_0})\,\frac{\Sigma_s^F}{\Sigma_t^F}\,P_{F_0} \qquad (10\text{-}52)$$

Likewise, if we assume the distribution of second collisions to be uniform as well, then

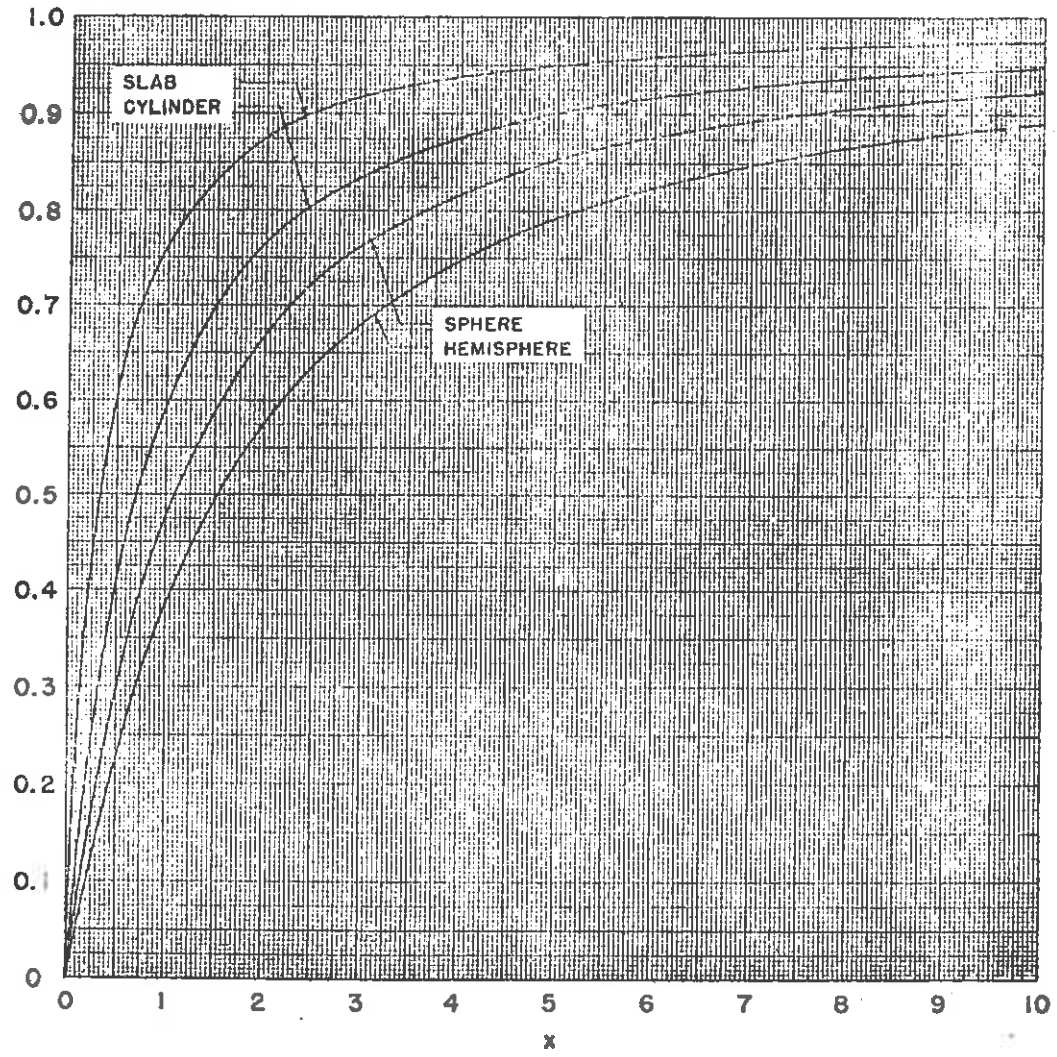

$(1 - P_{F_0})$

—Collision probabilities for uniform source density. For a cylinder, a sphere, and a hemisphere, x is the radius; for a slab, x is the half thickness. x is in units of mean free paths.

$$P_{F_2} = (1-P_{F_0}) \frac{\Sigma_s^F}{\Sigma_t^F} (1-P_{F_0}) \frac{\Sigma_s^F}{\Sigma_t^F} P_{F_0} \quad . \tag{10-53}$$

In a similar fashion, we find under the assumption of spatially uniform collision densities

$$\begin{aligned} P_F &= P_{F_0} + P_{F_1} + P_{F_2} + \cdots \\ &= P_{F_0} \left[1 + \alpha + \alpha^2 + \cdots \right] \end{aligned} \tag{10-54}$$

where $\alpha \equiv (1-P_{F_0}) \frac{\Sigma_s^F}{\Sigma_t^F} < 1$. Summing the geometric series, we obtain

$$P_F = \frac{P_{F_0}}{1-\alpha} = \frac{1}{1 + \frac{\Sigma_a^F}{\Sigma_t^F} \left(\frac{1-P_{F_0}}{P_{F_0}} \right)} \quad . \tag{10-55}$$

In the ABH method, this result is improved somewhat by using the actual distribution of first collisions. In this case, P_F is given by

$$P_F = \left\{ 1 + \frac{\Sigma_a^F}{\Sigma_t^F} \left[\frac{1-P_{F_0}}{P_{F_0}} - a \Sigma_t^F \right] \left[1 + \alpha \left(\frac{\Sigma_s^F}{\Sigma_t^F} \right) + \beta \left(\frac{\Sigma_s^F}{\Sigma_t^F} \right)^2 \right] + a \Sigma_a^F \right\}^{-1} \tag{10-56}$$

where the coefficients α and β are tabulated for cylindrical fuel elements as

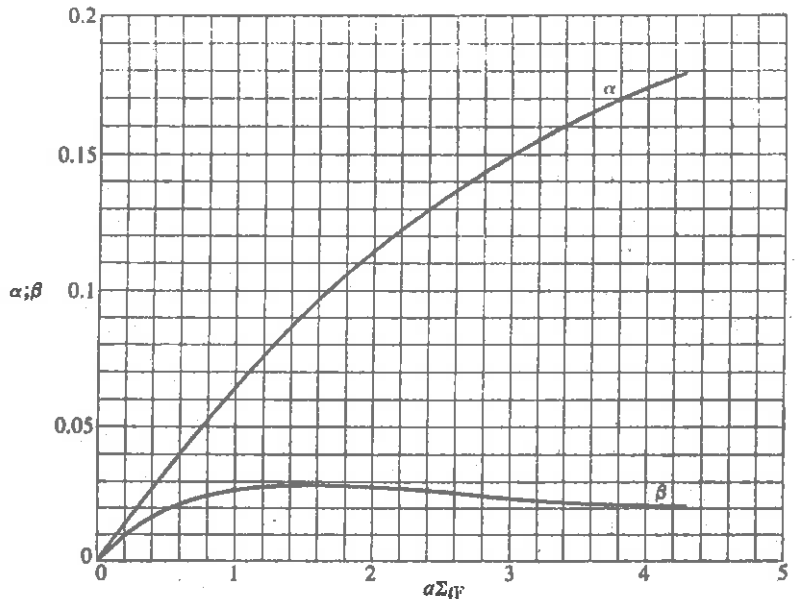

where a is the fuel rod radius. [Note that if $\alpha = \beta = 0$, this is identical to Eq. (10-55).] Now recall from the chord method that

$$P_{F_0} = \frac{S_F}{4V_F \Sigma_t^F} \int_{R_{min}}^{R_{max}} dR \left(1 - e^{-\Sigma_t^F R}\right) \phi(R) \qquad (10\text{-}57)$$

For a "black" fuel rod, we have

$$1 - e^{-\Sigma_t^F R} \cong 1 \qquad (10\text{-}58)$$

and since

$$\int_{R_{min}}^{R_{max}} \phi(R) dR = 1 \qquad (10\text{-}59)$$

we have

$$P_{F_a}\Big|_{\substack{\text{black}\\ \text{lump}}} = \frac{S_F}{4V_F \Sigma_t^F} \qquad (10\text{-}60)$$

a result we used earlier.

Our final task is to determine

P_M = probability that a neutron born uniformly and isotropically in the moderator is absorbed in the fuel (which is assumed to be black to all incident neutrons)

We will use diffusion theory to calculate P_M, although we will insert a transport theory correction at the fuel-moderator interface. That is, we will solve

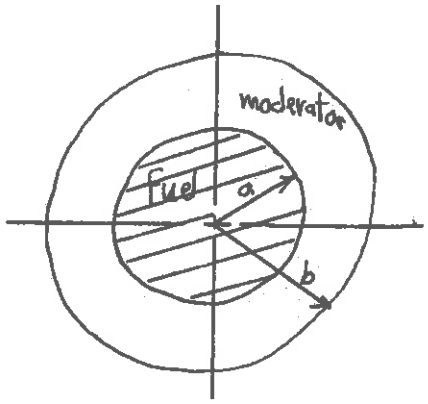

$$D_M \nabla^2 \phi_M(\vec{r}) - \Sigma_a^M \phi_M(\vec{r}) = -q(\vec{r})$$

b.c. (i) $\nabla \phi_M\Big|_b = 0$

(ii) $\frac{1}{\phi_M} \frac{d\phi_M}{dr}\Big|_a = \frac{1}{d}$

Here, we have used a transport boundary condition at r = a, involving a parameter d which is given below in terms of the fuel radius and the transport mean free path

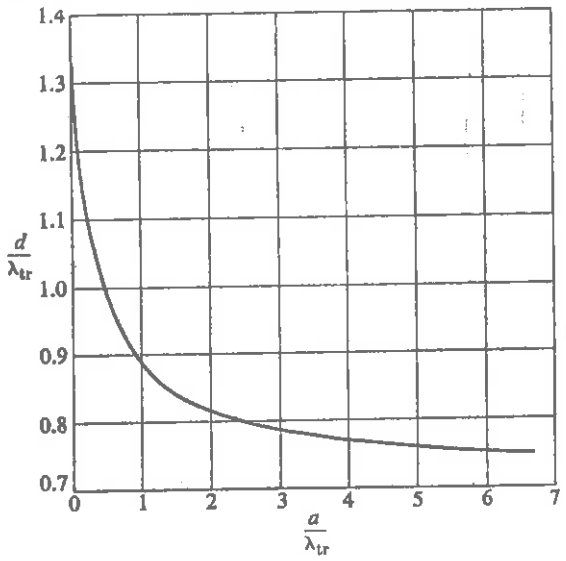

We need only solve this diffusion problem, and then use the fact that

$$P_M = \frac{2\pi a D_M}{q_o V_M} \left.\frac{d\phi_M}{dr}\right|_a \qquad (10\text{-}61)$$

In order to determine P_M. Avoiding the details, we will only give the final result here

$$\frac{1}{P_M} = \frac{V_M a d}{2 V_F L_M^2} + E(\kappa_M a, \kappa_M b) \qquad (10\text{-}62)$$

where

$$L_M^2 = 1/\kappa_M^2 = D_M/\Sigma_a^M \qquad (10\text{-}63)$$

and E is a lattice function, which for cylindrical geometries takes the form

$$E(\kappa_M a, \kappa_M b) = \frac{\kappa_M (b^2 - a^2)}{2a} \left[\frac{I_0(\kappa_M a) K_1(\kappa_M b) + K_0(\kappa_M a) I_1(\kappa_M b)}{I_1(\kappa_M b) K_1(\kappa_M a) - K_1(\kappa_M b) I_1(\kappa_M a)} \right] \quad (10\text{-}64)$$

Hence our final expression becomes

$$\frac{1}{f} - 1 = \frac{\Sigma_a^M V_M}{\Sigma_a^F V_F} \left\{ 1 + \frac{\Sigma_a^F A}{\Sigma_t^F} \left[1 + \alpha \left(\frac{\Sigma_s^F}{\Sigma_t^F} \right) + \beta \left(\frac{\Sigma_s^F}{\Sigma_t^F} \right)^2 \right] \right.$$

$$\left. + \left(\frac{ad}{2L_M^2} - a \Sigma_a^M \right) \frac{V_M}{V_F} + E(\kappa_M a, \kappa_M b) - 1 \right. \quad (10\text{-}65)$$

It is useful to present similar results for a three region cylindrical fuel cell in which the clad is taken into account. [One usually homogenizes the gap and clad together.] As we have seen, for this cell the thermal utilization is given in terms of two disadvantage factors as

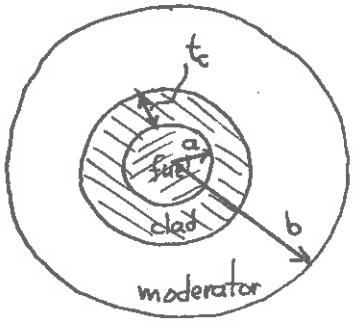

$$f = \frac{\Sigma_a^F V_F}{\Sigma_a^F V_F + \Sigma_a^C V_C \bar{\phi}_c / \bar{\phi}_F + \Sigma_a^M V_M \bar{\phi}_M / \bar{\phi}_F}$$

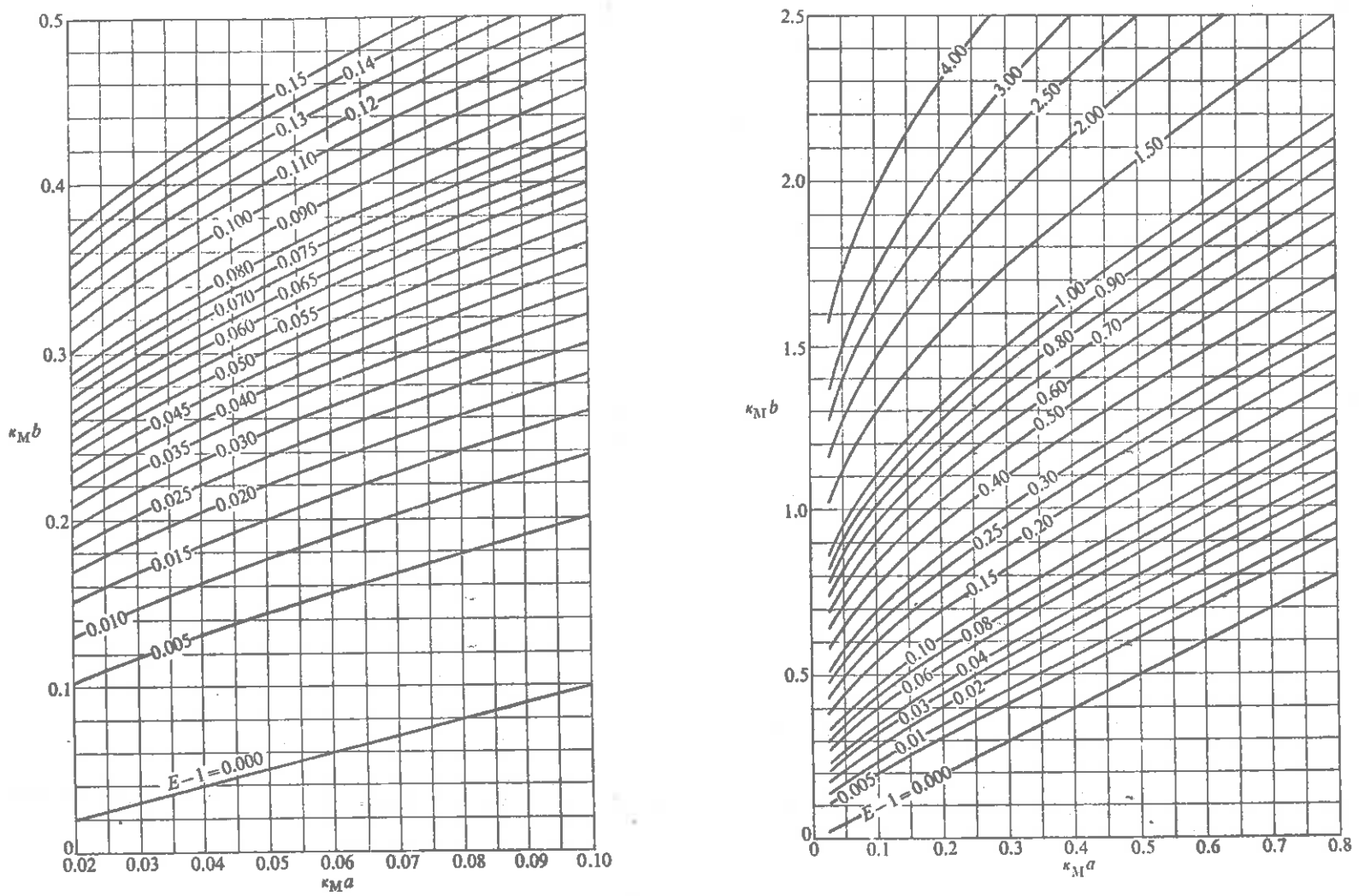

Contours of the lattice function $E(\kappa_M a, \kappa_M b) - 1$ for cylindrical rods. [From *The Reactor Handbook*, Vol. 1, p. 518, U. S. Atomic Energy Commission Report AECD-3645 (1955).]

The ABH method yields expressions for these disadvantage factors of the form

$$\frac{\bar{\phi}_c}{\bar{\phi}_F} = \frac{\phi_s}{\bar{\phi}_F} + \frac{\Delta\phi_c}{2\bar{\phi}_F} \tag{10-66}$$

where $\frac{\Delta\phi_c}{\bar{\phi}_F} = \kappa_c^2 t_c^2 \frac{\Sigma_a^F}{\Sigma_a^c}$, t_c = clad thickness

while

$$\frac{\phi_s}{\bar{\phi}_F} = 1 + \frac{\Sigma_a^F}{\Sigma_t^{F*}}\left[\frac{P_{F_0}}{1-P_{F_0}} - a\Sigma_t^{F*}\right]\left[1+\alpha\left(\frac{\Sigma_s^{F*}}{\Sigma_t^{F*}}\right)+\beta\left(\frac{\Sigma_s^{F*}}{\Sigma_t^{F*}}\right)^2\right] \tag{10-67}$$

Here $\Sigma_s^{F*} = \Sigma_s^F(1-\bar{\mu}_0)$ and $\Sigma_t^{F*} = \Sigma_s^F(1-\bar{\mu}_0)+\Sigma_a^F$, the transport corrected cross sections, while P_{F0} is the collision probability for a cylinder. Similarly

$$\frac{\bar{\phi}_M}{\bar{\phi}_F} = \frac{\phi_s}{\bar{\phi}_F} + \frac{\Delta\phi_c}{2\bar{\phi}_F} + \frac{3}{2}a^2\Sigma_a^F\left(1+\frac{V_M}{V_F}\frac{\Sigma_a^M}{\Sigma_a^F}\frac{\bar{\phi}_c}{\bar{\phi}_F}\right)\times$$
$$\times\left[\frac{2E(\kappa_M b, \kappa_M(a+t_c))}{3\Sigma_a^M\left(b^2-(a+t_c)^2\right)} + \frac{1}{a+t_c}\left(d-\frac{2}{3}\right)\right] \tag{10-68}$$

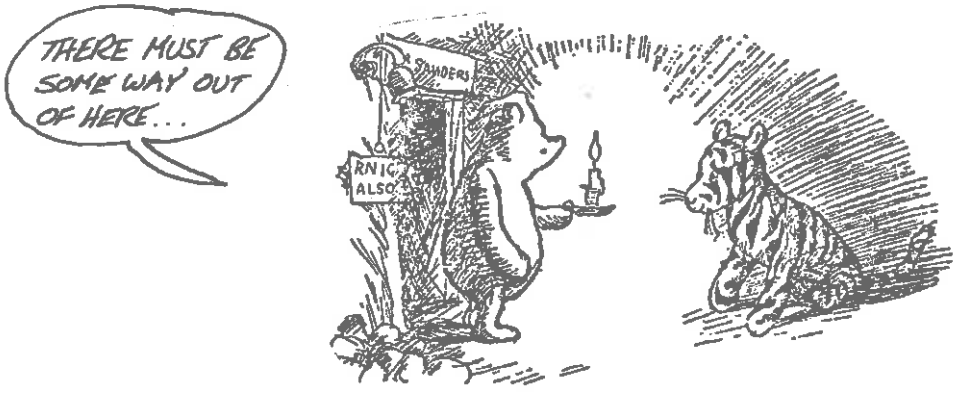

The ABH method actually gives remarkably good results. For a range of fuel-to-moderator ratios, the values of $\bar{\phi}_M / \bar{\phi}_F$ calculated by the ABH method are within 0.5% of those calculated by a transport theory analysis (DS_8).

It should be noted that the disadvantage factors calculated by the ABH method depend upon various macroscopic cross sections. The most common scheme is to consider these cross sections as being evaluated at the mean energy of the Maxwellian spectrum characterizing the moderator temperature. However, it is possible to also regard the disadvantage factors as depending implicitly upon energy via energy dependence of the cross sections which appear in them. That is, one can calculate a disadvantage factor for each energy point utilized in the thermal spectrum calculation. These energy dependent disadvantage factors can then be utilized to determine cell-averaged group constants as follows:

(i) Determine the macroscopic cross sections at each energy using the energy dependent disadvantage factors

$$\Sigma_a(E) = \sum_{\substack{\text{isotopes} \\ i}} \sum_{\substack{\text{regions} \\ r}} N_{ir}\ \sigma_a^{(i)}(E)\, \Phi_{ir}(E) \qquad (10\text{-}70)$$

(ii) Calculate the spectrum $\psi(E)$ (e.g., using SOFOCATE) using these cross sections.

(iii) Calculate the cell-averaged group constants as

$$\langle \Sigma_a \rangle_{cell} = \frac{\int dE\, \Sigma_a(E)\, \psi(E)}{\int dE\, \psi(E)} \qquad (10\text{-}71)$$

$$\langle \nu \Sigma_f \rangle_{cell} = \frac{\int dE\, \nu \Sigma_f(E) \Psi(E)}{\int dE\, \Psi(E)} \qquad (10\text{-}72)$$

$$\langle D \rangle_{cell} = \frac{\int dE\, D(E) \Psi(E)}{\int dE \Psi(E)} \qquad (10\text{-}73)$$

where

$$D(E) \equiv \left[3 \sum_{\substack{\text{isotopes} \\ i}} \sum_{\substack{\text{regions} \\ r}} N_{ir}\, \sigma_{tr}^{\omega}(E)\, \phi_{ir}(E) \right]^{-1}$$

It should be noted that in most cases, the use of energy-dependent disadvantage factors yields results which are quite comparable to those using the somewhat simpler disadvantage factors simply calculated at the mean energy of the spectrum.

C. Integral Transport Methods for Thermal Cell Calculations (THERMOS)

Thus far we have described methods for including lattice heterogeneities in thermal spectrum calculations which essentially separate the treatment of the spatial and energy dependence of the neutron flux. That is, the spatial behavior of the flux in the unit cell is treated in the one speed approximation (such as in the ABH method), and then the thermal disadvantage factors calculated from this spatial analysis are used to generate cell-averaged or "self-shielded" thermal group constants using the results of an infinite homogeneous medium thermal spectrum code. Such a scheme is characterized by a minimal calculational

effort while still producing results of sufficient accuracy for many reactor design calculations.

However, occasionally a more detailed analysis of the spatial dependence of the thermal spectrum in a fuel cell is required, for which the assumption of space-energy separability is inadequate. For such calculations it is usually also necessary to take into account the more detailed nature of thermal neutron scattering in the moderator using the scattering kernels generated by more elaborate methods (e.g., GASKET) than those such as the Wigner-Wilkins scheme.

Such an analysis usually requires a detailed solution of the energy-dependent transport equation characterizing the cell. Perhaps the most popular of such transport methods is the THERMOS code developed by Honeck, which uses an integral form of the transport equation to calculate the spatially dependent thermal neutron spectrum in a cell characterized by one-dimensional symmetry (usually cylindrical). The feasibility of the approach used in THERMOS relies heavily upon the assumption of isotropic scattering.

To sketch the method, let us first recall the form of the energy-dependent transport equation, assuming isotropic sources and scattering:

$$\hat{\Omega}\cdot\nabla\phi + \Sigma_t(\vec{r},E)\phi = \frac{1}{4\pi}\int_0^{E_c} dE' \int_{4\pi} d\hat{\Omega}'\, \Sigma_s(\vec{r},E'\to E)\phi(\vec{r},E',\hat{\Omega}') + \frac{S(\vec{r},E)}{4\pi}, \quad 0 \le E \le E_c \tag{10-74}$$

where we have noted that for such thermal spectrum problems, one is usually interested in energies E below some cutoff energy E_c (typically of the order of 1 eV). The source term actually represents neutrons slowing down below E_c from higher energies:

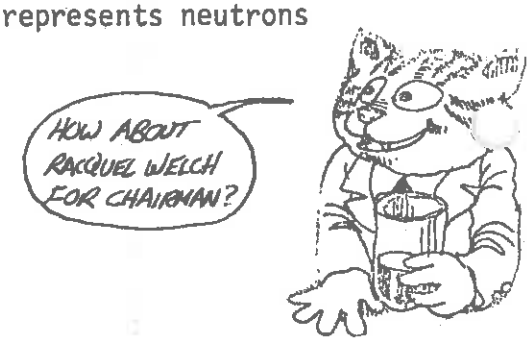

$$S(\vec{r},E) = \int_{E_c}^{\infty} dE' \, \Sigma_s(\vec{r},E' \to E) \, \Phi(\vec{r},E') \qquad (10\text{-}75)$$

Now notice that the transport Eq. (10-74) contains only a single derivative in space. Hence, one can use standard integrating factor techniques (see Appendix J for details) to integrate this equation over space. After a subsequent integration over angle, one arrives at the so-called "integral form" of the neutron transport equation

$$\Phi(\vec{r},E) = \int d^3r' \, T(\vec{r},\vec{r}',E) \left[\int_0^{E_c} dE' \Sigma_s(\vec{r}',E' \to E) \Phi(\vec{r}',E') + S(\vec{r},E) \right] \qquad (10\text{-}76)$$

where

$$T(\vec{r},\vec{r}',E) = \frac{\exp\left[-\int_0^{|\vec{r}-\vec{r}'|} ds \, \Sigma_t\left(\vec{r} - s\frac{\vec{r}-\vec{r}'}{|\vec{r}-\vec{r}'|}, E\right) \right]}{4\pi |\vec{r}-\vec{r}'|^2} \qquad (10\text{-}77)$$

Note here that $T(\vec{r},\vec{r}',E)$ is in fact the uncollided flux at $\vec{r}$ of energy E from a unit point source at $\vec{r}'$ of the same energy E. It is sometimes known as the "transport" or "first flight kernel", and we will later see that it is closely related to a collision probability.

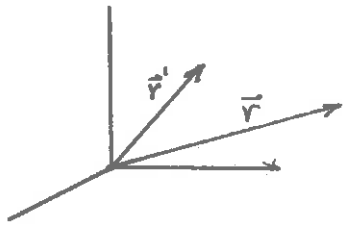

This equation is now solved numerically for a unit fuel cell, assuming zero net neutron current across cell boundaries and a

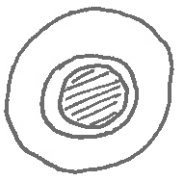

uniformly distributed slowing down source only in the moderator. The integral transport equation is first written in multigroup form

$$\bar{\Phi}^g(\vec{r}) = \int d^3r' \, T(\vec{r},\vec{r}',E_g)\left[\sum_{g'=1}^{G} \Sigma_s^{g\to g'}(\vec{r}')\,\bar{\Phi}^{g'}(\vec{r}') + S^g(\vec{r}')\right] \qquad (10\text{-}78)$$

$$1 \le g \le G$$

To handle the spatial variable, the cell is divided into N subregions. One then assumes that $\bar{\Phi}^g(\vec{r})$ is spatially independent within each subregion such that Eq. (10-78) can be written as

$$\phi_n^g = \sum_{m=1}^{N} T_{mn}^g \left[\sum_{g'=1}^{G} \Sigma_{sm}^{g\to g'}\phi_m^{g'} + S_m^g\right] \qquad (10\text{-}79)$$

$$1 \le g \le G, \quad 1 \le n \le N$$

where

$$T_{mn}^g = \frac{1}{V_m}\int_{V_m} d^3r \int_{V_n} d^3r' \; T(\vec{r},\vec{r}',E_g) \qquad (10\text{-}80)$$

Notice here that T_{nm}^g can be interpreted as the transfer or coupling coefficient characterizing neutron transport between subregions n and m.

The THERMOS method first calculates the coupling coefficients T_{nm}^g for the cell of interest, usually by numerically performing the integration indicated in Eq. (10-77). Then the N x G multigroup, spatially discretized equations are solved using standard iterative techniques (e.g., overrelaxation). As one might expect, the calculation of the T_{nm}^g is very time consuming. Furthermore, since we are actually solving

a discretized integral equation in space (as opposed to a differential equation), it is not surprising to find that the matrices involved are full (which restricts one in practice to using a small number of sub-regions).

THERMOS works best for small, highly absorbing lattices with rapidly spatially varying properties. Once having obtained the spatially dependent flux in the cell, $\Phi(\vec{r},E)$, one can directly calculate the cell-averaged or self-shielded cross sections as

$$\langle \Sigma_i^{(i)}(E) \rangle = \frac{\int_{V_{cell}} d^3r \; N_i(\vec{r}) \; \sigma^{(i)}(E) \; \Phi(\vec{r},E)}{\int_{V_{cell}} d^3r \; \Phi(\vec{r},E)} \tag{10-81}$$

Of course one can also calculate thermal disadvantage factors, e.g.,

$$\xi(E) = \frac{\frac{1}{V_M}\int_{V_M} d^3r \; \Phi(\vec{r},E)}{\frac{1}{V_F}\int_{V_F} d^3r \; \Phi(\vec{r},E)} \tag{10-82}$$

The problem with codes such as THERMOS which attempt to calculate in some detail the spatial dependence of the flux in a unit fuel cell is one of cost relative to less sophisticated schemes such as the ABH method. Typical running times for such detailed transport codes are several orders of magnitude longer than schemes based upon relative simple estimates of the disadvantage factors. Hence the typical procedure is to calculate the fine structure within fuel cells using THERMOS only in detailed design studies. These results are then used

to homogenize or self-shield group constants for a few group, 2-D diffusion or transport calculation performed on a fuel subassembly or group of subassemblies. The procedure is usually augmented by a few experimentally obtained corrections.

III. HETEROGENEOUS EFFECTS IN FAST NEUTRON PHYSICS

A. Resonance Escape Probabilities in Lumped Fuels

1.) The Slowing Down Equations for a Two-Region Cell

In our introductory discussion of lattice effects on core multiplication, it was stressed that fuel lumping can cause rather dramatic changes in resonance absorption due to self-shielding effects. Indeed, the effective resonance integrals for the fuel can be decreased from their homogeneous values by as much as an order of magnitude. Hence it is essential that we discuss schemes for calculating the resonance integrals characterizing heterogeneous lattices. It is evident that such schemes must account for the spatial dependence of the flux in the fuel cell. The method we will describe is based upon the concept of collision or escape probabilities--that is, the probability that a neutron originating in one region will make its next collision in another region.

For convenience, we will consider the fuel cell to be composed of only two species, fuel and moderator. [The extension to multiple isotopes or moderator admixed into the fuel is given in many of the standard references on this subject.] Our first task is to write a balance equation describing the neutron flux in the cell. Recall

that the balance equation describing neutron slowing down in an infinite, homogeneous medium is

$$\Sigma_t(E)\phi(E) = \int_E^{E/\alpha_A} \frac{\Sigma_s^A(E')\phi(E')dE'}{(1-\alpha_A)E'} + \int_E^{E/\alpha_M} \frac{\Sigma_s^M(E')\phi(E')dE'}{(1-\alpha_M)E'} \qquad (10\text{-}83)$$

We will develop a generalization of this equation to account for a heterogeneous fuel cell by defining the escape probabilities:

$P_F(E)$ = probability that a neutron of energy E originating in the fuel will make its next collision in the moderator (that is, will escape the fuel without suffering a collision)

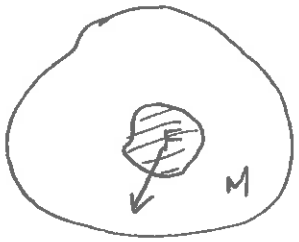

$P_M(E)$ = probability that a neutron of energy E originating in the moderator will make its next collision in the fuel

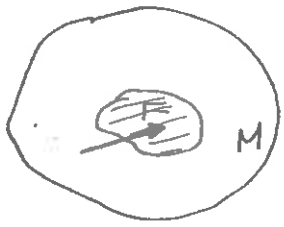

We can now use these escape probabilities to develop a generalization of Eq. (10-84). For suppose we interpret $\phi_F(E)$ and $\phi_M(E)$ as the volume averaged flux in the fuel and moderator, respectively. Then, for example,

$$V_M \int_E^{E/\alpha_M} \frac{\Sigma_s^M(E')\,\phi_M(E')dE'}{(1-\alpha_M)E'}$$

represents the average rate at which neutrons slow down to an energy E in the moderator. Hence, by mulitplying this expression by $P_M(E)$, we can compute the rate at which neutrons of energy E are transferred from the moderator into the fuel. In a similar fashion, one can calculate the rate at which neutrons slowing down to energy E in the fuel suffer their next collision in the fuel as

$$[1 - P_F(E)] V_F \int_E^{E/\alpha_F} dE' \frac{\Sigma_s^F(E') \phi_F(E')}{(1-\alpha_F)E'}$$

The sum of these two contributions must equal the total rate at which collisions are occurring in the fuel; hence we arrive at the balance relation for the fuel:

$$V_F \Sigma_t^F(E) \phi_F(E) = V_F [1 - P_F(E)] \int_E^{E/\alpha_F} dE' \frac{\Sigma_s^F(E') \phi_F(E')}{(1-\alpha_F)E'} + V_M P_M(E) \int_E^{E/\alpha_M} dE' \frac{\Sigma_s^M(E') \phi_M(E')}{(1-\alpha_M)E'} \quad (10\text{-}84)$$

We can write a similar balance relation for the moderator region:

$$V_M \Sigma_t^M(E) \phi_M(E) = V_M [1 - P_M(E)] \int_E^{E/\alpha_M} dE' \frac{\Sigma_s^M(E') \phi_M(E')}{(1-\alpha_M)E'} + V_F P_F(E) \int_E^{E/\alpha_F} dE' \frac{\Sigma_s^F(E') \phi_F(E')}{(1-\alpha_F)E'} \quad (10\text{-}85)$$

These two equations represent the generalization of the slowing down equation (10-83) for an infinite, homogeneous medium. As they stand,

these coupled integral equations are exact. However they are only formal until the escape probabilities $P_F(E)$ and $P_M(E)$ have been specified (in much the same sense that the multigroup equations were also exact but of only a formal significance until the multigroup constants were determined). We can (and will later) give an alternative derivation of these equations in an effort to arrive at a more explicit form for the escape probabilities. For now, however, we will proceed to apply Eq. (10-84) and (10-85) to the study of resonance absorption in lattices, deferring the calculation of the escape probabilities until later.

It is possible to decouple these equations by making the narrow resonance approximation for the moderator. That is, we will assume that

$$\Delta E\big|_M = \left(\frac{1-\alpha_M}{2}\right) E_1 << \Gamma_p \tag{10-86}$$

so that we can replace the average flux in the moderator by its asymptotic form

$$\phi_M(E) \sim \frac{1}{\overline{\xi\Sigma_p}\, E} \tag{10-87}$$

where

$$\overline{\xi\Sigma_p} \equiv \frac{\xi_F \Sigma_p^F V_F + \xi_M \Sigma_s^M V_M}{V_F + V_M} \tag{10-88}$$

If we now use this in the second term on the RHS of Eq. (10-84) corresponding to slowing down in the moderator, we find that it becomes

$$V_M P_M(E) \int_E^{E/\alpha_M} dE' \frac{\Sigma_s^M(E')\phi_M(E')}{(1-\alpha_M)E'} = V_M P_M(E) \frac{\Sigma_s^M}{\bar{\xi}\Sigma_p E} \quad . \tag{10-89}$$

Hence, by substituting this NR form into Eq. (10-84), we will have eliminated the appearance of the moderator flux in the equation for the fuel region, thereby decoupling this equation from the moderator region balance equation.

It is useful to make one further manipulation before inserting the NR approximation for the moderator into Eq. (10-84). Using the reciprocity theorem, one can demonstrate that the escape probabilities relating the fuel and moderator regions must satisfy

$$P_F(E)\Sigma_t^F(E)V_F = P_M(E)\Sigma_t^M(E)V_M \tag{10-90}$$

If we furthermore assume that absorption is negligible in the moderator [$\Sigma_t^M(E) \sim \Sigma_s^M(E)$], we can rewrite (10-89) as

$$V_M P_M(E) \int_E^{E/\alpha_M} dE' \frac{\Sigma_s^M(E')\phi_M(E')}{(1-\alpha_M)E'} = V_F P_F(E) \frac{\Sigma_t^F(E)}{\bar{\xi}\Sigma_p E} \tag{10-91}$$

Hence our slowing down equation for the fuel region becomes

$$\Sigma_t^F(E)\phi(E) = [1-P_F(E)] \int_E^{E/\alpha_F} dE' \frac{\Sigma_s^F(E')\phi_F(E')}{(1-\alpha_F)E'} + P_F(E)\frac{\Sigma_t^F(E)}{\bar{\xi}\Sigma_p E} \tag{10-92}$$

Once we know $P_F(E)$, we can solve this equation for $\phi_F(E)$--either using analytical approximations or brute force numerical methods--and thereby calculate the effective resonance integral for the resonance:

$$I = \overline{\xi\Sigma}_p \int_{E_1} dE\, \sigma_a^F(E)\phi_F(E) \qquad (10\text{-}93)$$

Notice that for a homogeneous system, $P_F \rightarrow 0$, and Eq.(10-89) reduces to our earlier slowing down equation (10-83).

2) The Rational Approximation

But we still need to calculate $P_F(E)$. To facilitate this calculation, it is customary to introduce the "flat flux approximation" in which $P_F(E)$ and $P_M(E)$ are obtained for uniform (spatially independent) sources of neutrons in the fuel or the moderator. Although this approximation might be reasonable far from the resonance energy, it is certainly not strictly valid at this energy since the flux in the fuel element is quite strongly varying due to self-shielding. However, once again we are saved by a fortunate cancellation of errors. [God watches out for drunks, fools, and reactor physicists.]

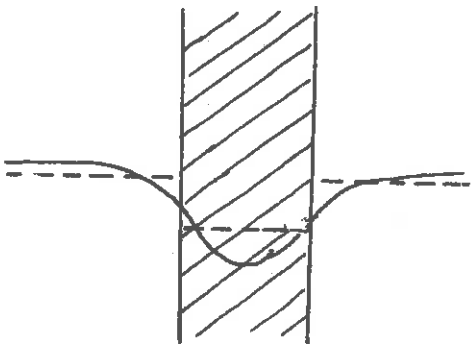

Hence we are now faced with calculating $P_F(E)$, the probability that a neutron born uniformly and isotropically in the fuel makes its next collision in the moderator. Fortunately, the resonance integral is not overly sensitive to the detailed behavior of $P_F(E)$. In fact, it is usually sufficient to introduce a particularly simple approximation

for $P_F(E)$ first suggested by Wigner. First notice that we know the limiting behavior of $P_F(E)$ for both small and large fuel lumps. For small fuel lumps, obviously

$$P_F(E) \rightarrow 1 \quad \text{as} \quad \frac{V_F}{S_F} \rightarrow 0 \tag{10-94}$$

For large fuel lumps, we can effectively use the black lump result

$$P_F(E) \rightarrow \frac{S_F}{4 V_F \Sigma_t^F} \quad \text{as} \quad \frac{V_F}{S_F} \rightarrow \infty \tag{10-95}$$

With these limits in mind, Wigner chose a simple interpolation formula between the limits (known as the "Wigner rational approximation")

$$P_F(E) = \frac{(S_F / 4 V_F \Sigma_t^F)}{1 + (S_F / 4 V_F \Sigma_t^F)} \tag{10-96}$$

It is customary to define a fictitious macroscopic cross section

$$\Sigma_e \equiv \frac{S_F}{4 V_F} \equiv \frac{1}{\langle R \rangle_F} \tag{10-97}$$

where $\langle R \rangle_F$ is the mean chord length of the fuel lump. One can similarly define its microscopic counterpart

$$\sigma_e \equiv \frac{\Sigma_e}{N_F} = \frac{S_F}{4 V_F N_F} \tag{10-98}$$

Notice that these quantities represent the effective cross section for neutron removal from the fuel lump via leakage to the moderator. Using this definition, we can now write Wigner's rational approximation as

$$P_F(E) = \frac{\Sigma_e}{\Sigma_t^F(E) + \Sigma_e} = \frac{\sigma_e}{\sigma_t^F + \sigma_e} \tag{10-99}$$

To proceed further, we can now return to Eq. (10-89) and introduce the standard approximations for the scattering integral characterizing the absorber. First, in the narrow resonance approximation (N.R.)

$$\int_E^{E/\alpha_F} dE' \frac{\Sigma_s^F(E')\phi_F(E')}{(1-\alpha_F)E'} \sim \frac{\Sigma_p^F}{\xi\bar{\Sigma}_p E} \tag{10-100}$$

Hence we can solve for the flux as

$$\phi_F(E) = \frac{[1-P_F(E)]\Sigma_p^F + P_F(E)\Sigma_t^F}{\Sigma_t^F\ \xi\bar{\Sigma}_p\ E} \tag{10-101}$$

The corresponding N.R. approximation to the resonance integral is then

$$I_{NR} = \int \frac{dE}{E} \frac{\sigma_a^F}{\sigma_t^F}\left[\sigma_p^F + P_F(E)(\sigma_t^F - \sigma_p^F)\right], \tag{10-102}$$

or using the rational approximation (10-99)

$$I_{NR} = \int \frac{dE}{E} \frac{(\sigma_p^F + \sigma_e)\sigma_a^F}{\sigma_t^F + \sigma_e} \tag{10-103}$$

In a similar fashion, the wide resonance or N.R.I.M. approximation for the absorber implies

$$\int_E^{E/\alpha_F} dE' \frac{\Sigma_s^F(E')\phi_F(E')}{(1-\alpha_F)E'} \sim \Sigma_s^F(E)\phi_F(E) \tag{10-104}$$

This approximation leads one to

$$I_{NRIM} = \int \frac{dE}{E} \frac{P_F \sigma_a^F}{1-(1-P_F)(\sigma_s^F/\sigma_t^F)} \tag{10-105}$$

or in the rational approximation

$$I_{NRIM} = \int \frac{dE}{E} \frac{\sigma_e \sigma_a^F}{\sigma_a^F + \sigma_e} \tag{10-106}$$

It is informative to compare these expressions with the earlier results we obtained for homogeneous systems:

$$I_{NR}^{hom} = \int \frac{dE}{E} \frac{\sigma_a^F}{1+(\sigma_a^F+\sigma_s^F)/\sigma_p} \tag{10-107}$$

$$I_{NRIM}^{hom} = \int \frac{dE}{E} \frac{\sigma_p \sigma_a^F}{\sigma_a^F + \sigma_p}$$

where we define the potential scattering cross section per fuel atom of the fuel-moderator mixture as

$$\sigma_p = \frac{\Sigma_s^M}{N_F} + \sigma_p^F \tag{10-108}$$

Notice that by replacing the potential scattering cross section in (10-107) by

$$\sigma_p \rightarrow \sigma_p^F + \sigma_e \tag{10-109}$$

we arrive at the same value of resonance integral. Hence we can very simply adapt the schemes used to calculate homogeneous resonance integrals to heterogeneous lattices by merely replacing σ_p by $\sigma_p^F + \sigma_e$.

It is useful to also give the resonance integrals for the more general case in which there is moderator (such as oxygen or carbon) admixed into the fuel. If we identify this element by a scattering cross section, σ_{pm}^F, then our two approximations to the resonance integral become

$$I_{NR} = \int \frac{dE}{E} \frac{\sigma_a^F}{1 + (\sigma_a^F + \sigma_s^F)/(\sigma_p^F + \sigma_e + \sigma_{pm}^F)} \tag{10-110}$$

$$I_{NRIM} = \int \frac{dE}{E} \frac{(\sigma_e + \sigma_{pm}^F)\sigma_a^F}{\sigma_a^F + \sigma_e + \sigma_{pm}^F} .$$

Two interesting limits of these resonance integrals are

(i) $\sigma_{pm}^F + \sigma_e << \sigma_i$; $\sigma_s^M << \sigma_e$

Then

$$I \cong A + B\sqrt{\frac{S_E}{M_F}} \quad , \quad M_F \equiv V_F N_F \tag{10-111}$$

(ii) $\sigma_{pm}^F + \sigma_e << \sigma_i$; $\sigma_s^M >> \sigma_e$

In this case

$$I \cong C + D\left(\frac{S_E}{M_F}\right) \tag{10-112}$$

3) Empirical Correlations for Resonance Integrals

Very similar expressions have been verified experimentally in a series of experiments by Hellstrand* who found the following empirical correlations for oxide fuels

$$I^{28} = 11.6 + 22.8\left(S_F/M_F\right) \quad , \qquad (10\text{-}113)$$

$$I^{28} = 4.15 + 26.6\sqrt{S_F/M_F}$$

for a temperature T = 20°C. These two forms have been found to work equally well over the range of S_F/M_F examined. Repeated experiments for the temperature range T = 20°C to 600°C can be fitted by

$$I^{28} = I^{28}(T=20°C)\left[1+\beta\left(\sqrt{T}-\sqrt{20°}\right)\right] \quad . \qquad (10\text{-}114)$$

Strawbridge and Barry** have proposed a single correlation to fit all of the Hellstrand data which is more commonly used in the analysis of light water reactors

$$I^{28} = 2.16x + 2.56 + \left[.0279x - .0537\right]\sqrt{T} \qquad (10\text{-}115)$$

Here

$$x \equiv \left[\frac{\Sigma_p^F}{N_{28}} P_F + \frac{D_{eff}}{\langle R\rangle_F N_{28}}\right]^{1/2} \quad .$$

---

*J. Hellstrand, J. App. Phys. 28, 1493 (1957)
Hellstrand, Blomberg, and Hörner, Nuc. Sci. and Eng. 8, 497 (1960)
**Strawbridge and Barry, Nuc. Sci. and Eng. 23, 58 (1965)

and

$\Sigma_p^F \equiv$ potential scattering cross section of fuel ($\sigma_p^u = 10.7$ b, $\sigma_p^O = 3.8$ b)

$N^{28} \equiv U^{238}$ number density in fuel

$\langle \bar{R} \rangle_F \equiv$ mean chord length

$D_{eff} \equiv$ effective shielding factor (Dancoff correction)

Typical results from this correlation are shown for several different fuel temperatures below:

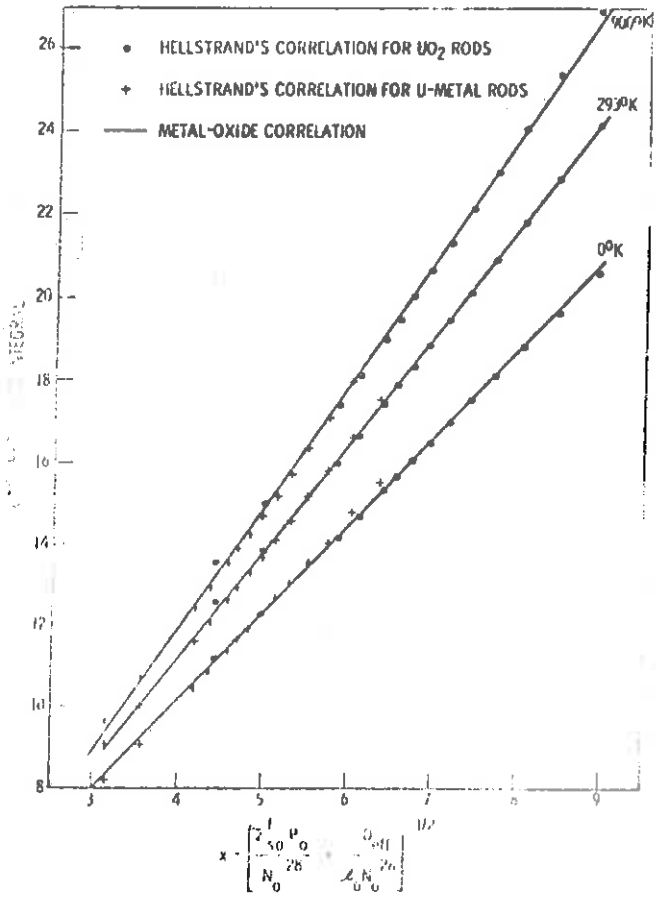

Comparison of metal-oxide resonance integral correlation with Hellstrand's correlations for isolated rods.

4) Rod Shadowing and the Dancoff Correction

Thus far we have treated resonance absorption in a fuel lump as if the unit fuel cell were truly isolated from other fuel cells. But, in fact, if the fuel rods in a lattice are separated by a moderator which is not many mean free paths thick, it is possible for neutrons with energies in the resonance region to pass from one fuel lump to another. This invalidates our earlier calculation based upon collision probabilities, for in that calculation we assumed that the escape probability from the fuel P_F implied that upon escaping from the fuel, the neutron would suffer its next collision in the moderator. But if other fuel lumps are nearby, this next collision might also occur in the fuel. Hence we should try to calculate a modified escape probability, P_F^*, that a source neutron born in the fuel suffers its next collision in the moderator--even though there may be fuel elements adjacent. Then we can use our earlier analysis, merely replacing P_F by P_F^*.

Recall that the escape probability for a given region could be written as

$$P_F = \frac{\int d\hat{\Omega} \int dA \; \hat{n}\cdot\hat{\Omega} \left(1 - e^{-R_s \Sigma_t}\right)}{\Sigma_t^F \langle R \rangle_F \int d\hat{\Omega} \int dA \; \hat{n}\cdot\hat{\Omega}} \qquad (10\text{-}116)$$

Now to handle a periodic array of fuel rods, we merely extend the chord under consideration in the integration to see whether it intercepts further fuel rods

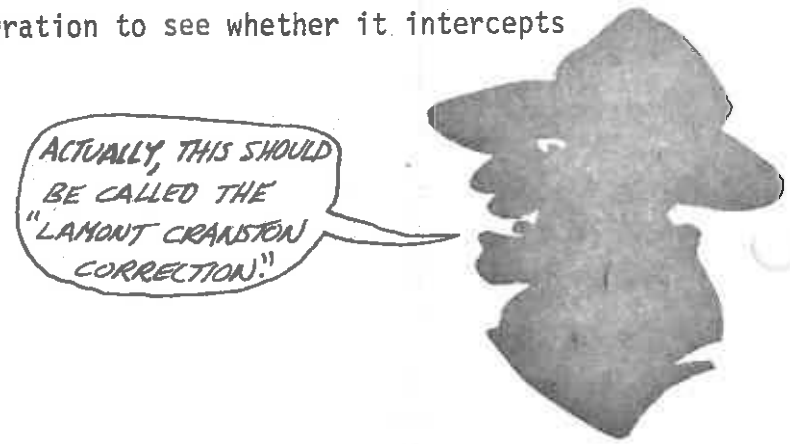

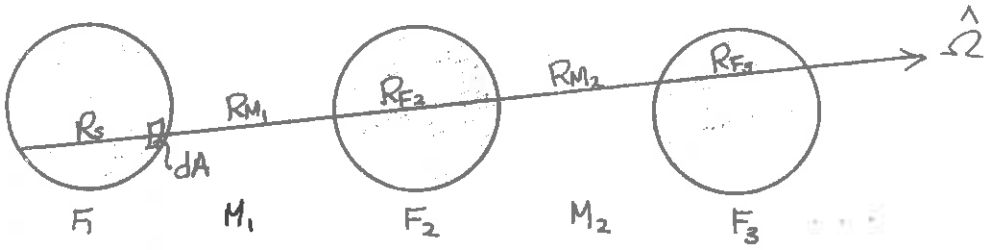

Hence the contribution to the integral from a given chord should be reduced by

$$\underbrace{\left(1 - e^{-\Sigma_t^M R_{M_1}}\right)}_{\substack{\text{collision probability} \\ \text{in region } F_2}} + \underbrace{e^{-\Sigma_t^M R_{M_1}} e^{-\Sigma_t^F R_{F_2}}}_{\substack{\text{transmission probabilities through} \\ M_1 \text{ and } F_2}} \left(1 - e^{-\Sigma_t^M R_{M_2}}\right) + \cdots \tag{10-117}$$

We can develop a useful approximation to the integral as follows:

Define the modified collision probabilities:

$P_M^i \equiv$ probability that a neutron incident on the moderator after i previous traversals of fuel will collide in the moderator

$P_F^i \equiv$ probability that a neutron incident on fuel after i previous traversals of fuel will collide in fuel

Then we can write

$$P_F^* = P_F \left[P_M^0 + (1-P_M^0)(1-P_F^0) P_M^1 + (1-P_M^0)(1-P_F^0)(1-P_M^1)(1-P_F^1) P_M^2 + \cdots \right] \tag{10-118}$$

If we replace all $P_M^i \sim P_M^o$ and $P_F^i \sim P_F^o$, then we can sum this series to find

$$P_F^* = P_F \frac{P_M^o}{1-(1-P_M^o)(1-P_F^o)} \qquad (10\text{-}119)$$

Usually one writes

$$P_M^o = (1-C) \qquad (10\text{-}120)$$

where C is referred to as the Dancoff correction. To handle P_F^o, one uses the approximate form

$$P_F^o \sim \Sigma_t^F \langle R \rangle_F P_F \qquad (10\text{-}121)$$

then one finds

$$P_F^* \cong P_F \frac{(1-C)}{1-C\left(1-\Sigma_t^F \langle R \rangle_F P_F\right)} \qquad (10\text{-}122)$$

The Dancoff factor has been tabulated in numerous references, among them ANL-5800.

One can now merely use P_F^* in place of P_F in the calculations of the resonance integrals for the lattice of interest. The effect of such a correction is to decrease the surface area of a single fuel element by a factor of 1-C. This fact is of particular use if one of the various correlations for the resonance integral is to be used.

Notice that decreasing the surface area of a fuel lump will reduce the corresponding resonance integral from its value for an isolated

fuel element. Hence one finds that the Dancoff correction for neighboring fuel elements corresponds effectively to a correction for the shadowing of one fuel element by another.

5) Generalized Slowing Down Equations for a Two-Region Cell

It is possible to give a more rigorous derivation of the coupled slowing down equations (10-84) and (10-85) characterizing a two-region fuel cell. We begin by recalling the integral form of the neutron transport equation under the assumption of isotropic scattering

$$\Phi(\vec{r},E) = \int d^3r' T(\vec{r},\vec{r}',E) \int_0^\infty dE' \Sigma_s(\vec{r}',E'\to E)\Phi(\vec{r}',E')$$

where

$$T(\vec{r},\vec{r}',E) = \frac{1}{4\pi|\vec{r}-\vec{r}'|^2}\exp\left[-\tau(\vec{r},\vec{r}',E)\right]$$

$$\tau(\vec{r},\vec{r}',E) = \int_0^{|\vec{r}-\vec{r}'|} ds\, \Sigma_t\left(\vec{r}-\frac{(\vec{r}-\vec{r}')}{|\vec{r}-\vec{r}'|}s, E\right)$$

Notice that the source term has been eliminated from the equation, consistent with our interest only in resonances which are many collision intervals below the source energy. In this spirit, one usually attaches the boundary condition

$$\lim_{E\to\infty} \Phi(\vec{r},E) = \gamma_E \,. \qquad (10\text{-}142)$$

Next we divide the volume integral into two contributions, one from the fuel volume V_F and one from the moderator volume V_M.

$$\Phi(\vec{r},E) = \int_{V_F} d^3r' \, T(\vec{r},\vec{r}',E) \int_E^{E/\alpha_F} dE' \, \frac{\Sigma_s^F(E')\,\Phi(\vec{r}',E')}{(1-\alpha_F)E'} + \int_{V_M} d^3r' \, T(\vec{r},\vec{r}',E) \int_E^{E/\alpha_M} dE' \, \frac{\Sigma_s^M(E')\,\Phi(\vec{r}',E')}{(1-\alpha_M)E'} \tag{10-143}$$

Now define

$$P_F(\vec{r},E) \equiv \Sigma_t^M \int_{V_M} d^3r' \, T(\vec{r},\vec{r}',E) \tag{10-144}$$

This is the probability of a first collision in the moderator due to a unit isotropic source at r in V emitting neutrons of energy E. Hence the general escape probability for the fuel lump is obtained by integrating this quantity over V_F and dividing by V_F

$$P_F(E) = \frac{1}{V_F} \int_{V_F} d^3r \, P_F(\vec{r},E) = \frac{1}{V_F} \int_{V_F} d^3r \, \Sigma_t^M \int_{V_M} d^3r' \, T(\vec{r},\vec{r}',E) \tag{10-145}$$

In a similar fashion, we can define the average escape probability for the moderator as

$$P_M(E) = \frac{1}{V_M} \int_{V_M} d^3r \, P_M(\vec{r},E) = \frac{1}{V_M} \int_{V_M} d^3r \, \Sigma_t^F \int_{V_F} d^3r' \, T(\vec{r},\vec{r}',E) \tag{10-146}$$

It is also useful to recall the definitions of the volume averaged fluxes

$$\phi_F(E) = \frac{1}{V_F}\int_{V_F} d^3r\, \Phi(\vec{r},E)$$

$$\phi_M(E) = \frac{1}{V_M}\int_{V_M} d^3r\, \Phi(\vec{r},E) \qquad (10\text{-}147)$$

Now volume average Eq. (10-143) over the fuel region

$$\frac{1}{V_F}\int_{V_F} d^3r\, \Phi(\vec{r},E) = \frac{1}{V_F}\int_{V_F} d^3r \int_{V_F} d^3r'\, T(\vec{r},\vec{r}',E)\int_E^{E/\alpha_F} \frac{dE'\,\Sigma_s^F(E')\,\Phi(\vec{r}',E')}{(1-\alpha_F)E'}$$

$$+\frac{1}{V_F}\int_{V_F} d^3r \int_{V_M} d^3r'\, T(\vec{r},\vec{r}',E)\int_E^{E/\alpha_M} dE'\,\frac{\Sigma_s^M(E')\,\Phi(\vec{r}',E')}{(1-\alpha_M)E'} \qquad (10\text{-}148)$$

or using our above definitions

$$\phi_F(E) = \frac{1}{\Sigma_t^F V_F}\int_{V_F} d^3r'\,\left[1-P_F(\vec{r}',E)\right]\int_E^{E/\alpha_F} dE'\,\frac{\Sigma_s^F(E')\,\Phi(\vec{r}',E')}{(1-\alpha_F)E'}$$

$$+\frac{1}{\Sigma_t^M V_F}\int_{V_F} d^3r'\,P_M(\vec{r}',E)\int_E^{E/\alpha_M} dE'\,\frac{\Sigma_s^M(E')\,\Phi(\vec{r}',E')}{(1-\alpha_M)E'} \qquad (10\text{-}149)$$

Here we have identified the number of first collisions in the fuel lump

$$1-P_F(\vec{r},E) = \Sigma_t^F(E)\int_{V_F} d^3r'\; T(\vec{r},\vec{r}',E) \tag{10-150}$$

Next, add and subtract $P_F(E)$ and $P_M(E)$ to rewrite this as

$$\Sigma_t^F\phi_F(E) = [1-P_F(E)]\int_E^{E/\alpha_F} \frac{dE'\,\Sigma_s^F(E')\phi_F(E')}{(1-\alpha_F)E'} + P_M(E)\int_E^{E/\alpha_M} dE'\,\frac{\Sigma_s^M(E')\phi_M(E')}{(1-\alpha_M)E'}$$

$$+\frac{1}{V_F}\int_{V_F} d^3r'\,[P_F(E)-P_F(\vec{r}',E)]\int_E^{E/\alpha_F} dE'\,\frac{\Sigma_s^F(E')\phi_F(\vec{r}',E')}{(1-\alpha_F)E'} \tag{10-151}$$

$$+\frac{1}{V_M}\int_{V_M} d^3r'\,[P_M(\vec{r}',E)-P_M(E)]\int_E^{E/\alpha_M} dE'\,\frac{\Sigma_s^M(E')\phi_M(\vec{r}',E')}{(1-\alpha_M)E'}.$$

One can write a similar equation for the moderator region by merely interchanging the F and M subscripts. Notice now that Eq. (10-151) would be identical to our earlier Eq. (10-84) were it not for the presence of the last two terms. These terms may be though of as a correction to the flat flux approximation, since they will vanish if the narrow resonance is applied to the terms, since then one assumes

$$\phi(\vec{r}',E') \sim \frac{1}{\Sigma_s E'} \tag{10-152}$$

is independent of position. Hence, in addition to providing a formal basis for the development of the volume-averaged slowing down equation (10-84), Eq. (10-151) also provides a consistent means to estimating the error introduced by making the flat flux approximation.

B. Modifications in the Treatment of Fast Fission

Although the number of fast fission events which occur in a thermal reactor is not large, such reactions can be quite significant since they can provide a sizeable fraction of the excess reactivity of a core. It is particularly important to take some account of the fact that the probability of a fast fission reaction occurring is enhanced somewhat by fuel lumping. Thus the fast fission factor ϵ is increased from its value for a homogeneous reactor core.

The calculation of heterogeneous modifications to the fast fission factor is a subject which is considered in detail in several of the standard references, e.g., Lamarsh, pp. 402-407 or Megreblian & Holmes, pp. 692-698. We will focus our attention instead on the more practical question of just how heterogeneous effects are included in the treatment of fast fission in conventional fast spectrum codes.

The rate at which fast fission reactions occur depends upon the magnitude of the fast neutron flux in the fuel region. From our earlier discussion, we expect this fast flux (say, in the energy range .821 MeV to 10 MeV) to be somewhat larger in the fuel than in the moderator, since once neutrons have entered the moderator, they are rapidly slowed down below the fast fission energy threshold. Hence we might expect that a homogeneous fast spectrum calculation will tend to underpredict the amount of fast fission occurring, since it will use the average flux characterizing a homogeneous system.

To correct this, we will follow a procedure* very similar to that used in our treatment of thermal fission--that is, we will define a "fast utilization factor" (similar to the thermal utilization factor) which is the ratio of the rate of neutron removal in the fuel to the total rate of fast neutron removal. Notice that we include in this definition all mechanisms for neutron removal, including neutron absorption, elastic and inelastic scattering. Then it is evident in analogy to our treatment of p that

$$f_F = \frac{\Sigma_r^F V_F \bar{\Phi}_F}{\Sigma_r^F V_F \bar{\Phi}_F + \Sigma_r^M V_M \bar{\Phi}_M} \qquad (10\text{-}123)$$

Here, Σ_r is the removal cross sections for fast neutrons. We will now introduce a flux "fast advantage factor", defined as

$$\xi_F \equiv \bar{\Phi}_F / \bar{\Phi}_M \qquad (10\text{-}124)$$

(Notice that in the fast range, the fuel is now at an advantage in competing with the moderator for neutron absorption). Using this definition and our expression for f_F, we can solve for the fast advantage factor in terms of the fast utilization factor as

$$\xi_F = \frac{\Sigma_r^M V_M}{\Sigma_r^F V_F}\left(\frac{f_F}{1-f_F}\right) = \frac{\Sigma_t^M (1-C_M) V_M}{\Sigma_t^F (1-C_F) V_F}\left(\frac{f_F}{1-f_F}\right), \qquad (10\text{-}125)$$

where we have defined

$$1 - C \equiv \Sigma_r / \Sigma_t \; . \qquad (10\text{-}126)$$

---

*Proposed by R. C. Hellens and described by Strawbridge and Barry.

One usually normalizes the fluxes appearing in this ratio such that

$$\bar{\phi}_F V_F + \bar{\phi}_M V_M = 1 \quad . \tag{10-127}$$

Once we have determined ξ_F , we can calculate new group constants characterizing the fast range which include the effect of fast flux enhancement due to fuel lumping.

Of course, the success of this technique hinges upon our ability to calculate P_F. One could always use brute force methods based upon Monte Carlo calculations. But we will instead introduce an alternative technique based upon the methods of successive generations using collision probabilities for the moderator and fuel regions.

To this end, we will define the following collision probabilities for a given fast energy micro-group in the fast spectrum code energy mesh

P_F = probability that a neutron born uniformly and isotropically in the fuel will escape the fuel region if every collision removes the neutron from the fast group

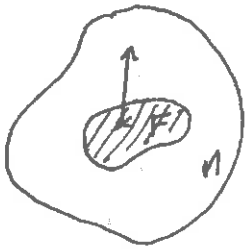

P_M = probability that a neutron born uniformly and isotropically in the moderator will escape the moderator region if every collision removes the neutron from the fast group

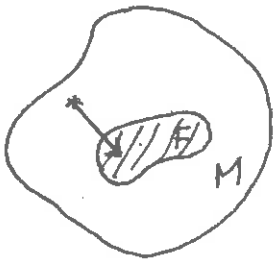

We will also introduce two additional quantities

β_F = probability that a neutron entering the fuel region will be removed from the group if every collision removes the neutron

β_M = probability that a neutron entering the moderator region will be removed from the group if every collision removes the neutron

Here β_F and β_M are referred to as the "blackness" coefficients of the fuel and moderator regions respectively. Notice we have modified the usual definitions of P_F and P_M by specifying that all collisions remove neutrons from the fast group. But of course this is not strictly true. In general, only a fraction $1-C = \Sigma_r/\Sigma_t$ of the collisions result in removals, while a fraction C remain in the region. For example, in the first generation, if one neutron is born in the fuel,

P_F	escape fuel region
$(1-P_F)$	have a collision in fuel
$(1-P_F)(1-C_F)$	are removed from fast group

Continuing on in this fashion, in the second generation, assuming after each collision the neutrons are still uniformly distributed,

$(1-P_F)C_F$	remain in rod
$(1-P_F)C_FP_F$	escape fuel region
$(1-P_F)C_F(1-P_F)(1-C_F)$	are removed from group

and so on. Hence we can sum the escapes from all generations to calculate the effective escape probabilities:

$$P_F^* = P_F + (1-P_F)C_F P_F + (1-P_F)C_F(1-P_F)C_F P_F + \cdots$$

$$= \frac{P_F}{1 - C_F(1-P_F)} \qquad (10\text{-}128)$$

Similarly

$$P_M^* = \frac{P_M}{1 - C_M(1-P_M)} \qquad (10\text{-}129)$$

[Note that an essential ingredient in this calculation was the assumption that each generation remained uniformly and isotropically distributed.]

We can perform the same stunt to calculate the effective blackness coefficients. Suppose one neutron is incident at the fuel surface. Then

β_F have a collision

β_F $(1-C_F)$ are removed from fast group

In the second collision generation

$\beta_F C_F$ remain in the fast group

$\beta_F C_F P_F^*$ escape fuel region in all successive generations

$\beta_F C_F (1-P_F^*)$ are removed from group in all successive generations

Hence we can add all removals to find

$$\beta_F^* = \beta_F(1-C_F) + \beta_F C_F (1-P_F^*) \qquad (10\text{-}130)$$

$$= \beta_F (1 - C_F P_F^*)$$

and

$$\beta_M^* = \beta_M (1 - C_H P_M^*) \tag{10-131}$$

Now to calculate the fast utilization f_F, we will use the above quantities to follow a neutron born in the fuel as it suffers collisions in the fuel or passes back and forth between fuel and moderator

1	neutron born in fuel
$1-P_F^*$	removed from fast group in fuel
P_F^*	enter moderator
$P_F^* \beta_M^*$	removed from fast group in moderator
$P_F^*(1-\beta_M^*)$	reenter fuel
$P_F^*(1-\beta_M^*)\beta_F^*$	removed from fast group in fuel
$P_F^*(1-\beta_M^*)(1-\beta_F^*)$	enter moderator
⋮	

Thus, summing all removals in the fuel due to this source neutron to calculate a fast utilization for the fuel

$$f_{F_F} = 1 - P_F^* + P_F^*(1-\beta_M^*)\beta_F^* + P_F^*(1-\beta_M^*)(1-\beta_F^*)(1-\beta_M^*)\beta_F^* + \cdots$$

or summing

$$f_{FF} = 1 - \frac{P_F^* \beta_M^*}{1-(1-\beta_F^*)(1-\beta_M^*)} \tag{10-132}$$

In a similar fashion, we can calculate a fast utilization factor for the moderator

$$f_{MF} = \frac{P_F^* \beta_M^*}{1-(1-\beta_F^*)(1-\beta_M^*)} \quad (10\text{-}133)$$

We can calculate similar fast utilization factors for the situation in which the source neutron is born in the moderator by simply reversing region subscripts

$$f_{FM} = \frac{P_M^* \beta_F^*}{1-(1-\beta_F^*)(1-\beta_M^*)} \quad (10\text{-}134)$$

and

$$f_{MM} = 1 - \frac{P_M^* \beta_F^*}{1-(1-\beta_F^*)(1-\beta_M^*)} \quad (10\text{-}135)$$

Hence, to calculate the fast utilization characteristic of the fuel, we simply weight the utilizations by the fractional source in each region

$$f_F = \frac{f_{FF} Q_F V_F + f_{FM} Q_M V_M}{Q_F V_F + Q_M V_M} \quad (10\text{-}136)$$

where Q_j is the source in region j. The source Q_F is the sum of the direct fission source, $\chi(E)$, and the slowing-down source in the fuel region of all upper groups. The source Q_M is simply the slowing down source from the moderator regions of all upper groups.

To calculate P_F, P_M, β_F, β_M, one uses our earlier work on collision probabilities, with liberal help from Case, de Hoffmann, and Placzek. Here we merely note

$$P_F = 1 - P_c \tag{10-137}$$

where P_c is tabulated in Case, et. al. Then

$$\beta_F = \langle R \rangle_F \Sigma_t^F P_F \tag{10-138}$$

where $\langle R \rangle_F$ is the mean chord length in the fuel. Next, β_M is calculated as a Dancoff factor for the moderator

$$\beta_M = 1 - \frac{e^{-\tau \Sigma_t^M \langle R \rangle_M}}{1 + (1-\tau)\Sigma_t^M \langle R \rangle_M} \tag{10-139}$$

$$\tau = \left\{ \left[\pi \left(1 + \frac{V_M}{V_F} \right)^{1/2} - 1 \right\} \frac{V_M}{V_F} - .08 \right.$$

(for a square lattice)

while

$$P_M = \frac{\beta_M}{\langle R \rangle_M \Sigma_t^M} \tag{10-140}$$

One can now calculate this fast utilization and the corresponding fast advantage factor for each of the fast groups, and then use these quantities to adjust the cross sections in these groups for heterogeneous effects.

Actually, the inclusion of lattice effects in fast fission is not nearly so critical as in thermal group constant generation, since errors in the treatment of fast fission rarely lead to an error of over several

tenths of a per cent in core multiplication. Hence rather crude methods are usually sufficient for accounting for lattice heterogeneities in fast fission for thermal reactor design.

C. The Inclusion of Heterogeneous Effects in Fast Spectrum Codes

As we have seen, the most significant effects of a heterogeneous fuel arrangement on the calculation of fast group constants enter into the treatment of resonance absorption, although modifications are frequently also included in the treatment of fast fission.

The dominant heterogeneous effect in resonance absorption is that of self-shielding which substantially reduces the value of the resonance integral. One can include this effect in the calculation of resonance integrals by using the expressions obtained in section 10-2-1 utilizing the rational approximation for the escape probability from a fuel lump. [One could also simply use one of the various empirical correlations for I.] It is customary to account for rod shadowing effects as well by including the Dancoff correction factor in the calculation of I.

The resonance integral can then be used to obtain the corresponding resonance escape probability

$$p = \exp\left[-\frac{NI}{\xi\Sigma_s}\right] \tag{10-153}$$

which enters into the fast spectrum calculation.

Frequently, the resonance escape probabilities for each group are adjusted (fudged) so that the total resonance integral agrees with an empirical correlation (although the amount of resonance absorption

assigned to each microgroup in the fast spectrum code will vary with the details of the calculation). For example, one scheme might be to multiply every resonance escape probability P_n for U^{238} by the same fudge factor L, and then vary L until I^{28} when calculated assuming zero absorption for all other elements agrees with the Strawbridge and Barry correlation (this is known as the "ω^*-search", where

$$\omega^* \equiv \frac{1-p^{28}}{p^{28}} \quad)$$

One also scales the cross sections in the fast microgroups to account for fast flux peaking in the fuel which tends to enhance fast fission.

With these adjusted resonance escape probabilities and cross sections, one can now calculate the fast neutron energy spectrum and generate the fast few group constants.

PART IV

AN INTRODUCTION

TO

NUCLEAR REACTOR CORE DESIGN

CHAPTER 11: GENERAL ASPECTS OF NUCLEAR REACTOR CORE DESIGN

I. A SURVEY OF DESIGN PROBLEMS FACED BY THE NUCLEAR ENGINEER

A. Introductory Comments on Nuclear Design

The primary responsibility for the nuclear design of a reactor core rests with the nuclear engineer. This design must be accomplished within numerous constraints imposed upon the reactor operation. The neutronic analysis and design of a reactor core is highly interdependent upon other areas of core design, including thermal-hydraulic design, structural analysis, economic performance, and so on. The primary tools used by the nuclear engineer in his analysis of the reactor core consist of a multiplicity of computer programs or codes which are used to simulate the nuclear behavior of the reactor.

The complete nuclear design of a given core configuration is performed many times--initially to identify design constraints, then to refine the design while interacting with thermal-hydraulic and plant design--then, finally, to establish a reference design which provides a calculational base against which optimization calculations can be compared. Naturally, during the latter stages of the design process, the analysis becomes much more detailed (and expensive) as one narrows in on the final design configuration.

This design process is very similar to those utilized in other fields of engineering. One first must attempt to define the various design constraints which include considerations of system performance (both from the aspect of reliability as well as economic performance)

and safety criteria. One then attempts to synthesis a preliminary design, drawing on available information such as plants already in operation, experimental mockups, and frequently, old-fashioned intuition. The preliminary design results in a set of specifications involving quantities such as fuel enrichment, coolant flow rates, core configuration, reload patterns, etc.

One next performs a detailed analysis of this preliminary design in order to evaluate its predicted performance and verify whether it conforms to the constraints imposed upon the system. For example, one would want to calculate the core power and temperature distribution, the pressure drop of the coolant, the fuel lifetime, coolant flow conditions (e.g., DNBR). When possible, these calculations are compared against experiments in order to validate the computational models which are used. A detailed evaluation of the preliminary design will then lead to more detailed designs and analyses as one attempts to optimize the tradeoff between system performance and design constraints. As a final design is approached, one attempts to define detailed system specifications (frequently allowing for several alternative subsystem designs) as a preliminary to actual core fabrication.

B. Types of Design Problems

The various functions of a nuclear designer can be grouped into one of several classifications:

(i) Core criticality and power distributions: Of course the first concern of the nuclear engineer is to determine the multiplication factor or criticality of a given core configuration. He is concerned as well with the determination of the core power distributions since these are of central importance in

the corresponding thermal analysis of the core. For example, one would like to design a core which will result in a flat radial and axial power distribution through core lifetime while at the same time providing sufficient reactivity to yield adequate fuel burnups while maintaining adequate reactor control over core life. The analysis of the core power distribution or flux distribution involves consideration of the arrangement of fuel assemblies, control elements, fission product concentrations, and moderator densities (e.g., moderator void distributions).

(ii) Reactivity coefficients: A closely related analysis is concerned with the various mechanisms which affect core reactivity. One is particularly interested in the various reactivity coefficients which characterize the transient behavior of the reactor. In order to determine such coefficients, some information concerning the temperature distribution through the reactor is necessary. Then one needs to determine the effect of coolant density changes--that is, the so-called coolant void coefficient of reactivity. Of comparable concern is the Doppler coefficient of reactivity, which of course involves the study of resonance absorption in the reactor. One must also study reactivity coefficients characterizing thermal expansion of the structural material comprising the core. Such calculations are of vital importance to reactor safety studies.

(iii) Fuel Loading Requirements and core arrangement: Of course the nuclear designer must determine that fuel loading which will guarantee reactor criticality over the desired core

lifetime. This requires compensating for both fuel depletion as well as reactivity effects due to both temperature feedback and fission product buildup. At this point various details of the fuel design enter such as the moderator to fuel volume ratio, the fuel element dimensions and configuration, enrichment, and so on.

(iv) Reactivity control calculations: Closely related analyses must be performed to determine the amount of negative reactivity which must be included to compensate for the excess reactivity contained in the initial fuel loading as well as to allow for flexible and safe reactor operation. One must allocate this reactivity among several different control mechanisms, including movable control rods, soluble neutron poisons in the coolant (chemical shim), and neutron poisons which burn out over core life (burnable poisons or mechanical shim). The study of such control mechanisms involves a fair degree of black magic, coupled with both diffusion and transport theory calculations to account for the very highly absorbing control elements. Such calculations are necessary to perform the detailed design of individual control rods, as well as control rod patterns and withdrawal and insertion sequences (rod programing).

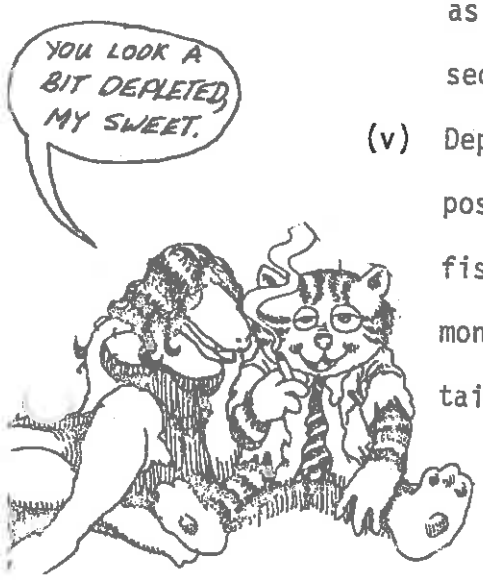

(v) Depletion analysis: During reactor operation the fuel composition will change as fissile isotopes are consumed and fission products are produced. The nuclear designer must monitor these processes over core life in an effort to ascertain fuel composition and reactivity vs. energy removal.

This requires studying the depletion and production chains for the principal isotopes (e.g., U^{235}-U^{238} or U^{233}-Th^{232} systems) coupled with the equations determining the neutron flux in the core. This analysis is closely related to the topic of nuclear fuel management in which one tries to optimize the fuel loading, arrangement, and reloading in order to achieve the most economical power generation within the design constraints (e.g., safety margins) placed upon reactor operation. The so-called "fuel cycle" is characterized by the fuel lifetime, the fraction of the core refueled from time to time, the power density and specific power, and the method of managing the bred fissile material. The choice of a fuel cycle will invariably represent a compromise between economic and engineering considerations. The primary engineering limitions are usually the maximum fuel temperatures, maximum coolant temperatures, control margins, and the maximum allowable exposure of the fuel. Such quantities must be monitored throughout core life.

From this discussion it is apparent that the responsibilities of the nuclear designer are quite varied and numerous. He must establish the limits upon and determine the values of the fuel-to-moderator volume ratio, the fuel rod diameter, and the fuel element arrangement. The fuel loading requirement must then be determined taking into account temperature and power reactivity defects, fuel depletion, and fission product buildup. Next control requirements must be established, including reactivity requirements, control rod geometry and patterns, and the

possible use of chemical shim and burnable poisons. The fuel distribution and refueling arrangement must then be studied in order to achieve economic fuel management within the constraints imposed by safe reactor operation. The kinetic characteristics of the reactor must be determined for safety analyses of core operation, including the various reactivity coefficients which arise, fission product poisoning, and the analyses of various hypothetical accidents.

All of these design functions rely upon the basic theory of nuclear chain reactions that we have developed in the preceding chapters. However because of the accuracy and detail of the information required for actual reactor design, rather sophisticated applications of this theory are necessitated, which, in turn, require the extensive use of modern digital computers.

C. Reactor Calculational Models

As we have mentioned, modern nuclear reactor design depends heavily upon various mathematical models of the nuclear fission chain reaction which are studied and analyzed using digital computers. The computer programs or "codes" which represent these mathematical simulations of the reactor core are generally quite complex and frequently are the result of many years of extensive development and testing at the various nuclear laboratories in this country and abroad. More recently, such codes have become the subject of various proprietary restrictions and while their general features are usually common knowledge, the details of the codes used in present day reactor design are classified as proprietary information by the reactor manufacturers. Hence our discussion here must be of a general nature.

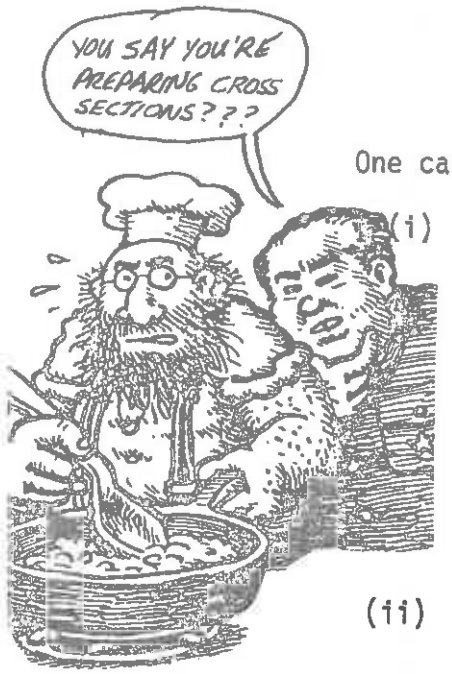

One can generally group such codes into one of four different types:

(i) cross section library handling codes: Such codes are used to manipulate and arrange the massive amount of data on nuclear cross sections contained in such sources as ENDF/B. In particular, such codes must be used to prepare this data in a form suitable for input into other reactor design codes.

(ii) multigroup constant generation codes: As we have seen, most analyses of nuclear reactor cores are based upon the multigroup treatment of the neutron energy. The group constants necessary for such treatment must themselves be generated by neutron energy spectra codes.

(iii) static design codes: The most common type of calculation involves the steady state analysis of the reactor criticality or the determination of the neutron flux distribution within the core. Such information is required for accurate predictions of the fuel loading, power distribution, temperature dependence of reactivity, excess reactivity, shutdown margins, shielding requirements, and other quantities.

(iv) time dependent codes: One is basically concerned with two types of time-dependent calculations. The first of these concerns changes in the reactor properties over the core life such as fuel depletion or fission product buildup. Hence the time scale is of the order of weeks or months. The second type of calculation is concerned with the short time response of the reactor to reactivity perturbations on time

scales of minutes, seconds, or less and is of considerable relevance to both reactor operation and safety analyses.

D. Design Responsibilities

As we have repeatedly emphasized, the neutronic analysis of a reactor core is only one facet of core design. And the core design itself is only a part of the myriad of considerations which are required for the design of a modern nuclear power plant. A very rough classification of these design responsibilities are as follows:

(i) User (utility): The electrical utility owns and operates the plant. Their primary concerns are minimum energy costs, plant reliability and safety, and minimum environmental impact. Hence the user establishes the gross system requirements and evaluates the proposals submitted by the various reactor manufacturers.

(ii) Nuclear equipment manufacturer: Designs and manufactures the nuclear steam supply system (the reactor, steam generator, and primary coolant system).

(iii) Architect-engineer: Designs the non-nuclear portion of the plant, including the containment building, piping, turbo-generator, condensor, and electrical switchgear. (If the nuclear equipment manufacturer supplies these non-nuclear components as well as the NSSS, the plant is said to be constructed on a "turnkey" basis.) The architect engineer also coordinates the engineering details, supervises the construction and inspection of the various contractors working on the plant. It subcontracts the manufacture of the non-nuclear equipment and the plant construction.

It is evident from these descriptions of various design responsibilities that the design and construction of a modern nuclear plant is an extremely complicated business involving the coordination of many different disciplines. Although our concern in this text has been with the nuclear design of the nuclear reactor itself, it is important to keep in mind the intimate relationship between nuclear design and non-nuclear aspects of the plant design.

E. How to Design a Reactor--Revisited

Perhaps the simplest way to illustrate the various ways in which the design of a nuclear reactor is constrained within various engineering limitations is to review our earlier discussion in Chapter 3 of the steps involved in reactor design.

1. Determine the plant electrical output

The electrical output of the plant is usually chosen by the utility ordering the plant. Since the cost per unit of electrical energy generated decreases with increasing plant size, there is incentive to build as large a nuclear plant as would be allowed by the A.E.C. However, there is also the rough rule of thumb that a utility is reluctant to build a single generating unit that is larger than 10% of its present generating capacity--a feature which many nuclear plants exceed.

2. Determine the maximum linear power density

We will see later in section 12-2 that the linear heat flux passing from the fuel rod into the coolant is given by a simple relationship

$$q' = 4\pi k_f (T_\ell - T_{fl})$$

where T_{fl} is the coolant temperature and T_{ℓ} is the centerline temperature of the fuel element. Since the coolant temperature T_{fl} is usually determined by other considerations, one must limit the linear heat flux in order to prevent the fuel temperature from exceeding the fuel melting point (roughly 5000°F for UO_2). For example, this corresponds to roughly

$$q'_{max} \sim 20 \text{ kw/ft}$$

in light water reactors.

3. Determine the maximum-to-average power density ratio

The maximum-to-average power density ratio depends upon a number of factors such as fuel arrangement, the spaces between the fuel assemblies, the presence of coolant slots when control rods are withdrawn, and so on. Furthermore, this ratio will change as a function of core burnup. One must determine the maximum value of this ratio over the operating life of the core.

4. Determine the fuel rod size and pitch

A number of factors must be considered in determining the fuel rod diameter and spacing. For example, an increase in fuel rod size implies more fuel per rod--hence more energy from the rod for the same burnup. But the effective heat transfer area of the fuel assemblies is correspondingly decreased, implying a lower power density. In a similar fashion, the effects of changing the fuel-to-moderator volume ratio must be considered. Since most LWR cores are undermoderated,

decreasing this ratio will increase the core reactivity for fixed fuel enrichment. It will also increase the coolant channel cross sectional area, hence decreasing the coolant pressure drop through the core and thereby decreasing the required coolant pumping power. Increasing the fuel rod diameter for a fixed fuel-to-moderator volume ratio will increase the core diameter, thereby implying increased pressure vessel size, as well as a larger fuel inventory. Many such factors must be weighed against each other in the determination of the fuel configuration.

5. Determine the thermal efficiency of the plant

In order to determine the thermodynamic efficiency of the nuclear plant, one must study the thermodynamic cycle efficiency of the various thermal processes (both heat generation, heat transfer, and the conversion of heat energy into mechanical and finally electrical energy).

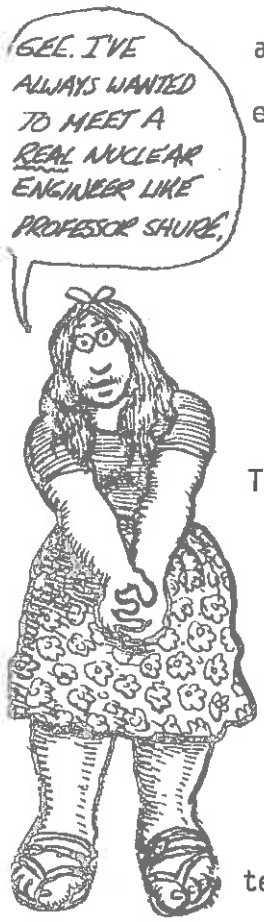

6. Establish the core volume

Here one can simply use

$$\text{core volume} = \frac{\text{plant electrical output}}{\text{efficiency} \times \text{power density}}$$

To determine the core power density, one can estimate

$$\text{power density} = \frac{\text{average linear power density}}{(\text{fuel rod pitch})^2}$$

7. Determine the excess reactivity requirements and the fuel enrichment

Here we need to consider a number of reactivity effects such as temperature and power defects, fission product poisoning, fuel depletion,

as well as allowing sufficient reactivity control for power level changes and for computational uncertainties.

8. Optimization

Certainly the most difficult and expensive facet of the design involves optimization to achieve minimum electrical generation costs consistent with operational requirements. Numerous parametric studies over a broad range of variables must be made in order to zero in on an optimum design.

II. CONSTRAINTS ON REACTOR CORE DESIGN

A. Nuclear Analysis

We have already outlined the various types of calculations required in the nuclear analysis and design of a reactor core. These include the calculation of core criticality and power distributions, the determination of reactivity coefficients, fuel loading requirements and core arrangement, reactivity control calculations, fuel depletion studies, and reactor safety analysis. There are numerous constraints imposed on such nuclear design. Of course, the core composition and configuration must be chosen such that sufficient excess reactivity is available for power generation over a reasonable time period (usually on the time scale of years). The reactivity control must be capable of insuring the safe and reliable operation of the reactor over core life. And these requirements must be met while at the same time minimizing the economic cost of the power generation. These constraints are frequently in conflict with one another. For example, there is

incentive to operate the reactor at the largest possible power density consistent with maintaining fuel and coolant temperatures below limits set by safety considerations. Yet such a high power density is frequently not consistent with economic power generation over the entire core life, since the flux and hence the power distribution will shift as the fuel is depleted.

The nuclear analysis and design of the core cannot be decoupled from other considerations such as the thermal behavior of the core or the behavior of the various materials which comprise the core. This can perhaps be understood more clearly by briefly describing the other types of analysis which arise in reactor core design.

B. Thermal Core Analysis

The energy released in nuclear fission appears as kinetic energy of fission reaction products and eventually as heat generated in the reactor fuel elements. This heat must be removed from the reactor core and used to generate electrical power. Below we have sketched the sequence of processes involved in the transport and utilization of fission heat energy:

fission product energy in fuel

thermal conduction across fuel, gap, and clad

thermal conduction-convection from clad surface into coolant

forced thermal convection in coolant primary loop

production of steam in steam generator in PWR NSSS (this occurs in the reactor vessel in a BWR NSSS)

conversion of steam energy into mechanical energy in turbine

condensation of wet steam discharged from turbine (and subsequent return as feedwater to steam generator)

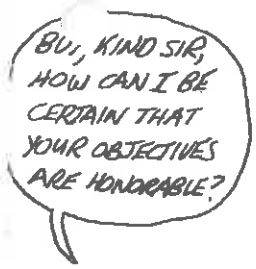

The study of each of these processes is most properly the concern of the mechanical engineer. However since they have such a significant bearing on the nuclear design of the core, we will devote a considerable portion of Chapter 12 to a summary of the thermal analysis of nuclear reactor cores.

The primary objectives of the thermal analysis are three-fold:

(i) high power density (kw/liter): This will minimize the core pressure vessel size.

(ii) high fuel specific power (kw/kgU): This minimizes fuel inventory.

(iii) high coolant outlet temperature: This maximimizes the thermodynamic efficiency.

These objectives are subject to several very important constraints. First, one must always insure that the fuel temperatures remain below the fuel melting point. There are also limits on the amount of heat transfer which can occur between the fuel element clad and the coolant, since if this heat transfer rate becomes too large, film boiling of the coolant may occur which will result in a rapid rise in clad (and hence fuel) temperatures. One must also insure that the coolant pressures always remain below those which can be safely constrained by the core pressure vessel.

Such constraints must be studied over core life, since as the power distribution in the core changes due to fuel burnup or core reloading, the temperature distribution will similarly change. Furthermore, since the cross sections which govern the neutronics of the core are strongly temperature and density dependent, there will be a strong

coupling between the thermal-hydraulic and neutronic behavior of the reactor core. We will see in the next chapter that this coupling has a strong influence on the manner in which reactor criticality calculations must be performed.

C. Mechanical Analysis of Reactor Cores

It is of vital importance to choose materials and design core components which can withstand the intense radiation, high pressure, and high thermal gradient environment of a reactor core. Of central concern is the mechanical behavior of fuel elements--which are subjected to severe stresses, both internally due to fission gas and fuel swelling, and externally due to high external pressures in the coolant or large thermal gradients across the clad or clad-fuel interactions. But the mechanical design of additional core components must also be considered. For example, the various internal structure required to support the fuel, flow baffles, and control rod assemblies must be designed to withstand the intense core environment. And of course the reactor pressure vessel itself represents a formidable mechanical design problem, since it must withstand extremely high pressures over the operating lifetime of the reactor. Related mechanical design problems concern the fabrication and maintenance of the mechanical assemblies in the core. Particular attention must be made to refueling operations.

D. Materials Problems in Reactor Core Design

Materials used in nuclear reactor construction are subjected to intensive bombardments by nuclear radiation. Over a period of time, such radiation can dramatically alter the properties of these materials.

For example, metals will become brittle and swell, corrosion is enhanced, and so on. The reactor engineer must be very careful to anticipate such radiation damage in his design.

These effects of radiation on reactor materials have become particularly important in today's maturing nuclear reactor industry. In order to achieve the lowest possible power costs, nuclear fuel elements must be used in a reactor as long as possible (i.e., high burnup). Actually, the principal limitation on the amount of burnup is not the loss of U^{235} or Pu^{239} nuclei through fission, but rather the attendant radiation damage to the fuel and the cladding material which would lead to fuel element failure if the fuel is left in the core too long. Hence, whereas nuclear reactors were limited by nuclear considerations during the 1950's, and by thermal design during the 1960's, today's modern power reactors are primarily limited by the radiation damage which can be withstood by reactor materials.

Life will get even more difficult in fast breeder reactors because of the intensity of fast neutron radiation. Several years ago it was found that stainless steel (a major structural component of the fast breeder) swells rather dramatically (several per cent) when irradiated over long periods of time by fast neutrons. Such swelling must be accounted for in the mechanical design of the fast reactor core (no mean feat).

There are several types of high energy radiation present in a nuclear reactor core. Most of these result from the nuclear fission reaction itself, although lesser amounts arise from associated reactions such as radiative neutron capture. Of course most fission energy is carried by

the massive fission fragment nuclei. These cause catastrophic damage to the adjacent fuel material. But because of their large electrical charge, the range of the fission fragments is extremely short (less than 20 microns), and hence this damage is localized in the fuel to the immediate vicinity of the fission event. A potentially more serious type of radiation is that due to fast neutrons. Because of their neutrality, neutrons have rather long ranges (as much as several meters). Hence they can damage material located anywhere in the reactor core. Gamma radiation is also characterized by large ranges, but is of secondary importance to fast neutron damage.

The actual effect of radiation on a material depends sensitively on the type of material, the type of radiation, and the conditions during the time of irradiation (such as temperature). However some general observations can be made. For example, for irradiated metals, hardness, tensile strength and impact resistance increase, while ductility decreases (corresponding to an increase in brittleness).

The significance in radiation damage in reactor core design becomes particularly apparent when one examines nuclear fuel performance in light water reactors. As we have seen, it is the low cost of nuclear fuel (relative to the electrical power produced) which is the principal factor in the low cost of nuclear power. That such costs are realizable is due in no small measure to the significant advances made in nuclear fuel design and performance since the mid-1960's. Nuclear fuel elements must be designed subject to several criteria intended to guarantee the fuel performance up the lifetime limit:

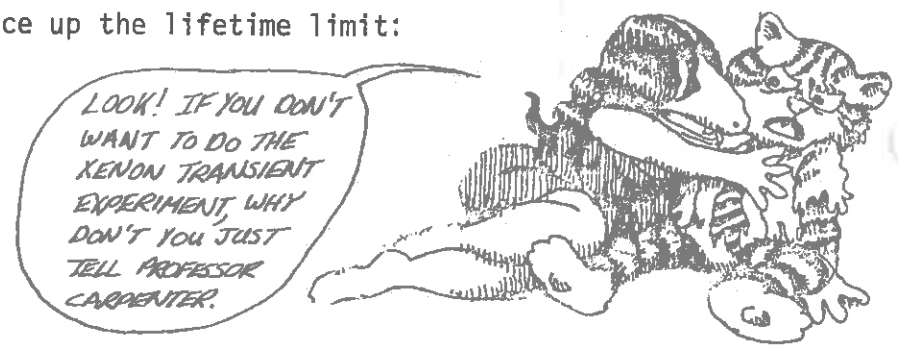

(i) The fuel temperature at the hottest point always must be below the melting point.

(ii) Axial fuel displacement influencing temperature distribution and multiplication are tolerable only to a very small extent.

(iii) The cladding must remain leak tight.

(iv) The outer geometry of the fuel pin (length, diameter, straightness) is subject to very small tolerances.

As we have seen, nuclear fuel elements are subjected to enormous irradiation. They are furthermore subject to extremely large temperature variations. This is caused to a large degree by the rather poor ability of the principal type of nuclear fuel, uranium oxide, to conduct heat. Such temperature variations place enormous thermal stresses on the fuel elements and interact strongly with the changes in the fuel induced by irradiation.

The principal radiation effects which must be accounted for in fuel element design include:

fuel: creep and swelling, fission gas release, pore migration, chemical changes, change in radiation and axial fuel density profile

cladding: mechanical properties, swelling by void formation, corrosion

fuel pins: radial heat transfer and temperature distribution, mechanical and chemical interaction between fuel and cladding, swelling and bowing of the pin

fuel bundle: changes of component geometry, interaction of pin and spacers

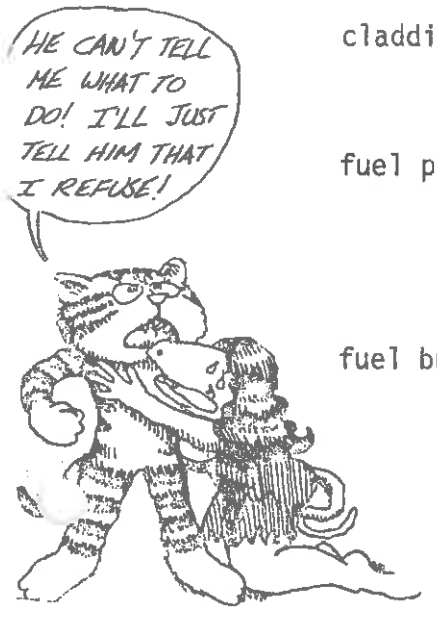

Such considerations have led to a number of modifications in fuel element designs for LWR's. Current designs provide for increased void volume to accomodate fuel swelling and fission gas release associated with the higher burnups used in today's power reactors. The excellent corrosion resistance of zirconium alloys has led to their almost exclusive use as a cladding material. As the nuclear power industry obtains more operating experience with fuel design and behavior under long term irradiation, it is able to develop advanced designs capable of very high burnups and power densities.

The commercial success of the LMFBR will also be critically dependent on the attainment of low fuel-cycle costs and therefore on the satisfactory behavior of the fuel to high burnup. Only rather recently has any experience at all in the behavior of materials in high fast neutron flux environments been available. Perhaps the most dramatic effect thus far observed occurs in structural materials such as stainless steel. After long periods of irradiation by fast neutrons, the steel is observed to swell. Closer examination indicates the presence of small voids in the irradiated material. Of course, such swelling and void formation are highly undersirable in a reactor core in which mechanical and structural tolerances must be kept very refined over the lifetime of the core (up to 30 years).

The voids are caused by fast neutrons which rip through the crystal lattice knocking atoms out of their lattice positions. These vacancies tend to migrate together to form voids and hence induce the swelling. By raising the steel to high temperatures the voids can be annealed out. Unfortunately, at the anticipated operating temperatures of the LMFBR, such swelling is quite pronounced and is still not thoroughly understood.

E. Economic Analysis

The justification for nuclear power plants must reside in their economic advantages over more conventional sources of electrical power. The cost of electrical power can be broken down into a number of factors including the capital cost of constructing the plant, the annual cost of operating and maintaining the plant, and the annual costs for fuel. The capital investment required for the construction of nuclear power plants is equal to or greater than that required for conventional power plants. Furthermore, operating and maintenance costs account for only a small fraction of the total cost of producing electricity. Hence the primary advantage enjoyed by nuclear power is in the lower cost of its fuel.

Nuclear fuel costs are much different than fossil fuel costs. A number of charges other than direct materials costs are involved, and these may lead or lag utilization of the fuel material by several years. There are a large number of rather sophisticated and expensive processing operations required by the fuel before it is inserted into the reactor core, and by the spent fuel after it is removed from the core. The major portions of the fuel cycle costs include the charges for uranium consumption (burnup charges), the cost of fabricating the fuel element, the cost for recovery of spent fuel (reprocessing and shipping charges), and working capital charges for the fuel fabrication cost and the fuel inventory. [Working capital charges are interest charges to be paid for the invested capital and are based on all of the fuel in the reactor.]

Needless to say, the complexity of accounting for nuclear fuel costs and capital plant investment requires rather sophisticated

and expensive processing operations required by the fuel before it is inserted into the reactor core and by the spent fuel after it is removed from the core. The major portions of the fuel cycle costs include the charges for uranium consumption (burnup charges), the cost of fabricating the fuel elements, the cost for recovery of spent fuel (reprocessing and shipping charges), and working capital charges for the fuel fabrication cost and the fuel inventory. [Working capital charges are interest charges to be paid for the invested capital and are based on all of the fuel in the reactor.]

Needless to say, the complexity of accounting for nuclear fuel costs and capital plant investment requires rather sophisticated economics analysis of the plant design. Nuclear power costs will depend upon parameters that vary widely, depending upon the location of the plant, the type of the reactor, and even the time at which the economic study is performed. Such considerations make it apparent that each reactor manufacturer and utility have access to a technical group capable of predicting the behavior of the nuclear fuel, performing an economic analysis of such fuel utilization, and analysing the total power system requirements involving the plant (including other conventional and nuclear plants in the system).

F. Safety and Regulatory Considerations

Of course, all reactor designs are subjected to extremely thorough studies to insure that they are compatible with existing safety and regulatory standards. For example, the response of the reactor design to reactivity insertions resulting from severe disturbances which could arise only under the most extreme circumstances must be determined. Other topics

include the analysis of accidents initiated by local fuel element failure (and subsequent failure propagation), loss of coolant accidents, failure of control systems, and so on.

Such analyses are important not only for determining the necessary engineered safeguards systems, but to study as well the performance and interaction of these systems under various postulated accident conditions.

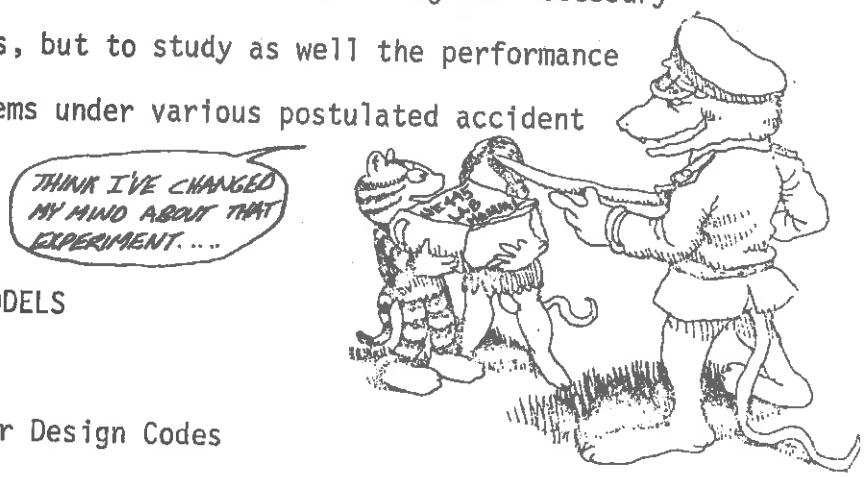

III. REACTOR CALCULATIONAL MODELS

A. An Overview Of Reactor Design Codes

We have mentioned that reactor design codes can be classified into one of several groups, namely, cross section library codes, multigroup constant (MGC) generation codes, static design codes, and time-dependent codes. Of course the latter three types of codes are based upon models which can be traced back to the neutron transport equation. But as we have repeatedly emphasized, the direct solution of this equation is usually quite intractible, hence numerous approximations are usually required in order to develop the mathematical models which serve as the basis of reactor design codes. Typically, these codes suppress certain independent variables in order to allow a detailed analysis of the process of interest. For example MGC generation codes usually suppress spatial dependence--either by assuming an infinite medium or a single diffusion mode--in order to facilitate a detailed treatment of the neutron energy. In a similar sense, static design codes employ a rather course multigroup structure in order to allow a detailed study

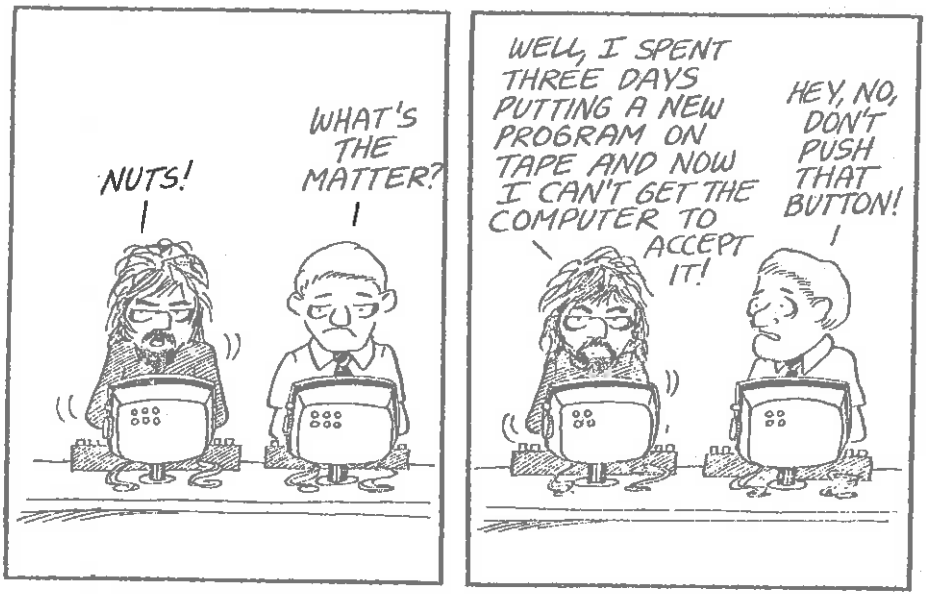
NUTS!
WHAT'S THE MATTER?
WELL, I SPENT THREE DAYS PUTTING A NEW PROGRAM ON TAPE AND NOW I CAN'T GET THE COMPUTER TO ACCEPT IT!
HEY, NO, DON'T PUSH THAT BUTTON!
attention: your entire program has been destroyed
AARRGG!
YOU'VE GOT TO RELAX..
GBTrudeau

of the spatial dependence of the neutron flux. In time-dependent codes one frequently ignores both spatial and energy dependence.

The proper utilization of such nuclear reactor codes requires not only a thorough knowledge of the various approximations which have entered into the development of the code, but as well a good deal of common sense, experience, and just plain old-fashioned good luck. In this brief summary, we will attempt to review the function of each of the major types of nuclear design codes as well as the approximations which usually enter them. We will also discuss how these codes are interrelated and how they are blended together in a reactor design. In the next section we will discuss how the codes are verified and/or "fudged" using experimental measurements.

B. Cross-Section Preparation Codes

The basic ingredient in any nuclear analysis is a set of cross sections characterizing the probabilities of various neutron-nuclear reactions which might occur. Most generally this would consist of a tabulation of cross section data covering the energy range from 0 to 10 MeV for (n,γ), (n,α), (n, fission), (n,p), (n,2p), (n,2n), and (n,n') reactions as well as differential scattering cross sections describing neutron energy and angle transfers in scattering collisions. Such cross section data is provided by a plethora of diverse experiments, approximate theoretical calculations, and extrapolations of experimental measurements. In any collection of raw cross section data there exist many duplications, disagreements, and gaps in the tabulated cross sections. It is the job of a cross section evaluator to select the most consistent set of cross section data. The standard source of cross

sections for nuclear design in this country is the Evaluated Nuclear Data File/Version B which contains data compiled and evaluated from all known cross section information. The amount of such data requires that it be stored on magnetic tape and manipulated using complex data handling codes. Such codes not only select out the cross section data of interest and prepare it into a form suitable for input to reactor design codes, but as well they interpolate existing data to fill in any gaps which may exist, as well as apply various theoretical models (such as the optical model of the nucleus) to generate cross section data in those regimes in which no experimental data exists. These library codes also generate differential scattering cross sections, resonance integrals, and thermal energy scattering kernels.

The differential scattering cross sections for elastic scattering are usually generated as a sequence of terms in a Legendre polynomial expansion. By way of contrast, inelastic scattering and (n,2n) processes are usually assumed to be isotropic in the laboratory system and calculated using available data on the appropriate nuclear states or the evaporation model of the nucleus.

One of the more difficult aspects of cross section generation concerns the treatment of resonance cross sections. Because such resonances are usually quite large in magnitude and yet quite narrow compared to even energy intervals characterizing the cross section data, it is necessary to make some attempt to account for flux depression in the resonances in order to include effective resonance integrals in the cross

---

Ref: ANL-7411 Computer Code Abstracts
ANL-5800 Reactor Physics Constants (Chapter 10)
Advances in Nuclear Science & Technology, Vol. 2 (1954); Roos and Sangren

section data set. In the regime in which the resonances are isolated and measured, this can be accomplished using the standard techniques (e.g., the NR or NRIM approximations). Various nuclear models can be used to generate resonance parameters for the energy range in which the resonances are still isolated but not measured. The most difficult area to treat is the energy range in which the resonances are not only unresolved, but overlap as well so appreciably that they cannot be considered independently. It is also usually necessary to account for heterogeneous effects (a la Chapter 10), temperature effects on the resonance structure, and overlap of resonances of different materials.

C. Multigroup Constant Generation Codes

As we have seen, the energy range spanned by the neutrons as they are born in fission and slow down to eventual capture or leakage at thermal energies (at least in thermal reactors) is enormous, covering some eight orders of magnitude. Since the cross sections themselves depend sensitively upon energy, it is apparent that one must proceed rather carefully in generating few group constants for use in multigroup diffusion calculations.

One usually proceeds in two steps. The energy range of interest is first divided up into a very fine multigroup structure, and the cross section data supplied by a library code is simply averaged over these groups (for example, in the slowing down range one might use a 1/E spectrum). Appropriate approximations to the effective resonance integrals of interest are also included in this set of "fine group constants". These fine group constants then serve as the microscopic

cross section data used in fast and thermal spectrum codes which perform an approximate calculation of the neutron energy dependence for the nuclear assembly of interest, and then average or collapse the fine group constants into few group constants over these approximate spectra. It should be noted that whereas fine group constants are usually evaluated without reference to the detailed system under consideration, the spectrum generation codes generate few group MGC for the specific system of interest. These MGC are then used in static and kinetic design analysis.

Of course the trick enabling one to perform a detailed study of the neutron energy spectrum is the temporary neglect of the detailed spatial dependence of the neutron flux. It is customary to assume a simple single mode flux shape--that is, to assume a buckling which characterizes the region of the core under consideration. The angular flux dependence is simplified using either the P_1 or B_1 approximation (although sometimes higher order B_N methods may be used).

However the success of MGC generation codes frequently depends on how these codes are corrected for the rather strong spatial dependence of the flux which occurs in the vicinity of the fuel rod or control rod. We have already examined several methods for correcting cross section group constants for these heterogeneous effects--e.g., disadvantage factors, collision probabilities, and such. In the fast region, it is usually sufficient to merely correct the calculation of the resonance integrals for self-shielding effects using escape probabilities calculated for the cell geometry of interest. In the thermal range, one may either use approximate techniques such as the ABH method to determine

disadvantage factors, or use more elaborate cell calculation techniques such as THERMOS to directly calculate the self-shielded cross sections.

We have seen that these MGC are usually then spatially averaged over the fuel cell or perhaps a fuel assembly in order to generate "homogenized" cross sections most consistent with the spatial mesh to be used in the few-group multigroup diffusion calculation.

We have already referred to the various common schemes to generate few group constants for light water reactors--namely, MUFT-type calculations for the fast spectrum, and SOFOCATE or TEMPEST-type calculations for the thermal spectrum, including perhaps a THERMOS calculation for cell analysis. The corresponding types of codes for HTGR's include GAM for the fast group constants and GATHER for thermal group constants. The group structure necessary for fast reactor analysis must be considerably more detailed, and ultrafine group structures such as those employed in MC^2 are used to generate MGC for fast assembly analysis.

The corresponding codes for MGC generation in the University of Michigan Nuclear Engineering library include MIFS, a MUFT-type fast spectrum code, and MITS, a SOFOCATE-type thermal spectrum code.

A sequence of calculations used in the generation of few group MGC are illustrated schematically in Figure 11-1.

D. Static Design Codes

Static design codes are commonly used to obtain the most detailed description of the energy-dependent neutron flux through the core. This information is required for accurate predictions of the fuel loading, power distributions, temperature dependence of reactivity, excess reactivity, shutdown margins, shielding requirements, and other

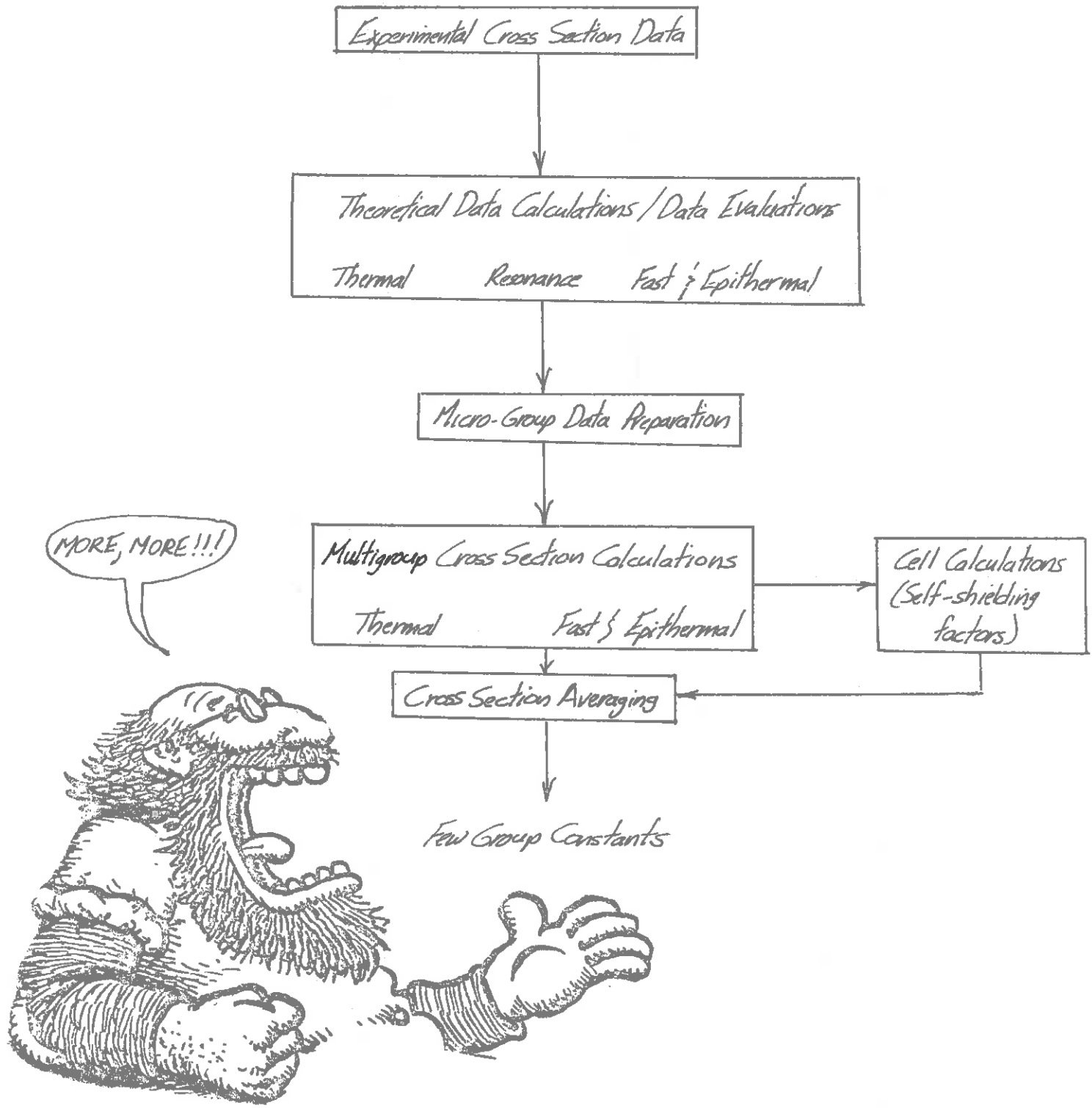

Figure II-1: Generation of Few Group Constants

quantities. These codes are usually few-group diffusion or transport codes which utilize the MGC generated by the spectrum codes discussed in the previous section. One customarily uses such codes to determine the multiplication factor (eigenvalue) and flux distribution in the system of interest. Usually multidimensional diffusion codes are sufficient for this task. However occasionally transport codes are necessary to determine cell correction factors in the vicinity of strong absorbers or voids.

Indeed, before a diffusion theory calculation can be performed, the heterogenieties in the core must be homogenized. Although MGC generation codes usually provide sufficient accuracy for this purpose, it is occasionally necessary to use a transport code such as ANISN or 2DF for this purpose. With such corrections, multigroup diffusion codes are usually adequate for a wide class of problems, including the determination of the over-all flux distribution, the effects of fuel zoning, reactivity predictions, and so on.

In light water moderated reactors, a four-group diffusion model (3 fast groups, one thermal group) usually provides sufficient accuracy. In HTGR's the use of 3 fast groups and 4 thermal groups has proven to be adequate. By way of contrast, the design of fast reactors may require as many as 20 or 30 groups for an adequate treatment of the energy dependence of the flux.

Such codes can also be used to calculate temperature and power coefficients of reactivity. This is usually performed by merely calculating the core multiplication for several different core temperatures or power levels (using different MGC for each temperature, of course).

A schematic of the manner in which static design codes are utilized in core analysis is shown in Figures 11-2 and 11-3.

E. Time-Dependent Design Codes

The fourth class of codes attempt to explicitly treat the time dependence of the nuclear behavior of the core. Of course by including this additional variable, one is usually forced to utilize a coarser description of the remaining variables--e.g., space and energy. Such codes can themselves be broken into three separate classifications:

1.) Depletion Codes

In a depletion calculation, one is concerned with monitoring the core composition and flux distribution in the reactor over the core life. In particular, one must take into account the time and space dependence of

(i) fissile material buildup (from fertile materials) and depletion

(ii) fertile material depletion

(iii) burnable poison depletion

(iv) fission product buildup

(v) the buildup and depletion of heavy metal nuclides such as U^{234}, U^{236}, Pu^{240}

(vi) the movement of control rods to maintain criticality

Depletion codes involve first the solution of the balance equations describing isotope concentrations, e.g.,

$$\frac{dN_i}{dt} = \sum_j \gamma_{j,i}\,\sigma_f^j N_j \phi + \sigma_\gamma^{i-1} N_{i-1}\phi + \lambda_{i'} N_{i'} - \sigma_f^i N_i \phi - \sigma_\gamma^i N_i \phi - \lambda_i N_i \qquad (11\text{-}1)$$

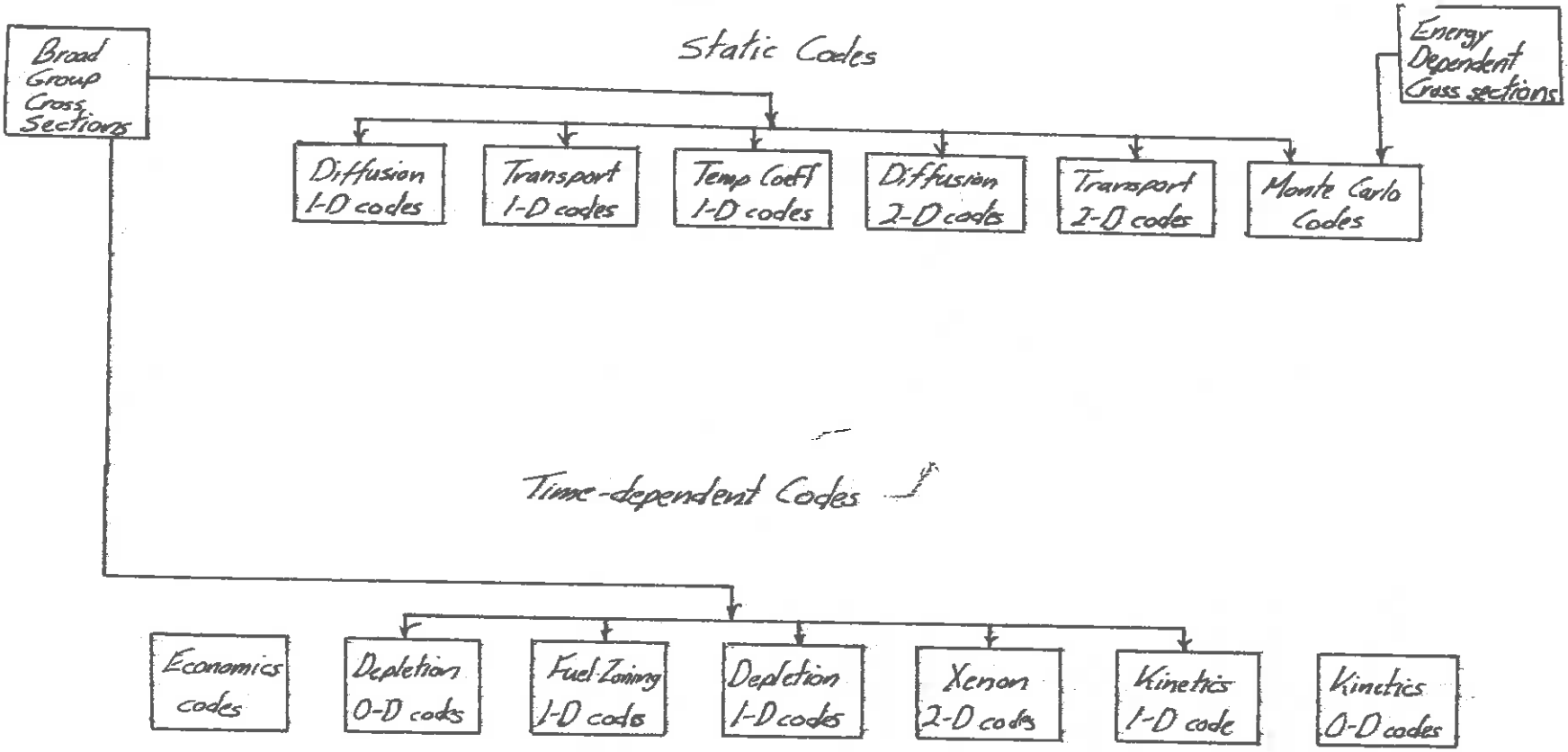

Figure II-2: Classification of Static & Time-dependent codes

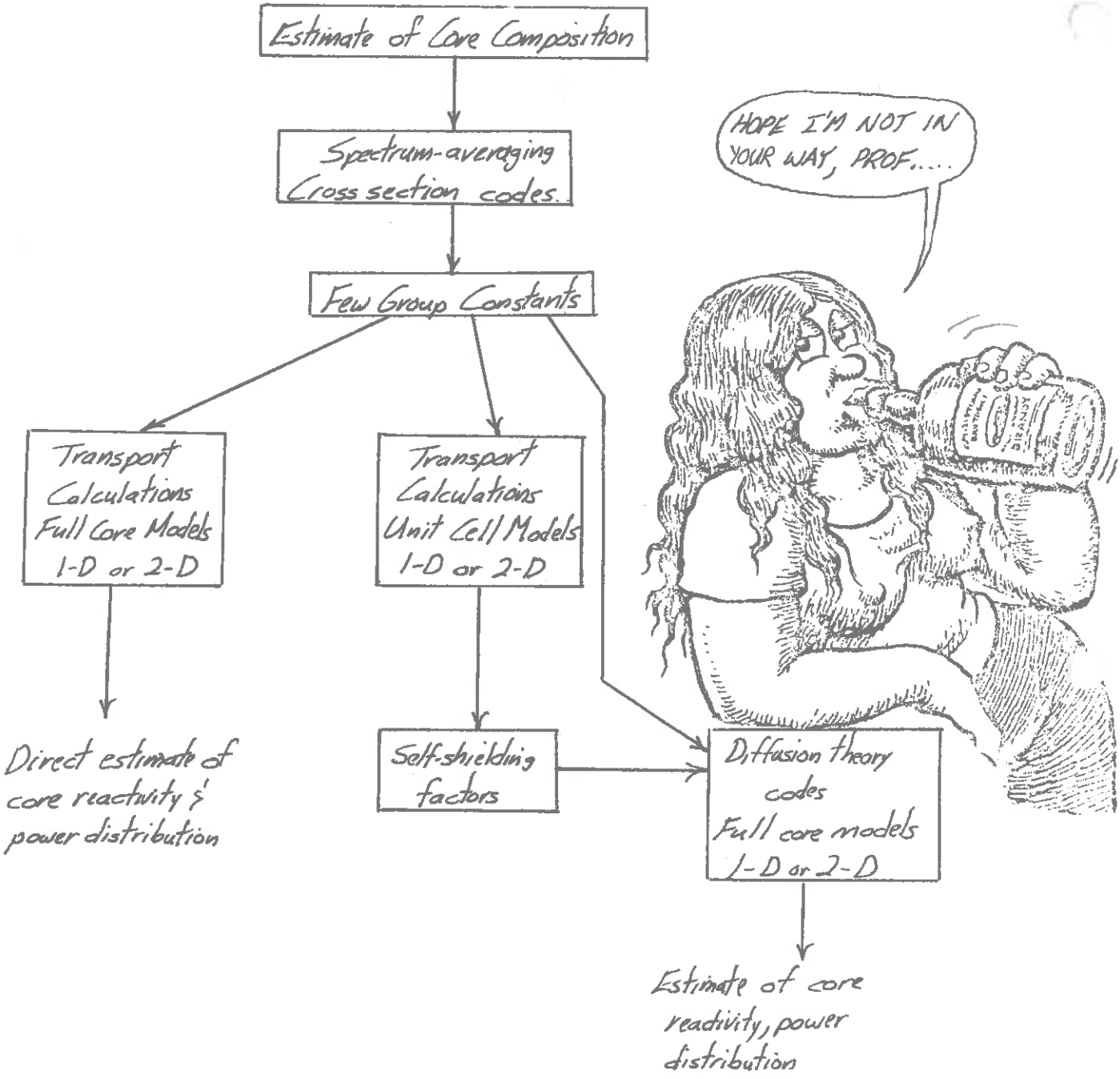

Figure II-3: Static Core Calculations

as well as the neutron balance equations describing core criticality. Because of the many variables involved, such as power density, rate of reload, excess reactivity requirements, and varying reload patterns, even the simplest depletion problem may require solutions at many points in time.

Because of their low computer cost and general flexibility, extensive use is made of zero-dimensional depletion codes for survey calculations. However, more detailed analyses will require the use of 1-D or 2-D depletion codes in order to account for the spatial flux variation and control rod and reload patterns. A rough schematic of depletion analysis is shown in Figure 11-4.

2.) Fuel Cycle Analysis

One of the major applications of fuel depletion codes is to the analysis of fuel cycle strategy--that is, a determination of the optimum fuel reloading strategy for minimizing fuel cycle costs. Such estimates of initial core composition and reload fuel composition must take into account the requirements for heat removal, coolant pumping power, peak fuel temperatures, etc., and hence are invariably a compromise between that core composition which gives the lowest fuel cycle cost and that composition which results in acceptable system temperatures. A schematic of the various steps involved in fuel cycle analysis are shown in Figure 11-5.

3.) Reactor Kinetics Analysis

In order to analyze the transient response of the reactor to both normal operating conditions and postulated accident situations, one must utilize codes based upon the nuclear reactor kinetics equations discussed in Chapter 6. Such calculations differ dramatically from

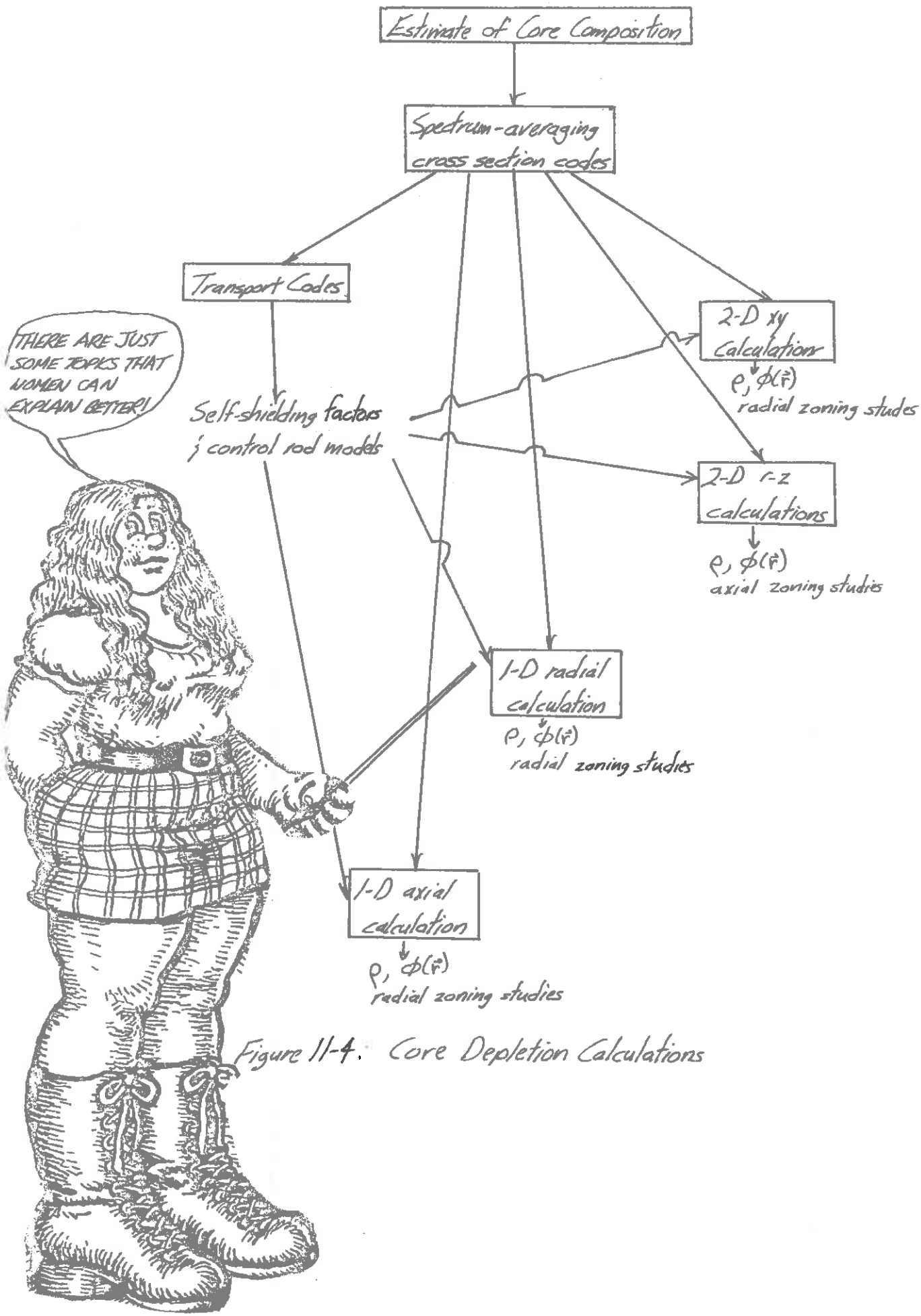

Figure II-4. Core Depletion Calculations

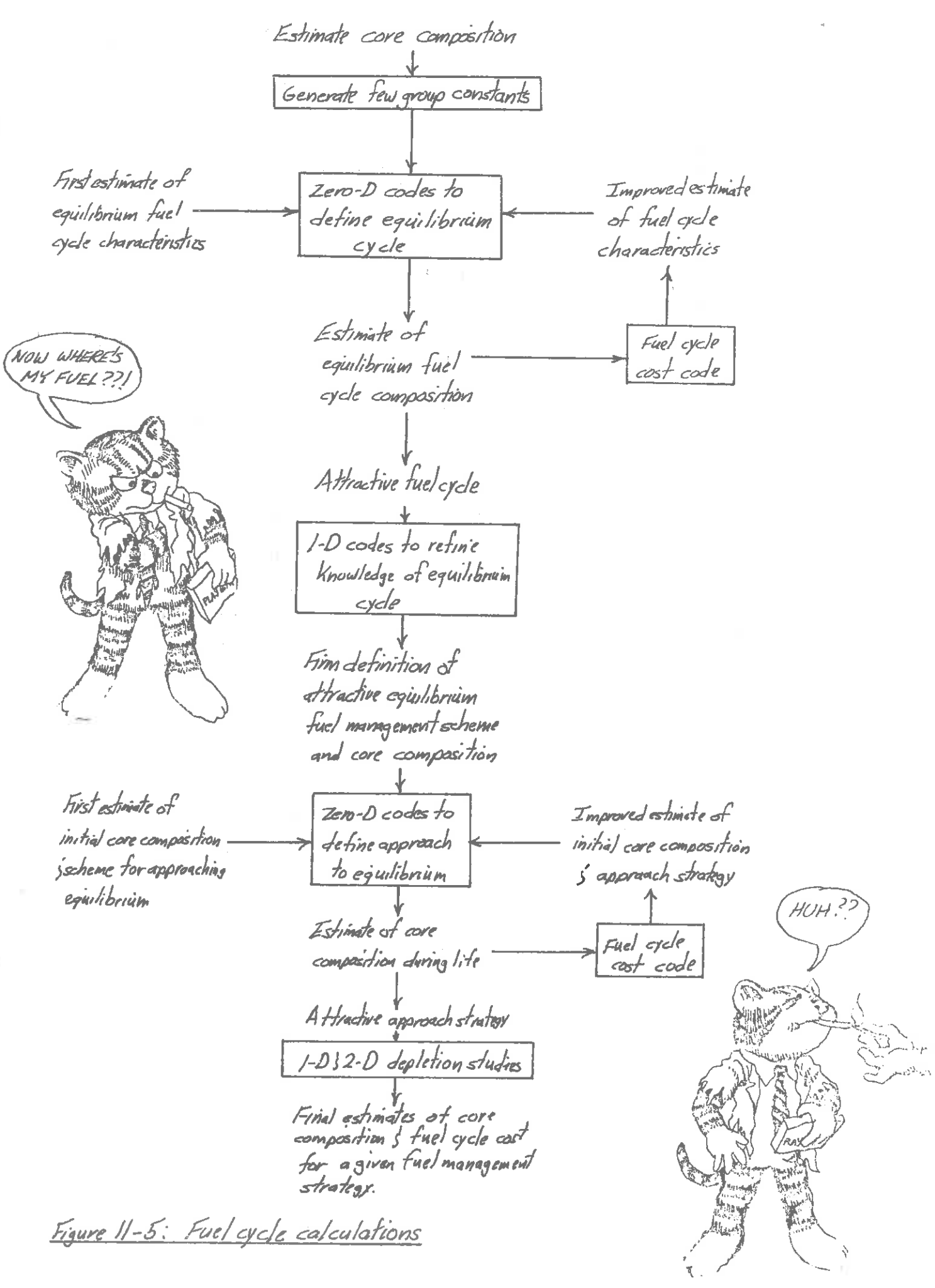

Figure II-5: Fuel cycle calculations

depletion calculations in two respects: first, the time scale of reactor transient behavior is usually of the order of minutes or less, whereas depletion calculations are concerned with core behavior over times as long as several years. Second, in kinetics calculations, the reactor is usually subject to a non-zero net reactivity (due to control, operating conditions, etc.). In a depletion calculation, one always assumes that control is adjusted to hold the core critical at all times. Hence in a depletion calculation, one is actually only concerned with the steady-state equations describing the neutronics.

Reactor kinetics analysis plays an important role in core design since it is necessary to assess safety margins, to select and place control and safety instrumentation, to design the control and protective system, and to determine the need and effectiveness of engineered safeguards.

Of course at the heart of such codes is a numerical solution of the reactor kinetics equations describing the neutron flux time behavior in the core. However one must as well account for coolant flow and heat transfer in order to determine feedback reactivity. In addition, there is strong coupling to other dynamic processes in the NSSS, such as the primary coolant loop, steam generator, coolant pumps, feedwater system, and so on. Hence the study of reactor dynamics can become quite complicated.

As input to such codes one requires not only basic nuclear data, such as cross sections, temperature coefficients, and so on, but as well thermal-hydraulic information. These latter quantities are usually determined using static design codes.

The simplest level of description would be the use of point reactor kinetics to describe the core neutronics. However in many instances, the spatial dependence of the flux is important, and then either brute force multigroup diffusion codes or hybrid schemes such as synthesis must be utilized for an adequate description. A schematic of a typical reactor kinetics analysis is shown in Figure 11-6.

F. Code Packages

Such reactor design codes frequently are designed as modules to fit into a more general overall design code package capable of a variety of design functions. A very simple example of such a package is the reactor calculational model used at the U of M. A diagramatic sketch of this reactor calculation model is shown in Figure 11-7. The principal codes involved are described briefly below:

CONLIB: A cross section library generation code which selects out of the general MUFT library a subset of isotopes of interest in a particular design.

MITS: Thermal spectrum code

Input library: MITL (54 elements, σ_s, σ_f, σ_a vs. E)

Solves infinite medium thermalization equation

Assumes proton gas (similar to SOFOCATE)

Uses ABH method of calculate disadvantage factor

Generates one-group thermal cross sections

MIFS: Fast spectrum code

Input library: MIFL (40 elements, 54 groups, σ_f, σ_a, σ_s, resonance data, inelastic scattering matrices, source spectra)

Solves ∞-homogeneous medium slowing down equation

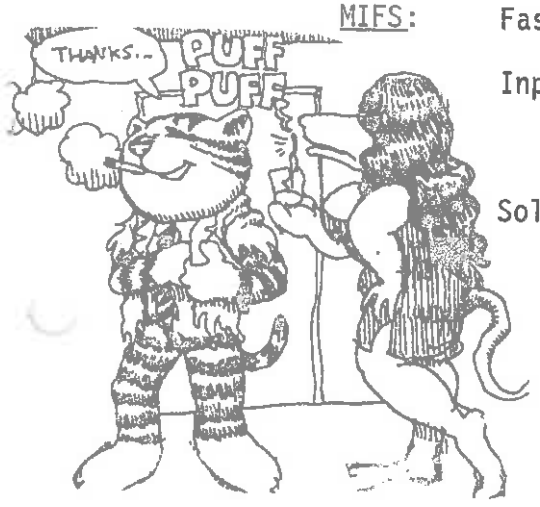

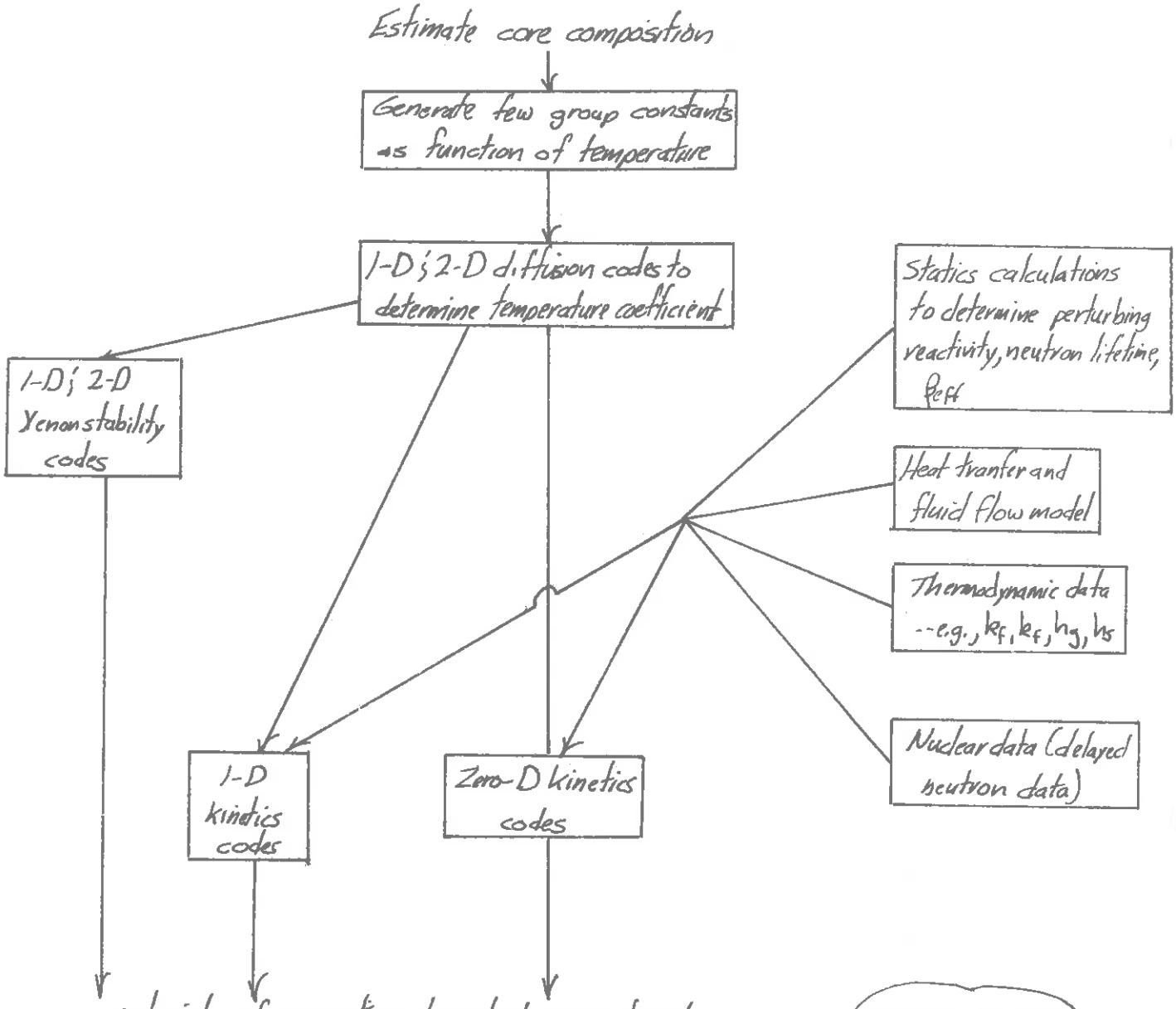

Figure II-6: Kinetics Calculations

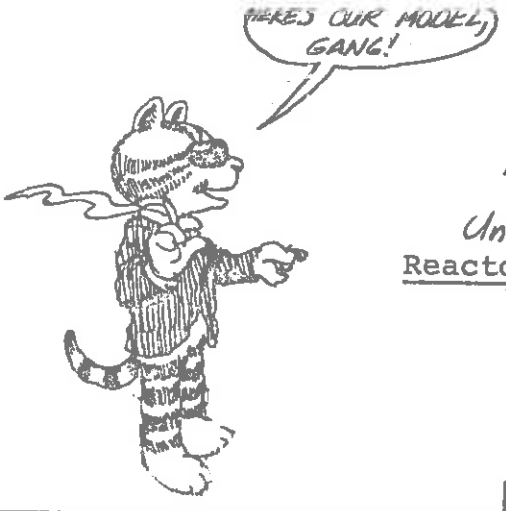

Figure II-7

University of Michigan
Reactor Calculational Model

Uses P-1 or B-1 treatment of angle, exact treatment of hydrogen, and either age theory or Goertzel-Grueling treatment for A > 1 (similar to MUFT)

Includes heterogeneous effects on resonances

SLØDØG: 1-D, modified 1-group diffusion code (neglects thermal leakage)

Calculates slab or cylinder geometry

Handles up to 10 regions

Determines k_{eff}, flux, and power profiles

Analyses outer (source) interactions (uses non-iterative Gaussian elimination to avoid inner iterations)

ØNE: 1-D, 1 to 10 group diffusion code

Calculates slab, cylinder, or sphere

criticality options include k_{eff}, transverse buckling search, poison search, or subcritical assembly with external source

Calculates adjoint equations

Calculates flux, adjoint flux, and power

Handles 25 regions (9 different zones)

MITH: Single-channel thermal hydraulic code

Calculates both average and hot channel for LWR

Gives temperature, densities, and DNBR

IV. RELATION OF DESIGN CALCULATIONS TO CORE PHYSICS MEASUREMENTS

A. Overview

It is extremely important to check the calculational model against experiments, since not only have numerous approximations been introduced in performing the design calculations, but as well even the

necessary input data (i.e., microscopic cross sections) have limited accuracy. There are a variety of such experiments which can provide "integral data" useful for checking or even renormalizing computer code models"

(i) Zero-power experiments: These are initially performed on a simplified mockup of the new design (although in more standard designs, the actual plant core may be used). Typically one can either perform so-called exponential experiments in which $k_{eff} < 1$ and a source is inserted to maintain a neutron flux, or a critical experiment in which the core loading is adjusted until $k_{eff} = 1$.

(ii) Measurements performed at power: flux and power profiles, temperature and power defects, control rod and chemical shim worth

(iii) Dynamic reactor measurements, rod drop, rod oscillator, and pulsed neutron measurements, transfer function measurements, reactor noise studies.

NOTE: Additional material will be added

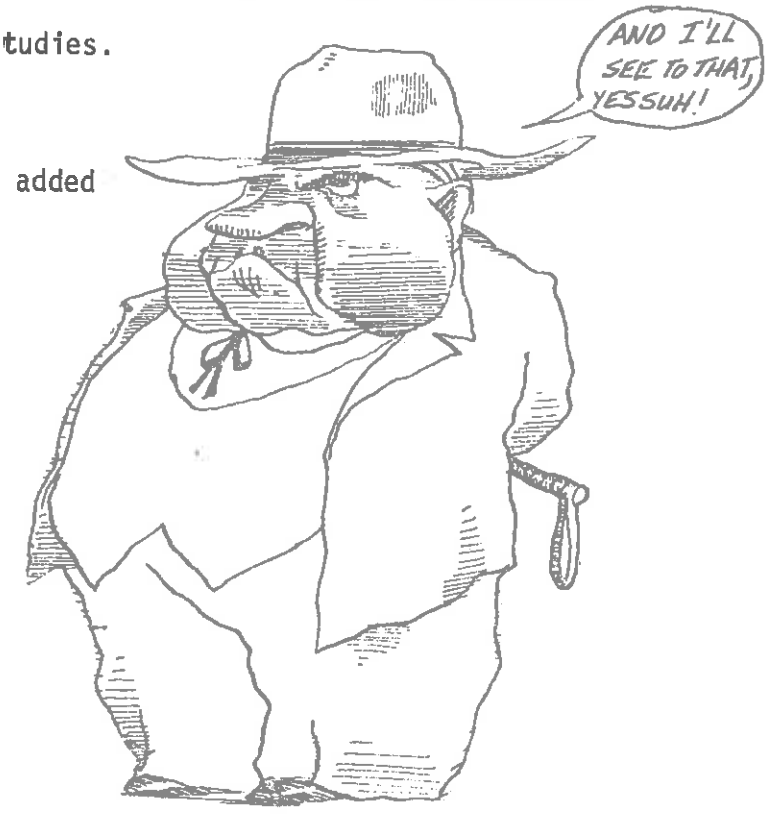

CHAPTER 12: THERMAL ANALYSIS OF NUCLEAR REACTOR CORES

I. INTRODUCTION

A. The Relationship of Thermal Core Analysis to Nuclear Design

A nuclear power reactor is designed to produce heat which can then be used to produce electrical energy, usually by way of an associated steam thermal cycle in which the reactor heat is used to produce high pressure, high temperature steam which can then be used to drive turbo-generators. Once we have acknowledged the fact that the primary function of the reactor core is really just that of a rather exotic heat source, then it becomes apparent that the thermal analysis of this core must play a very important role in its design. Indeed, the design of a reactor core depends as much on thermal as nuclear considerations. There is really no limit to the quantity of heat that a nuclear reactor is capable of generating, so long as sufficient cooling is provided to keep the temperatures of the core elements within safe limits. Hence the power level of a given reactor design is limited by thermal rather than nuclear considerations.

Furthermore, the neutronic analysis of the reactor core is rather intimately related to its thermal analysis, since we have seen that nuclear cross sections which influence core reactivity depend sensitively upon temperature. On the other hand, since the fission heat generated in the core is proportional to the neutron flux, the temperature distribution in the core will depend sensitively upon its neutronic behavior.

Thermal considerations also dominate the safety analysis of the reactor design. Indeed, one of the most critical aspects of modern power reactor designs is that of providing backup cooling systems which can continue to remove heat from the reactor core should the primary coolant system fail.

A nuclear designer will frequently require information concerning the thermal behavior of the reactor core. Hence he must either be prepared to interface with the mechanical engineers responsible for thermal core analysis, or he must be prepared to undertake this analysis himself.

For these reasons, we have felt it advisable to include a rather brief overview of thermal core analysis in this text. Our intent is not to provide a complete development of this topic, but rather to indicate those areas in which thermal analysis will interact with nuclear design and hence drift into the domain of nuclear engineering.

Our presentation will essentially follow the path traced out by thermal energy in the reactor, from its origin as fission heat energy in the fuel until it is finally removed from the reactor core by the coolant. The thermal transport path is sketched below:

fission product energy in fuel → conduction through fuel → transfer across fuel-clad gas gap ↓ conduction across clad → transfer from clad surface to coolant → forced convection in coolant out of core ↓ steam generator → turbine → condensor

As we will see later, the energy released by the nuclear fission reactions appears primarily as kinetic energy of the various fission reaction products.

The bulk of this fission product energy is rapidly deposited as heat in the fuel material very close to the location of the fission event. This heat is then transported via thermal conduction across the fuel element, across the gap separating the fuel from the clad, and then across the clad to the clad surface. It is then transferred from the clad surface to the coolant by forced convection. The mass motion of the coolant then carries the thermal energy up and out of the reactor core, either as sensible heat (i.e., coolant temperature rise) or latent heat (i.e., thermally induced phase change--boiling).

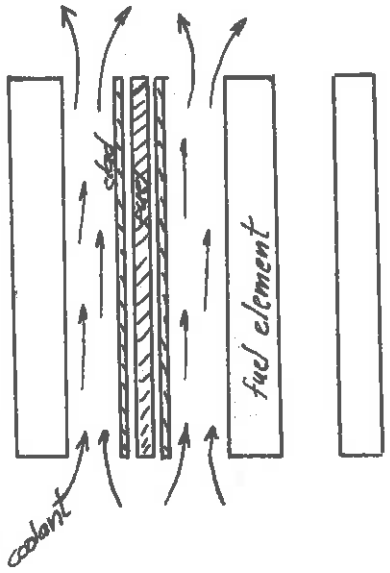

At this point, the nuclear core designer can jump off, although the power plant engineer must continue to follow the heat energy as it is used to convert feedwater into steam, then as the steam is used to drive a turbo-generator, and then finally recondensed into feedwater.

Before we dive into the analysis of various aspects of this thermal path, it is of interest to give several illustrations of just how thermal core behavior can limit reactor core design.

B. Examples of Thermal Limitations on Core Performance

1. Centerline Fuel Melting

We will see later that one of the principal limitations on allowable power densities in a nuclear reactor core arises from the desire to prevent the fuel centerline temperature at any point in the core from

exceeding its melting point. For ceramic fuels, the fuel melting temperature is quite high, e.g., 5000°F for UO_2. Nevertheless, the present power densities of modern power reactors are such that the maximum temperature occurring in the core can approach this limit. Since the power level of the reactor is not really limited by nuclear considerations, we find that in fact such temperature limitations will determine the maximum permissible power generated by the reactor.

2. Cladding Failure

Although the cladding in a nuclear reactor core will rarely experience temperatures approaching its melting point (unless so-called critical heat flux or burnout conditions are exceeded), the clad thermal behavior does place limitations on the core power density. The clad serves as a containment barrier to prevent radioactive fission products produced in the fuel from being released into the coolant (and subsequently being swept out of the reactor core). The cladding is subjected to rather severe stresses, both from the high pressure coolant surrounding the fuel element, as well as by fission gas pressure and fuel swelling inside the fuel element. Furthermore, it is subjected to high thermal stresses due to the enormous thermal gradients across the clad thickness. Since clad strength is a sensitive function of temperature and thermal history, one must limit this temperature in order to prevent clad failure. We will find later that a more critical limitation is placed upon the heat flux which can be transferred from the clad to the coolant, since above certain heat flux magnitudes, the heat transfer to the coolant becomes unstable, and the clad temperature rises dramatically leading to clad failure. This limitation, known as the critical or DNB heat flux, will be studied in some detail in Section 12-5.

3. Reactivity Void Coefficients

We have seen that the core multiplication depends sensitively upon the coolant density. For example, in á LWR, the coolant serves as a moderator. Decreasing the coolant density will reduce moderation and hence reactivity. By way of contrast, in a LMFBR, decreasing coolant density will cause a hardening of the neutron energy spectrum and hence enhance reactivity. Since the coolant density depends sensitively upon temperature, there is a very strong coupling between the thermal and nuclear behavior of a reactor. It is essential to account for such coupling, both in static reactor design as well as in reactor stability studies. Indeed, stability considerations will frequently place restrictions on the allowable temperatures or heat fluxes achieved in the core.

B. Objectives and Limitations of Thermal Reactor Design

Perhaps the three most obvious objectives in thermal core design are those of achieving:

(i) high core power density (Since this will minimize the required core size and hence the size of related equipment such as pressure vessels.)

(ii) high fuel specific power (This will minimize the fuel inventory.)

(iii) high coolant outlet temperature (This will lead to higher thermodynamic efficiency, as well as to the production of higher quality steam.)

Unfortunately, one's ability to achieve these objectives is restricted by a number of limitations imposed by the thermal behavior of the core. Such thermal limitations include:

1. Fuel Temperature Limitations

As we mentioned earlier, one designs a reactor core such that at no point does the fuel temperature exceed its melting point. The melting point for ceramic fuels such as UO_2 or UC are quite high, ranging as high as 5000°F. [In metallic fuels, one is more concerned about holding fuel temperatures below those points at which metallic phase changes in the fuel occur. For example, in uranium metal, there is a phase change at T = 1080°F.] These temperature limits are sensitive to irradiation fluences, and tend to decrease with increasing fuel exposure.

It should be mentioned that nothing really catastrophic will happen if an isolated fuel element experiences temperatures above its melting point. However, experience has indicated that the probability of fuel failure is much higher for those elements in which partial melting has occurred. Hence there is strong motivation to limit temperatures throughout the core below the fuel melting point.

We will find later that the maximum temperature achieved in the fuel is relatively insensitive to the diameter of the fuel rod and depends primarily upon the thermal conductivity of the fuel and the linear power density in the core. Therefore, one usually expresses the thermal limits imposed by fuel melting in terms of a limitation on the maximum achievable linear power density in the core. For example, in a modern PWR, this limitation is about 20 kw/ft. Present power reactors of this type are usually designed to operate with a maximum linear power density of 16-17 kw/ft.

2. Clad Thermal Limitations

The cladding material serves to separate the fuel from the coolant, thereby entraining fission products in the fuel and providing structural

strength to the fuel assembly. But as the clad temperature increases, its strength decreases and its susceptibility to corrosion is enhanced. One must insure that the clad temperature does not exceed those limits above which an appreciable probability of clad failure exists. One manner in which these temperature limits may be exceeded will occur if the heat flux transferred across the clad exceeds the critical heat flux at which burnout occurs, for then the clad temperature will immediately rise several hundred degrees, almost certainly leading to clad failure.

3. Coolant Temperature Limitations

In many reactor types, one wishes to limit the coolant temperature in order to achieve suitable coolant characteristics. For example, in a PWR, one desires to keep the bulk coolant temperature below its saturation temperature so that no bulk boiling occurs. Similarly, in a LMFBR there is motivation to keep the sodium temperature sufficiently low that the heat transfer capability of the coolant is maximized.

There are also limitations on the allowable temperature rise of the coolant as is passes through the core. On the one hand, one would like this temperature rise to be large enough so that one can achieve efficient heat transfer in the steam generator. But there is also strong motivation to minimize this temperature rise in order to lessen thermal shocks in the reactor core (such as during scram conditions). The temperature rise in water moderated reactors is kept quite small--for example, in a PWR, the coolant typically rises from an entrance temperature of 560°F to a exit temperature of 600°F--a temperature increase of only 40°F. In an LMFBR, this temperature rise is somewhat larger, amounting to some 300 °F while in a HTGR, the helium temperature rises by as much as 1200°F, as shown in the table below:

Coolant	T_{in} [°F]	ΔT [°F]	pressure [psia]
water	560	40	1000-2200
sodium	700	250	15
helium	600	1800	1000

It should be noted that while such temperature limitations set upper limits upon the temperatures achieved in the core, there are also lower limits set upon the inlet coolant temperature due to the available condensor cooling. The size of a reactor core will be determined primarily by the amount of heat transfer area necessary to transfer the desired thermal power utilizing the given temperature differences.

It is apparent that the first goal in thermal analysis is to determine for a given fission power distribution and coolant inlet condition the temperature distribution throughout the core, since one must insure that the maximum temperatures achieved in the core do not exceed any of the thermal limitations. It should be kept in mind that the fission power density is highly nonuniform. Hence the temperature distribution is similarly nonuniform--and, indeed, will depend upon time, since the fission power distribution will change over core life as the fuel burns nonuniformly. The usual procedure is to estimate the set of local operating conditions which represent the most extreme case, e.g., highest temperatures, and then to design the core so as to guarantee satisfactory

performance for this "hot spot", although it should be recognized that this may in fact yield an overconservative design.

The thermal analysis begins by determining the volumetric source of fission heat throughout the core. Since this is proportional to the fission rate density, one requires an initial estimate of the neutron flux distribution in the core. For the purpose of most thermal analysis, it is assumed that this fission heat source is confined to the fuel elements.

Since in the steady state this fission heat energy must be removed by the coolant, one can use a simple energy balance to calculate the coolant temperature as it passes up through the core using the inlet coolant temperature (presumed known). Then one can work backwards to determine the temperature rise across the clad, gap, and fuel element to the fuel centerline using the equations of thermal conduction (Fourier's law) and forced convection (Newton's law of cooling). In simple analyses, one performs such a calculation only for an average coolant channel and a hot coolant channel which is chosen to represent the worst possible case. In more realistic analyses, one must also take into account flow conditions and the intermixing of flow between coolant channels.

In this chapter we will sketch the basic concepts and procedures involved in the thermal analysis of a nuclear reactor core. Although we will usually try to relate these concepts and methods to well-known laws, we will give very few derivations. We do not intend this chapter to be a thorough development of heat transfer and fluid flow, but rather a brief description of how standard concepts from these disciplines are applied to nuclear reactor analysis. We have attempted to include sufficient explanation and discussion of these methods to allow the reader with

only rudimentary exposure to heat transfer and fluid flow to still benefit from the chapter. For more detailed treatments of many of these topics, we must refer the reader to one of several standard references.*

II. POWER GENERATION IN NUCLEAR REACTOR CORES

A. Fission Energy Deposition

The energy released in a nuclear fission reaction is distributed among a variety of reaction products. We have classified these reaction products both as to range and time of emission, and indicated the approximate percentage of the fission energy (some 200 MeV) carried by each:

Reaction Product	% energy	range	time delay
kinetic energy of fission fragments	80%	< .01 cm	instantaneous
fast neutrons	3%	10-100 cm	"
fission gamma energy	4%	100 cm	"
fission product decay	4%	short	delayed
neutrinos	5%	nonrecoverable	"
nonfission reactions due to neutron capture	4%	100 cm	

---

*Kreith

Bird, Stewart, and Lightfoot

El-Wakil

Tong and Weisman

Graves

The majority of the fission energy appears as the kinetic energy of the fission fragments, and is deposited essentially at the point of fission in the fuel. Note, however, that some of the fission energy appears as kinetic energy of neutrons (3%) and gammas (4%) which have relatively long ranges. This energy will be distributed over the core and adjacent material (shield, blanket, reflector, etc.).

Furthermore, it should be noted that some 4% of the fission energy appears in the form of heat generated by the decay of radioactive fission products. If the reactor were to be suddenly shut down, this decay heat would continue to be produced and would have to be removed (otherwise the reactor core temperature would rise dramatically, causing fuel element melting and failure). The removal of decay heat is one of the most serious problems in reactor safety studies.

It is customary to use an effective energy release per fission, usually some 192 MeV/fission, in determining the portion of the total energy of fission which is recovered in the primary coolant stream and hence contributes to the thermal power of the reactor. Of this 192 MeV, some 168 MeV appears as fission fragment energy, while 7 MeV appears as beta energy. These short range contributions deposit their energy in the fuel--and indeed, can be assumed to be proportional to the microscopic flux profile in the fuel pellet. If we also take into account the energy deposited in the fuel due to fast neutrons and gammas, we find that some 97% of the recoverable fission energy is deposited in the fuel. The remainder is deposited in the moderator or structural materials by neutrons and gamma radiation, with less than 1% being deposited in shielding due to gamma radiation.

In thermal design, the energy deposition distributed over the coolant and structural materials is usually reassigned to the fuel in order to simplify the thermal analysis of the core. If we then recall that the reaction rate density of fissions is given in terms of the neutron flux $\Phi(\vec{r},t)$ as

$$\text{fission rate} = \Sigma_f(\vec{r},t)\,\Phi(\vec{r},t) \tag{12-1}$$

where $\Sigma_f(\vec{r},t)$ is the one-group fission cross section, then we can multiply by

$$w_f = \text{energy released per fission} = 192 \text{ MeV}$$

to find the volumetric fission heat source in the reactor as

$$q'''(\vec{r},t) = w_f \Sigma_f(\vec{r},t)\,\Phi(\vec{r},t) \quad [\text{MeV/sec-cm}^3] \tag{12-2}$$

$$= 1.548 \times 10^{-8}\, w_f \Sigma_f(\vec{r},t)\,\Phi(\vec{r},t) \quad [\text{BTU/hr-ft}^3] .$$

Of course, since the flux and number density of the fuel vary across the reactor core, there will be a corresponding variation in the fission heat source.*

---

*A word here about notation: we will utilize the more or less conventional notation of mechanical engineers when referring to heat densities in which the number of primes on q indicates the dimensionality of the density. Hence, q"' represents a volumetric heat source; q" represents a heat flux per unit area; while q' represents a linear heat density, i.e., heat generated per unit length.

B. Fission Heat Distributions

The simplest model of fission heat distribution would correspond to a bare, homogeneous core. Then we know that the one-group flux distributions are as given below for several typical geometries:

rectangular parallelpiped:

$$\Phi(\vec{r}) = \Phi_0 \cos\frac{\pi x}{a_x} \cos\frac{\pi y}{a_y} \cos\frac{\pi z}{a_z} \qquad (12\text{-}3)$$

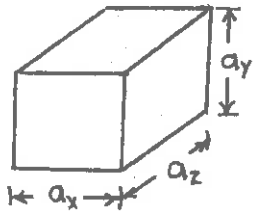

infinite slab:

$$\Phi(x) = \Phi_0 \cos\frac{\pi x}{a} \qquad (12\text{-}4)$$

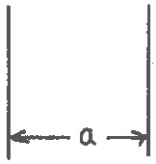

cylinder:

$$\Phi(\vec{r}) = \Phi_0 J_0\left(\frac{2.405r}{R}\right)\cos\frac{\pi z}{H} \qquad (12\text{-}5)$$

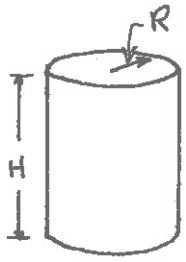

sphere:

$$\Phi(\vec{r}) = \Phi_0 \frac{\sin \pi r/R}{r} \qquad (12\text{-}6)$$

Of course the geometry of most interest will be the cylindrical core, for which we have sketched below the radial and axial flux profiles. We have also indicated the modifications to these profiles resulting from the addition of reflectors (although most thermal power reactor designs are unreflected).

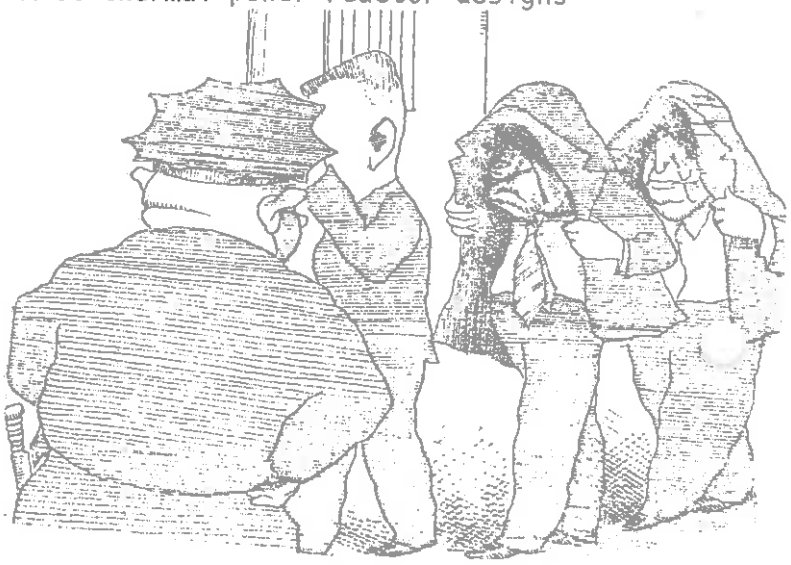

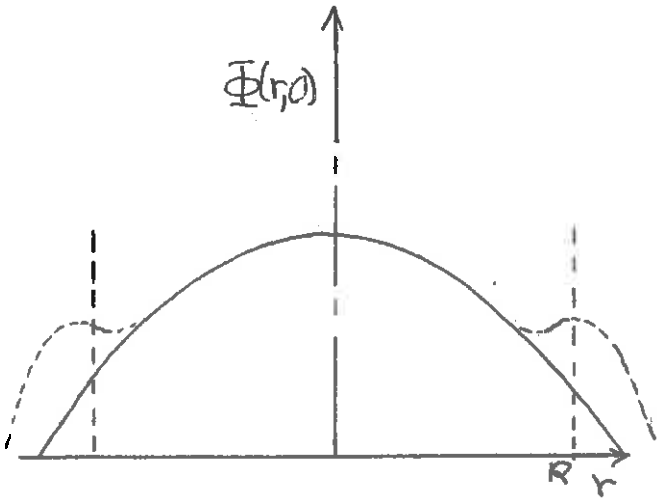

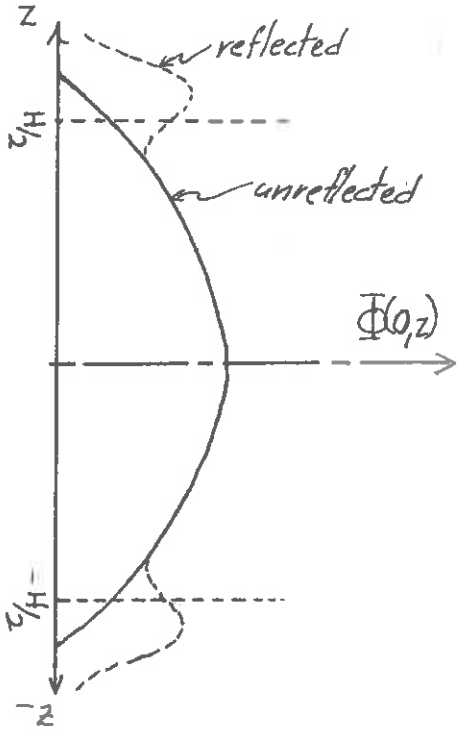

To account for heterogenieties in the core lattice, one can use the gross flux profiles to determine the flux in each of the fuel elements of the core. For example if we assume that this profile is that characterizing a bare cylindrical core

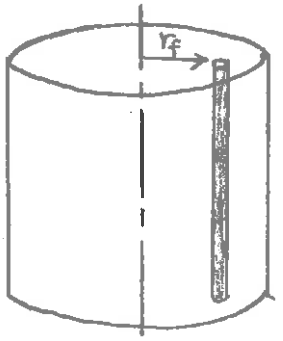

$$\Phi(\vec{r}) = \Phi_0 J_0\left(\frac{2.405r}{R}\right)\cos\frac{\pi z}{H}, \qquad (12\text{-}7)$$

then the flux for a fuel element at a radius r_f is given by

$$\Phi(r_f,z) = \Phi_0 J_0\left(\frac{2.405 r_f}{R}\right)\cos\frac{\pi z}{H} \qquad (12\text{-}8)$$

Usually, the fuel element cross section is so small compared to the core size that we can assume q"'(r) is constant across the width of the fuel rod. We would then take the fission heat source in the rod to be given by

$$q'''(\vec{r}) = w_f \Phi_0 J_0\left(\frac{2.405 r_f}{R}\right) \cos\frac{\pi z}{H} \qquad (12\text{-}9)$$

Notice that while we can usually neglect the radial variations in the fission heat generated in the fuel rod, we cannot ignore the axial variation. In fact, if we remember that there is an appreciable depression of the thermal flux in the fuel rod due to self-shielding, then it is apparent that there may even be situations in which we may want to account for radial variation of the fission heat generated in the rod.

There are numerous other factors which will perturb the power distribution of the reactor core. For example, the reactor is usually not loaded with fuel of uniform enrichment. At the beginning of core life, higher enrichment fuel is usually loaded toward the edge of the core in order to flatten the power distribution. During core operation, the fuel will burn nonuniformly, leading to power nonuniformities which must be accounted for in thermal core analysis. Furthermore, subsequent refueling of the core will not be uniform and will lead to further variation in the power distribution. Typical power profiles for zone and scatter loading are shown in Figures 12-1 and 12-2 .

Control rods will also have a major effect of the axial and radial flux profiles. The effect of flux variation with control rod insertion in PWR's is illustrated in Figures 12-3 and 12-4 . There will also be local peaking of the flux, for instance in water gaps in LWR's or near reflectors. All of these variations in the flux and power distributions

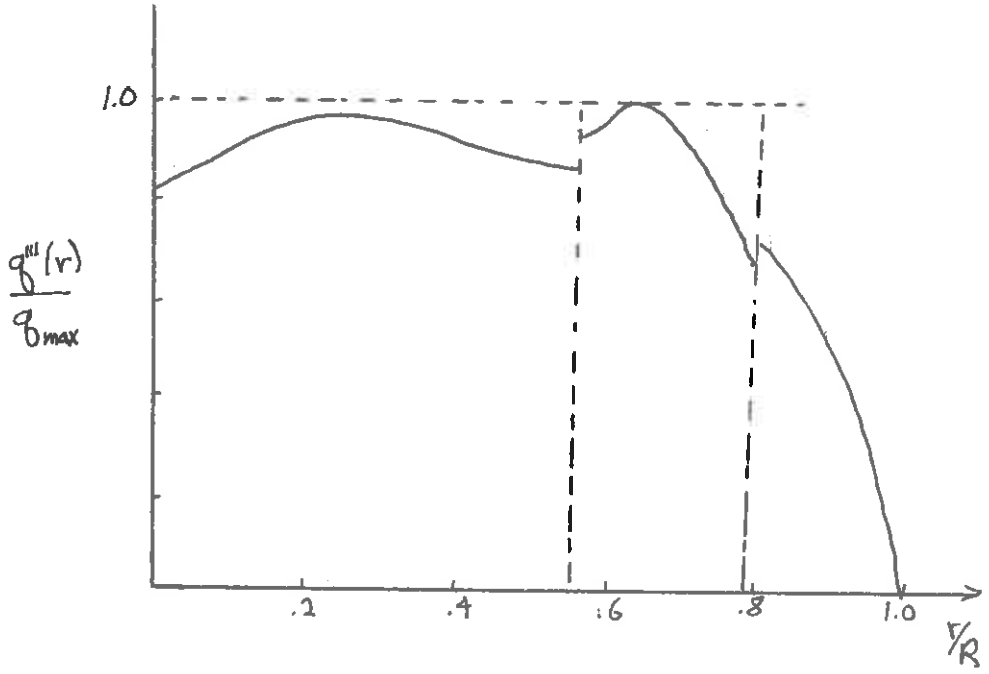

Figure 12-1: Radial Power Profile for Zonal Loaded Core

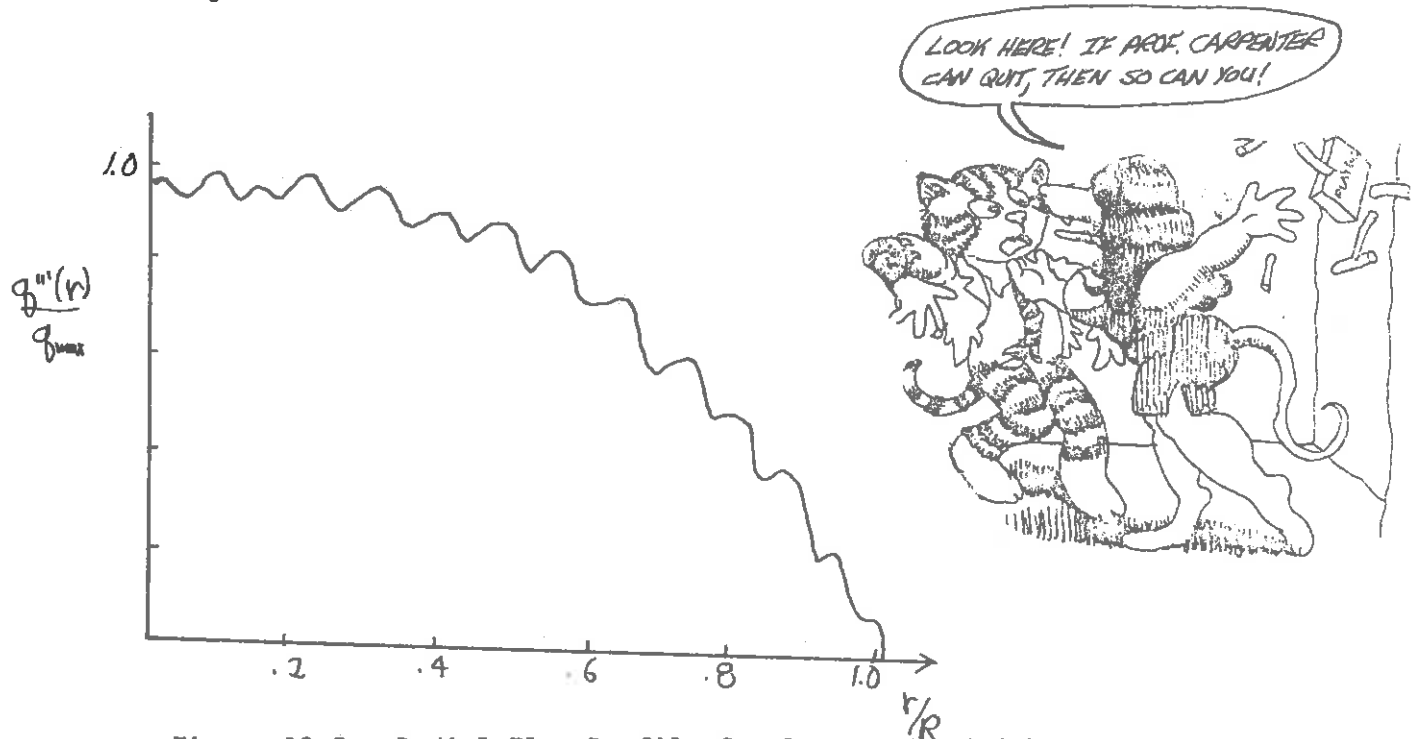

Figure 12-2 Radial Flux Profile for Scatter Loaded Core

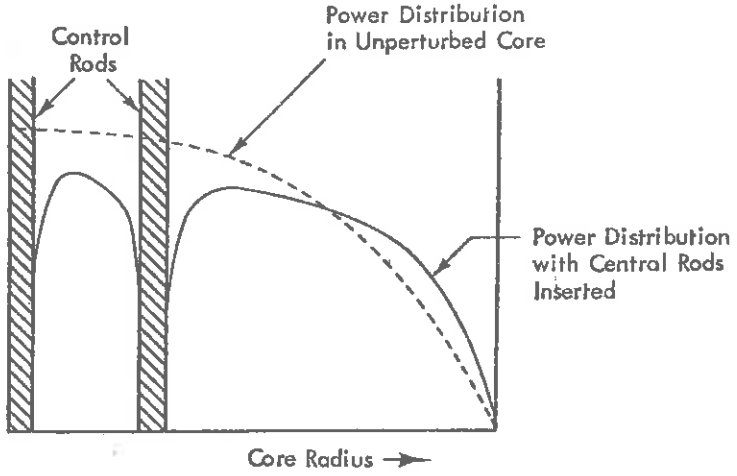

Radial power distribution in a cylindrical reactor with and without control rods.

Figure 12-3

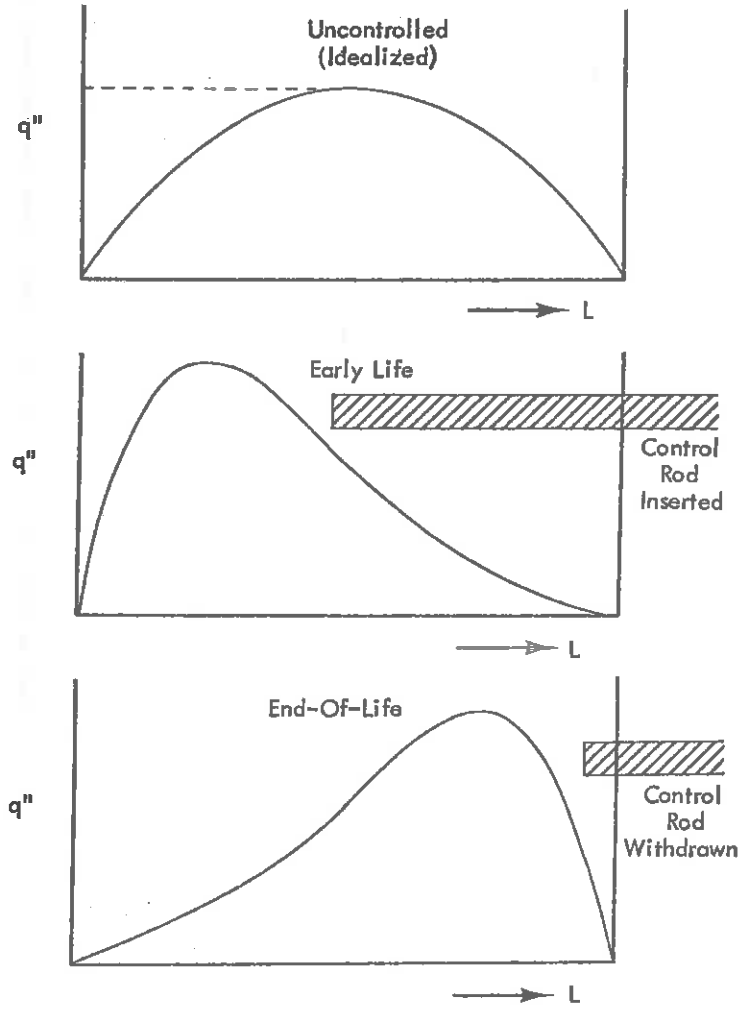

Axial power distribution.

Figure 12-4

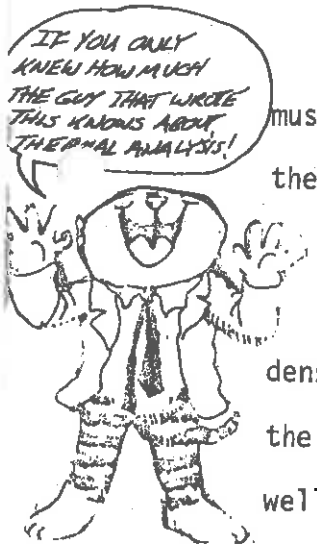

must be predicted by the nuclear engineer and included in a subsequent thermal analysis of the core.

C. Thermal Core Analysis

From the above discussion, it is apparent that the fission power density will vary over the core. Such variations occur not only from the usual flux variations in a bare, homogeneous reactor core, but as well due to the heterogeneous nature of the core, the nonuniformities of fuel burnup and fuel loading, the presence of coolant gaps and control elements, and also small variations due to manufacturing tolerances of core components. These will cause corresponding variations in the temperature distribution in the core. A common technique for accounting for these variations is to estimate a set of local operating conditions for the "worst case" ("worst" in the sense of most closely approaching thermal limitations), and to evaluate the reactor performance for this set of conditions. Associated with such local conditions are so-called "hot channel" factors which relate this extreme case to the average core behavior.

One most commonly defines the hot channel of the core as that coolant channel where the core heat flux and enthalpy rise is a maximum. Conditions in the hot channel are defined by several ratios of local conditions to average conditions, and these ratios are termed the "hot channel factors". We will discuss hot channel factors in more detail in section 12-7; at this time, it is appropriate however, to introduce the hot channel factors which characterize the variations in the fission heat generation in the reactor core. Three such nuclear hot channel factors are usually introduced:

$$\text{Radial nuclear factor} = \frac{\text{mean heat flux in hot channel}}{\text{mean heat flux in average channel}} \equiv F_N^R$$

$$\text{Axial nuclear factor} = \frac{\text{maximum heat flux in hot channel}}{\text{mean heat flux in hot channel}} \equiv F_N^A$$

$$\text{Nuclear heat flux factor} = \frac{\text{maximum heat flux in the core}}{\text{mean heat flux in core}} \equiv F_q^N$$

From these definitions, it is obvious that

$$F_q^N = F_N^R \, F_N^A \tag{12-10}$$

The major results of the nuclear calculations on a core can frequently be relayed to the thermal designer in terms of nuclear hot-channel factors. These factors, together with an estimate of the axial power distribution shape, can serve as the basis for the initial plant thermal design, although there will be later interaction between the thermal and nuclear designs.

Once we are given an axial flux or power distribution and the coolant inlet conditions (e.g., temperature and pressure), we can compute the conditions of the coolant as it passes up the coolant channel through the core of the reactor. Such a calculation involves only a simple energy balance equating the heat flux passing into the coolant from the fuel element to the change in temperature (or, more generally, the enthalpy) of the coolant as it absorbs this heat.

The more difficult analysis concerns the determination of the radial temperature rise from the coolant to the clad surface, then across the clad and the gap to the fuel itself. Such a calculation involves a study

of heat conduction through the fuel element and forced convection heat transfer from the clad surface to the coolant. This analysis is frequently complicated by a phase change of the coolant as it passes up the channel. Finally, we are usually also concerned with the hydrodynamic flow conditions of the coolant, such as the pressure drop along the channel, flow mixing, and other characteristics of the coolant.

We will consider each of these topics in turn, first developing the relations between the temperature drop across the fuel, gap, and clad using the thermal conduction equation; then studying the transfer of heat from the clad surface to the coolant via forced convection considering both single phase and two-phase coolants; and finally giving a brief outline of the hydraulic analysis of the core.

III. RADIAL HEAT CONDUCTION IN REACTOR FUEL ELEMENTS

A. The Equation of Thermal Conduction

Let us first briefly review the transfer of heat in solids via thermal conduction. Consider an arbitrary volume V of surface area S (sound familiar?), each point of which is characterized by a temperature $T(\vec{r},t)$. Suppose that there is a distributed source of heat in the body, say $q'''(\vec{r},t)$. We can quickly arrive at the equation of thermal conduction by performing a simple energy balance for this arbitrary volume V. That is, we equate

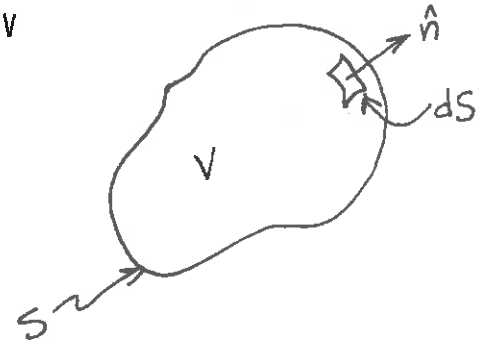

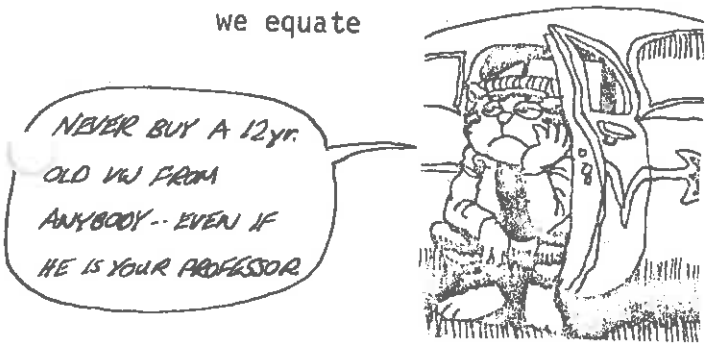

$$\begin{pmatrix}\text{time rate of change}\\ \text{of internal energy}\\ \text{of } V\end{pmatrix} = \begin{pmatrix}\text{rate of}\\ \text{energy addition}\\ \text{due to heat}\\ \text{source}\end{pmatrix} - \begin{pmatrix}\text{rate of energy}\\ \text{loss due to heat}\\ \text{flux through}\\ \text{surface } S\end{pmatrix} \tag{12-11}$$

We can identify a mathematical expression for each of these terms as

$$\frac{\partial}{\partial t}\int_V d^3r\, \rho c T = \int_V d^3r\, q''' - \int_S dS\, \vec{q}''\cdot\hat{n} \tag{12-12}$$

where $\rho(\vec{r},t)$ is the density of the material, c is its specific heat, and $q''(\vec{r},t)$ is the heat flux vector. If we use Gauss' law on the last term

$$\int_S dS\, \vec{q}''\cdot\hat{n} = \int_V d^3r\, \nabla\cdot\vec{q}'', \tag{12-13}$$

we can group all terms under the volume integral, and then use the fact that since the volume we chose to consider was arbitrary, we must require

$$\int_V d^3r \left[\frac{\partial}{\partial t}(\rho c T) - q''' + \nabla\cdot\vec{q}''\right] = 0 \Rightarrow \left[\frac{\partial}{\partial t}(\rho c T) - q''' + \nabla\cdot\vec{q}''\right] = 0 \tag{12-14}$$

Notice that this energy conservation equation was derived in a manner very analogous to that which we used to derive the neutron transport equation. We will now introduce an approximation which is the direct analogue to the diffusion approximation in neutron transport. We will assume that the heat flux is proportional to the gradient of the temperature:

$$\vec{q}''(\vec{r},t) = -k\,\nabla T(\vec{r},t) \qquad (12\text{-}15)$$

This relationship, known as Fourier's law of thermal conduction, is a very good approximation for most materials. [Of course, it is the analogue to Fick's law.] When we substitute it into the energy conservation equation, we arrive at the equation of thermal conduction:

$$\frac{\partial}{\partial t}(\rho c T) - \nabla\cdot k\nabla T = q'''(\vec{r},t) \qquad (12\text{-}16)$$

We need both initial conditions and boundary conditions to complete the mathematical description of heat conduction. These conditions can be derived using similar energy balance ideas, but we will only state them here:

Initial condition: Specify $T(\vec{r},0)$ for all $\vec{r}$

Boundary conditions:

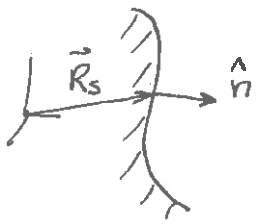

(i) **specify** the surface temperature

$$T(\vec{r},t)\big|_{\vec{R}_s} = f(\vec{R}_s,t)$$

(ii) specify the surface heat flux

$$\vec{q}''\cdot\hat{n}\big|_{\vec{R}_s} = -k\,\hat{n}\cdot\nabla T\big|_{\vec{R}_s} = g(\vec{R}_s,t)$$

(iii) heat transfer boundary condition

$$\vec{q}''\cdot\hat{n}\big|_{\vec{R}_s} = -k\,\hat{n}\cdot\nabla T\big|_{\vec{R}_s} = h\left[T(\vec{R}_s,t) - T_\infty\right]$$

(iv) interface conditions

(a) continuity of temperature

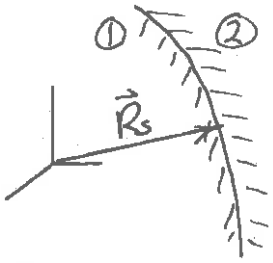

$$T_1(\vec{R}_s) = T_2(\vec{R}_s)$$

(b) continuity of heat flux

$$\hat{n} \cdot \vec{q}''_1 \big|_{\vec{R}_s} = \hat{n} \cdot \vec{q}''_2 \big|_{\vec{R}_s}$$

or

$$k_1 \hat{n} \cdot \nabla T_1 \big|_{\vec{R}_s} = k_2 \hat{n} \cdot \nabla T_2 \big|_{\vec{R}_s}$$

The thermal conductivity k is temperature dependent in most materials. Although this temperature dependence is usually ignored in studying thermal conduction in materials such as the gap or the clad in which a relative small temperature drop occurs, it must be considered in treating thermal conduction through the fuel, since in this case we may have a temperature drop of several thousand degrees.

We will simplify the analysis of thermal conduction by considering only steady state phenomena such that the thermal conduction equation becomes

$$-\nabla \cdot k \nabla T(\vec{r}) = q'''(\vec{r}) \qquad (12\text{-}17)$$

[Transient problems are treated in detail by El-Wakil and Tong & Weisman.]

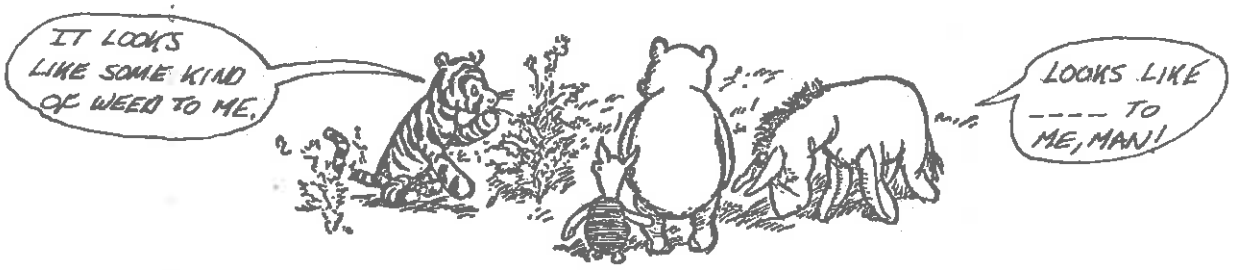

B. Heat Transfer in Cylindrical Fuel Elements

Most modern power reactor cores are composed of cylindrical fuel elements which usually contain ceramic fuel elements contained in metallic tubes (i.e., cladding). Our goal will be to calculate the temperature drop from the centerline of the fuel, where the maximum temperature normally occurs, to the surface of the clad in terms of the various physical properites of the fuel element. For the purposes of this calculation, we can regard the clad surface temperature as a reference temperature, since it will be determined in terms of the coolant temperature and eventually in terms of the coolant inlet conditions and the reactor power level.

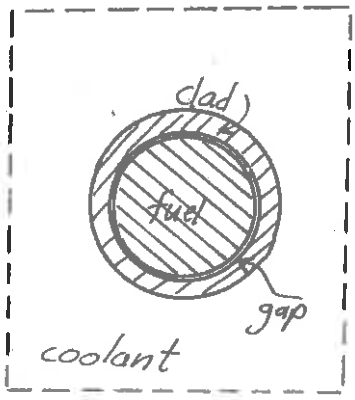

To simplify this calculation, we will make several useful assumptions:

(i) We will assume that we can neglect thermal conduction in the axial direction. This is a valid assumption since the temperature gradient across the fuel element in the radial direction is several orders of magnitude larger than that in the axial direction. Axial heat transfer will occur outside the fuel element via forced convection in the coolant.

(ii) The fission energy will be assumed to appear as a uniform heat source distributed through the fuel. Actually, there is some variation in this heat source since it is proportional to the flux in the fuel, and we have seen in Chapter 10 that there

is an appreciable flux depression in the fuel due to self-shielding effects. However, neglect of this spatial variation is usually adequate for most thermal core analysis.

(iii) Only steady state heat transfer in the core will be considered. We will now consider the radial heat transfer in each region of the reactor fuel element.

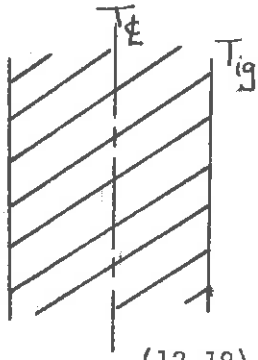

1. Fuel

The heat conduction equation for a cylindrical fuel rod takes the form

$$\frac{1}{r}\frac{d}{dr}\,k_f\,r\frac{dT}{dr} = -q''' \qquad (12\text{-}18)$$

where we have noted the axial symmetry to omit the angular dependence. The corresponding boundary conditions are

(i) $$T(0) = T_\ell$$

(ii) $$\left.\frac{dT}{dr}\right|_{r=0} = 0$$

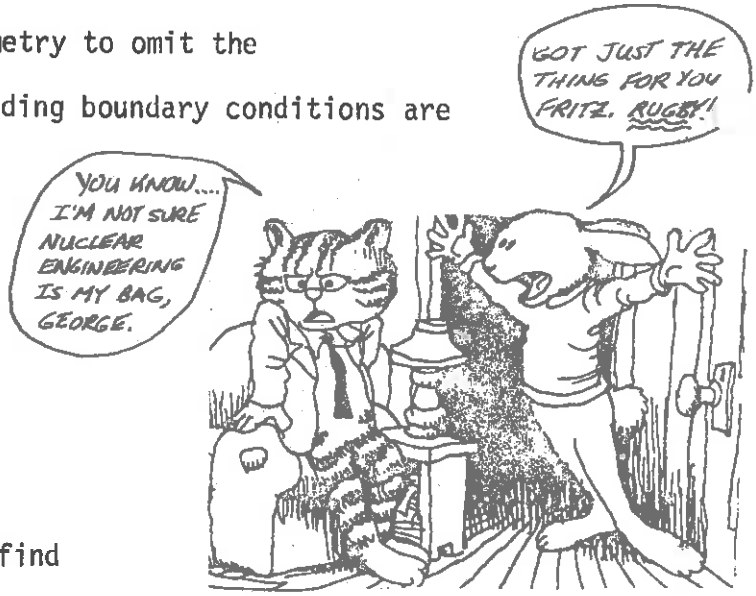

We can integrate this equation to find

$$k_f\,r\frac{dT}{dr} = -\int_0^r dr\,r q''' = -\frac{r^2}{2}q''' \qquad (12\text{-}19)$$

Now recall in general that the thermal conductivity depends upon the fuel temperature, i.e., $k_f(T)$. Hence it is not possible to obtain an explicit

form for T(r) until we have specified the functional dependence of $k_f(T)$. We can derive an expression for the temperature drop across the fuel however. Rewrite (12-19) as

$$k_f dT = -\frac{r}{2} q''' dr \tag{12-20}$$

and integrate this equation between r = 0 and r = R to find

$$\int_{T_\ell}^{T_{ig}} k_f(T)\, dT = -\int_0^R dr\, \frac{r q'''}{2} = -\frac{R^2}{4} q''' \tag{12-21}$$

Now define an average thermal conductivity for the fuel as

$$\overline{k_f} \equiv \frac{1}{T_\ell - T_{ig}} \int_{T_{ig}}^{T_\ell} k_f(T)\, dT \,. \tag{12-22}$$

Hence we can rewrite (12-21) as

$$T_\ell - T_{ig} = \frac{q''' R^2}{4 \overline{k_f}} \tag{12-23}$$

[In the situation where k_f can be assumed constant, one can actually determine the functional form of T(r) by integrating (12-19) directly to find

$$T(r) = T_\ell - \frac{q''' r^2}{4 \overline{k_f}} \tag{12-24}$$

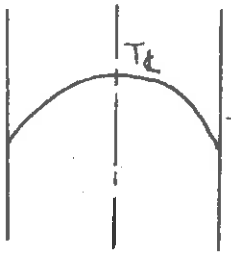

]

Let us define the linear power density of the fuel element as

$$q' \equiv \pi R^2 q''' \tag{12-25}$$

Here, of course q' is the power generated per unit length of the fuel element. In terms of this quantity, the temperature drop across the fuel becomes

$$\Delta T\Big|_{fuel} = T_\ell - T_{ig} = \frac{q'}{4\pi k_f} \tag{12-26}$$

In particular, we should note that the fuel temperature drop is not dependent upon the fuel radius. This temperature drop only depends upon the linear power density q' and the thermal conductivity of the fuel.

The fuel thermal conductivity is usually quite low for ceramics such as UO_2. In Figure 12-5 we have plotted the average thermal conductivity for UO_2. This low thermal conductivity leads to rather large temperature differences across the fuel element. For example, a linear power density of 15 kw/ft in a typical LWR would lead to a temperature difference of 2500°F.

Since the fuel centerline temperature T_ℓ is limited by the fuel melting point, some 5000°F for UO_2, it becomes apparent that one must limit the linear power density in order to avoid fuel centerline melting. For UO_2 fuel elements, the limit on linear power density is roughly 20 kw/ft. Most power reactors operate such that the maximum linear power density is 16-17 kw/ft.

It should also be noted that the fact that the temperature drop does not depend upon the fuel radius suggests that, at least from a

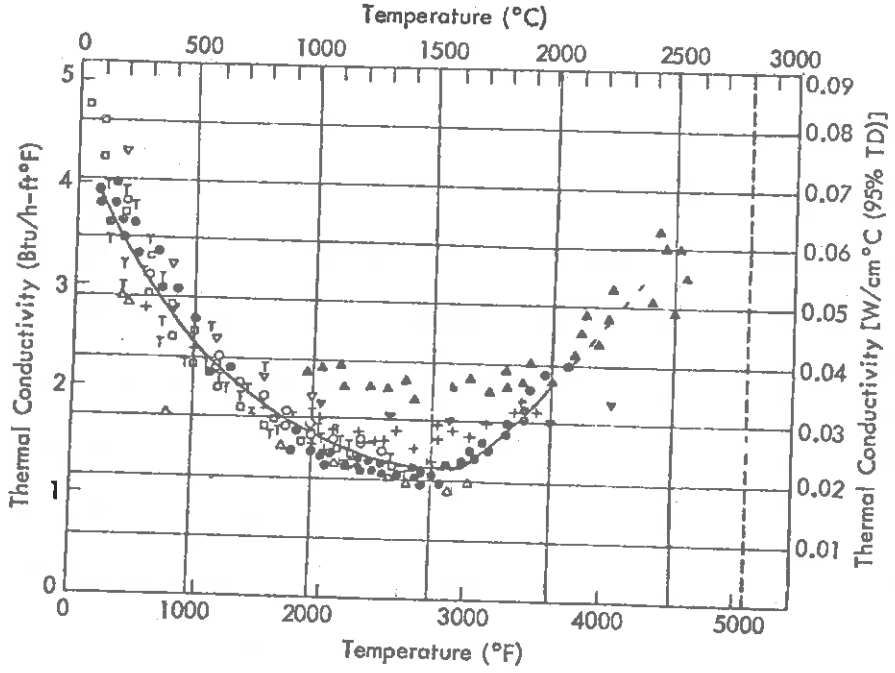

Thermal conductivity of unirradiated UO_2.
Notation ○ Godfrey et al., Ref. 27, 1964.
□ Dayton & Tipton, Battelle Memorial Institute Report BMI-1448, 1960.
▽ Kingery et al., *J. Am. Ceram. Soc.*, **37**, 107, 1954.
T Howard & Galvin, UKAEA IG Report 51, 1960.
⊢ Reiswig, *J. Am. Ceram. Soc.*, **44**, 48, 1961.
● Nishijima, Ref. 31, 1965.
+ Bush et al., *Trans. Am. Nucl. Soc.*, **7**, 392, 1964.
▼ Feith, Ref. 32, 1963.
▲ Feith unpublished data.

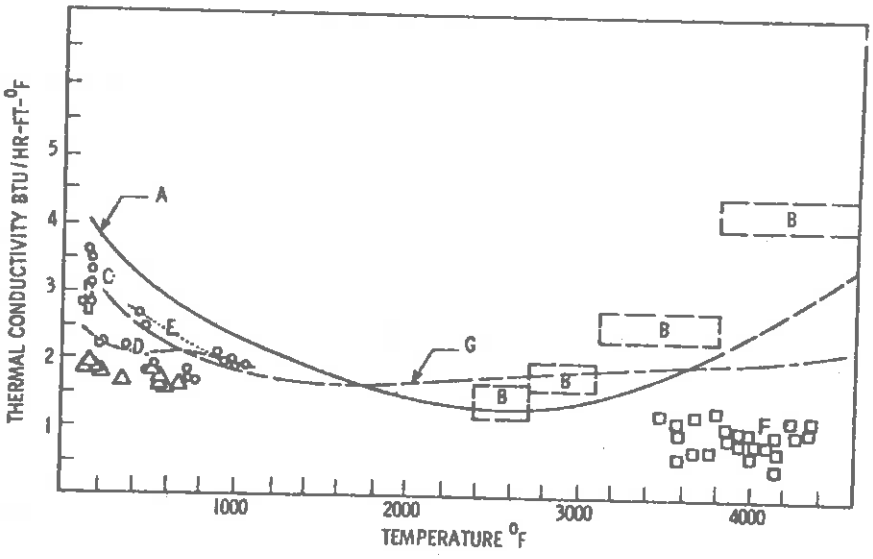

Irradiated UO_2 thermal conductivity and out-of-pile data. (From *Nucl. Eng. Design*, **6**, 301, 1967.)
Notation A. Curve based on unirradiated data
B. Bates, Ref. 30, post-irradiation measurements, 1961.
C. Bain & Robertson, *J. Nucl. Mater.*, **1**, 109, 1959, post-irradiation data.
D. Dayton & Tipton, Battelle Memorial Institute Report BMI-1448 (Rev.), 1960, post-irradiation data, (---- heating; .... cooling).
E. Ibid., 1961 post-irradiation data (△ first cycle heating; ○ second-cycle heating; □ third-cycle cooling).
F. Lyons et al., Ref. 34, 1964 post-irradiation data.
G. Robertson et al., *J. Nucl. Mater.*, **7**, 225, 1962, $\int_0^{2800°C} K dt = 97$ W/cm.

thermal standpoint, one can achieve the same linear power density without exceeding core temperature limitations by using smaller fuel rods. Since the use of smaller rods can reduce fuel inventory, this feature can have an important bearing on the economics of core design.

It is possible to repeat our analysis of the heat transfer in the fuel for the situation in which the flux depression is explicitly accounted for. Such an analysis indicates that the assumption of a uniform heat source q''' actually implies a somewhat larger $\Delta T)_{fuel}$ than that corresponding to a distributed heat source. Therefore our calculations above are somewhat on the conservative side.

2. Gap

The ceramic fuel pellets are encased in a metallic tube or clad. There will be a small clearance or gap between the fuel and the clad several thousands of an inch in thickness which is usually filled with some inert gas such as helium. Although the thickness of the gap is quite small, the rather low thermal conductivities of gases will cause a rather large temperature drop across the gap. If the gap spacing was uniform, then we could simply solve the equation of thermal conduction for the gas in the gap to find the temperature drop across the gap as

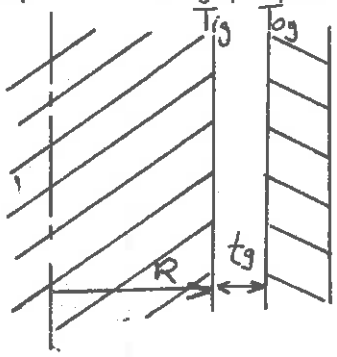

$$\Delta T\Big|_{gap} = T_{ig} - T_{og} = \frac{q'}{2\pi R}\frac{t_g}{k_g} \qquad (12\text{-}27)$$

But after a period of reactor operation, the fuel pellets swell and crack, and will actually come into contact with the clad in many places. For

this reason, one usually expresses the temperature drop across the gap by using an effective coefficient of gap conductance, defined such that

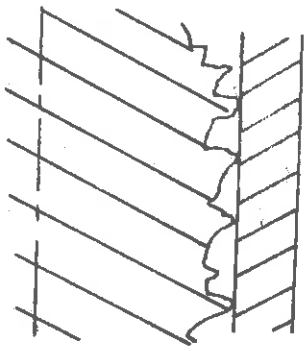

$$q'' = h_g (T_{ig} - T_{og}) . \qquad (12\text{-}28)$$

This coefficient will be a function of gap thickness, gas conductivity, and also of contact pressure, surface roughness, clad material, and fuel life. It typically ranges in value between 1000 to 2000 BTU/ht-ft-°F. Plots of the contact conductance are given in Figure 12-6 . A correlation giving h_g in terms of the contact pressure and the thermal conductivity of the gas is

$$h_g = \alpha_p + k_g / (14.4 \times 10^{-6}) \qquad (12\text{-}29)$$

where $\alpha = 0.60$ for Zr, and $\alpha = 0.48$ for stainless steel. Using this correlation, one can obtain the dependence of gap conductance on linear power density in Figure 12-7 .

If we recognize that the heat flux across the gap in the steady state must be just that amount of heat produced in the fuel divided by the surface area of the fuel

$$q'' = \frac{q''' (\pi R^2 L)}{2\pi RL} = q''' \frac{R}{2} , \qquad (12\text{-}30)$$

then we can calculate the temperature drop across the gap as

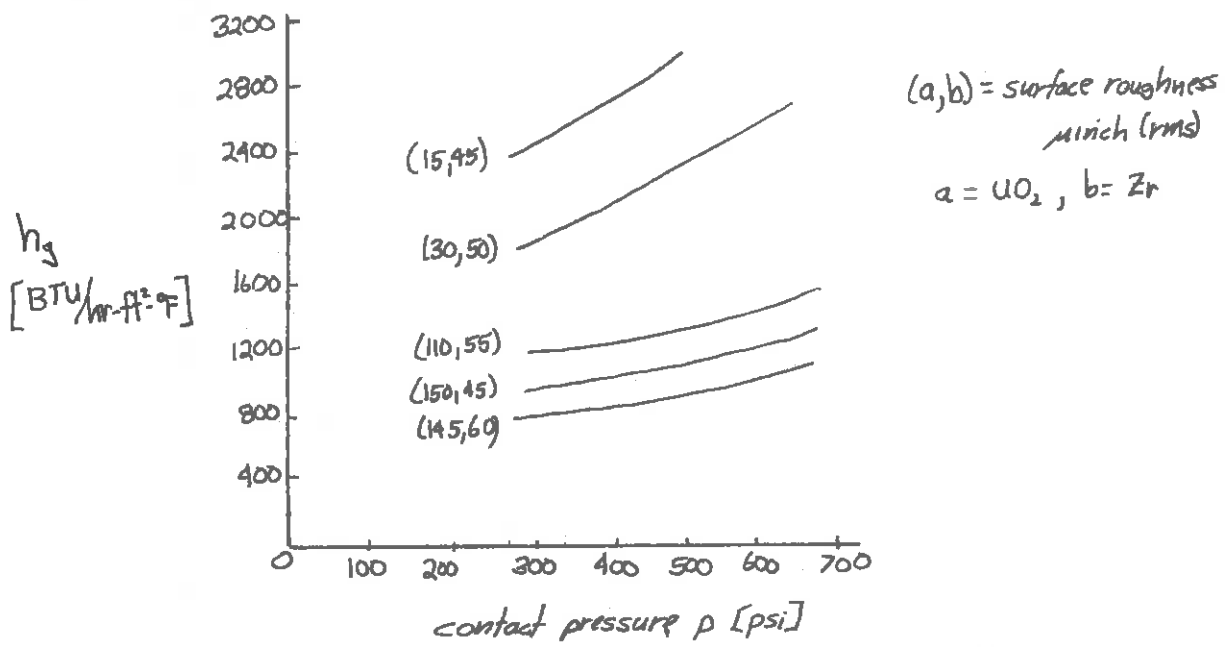

Figure 12-6: Gap heat transfer coefficient

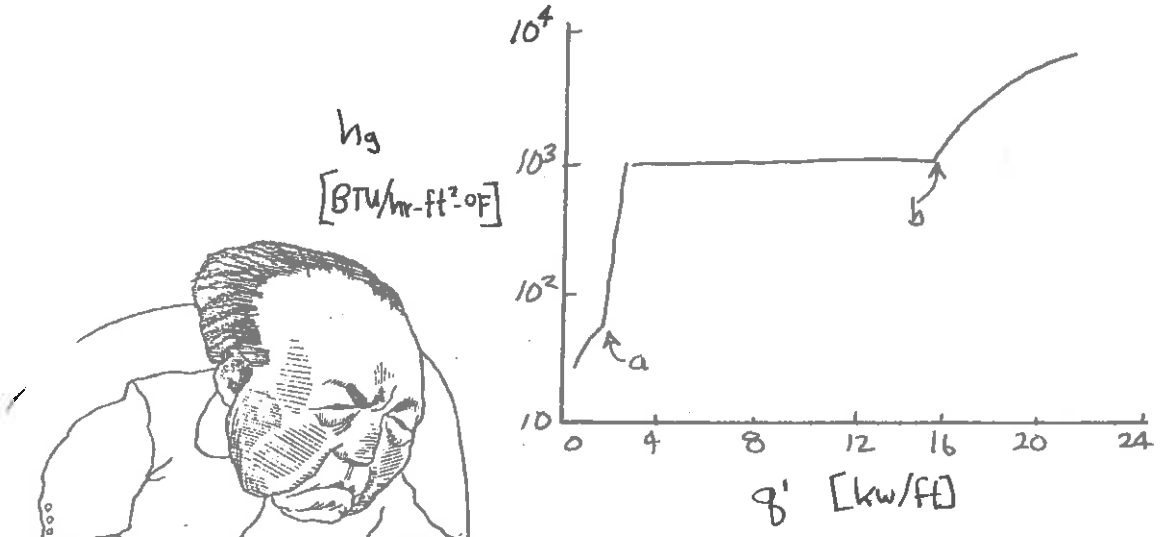

Figure 12-7

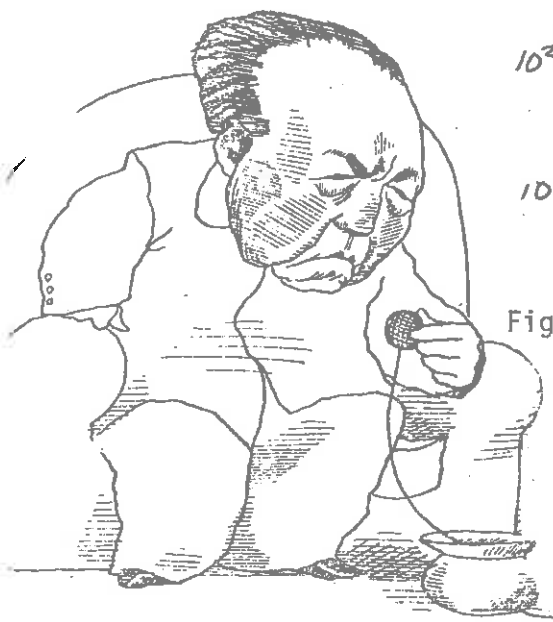

$$\Delta T\Big|_{gap} = \frac{q''' R}{2 h_g} = \frac{q'}{2\pi R h_g} \qquad (12\text{-}31)$$

For a linear power density of 15 kw/ft, this temperature difference can range between 250 to 500°F, depending upon the value chosen for h_g.

3. Clad

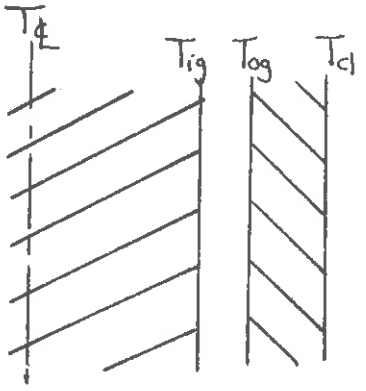

To simplify the analysis of the clad, we will assume that the clad thermal conductivity is essentially constant and that there is no heat production in the clad. Then the thermal conduction equation becomes

$$k_c \frac{1}{r} \frac{d}{dr}\left(r \frac{dT}{dr}\right) = 0 \qquad (12\text{-}30)$$

subject to boundary condition

(i) $T(R) = T_{og}$ $\qquad [R + t_g \sim R]$

(ii) $-k_c \left.\frac{dT}{dr}\right|_R = q''$

We can immediately integrate this equation to find

$$T(r) = T_{og} - \frac{q'''}{k_c} \frac{R^2}{2} \ln \frac{r}{R}$$

or

$$\Delta T|_{clad} = T_{og} - T_{cl} = \frac{q''' R^2}{2k_c} \ln \frac{R+t_c}{R} \qquad (12\text{-}32)$$

where t_c is the clad thickness. In practice, the clad thickness is quite small compared to the fuel rod diameter--usually on the order of 1/20. Hence it is customary to expand the log term to write

$$\Delta T|_{clad} = \frac{Rq'''}{2}\left(t/k_c\right) = \frac{q'}{2\pi R}\left(t/k_c\right) \qquad (12\text{-}33)$$

for the temperature drop across the clad.

4. Clad Surface to Coolant

Heat transfer from the clad surface to the coolant is described by Newton's law of cooling

$$q'' = h_s \left(T_{cl} - T_{fl}\right) \qquad (12\text{-}34)$$

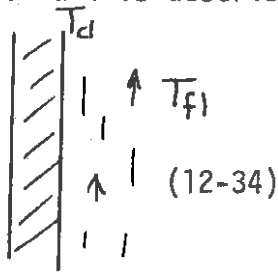

where h_s is the convective heat transfer coefficient. This coefficient will depend upon the properties and flow conditions of the coolant, and its determination will be the subject of the next section of this chapter. For now, however, we will assume that it is known, and proceed to calculate the temperature drop to the coolant using Eq. (12-30) for q'' to find

$$\Delta T|_{cool} = T_{cl} - T_{fl} = \frac{q''}{h_s} = \frac{q''' R}{2h_s} = \frac{q'}{2\pi R h_s} \qquad (12\text{-}35)$$

5. Total Temperature Drop Across the Fuel Element

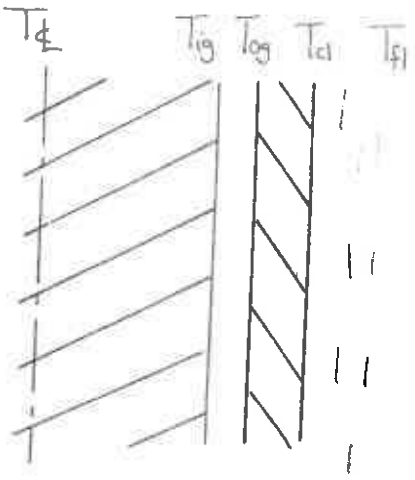

We can now calculate the total temperature drop from the fuel centerline to the coolant as

$$T_\ell - T_{fl} = (T_\ell - T_{ig}) + (T_{ig} - T_{og}) + (T_{og} - T_{cl}) + (T_{cl} - T_{fl})$$

$$= \Delta T|_{fuel} + \Delta T|_{gap} + \Delta T|_{clad} + \Delta T|_{cool} \qquad (12\text{-}36)$$

$$[(3100°) = (2500°) + (500°) + (100°) + (10°)]$$

[For purposes of later reference, we have indicated typical temperature drops for a linear power density of 15 kw/ft.] If we use our earlier expressions for the individual temperature drops, we find

$$T_\ell - T_{fl} = \frac{q'''R}{2}\left[\frac{R}{2k_f} + \frac{1}{h_g} + \frac{t_c}{k_c} + \frac{R}{h_s(R+t_c)}\right] \qquad (12\text{-}37)$$

It is also useful to rewrite this in terms of the linear power density q':

$$T_\ell - T_{fl} = \frac{q'}{2\pi R}\left[\frac{R}{2k_f} + \frac{1}{h_g} + \frac{t_c}{k_c} + \frac{R}{h_s(R+t_c)}\right], \qquad (12\text{-}38)$$

Now, in general, the coolant temperature is essentially fixed by the remaining thermal components of the plant (such as the steam generator and condensor). Furthermore, regardless of where we are along the axis of the core, the coolant temperature varies comparatively little (e.g., in a LWR, the coolant rises from 560 to 600°F, while in a HTGR it rises from 600 to 1800°F). The fuel centerline temperature is constrained to remain below the melting point of the fuel (e.g., 5000°F). Hence the

allowable temperature drop across the fuel element is limited by the fuel melting restrictions; there will be corresponding limits on the allowable linear power density. This maximum allowable linear power density essentially determines the size of the reactor core required for a desired power level.

$$q' = \frac{2\pi (T_\ell - T_{fl})}{\left[\frac{1}{2k_f} + \frac{1}{Rh_g} + \frac{t_c}{k_c R} + \frac{1}{h_s(R+t_c)}\right]} \qquad (12\text{-}37)$$

We can see that there is strong motivation to maximize the heat transfer coefficients h_g, h_s, k_c, and k_f in order to maximize the allowable linear power density and hence minimize the required core size.

In Table 12-2 we have listed typical operating system temperatures for a LWR operating at a linear power density of 17 kw/ft. It should be noted from this table that over 90% of the temperature drop occurs across the fuel and the gap. Hence a small error in the treatment of these regions can swamp out the analysis of the clad and the clad-coolant interface.

Since most of the temperature drop is across the fuel, we can infer that the maximum centerline temperature of fuel elements in a reactor core do not depend appreciably upon the diameter of the fuel elements. This suggests that the selection of the fuel diameter will involve nuclear rather than thermal considerations.

TABLE 12-2

EXAMPLE: $q' = 17$ kw/ft

$T_{fl} = 600°F$

UO_2 = pellet diameter = 0.37"

Zr tube diameter = 0.42"

	T[°F]	ΔT
coolant	600 °	—
clad outer surface	657 °	57 °
clad inner surface	786 °	129 °
pellet surface	1189 °	403 °
fuel centerline	3958 °	2769 °

IV. FORCED CONVECTION HEAT TRANSFER IN SINGLE PHASE COOLANTS

A. Introduction

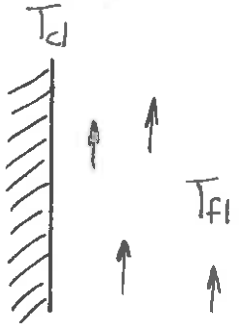

In the preceding section we treated the transfer of heat from the clad surface to the coolant using Newton's law of cooling:

$$q'' = h_s (T_{cl} - T_{fl}) \qquad (12\text{-}40)$$

where h_s is the coefficient of convective heat transfer. The magnitude of h_s varies greatly for different types of coolants and flow conditions. For example

	h_s [BTU/hr-ft^2-°F]
flowing air	2-50
flowing water	100-1000
boiling water	500-5000

We will be concerned here with forced convection--namely, that situation in which heat is transported away from a surface by mass motion of a coolant adjacent to the surface maintained by an externally induced flow (e.g., coolant pumps), as contrasted with natural convection in which the density variation in a temperature gradient induces a flow (e.g., in a swimming pool reactor).

Before we begin a detailed discussion of how the convective heat transfer coefficient h is determined for various coolant and flow conditions characteristic of nuclear power reactors, it is useful to briefly review several useful concepts involving the flow of an incompressible

fluid in a channel--that is, hydraulics. Actually, we will begin our discussion of incompressible fluid flow by first writing down once and for all the full set of equations describing hydrodynamics. We will avoid a discussion of the derivation of these equations (although such a derivation can be given by simply adding liberal doses of vector calculus to the conservation laws governing mass, momentum, and energy), and immediately apply them to the special case of a steady state, incompressible flow. We would hope to comfort the student with no previous exposure to fluid dynamics by admitting that we are not going to do much with the full set of hydrodynamics equations. So just sit back and relax, avoid panicking, and "enjoy" our review as a cultural experience.

B. The Equations of Hydrodynamics

The flow of mass, momentum, and energy in a fluid can be described by the equations of hydrodynamics. These equations are derived in a great many standard references by setting up balance equations expressing the conservation of mass, momentum, and energy for the fluid, much in the same manner in which we derived the equations of neutron transport. We will merely state the equations of hydrodynamics here:

Equation of continuity: (conservation of mass)

$$\frac{\partial \rho}{\partial t} + \nabla \cdot (\rho \vec{u}) = 0 \qquad (12\text{-}41)$$

Equation of motion: (conservation of momentum)

$$\rho \left[\frac{\partial \vec{u}}{\partial t} + (\vec{u} \cdot \nabla) \vec{u} \right] = \vec{f} - \nabla p + \nabla \cdot \overleftrightarrow{\tau} \qquad (12\text{-}42)$$

Equation of energy transport: (conservation of energy)

$$\rho\left[\frac{\partial e}{\partial t} + (\vec{u}\cdot\nabla)e\right] = -\nabla\cdot\vec{q}'' - p\nabla\cdot\vec{u} + \overleftrightarrow{\tau}:\nabla\vec{u} + q''' \qquad (12\text{-}43)$$

Here, the hydrodynamic variables characterizing the fluid are

$\rho(\vec{r},t)$	mass density
$\vec{u}(\vec{r},t)$	local fluid velocity
$e(\vec{r},t)$	internal energy density
$\vec{q}''(\vec{r},t)$	heat flux
$\overleftrightarrow{\tau}(\vec{r},t)$	viscous stress tensor
$p(\vec{r},t)$	pressure
$\vec{f}(\vec{r},t)$	body force density
$q'''(\vec{r},t)$	volumetric source density

These equations must augmented by two transport laws which give the viscous stress tensor and the heat flux in terms of other hydrodynamic variables:

Newton's law:

$$\overleftrightarrow{\tau} = \lambda(\nabla\cdot\vec{u})\overleftrightarrow{I} + \mu\left[\nabla\vec{u} + (\nabla\vec{u})^T\right] \qquad (12\text{-}44)$$

Fourier's law:

$$\vec{q}'' = -k\nabla T \qquad (12\text{-}45)$$

where we have introduced the transport coefficients of bulk and shear viscosity, λ and μ, and the thermal conductivity k. It should be noted that unlike the hydrodynamics equations, the transport equations

are no longer exact relations and must be regarded as approximate laws (although very good approximations for all of the situations we will encounter).*

These five equations must be accompanied by a sixth equation in order to complete the system. This last equation is the equation of state for the fluid which relates the pressure to the density and the fluid temperature

$$p = p(\rho, T) \quad \text{[e.g., for an ideal gas, } p = \rho R\, T] \tag{12-46}$$

In this chapter, we will be concerned with the application of these equations to the study of incompressible fluid flow (i.e., hydraulics with spatially independent transport coefficients. In this case, the hydrodynamics equations reduce to

Continuity:
$$\nabla \cdot \vec{u} = 0 \tag{12-47}$$

Navier-Stokes:
$$\rho\left[\frac{\partial \vec{u}}{\partial t} + (\vec{u}\cdot\nabla)\vec{u}\right] = -\nabla p + \mu \nabla^2 \vec{u} \tag{12-48}$$

Heat conduction & convection:

$$\rho c\left[\frac{\partial T}{\partial t} + (\vec{u}\cdot\nabla)T\right] = k\nabla^2 T + q''' \tag{12-49}$$

Notice that if we set the flow velocity $\vec{u} \equiv 0$, then we return to our earlier form of the thermal conduction equation.

---

*One occasionally defines:

$\nu \equiv \mu/\rho \equiv$ kinematic viscosity

$D_T \equiv k/\rho c \equiv$ thermal diffusivity

C. Incompressible Fluid Flow

Let's begin by studying the "simple" problem of a fluid flowing through a long pipe of uniform cross section. Suppose we imagine an experiment in which a dye is injected into the fluid and is swept along by the flow such that we can follow the streamlines traced out by the motion of the fluid. Then two quite different flow patterns will be observed, depending upon the flow velocity of the fluid.

For low flow velocities, the flow pattern is quite uniform,

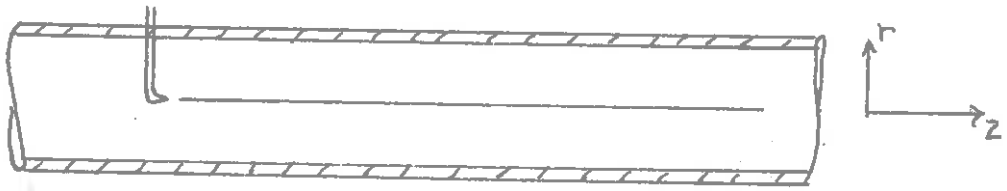

staying parallel to the walls. There is no radial motion of the fluid. We refer to such a situation as "laminar" flow.

For sufficiently high flow velocities, the flow pattern becomes quite irregular. There are fluctuations in the radial fluid velocity

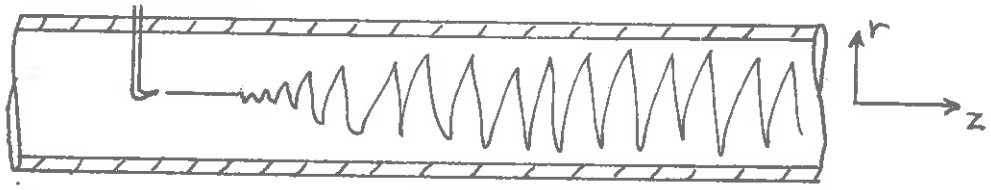

about zero. One can also distinguish "eddy" patterns of the fluid which move back and forth across the tube. Such a situation is known as "turbulent" flow.

The transition from laminar to turbulent flow was found by Reynolds to depend upon the magnitude of the following dimensionless parameter

$$Re \equiv \frac{\rho u D}{\mu} \qquad (12\text{-}50)$$

known appropriately enough as the "Reynold's number" characterizing the flow. Here, u is the flow velocity and D is the diameter of the pipe. The Reynold's number is actually the ratio of the inertial forces present in the fluid to the viscous forces. If we think of viscosity as a mechanism which tends to damp out disturbances in the flow, while inertial forces tend to enhance such disturbances, then we might expect that for sufficiently large flow velocities, the viscosity of the fluid is no longer able to damp out flow fluctuations, and the flow will become unstable. The Reynold's number characterizing this transition from stable, laminar flow to unstable, turbulent flow is usually of the order of 1000 (although it may vary considerably, depending upon the flow characteristics).

The study of turbulent flow is quite complicated. It is now believed that the equations of hydrodynamics contain all of the complexities of turbulent behavior, but nobody has been able to extract these turbulent solution from the equations to date. For this reason, most descriptions of turbulent flow are highly empirical in nature and rely heavily upon experimental measurement.

All fluid flow in reactors is highly turbulent in nature. Hence we will be forced to rely upon an empirical approach to our study of hydraulics in reactor cores. However, to introduce the concepts involved

in analyzing turbulent flow and heat transfer, we will find it useful to first consider several simple problems in laminar flow.

1. Plane Couette Flow

We will begin by considering a fluid contained between two infinite, parallel plates:

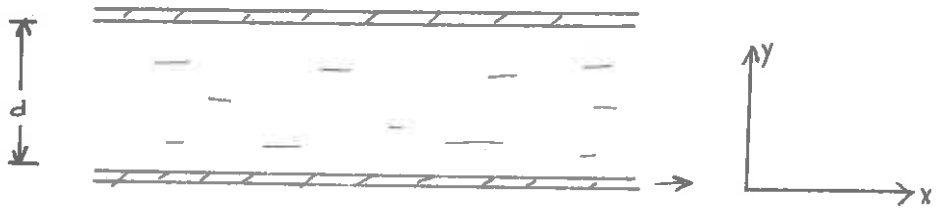

Now suppose at t = 0, the lower plate begins to move with a velocity V. One then finds that the fluid also begins to move (i.e., it tends to "stick" to the plates) in such a way that the fluid velocity "profile" looks as shown below:

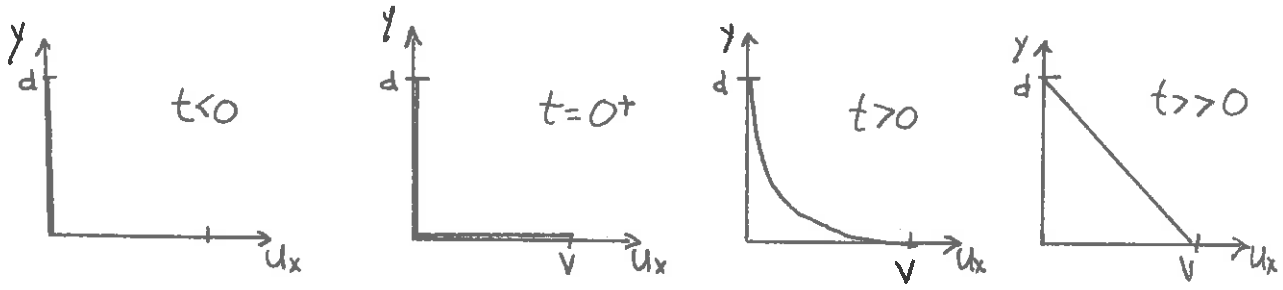

For sufficiently long times, one finds a linear velocity profile $u_x(y)$. Such a profile is also predicted by the steady-state solution of the Navier-Stokes equation:

$$\rho\left[\frac{\partial \vec{u}}{\partial t} + (\vec{u}\cdot\nabla)\vec{u}\right] = \vec{f} - \nabla p + \mu\nabla^2\vec{u} \qquad (12\text{-}51)$$

or

$$0 = \mu \frac{\partial^2 u_x}{\partial y^2} \tag{12-52}$$

We want to solve this equation subject to the boundary condition that the fluid adjacent to the plates is at rest:

$$u_x(d) = 0 \quad \text{and} \quad u_x(0) = V$$

The general solution to Eq. (12-52) is just

$$u_x(y) = ay + b$$

Applying the boundary conditions, we find

$$u_x(0) = b = V, \quad u_x(d) = ad + V = 0 \Rightarrow a = -V/d$$

Hence we find the velocity profile

$$u_x(y) = V\left(1 - y/d\right) \tag{12-53}$$

as we expected. This flow situation is known as "plane Couette flow".

2. Laminar Flow in a Circular Pipe

We will now generalize this situation a bit by considering laminar flow in a long pipe with circular cross section of radius R

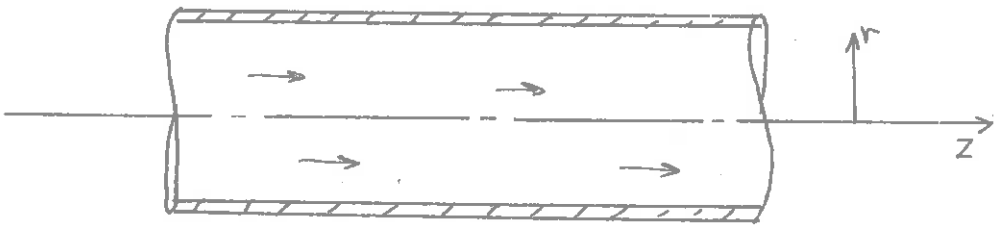

We will once again proceed by applying the Navier-Stokes equation. First, note that the flow velocity for laminar flow can only be in the longitudinal direction

$$\vec{u} = u_z(r)\ \hat{e}_z \tag{12-54}$$

Hence only the z-component of the Navier-Stokes equation remains

$$-\frac{\partial p}{\partial z} + \mu \frac{1}{r}\frac{\partial}{\partial r} r \frac{\partial}{\partial r} u_z(r) = 0 \tag{12-55}$$

Notice that this equation implies that each term in the equation must be equal to a constant, since otherwise a function of z could never be equal to a function of r for all z and r (you might recall that this is the same argument that is used in separation of variables solutions of partial differential equations). Hence we must have

$$\frac{\partial p}{\partial z} = \frac{dp}{dz} = \text{constant} = -\left(\frac{p_2 - p_1}{L}\right) = +\frac{\Delta p}{L} \tag{12-56}$$

where L is the length of the pipe.

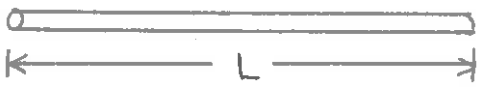

Returning to Eq. (12-55), we find

$$\mu \frac{1}{r}\frac{d}{dr} r \frac{du_z}{dr} = +\frac{\Delta p}{L} \tag{12-57}$$

We must solve this equation subject to the boundary conditions:

(i) $u_z(R) = 0$

(ii) $\left.\frac{du_z}{dr}\right|_0 = 0$

To construct a general solution, we just integrate

$$\frac{d}{dr} r \frac{du_z}{dr} = + \frac{\Delta p}{\mu L} r$$

to find

$$r\frac{du_z}{dr} = + \frac{\Delta p}{\mu L} \frac{r^2}{2} + C_1$$

or integrating once again

$$u_z(r) = + \frac{\Delta p}{\mu L} \frac{r^2}{4} + C_1 \ln r + C_2$$

Now the requirement that $u_z(0) < \infty$ **implies that** we choose $C_1 = 0$.

The boundary condition at r = R implies

$$u_z(R) = 0 \Rightarrow C_2 = \frac{\Delta p}{\mu L} \frac{R^2}{4}$$

Hence our general solution can be written as

$$u_z(r) = \frac{1}{4\mu} \frac{\Delta p}{L} (R^2 - r^2). \qquad (12\text{-}58)$$

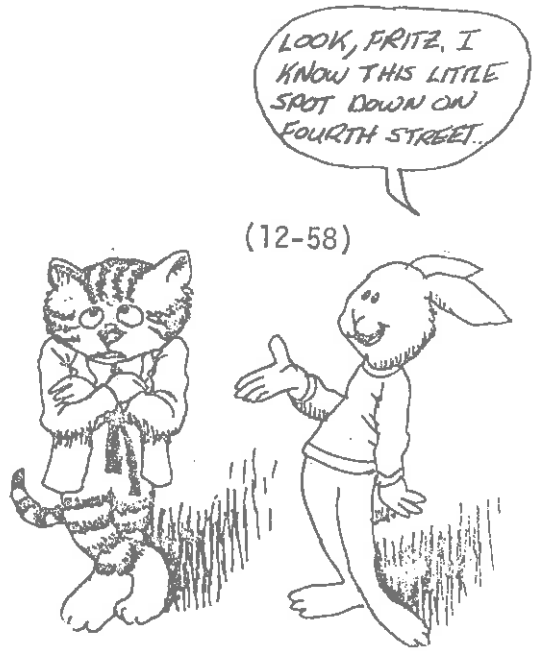

This parabolic flow profile is known as "Hagen-Poiseuille" flow.

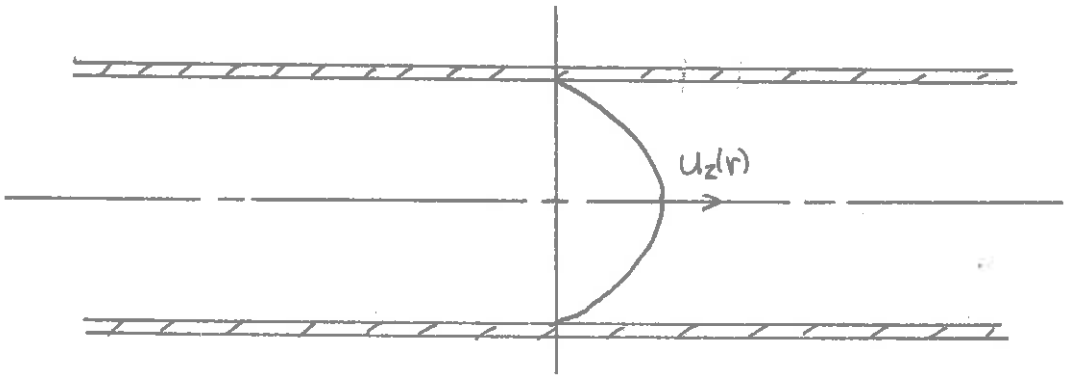

Several useful quantities characterizing such laminar pipe flow are

Maximum flow velocity:

$$u_z|_{max} = \frac{1}{4\mu}\left(\frac{P_1 - P_2}{L}\right)R^2 \tag{12-59}$$

Average flow velocity:

$$\langle u_z \rangle = \frac{1}{\pi R^2}\int_0^R u_z(r)2\pi r dr = \frac{1}{8\mu}\left(\frac{P_1 - P_2}{L}\right)R^2 = \frac{1}{2}u_z|_{max} \tag{12-60}$$

Volumetric flow rate:

$$Q = \pi R^2 \langle u_z \rangle = \frac{\pi}{8\mu}\left(\frac{P_1 - P_2}{L}\right)R^4 \tag{12-61}$$

Force on pipe of length L:

$$F = 2\pi RL\,\tau_{rz}|_{r=R} = 2\pi RL\left(\frac{P_1 - P_2}{2L}\right)R = \pi R^2(P_1 - P_2) \tag{12-62}$$

Pressure drop:

$$\Delta p = P_1 - P_2 = \frac{8\mu LQ}{\pi R^4} \tag{12-63}$$

3. Flow in Non-Circular Channels

Frequently it becomes useful to extend these results to flow in noncircular channels. For this purpose, one replaces D by an "equivalent hydraulic diameter", D_h, defined by

$$D_h = 4\,S/Z \tag{12-64}$$

where S is the flow area and Z is the wetted perimeter of the flow.

EXAMPLE: Consider flow among a number of rods of diameter d. Then one defines the equivalent hydraulic diameter by locating a "unit cell" and calculating S and Z as

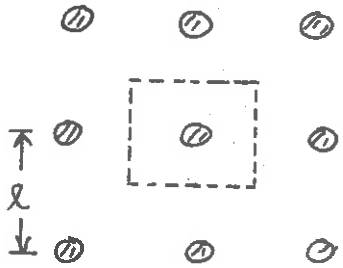

$$S = \ell^2 - \frac{\pi}{4}d^2$$

$$Z = \pi d$$

Hence for this geometry, we find

$$D_h = 4\left(\frac{\ell^2 - \frac{\pi}{4}d^2}{\pi d}\right) \tag{12-65}$$

4. Turbulent Flow

The study of laminar flow is of limited usefulness in reactor applications in which the coolant flow is highly turbulent. One can "fudge" up some of our laminar flow to account for turbulent by defining the Fanning "friction factor f" by

$$\text{friction factor } f = \frac{\text{force on pipe}}{(\text{flow contact area}) \times (\text{kinetic energy density})}$$

$$= \frac{F}{A_c \times K} \tag{12-66}$$

If we substitute in our earlier expressions for F, A_c, and K,, we find

$$f = \frac{\pi R^2 (P_1 - P_2)}{(2\pi RL)(\frac{1}{2}\rho \langle u_z \rangle^2)} \tag{12-67}$$

for a circular pipe. Notice now that if we can determine f for the flow, then we can calculate the pressure drop in the pipe as

$$\Delta p = P_1 - P_2 = 4\left(\frac{L}{D}\right)\frac{1}{2}\rho\langle u_z\rangle^2 f. \tag{12-68}$$

EXAMPLE: For laminar flow, we know that

$$\langle u_z \rangle = \frac{1}{8\mu}\left(\frac{P_1 - P_2}{L}\right)R^2$$

Hence we can calculate

$$f = \frac{P_1 - P_2}{4\left(\frac{L}{D}\right)\frac{1}{2}\rho\langle u_z\rangle^2} = \frac{8\mu}{\rho\langle u_z\rangle R}$$

$$= \frac{16}{\left[\rho\langle u_z\rangle D/\mu\right]} = \frac{16}{Re} \tag{12-69}$$

which is the Fanning friction factor for laminar flow. [Note: One occasionally sees the expression f = 64/Re for laminar flow. This latter parameter is known as the "Darcy-Weisbach" friction factor. Hence, $f_{Fanning} = 1/4\ f_{Darcey\text{-}Weisbach}$.]

In turbulent flow, f is usually measured experimentally as a function of the Reynold's number Re and the pipe roughness. The latter quantity is measured by the ratio of the average fluctuation in pipe diameter over the diameter D:

The friction factor f is plotted vs. Re and k/D in a chart known as the "Moody diagram":

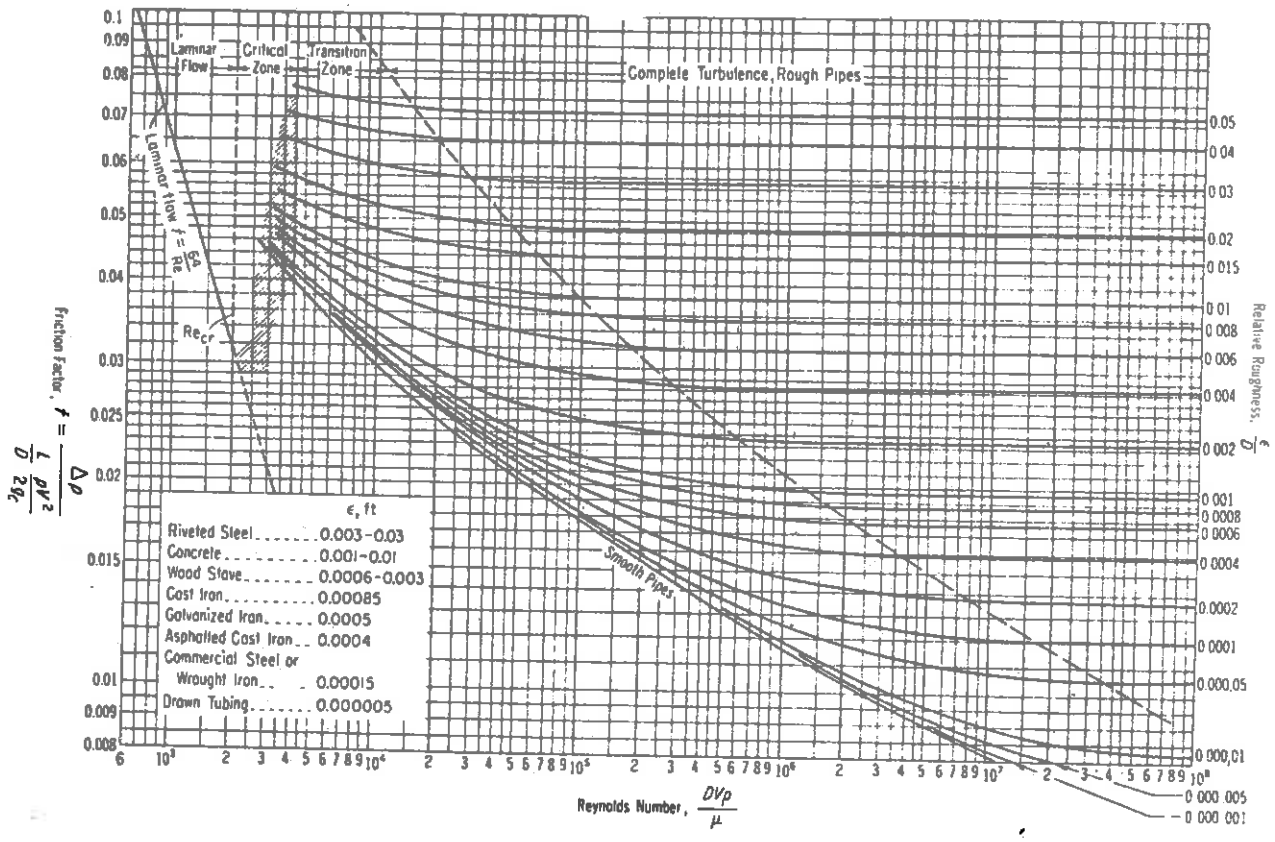

In this diagram, the transition from laminar to turbulent flow occurs at

$$Re^* = 2100$$

Various correlations have been developed for the friction factor. In particular, for turbulent flow in smooth pipes, one customarily uses the "Blasius" formula for single-phase coolant reactor calculations:

$2100 < Re < 10^5$: $\quad f = .0791\, Re^{-0.25}$ (12-70)

An interesting comparison between laminar and turbulent flow can be made by considering the pressure drop in each case. Noting that the mass flow rate W is proportional to the average flow velocity, we find

$$\Delta p \sim \langle u_z \rangle \sim W \qquad \text{laminar}$$

$$\Delta p \sim \langle u_z \rangle^{1.75} \sim W^{1.75} \qquad \text{turbulent} \tag{12-71}$$

Hence there is considerably more pressure drop in turbulent flow. This can be understood by comparing the velocity profiles for the two cases:

laminar: $\dfrac{u_z}{u_z|_{max}} = 1 - \left(\dfrac{r}{R}\right)^2$

turbulent: $\dfrac{u_z}{u_z|_{max}} = \left[1 - \dfrac{r}{R}\right]^{1/7}$

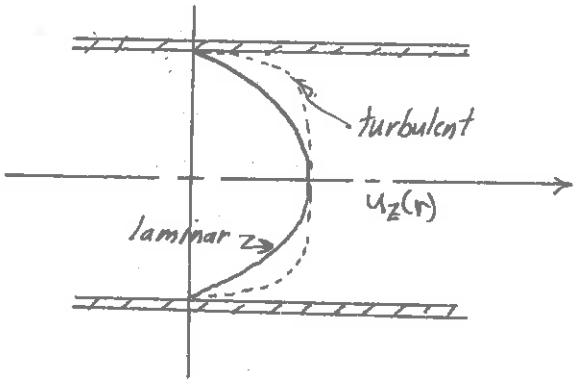

The much steeper velocity gradient near the wall in turbulent flow causes a much larger shear stress on the wall,

$$\tau_{yz} = -\mu \left.\frac{\partial u_z}{\partial r}\right|_{r=R} \tag{12-71}$$

and hence a larger pressure drop.

In summary then, one can use these results to calculate the pressure drop for either laminar or turbulent flow of a fluid in a channel.

EXAMPLE: Water at 1 atm, 70°F

Smooth, circular pipe, 1" I.D.

L = 10 ft

Fully developed turbulence

$\langle u_z \rangle$ = 10 fps

Suppose we want to determine the pressure drop along the pipe, and the pumping power necessary to maintain the flow in this pipe. We first calculate

$$Re = \frac{\rho D \langle u_z \rangle}{\mu} = \frac{(62.3\ lb/ft^3)(1/12\ ft)(10\ ft/sec)}{(.658 \times 10^{-3}\ lb/ft\text{-}sec)}$$

$$= 7.9 \times 10^4 > 2100.$$

which confirms that the flow is indeed turbulent. Using the Blasius formula,

$$f = \frac{.0791}{(7.9 \times 10^4)^{1/4}} = .00471$$

Thus, the pressure drop is

$$\Delta p = 4\left(\frac{L}{D}\right)\frac{1}{2}\rho\langle u_z\rangle^2 f = 4\left(\frac{10}{1/12}\right)\frac{1}{2}\left(62.3\ lb/ft^3\right)\left(100\ ft^2/sec^2\right)(.00471)\frac{1}{32.2\ ft/sec^2}$$

$$= 219\ lb/ft^2 = 1.52\ psi$$

Finally, we calculate the pumping power as

pumping power = force x velocity = $A_c \Delta p \langle u_z \rangle$

$$= 11.2\ \frac{ft\text{-}lb}{sec} = 717\ \frac{ft\text{-}lb}{min} = .0217\ hp = 16.2\ watts$$

D. Forced Convection Heat Transfer

1. Laminar Flow

We have indicated that coolant flow in nuclear reactor cores is highly turbulent. This turbulence tends to greatly enhance heat transfer from the clad surface to the coolant over that which would be present if the flow were laminar. However, the complexity of fluid turbulence once again forces us to rely upon various empirical correlations for calculating quantities such as the convective heat transfer coefficient. However, in order that we may better understand the assumptions that have gone into such correlations, we will first indicate how h may be calculated for various simple laminar flows.

We will first consider the case of heat transfer to an incompressible fluid flowing in a pipe of circular cross section:

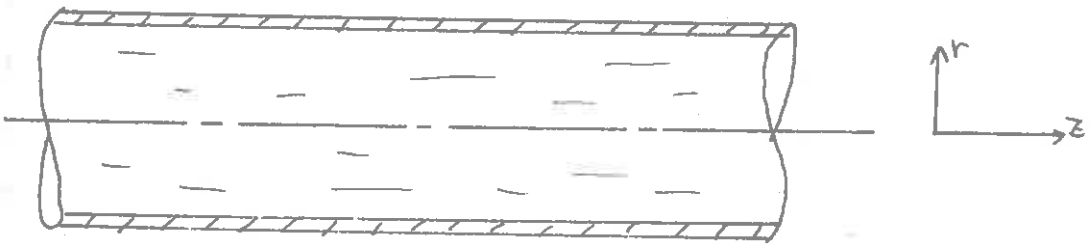

We have already determined that such a flow will be characterized by a parabolic velocity profile

$$u_z(r) = \frac{1}{4\mu}\left(\frac{P_1 - P_2}{L}\right)(R^2 - r^2) = 2\langle u_z\rangle\left(1 - \frac{r^2}{R^2}\right). \qquad (12\text{-}72)$$

We now want to consider the temperature distribution in such a flowing fluid due to heat flow through the walls of the pipe. We begin by recalling the energy equation for such an incompressible fluid:

$$\rho c_p \left[\frac{\partial T}{\partial t} + \vec{u} \cdot \nabla T \right] = k \nabla^2 T + q''' \qquad (12\text{-}73)$$

Now for laminar flow, we note the following simplifications

(i) steady-state flow: $\partial T/\partial t = 0$

(ii) laminar flow: $\vec{u} \cdot \nabla T = u_z \partial T/\partial z$

(iii) no heat sources in the fluid: $q''' \equiv 0$

Hence our energy equation becomes

$$\rho c_p u_z \frac{\partial T}{\partial z} = k \left[\frac{1}{r} \frac{\partial}{\partial r} \left(r \frac{\partial T}{\partial r} \right) + \frac{\partial^2 T}{\partial z^2} \right] \qquad (12\text{-}74)$$

Now usually the axial heat conduction will be much less than the radial heat conduction, since axial heat transfer is primarily by convection. Hence we can simplify (12-74) even further by writing

$$\rho c_p u_z \frac{\partial T}{\partial z} = k \left[\frac{1}{r} \frac{\partial}{\partial r} \left(r \frac{\partial T}{\partial r} \right) \right] \qquad (12\text{-}75)$$

We will now make use of several important assumptions:

(i) constant wall heat flux $q''_{wall} \neq q''_{wall}(z)$

(ii) "fully developed" velocity profile:

$$u_z(r) = 2\langle u_z \rangle \left[1 - \left(\frac{r}{R} \right)^2 \right] \qquad (12\text{-}76)$$

(iii) "fully developed" temperature profile. This latter profile is characterized by a temperature dependence such that

$$\frac{T(r,z) - T_{wall}(z)}{T_{fl}(z) - T_{wall}(z)} = \text{function}(r) \equiv f(r) \tag{12-77}$$

where $T_{wall}(z)$ = wall temperature

$$T_{fl}(z) = \frac{1}{\pi R^2 \langle u_z \rangle} \int_0^R u_z(r)\, T(r,z)\, 2\pi r\, dr$$

= "mixed mean" or "bulk fluid" temperature

Before solving the energy equation subject to these assumptions, let us recall for a moment Newton's law of cooling

$$q_{wall} = h\,(T_{wall} - T_{fl}) \tag{12-78}$$

We will turn this around and use it as a definition in order to calculate h. First note that

$$q_{wall} = -k \left.\frac{\partial T}{\partial r}\right|_{r=R} \tag{12-79}$$

Next, from our definition of a fully developed temperature profile, we can write

$$\left.\frac{\partial T}{\partial r}\right|_{r=R} = (T_{fl} - T_{wall}) \left.\frac{df}{dr}\right|_{r=R} \tag{12-80}$$

If we now combine Eq. (12-78) and Eq. (12-79)

$$h(T_{wall} - T_{fl}) = -k \frac{\partial T}{\partial r}\Big|_{r=R} \tag{12-81}$$

and use Eq. (12-80), we find

$$h(T_{wall} - T_{fl}) = k(T_{wall} - T_{fl}) \frac{df}{dr}\Big|_{r=R} \tag{12-82}$$

Hence we must conclude that

$$h = k \frac{df}{dr}\Big|_{r=R} = \text{constant} \tag{12-82}$$

Thus the convection heat transfer coefficient, h, is a constant along the length of the pipe for a fully developed laminar temperature profile.

Continuing, we can differentiate Eq. (12-77)

$$\frac{\partial}{\partial z}\left[\frac{T(r,z) - T_{wall}(z)}{T_{fl}(z) - T_{wall}(z)}\right] = 0$$

or rearranging

$$(T_{fl} - T_{wall})\left(\frac{\partial T}{\partial z} - \frac{dT_{wall}}{dz}\right) - (T - T_{wall})\left(\frac{dT_{fl}}{dz} - \frac{dT_{wall}}{dz}\right) = 0$$

or

$$\frac{\partial T}{\partial z} = \frac{dT_{wall}}{dz} + \left(\frac{T - T_{wall}}{T_{fl} - T_{wall}}\right)\left(\frac{dT_{fl}}{dz} - \frac{dT_{wall}}{dz}\right)$$

But we have assumed that the wall heat flux is constant

$$q''_{wall} = h(T_{wall} - T_{fl}) = \text{constant} \qquad (12\text{-}83)$$

Hence we conclude that

$$T_{wall}(z) - T_{fl}(z) = \text{constant}$$

and thus

$$\frac{dT_{wall}}{dz} = \frac{dT_{fl}}{dz}$$

or

$$\frac{\partial T(r,z)}{\partial z} = \frac{dT_{wall}}{dz} = \frac{dT_{fl}}{dz}$$

We can utilize this relation to determine the axial temperature distributions by writing an energy balance for a segment of the pipe

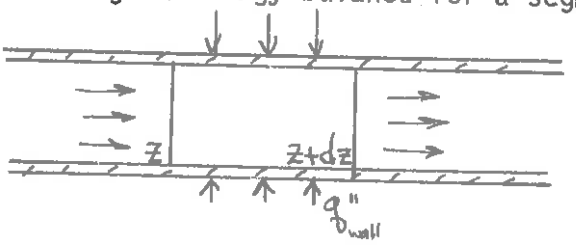

Evidently, then,

$$\rho \langle u_z \rangle \pi R^2 c_p \, dT_{fl} = q''_{wall} \, 2\pi R \, dz \qquad (12\text{-}84)$$

or

$$\frac{dT_{fl}}{dz} = \frac{2q''_{wall}}{\rho \langle u_z \rangle c_p R} = \text{constant} \qquad (12\text{-}85)$$

Thus we find

$$\frac{dT_m}{dz} = \frac{dT_{wall}}{dz} = \text{constant}$$

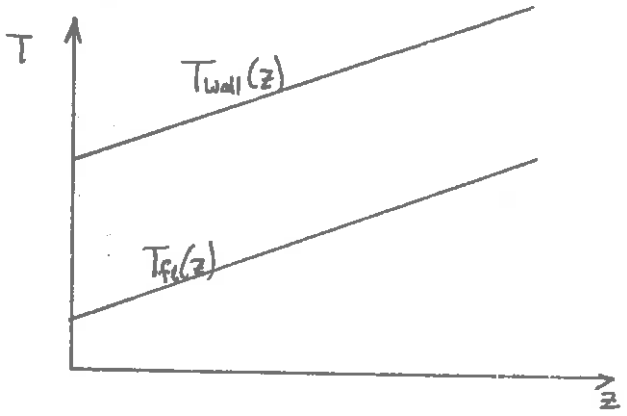

We are now ready (finally!) to return to our energy equation (12-75)

$$\rho c_p u_z \frac{\partial T}{\partial z} = k\left[\frac{1}{r}\frac{\partial}{\partial r}\left(r\frac{\partial T}{\partial r}\right)\right] \qquad (12\text{-}75)$$

Using the Hagen-Poiseuille velocity profile, Eq. (12-75) becomes

$$\rho c_p 2\langle u_z\rangle\left[1-\left(\frac{r}{R}\right)^2\right]\frac{dT_{fl}}{dz} = \rho c_p 2\langle u_z\rangle\left[1-\left(\frac{r}{R}\right)^2\right]\frac{2q''_{wall}}{\rho\langle u_z\rangle c_p R}$$

Hence

$$\frac{1}{r}\frac{\partial}{\partial r}\left(r\frac{\partial T}{\partial r}\right) = \frac{4q''_{wall}}{Rk}\left[1-\left(\frac{r}{R}\right)^2\right] \qquad (12\text{-}86)$$

We will solve this subject to boundary conditions:

(i) $T(R,z) = T_{wall}(z)$

(ii) $T(0,z) < \infty$

We can easily integrate this equation and apply the boundary conditions to find a temperature profile:

$$T(r,z) - T_{wall}(z) = \frac{4q_{wall}}{Rk}\left[\frac{r^2}{4} - \frac{r^4}{16R^2} - \frac{3R^2}{16}\right] \qquad (12\text{-}87)$$

which characterizes fully developed laminar flow in a circular pipe.

Now to determine the convective heat transfer coefficient, h, we calculate

$$T_{fl}(z) = \frac{1}{\pi R^2 \langle u_z \rangle}\int_0^R 2\langle u_z\rangle\left[1-\left(\frac{r}{R}\right)^2\right] T(r,z)\,2\pi r\,dr$$

$$= T_{wall}(z) + \frac{11}{24}\frac{R}{k}q''_{wall} \qquad (12\text{-}88)$$

Thus

$$q''_{wall} = \frac{24k}{11R}\left[T_{wall} - T_{fl}\right] \qquad (12\text{-}89)$$

such that we can identify

$$h = \left(\frac{48}{11}\right)\frac{k}{D} \qquad (12\text{-}90)$$

It is convenient to rewrite this expression for h in terms of a dimensionless parameter

$$\frac{hD}{k} \equiv Nu \equiv \text{"Nusselt number"} \qquad (12\text{-}91)$$

That is, one determines the Nusselt number for a flow process and then uses this to infer the value of the convective heat transfer coefficient, h. For flow which is: (i) laminar, (ii) with fully developed velocity and temperature profiles, and (iii) with a constant wall heat flux, we have just found that the Nusselt number is given by

$$Nu = \frac{48}{11} = 4.364$$

Notice that the Nusselt number can be interpreted as kind of a dimensionless temperature gradient at the wall

$$Nu = \frac{hD}{k} = \frac{q_{wall}\left(\frac{D}{T_{wall} - T_{fl}}\right)}{-q_{wall}/\frac{\partial T}{\partial r}\Big|_R} = \frac{-\frac{\partial T}{\partial r}\Big|_{r=R}}{\frac{T_{wall} - T_{fl}}{D}}$$

$$= \frac{\partial\left(\frac{T - T_{wall}}{T_{fl} - T_{wall}}\right)}{\partial(r/D)}\Bigg|_{r=R} \qquad (12\text{-}92)$$

It will be useful to define another dimentionless parameter,

$$Pr \equiv \frac{\mu}{\rho D_T} = \frac{\nu}{D_T} \equiv \text{"Prandtl number,"} \qquad (21\text{-}93)$$

which is essentially a measure of the ratio of the molecular momentum transfer to the molecular heat transfer. In particular, note that

$$Pr < 1 \Rightarrow \frac{\partial T}{\partial r} < \frac{\partial u}{\partial r}$$

--that is, the temperature gradient is not as steep as the velocity gradient. Prandtl numbers characterizing various types of fluids are shown below

TABLE 9-2
Prandtl Numbers of Some Reactor Coolants

Category	Coolant	Prandtl number
I	Water	4.25 at 100°F 0.87 at 500°F
	Organic coolants (Santowax O-M)	8.55 at 500°F 4.57 at 800°F
	Gases	0.68 to 0.77
II	Liquid metals	0.004 to 0.03

To tie together these two parameters with the Reynold's number, one can define the Stanton number

$$St \equiv \frac{Nu}{Re\,Pr} = \frac{hD/k}{\left(\frac{\rho\langle u_z\rangle D}{\mu}\right)\left(\frac{\mu}{\rho k/\rho C_p}\right)} = \frac{h}{\rho\langle u_z\rangle C_p} \quad (12\text{-}94)$$

If we rewrite this as

$$St\,Pr = \frac{Nu}{Re} = \frac{48/11}{Re} = \frac{3}{11} f, \quad (12\text{-}95)$$

then it becomes apparent that the convective heat transfer coefficient is proportional to the friction factor f.

2. Turbulent Flow Heat Transfer

As we have repeatedly stressed, coolant flow in nuclear reactors is highly turbulent. This turbulence dramatically affects convective heat transfer and the value of h. In the preceding section it was noted that h is usually determined by specifying the Nusselt number

characterizing the flow. It can be shown by dimensional analysis that the Nusselt number is a function of the Reynolds and the Prandtl numbers:

$$Nu = Nu(Re,Pr) \tag{12-96}$$

This is particularly interesting, since the Prandtl number is made up entirely of physical properties of the coolant fluid and is not characteristic of the flow. For this reason, the influence of turbulence must enter through the dependence of Nu upon the Reynolds number. That is, for a given fluid characterized by a given temperature, the heat transfer coefficient h is determined only by the Reynolds number.

Due to the complicated nature of turbulent flow, one is forced to rely upon empirical formulas or "correlations" which express Nu as a function of Pr and Re. The correlation which should be applied depends upon the value of Pr. We have noted that for water or gases, the Prandtl number is close to unity. This implies essentially that the molecular transport of momentum (governed by ν) is comparable to the molecular transport of heat (D_T). Such considerations allow one to derive a particularly simple correlation for Nu called the Dittus-Boelter equation

$$Nu = 0.023\ Re^{0.8}\ Pr^{0.4} \tag{12-97}$$

Before sketching the derivation of this result, it should be noted that the Prandtl numbers for liquid metals are quite small (due to their very large thermal conductivities) and the above correlation will not apply. We will discuss heat transfer for liquid metal coolants in a later section.

In order to account for the transport of momentum and heat due to turbulent motions (eddys), we will insert "anomalous" corrections to the viscosity and thermal conductivity in Newton's law and Fourier's law:

$$\tau_{rz} = -\rho(\nu + \epsilon_M)\frac{\partial u_z}{\partial r}$$

$$q_{0r} = -\rho C_p (D_T + \epsilon_M)\frac{\partial T}{\partial r} \qquad (12\text{-}98)$$

Here, we define

$\epsilon_M \equiv$ eddy diffusivity for momentum transport

$\epsilon_H \equiv$ eddy diffusivity for heat transport

It should be noted that the eddy diffusivities will be very strong functions of position across the pipe.

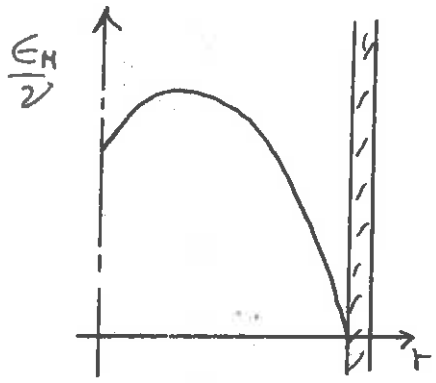

We will now assume that the coolant is characterized by a Prandtl number of unity, Pr = 1, such that

$$\nu = D_T$$

Furthermore, we will assume that

$$\epsilon_H = \epsilon_M$$

[It turns out that there is good reason to believe that this is rigorously true.] Now we know

$$\tau_{rz} = \tau_{wall}(r/R) \qquad (12\text{-}99)$$

We will assume in analogy that

$$q_r = -q_{wall}(r/R) \qquad (12\text{-}100)$$

[This is equivalent to assuming that the temperature and velocity profiles are equivalent.] Then taking the ratio of (12-99) and (12-100), we find

$$\frac{\tau_{rz} C_p}{q_r} = \left(\frac{\nu + \epsilon_M}{D_T + \epsilon_H}\right) \frac{\partial u_z}{\partial T} \qquad (12\text{-}101)$$

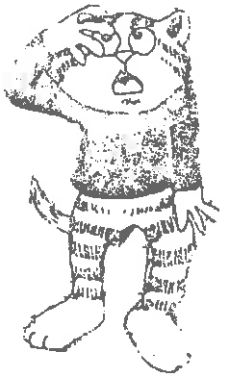

or

$$-\frac{\tau_{wall} C_p}{q''_{wall}} = \frac{\partial u_z}{\partial T} \qquad (12\text{-}102)$$

If we now integrate this from the centerline r = 0 to the wall r = R,

$$-\frac{\tau_{wall} C_p}{q''_{wall}} = \frac{u_z(0)}{T(0,z) - T_{wall}} \qquad (12\text{-}103)$$

But we have seen that the velocity profile for turbulent flow is quite flat. Hence the average flow velocity $\langle u_z \rangle$ is essentially equal to the centerline flow velocity, with a similar argument holding for T(0) and $\langle T \rangle = T_{fl}$

$$\langle u_z \rangle \cong u_z(0), \quad \langle T \rangle \equiv T_{fl} \cong T(0,z)$$

Hence (12-103) becomes

$$-\frac{\tau_{wall} C_p}{q_{wall}} = \frac{\langle u_z \rangle}{T_{fl} - T_{wall}} \qquad (12\text{-}104)$$

But we recall from our earlier work

$$2\pi RL\,\tau_{wall} = (P_1 - P_2)\pi R^2 \tag{12-105}$$

$$P_1 - P_2 = 4\left(\frac{L}{D}\right)\tfrac{1}{2}\rho\langle u_z\rangle^2 f \tag{12-106}$$

$$q_{wall} = h\left[T_{wall} - T_{fl}\right] \tag{12-107}$$

Hence we can calculate

$$St = \frac{h}{\rho C_p \langle u_z\rangle} = \frac{f}{2} = \frac{Nu}{Re\,Pr} \tag{12-108}$$

or since we have assumed Pr = 1,

$$Nu = \tfrac{1}{2} f\,Re \tag{12-109}$$

We can use the Blasius formula for the friction factor in the range $2100 < Re < 10^5$

$$f \cong .046\,Re^{-.2}$$

to find (after reinserting an empirical dependence upon the Prandtl number)

$$Nu = .023\,Re^{.8}\,Pr^{.4} \tag{12-110}$$

which is the advertised Dittus-Boelter correlation good for flows in which $Pr \sim 1$. Since this correlation does not take into account the

effect of the variation in temperature from the tube wall to the fluid centerline on the physical properties, it is most appropriate for near isothermal flow (which, fortunately, coolant flow in a nuclear reactor core closely approximates).

There are many other correlations for more specialized flow situations (e.g., for organic coolants or superheated steam). For example, for water flow parallel for flow rod bundles, a correlation due to Weisman is occasionally used:

$$Nu = c\, Re^{.8}\, Pr^{.33} \qquad (12\text{-}111)$$

where

$$c = .042\frac{\ell}{D} - .024$$

for square lattices such that

$$1.1 \leq \ell/D \leq 1.3$$

3. Liquid Metal Coolants

The very high power densities achieved in fast reactor cores necessitate extremely efficient heat transfer which motivates the use of liquid metal coolants. Such coolants are also desirable for their weak moderating properties.

The primary coolant of interest in LMFBR development is liquid sodium. This coolant is characterized both by high thermal conductivity and low viscosity (and hence low Prandtl numbers, $Pr \sim 0.004$) which implies excellent heat transfer capability along with low pumping powers. [The thermal conductivity of sodium is k = 43.3 BTU/hr-ft-°F compared with a value of k = 0.356 for water.]

The very small Prandtl number liquid sodium implies that the thermal diffusivity is so large that it overshadows the turbulent diffusivity. Hence our earlier correlations for h no longer apply. Instead one uses either:

Constant wall heat flux:

$$Nu = 7 + .025\ Pe^{.8} \qquad (12\text{-}112)$$

(Lyon-Martinelli correlation)

Constant wall temperature:

$$Nu = 5 + .025\ Pe^{.8} \qquad (12\text{-}113)$$

(Seban-Shimazaki correlation)

Here, Pe is the so-called Peclet number

$$Pe = Re\,Pr = \frac{D\langle u_z\rangle \rho c_p}{k}. \qquad (12\text{-}114)$$

4. Choice of Reactor Coolants

There are a variety of considerations which come into play when choosing a reactor coolant. From a nuclear standpoint, one desires coolants with low neutron absorption cross sections, low induced radioactivity, good radiation stability, and, depending on whether one is concerned with thermal or fast reactors, strong or weak moderating properties. One also desires coolants with low melting points, low vapor pressures, and good thermal stability. And of course, one desires high heat transfer coefficients, low pumping losses, and low cost.

Clearly, two of the characteristics of most concern are the magnitude of the heat transfer coefficient, h, and the size of the pumping work required to pump the coolant through the coolant loop (reactor core,

piping, heat exchangers, etc.). The value of the heat transfer coefficient depends upon many factors, such as the geometrical shape of the channel, the flow rate, the heat flux, the temperature, as well as the physical properties of the coolant itself. The pumping work can be calculated in terms of the pressure drop around the primary coolant loop as

$$P.W. = \Delta p \, A_c \, u \qquad (12\text{-}115)$$

where

p = pressure drop around loop

A_c = cross-sectional area of coolant passage

u = coolant velocity

We can get some idea of the suitability of various typical reactor coolants by comparing typical values of h as well as relative (pumping work/heat transferred):

	h [BTU/hr-ft^2-°F]	PW/q [relative]
light and heavy water	5000-8000	1.0
organic liquids	2000-3000	4-10
liquid metals	4000-10,000	3-7
gases (He)	10-100	~100

Clearly in terms of these quantities, liquid metals would make the best coolants. But, of course, there are a number of nuclear advantages to coolants such as water which often outweigh the heat transfer capability of liquid metals (e.g., moderating power).

It is also of interest to compare the three principal coolants used in power reactors in a number of other areas:

coolant	T [°C]	Pressure [atm]	ΔT [°C]	$\langle u_z \rangle$ [cm/sec]	ρ [gm/cc]	$\rho \langle u_z \rangle c_p \Delta T$
water	300	100	20	400	.70	7,000
helium	500	40	400	16,000	.0024	7,150
sodium	400	1	150	400	.85	15,300

Here, the last parameter is

$$\rho \langle u_z \rangle c_p \Delta T = \frac{\text{heat removal rate}}{\text{flow area}}$$

and is a measure of heat transfer effectiveness. One should particularly note here the very high flow rates required in order for a gas coolant to achieve a heat transfer capability comparable to that of a liquid. Such flow rates require rather large pumping powers. Indeed, in an HTGR, roughly 5 to 10% of the power output is required just to pump the coolant through the core.

E. Axial Temperature Distributions

1. Analysis for Bare, Homogeneous Cores

We will now turn our attention to the determination of the axial temperature distribution in a channel containing a single phase coolant. For the purposes of illustration, we will first assume that the axial power distribution is that characterizing a bare, homogeneous cylindrical core:

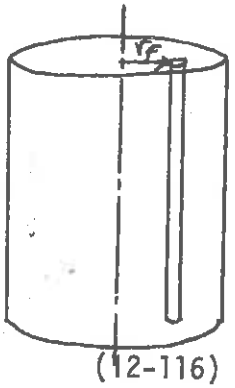

$$q''' = \underbrace{w_f \Phi_0 J_0\left(\frac{2.405\, r_f}{R}\right)}_{G_c} \cos\left(\frac{\pi z}{H}\right) \qquad (12\text{-}116)$$

For more general axial power distributions, one usually will have to resort to numerical methods, such as those we will discuss in the next section.

To compute the temperature of the coolant (or more generally, its enthalpy) as it passes up the coolant channel, we simply perform an energy balance by equating the heat energy gained by the coolant to that produced in the fuel over a small distance dz:

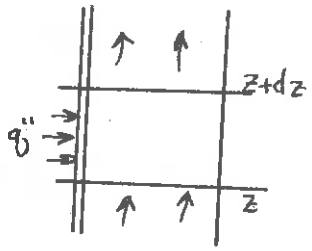

$$wc_p dT = G_c(\pi R^2)dz \equiv q' dz \equiv q'_c \cos\left(\frac{\pi z}{\tilde{H}}\right) dz \qquad (12\text{-}117)$$

[It should be noted that by restricting ourselves to a single phase coolant, we have assumed that all the heat is absorbed as sensible heat and that no coolant phase change is allowed to occur in the channel. In the more general case, we would use the specific enthalpy h to write (12-117) as

$$wdh = q' dz \quad] \qquad (12\text{-}118)$$

We can now integrate this relation up the channel to find

$$wc_p \int_{T_{inlet}}^{T_{fl}} dT = q'_c \int_{-H/2}^{z} dz' \cos\left(\frac{\pi z'}{\tilde{H}}\right) \qquad (12\text{-}119)$$

or

$$T_{fl}(z) - T_{inlet} = \frac{q'_c \tilde{H}}{\pi c_p w}\left[\sin\left(\frac{\pi z}{\tilde{H}}\right) + \sin\left(\frac{\pi H}{2\tilde{H}}\right)\right] \qquad (12\text{-}120)$$

In particular, the exit coolant temperature is given by

$$T_{exit} - T_{inlet} = \frac{2 q_c' \tilde{H}}{\pi C_p w} \sin\frac{\pi H}{2\tilde{H}} \sim \frac{2 q_c' \tilde{H}}{\pi C_p w} \quad \text{for } \tilde{H} \sim H. \qquad (12\text{-}121)$$

We have now evaluated the coolant temperature distribution at any point z in the channel:

$$T_{fe}(z) = T_{inlet} + \frac{q_c' \tilde{H}}{\pi C_p w}\left[\sin\frac{\pi z}{\tilde{H}} + \sin\frac{\pi H}{2\tilde{H}}\right] \qquad (12\text{-}122)$$

Hence using our earlier work on thermal conduction, we can work back to calculate the temperatures in the fuel and clad. First, recall that balancing the heat produced in a small length dz against that transferred into the coolant demands

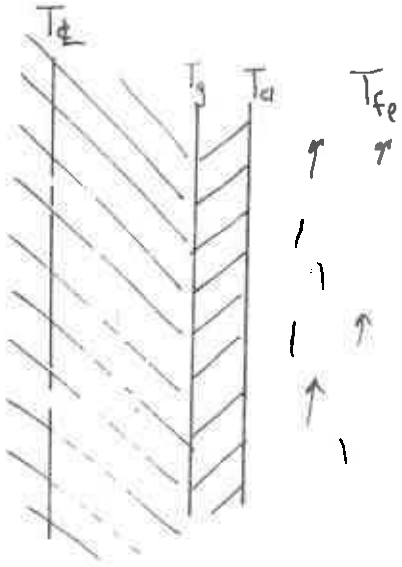

$$q' dz = h 2\pi(R+t_c) dz (T_{cl} - T_{fe}) \qquad (12\text{-}123)$$

Hence we can find the clad surface temperature as

$$T_{cl}(z) = T_{fe}(z) + \frac{q_c'}{h 2\pi(R+t_c)} \cos\frac{\pi z}{\tilde{H}} \qquad (12\text{-}124)$$

$$= T_{inlet} + q_c' \left[\frac{\tilde{H}}{\pi C_p w}\left(\sin\frac{\pi z}{\tilde{H}} + \sin\frac{\pi H}{2\tilde{H}}\right) + \frac{1}{h 2\pi(R+t_c)} \cos\frac{\pi z}{\tilde{H}}\right]$$

One can now work back to find the fuel surface and centerline temperatures as

$$T_{ig}(z) = T_{cl}(z) + q'_c\left[\frac{1}{2\pi R h_g} + \frac{t_c}{2\pi R k_c}\right]\cos\frac{\pi z}{H}$$

$$= T_{inlet} + q'_c\left[\frac{\tilde{H}}{\pi c_p w}\left(\sin\frac{\pi z}{\tilde{H}} + \sin\frac{\pi H}{2\tilde{H}}\right) + \left(\frac{1}{2\pi(R+t_c)h_s} + \right.\right. \qquad (12\text{-}125)$$

$$\left.\left. + \frac{1}{2\pi R h_g} + \frac{t_c}{2\pi R k_c}\right)\cos\frac{\pi z}{H}\right]$$

and

$$T_f(z) = T_{ig}(z) + \frac{q'_c}{4\pi k_f}\cos\frac{\pi z}{H}$$

$$= T_{inlet} + q'_c\left[\frac{\tilde{H}}{\pi c_p w}\left(\sin\frac{\pi z}{\tilde{H}} + \sin\frac{\pi H}{2\tilde{H}}\right) + \left(\frac{1}{4\pi k_f}\right.\right. \qquad (12\text{-}126)$$

$$\left.\left. + \frac{1}{2\pi(R+t_c)h_s} + \frac{1}{2\pi R h_g} + \frac{t_c}{2\pi R k_c}\right)\cos\frac{\pi z}{H}\right]$$

Plotting these temperature distributions out, one notes that the maximum temperatures occur slightly above the centerline of the core:

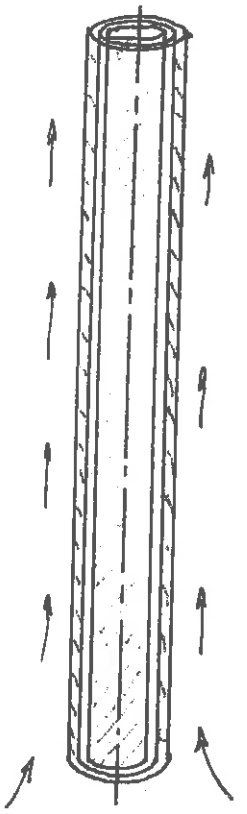

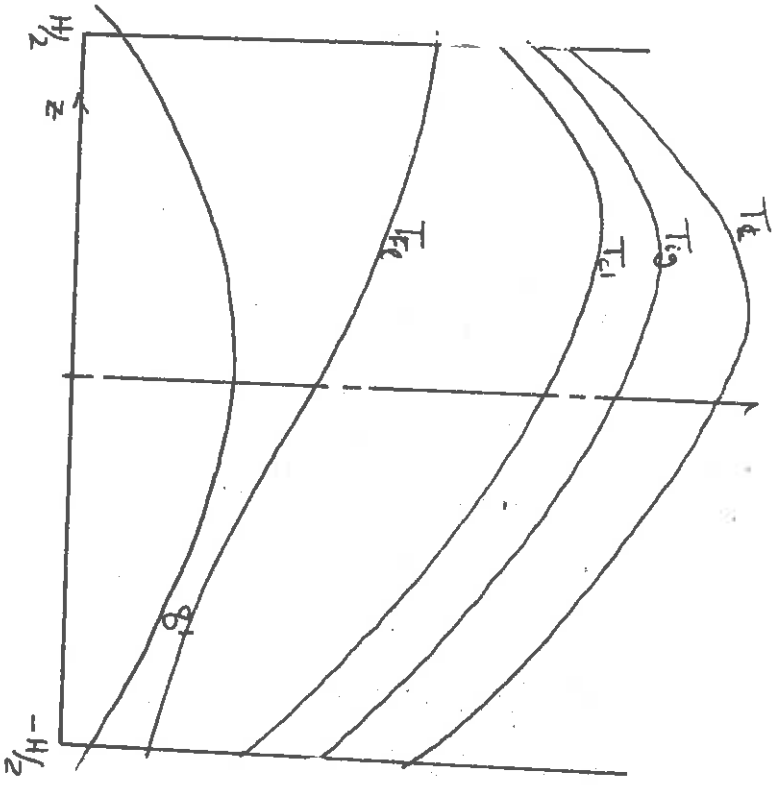

For example, one can calculate the point at which the maximum clad temperature occurs by computing

$$\frac{dT_{cl}}{dz} = 0$$

and then finding

$$z_{clad} = \frac{\tilde{H}}{\pi} \tan^{-1}\left[\frac{h\, 2(R+t_c)\tilde{H}}{c_{pw}}\right] \qquad (12\text{-}127)$$

Similarly

$$z^{\ell}_{max} = \frac{\tilde{H}}{\pi} \tan^{-1}\left\{\frac{\tilde{H}/c_{pw}}{\frac{1}{4k_f} + \frac{1}{2Rh_g} + \frac{t_c}{2Rk_c} + \frac{1}{2h_s R(R+t_c)}}\right\} \qquad (12\text{-}128)$$

2. Numerical Studies of Single Channel Flow

In single-phase flow, the temperature and pressure distributions in a coolant channel can easily be calculated numerically. The channel length is divided into segments, and the solution of the corresponding heat balance equation is obtained by marching from the coolant inlet up the channel. For example, suppose we divide the channel into equal segments of length Δz:

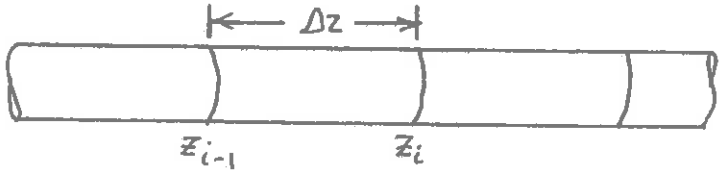

Then, given the inlet condition at a point $z_0 = 0$, we must determine the coolant conditions up the channel. Define the flow variables at each point:

w = mass flow rate

p_i = pressure at z_i

h_i = enthalpy at z_i

T_i = bulk (mean) temperature at z_i

Now consider a typical segment from z_{i-1} to z_i. We begin by writing the heat balance in difference form as

$$w\Delta h = 2\pi R\,\Delta z\left[\frac{q''_{bi-1} + q''_{bi}}{2}\right]. \qquad (12\text{-}129)$$

The heat flux q''_i will be known from the axial flux or power profile. Hence, we can solve for the enthalpy at z_i in terms of the enthalpy at z_{i-1}

$$h_i = h_{i-1} + \frac{\pi R\Delta z}{w}\left[q_{bi-1} + q_{bi}\right] \qquad (12\text{-}130)$$

Next, we calculate the Reynold's number of the flow:

$$Re = \frac{\rho\langle u_z\rangle D}{\mu} = \frac{\rho\langle u\rangle \frac{\pi}{4}D^2}{\mu}\frac{4}{\pi D} = \frac{4w}{\pi D\mu} \qquad (12\text{-}131)$$

where the viscosity will be a tabulated function of pressure and temperature, $\mu = \mu(p_{i-1}, T_{i-1})$. This will determine the appropriate friction factor. For example, if $2100 < Re < 10^5$, then we can use the Blasius formula

$$f = .0791\,Re^{-.25} \qquad (12\text{-}132)$$

Once we know the friction factor f, we can then calculate the frictional pressure drop up the segment

$$\Delta p\,(\pi R^2) = 2\pi R\,\Delta z\;\tfrac{1}{2}\rho\langle u_z\rangle^2 f$$

or

$$\Delta p = \frac{\Delta z}{R}\,w^2\frac{f}{\rho A^2}\,, \quad A = \frac{\pi}{4}D^2 \tag{12-133}$$

Here we have used the equation of state to find $\rho(p_{i-1}, T_{i-1})$. Note also that for vertical flow, one must always subtract the hydrostatic pressure difference Δp.

Next, the temperature can be calculated from an equation of state, $T = T(p_{i-1}, h_{i-1})$ [which is usually tabulated]. This allows one to calculate the heat transfer coefficient from

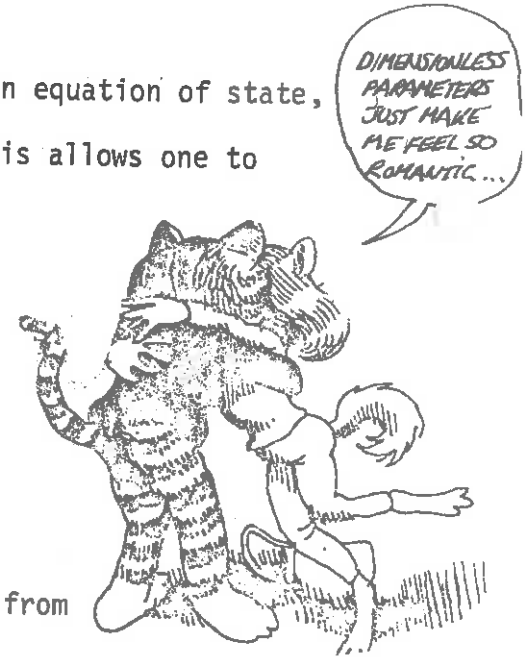

$$Nu = Nu\,(Re, Pr)$$

for example,

$$Nu = 0.0155\,Pr^{.5}\,Re^{.83}$$

Then, since T_i and p_i are known, one can evaluate h from

$$h = Nu(k/D)$$

Finally one can calculate the clad wall temperature using Newton's law of cooling

$$T_{cl_i} = T_i + q''_i/h \,. \tag{12-134}$$

This very simple single channel scheme is frequently used in thermal hydraulic codes which ignore flow mixing between channels and attempt to treat an average channel and a hot channel (using the hot channel factors to determine the heat flux in this channel).

V. BOILING HEAT TRANSFER IN NUCLEAR REACTOR CORES

A. Introduction

Thus far we have restricted our analysis of heat transfer between the clad surface and the coolant to situations in which there is no phase change. However, most present day power reactor cores are designed to operate such that there will in fact be localized boiling at the clad surface, since boiling heat transfer is perhaps the most efficient heat transfer mechanism. Such localized boiling does not necessarily lead to bulk boiling of the coolant, however. For example, in a PWR, although the clad surface temperature is allowed to exceed the saturation temperature of the coolant, the bulk coolant temperature always remains below this temperature. Hence, although small vapor bubbles will form on the clad surface, they quickly collapse as they leave this surface. This phenomenon known as subcooled boiling is an extremely efficient heat transfer mechanism.

By way of contrast, in boiling water reactors the coolant temperature is allowed to exceed the saturation temperature. Bulk or saturated boiling occurs and results in appreciable vapor (steam) formation within the core.

The primary form of boiling heat transfer used in nuclear reactors is so-called nucleate boiling in which many small bubbles form around

small nucleation points on the clad surface and then break away into the coolant. Power reactors are designed to operate in the nucleate boiling regime since this is the most efficient form of heat transfer. Indeed, the efficiency of heat transfer in the nucleate boiling regime is so high that the clad surface temperature will rise no more than 6 to 8°F above the fluid saturation temperature.

One must take care, however, that the heat flux does not become sufficiently large that these bubbles coalesce into a vapor film which covers the surface, since then the heat transfer efficiency drops dramatically, and the clad surface temperature will rise by several hundred degrees. This situation is known as the DNB (departure from nucleate boiling) condition and will be discussed in more detail later.

In this section we will briefly discuss several more general aspects of boiling heat transfer, and then we will introduce the various methods used to analyze this phenomenon in thermal core analysis.

B. Boiling Heat Transfer

Suppose we first consider a heating element submerged in a pool of stationary fluid. A sketch of the heat flux transferred from the heating surface to the fluid versus the temperature difference between the surface and the bulk fluid temperature is shown below:

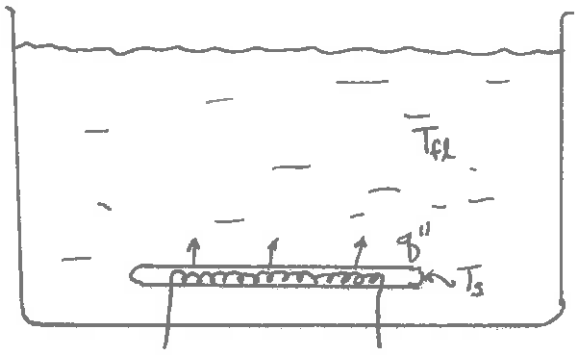

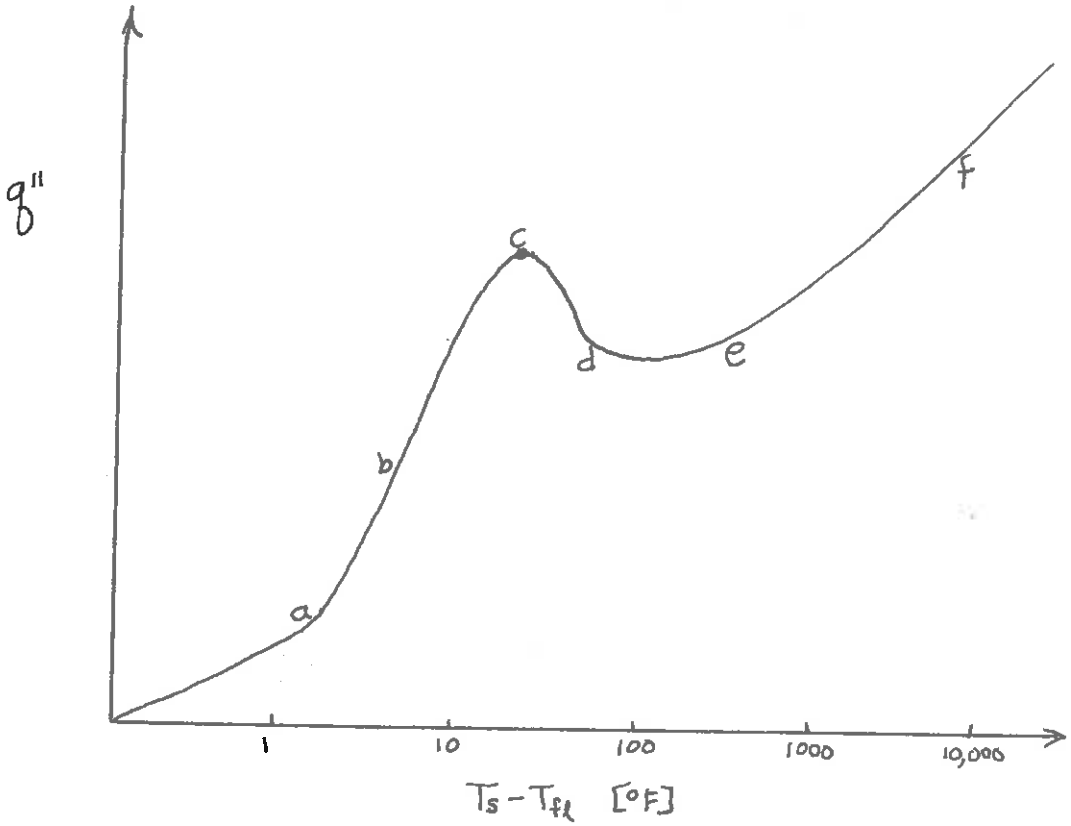

One can distinguish several distinctly different heat transfer regimes. In the region

0-a: Little liquid superheat; heat transfer by natural convection

a-b: a few bubbles are formed, but these collapse after leaving the surface (although aggitation will increase heat transfer)

b-c: the number of bubbles formed increases rapidly--this is the nucleate boiling regime

c: burnout point or departure from nuclear boiling (DNB)

c-d: bubbles become so numerous that they begin to coalesce and clump near the heating surface (the vapor covering the surface acts as a heat insulator)--this is known as partial nucleate boiling

d-e: a continuous blanket of vapor forms over the heating surface--film boiling regime

e-f: now thermal radiation from the surface comes into play--film and radiation regime

It should particularly be noted that if the heat flux q" is the independent variable, then increasing q" beyond the DNB point will result in a large increase in the surface temperature for a given coolant temperature. This phenomenon is known as burn-out and must be avoided in reactor operation.

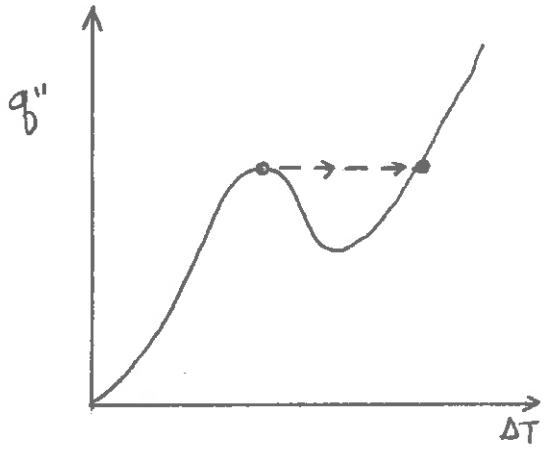

These concepts also apply in a flowing channel. Suppose we consider a channel with a uniform wall heat flux q''_{wall}. Then one will find temperature profiles up the channel as shown below:

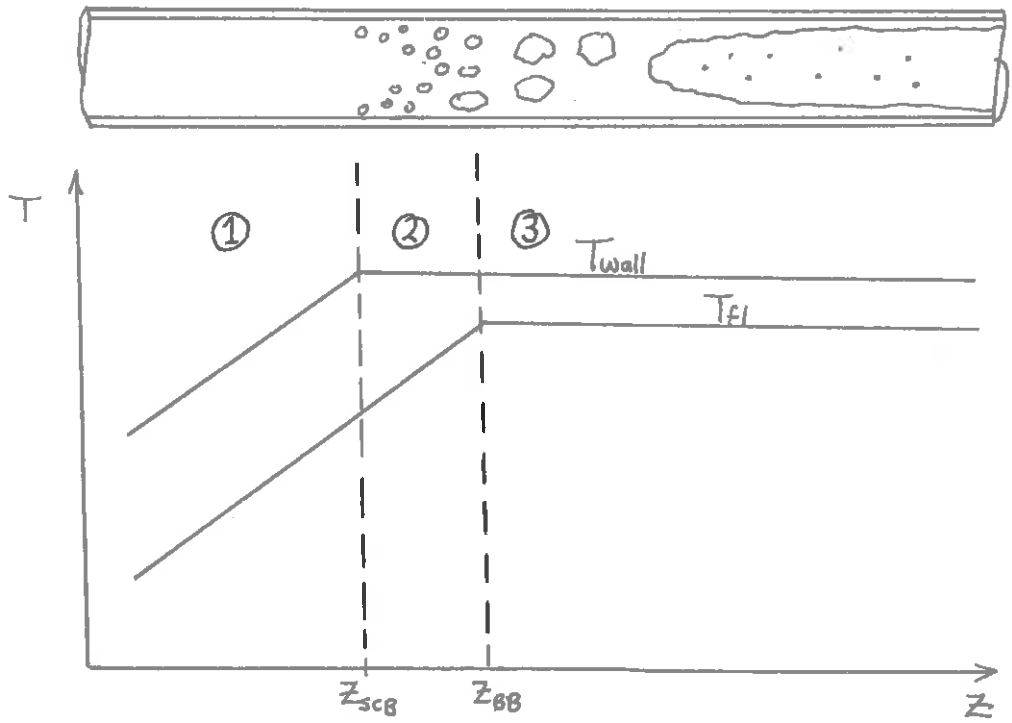

Once again we can distinguish several regions of heat transfer:

Region ①: single phase convection

In this region, we can use the analysis we developed in the previous section to determine the convective heat transfer coefficient, h_s, arising in Newton's law of cooling

$$q'' = h_s(T_{cl} - T_{ff}) \tag{12-135}$$

For example, for turbulent flow, one customarily would use the Dittus-Boelter equation to determine Nu and hence h_s

$$Nu = \frac{h_s D}{k} = .0155\, Re^{.83}\, Pr^{.5} \tag{12-136}$$

For such a single phase forced convection, h_s, is relatively constant for fixed values of coolant velocity, fuel geometry, and coolant properties. Since the coolant flow is outside the parallel to the fuel elements, one must use the equivalent hydraulic diameter in these expressions.

Region 2: subcooled boiling: $T_{cl} \geq T_{sat}$ but $T_f < T_{sat}$

Once the clad surface temperature reaches the saturation temperature of the coolant, the temperature drop is no longer linear in the heat flux. In this region, the heat transfer process is extremely efficient, and the temperature difference is quite small compared to the other temperature differences in the core. In light water reactors, it is customary to use an empirical correlation developed by Jens and Lottes in order to calculate the temperature difference between the clad surface and the coolant:

$$\Delta T\big|_{cool} = T_{cl} - T_{fl} = 60e^{-P/900}\left(\frac{q''}{10^6}\right)^{1/4} \qquad (12\text{-}137)$$

where p is the pressure in units of psia and q" is the heat flux in units of BTU/hr-ft^2. This correlation is valid for pressures, temperatures, and coolant flow rates characteristic of both PWR's and BWR's. For example, in a PWR at 2000 psia with a heat flux of 5 x 10^5 BTU/hr-ft^2, one would find a temperature difference of only 5.5°F. There will be very little change in the temperature difference with heat flux in this boiling regime. Once the clad surface temperature reaches the saturation temperature of the coolant, it tends to remain near that level unless the heat flux reaches the DNB value.

One can use these relationships to determine the position at which subcooled boiling begins. We equate

$$T_{cl} - T_{sat} = 60e^{P/900}\left(\frac{q''}{10^6}\right)^{1/4} \qquad (12\text{-}138)$$

Then noting also that

$$q'' = h_s(T_{cl} - T_{fl}) \qquad (12\text{-}139)$$

we can find

$$T_{fl}\big|_{z_{SCB}} = T_{cl} - q''/h$$
$$= T_{sat} + 60e^{-P/900}\left(\frac{q''}{10^6}\right)^{1/4} - q''/h \qquad (12\text{-}140)$$

and then solve this for the position, z_{SCB}.

Region 3: Saturated or bulk boiling: $T_f = T_{sat}$

Eventually, sufficient heat is transferred to the coolant that it reaches its saturation temperature and begins bulk boiling. Subsequent heat addition will cause further boiling, and hence the coolant temperature will remain essentially constant and equal to T_{sat} up the remainder of the channel.

C. Two Phase Flow

When the coolant is a two phase mixture of liquid and vapor, the coolant flow pattern can become quite complicated. One can distinguish several types of two-phase flow:

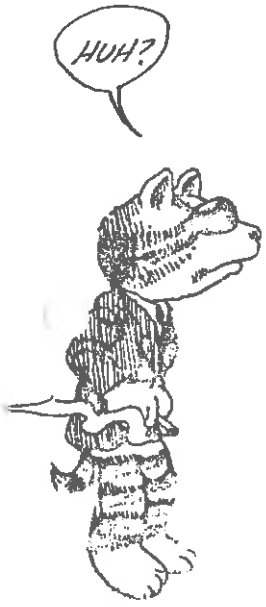

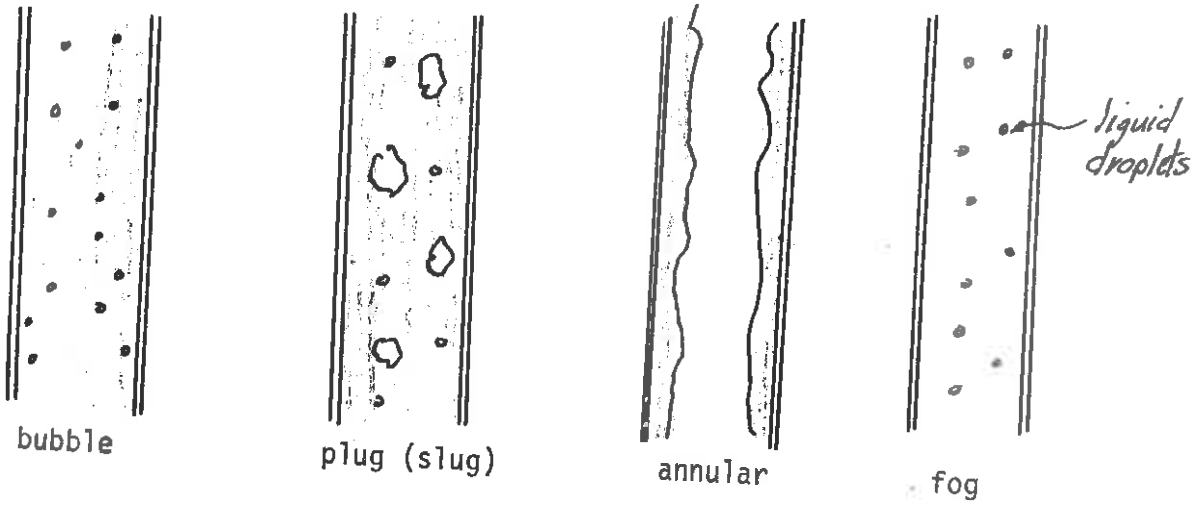

bubble plug (slug) annular fog

It is useful to introduce some definitions characterizing the condition of the coolant:

$$\text{static quality} \equiv \chi_s \equiv \frac{\text{mass of vapor in mixture}}{\text{total mass of mixture}}$$

$$\text{void fraction} \equiv \alpha \equiv \frac{\text{volume of vapor in mixture}}{\text{total volume of liquid-vapor mixture}}$$

We can compute these quantities in terms of the cross-sectional areas occupied by liquid and vapor. First,

$$\alpha = \frac{A_g}{A_g + A_l}$$

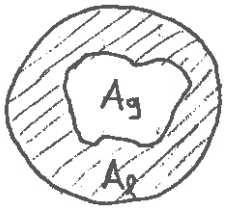

(12-141)

Also

$$\chi_s = \frac{\rho_g A_g}{\rho_g A_g + \rho_l A_l} = \frac{1}{1 + \frac{\rho_l}{\rho_g}\frac{A_l}{A_g}} = \frac{1}{1 + \frac{\rho_l}{\rho_g}\left(\frac{1-\alpha}{\alpha}\right)} \quad (12\text{-}142)$$

For example, water at STP conditions has χ = 2%, α = 97%. Other values of void fraction vs. quality are indicated below:

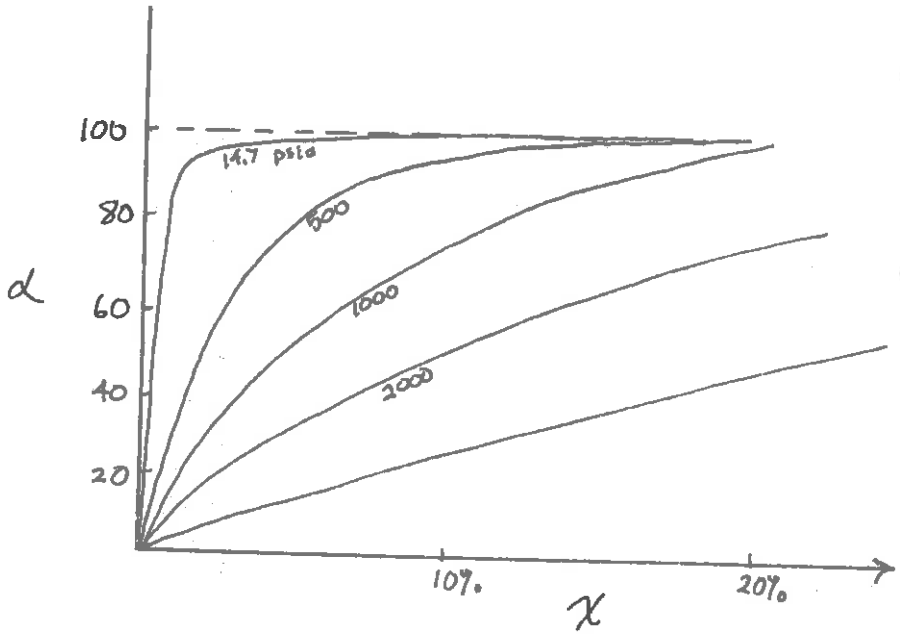

When the two phase mixture is flowing, we must be more careful in our definitions since the vapor has a tendency to slip past the liquid. We

define the slip ratio as

$$\text{slip ratio} \equiv S \equiv V_g/V_f \tag{12-143}$$

Then

$$x = \frac{\text{mass flow rate of vapor}}{\text{total mass flow rate}} = \frac{w_g}{w_g + w_\ell}$$

$$= \frac{A_g \rho_g V_g}{A_g \rho_g V_g + A_\ell \rho_\ell V_\ell} = \frac{1}{1 + \frac{\rho_\ell}{\rho_g}\frac{A_\ell}{A_g}\frac{V_\ell}{V_g}} \tag{12-144}$$

or

$$x = \frac{1}{1 + \frac{\rho_\ell}{\rho_g}\left(\frac{1-\alpha}{\alpha}\right)\frac{1}{S}} \tag{12-145}$$

This latter equation is known as the "S-α-x" relationship.

D. Heat Addition To Boiling Flow

Consider a fluid flowing through a channel of diameter D with wall heat addition $q''_{wall}(z)$

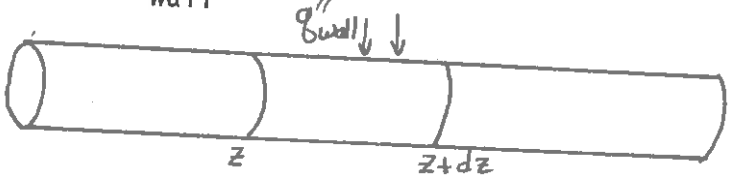

Our simple energy balance will yield

$$w\,dh = q''_{wall}(\pi D)\,dz \tag{12-146}$$

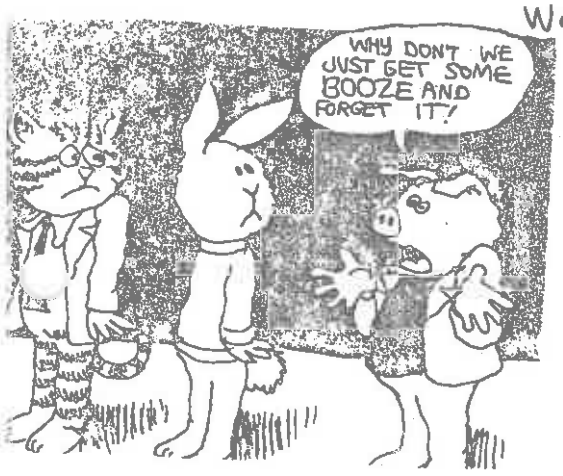

If we integrate this in the usual manner, we can find the enthalpy at any point in the coolant channel as

$$h(z) = h_{inlet} + \frac{\pi D}{w} \int_0^z q''_{wall}(z)\, dz \qquad (12\text{-}147)$$

Now suppose that bulk boiling begins at a point z_{BB} up the channel:

Then if we define

h_f = enthalpy of saturated liquid = $h_f(p)$

we can determine z_{BB} from

$$h = h_f + \chi h_{fg} \qquad (12\text{-}148)$$

where $\chi \equiv$ flow quality

$h_{fg} \equiv$ heat of vaporization = $h_{fg}(p)$

Thus we can turn this around to calculate the fluid quality as

$$\chi(z) = \frac{1}{h_{fg}} \left[h_{inlet} - h_f + \frac{\pi D}{w} \int_0^z q''_{wall}(z)\, dz \right], \quad z > z_{BB}$$

or

$$\chi(z) = \frac{\pi D}{w h_{fg}} \int_{z_{BB}}^z q''_{wall}(z)\, dz \qquad (12\text{-}149)$$

Once we know $\chi(z)$, then we can determine the void fraction $\alpha(z)$--provided we know the slip ratio S(z). In general, S has a value of about 1 near z_{BB} and tends to increase from the value as one passes up the channel.

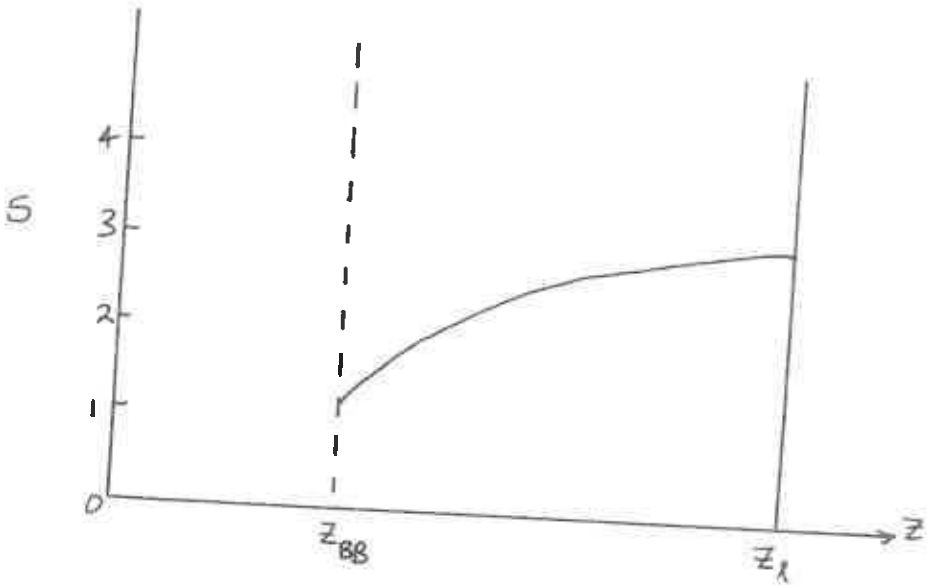

A knowledge of the void fraction is vital to the nuclear analysis of the core, since α determines the coolant density and hence the macroscopic coolant cross section.

EXAMPLE:

channel length z = 5 ft

liquid velocity at inlet = 10 fps

constant wall heat flux = 5×10^5 BTU/hr-ft^2

channel diameter = 0.5 inches

constant slip ratio S = 3

pressure = 1000 psia

T_{inlet} = 500°F

Suppose we wish to determine z_{BB}, $\chi(z)$, and α (z). From the steam tables, we can find

$$h_f(1000) = 542.4 \text{ BTU/lb}$$
$$h_{fg}(1000) = 649.4 \text{ BTU/lb}$$
$$h_{inlet} = 487.6 \text{ BTU/lb}$$
$$v_f = 1/\rho_f = .0216 \text{ ft}^3/\text{lb}$$
$$v_g = 1/\rho_g = .4456 \text{ ft}^3/\text{lb}$$

Hence the mass flow rate is

$$w = \langle u_z \rangle \rho_\ell A = (10 \text{ ft/sec})\left(\frac{1\text{b}}{.0216 \text{ ft}^3}\right)\left(\frac{\pi}{4}\left(\frac{.5}{12}\right)^2 \text{ft}^2\right) = .631 \text{ lb/sec} = 2270 \text{ lb/hr}$$

For uniform heat addition, Eq. (12-149) becomes

$$h_f - h_{inlet} = \frac{\pi D}{w} z_{BB} q''_{wall}$$

Hence we can solve for z_{BB} as

$$z_{BB} = \frac{w(h_f - h_{sat})}{\pi D q_{wall}} = \frac{(2270 \text{ lb/hr})(542.4 - 487.7) \text{ BTU/lb}}{\pi(.5/12 \text{ ft})(5)(10^5 \text{ BTU/hr ft}^2)}$$

$$= 1.91 \text{ ft}$$

Now
$$\chi(z) = \frac{\pi D}{w h_{fg}}(z - z_B)$$

$$= \frac{\pi(.5/12)\text{ft}(5.105)\frac{\text{BTU}}{\text{hr ft}}(z - z_{BB})}{(2270 \text{ lb/hr})\ 649.4 \text{ BTU/lb}}$$

$$= .0444\ (z - z_{BB}), \quad z > z_{BB}$$

In particular, the exit quality is $\chi_\ell = .0444(5-1.91) = .137 \approx 13.7\%$

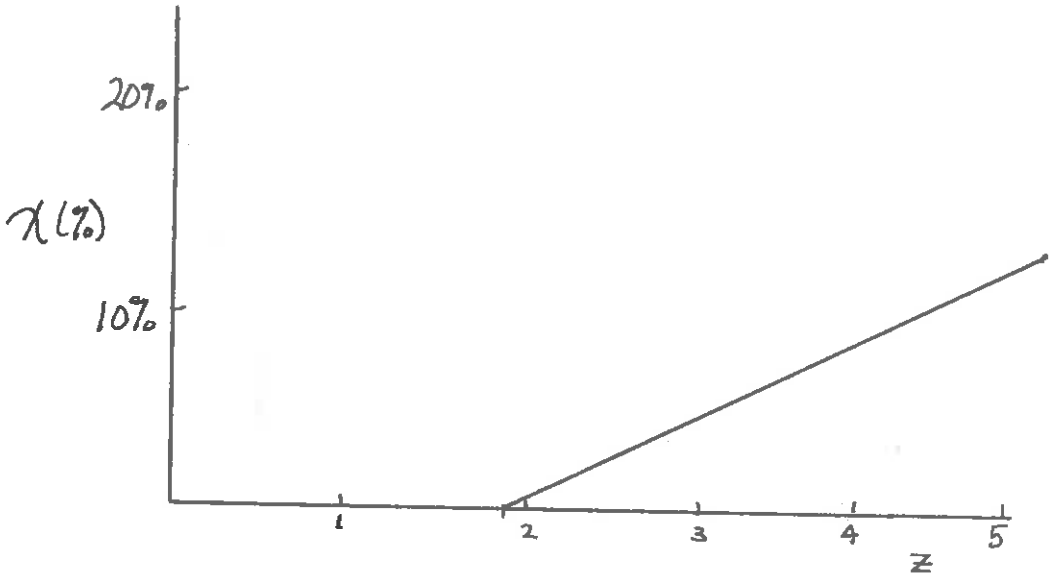

To find the void fraction, use the S- χ - α relationship

$$\alpha(z) = \frac{1}{1+S\left(\frac{\rho_g}{\rho_\ell}\right)\left(\frac{1-\chi}{\chi}\right)} = \frac{1}{1+3\left(\frac{.0216}{.4456}\right)\left(\frac{1-\chi}{\chi}\right)}$$

Hence we find

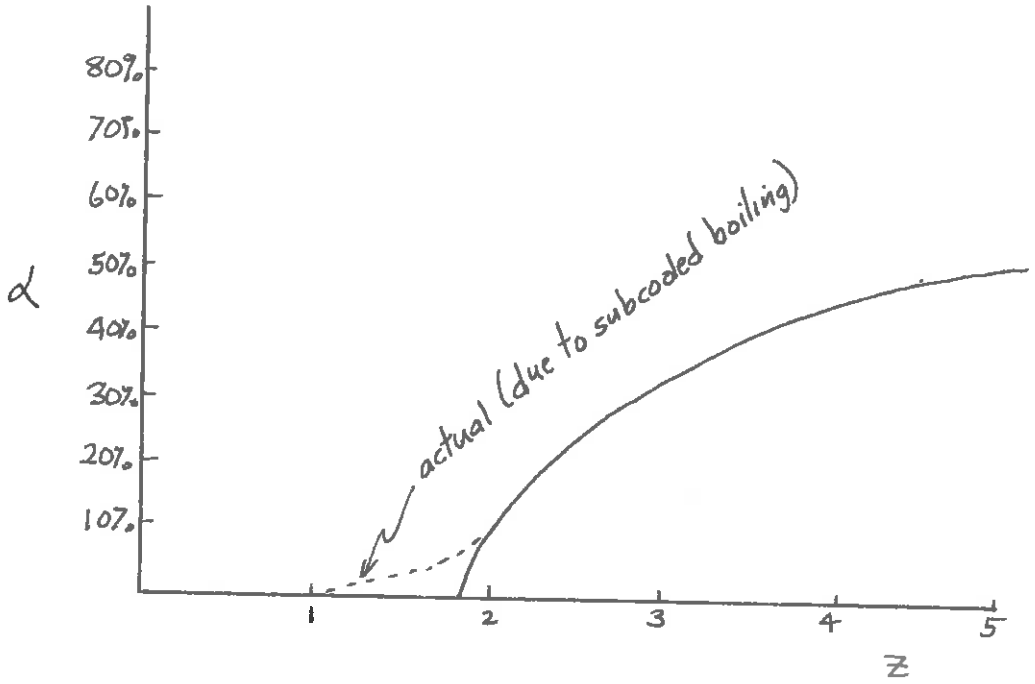

As we mentioned earlier, the void fraction is extremely important in the calculation of the void coefficient of reactivity. There is a very strong coupling between the thermal core behavior which determines $\alpha(z)$, and the axial flux profile in boiling water reactors.

E. Flow Boiling Crisis or DNB

Our earlier discussion of boiling heat transfer indicated that if the wall heat flux exceeded a certain magnitude, there would be an unstable transition from nucleate boiling to film boiling with a corresponding increase in wall surface temperature. This "boiling crisis" corresponds to a sudden drop in the heat transfer coefficient h_s due to a change in the boiling mechanism from nucleate boiling to film boiling. The boiling crisis is known by a number of names, including burnout, critical heat flux, DNB (departure from nuclear boiling). Flow boiling crisis is more complicated that pool boiling crisis due to the added effects of convection (forced) and bubble clouding which tends to shield the heat transfer surface

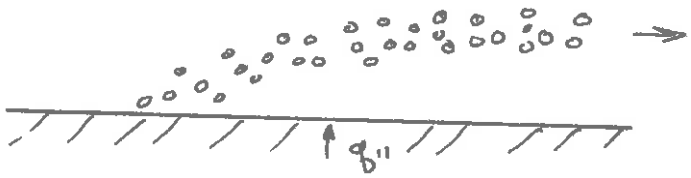

Flow instabilities can also complicate the situation. For example, a sudden drop in pressure can increase the local super heat and perhaps lead to DNB.

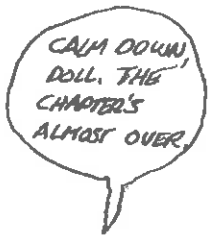

The burnout mechanism is closely related to the flow pattern. There are basically two catagories of interest in reactor design.

(i) subcooled or low quality DNB: Here DNB is probably caused by detachment of the bubble boundary layer. This is the type of DNB that one would design against in a PWR.

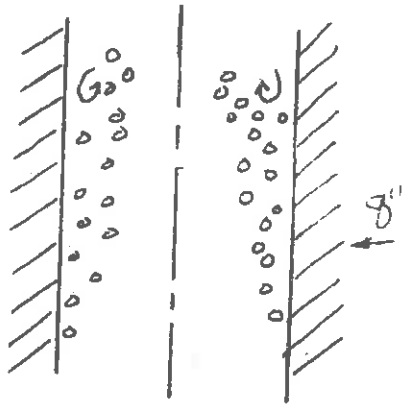

(ii) burnout in high quality region: In this phenomenon, burnout occurs in a liquid film which covers the heat transfer surface. Such a process is of concern in BWR's. Burnout in the high quality region will occur when the liquid film "dries out". This process is slow compared to subcooled DNB, the high velocity vapor core provides fairly good single-phase convection heat transfer.

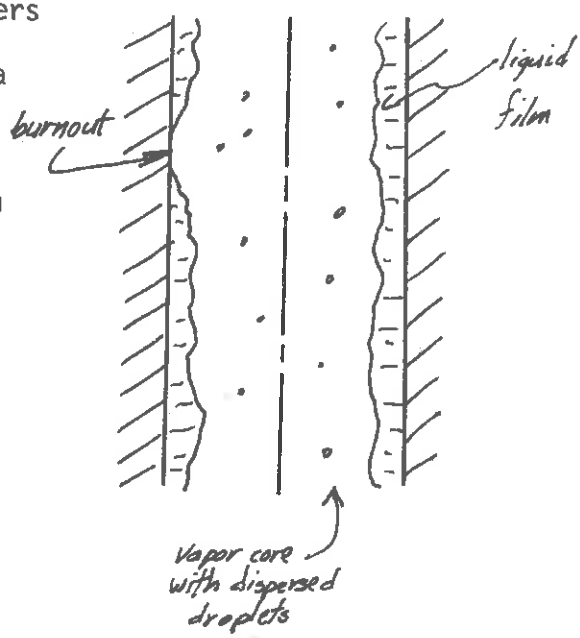

It is extremely important to be able to determine the critical heat flux at which DNB will occur. Unfortunately, this heat flux depends upon a large number of factors, such as channel shape, surface condition, physical properties of the coolant, flow conditions, and so on. Various empirical correlations based upon experimental data have been developed for those range of conditions encountered in modern power reactors. Of particular interest are two correlations characterizing light water reactors.

W-3 Correlation

This correlation was developed by L. S. Tong for the prediction of critical heat flux in PWR's. For a uniformly heated channel, the correlation predicts

$$q''_{DNB}/10^6 = F_1(p,\chi)\, F_2(G,\chi)\, F_c(\chi)\, F_4(D_h)\, F_5(h_{sat}=h_{in}) \qquad (12\text{-}150)$$

where

$$F_1(p,\chi) = (2.022 - 4.302\ p \times 10^{-4}) + (0.1722 - 9.84\ p \times 10^{-5}) \times \\ \times \exp\,(18.177 - 4.129\ p \times 10^{-3})\,\chi$$

$$F_2(G,\chi) = (0.1484 - 1.594\chi + 0.1729\,\chi^2)\ G/10^6 + 1.037$$

$$F_3(\chi) = 1.157 - 0.896\,\chi$$

$$F_4(D_h) = 0.2664 + 0.8357 \exp(-3.151\ D_h)$$

$$F_5(h_{sat} - h_{in}) = 0.8357 + 7.94 \times 10^{-4}\ (h_{sat} - h_{in})$$

This correlation is valid for a range of parameters:

pressure p: 1000 to 2300 psi

flow rate G: 1.0×10^6 to 5.0×10^6 lb/hr-ft^2

hydraulic diameter D_h: 0.2 to 10.7 inches

quality χ: -0.15 to 0.15

inlet enthalpy = 400 BTU/lb

channel length L = 10 to 144 inches

This correlation is intended as a best estimate of the critical heat flux for the situation in which the channel experiences a uniform heat flux.

Janssen-Levy Correlation

A similar correlation has been developed for BWR's:

$$q''_{DNB}/10^6 = 0.705 + 0.237\ (G/10^6),\ \chi < \chi_1$$
$$= 1.634 - 0.270\ (G/10^6) - 4.710\chi,\ \chi_1 < \chi < \chi_2$$
$$= 0.605 - 0.164\ (G/10^6) - 0.653\chi,\ \chi_2 < \chi \qquad (12\text{-}151)$$

where

$$\chi_1 = 0.197 - 0.108\ (G/10^6)$$
$$\chi_2 = 0.254 - 0.026\ (G/10^6)$$

at other pressures

$$q''_{DNB}(p) = q''_{DNB}(1000) + 440\ (100-p)$$

The ranges of parameters for which this correlation is valid are

pressure p: 600 to 1450 psi

flow rate G: 0.4×10^6 to 6.0×10^6 lbs/hr-ft^2

quality χ: negative to 0.45

hydraulic diameter D_h: 0.245 to 1.25 inches

channel length L: 29 to 108 inches

In contrast to the W-3 correlation, the Janssen-Levy correlation is designed to give a somewhat conservation estimate of the critical heat flux.

The core designer must use such correlations to insure that the critical heat flux is not exceeded during core operation. One usually defines the minimum ratio of the critical heat flux to the heat flux achieved in the core as the DNB ratio (DNBR).

$$DNBR = \left[q''_{DNB}(z)/q''(z)\right]_{min} \qquad (12\text{-}152)$$

Minimum values for this ratio of 1.25 to 1.5 are usually maintained under a high heat flux transient condition for the most adverse combination of mechanical and coolant conditions.

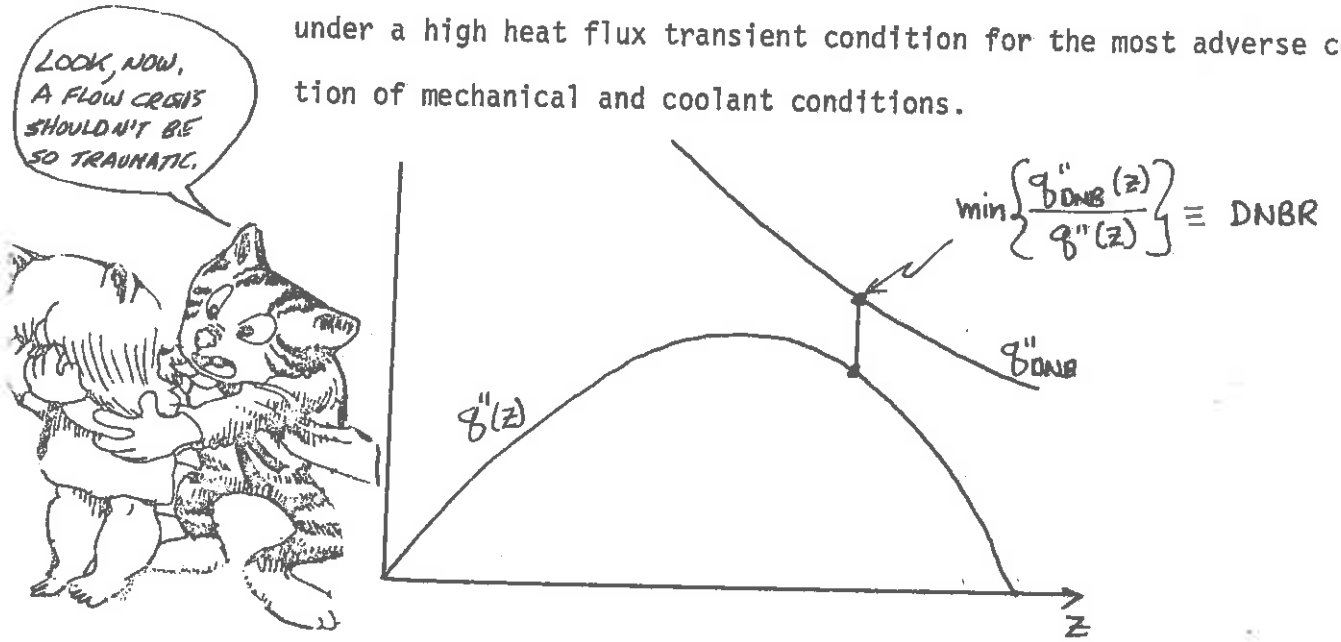

F. Axial Temperature Distributions

Thus far we have confined our discussion of axial temperature distributions to channels containing a single phase coolant. Let us now consider how such temperature distributions would be altered when coolant boiling is present. First, consider the "hot" channel of a PWR in which nucleate boiling occurs. The coolant enters the channel with a temperature $T < T_{sat}$. After passing some distance up the channel, the clad surface temperature reaches T_{sat} (although the bulk coolant temperature T_f remains below T_{sat} throughout the channel), and nucleate boiling heat transfer begins. Such heat transfer is so efficient that the clad surface temperature remains essentially constant the rest of the way up the channel.

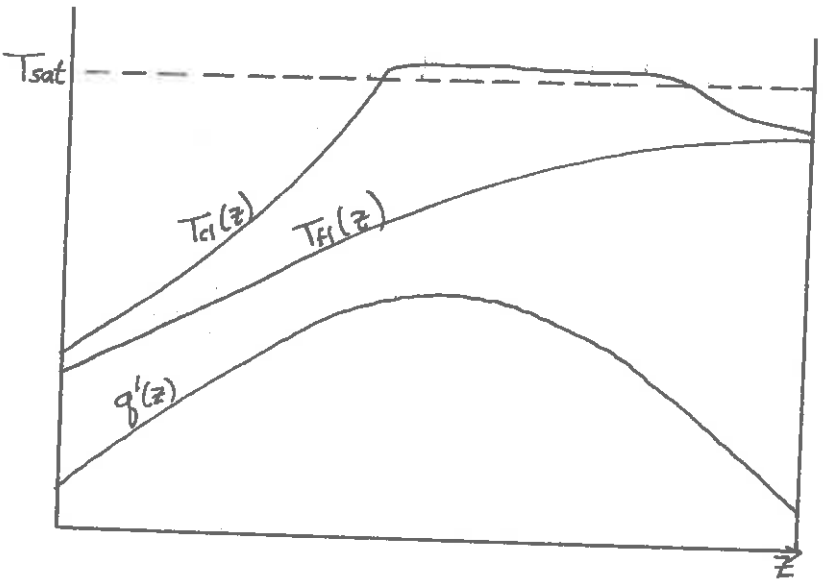

Consider now a coolant channel in a BWR. Once again the coolant enters below saturation temperature, and the clad surface temperature will eventually reach T_{sat} before the bulk coolant temperature. However, now further up the channel, the coolant reaches saturation, and additional heat added to the channel increases its quality.

Both the clad surface and coolant temperatures

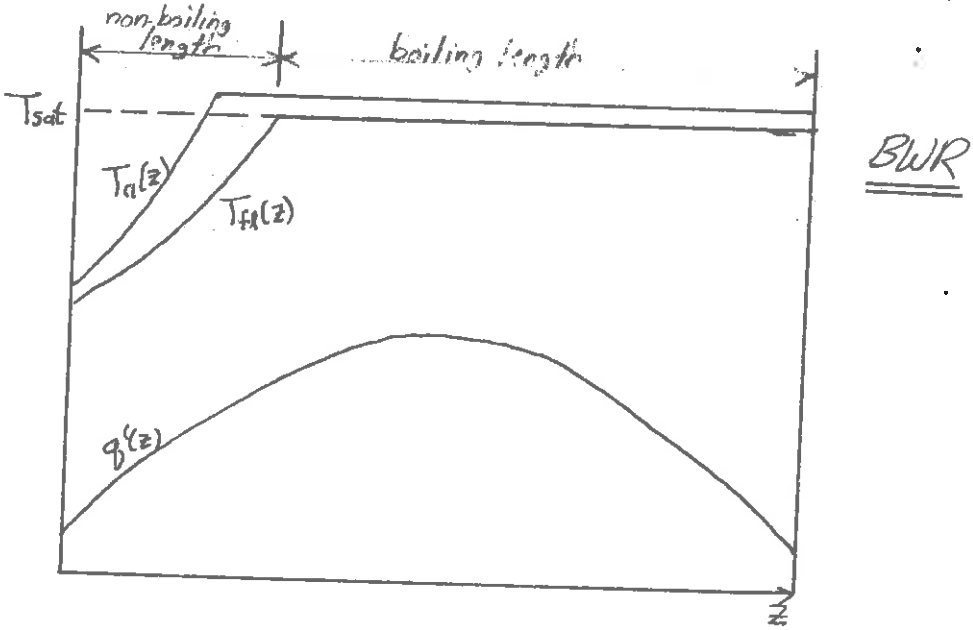

remain relatively constant after the inception of boiling.

VI. HYDRODYNAMIC CORE ANALYSIS

The thermal performance will depend strongly upon the coolant flow behavior. In particular, one must determine the coolant flow rate, pressure drop across the core, and the pumping power required to maintain the coolant flow. Since the flow in the core is highly turbulent, we are forced to employ once again various empirical correlations in order to analyze the coolant hydrodynamic behavior.

A. Pressure Drop in Core

One can classify several mechanisms which will cause a pressure drop along the coolant channel

(i) friction losses from the fuel rod bundle

(ii) friction losses from the spacer grids

(iii) friction losses at the core inlet and exit (contraction or expansion)

(iv) acceleration pressure drop due to phase change

(v) elevation

To determine the pressure drop due to channel friction, we can use the friction factor to write

$$\Delta p\Big|_{friction} = f\left(\frac{L}{D_h}\right)\rho\frac{\langle u_z\rangle^2}{2g} \qquad (12\text{-}153)$$

where, for $2100 < Re < 10^5$, we can use

$$f = .0791\ Re^{-0.25} \qquad (12\text{-}154)$$

Friction losses due to spacer grids or inlet or exit geometry are classified as form losses, since they correspond to a change in the coolant momentum due to a change in the coolant channel geometry. One usually writes

$$\Delta p|_{form} = \Delta p|_{grids} + \Delta p|_{\substack{inlet \\ ; exit}} = \sum_i K_i \rho \frac{\langle u_z \rangle^2}{2g} \qquad (12\text{-}155)$$

where K_i is a form friction factor which is due to a change in the coolant channel cross sectional area of the ith type. K_i is quite complicated for spacer grids, and must be determined experimentally for each spacer grid design.

The acceleration pressure drop is due to a differential velocity between the liquid and vapor phases of the coolant and a corresponding coolant expansion. One can show

$$\Delta p|_{acc} = \frac{G^2}{\rho_g} \left[\frac{(1-\chi)^2}{1-\alpha} + \frac{\chi^2}{\alpha} \frac{\rho_l}{\rho_g} - 1 \right] \qquad (12\text{-}156)$$

where $G = \rho \langle u_z \rangle$.

When two phase flow is present, a somewhat different friction and form pressure drop must be used. For the channel friction, it is customary to use the Martinelli-Nelson correlation

$$\Delta p \Big|^{2phase}_{friction} = R_{MN} f \left(\frac{L}{De} \right) \frac{\langle u_z \rangle^2}{2g} \qquad (12\text{-}157)$$

where R_{MN} is a tabulated parameter depending on pressure and flow quality. For example:

P \ R_{MN}	10%	20%
1000 psi	3.10	4.92
2000 psi	1.72	2.27

The form losses are written as

$$\Delta p\Big|_{form}^{2\,phase} = \rho \frac{\langle u_z \rangle^2}{2g} K_g \left[\frac{(1-\chi)^2}{(1-\alpha} + \frac{\chi^2}{\alpha} \frac{\rho_f}{\rho_g} \right] \qquad (12\text{-}158)$$

Finally, the elevation pressure drop is calculated as

$$\Delta p\Big|_{elevation} = \int_{-H/2}^{H/2} \rho(z)\, dz \qquad (12\text{-}159)$$

--although this term is usually quite small.

The total pressure drop across the core is the sum of these various contributions. We have indicated typical magnitudes below for a PWR

$$\Delta p = \Delta p\Big|_{friction} + \Delta p\Big|_{form} + \Delta p\Big|_{acc} + \Delta p\Big|_{elevation} \qquad (12\text{-}160)$$

B. Multi-channel Analysis

Our earlier single channel analysis has not accounted for phenomena such as flow mixing between channels which is caused by both

turbulence and pressure gradients. Such mixing can lead to energy transfer between channels as well as pressure losses.

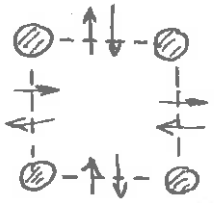

One could characterize such coupling between channels by writing a generalized energy balance equation for a channel m

$$\underbrace{W_m \frac{dh_m}{dz}}_{\text{axial mass flow rate}} = \underbrace{W_{n-m}(H_n - h_m)}_{\text{cross flow rate/length}} + \underbrace{\rho\epsilon(h_n - h_m)}_{\text{mixing coefficient}} + q' \quad (12\text{-}161)$$

Here, the cross channel coupling coefficients W_{n-m} and ϵ must be evaluated from empirical correlations based upon experiment.

One can also have flow redistribution effects in the inlet plenum such that there is not a uniform inlet velocity to each channel. Such flow redistribution could in fact lead to instabilities, and must be accounted for in more detailed core hydraulic analysis.

VII. THERMAL-HYDRAULIC CORE ANALYSIS

A. Hot Channel Factors

One of the principal goals of the reactor designer is to assure that none of the thermal limitations on the core behavior is exceeded. Thus far we have discussed two such limitations. First, one must design the core so that the fuel centerline temperature does not exceed the fuel melting point. This limitation is usually expressed as a restriction on the linear power density

$$q'(r) < q'_{max} \quad [16 \text{ kw/ft in LWR's}]$$

Yet another limitation arises from requiring that the clad surface heat flux always remain below its DNB limit:

$$q''(r) < q''_{DNB}$$

There are usually other thermal limitations placed upon core performance. For example, thermal and fission gas stresses on the clad can limit power generation. Furthermore, thermal-hydraulic performance is also frequently limited by nuclear stability considerations (particularly in BWR's which experience an appreciable variation in moderator density throughout the core).

Certainly one approach to thermal-hydraulic analysis of the core would be to first perform a detailed three dimensional calculation of the core power distribution, taking into account the effects of fuel burnup, fission product buildup, control distributions, and moderator density variations over core life. This information could then be used to determine the coolant flow and temperature distribution throughout the core. However, such a calculation is usually prohibitively expensive for routine design applications.

A more common approach is to investigate how closely the "hot-channel" in the core approaches the operating limitations. Then if one can assure that the thermal conditions of this channel remain below the core limitations, then the remaining channels in the core will presumably fall within design limitations. One usually defines the hot channel in the core as that coolant channel in which the core heat flux and enthalpy

rise is a maximum. Associated with this channel are various "hot channel" or "hot spot" factors which relate the performance of this channel to the average behavior of the core.

We have already been introduced to the concept of nuclear hot channel factors which take into account the variation of the neutron flux and fuel distribution within the core. For example, the radial nuclear factor was defined as

$$F_R^N = \frac{\text{average heat flux of the hot channel}}{\text{average heat flux of the channels in core}} \qquad (12\text{-}162)$$

$$= \frac{\int_{-H/2}^{H/2} q''(\vec{r}_{Hc})\,dz}{\frac{1}{I}\sum_{i=1}^{I}\int_{-H/2}^{H/2} q''(\vec{r}_i)\,dz} \qquad \text{for I channels (pins)}$$

Similarly, the axial nuclear factor is

$$F_Z^N = \frac{\text{maximum heat flux of hot channel}}{\text{average heat flux of hot channel}} \qquad (12\text{-}163)$$

$$= \frac{\max_z q''(\vec{r}_{Hc})}{\frac{1}{H}\int_{-H/2}^{H/2} q''(\vec{r}_{Hc})\,dz}$$

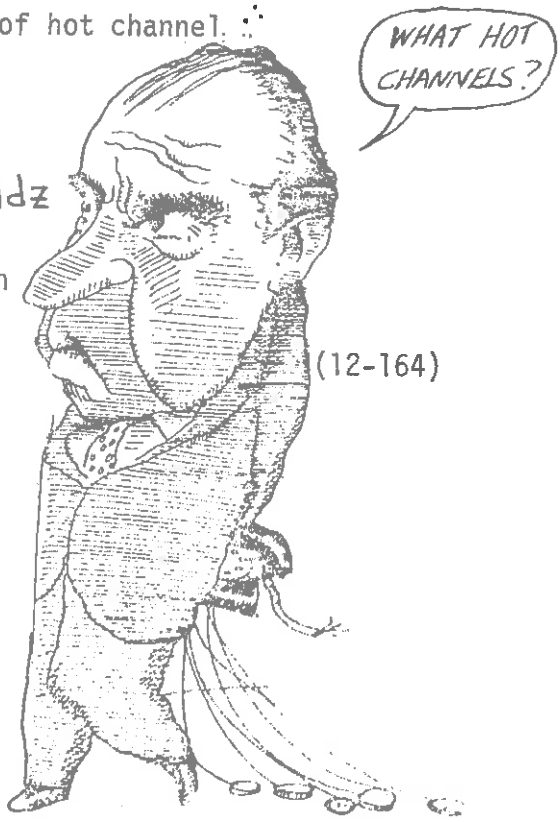

The total nuclear hot channel factor is then

$$F_q^N = F_Z^N F_R^N \qquad (12\text{-}164)$$

By way of example, consider a homogeneous, bare cylindrical core described by a power distribution

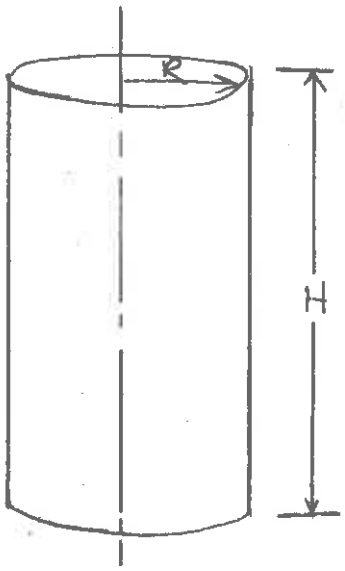

$$q'''(\vec{r}) = Q_0 J_0\left(\frac{2.405r}{R}\right)\cos\left(\frac{\pi z}{H}\right) \qquad (12\text{-}165)$$

Then we can calculate

$$F_R^N = \frac{\int_{-H/2}^{H/2}\cos\left(\frac{\pi z}{H}\right)dz\; J_0(0)}{\int_{-H/2}^{H/2}\cos\left(\frac{\pi z}{H}\right)dz\int_0^R J_0\left(\frac{2.405r}{R}\right)2\pi r dr} = 2.32 \qquad (12\text{-}166)$$

and

$$F_z^N = \frac{\cos(0)\,J_0(0)}{\frac{1}{L}\int_{-H/2}^{H/2}\cos\left(\frac{\pi z}{H}\right)dz\; J_0(0)} = 1.57 \qquad (12\text{-}167)$$

This implies an overall nuclear hot channel factor of

$$F_q^N = (2.32)(1.57) = 3.638 \qquad (12\text{-}168)$$

[This is actually quite conservative. A zone-loaded PWR will typically have a nuclear hot channel factor of $F_q^N = 2.6$.]

One next can define an enthalpy hot channel factor

$$F_{\Delta H} \equiv \frac{\text{maximum coolant enthalpy rise}}{\text{average coolant enthalpy rise}} \qquad (12\text{-}167)$$

This factor is a function both of variations in the power distribution and coolant flow. For example, some 3-10% of the coolant flow bypasses the fuel assemblies, due to leaks past mechanical seals or the presence of other core components. There will be nonuniformities in the coolant flow from channel to channel, although these are reduced somewhat by the lower inlet plenum. Flow mixing between coolant channels can also occur, as well as flow redistribution in which pressure variations due to coolant expansion or variations in nucleate boiling cause variations.

By way of example, we can calculate the enthalpy hot channel factor taking into account only the power variation in a bare, homogeneous cylindrical core as

$$\Delta H(r) = \frac{1}{W}\int_{-H/2}^{H/2} q''(r,z)\,dz = \frac{2HA}{\pi W} J_o\left(\frac{2.405r}{R}\right) \qquad (12\text{-}168)$$

or

$$\Delta\overline{H} = \frac{1}{\pi R^2}\int_0^R \Delta H(r)\,2\pi r\,dr = .862\frac{HA}{\pi W} \Rightarrow F_{\Delta H} = \frac{\Delta H_{max}}{\Delta\overline{H}} = 2.32 \qquad (12\text{-}169)$$

A more detailed example of enthalpy hot channel factors for a typical PWR are given below

Engineering Hot Channel Factors

Enthalpy Rise:

Inlet plenum sub-factor	1.03
Flow redistribution sub-factor	1.03
Flow mixing sub-factor	.95
Statistical factors	1.08
$F_{\Delta H}$ Total	1.09

The third hot channel factor frequently introduced is that characterizing the clad surface temperature

$$F_A = \frac{(T_{clad} - T_{coolant})_{max}}{(T_{clad} - T_{coolant})_{ave}} \qquad (12\text{-}170)$$

Actually, this factor is usually inconsequential in LWR's in which nucleate boiling keeps the clad surface temperature quite close to the coolant temperature. However it can be of more significance in HTGR's and LMFBR's in which the temperature from the clad surface to the coolant is much larger.

B. Determination of Reactor Core Size

It is instructive to examine how the thermal design influences the determination of the reactor core size. One usually proceeds in several steps:

(i) One first determines the various hot channel factors characterizing the core, using both computer codes describing the core neutronics and thermal hydraulic behavior, as well as experience from earlier designs.

(ii) Next, one determines the maximum acceptable power level in the hot channel, taking into account both steady state and transient operating conditions.

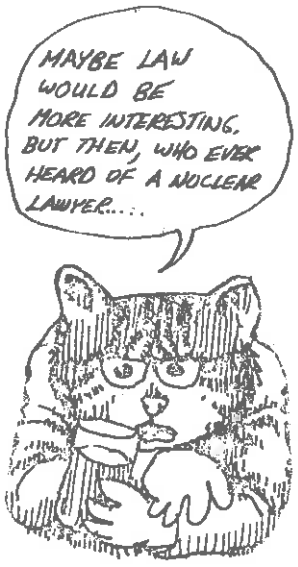

(iii) Using the hot channel factors and core performance limitations, one can now determine the average linear power density, outlet coolant temperature, average pressure drops, and so on. These can then be used to compute the core volume as

$$\text{Core volume} = \frac{\text{Core thermal power level}}{q'} \times \frac{\text{channel volume}}{\text{fuel rod length}} \quad (12\text{-}171)$$

C. Thermal-Hydraulic Design Codes

A variety of computer codes have been developed to analyze the thermal hydraulic behavior of nuclear reactor cores. In order to illustrate such models, we will consider only a very simple code designed to perform a single channel thermal-hydraulic analysis on the hot channel of a light water moderated core.

Problem geometry: Fuel: metal clad oxide rods
pellet diameter
clad outside diameter
clad thickness

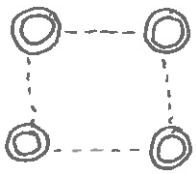

Coolant channel: square or triangular pitch

Assumptions: 1.) constant coolant flow in each channel
2.) same axial power shape in all channels
3.) no pressure drop in active channel due to spacer grids

Calculational sequence:

Divide active channel into equal length segments. Assume uniform power generation in each segment:

$$q'(z) = \frac{\text{Power/rod}}{\text{rod length}} \times \text{shape factor}$$

$$\text{shape factor} = \begin{cases} \sin \pi z/L \\ \frac{L-z}{L} \sin \pi z/L \quad \text{(bottom peaked)} \\ z/L \sin \pi z/L \quad \text{(top peaked)} \\ \text{pointwise} \quad \text{(arbitrary)} \end{cases} \qquad (12\text{-}172)$$

in an increment, i

$$q_i = \text{power input in length } \Delta z = \int_{z_{i-1}}^{z_i} q(z)\, dz \qquad (12\text{-}173)$$

(i) Enthalpy calculation

$$h_i = h_{i-1} + \frac{q_i}{w}, \quad h_0 = h_{inlet} \qquad (12\text{-}174)$$

The physical data for the coolant is stored in tables as a function of pressure and temperature. Intermediate values obtained by interpolation. Then coolant temperature is determined by

$$T_{fl_i} = f(h_i, p) \qquad (12\text{-}175)$$

Clad temperature is given by

$$T_{cl_i} = T_{fl_i} + \frac{q_i/\Delta z}{\pi D} \frac{1}{h_s} \qquad \text{forced convection}$$

or

$$T_{cl_i} = T_{sat} + 1.9\, e^{-p/900} \left(\frac{q''_i}{10^6}\right)^{1/4} \qquad \text{Jens-Lottes} \tag{12-176}$$

Fuel surface temperature by

$$T_{s_i} = T_{cl_i} + \frac{q_i/\Delta z}{\pi D}\left[\frac{t_c}{k_c} + \frac{1}{h_g}\right] \tag{12-177}$$

Fuel centerline temperature as

$$T_{\ell} = T_{s_i} + \frac{q_i/\Delta z}{4\pi k_f} \tag{12-178}$$

(ii) Pressure calculations:

$$p_i = p_o - \Delta p_{AB} + \Delta p_{OB} + \sum_{i=1}^{I} \Delta p_i$$

$$\Delta p_i = f_i \frac{\Delta z}{D} \frac{G^2}{2g_c \rho} - \rho \Delta z - p_{acc} \tag{12-179}$$

Here, f_i accounts for flow regime.

CHAPTER 13: NUCLEAR ANALYSIS OF REACTOR CORES

I. INTRODUCTORY REMARKS

A. An Overview of Nuclear Core Analysis

In this chapter we will consider in some detail the application of the concepts and methods developed in the first ten chapters of this text to the neutronic analysis of nuclear reactor cores. Our primary concern will be with the study of static calculations of the core power distribution and with the time-dependent analysis of fuel depletion and isotope buildup. Such calculations interact to a very considerable degree with other facets of the core analysis--particularly those involving thermal-hydraulic design and the economics of electrical power generation.

In fact, the predicted nuclear behavior of the core frequently serves as the input to other aspects of core design. For example, the determination of the neutron flux in the core implies the core power distribution which is necessary for thermal-hydraulic analysis, fuel depletion studies, and the optimization of plant economic parameters:

There will of course be considerable feedback from these latter design functions to the nuclear core analysis, since they determine core composition.

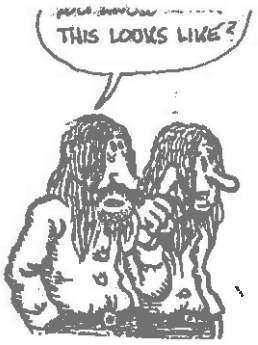

It is possible to distinguish three types of nuclear core analysis:

(i) Calculation of the core power distribution:

The calculation of the core multiplication and flux or power distribution is, of course, the most common type of analysis performed in nuclear core studies. This explains our preoccupation with this subject during the earlier chapters of this text. This calculation depends sensitively upon core enrichment, moderator-to-fuel ratio, core geometry, the location and types of reactivity control, fuel element design, and so on. The core power density will, of course, depend upon both space and time (because of fuel burnup and isotope production over core life).

We have seen that the parameters of most interest to the core thermal designer are the nuclear hot channel factors (the "power peaking factors"), F_R^N and F_z^N, which along with the axial core power profile, allow the determination of whether the thermal limitations on core performance will be exceeded by a given core design. But, as we will see later in this chapter, there is a strong feedback from the thermal analysis, since the core temperature will strongly affect coolant density and resonance absorption, which, in turn, will affect reactivity.

(ii) Reactivity and control analyses:

A variety of mechanisms are used to control reactivity in a nuclear reactor. These include moveable absorbers, fixed or burnable poisons in the core, and absorbers dissolved in the reactor primary coolant. It is important to study how such control elements interact with the nuclear behavior of the core, both in static and dynamic situations. We will consider this aspect of reactor core analysis in some detail in the next chapter.

(iii) Fuel depletion analysis:

The calculation of the core multiplication and power distribution must be made many times over the operating lifetime of the core, since as power is produced, fuel is depleted and isotopes are produced either directly by fission or by neutron capture. The study of the interaction of the core power distribution with the time dependent production or depletion of nuclei in the core is known as depletion or burnup analysis. It is perhaps the most time-consuming and expensive aspect of nuclear reactor analysis--and also perhaps the most important (aside from reactor safety analysis) since it will determine the economic performance of the nuclear reactor. We will consider this subject in detail in the last section of this chapter, and then we will imbed it within the more general topic of nuclear fuel management in Chapter 16.

B. Calculational Models Used in Nuclear Core Analysis

We have already given an overview of the various components of the models used to analyze core neutronic behavior. However, it is useful to review these components by considering in more detail a typical code package used to determine core static power distributions and fuel depletion. To be specific, we will outline the component modules of code packages used for the neutronic and depletion analysis of light water reactors (such as LEØPARD, LASER, or FLARE). The differences which appear in code packages used for comparable analysis of HTGR's and LMFBR's will be discussed in later sections of this chapter.

Such a code package might consist of six major code modules, each of which is responsible for a particular aspect of the core analysis:

(i) Macroscopic cross section module

One of the most important aspects of calculations based upon the multigroup treatment of the neutron energy dependence (as is essentially all nuclear design) is the generation of few group constants. As we have seen, such group constants are formed by averaging the microscopic cross section information obtained from evaluated data sets such as ENDF/B over not only a neutron energy spectrum hopefully characterizing that in the reactor core of interest, but averaging these cross sections as well over the detailed spatial dependence of the flux in a unit fuel cell in order to account for heterogeneous effects (such as self-shielding). As input, such modules require the number densities characterizing the materials in the fuel cell to be analyzed. The coolant density and average moderator, structure, and fuel temperatures are provided from a thermal hydraulic module while the fuel density (as well as fission product densities) are provided by the depletion module, while the densities of other materials such as structure are provided by input specifications.

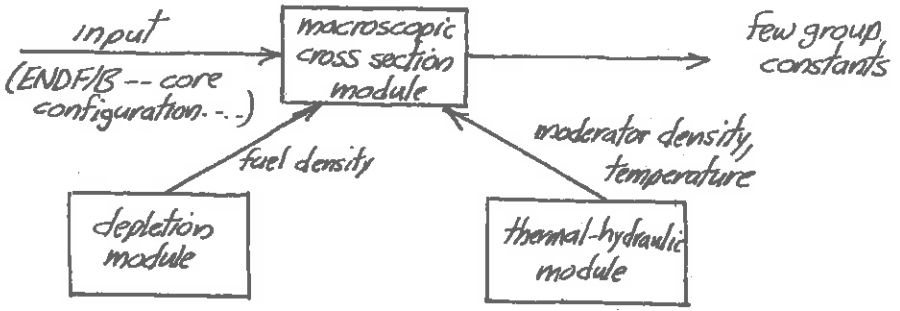

The energy-averaged, self-shielded microscopic group constants are then determined either by performing fast and thermal spectrum calculations for the fuel cell of the specified composition, or by computing a small number of descriptive parameters which can then be used to obtain the

microscopic group constants from suitable tables which have been constructed for the reactor core of interest. [The business of group constant parameterization is a very useful and important topic in depletion calculations because of the large number of times such group constants must be generated over core life. We will return to consider it in more detail later in this chapter.]

Such group constants must be generated for each region of the core in which the composition is different. One must account as well for the contributions of fission products such as xenon and samarium and also for control absorption which might be present in the cell of interest. As we will see in Chapter 14, the effect of control elements or burnable or soluble poisons in the cell are usually included by generating effective absorption cross sections characterizing the control absorber and then adding these to the absorption group constant characterizing the cell. These effective control cross sections can also frequently be parameterized at considerable computational savings.

(ii) Flux-power module

At the heart of the neutronics code package is the module which solves the multigroup diffusion equations to determine the flux and power distribution in the core as well as the core multiplication. We will examine this particular module in some detail in the next section since the calculation of the power distribution in a realistic reactor core can be an extremely complicated problem. We will examine two different approaches to this calculation: the first based upon the conventional finite-difference solution of the multigroup diffusion equations, and the second based upon so-called nodal methods which decompose the

core into "node cells" and then calculate only the average power or flux for each of these cells. The latter scheme is particularly useful when information is required about the 3-dimensional flux distribution in the core, but a direct finite difference solution of the multigroup diffusion equations would be prohibitively expensive.

(iii) Control adjustment module

The control adjustment module takes the core multiplication calculated by the flux-power module and estimates the amount of control insertion or withdrawal necessary to return the reaction to a critical state. In determining how to adjust the control reactivity (e.g., moveable rods or chemical shim), the control module may be guided by a prespecified control management scheme. It then returns the effective control group constants for the new control pattern to the macroscopic cross section module.

(iv) Depletion module

The depletion module solves the rate equations describing the isotopic changes in core composition during reactor operation. Such equations must account for fuel burnup, the conversion of fertile to fissile material, and the buildup of nonsaturating fission products. The input to the depletion module is the flux profile provided by the flux-power module. The number densities calculated by this module must then be returned to the macroscopic cross section module.

(v) Thermal hydraulic module

The flux-power module provides the power distribution required by the thermal-hydraulic module which then calculates core temperatures and heat fluxes in order to make certain that the thermal limitations

placed on core performance are not exceeded. The core temperatures and coolant density profiles are returned to the macroscopic cross section module. As we will see in the next section, usually source iteration between the thermal-hydraulic and nuclear core analysis is necessary.

(vi) Economics module

Such code packages will frequently also contain a module which uses information from the depletion analysis to determine the cost of the power generation (i.e., fuel costs) for the period under study. Such calculations will be discussed in Chapter 16.

A schematic diagram of the various modules of such a code package and their interaction is shown in Figure 13-1.

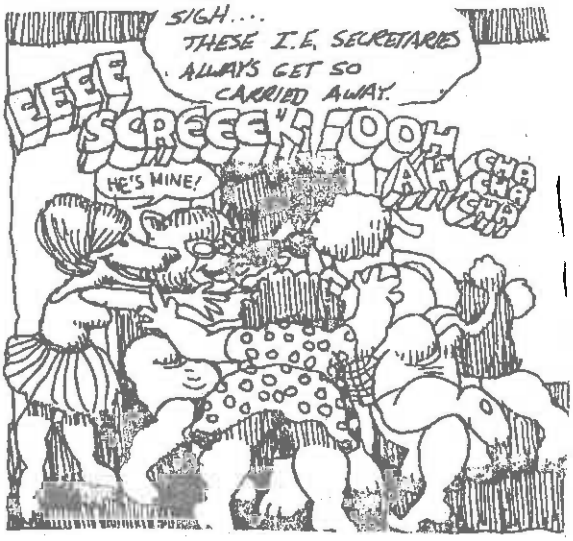

II. THE CALCULATION OF CORE POWER DISTRIBUTIONS

A. Multigroup Diffusion Methods

Of central concern in reactor core analysis is the calculation of the neutron flux and power distribution in the core. The power distribution is essential for the subsequent thermal hydraulic analysis of the core. In particular, we have seen that the nuclear hot channel factors and axial power profile determine how close the core performance approaches thermal design limitations. The neutron flux distribution is necessary for the determination of fuel burnup and isotope buildup. The reactor designer would like to utilize information provided by such core analysis to achieve a flat power profile (desirable from a thermal standpoint) while providing sufficient excess reactivity to yield long core lifetimes and hence high fuel exposure (desirable from an economic standpoint) while maintaining adequate reactor control requirements for safe reactor operation.

The calculation of the global power distribution is most commonly accomplished by solving the few group diffusion equations

$$-\nabla\cdot D_g(\vec{r})\nabla\phi_g(\vec{r}) + \left[\Sigma_{a_g}(\vec{r})+\Sigma_{R_g}(\vec{r})\right]\phi_g(\vec{r}) = \sum_{g'=1}^{g-1}\Sigma_{s_{g'g}}\phi_{g'}(\vec{r}) + \frac{1}{k}\chi_g\sum_{g'=1}^{G}\nu_{g'}\Sigma_{f_{g'}}\phi_{g'}(\vec{r}) \tag{13-1}$$

These equations are solved by using finite difference methods to discretize the spatial variable and then following the usual inner-outer iteration strategy to solve for the criticality eigenvalue k and the corresponding flux $\phi_g(\vec{r})$. To be more precise, the reactor core is broken up into a

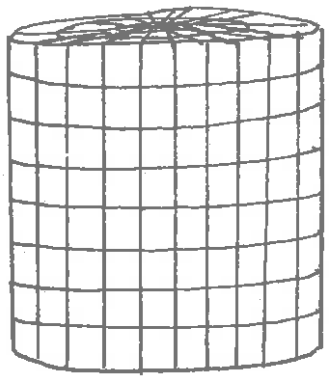

spatial grid or mesh--say with M mesh cells. Then the multigroup diffusion equation is integrated over a typical cell, and standard sum and difference formulas are used to represent the terms in the equation. Hence the multigroup diffusion equations are replaced by an MxG set of algebraic equations--that is, an (MxG) dimension matrix eigenvalue problem

$$\underline{\underline{M}}\,\underline{\phi} = \frac{1}{k}\,\underline{\underline{F}}\,\underline{\phi}$$

The elements of the matrices $\underline{\underline{M}}$ and $\underline{\underline{F}}$ are the few group constants supplied by a macroscopic cross section module. The matrix eigenvalue problem can then be solved by standard power iteration methods (usually accelerated by source extrapolation). (Recall the discussion of Chapter 7).

The complexity of such calculations depend sensitively upon the nature of the design information required. During the final phases of a core design, one may be required to perform very detailed 2-D or 3-D calculations in which one or more mesh points are assigned to each fuel element in the core (some 40,000 elements in a modern PWR), coupled with a correspondingly detailed axial mesh. Codes available for such multigroup, multidimensional diffusion calculations such as the PDQ series developed at BAPL and KAPL are extremely expensive to run.

For core lifetime studies in which the power and flux distributions must be calculated at many time steps during core life, one is usually forced to use either simpler treatments of the core (e.g., one-dimensional

(e.g., LASER) or even zero-dimensional (e.g., LEØPARD) models . Unfortunately, the detailed study of core depletion usually requires a 3-D analysis. For large reactors, even crude 3-D studies would require on the order of 100x100x100 mesh points for each group--and hence incur considerable computer storage and calculational running time expenses.

For this reason, there has been strong motivation to develop alternatives to the standard finite difference treatment of the multigroup diffusion equations. It is desirable to discuss two of the more popular of such alternative schemes for calculating core power distributions: nodal methods and flux synthesis.

B. Nodal Methods

We desire a scheme for determining the 3-D core power distribution which avoids the prohibitive storage and execution time requirements of the finite difference treatment of the multigroup diffusion equations. Such a scheme was first developed for the treatment of BWR cores and implemented in the FLARE code. The general idea is to decompose the reactor into relatively large volumes or "nodes cells" in which the composition and fluxes are assumed uniform. One then attempts to determine the coupling coefficients characterizing node cell to node cell leakage, and then to determine the nodal fluxes themselves.

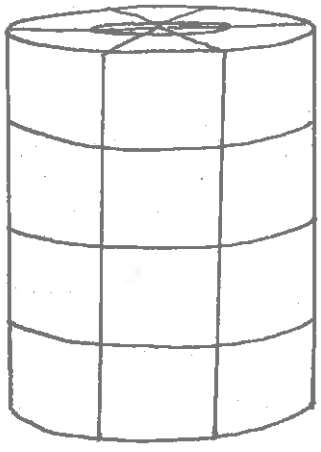

To develop these equations, first rewrite the multigroup diffusion equations as

$$-\nabla \cdot D_g \nabla \phi_g + \Sigma_{tg} \phi_g = S_g \tag{13-2}$$

where the effective source term S_g is given by

$$S_g \equiv \sum_{g'=1}^{g-1} \Sigma_{sg'g} \phi_{g'} + \frac{1}{k} \chi_g \sum_{g'=1}^{G} \nu_{g'} \Sigma_{fg'} \phi_{g'} \tag{13-3}$$

Now before introducing our nodal mesh, we first rewrite Eq. (13-2) by formally solving for $\phi_g(\vec{r})$

$$\phi_g(\vec{r}) = \int_V d^3r' \, G_g(\vec{r},\vec{r}') S_g(\vec{r}') \tag{13-4}$$

in terms of the Green's function $G_g(\vec{r},\vec{r}')$ satisfying

$$-\nabla \cdot D_g \nabla G_g + \Sigma_{tg} G_g(\vec{r},\vec{r}') = \delta(\vec{r}-\vec{r}') \tag{13-5}$$

$g = 1, \ldots, G$

[Note that $G_g(\vec{r},\vec{r}')$ ≡ flux at $\vec{r}$ due to unit source at $\vec{r}'$ (all in group g)

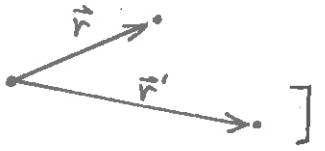

]

We now introduce the principal aspect of nodal methods by dividing the reactor core into N node cells and integrating Eq. (13-4) over the volume V_n of the n'th cell to obtain

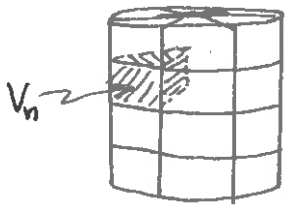

$$\phi_{gn} = \sum_{n'} K_{gnn'} S_{gn'} \tag{13-6}$$

where we define the nodal fluxes ϕ_{gn} and sources S_{gn}, as spatial averages over the cell volumes

$$\phi_{gn} \equiv \frac{1}{V_n} \int_{V_n} d^3r \; \phi_g(\vec{r}) \tag{13-7}$$

$$S_{gn} \equiv \frac{1}{V_n} \int_{V_n} d^3r \; S_g(\vec{r}) \tag{13-8}$$

while the node-to-node transfer kernel is given (formally at least) by

$$K_{gn'n} = \frac{\frac{1}{V_n} \int_{V_n} d^3r' \int_{V_{n'}} d^3r \; G_g(\vec{r},\vec{r}') S_g(\vec{r}')}{\frac{1}{V_{n'}} \int_{V_{n'}} d^3r' \; S_g(\vec{r}')} \tag{13-9}$$

Note that $K_{gnn'}$ can be interpreted as the probability of a neutron born in group g in cell n' diffusing to cell n. Unfortunately, as it stands, the definition of $K_{gnn'}$ requires a knowledge of the source $S_g(\vec{r})$--which in turn depends upon the flux $\phi_g(\vec{r})$. Our success in utilizing nodal methods will hinge upon our ability to guess $K_{gnn'}$.

But enough of such worries for the moment. Suppose we can somehow determine $K_{gnn'}$. Then we must solve a system of equations represented by

$$\underline{\phi} = \underline{\underline{K}} \left[\underline{\underline{S}} + \frac{1}{k} \underline{\underline{F}} \right] \underline{\phi} \tag{13-10}$$

Once again, we can solve this by the standard power method--but unlike the finite difference approach which yields

$$\underline{\underline{M}} \, \underline{\phi} = \frac{1}{k} \underline{\underline{F}} \, \underline{\phi} \tag{13-11}$$

an iterative inversion of $\underline{\underline{M}}$ (i.e., the inner iterations) is no longer required. By assuming a knowledge of $\underline{\underline{K}}$--and hence $G_g(\vec{r},\vec{r}')$,--we have bypassed this step.

Of course, from a formal point of view, as the number of nodal cells N approaches the number of mesh cells M, the nodal method becomes equivalent to the finite difference shceme--and hence loses any calculational advantages. The real power of the nodal approach is realized only when the number of the node cells N is small, since then the cells are large enough that they become only coupled via neutron leakage to nearby cells--that is, the transfer matrix $\underline{\underline{K}}$ is sparse. But choosing large node cells places the burden of the calculational effort on an estimate of the transfer kernels $K_{gnn'}$.

The determination of this kernel is usually accomplished in a most empirical fashion (a nice way of saying it is fudged). Note that

$$\Sigma_{a_n} K_{nn'} \equiv \text{rate of neutron absorption in node cell n due to a unit source in node cell n'} \tag{13-12}$$

Hence, one scheme to determine $K_{nn'}$ is to set up a prototype problem in which a source is located in a region n', and one then calculates the absorption rate in another region n. Typically, one assumes a one dimensional geometry, and then solves the one speed neutron diffusion equation for very simple source shapes. For example, the absorption rate resulting from a flat source in a slab geometry as shown is

$$\Sigma_{an} K_{nn'} = \frac{\Sigma_{an}}{\frac{\Delta}{L_{n'}}\left[\left(\frac{1+e^{-\Delta/L_{n'}}}{1-e^{-\Delta/L_{n'}}}\right)+\frac{L_{n'}\Sigma_{an'}}{L_n\Sigma_{an}}\right]} \qquad (13\text{-}13)$$

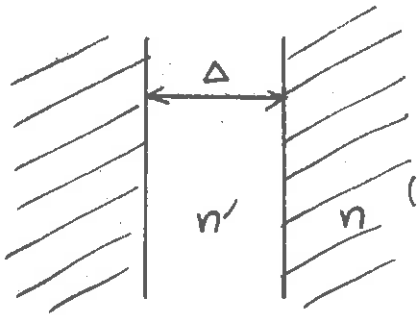

where the subscripts n' and n refer to the source and the absorption regions, respectively. Other possible source shapes might be exponential or parabolic.

In any event, the usual scheme is to blend several of these kernels together with arbitrary coefficients--e.g.,

$$K_{nn'} = \alpha K^{I}_{nn'} + \beta K^{II}_{nn'} + \gamma K^{III}_{nn'} + \cdots \qquad (13\text{-}14)$$

One can also superimpose one-dimensional forms to synthesize three-dimensional kernels. The blending coefficients are then determined by comparison with various benchmark calculations (and lots of experience, fiddling, and fudging). [It should be mentioned that there have been numerous schemes proposed for more rigorous calculations of $K_{gnn'}$, such as those utilizing variational methods.]

C. Synthesis Methods

Spatial flux synthesis is a technique whereby one or two-dimensional diffusion calculations are combined to yield a representation of a three-dimensional flux distribution. There are a variety of techniques, both heuristic and formal, for blending such lower dimensional calculations together. For purposes of illustration, let us first consider a simple example:

EXAMPLE: We will illustrate how one-dimensional calculations can be utilized to analyze a zone-loaded cylindrical core with, say, 3 radial zones and 2 axial zones. (ℓ = radial zone, m = axial zone).

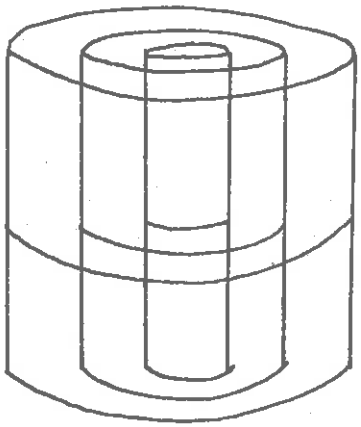

One begins by assuming an axial profile of the form $\cos B_z z$, where the axial buckling B_z^2 must initially be guessed. For each axial zone m one then has a flux

$$\phi_g^m(\vec{r}) = \phi_g^m(r)\cos B_z z \qquad (13\text{-}15)$$

The diffusion term in the multigroup diffusion equations then becomes

$$\nabla \cdot D_g^m \nabla \phi_g^m = \left[\frac{1}{r}\frac{\partial}{\partial r} D_g^m(r) \frac{\partial \phi_g^m}{\partial r} - D_g^m(r) B_z^2 \phi_g^m(r)\right]\cos B_z z \qquad (13\text{-}16)$$

Hence we arrive at a one-dimensional problem for the radial flux profile

$$-\frac{1}{r}\frac{d}{dr} D_g^m(r) \frac{d\phi_g^m}{dr} + \left[\Sigma_{tg}^m(r) + D_g^m(r) B_z^2\right]\phi_g^m(r) = \sum_{g'=1}^{g-1} \Sigma_{sg'g}^m \phi_{g'}^m + \frac{1}{k}\chi_g \sum_{g'=1}^{G} \nu_{g'} \Sigma_{fg'}^m \phi_{g'}^m \qquad (13\text{-}17)$$

which is characterized by an effective total cross section

$$\Sigma_{effg}^m \equiv \Sigma_{tg}^m + D_g^m B_z^2 \qquad (13\text{-}18)$$

(here, $D_g^m B_z^2$ represents removal of neutrons due to axial diffusion).

We can now solve this 1-D problem to determine the radial flux profile ϕ_g^m, and from this calculate the radial buckling for each region (ℓ, m) as

$$B_{r_{\ell m}}^2 = \frac{\sum_g \int_{r_{\ell-1}}^{r_\ell} \nabla^2 \phi_g^m(r)\, dr}{\sum_g \int_{r_{\ell-1}}^{r_\ell} \phi_g^m(r)\, dr} \tag{13-19}$$

An analogous approach can be taken to determine the axial profile. That is, one solves the axial 1-D diffusion equations assuming an effective cross section

$$\Sigma_{eff_g} = \Sigma_{t_g}^\ell + D_g^\ell B_{r_\ell}^2(z) \tag{13-20}$$

where

$$B_{r_\ell}^2(z) = B_{r_{\ell m}}^2 \quad \text{for } z \text{ in region } m. \tag{13-21}$$

Having determined this axial profile, one can then calculate an axial buckling $B_{z_{\ell m}}^2$ for each region. This can be used to re-adjust the effective cross section in the radial MGD equations, and hence allow one to determine a new radial profile. By iterating back and forth between 1-D radial and axial profiles, one can eventually converge on a 3-D solution in each region of the form

$$\phi_g^{\ell m}(\vec{r}) = \phi_g^{\ell m}(r)\, \psi_g^{\ell m}(z) \tag{13-22}$$

To the extent that the flux in each region can be approximated as a separable function of r and z, this scheme will yield adequate results.

One can generalize this scheme by alternating back and forth between a 2-D radial calculation and a 1-D axial calculation. In single channel synthesis methods, one performs radial calculations at a relatively small number of axial positions, and then such radial fluxes are superimposed with axial position dependent weighting coefficients to synthesize the overall 3-D flux profile in the core. One can extend such schemes by performing axial calculations as well to determine the appropriate choice of blending coefficients (multichannel synthesis).

The general synthesis process of building up a complicated solution out of simpler, but not elementary, component parts has received a great deal of attention in other aspects of core analysis. There are, for example, problems in which significant details of the flux distribution can be predicted in advance, and in these situations the full calculation of the flux using standard multigroup finite difference equations generates (at great expense) large amounts of redundant information. For example, an accurate calculation of the flux distribution in a fast reactor using the finite difference multigroup equations would require the use of a great many groups (20 to 30) to treat the energy dependence at each spatial point, when in fact it is known that the energy spectrum shifts fairly smoothly in space from one typical mode to another. The actual "information content" consists of these modal spectra and their relative strengths at each point, so effort is wasted in the finding of the multigroup solution.

Synthesis techniques can be used to attack such a problem. A synthesis typically involves a series expansion in which each term is the product of a known function of a few of the free variables multiplied by an unknown function not depending on those variables. Both the spherical harmonics expansion of the angular flux and the multigroup representation fit this description; generally, however, the term "synthesis" is reserved for short series in which the known functions are detailed and tailored to the particular problem, rather than large expansions in relatively simple base functions.

The accuracy of a particular synthesis approximation will depend not only on the choice of the expansion functions, but also on the method used to find the expansion coefficients. Occasionally orthogonality properties can be used, but usually some less direct procedure is necessary, such as a variational approximation technique.

Thus far we have confined our attention to synthesis in the spatial variables. But the energy variable as well is amenable to such a treatment. In the sense that the multigroup approximation is a synthesis method, synthesis of the energy dependence of the flux has been used for a long time. In the derivation of the multigroup equations it is implicitly assumed that the fine structure of the energy dependence is fairly constant over larger spatial regions, and that it is only necessary to compute scale factors to be applied to pre-calculated spectra for each disjoint energy group. This proves very successful in applications to thermal spectrum reactors, where indeed the domanant energy effect is the coupling of the neutron "birth" region through the resonance region to the thermal region, but it is not so useful in fast reactor analysis.

The weakness of the standard multigroup theory is not an inability to produce sufficiently accurate results; it is rather the inability to do this cheaply in situations when the details of the energy dependence cannot be assumed to be reasonably constant over large regions of space or when the details cannot be predicted over broad groups in energy. In the former situation, calculations must be performed carrying data for many regions (each with its own characteristic spectrum) (an expensive process). In the latter situation, calculations must be performed with a large number of groups (in order to resolve the unknown detail) (an even more expensive process).

To do a proper multigroup analysis of a fast reactor requires calculations in 20 to 30 groups because of the effects of the resonances in the fast region. The spatial variations of the flux, however, are fairly smooth because the long mean free paths of fast neutrons make fine structural detail "invisible". This effect compensates somewhat, but not entirely, for the greater number of energy variables (because the number of spatial variables can be reduced) but does not affect the fact that the spectrum is everywhere in transition, so that many material regions should be used. Using 20 groups makes a two-dimensional diffusion code expensive to run and makes three-dimensional analyses almost impossible.

Spectral synthesis involving the use of overlapping, rather than disjoint, energy expansion functions seems to hold out the promise of solving the space and energy fast flux problem without doing all of the (diffusion theory) work. The usual spectral synthesis equations are derived in the same way as the multigroup equations, i.e., by expanding

$$\phi(\vec{r},E) = \sum_m \psi_m(r)\chi_m(E) \qquad (13\text{-}23)$$

but with the difference that the $\chi_m(E)$ are functions of energy which span the whole energy range rather than discrete regions only. Thus the unknown space-dependent functions $\psi_m(\vec{r})$ now represent combining coefficients --relative proportions of the trial modes--rather than scale factors to be applied to each energy group.

The most important question about synthesis, whether it really is an accurate alternative to multigroup theory, seems to have been answered in the affirmative. Several different studies have shown that spectral synthesis approximations using three or four trial modes can achieve (except in occasional cases of anomalous failure) accuracies of a few tenths of a percent in criticality and reaction rate, provided that good flux trial modes and adjoint trial modes (weight functions) are used.

Despite the formal incentives for using synthesis and the demonstrations of its reasonable accuracy, this method has received only very limited application to practical problems of reactor analysis. The primary deterrent has been the occasional occurrence of "anomalous failures" of synthesis methods--cases in which the approximate solutions turn out to be extraordinarily poor. Examples of this have been reported for various group collapsing, and for spectral synthesis. The effect of these reports has been to scare off potential users of synthesis since it is hard to justify an element of risk when trying to solve genuine, practical problems.

This lack of confidence has been aggravated by the lack of any formal method of analysis which could identify the causes of the anomalies or predict their occurance. When using the finite difference multigroup approximation, one can rely on a large body of mathematical analysis giving assurance that iterations will converge, fluxes will be positive, eigenvalues will be real, etc. Unfortunately the synthesis approximation is not susceptible to similar mathematical analysis. The goal, after all, is to develop a method whereby detailed guesses at the solution of a particular problem can be incorporated into the approximation; but the formal equations for the remaining unknown functions thereby are written in terms of a large amount of unknown information (the detail guesses) about which any analysis must make the most conservative (worst) assumptions.

All this uncertainty would quickly be put out of mind if the spectral synthesis method proved to be significantly cheaper than the competing multigroup methods. A cheap calculation can be repeated or replaced if it turns out badly and furthermore allows the rapid accumulation of experience in how to avoid dangerous situations. Thus it has been disappointing to find that the spectral synthesis methods do not seem to achieve the savings implied by the fact that they require only about one-tenth as many unknowns as are required for the multigroup methods. The reason for this is that although the number of energy variables is reduced, the nature of the equations coupling them is made more complicated, and thus more effort is required to solve them. Comparisons of alternative solutions of a given problem have shown that the synthesis methods used required from one-sixth to one-half of the calculational

time required by multigroup programs. This is not a sufficient savings to justify the abandonment of the experience with and confidence in the finite difference multigroup diffusion methods.

The net evaluation of spectral synthesis has been that although it is useful, it will not suddenly supplant the more traditional methods. The reasons for this is not really due to the anomalies, since these occur very infrequently and are easy to recognize. The real resistance to synthesis is due to the lack of strong economic incentives (the investment in multigroup codes balances the savings of synthesis methods) and also a degree of "mental inertia"--unwillingness to abandon all the accumulated experience in preparing and analyzing multigroup diffusion models.

D. Parameterization of Few Group Constants

The group constants necessary for a multigroup diffusion calculation must be generated hundreds or perhaps even thousands of times in a core lifetime study. Not only must they be generated for each region (e.g., node cell) of the reactor core characterized by different composition, but as well they must be regenerated for each of these regions whenever the composition changes (e.g., via fuel burnup or moderator density changes). If detailed fast and thermal spectra were required for each change in composition, the computing costs for group constant generation would be formidable.

In practice, it is found that few group constants frequently depend on a relatively few parameters involving core temperatures and material densities. Hence it is far more efficient to construct tables of the values of the few group constants for several values of these parameters,

and then to use interpolation schemes to evaluate the group constants when necessary. To provide an illustration of how such a parameterization might work, we will give a very simple discussion of the generation of group constants for light water reactors within the MUFT-SØFØCATE approach.

1. Thermal Group Constant Parameterization

Recall that thermal group constants were defined as spectrum averages of the form

$$\overline{\sigma_x^j} = \frac{\int_0^{E_c} dE\, \phi(E)\, \sigma_x^j(E)}{\int_0^{E_c} dE\, \phi(E)} \qquad (13\text{-}24)$$

where E_c is the upper cutoff of the thermal group, $\phi(E)$ is the thermal spectrum, and σ_x^j is the microscopic cross section characterizing reactions of type x in materials j. The corresponding macroscopic cross section would then be calculated as

$$\Sigma_x = \sum_j N_j\, \overline{\sigma_x^j} \qquad (13\text{-}25)$$

In the SØFØCATE approach, the thermal spectrum is obtained by solving the Wigner-Wilkins equation characterizing a free proton gas. For $1/v$-absorption, this equation can be cast in the form (recall Section 9-3)

$$-\frac{d}{dx}\left\{\frac{1}{P(x)}\frac{d}{dx}\left(V(x)+\Gamma\right)\nu(x)\right\}+\left\{W(x)\left(V(x)+\Gamma\right)-\frac{4}{\sqrt{\pi}}\right\}\nu(x)=0 \qquad (13\text{-}26)$$

Here, we recall

$$\Gamma = \frac{\Sigma_a(kT)}{\xi \Sigma_s}$$

It should be noted that the only parameters which enter this equation are the temperature T and the ratio of absorption to scattering Γ. Hence we might expect that the thermal group constants generated by a SØFØCATE like code will depend only on the parameters Γ and T. This dependence is in fact rather smoothly varying, as shown, for example, in Figures (13-2) and (13-3) which show the dependence of $\overline{\sigma_a}^{25}$ upon Γ and T. Actually such behavior is also easily understood. If we model the thermal spectrum as a Maxwellian

$$\phi(E) = \phi_M(E, T_n) = \frac{E}{kT_n^2} e^{-E/kT_n} \qquad (13\text{-}27)$$

characterized by an effective neutron temperature

$$T_n = T(1+c\Gamma) \qquad (13\text{-}28)$$

then cross sections such as $\overline{\sigma_a}^{25}$ which are characterized by $1/v$ behavior yield a Γ dependence of the form

$$\overline{\sigma_a}^{25} \sim \frac{\sqrt{\pi}}{2} \frac{\sigma_a^{25}(kT)}{\sqrt{1+c\Gamma}} \qquad (13\text{-}29)$$

The temperature dependence is also easily explained by this model.

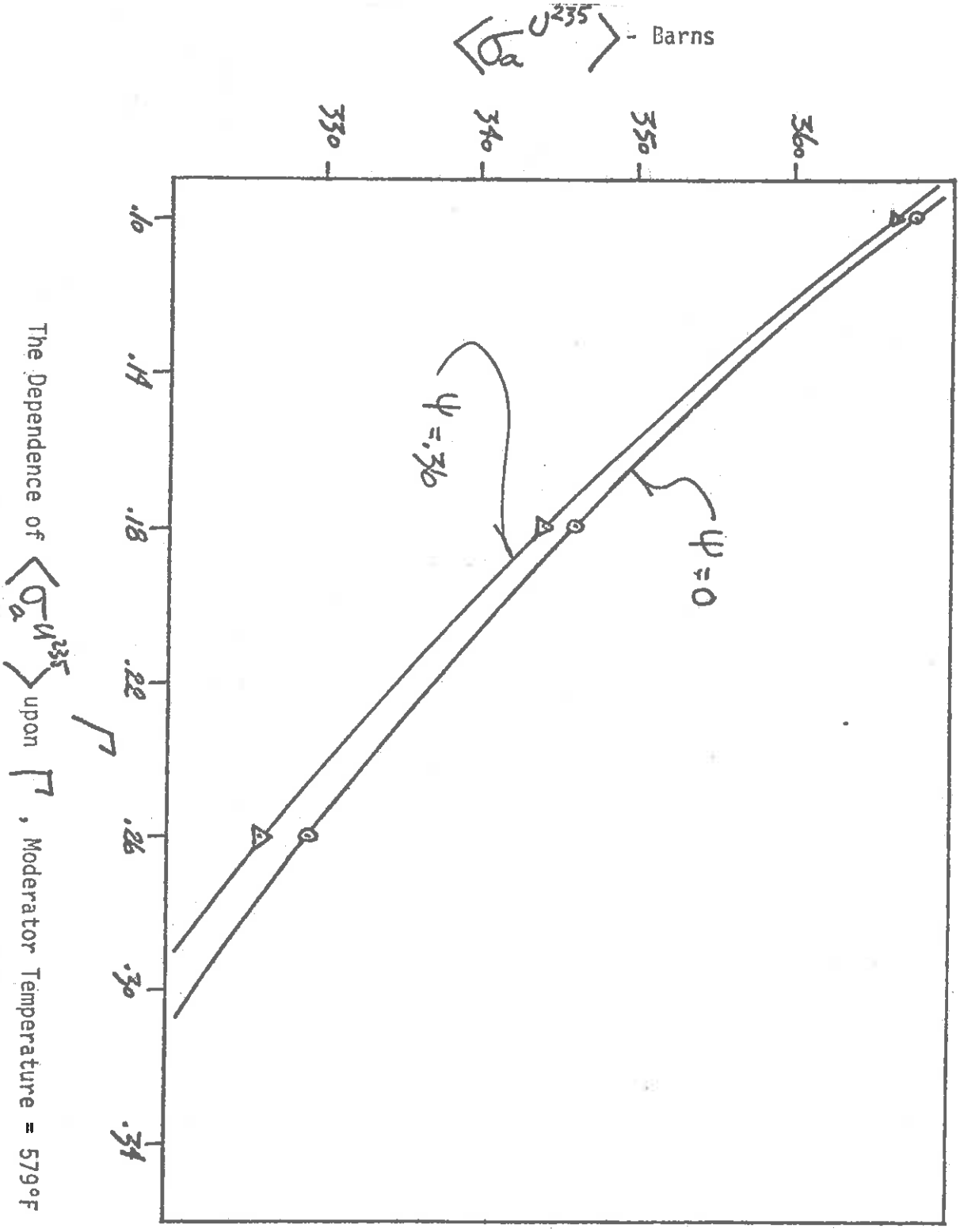

The Dependence of $\langle \sigma_a^{235} \rangle$ upon Γ, Moderator Temperature = 579°F

FIGURE 13-2

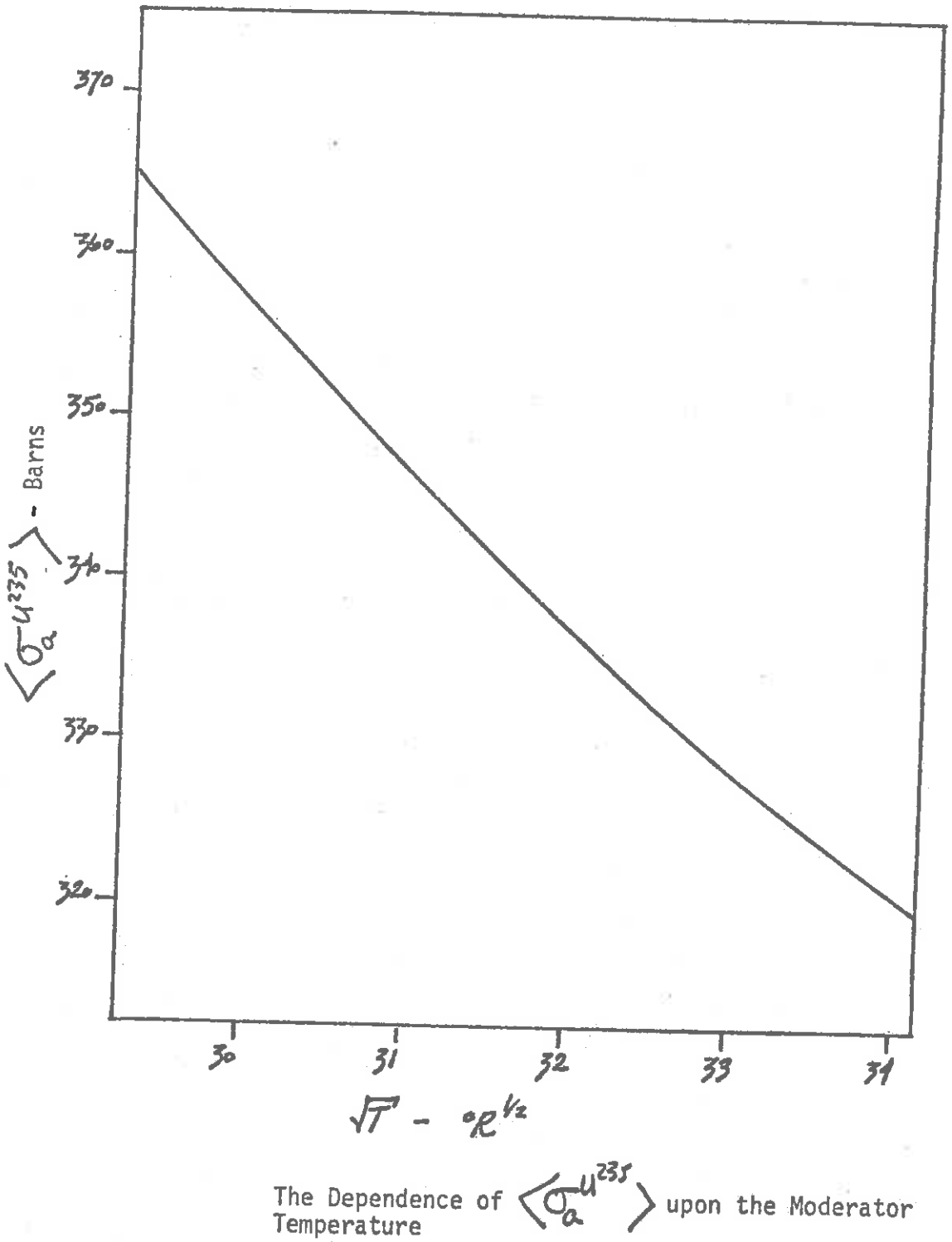

The Dependence of $\langle \sigma_a^{U^{235}} \rangle$ upon the Moderator Temperature

FIGURE 13-3

The Wigner-Wilkins equation can also be applied for non $^1/_v$-absorption. However the above two parameters will not suffice in this more general situation. This is particularly relevant to high burnup cores, since the appreciable amount of Pu^{239} in such cores is characterized by a highly non-$^1/_v$ behavior

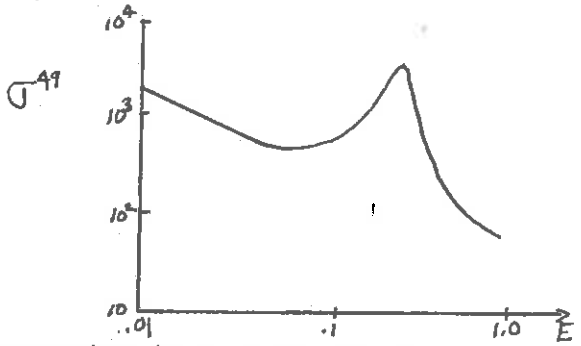

One possible parameter to account for the presence of Pu^{239} is

$$\Psi = \frac{\Sigma_a^{49}(kT)}{\Sigma_a(kT)} \qquad (13\text{-}30)$$

The dependence of group constants on this parameter is essentially linear, as shown in Figure (13-4) for $\overline{\sigma_a}^{25}$.

The above discussion suggests that it should be possible to construct three dimensional tables of thermal group constants dependent upon T, Γ, and Ψ. A macroscopic cross section module would then use data from thermal hydraulic and depletion modules to compute these parameters and then use the precalculated group constant tables, along with the appropriate interpolation schemes, to calculate the required thermal group constants.

2. Fast Spectrum Group Constant Parameterization

Recall that MUFT type calculations solve the exact slowing down equation for hydrogen coupled with the age or Goertzel - Greuling

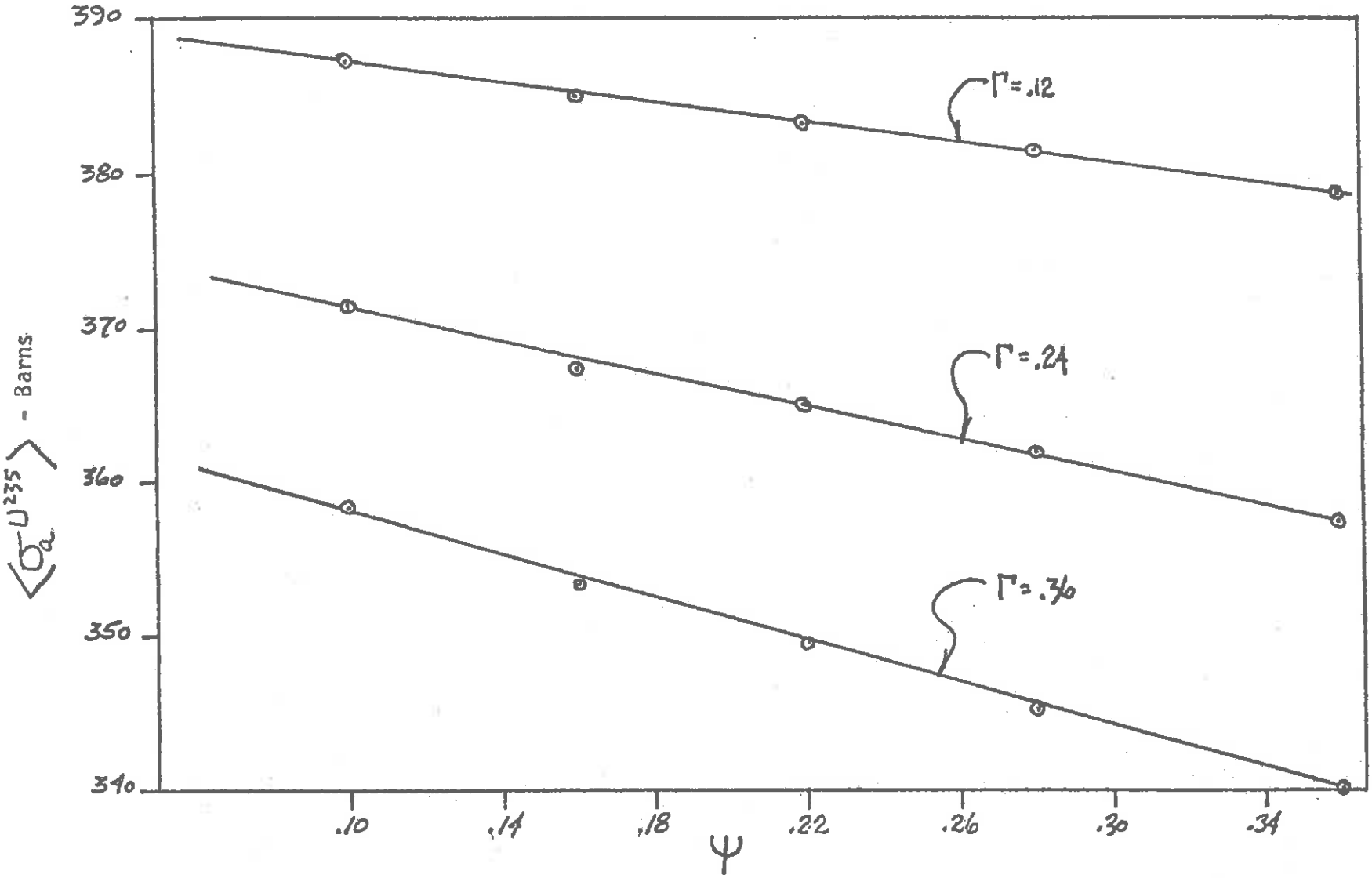

The Dependence of $\langle \sigma_a^{U^{235}} \rangle$ upon Ψ, Moderator Temperature = 545°F

FIGURE 13-4

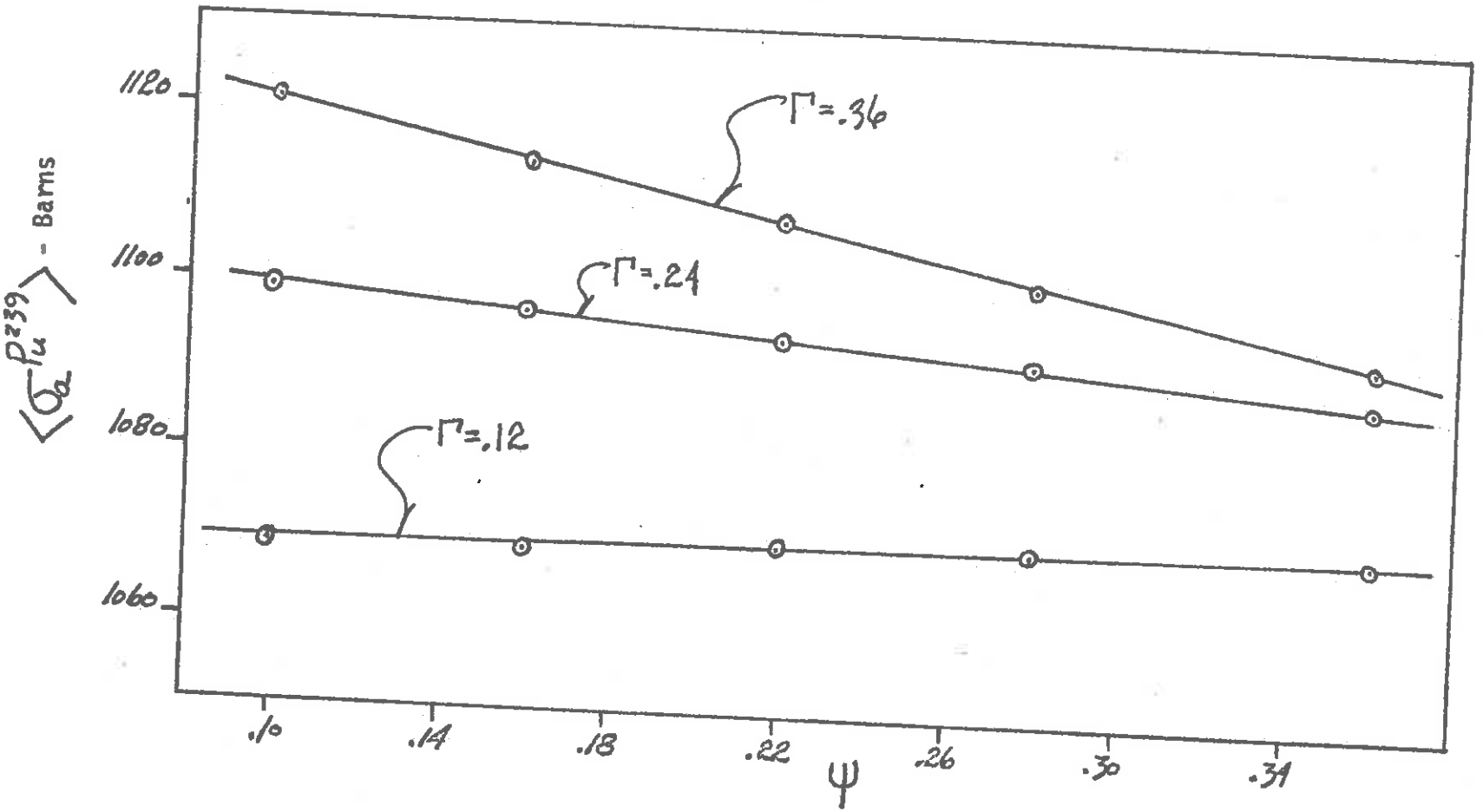

The Dependence of $\langle \sigma_a^{Pu^{239}} \rangle$ on Ψ, Moderator Temperature=545°F

FIGURE 13-4'

approximation for mass numbers A>1 to generate the fast spectrum. Inelastic scattering is treated by a direct micro-group approach, while resonance absorption is typically treated within the NR or NRIM approximations (with appropriate heterogeneous corrections).

Perhaps the key parameter of use in characterizing fast group constants is the ratio of moderator to fuel density. [One occasionally also uses the ratio of moderator volume to fuel volume--which gives essentially the same results.] Such a parameter characterizes the effectiveness of neutron moderation in the core. We have plotted the dependence of various fast group constants upon this ratio in Figure (13-5). Such a parameterization works quite well, provided the moderator densities are not too low.

Unfortunately, no comparable parameter exists for characterizing resonance integrals (aside from the fuel temperature). If such parameterizations are desired, it is usually necessary to rely upon various empirical correlations for the resonance integrals (such as those discussed in Chapter 10).

E. Thermal-Hydraulic Interaction With Neutronic Calculations

Water moderated reactors are characterized by a very strong coupling between coolant density and neutronic behavior. The presence of subcooled or bulk boiling in cooling channels gives rise to a large variation in coolant void fraction and hence density. Since most light water reactors are undermoderated, a local decrease in water density will cause a corresponding decrease in power density.

A similar effect can occur in LMFBR's, since a decrease in sodium density can lead to a spectrum hardening, hence a larger value of η, and

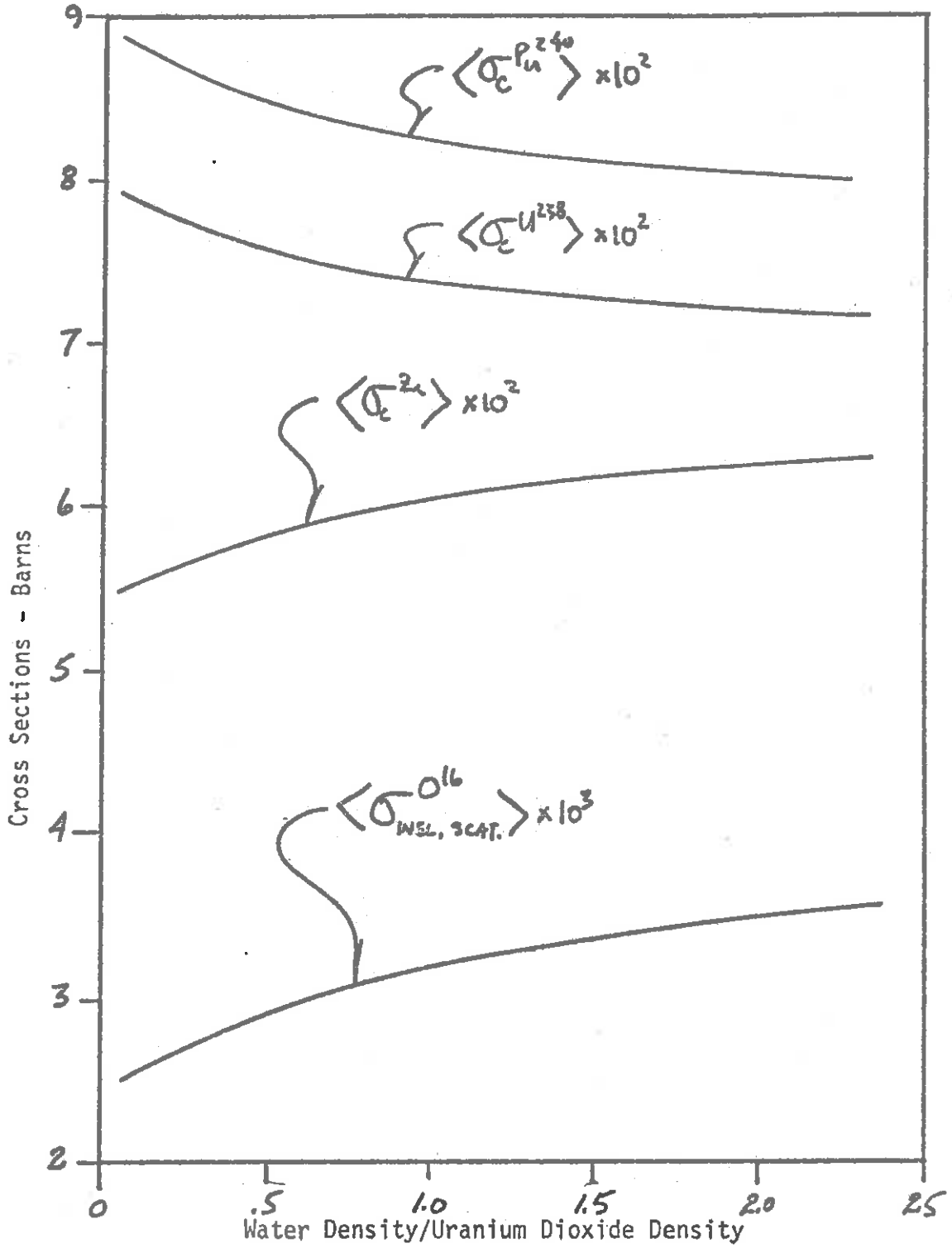

Group 1 Averaged Cross Sections

FIGURE 13-5

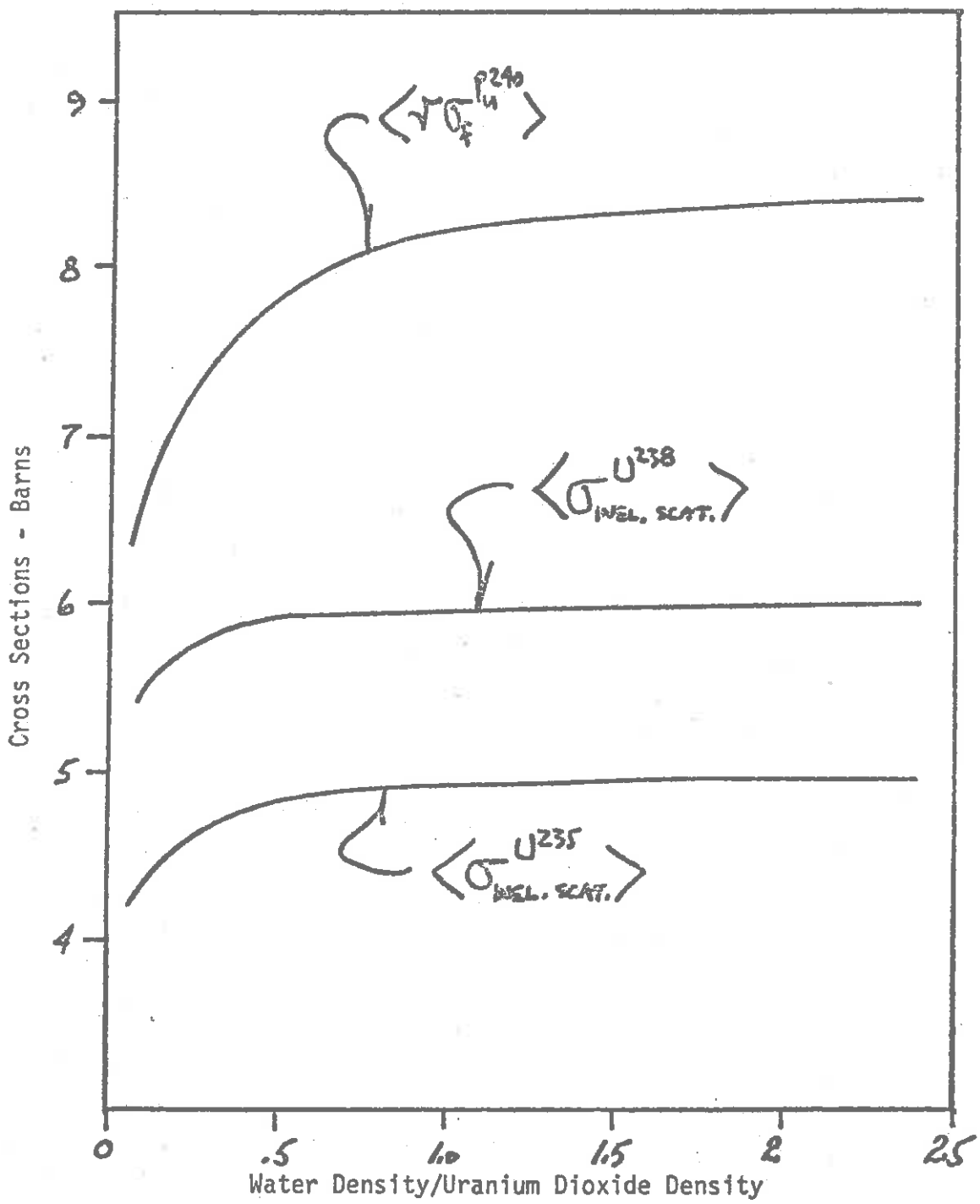

Group 2 Averaged Cross Sections

FIGURE 13-5'

hence power density increases (note this effect is in the opposite direction of coolant void reactivity effects in LWR's).

The coupling between coolant properties and core neutronic behavior is very much weaker in HTGR's--both because coolant phase change cannot occur, as well as because the coolant does not provide appreciable moderation (the graphite structure of the core serves this function).

To illustrate the interactions between thermal-hydraulic and neutronic calculations, let us consider a typical sequence of calculations in determining the power distribution in a PWR. The first step in such an analysis is for the nuclear designer to supply an approximate power distribution during core life, both under steady-state and transient operating conditions. These power distributions will determine the peak power that limits the reactor power output. The thermal designer needs as well information on the physical layout of the core (fuel element size, assembly geometry, etc.).

Using this information, the thermal analysis can then generate the core temperatures at various power levels, as well as the coolant void distributions including local boiling voids and bulk boiling voids.

Actually, this interaction is usually automated in most code packages, so that an iteration between neutronics and thermal hydraulics calculations is necessary

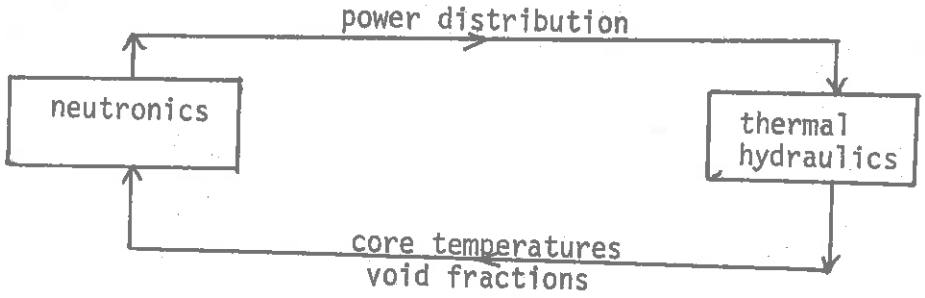

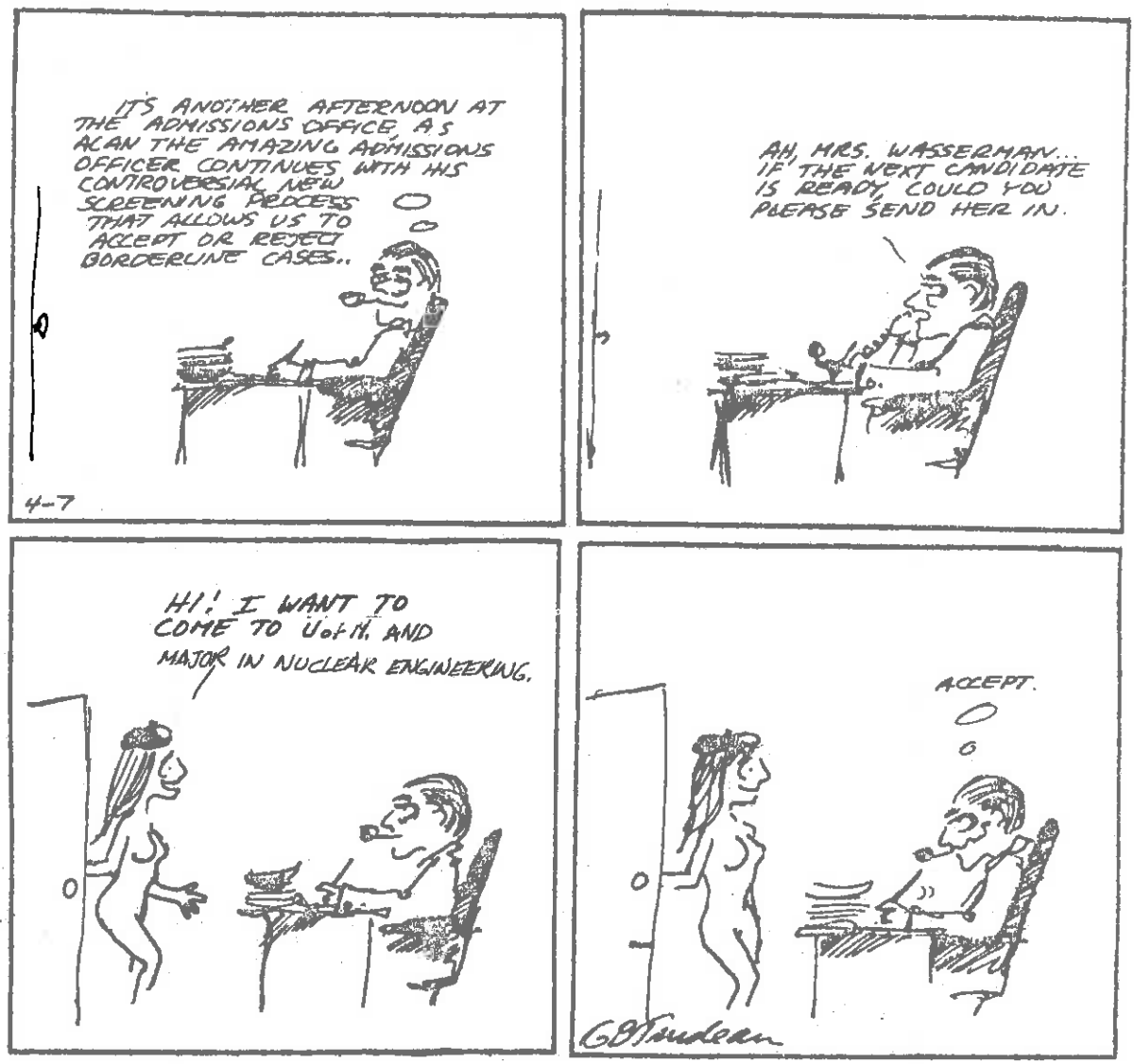
IT'S ANOTHER AFTERNOON AT THE ADMISSIONS OFFICE AS ALAN THE AMAZING ADMISSIONS OFFICER CONTINUES WITH HIS CONTROVERSIAL NEW SCREENING PROCESS THAT ALLOWS US TO ACCEPT OR REJECT BORDERLINE CASES..
4-7
AH, MRS. WASSERMAN... IF THE NEXT CANDIDATE IS READY, COULD YOU PLEASE SEND HER IN.
HI! I WANT TO COME TO U of M AND MAJOR IN NUCLEAR ENGINEERING.
ACCEPT.
GBTinderen

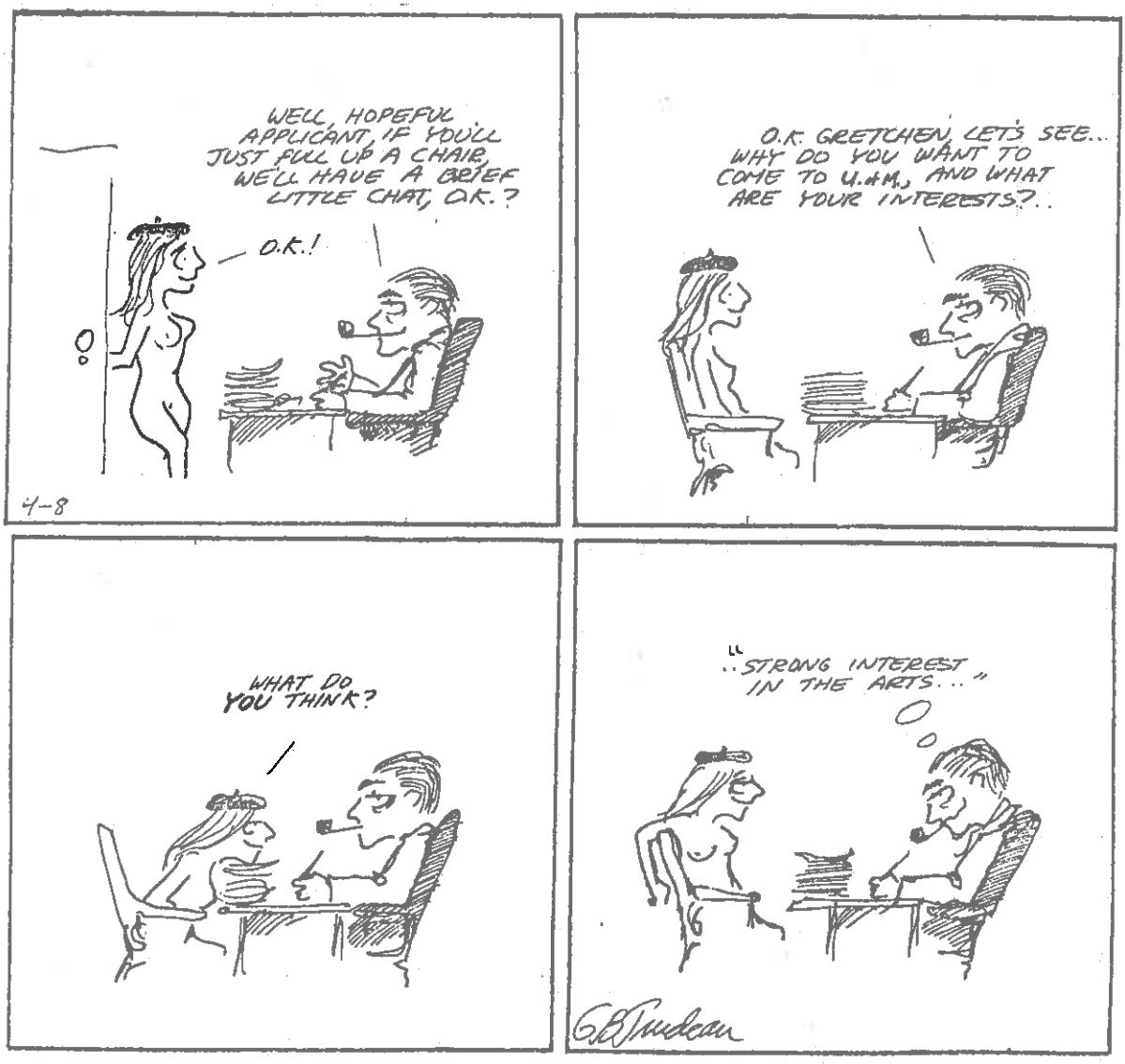
WELL, HOPEFUL APPLICANT, IF YOU'LL JUST PULL UP A CHAIR, WE'LL HAVE A BRIEF LITTLE CHAT, O.K.?
O.K.!
4-8
O.K. GRETCHEN, LET'S SEE.. WHY DO YOU WANT TO COME TO U.of M., AND WHAT ARE YOUR INTERESTS?..
WHAT DO YOU THINK?
"..STRONG INTEREST IN THE ARTS.."
G.E. Tudeau

Such an iterative approach is extremely important in BWR's, since the void fraction in a boiling channel varies quite dramatically from inlet to exit. We have sketched typical coolant density variations (in the average channel) and power distributions in a BWR. We have noted as well the convergence of these profiles as one iterates between thermal hydraulic and neutronic calculations.

F. Local Power Peaking

- to be inserted later -

III. SPECIFIC CONSIDERATIONS IN REACTOR CORE DESIGN

A. General Design Parameters

We have seen that the size of a reactor core is primarily determined by thermal considerations. That is, temperature limitations on core components (primarily fuel melting temperatures) combined with heat transfer limitations such as DNB determine the maximum allowable power density in the core. Hence, if one knows the corresponding maximum-to-average power peaking (hot channel) factor F_q^N, and can estimate the thermodynamic efficiency of the associated thermal cycle, then the core size required for a given electrical output can be determined.

Nuclear considerations are involved in a number of other aspects of core design, however. For example, the desired excess reactivity (which, in turn, depends upon the intended core lifetime) determines the amount of fuel loaded into the core, as well as its initial enrichment. Other nuclear considerations influence the ratio of moderator to fuel, the distribution of fuel enrichment in the core, the detailed fuel element

geometry, and so on. In this section we will examine several aspects of such design considerations.

1. Excess Reactivity Requirements

A nuclear reactor core must be loaded with considerably more fuel than that merely required for core criticality. The excess reactivity contributed by the fuel loading is required to compensate for a number of negative reactivity effects which arise during reactor operation, such as fuel burnup, temperature feedback, fission product poisoning, and so on. In the next chapter we will study several of these reactivity effects in more detail, as well as investigate the means by which one controls the rather sizeable amount of excess reactivity present in a power reactor core in order to keep the reactor critical. In this section, we will only briefly touch upon the requirements for excess reactivity in an effort to lay a foundation for our further discussion of nuclear core design.

a) Fuel Depletion: Of course the most obvious requirement for excess reactivity is that necessary to compensate for reactivity loss due to fuel burnup during reactor operation. Actually there are several competing effects which determine the loss in core reactivity due to fuel depletion. First there is the loss in the original fissile isotope (e.g., U^{235}) due to fission or capture. But there is also a positive reactivity effect resulting from the conversion of fertile to fissile nuclei (e.g., $U^{238} \longrightarrow Pu^{239}$). The significance of this effect is determined by the conversion ratio (fertile captures/fissile absorptions) which ranges between 0.5 for light water reactors to greater than 1.0 for fast breeder reactors. Finally, there is also a negative

reactivity effect due to the buildup of non-saturating fission products with appreciable cross sections. Typical excess reactivity requirements are tabulated below:

b) Equilibrium Fission Product Poisons: In thermal reactors, one must compensate for the rather sizeable negative reactivity introduced by saturable fission products such as xenon and samarium. As we have seen, the negative reactivity attributable to xenon is flux dependent, and can range as high as $\Delta\rho^{Xe} \cong -3.5\%$ for a thermal flux of $\phi_0 = 10^{14}$ sec^{-1}cm^{-2}. The samarium contribution is typically around $\Delta\rho^{Sm} = 0.7\%$.

c) Temperature and Power Reactivity Feedback: In our discussion of reactivity feedback in Chapter 6, we indicated that temperature variations in the core could affect reactivity, both through material expansion effects, as well as by modifying the microscopic cross sections themselves (e.g., the Doppler effect). For most reactors, an increase in core temperature will result in a negative reactivity effect. The negative reactivity introduced by raising the core temperature from ambient to operating temperature is known as the reactor temperature defect, while the reactivity change in going from zero power to full power is known as the power defect. Both temperature and power defects must be accounted for in determining excess reactivity requirements.

Typical values are:

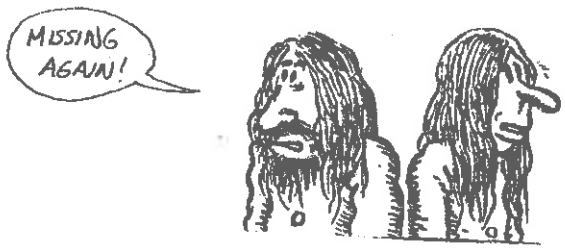

d) Other Effects: One must include sufficient reactivity to allow for power level changes and maneuvering. For example, a reduction in power level will cause an increase in xenon concentration, and hence a negative reactivity which must be overriden by the excess reactivity available in the fuel.

The magnitudes of each of these reactivity requirements are illustrated below for several reactor types:

It is apparent that the excess reactivity requirements are considerable, particularly in thermal reactors. These are usually met by adjusting fuel enrichment. Typically, this enrichment ranges from 50% to 100% more than that required merely for core criticality in order to supply the excess reactivity.

2. Moderator-To-Fuel Ratio

One of the key parameter which must be determined by the nuclear engineer in thermal reactor core design is the ratio of moderator density to fuel density. This parameter is primarily influenced by nuclear factors. Perhaps the most straightforward manner to illustrate the considerations involved in determining N_M/N_F is to investigate the dependence of each of the terms in the four factor formula $k=\eta f p \epsilon$. To be specific, we will consider light water reactors.

To first order, η is independent of this ratio (although it does enter through spectrum effects upon the thermal group constants appearing in η). The thermal utilization f clearly involves this ratio:

$$f = \frac{\Sigma_a^F}{\Sigma_a^F + \Sigma_a^M} = \frac{\sigma_a^F}{\sigma_a^F + \frac{N_M}{N_F}\sigma_a^M} \tag{13-31}$$

As we increase N_M/N_F, we find f decreases (obviously more absorption occurs in the moderator).

To investigate the resonance escape probability p, we can use the form

$$p = \exp\left[-\frac{N_F}{\xi\Sigma_s} I\right]$$

$$= \exp\left[-\frac{1}{\xi}\left(\frac{N_F}{N_M}\right)\frac{1}{\sigma_s^M} I\right] \tag{13-32}$$

Thus as N_M/N_F increases, the resonance absorption decreases (the neutrons slow down more readily), and p increases.

Finally, since the fast fission factor ϵ represents the ratio of total fissions to thermal fissions, we would expect that ϵ would decrease as N_M/N_F increases, since the neutrons are removed more rapidly from the fast group.

We can summarize these effects in the sketch below:

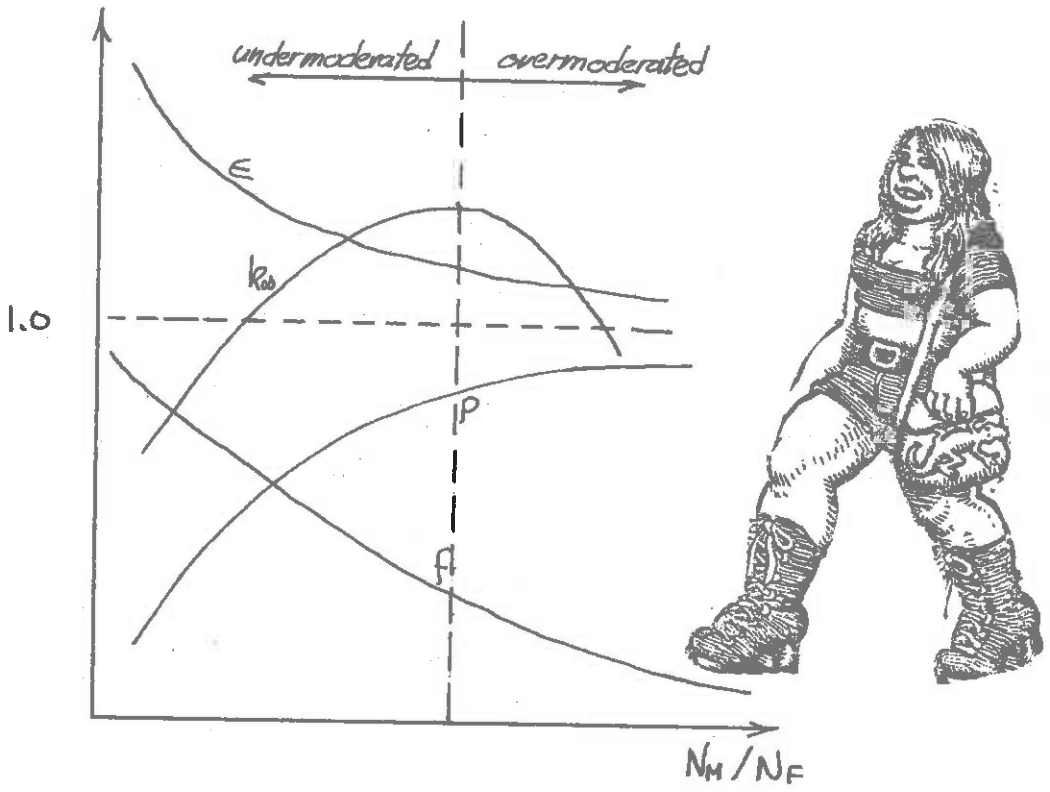

In particular, one should note that k_∞ has a maximum. Light water reactors are designed to operate with N_M/N_F slightly below this point, however, for two reasons. If the core is undermoderated, then a power increase resulting in coolant void formation will cause N_M/N_F to drop, hence decreasing reactivity. If the core were designed to be overmoderated, then a power increase would cause an increased reactivity due to a positive void coefficient. One finds that an undermoderated core has a lower fuel cost, both due to reduced thermal capture and a larger conversion ratio.

3. Enrichment

The fuel enrichment is varied to achieve the required excess reactivity. But again optimization is necessary. The increase in reactivity (through k_∞) due to an increase in core enrichment is larger at higher N_M/N_F ratios:

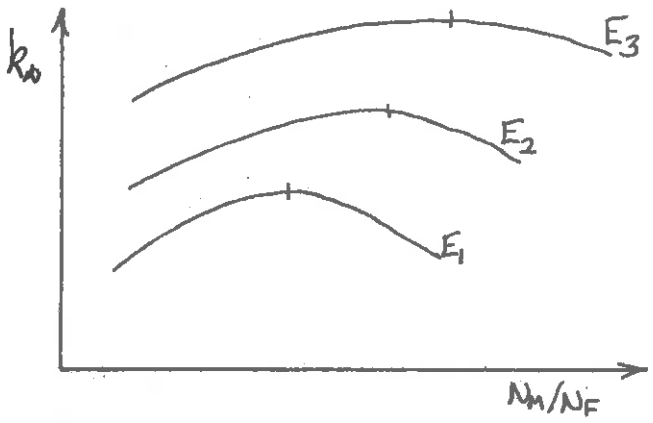

$E_3 > E_2 > E_1$

4. Heterogeneities

Local heterogeneities are essentially controlled by the fuel rod diameter, since this determines the fuel rod surface to mass ratio. Although this is usually selected using non-nuclear considerations, the dependence of k_∞ upon N_M/N_F will vary for different fuel rod diameters as sketched below

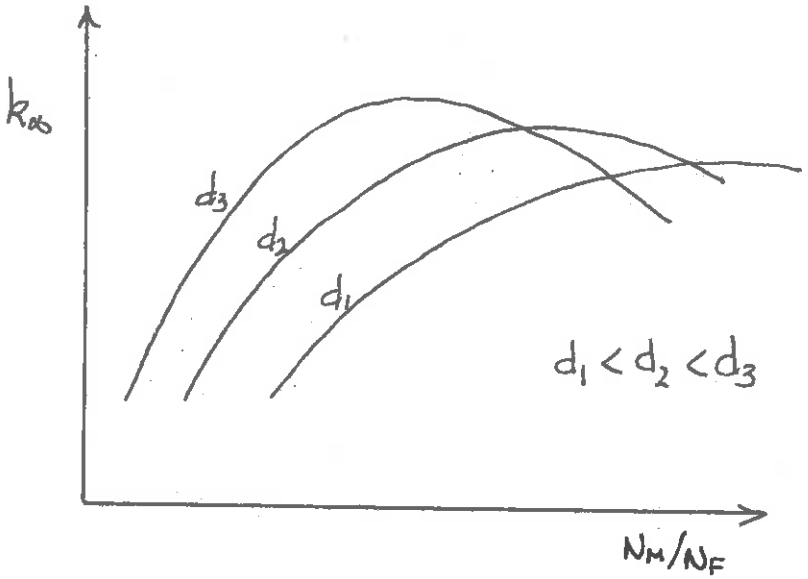

$d_1 < d_2 < d_3$

As the fuel rod becomes larger, self-shielding becomes more significant. In an undermoderated core, k_∞ decreases with a decrease in rod diameter, F, while the opposite holds true in an overmoderated core, since smaller rod diameters imply an increased surface to mass ratio and hence an increase in resonance absorption.

One can also consider the effects of gross heterogeneity such as fuel rod clustering. The influence of an increased Dancoff interaction, reduced resonance absorption, and the positive reactivity effects of water gaps tend to make reactivity coefficients less negative.

4. Chemical Shim

We will see in the next chapter that a common scheme used to control the excess reactivity in LWR's is to dissolve a poison such as B^{10} in the coolant. The behavior of k_∞ for various poison concentrations is shown below

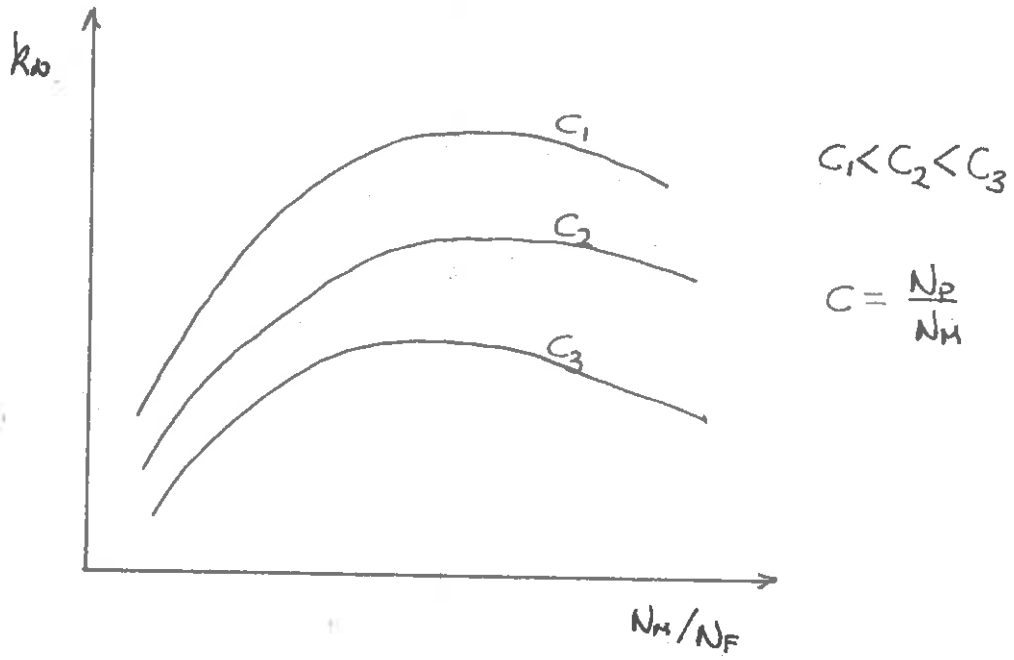

We might expect a strong interaction between the concentration of such soluble poisons and N_M/N_F, since for fixed concentration (say, ppm of boric acid), increasing N_M/N_F will correspond to an increase in absorption which will compensate to some degree for an increase in moderation. This will tend to make the moderator temperature coefficient of reactivity less negative. Such a compensation of moderation by parastic absorption in the poison frequently places an upper limit on allowable boron concentrations.

B. Pressurized Water Reactor Core Design

1. Core Layout

In an effort to illustrate more clearly the various aspects involved in nuclear core design, we will now briefly describe the specific core design and methods of analysis used for the more common types of large power reactors. We begin our discussion by considering the core design of a pressurized water reactor.

A cutaway view of the reactor vessel and a cross section of a typical PWR core is given in Figures 13-6 and 13-7. The detailed system parameters are listed in Table 13-1. The core of a modern PWR consists primarily of zircaloy-clad slightly enriched UO_2 fuel arranged in canless assemblies, such as those shown in Figure 13-8. The fuel pellets are composed of slightly enriched (2% - 3%) UO_2 powder that is compacted by cold pressing and then sintered to attain the required density. These pellets are inserted into zircaloy-4 tubes, and each end of the tube is sealed by welding an end plug to form a fuel rod. These fuel rods are pressurized to reduce cladding stress. The rods are then arranged into a square assembly fastened together by coolant nozzle plates at the top and bottom and by spring clip assemblies along the height of the fuel

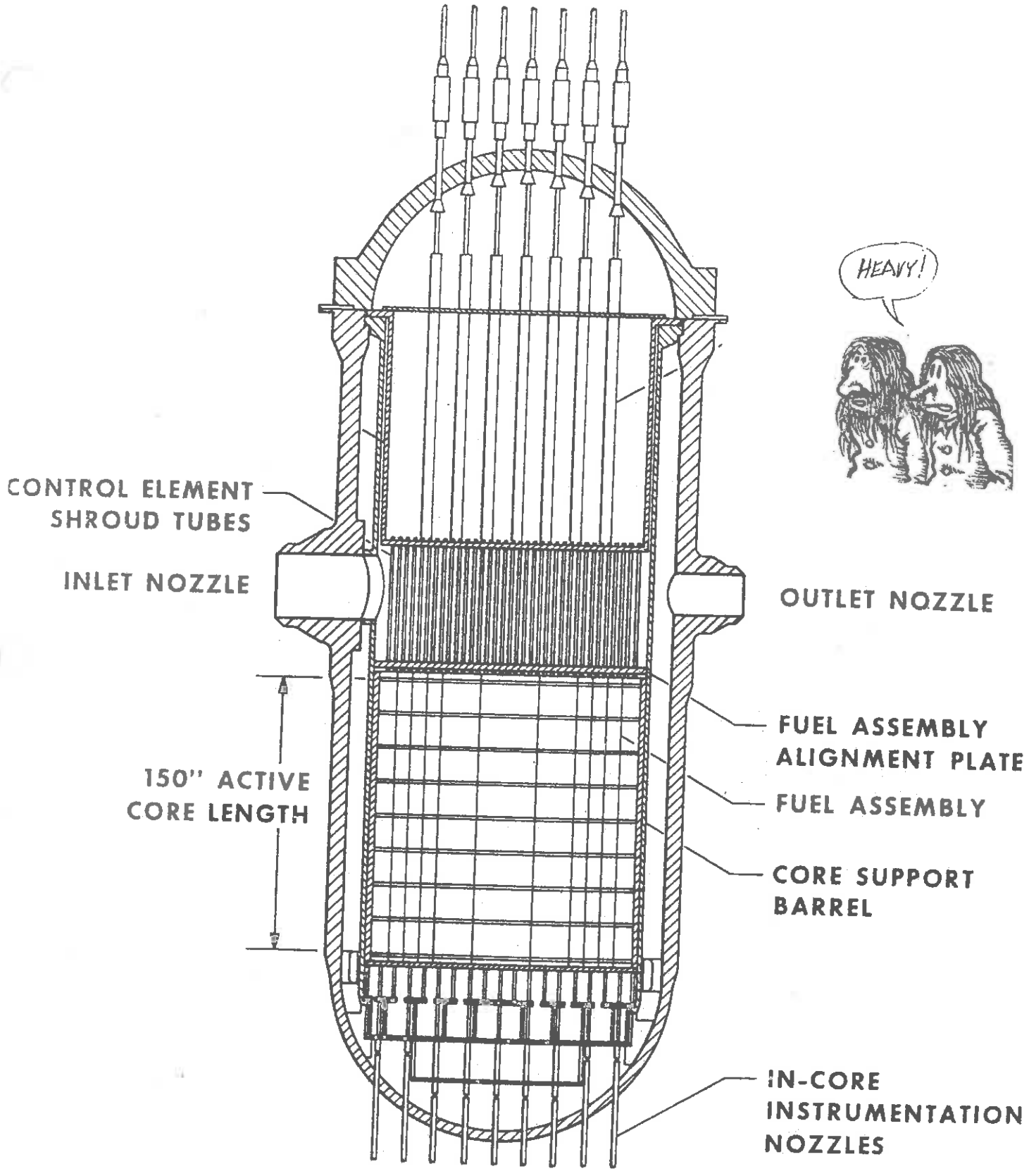

REACTOR ARRANGEMENT

FIGURE 13-6

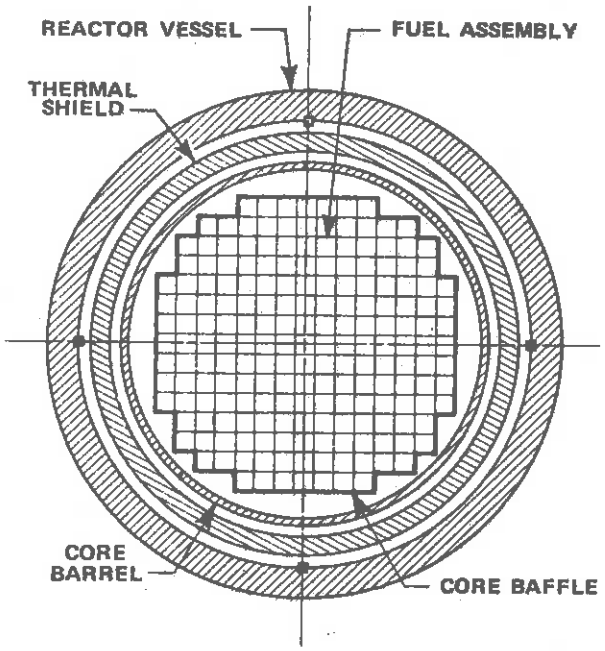

Cross Section of Typical Four-Loop Core (193 Fuel Assemblies)

TABLE

TYPICAL FOUR-LOOP REACTOR CORE PARAMETERS

Total heat output	~3250-3411 MWt
Heat generated in fuel	97.4%
Nominal system pressure	2250 psia
Total coolant flow rate	~138.4×10^6 lb per hr
Coolant temperature	
Nominal inlet	557.5°F
Average rise in vessel	61.0°F
Outlet from vessel	618.5°F
Equivalent core diameter	11.06 ft
Core length, between fuel ends	12.0 ft
Fuel weight, uranium (first core)	86,270 kg
Number of fuel assemblies	193

FIGURE 13-7

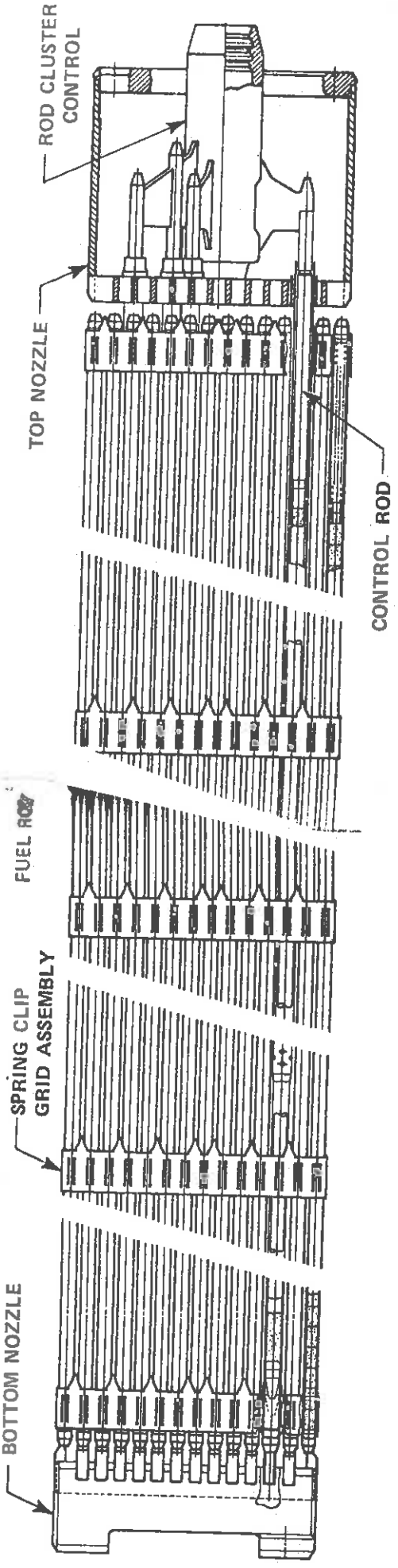

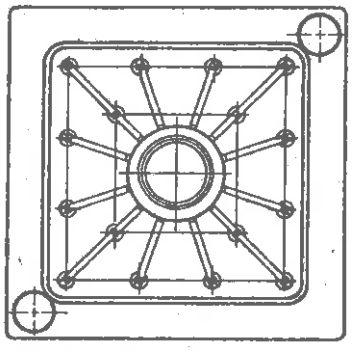

TOP VIEW

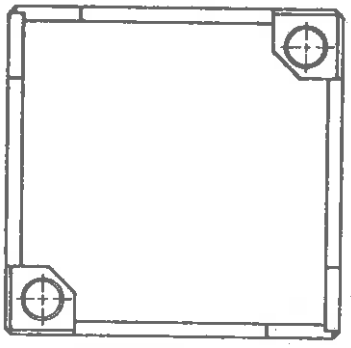

BOTTOM VIEW

FIGURE 13-8

FIGURE 13-8'

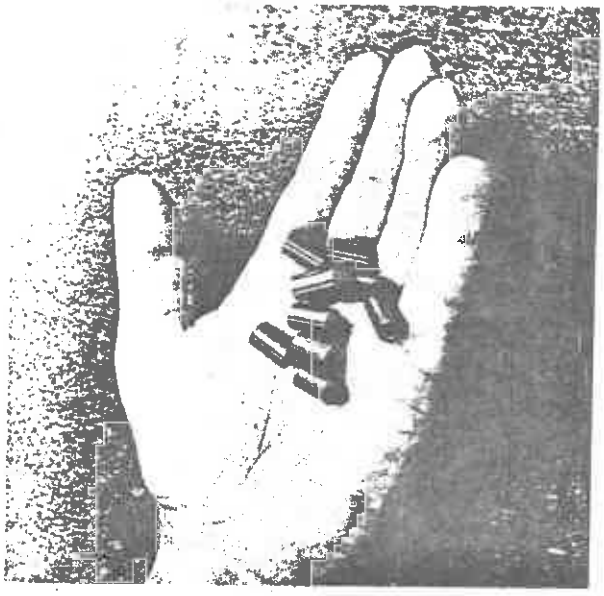

FUEL ROD PARAMETERS

Outside diameter	0.422 in.
Cladding thickness	0.0243 in.
Diametral gap (first and second region/other regions)	0.0075/0.0085 in.
Pellet diameter (first and second region/other regions)	0.3659/0.3649 in.
Pitch	0.563 in.
Rods array in assembly	15 x 15
Rods in assembly	204
Total number of fuel rods in core	39,372

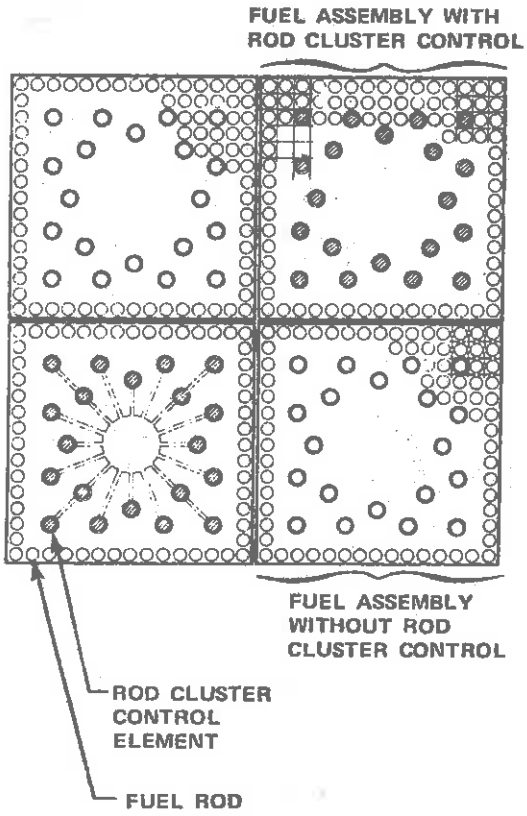

Cross Section of Fuel Assemblies with and without Rod Cluster Control

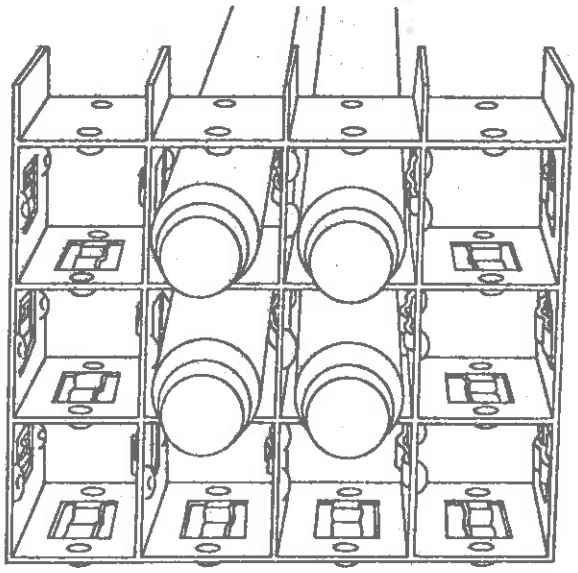

Portion of Spring Clip Grid Assembly

assembly. Mixing vanes are used to increase the heat transfer capability of the fuel rods. Typically, these structural components are zircaloy to reduce neutron capture.

The fuel enrichment is distributed over the core such that fuel assemblies with highest enrichment are placed on the periphery of the core, while those with lower enrichments are mixed in the central region of the core in a pattern that yields the most uniform power distributions.

Reactor control is provided by moveable control rod clusters, boric acid dissolved in the coolant, and, in the initial core loading, by using burnable poisons. In this scheme, the control rod clusters are used to follow load changes, to provide reactor scram, and to furnish control for slight deviations in reactivity due to temperature variations. The chemical shim is used to compensate for excess core reactivity and is reduced as fuel depletion occurs over core life. It is also used to compensate for the reactivity associated with xenon transients arising from power level changes. In the initial core loading, boro-silicate glass tubes are inserted into the core to compensate for the positive moderator void coefficient created by the chemical shim. The absorption due to these boron loaded tubes burns out over core life. We will return in the next chapter to give a much more thorough discussion of reactivity control in light water reactors.

2. Nuclear Analysis

The methods used in light water reactor analysis to determine power distributions and their stability, control requirements and load-following capability during core life, and core depletion effects are essentially those described in the earlier chapters of this text. Such methods have been refined to a high degree, primarily due to the

FIGURE 13-8"

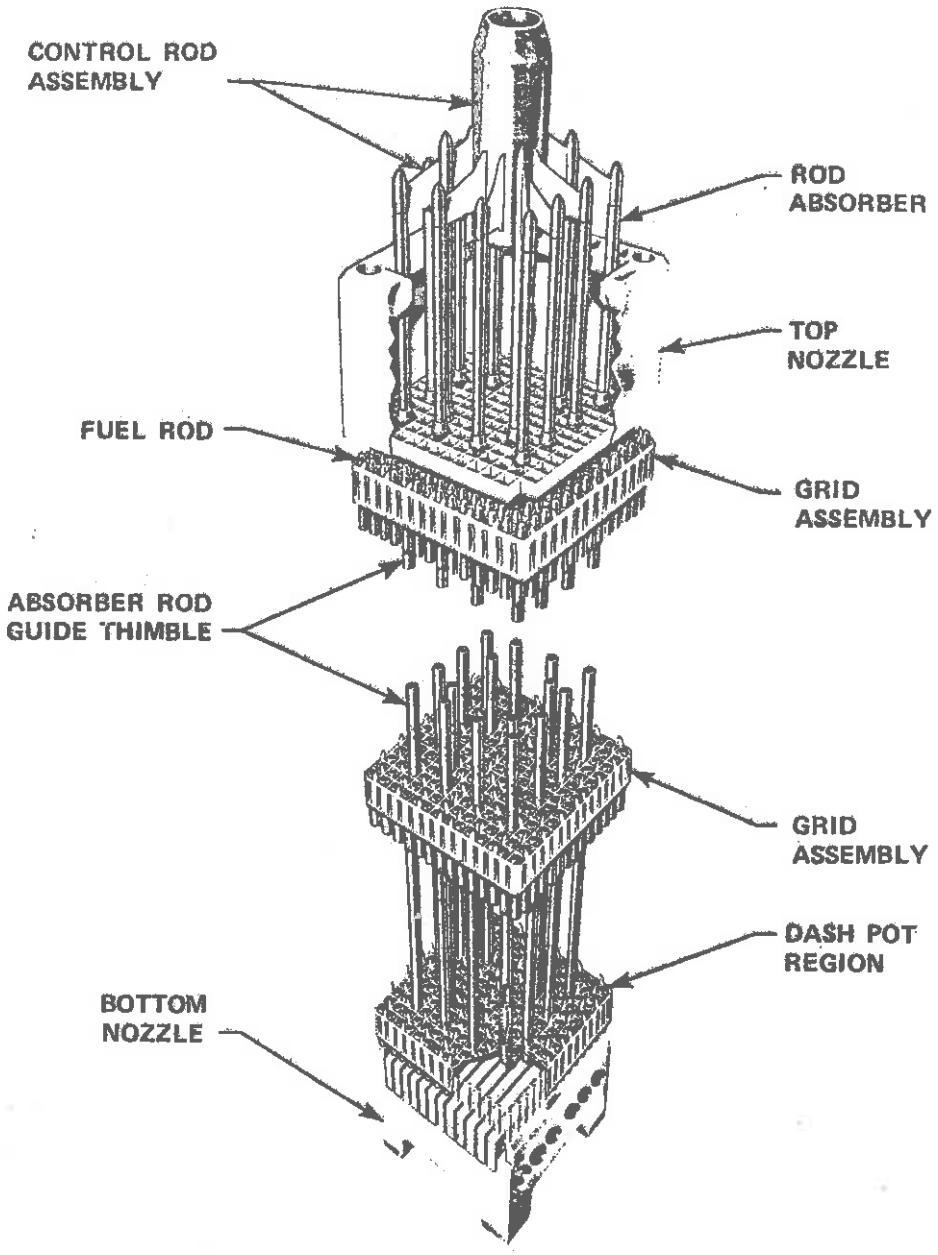

Cutaway of Typical Rod Cluster Control Assembly

substantial water reactor development program conducted by the naval reactor laboratories (BAPL and KAPL), and such methods have been repeatedly tested against both experimental cores and against actual power reactor experience.

Most PWR design calculations of power distribution, control rod and boron worth, temperature coefficients, and reactivity depletion are still performed using 2-D multigroup diffusion codes accompanied by an iteration with axial calculations. The motivation for this is twofold: The expense of a full 3-D calculation, although palatable for a benchmark or one-shot detailed design calculation, is still prohibitive for the more frequent power distribution calculations required by core depletion or optimization studies. Fortunately, PWR cores with chemical shim can be largely operated with the control rods out at a small bite position which results in a power distribution that is to first order separable into radial and axial shapes, particularly during the first fuel cycle.

As fission products accumulate and fuel depletion occurs, however, the separability disappears. In such cases, the 2-D + 1-D calculation scheme can lead to errors in the calculated multiplication. By way of illustration, the error between a 2-D + 1-D calculation and a 3-D calculation is shown in the figure below:

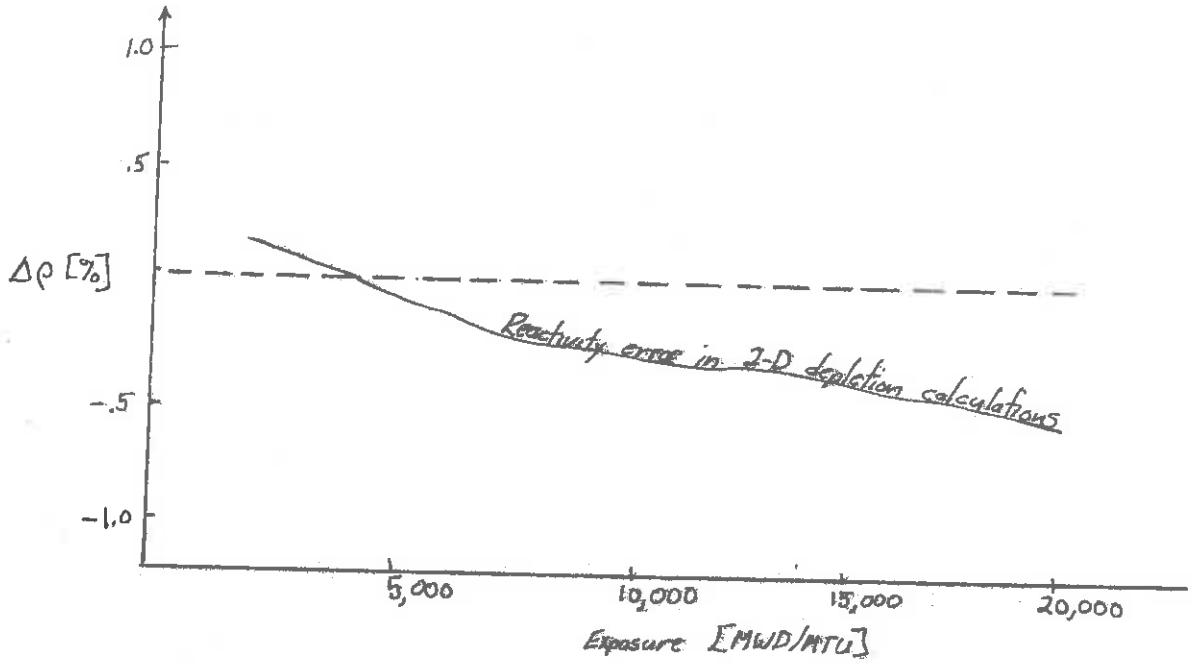

In this particular case, the error arises in the neglect of the correct axial weighting of the macroscopic cross sections of the various depleting isotopes.

The choice of an appropriate mesh size will vary depending on the type of calculation of interest. For example, if one wishes to account for the detailed local flux peaking which occurs in water gaps in the core, it may require one or more mesh points per fuel rod. On the other hand, for fuel depletion analysis, one may pass to a coarse mesh or nodal point.

It is usually possible to adequately represent the energy dependence by from 2 to 4 energy groups. This is usually sufficient because the very strong thermalizing nature of the water moderator tends to wash out the details of the energy dependence. In practice, most detailed design calculations of core power distributions are now performed with 4 energy groups (3 fast and 1 thermal).

The coupling between thermal-hydraulic effects and core neutronics behavior is relatively weak in a PWR (at least, compared to a BWR). This is a consequence of two things: first, the void fraction in a PWR core is quite small, customarily being only about 0.5% (due to subcooled boiling); second, the use of chemical shim tends to compensate for the usually strongly negative moderator temperature coefficient in light water reactors. Towards the end of core life, however, chemical shim is reduced and the moderator temperature coefficient becomes substantially more negative, resulting in a larger power and temperature defect. This will also result in a tendency for a bottom peaked axial flux profile near the end of cycle.

The amount of core leakage in any large thermal reactor is relatively small, being only about 3% in a large light water reactor (PWR or BWR). Hence the primary emphasis in treating neutron diffusion is to account for local heterogeneities and nonuniform power distributions in the core. Over the years there has been a refinement and extension of methods used to account for fuel assembly heterogeneities, with emphasis on more precise treatments of transport effects and cell-to-cell interactions. Although the improvements in the prediction of core power distributions and multiplication yield only small corrections, as the number of operating power reactors increases, the economic incentives for even small improvements in accuracy which permit better fuel cycle, power distribution, or fuel assembly design optimization become very large.

C. Boiling Water Reactor Core Design

1. Core Layout

A schematic of a typical large boiling water reactor is shown in Figure 13-9 along with a cross section of the reactor core in Figure

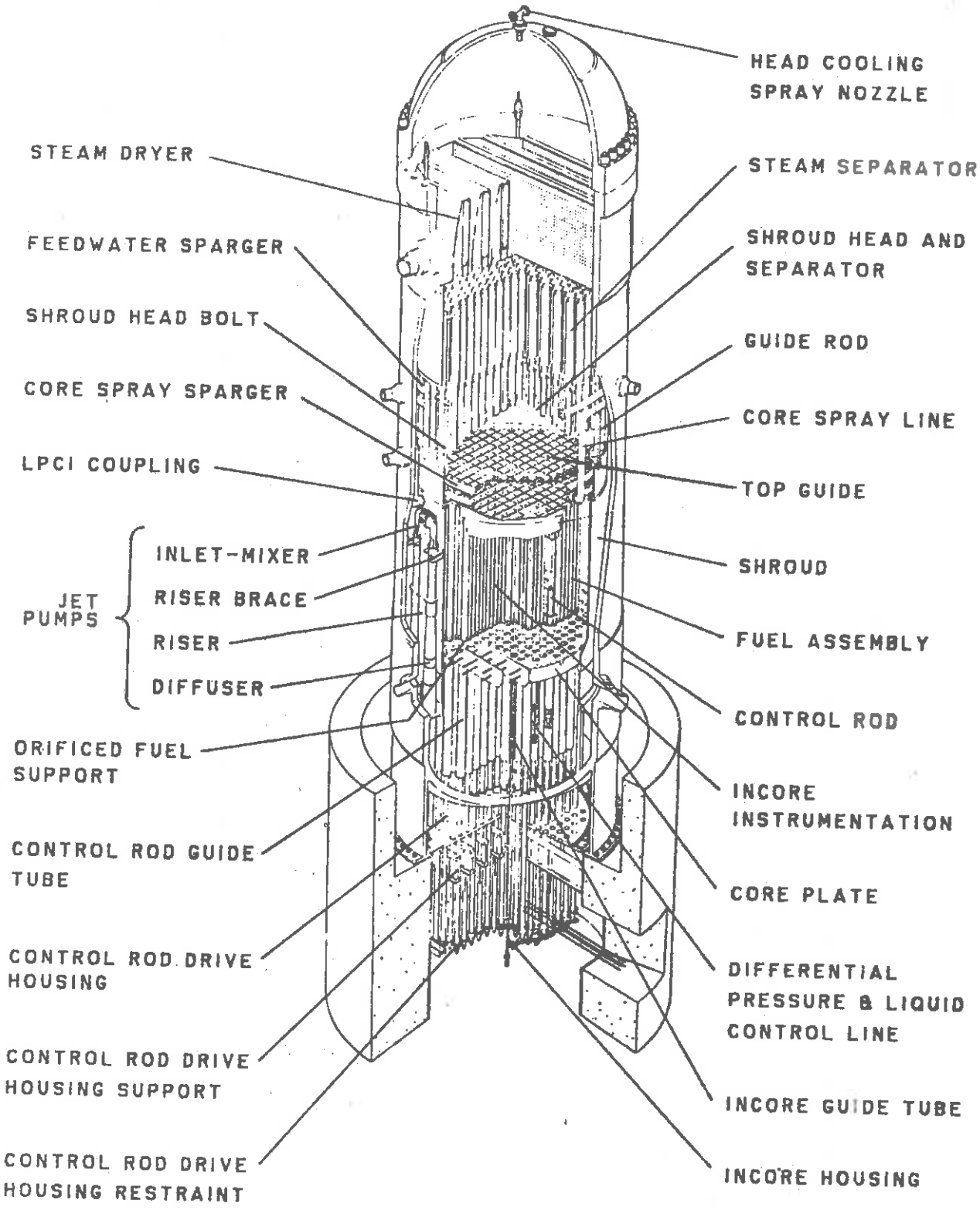

Reactor Vessel Cutaway

FIGURE 13-9

13-10. Like the PWR, the BWR core is composed of slightly enriched UO_2 fuel pellets encased in a zircaloy clad. The cladding tube is filled with helium and sealed with zicaloy end plugs. These fuel elements are then assembled into fuel bundles (typically in 8 x 8 arrays) which are supported by a lower and upoer tie place and surrounded by a can, as shown in Figure 13-11. Selected fuel rods in each assembly differ from the others in fuel enrichment in order to reduce power peaking near water gaps or flux depression near control elements.

The control rods are cruciform shaped blades fabricated of B_4C power in stainless steel tubes surrounded by a stainless steel sheath (see Figure 13-12) which are inserted form the bottom of the core (to avoid the steam separators at the top of the reactor pressure vessel). In addition, burnable poison is used for shim control in the form of gadolinia (Gd_2O_3) mixed with UO_2 in several fuel rods in each fuel bundle (replacing the burnable poison curtains used in earlier BWR designs).

2. Nuclear Analysis

The primary nuclear feature of a BWR core is a very large negative power coefficient of reactivity due to void formation (boiling) of the coolant. This effect is not only significant as a global stabilizing mechanism, but also acts on a local scale to provide inherent self flattening of the core power distribution in the event of a local power rise. It also provides sufficient damping to make the reactor core stable with respect to spatial xenon variations.

The short thermal neutron mean free path in a light water reactor lattice and the resultant sensitivity to geometry require a careful treatment of lattice effects. In general, one must use transport theory

FIGURE 13-10

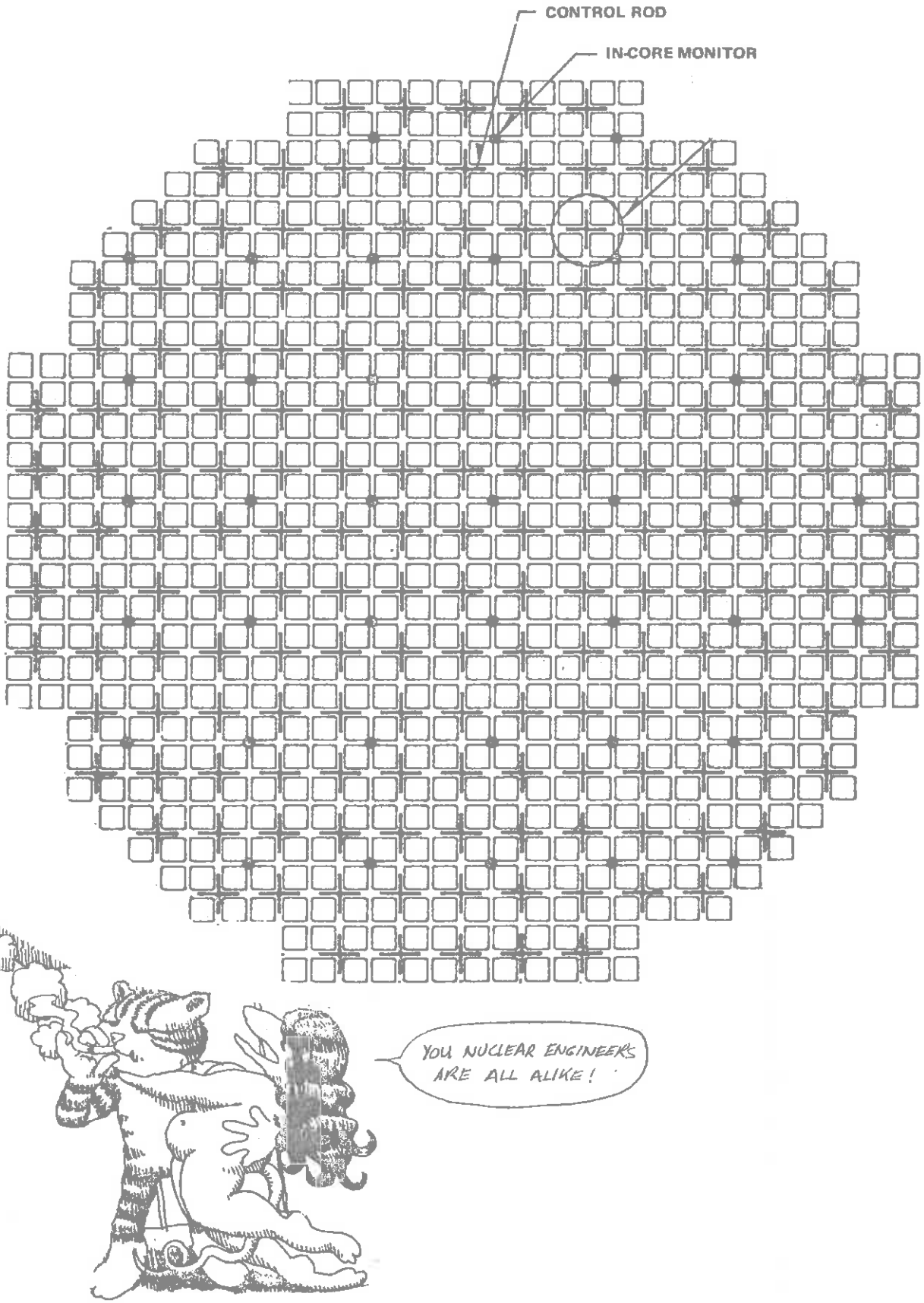
CONTROL ROD
IN-CORE MONITOR
YOU NUCLEAR ENGINEERS ARE ALL ALIKE!

FUEL DATA

Core Data

Fuel cell spacing (control rod pitch), in.	12
Number of fuel assemblies	732
Total number of fuel rods	46,116*
Total weight of UO_2, lb	345,500
Total weight of U, lb	304,600
Core power density (rated power), 1W/liter	56.0
Specific power (rated power), kW/kg U	25.9
Average linear rod power (rated power), kW/ft	6.29
Total core heat transfer area, ft^2	73,409
Core average heat flux, Btu/hr-ft^2	159,570

Fuel Assembly Data

Overall length, in.	176
Nominal active fuel length, in.	148
Fuel rod pitch, in.	0.640
Space between fuel rods, in.	0.147
Fuel channel wall thickness, in.	0.120
Fuel bundle heat transfer area, ft^2	100.3

Fuel Rod Data

Outside diameter, in.	0.493
Cladding thickness, in.	0.034
Pellet outside diameter, in.	0.416
Fission gas plenum length, in.	12.00
Pellet immersion density, gm/cc	10.42

FIGURE 13-11

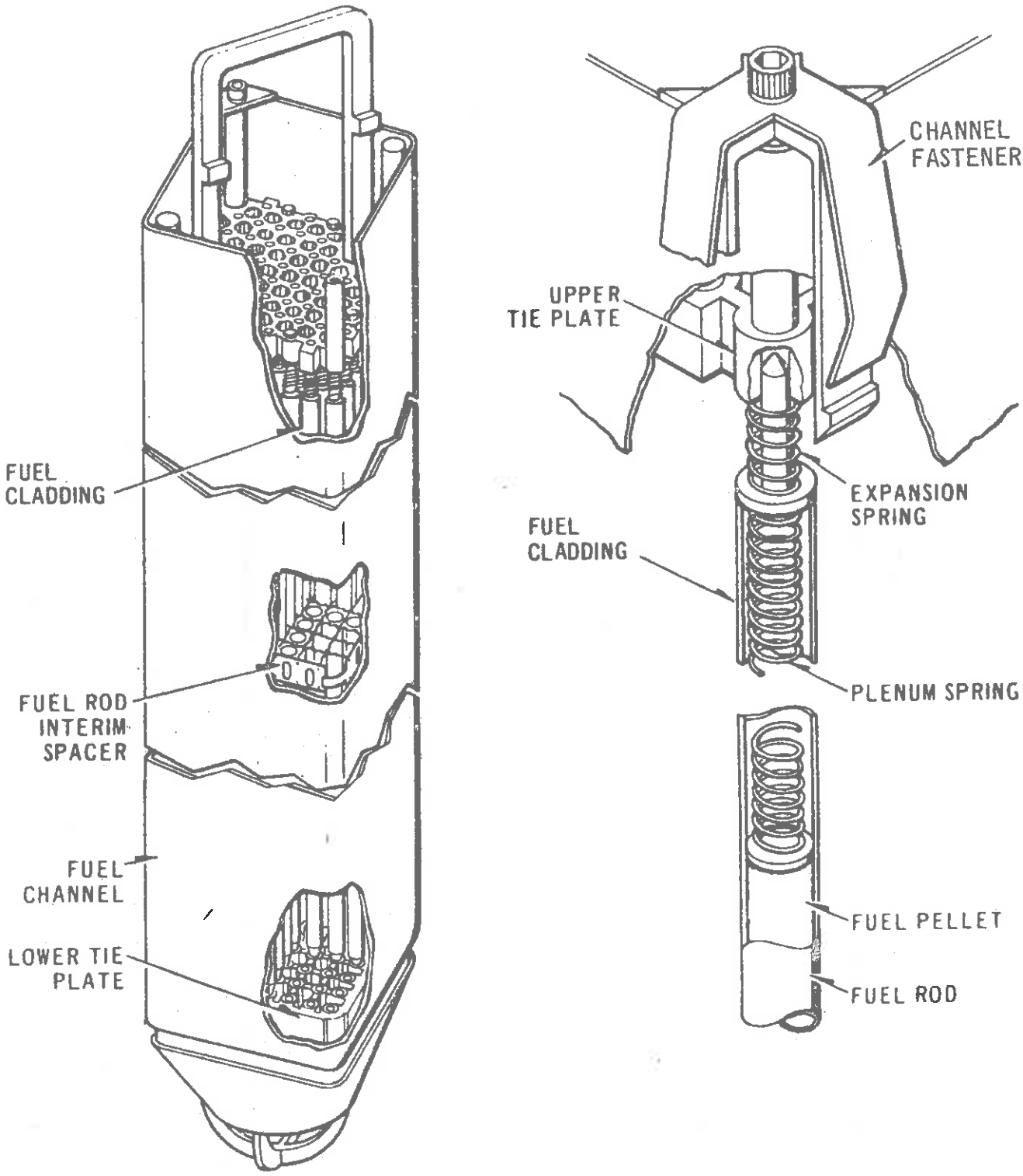

Fuel Assembly

FIGURE 13-11'

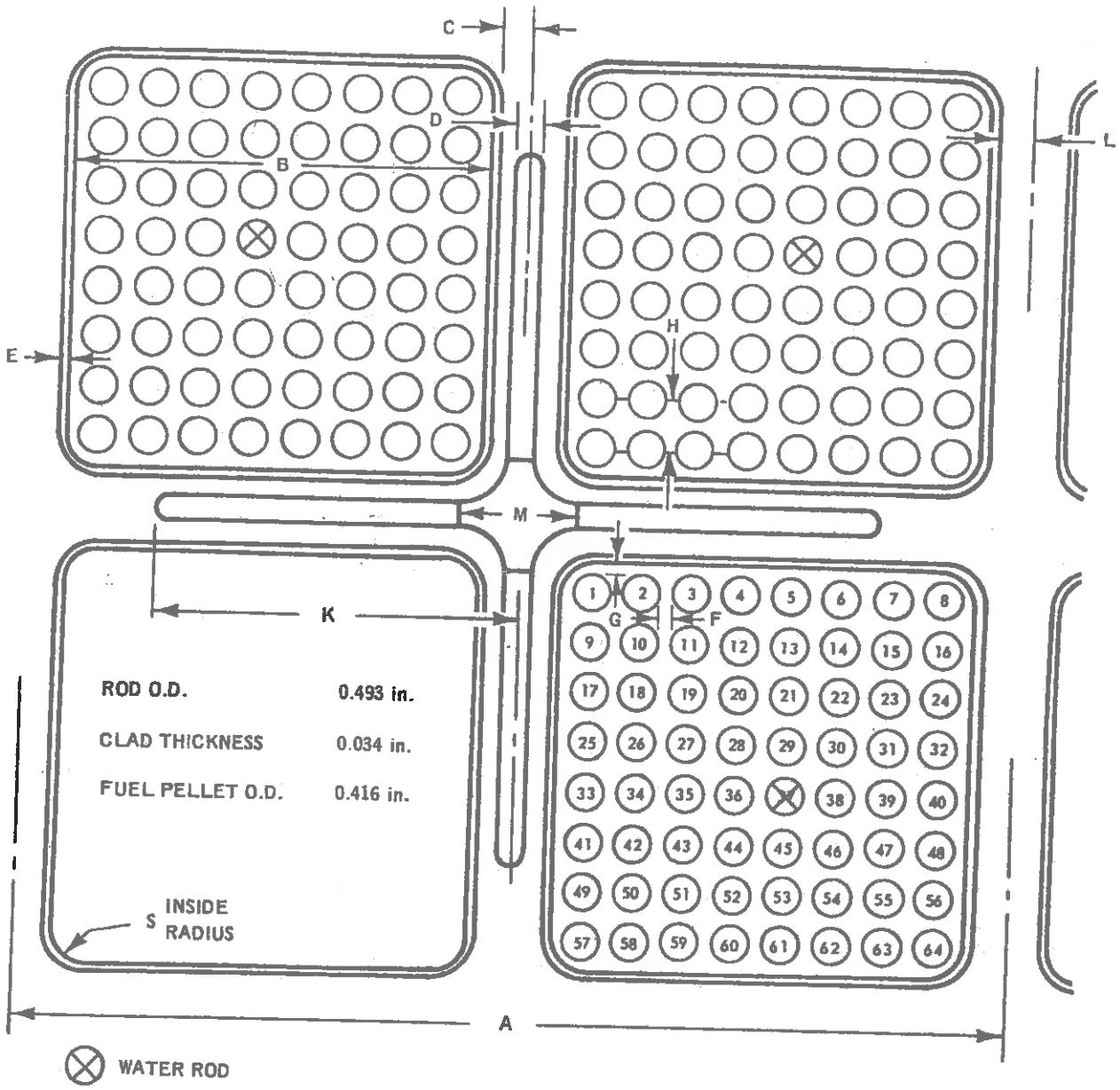

DIM. IDENTIFICATION	A	B	C	D	E	F	G	H	I	J
DIM. INCHES	12.0	5.278	0.241	0.260	0.120	0.147	0.1525	0.640		

DIM. IDENTIFICATION	K	L	M	N	O	P	Q	R	S	
DIM. INCHES	4.875	0.241	1.563						0.400	

Typical Core Cell

FIGURE 13-2

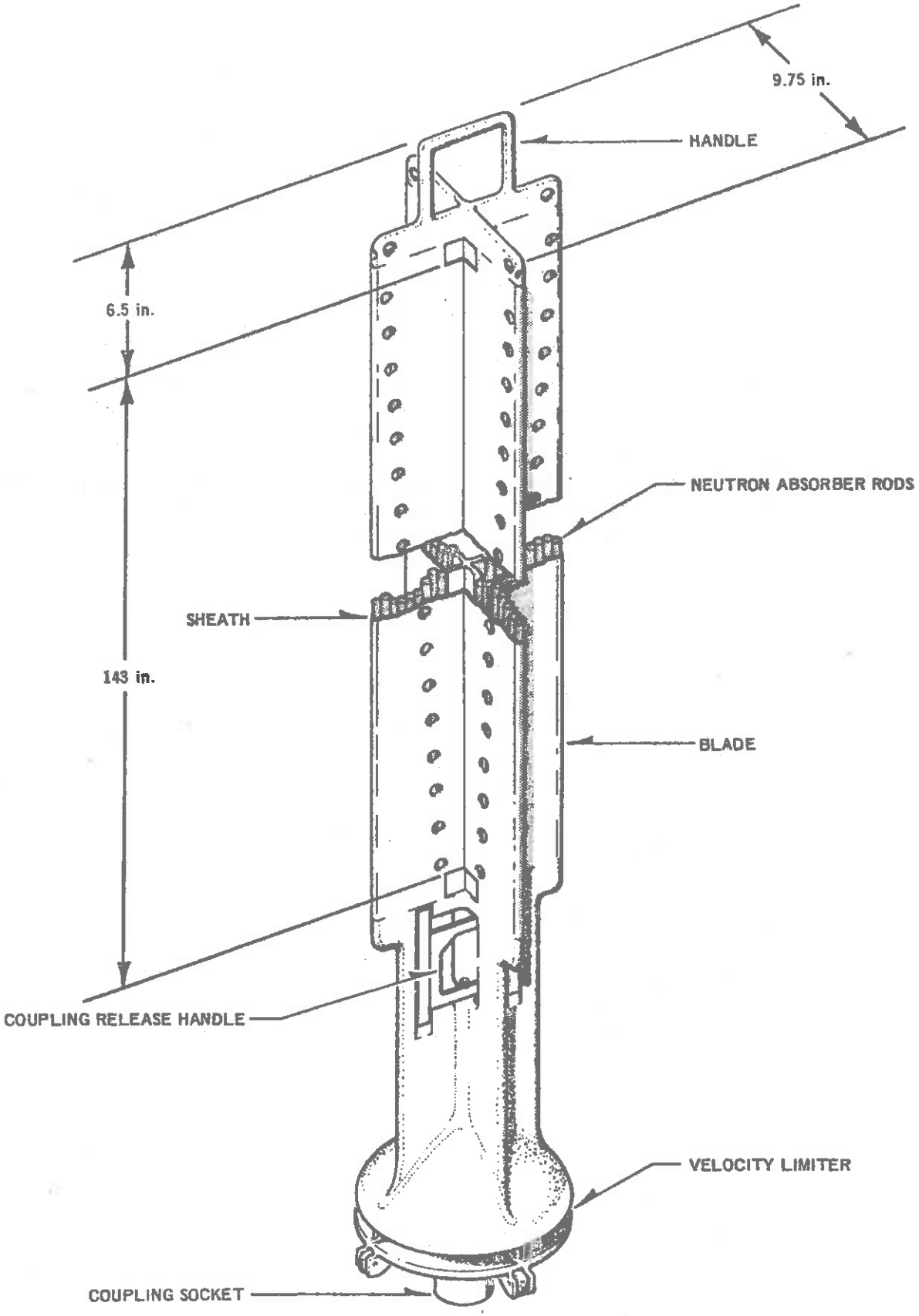

Control Rod Assembly

(e.g., via collision probability methods) to represent fuel rods, control rods, and burnable poisons. As with PWR's, the net neutron leakage from the core is a relatively small effect ($\sim$3%).

The local flux variation in the vicinity of control blades and particularly near the Gd_2O_3 burnable poison loaded pins is particularly difficult to describe.

The large negative moderator void coefficient causes very strong coupling between neutronic and thermal-hydraulic core analysis. One must utilize an iterative scheme in order to calculate the power distribution and void distribution simultaneously. Examples of this strong coupling are shown in the axial power profiles calculated for a typical BWR core in Figures 13-13 and 13-14. These calculations also illustrate the effect that control rod insertion can have on flattening the axial power variation. An actual measured axial power profile is also shown for comparison.

D. High Temperature Gas Cooled Reactors

1. Core Layout

The high temperature gas cooled reactor (HTGR) differs in a substantial way from both the LWR and the LMFBR in that its fuel elements are fabricated entirely out of ceramic materials (with no metallic cladding). The fuel materials are 93% enriched uranium in carbide form and fertile thorium in the oxide form (although the HTGR concept has the provision for the use of recycle U-233 as a feed material when it becomes available). Tiny particles (roughly 100 to 300 microns in diameter) of UC_2 are coated with pyrolytic carbon and silicon carbide, while the thorium oxide particles are coated with pyrolytic carbon. These particle coatings provide the

FIGURE 13-13

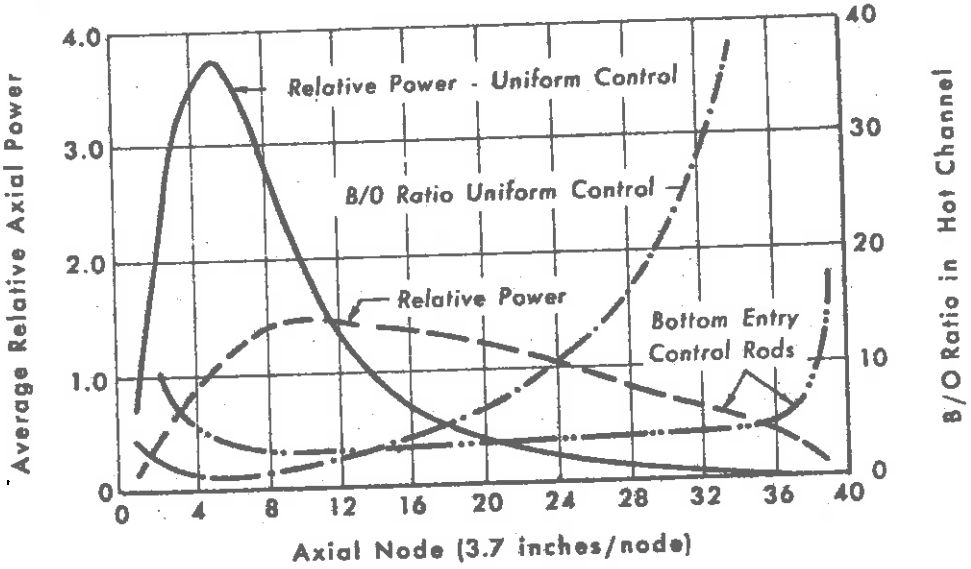

FIGURE CONTROL DISTRIBUTION EFFECT

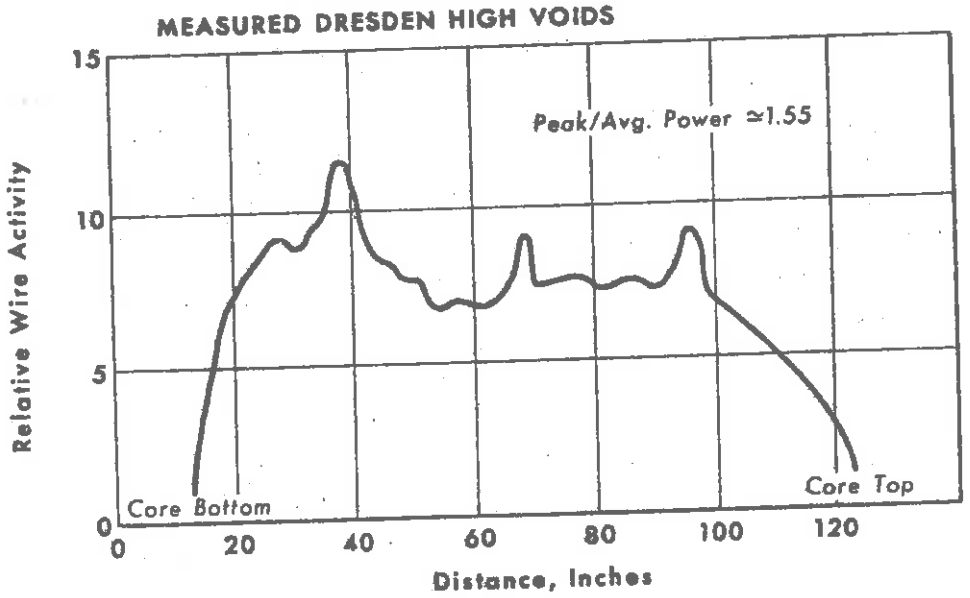

FIGURE AXIAL FLUX DISTRIBUTION

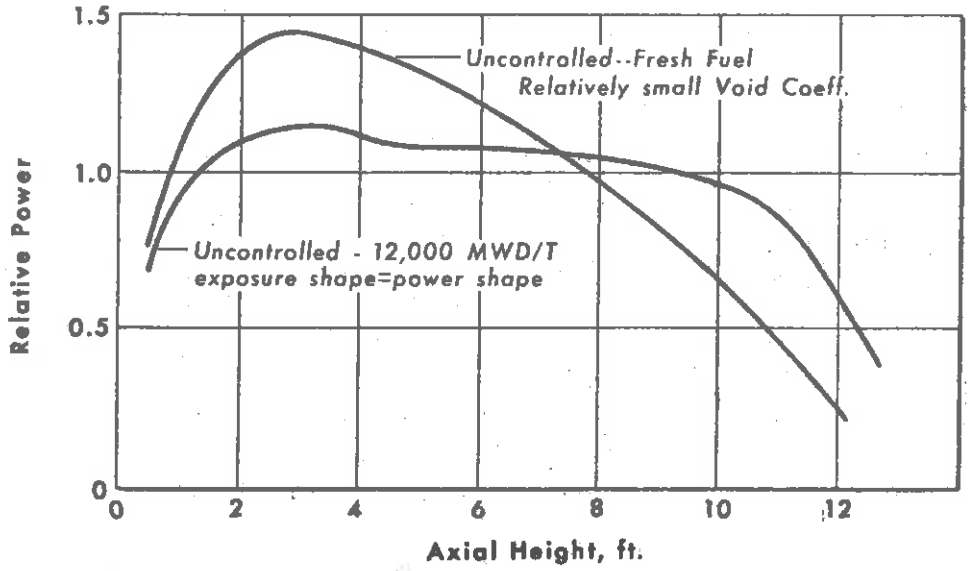

FIGURE 9 EXPOSURE EFFECTS ON AXIAL POWER

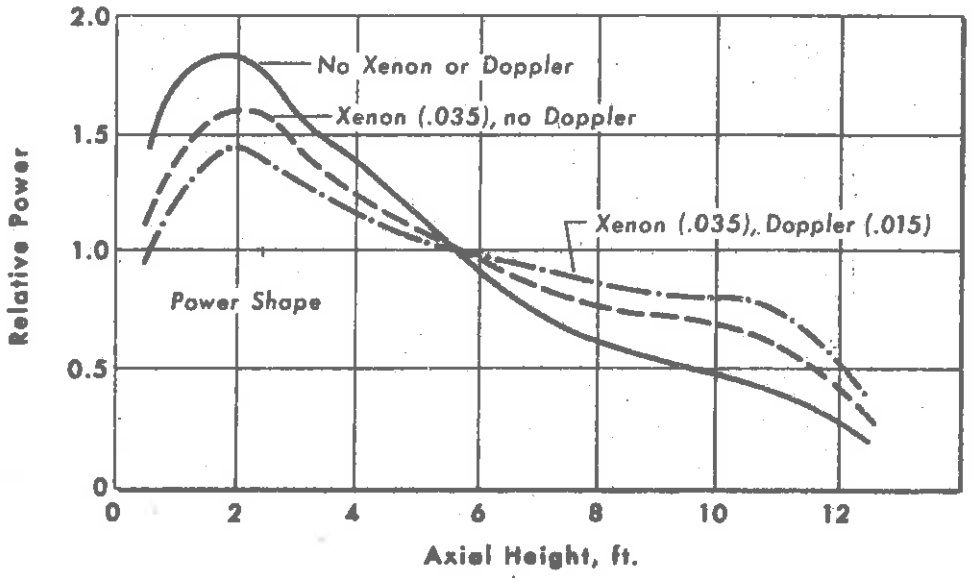

FIGURE 10 XENON-DOPPLER EFFECTS ON AXIAL POWER

Reactor Data Sheet

	PWR RG&E Ginna Sta	BWR J.C. Operating	LMFBR URREA - PFR	[illegible]
General Data				
Thermal Output Mw	1300	1600	600	2
Electrical Output Mw	420	515	250	—
Fuel Material	UO_2	UO_2	$Pu O_2 - UO_2$	14.1% U — al
Structural Material	Zircaloy	Zircaloy	316 SS	Al
Coolant	H_2O	H_2O	N_a	H_2O
Fuel Element Data				
Shape	Rod	Rod	Rod	Curved Plate
Cross Section Dimensions, in.	0.422	0.570	0.230	0.060 x 3
Fuel Dimension, in.	0.3699	0.488	0.200	0.020 Thick
Fuel Density g/cc	10.2	10.4	8.8	~3.1
Clad Thickness, in.	0.0243	0.0355	0.015	0.020
Fuel Element Pitch, in.	0.556 □	0.738 □	0.29 △	
Fuel Assembly Data				
Number of Assbys	121	560	78 FUEL 13 CONTROL	25/6 cm
Elements / Assby	179	49	325	18
Assby Pitch, in.	7.803	12"/4 assby apart	5.7 △	3.035
Grids / Assby	9		every 4"	
Active Fuel Height, in.	144	144	36 CORE 9 EA. BLANKET	24.585
Heat Transfer Data				
System Pressure, psia	2250	1015		
Total Flow 10^6 lbs/hr	67.1	66.85	23	
Effective Flow, 10^6 lbs/hr	61.1			
Tinlet °F	552			
Toutlet °F				

FIGURE 13-15

FISSILE COATED FUEL PARTICLE

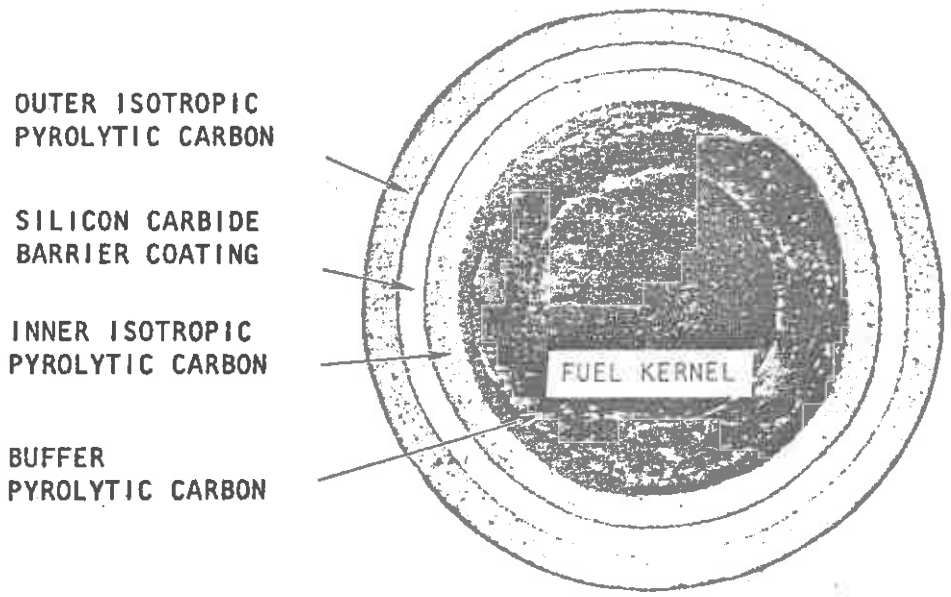

TRISO

FERTILE COATED FUEL PARTICLE

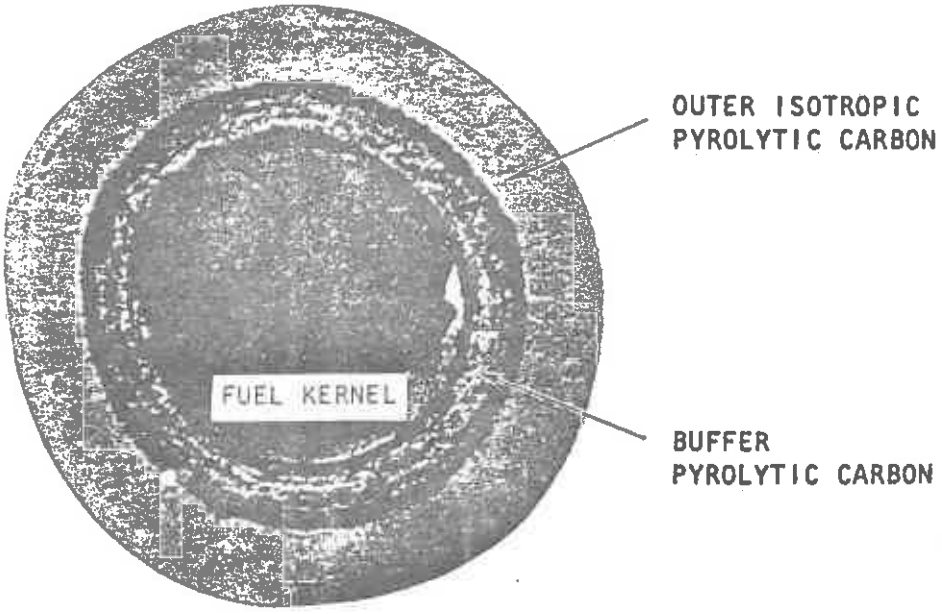

BISO

FIGURE 13-16

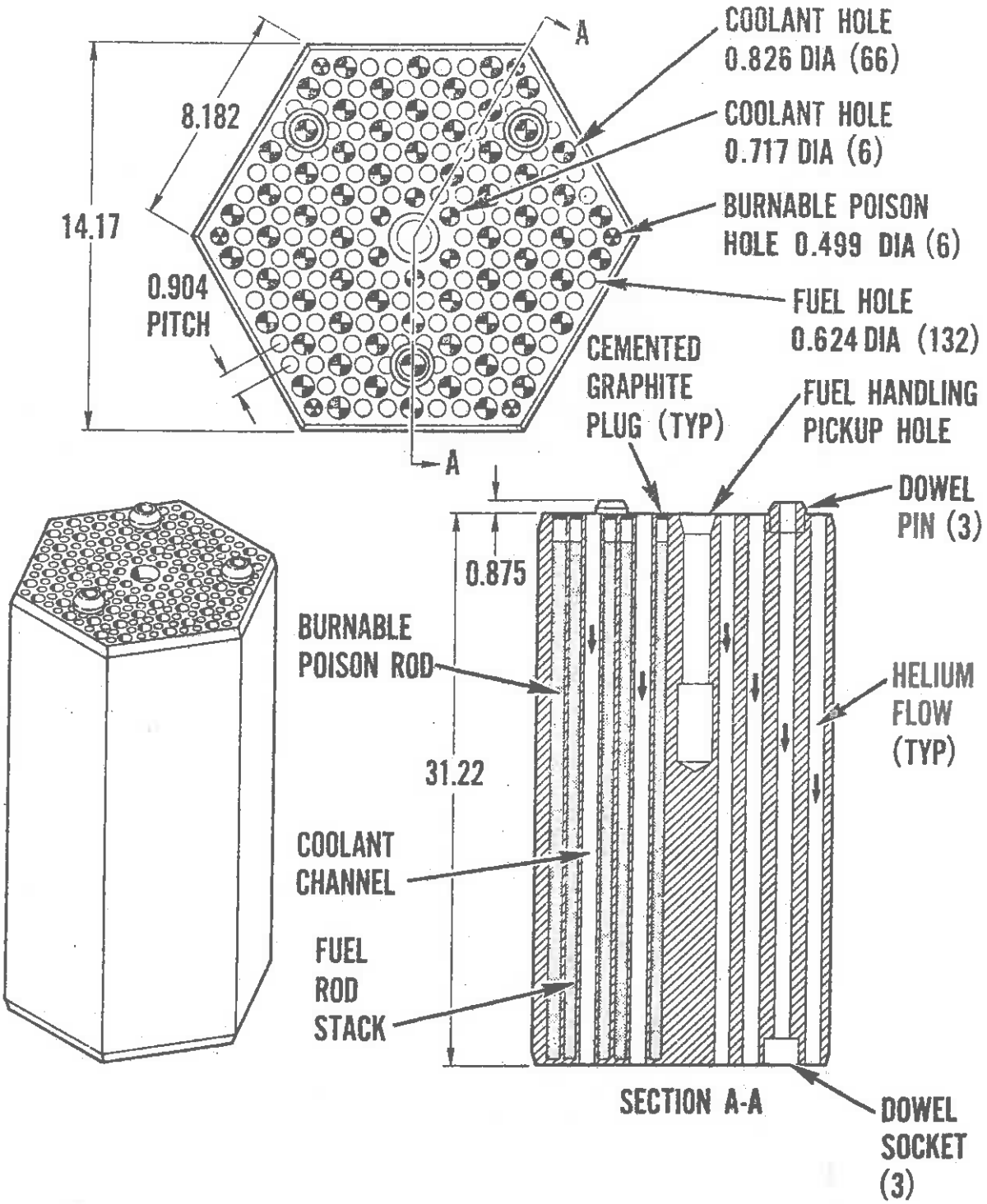
A
COOLANT HOLE
0.826 DIA (66)
COOLANT HOLE
0.717 DIA (6)
BURNABLE POISON
HOLE 0.499 DIA (6)
FUEL HOLE
0.624 DIA (132)
8.182
14.17
0.904
PITCH
CEMENTED
GRAPHITE
PLUG (TYP)
FUEL HANDLING
PICKUP HOLE
DOWEL
PIN (3)
0.875
BURNABLE
POISON ROD
HELIUM
FLOW
(TYP)
31.22
COOLANT
CHANNEL
FUEL
ROD
STACK
SECTION A-A
DOWEL
SOCKET
(3)

FIGURE 13-17

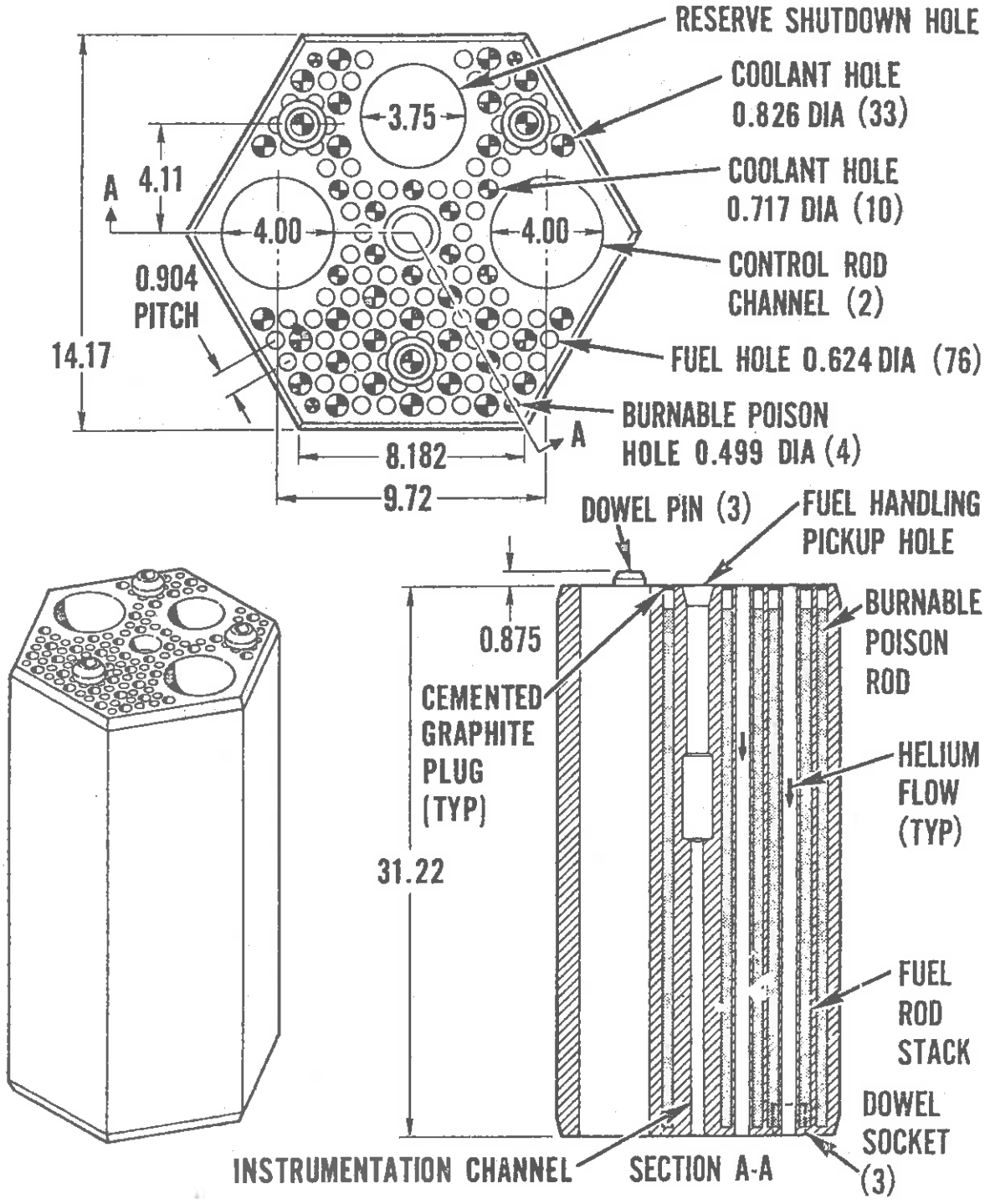
RESERVE SHUTDOWN HOLE
COOLANT HOLE 0.826 DIA (33)
COOLANT HOLE 0.717 DIA (10)
CONTROL ROD CHANNEL (2)
FUEL HOLE 0.624 DIA (76)
BURNABLE POISON HOLE 0.499 DIA (4)
3.75
4.11
A
4.00
4.00
0.904 PITCH
14.17
8.182
9.72
A
DOWEL PIN (3)
FUEL HANDLING PICKUP HOLE
0.875
CEMENTED GRAPHITE PLUG (TYP)
31.22
BURNABLE POISON ROD
HELIUM FLOW (TYP)
FUEL ROD STACK
DOWEL SOCKET (3)
INSTRUMENTATION CHANNEL
SECTION A-A

FIGURE 13-18

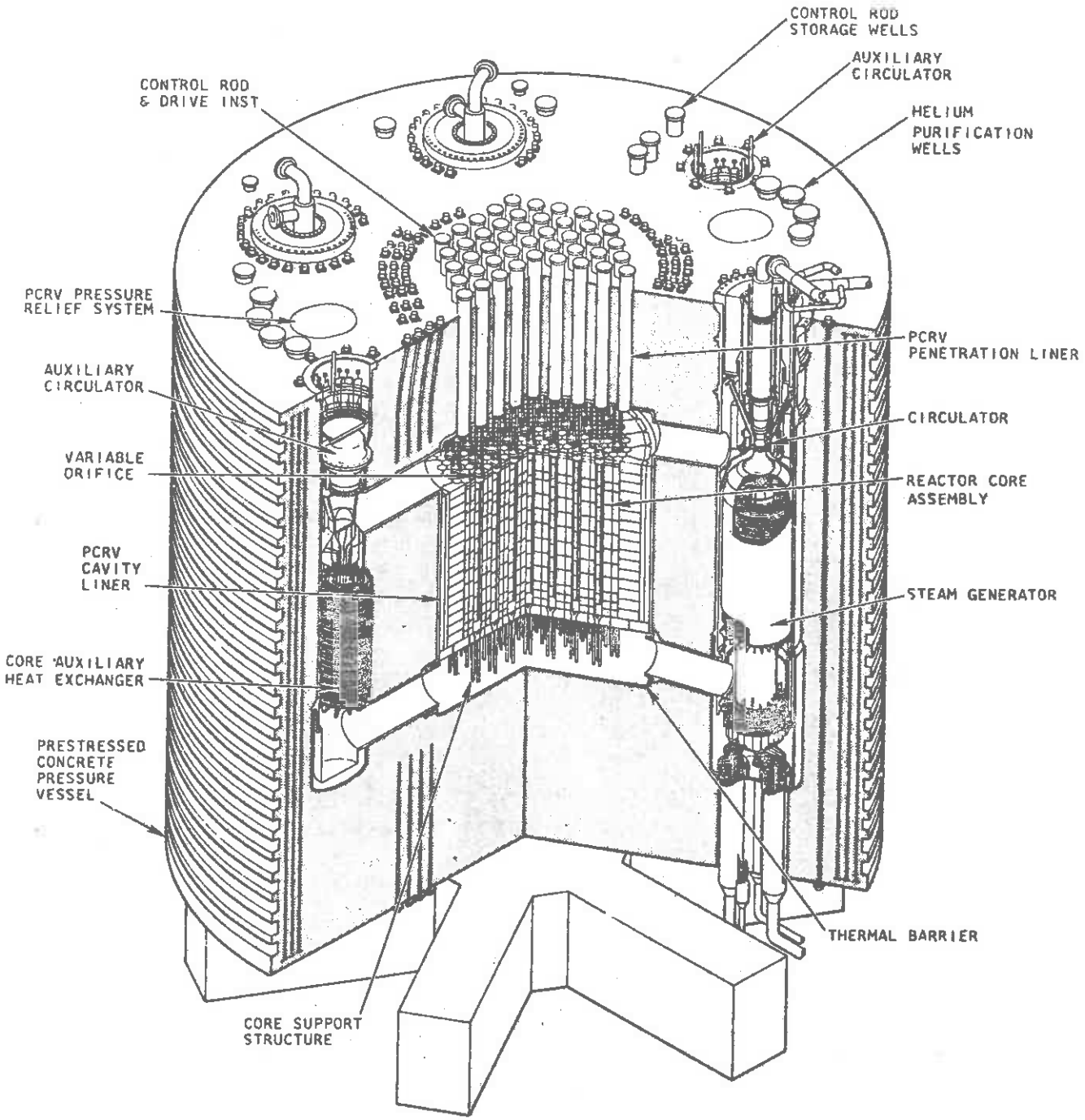
CONTROL ROD STORAGE WELLS
AUXILIARY CIRCULATOR
HELIUM PURIFICATION WELLS
CONTROL ROD & DRIVE INST
PCRV PRESSURE RELIEF SYSTEM
PCRV PENETRATION LINER
AUXILIARY CIRCULATOR
CIRCULATOR
VARIABLE ORIFICE
REACTOR CORE ASSEMBLY
PCRV CAVITY LINER
STEAM GENERATOR
CORE AUXILIARY HEAT EXCHANGER
PRESTRESSED CONCRETE PRESSURE VESSEL
THERMAL BARRIER
CORE SUPPORT STRUCTURE

FIGURE 13-18'

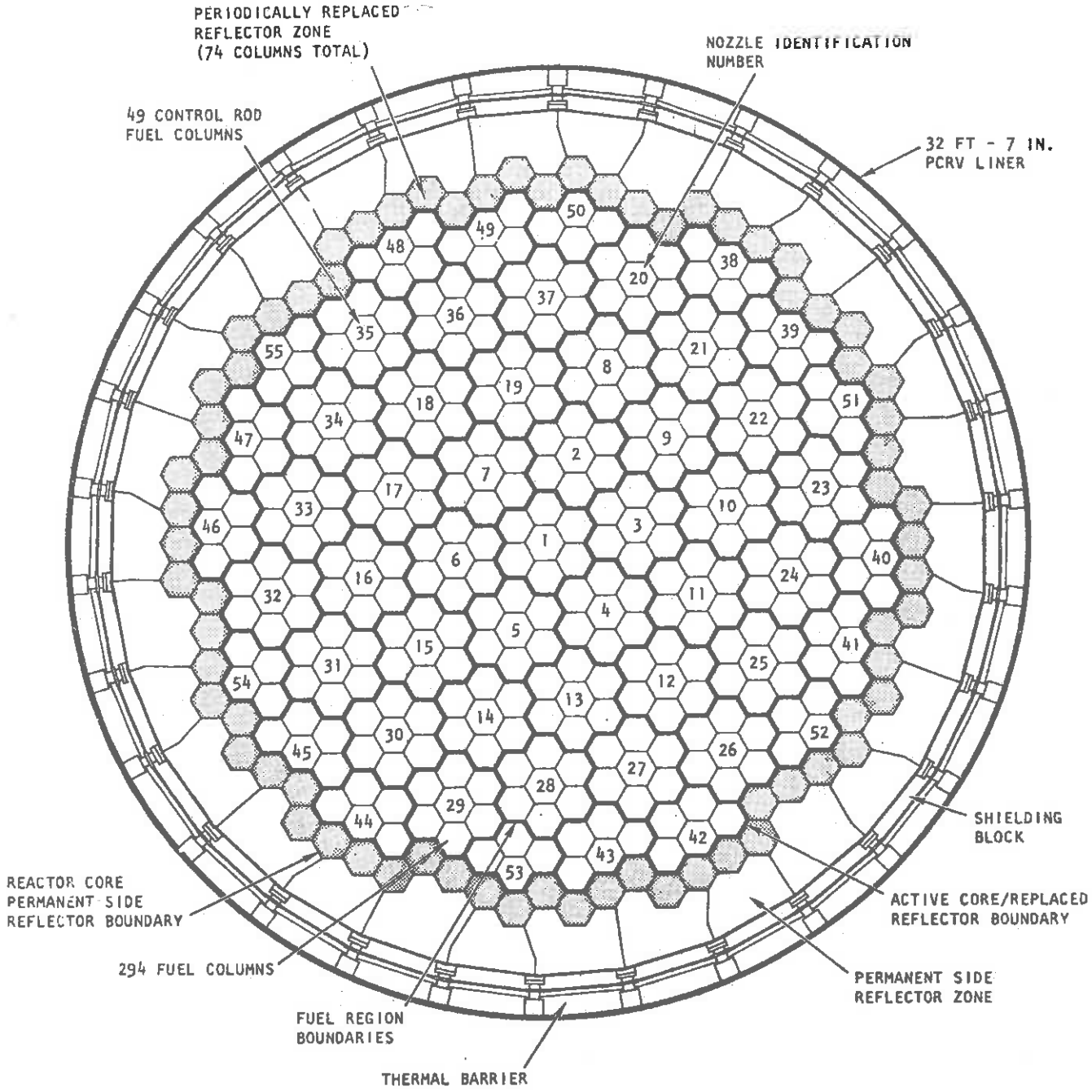
PERIODICALLY REPLACED REFLECTOR ZONE (74 COLUMNS TOTAL)
NOZZLE IDENTIFICATION NUMBER
49 CONTROL ROD FUEL COLUMNS
32 FT - 7 IN. PCRV LINER
SHIELDING BLOCK
REACTOR CORE PERMANENT SIDE REFLECTOR BOUNDARY
ACTIVE CORE/REPLACED REFLECTOR BOUNDARY
294 FUEL COLUMNS
PERMANENT SIDE REFLECTOR ZONE
FUEL REGION BOUNDARIES
THERMAL BARRIER

FIGURE 13-18"

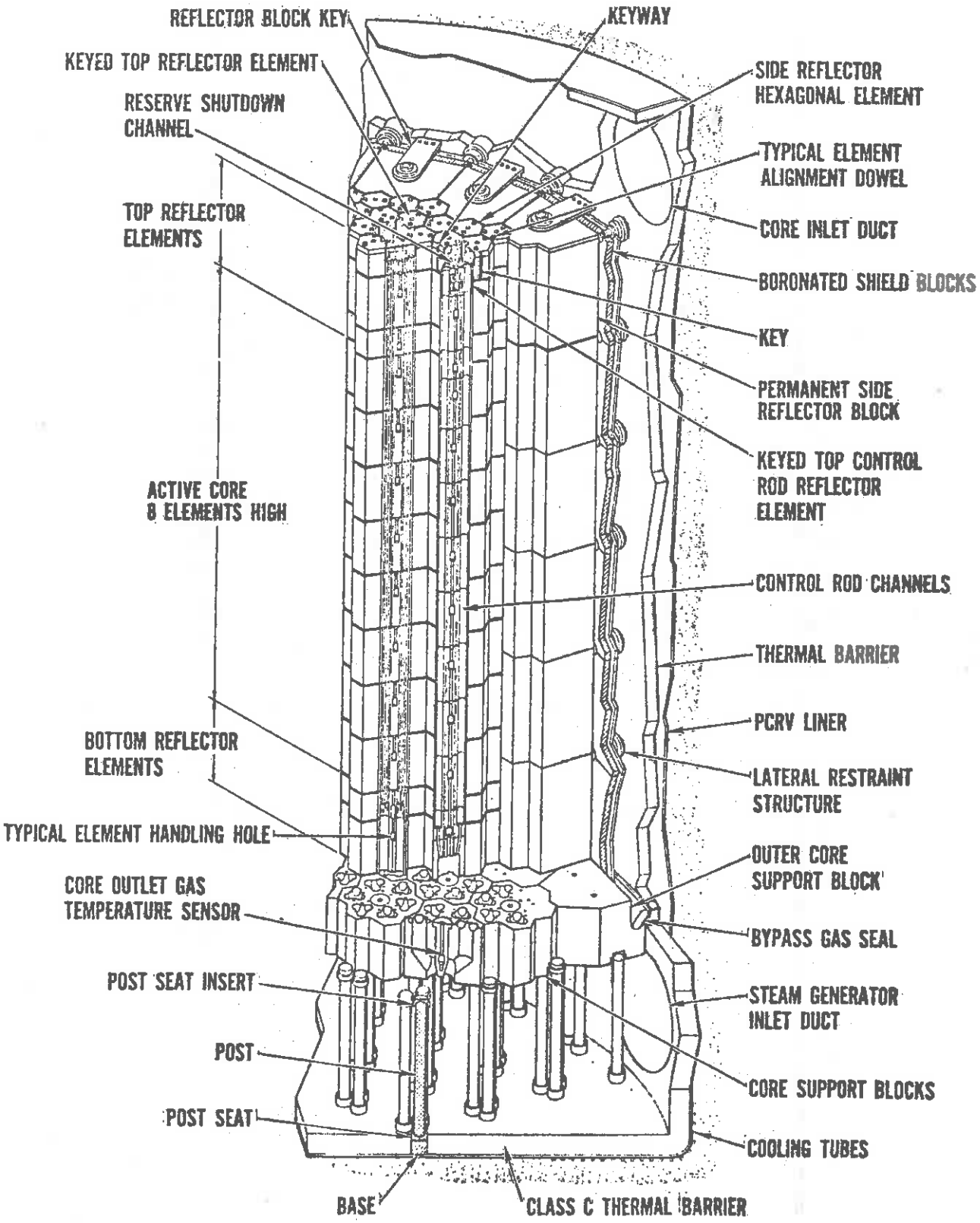
REFLECTOR BLOCK KEY
KEYWAY
KEYED TOP REFLECTOR ELEMENT
SIDE REFLECTOR HEXAGONAL ELEMENT
RESERVE SHUTDOWN CHANNEL
TYPICAL ELEMENT ALIGNMENT DOWEL
TOP REFLECTOR ELEMENTS
CORE INLET DUCT
BORONATED SHIELD BLOCKS
KEY
PERMANENT SIDE REFLECTOR BLOCK
KEYED TOP CONTROL ROD REFLECTOR ELEMENT
ACTIVE CORE 8 ELEMENTS HIGH
CONTROL ROD CHANNELS
THERMAL BARRIER
PCRV LINER
BOTTOM REFLECTOR ELEMENTS
LATERAL RESTRAINT STRUCTURE
TYPICAL ELEMENT HANDLING HOLE
OUTER CORE SUPPORT BLOCK
CORE OUTLET GAS TEMPERATURE SENSOR
BYPASS GAS SEAL
POST SEAT INSERT
STEAM GENERATOR INLET DUCT
POST
CORE SUPPORT BLOCKS
POST SEAT
COOLING TUBES
BASE
CLASS C THERMAL BARRIER

length (the distance from fission birth to absorption) is about 12 cm in an HTGR compared to 4-5 cm in a LWR. Hence the HTGR core is actually more tightly coupled and that thermal heterogeneity effects are less pronounced in an HTGR.

The nuclear characterstics of the HTGR core are also somewhat different because of the different core composition. The major core constituent, carbon, has a low absorption cross section, but somewhat weaker moderating ability than does hydrogen. This, coupled with the higher operating temperature of the HTGR core yields a fairly hard neutron spectrum which tends to interact more strongly with the low lying resonances of such nuclides as U-233 and Xe-135.

Yet another difference is the relatively weak interaction of the core neutronic behavior with the gas coolant, helium. The absence of a large moderator coefficient of reactivity implies that the principal contributer to the core temperature coefficient is the Doppler coefficient. This fact, coupled with a small positive moderator coefficient, yields a rather small net temperature coefficient of reactivity (about $-10 \times 10^{-5}/^{o}C$ at room temperature and -2×10^{-5} at operating temperatures). Fortunately, kinetics calculations show that the peak core temperatures during power excursions are very insensitive to the value of the temperature coefficient. Perhaps the principal reason for this is the immense heat capacity of the HTGR core. If all of the heat generated at full power were stored within the core (none of it being removed by the coolant), then the average core temperature would rise by only $8^{o}F$/sec.

Actually, the smaller temperature coefficient is an advantage since it results in less cold reactivity to be covered with control rods. Furthermore, even though the temperature coefficient is a sum of two fairly

small numbers, experience has indicated that it can be calculated with reasonable accuracy.

The longer migration length and harder energy spectrum characteristic of an HTGR tends to emphasize the treatment of neutron energy relative to lattice effects somewhat more than in light water reactors. For this reason, it is customary to use several thermal groups in multigroup diffusion analysis of such cores (typically, 3 thermal groups and 4 fast groups). Nuclear design of HTGR cores tends to rely a bit more on more detailed calculational models (using realistic descriptions of neutron thermalization, for example), in contrast to light water reactor calculations which tend to use more in the way of empirical correlations. This is due in part to the somewhat different nuclear characteristics of HTGR's, as well as to the limited amount of experimental and operational data available (at least compared to that available for light water reactors).

One final difference in HTGR nuclear analysis involves the use of a different fuel cycle--that in which Th-232 is the fertile material, and eventually U-233 will be the fissile reload fuel. The nuclear analysis of the U-235/Th-232/U-233 fuel cycle is somewhat different than that required by the U-235/U-238/Pu-239 fuel cycel used in light water reactors and fast breeder reactors. Such differences will be discussed in more detail in Chapter 16.

E. Liquid Metal Cooled Fast Breeder Reactors

1. Core Layout

In many ways the core of a LMFBR is similar to that of a LWR. It is made up of a lattice of metal tubes containing an oxide fuel (UO_2 and PuO_2) in a lattice having a pitch to diameter ratio of 1.2 to 1.4.

Control is provided by moveable rods containing absorbing materials such as boron. However, the coolant used in a liquid metal, and many of the nuclear characteristics of the core are quite different.

For purposes of illustration, we will discuss the core layout of the LMFBR demonstration plant under construction in the United States. Although this is only a 400 MWe system, its basic core geometry and component design are quite similar to those of a larger (1000 MWe) design, although, of course, the core size of the latter would be somewhat larger. The core of this LMFBR has a height and radius of about 3 ft. with axial and radial blankets of U^{238} which are from 1 to 2 ft. thick. Both core and axial blankets are made up of hexagonal subassemblies (5 inches across) containing bundles of fuel pins about 0.25 inches in diameter. The radial blanket subassemblies have larger diameter pins. Typical enrichment of the mixed oxide fuel (UO_2 and PuO_2) in the core is 17%. The fuel pins are clad in stainless steel. The core volume fractions are typically about 0.35 fuel and fertile material, 0.45 sodium coolant, and 0.20 structural and clad steel.

Control, both for safety and shim, is provided by moveable control rods of B_4O or tantalum. Shutdown reactivity is about 5% and the temperature plus power defect are about 2%. The main reactivity coefficients are those of the Doppler effect and the sodium void coefficient, although other important reactivity effects are provided by structural expansion and core motion.

2. Nuclear Core Analysis

The main advantage of the fast reactor is its potential for breeding--that is, producing more fissile material by transmutation of

fertile material than it consumes in the fission of fissile material. For a U^{235}-Pu^{239} fueled reactor, we have seen that the energy dependence of η implies that one should design such a reactor to operate with as fast a spectrum as possible. Hence one must avoid introducing material into the core which might moderate the neutrons. Even the presence of the oxygen atoms in the oxide fuel and the liquid metal coolant will cause a significant softening of the neutron spectrum below that which exists in a critical system made up of heavy metal atoms only. [We have compared the spectrum of a typical LMFBR with that of a pure U^{235} Godiva type assembly in Figure 13-17.]

One must also keep in mind tha fact that fast nuclear cross sections are some two orders of magnitude lower than those characterizing thermal neutrons. Hence the neutron mean free paths are correspondingly larger (15-20 cm as compared to 7-8 cm). Furthermore, the much smaller fission cross sections characterizing fast neutrons imply that a much higher concentration of fissile material is required for core criticality--which, in turn, implies a higher core power density.

Despite these differences, the methods used in the nuclear analysis of fast reactor cores bear remarkable similarity to those used in thermal reactor design. Once again, the principal tool is multigroup diffusion theory. However, the larger neutron mean free paths characteristic of fast neutrons means that heterogeneous lattice effects such as self-shielding are far less important than in thermal reactor analysis. Indeed, self-shielding is frequently neglected entirely in first order calculations. The local power peaking effects of concern in thermal reactor design do not arise in fast cores for the same reason. However, the absence

of strong heterogeneous effects is compensated by the much greater sensitivity of fast reactor nuclear performance to neutron energy spectrum effects. One must worry as well about a great many threshold-type nuclear reactions such as inelastic scattering and (n,α) reactions.

There are numerous other differences in fast core design. For example, the density of fissile material in a fast core is some 5 to 7 times that in a light water reactor in order to minimize neutron energy degradation and achieve the density required for core criticality. Since the core power density is high, and the fast neutron mean free path is long, there is sufficient neutron leakage from a fast reactor of even 1000 MWe size to make blankets of fertile material surrounding the core attractive. Over a period of time, fertile conversion in these blankets results in their producing some 10-20% of the total power generated by the LMFBR.

The excess reactivity requirements of a fast core are an order of magnitude below those of thermal cores. This is primarily due to the high conversion ratio and enrichment of such cores. Of course, one might expect that if the reactor is really breeding more fissile material that it utilizes, then the excess reactivity required to compensate for fuel depletion would be zero. However, although there is a net increase in fissile loading during operation, concentration of fissile material in the core actually decreases in most LMFBR designs, while that in the blanket increases. Hence the reactivity will decrease with burnup, although much more slowly than that in a thermal reactor. [It might be remarked that the gas-cooled fast reactor can actually be designed with an internal core conversion ratio greater than one.] The only other excess reactivity

requirements are those used to compensate for fission product buildup (which is relatively insignificant in fast reactors due to the much smaller cross section) and temperature and power defects.

For these reasons, a relatively modest amount of excess reactivity is required in LMFBR designs. Most of the fuel loading corresponds simply to that necessary to achieve core criticality.

The small magnitude of the excess reactivity requirements implies that control requirements are similarly smaller. This is fortunate, because the small absorption cross sections characterizing fast neutrons makes control much more difficult. Indeed, these cross sections are too low to allow the use of burnable poisons or soluble poisons in a fast core. Control is usually provided by moveable control rods of either boron or tantalum.

The kinetic characteristics of a fast reactor are also quite different. The most dramatic difference is in the prompt neutron lifetime which is typically some 2 orders of magnitude shorter than that characterizing thermal reactors. There is also a difference in the delayed neutron fraction β , this the Pu^{239} concentration in the core is quite appreciable. Finally, the methods of reactivity feedback, such as the Doppler effect and coolant void effects are much different. These topics will be discussed in some detail in the next chapter.

The higher specific power, fissile loading, and the use of Pu^{239} as fuel material all result in considerable increases in fuel fabrication and processing costs. The higher core specific power is usually achieved by increasing the surface-to-volume ratio (smaller fuel rod diameters), which increases fabrication costs even further (to some 4-5 times those

of thermal reactor fuels). Hence economic considerations will require a very high fuel burnup in LMFBR's, exceeding 100,000 MWD/MTU. Such high burnups place very stringent demands on fuel element performance, as we will see in Chapter 16.

The thermal design of the LMFBR is simplified somewhat by the absence of local flux peaking. Hence the achievable maximum-to-average power density ratios in the LMFBR are lower because of the smaller core size and the large blanket. ($F_q^N \cong$ 1.25-1.35 in a fast core as compared to 1.5 in a thermal core). The principal thermal limitation is that imposed by avoiding centerline fuel melting. Because the coolant is always several hundred degrees below its saturation temperature, there is no DNB limitation as there is in light water cores.

The large neutron mean free path in a fast core simplifies neutronic calculations to some degree by removing the strong sensitivity to lattice effects (self-shielding). However, the increased sensitivity of fast reactor performance to the neutron energy spectrum requires a much finer multigroup treatment (typically on the order of 20-30 groups).

The development of practical design methods are at a rather primitive stage of development. At this time, more emphasis is being placed on the development of rigorous, benchmark calculations in order to study core physics. The importance of spectrum effects makes ultrafine multigroup codes such as MC^2 (discussed in Chapter 8) important.

The geometrical complexity of fast reactor cores which contain many regions of different composition requires that effective methods by developed to calculate the three dimensional neutron flux distribution. Unfortunately, a 20-30 group, 3-D diffusion calculation is prohibitively

expensive. Hence the development of efficient approximate techniques such as synthesis or coarse-nodal methods for fast reactor analysis seems to be particularly important to the future design of such cores.

IV. FUEL DEPLETION CALCULATIONS

A. Introduction

Fuel depletion analysis is concerned with predicting the long term changes in reactor fuel composition caused by exposure to neutron flux during reactor operation. Such changes have an important bearing on the operating life of a reactor, as well as upon its stability and control. One must first insure that the shift in the core power distribution which accompanies fuel burnup does not result in the exceeding of core thermal limitations. Sufficient excess reactivity must be provided in the fresh core loading to achieve the desired fuel exposure (consistent with safety limitations). And, of course, a detailed analysis of core composition is necessary in order to optimize fuel exposure to achieve minimum power costs. Since the fuel costs over the operating lifetime of the reactor can exceed those of the capital cost of the plant itself, the incentive for accurate analysis of fuel depletion is quite high. It has been estimated that a difference of 0.25% in core reactivity in a 1000 MWe LWR typically will translate into $1,000,000 in fuel costs over a 10 year period. Since absolute reactivities cannot be predicted to this accuracy, fuel depletion calculations occupy a very important role in nuclear reactor analysis.

A variety of nuclear processes must be monitored during a depletion study. These include, of course, the consumption of fissile nuclides (fuel burnup). But as well, one must account for the conversion of fertile isotopes into fissile isotopes and the production of numerous fission products. Finally, one must monitor the reactivity balance to insure core criticality (usually by determining the change in reactivity over a period of core operation and then adjusting control to compensate for this reactivity change).

A complete burnup calculation would involve the solution of the coupled reaction rate equations describing such processes for the hundreds of different types of isotopes in a reactor core. In practice, one usually introduces two approximations which greatly simplify these calculations:

(i) The only fission products treated explicitly are those with large capture cross sections. These include Xe^{135} and Sm^{149}.

(ii) Any nuclide with a very short half-life is omitted from the burnup calculations (being treated as having effectively a zero half-life). The heavy nuclides typically treated in burnup problems are

uranium fueled reactors: U^{235}, U^{236}, U^{238}, Pu^{239}, Pu^{240}, Pu^{241}, Pu^{242}

thorium fueled reactors: U^{233}, U^{234}, U^{235}, U^{236}, Pr^{233}, Th^{232}

One also must include burnable poisons such as B^{10} or Gd.

EXAMPLE: Suppose the reactor were fueled with only a single isotope of density $N_F(\vec{r},t)$. Then the fuel burnup would be described by

$$\frac{dN_F}{dt} = - N_F(\vec{r},t)\,\sigma_a^F\,\phi(\vec{r},t)$$

We can formally solve this to find

$$N_F(\vec{r},t) = N_F(\vec{r},0)\,\exp\left[-\sigma_a^F \int_0^t \phi(\vec{r},t')\,dt'\right]$$

It is convenient to define a new variable, the time integrated neutron flux or "fluence"

$$\varphi(t) = \int_0^t \phi(t')\,dt'$$

Of course, this is still a formal solution since the flux, $\phi(\vec{r},t)$, depends upon the fuel density $N_F(\vec{r},t)$ through the equations describing reactor criticality (i.e., the multigroup diffusion equations).

We can use this result to illustrate the two standard approximations used in more elaborate depletion studies.

a) Constant flux approximation

Assume that over the time interval of interest, the flux can be treated as constant

$$\phi(\vec{r},t) = \phi_o(\vec{r})$$

Then we can solve for

$$N_F(\vec{r},t) = N_F(\vec{r},0)\,e^{-\sigma_a^F \phi_o(\vec{r})\,t}$$

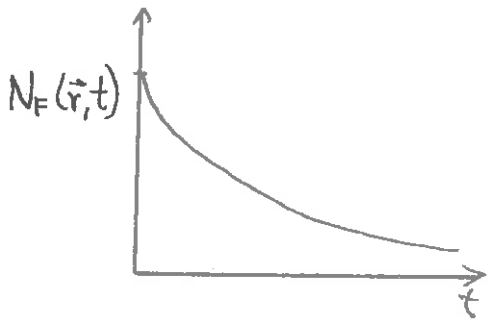

b) Constant power approximation:

One assumes instead that the reactor power is constant

$$P(\vec{r},t) = w_f N_F(\vec{r},t)\,\sigma_a^F\,\phi(\vec{r},t) = P_o(\vec{r})$$

Then one finds

$$N_F(\vec{r},t) = N_F(\vec{r},0)\left[1 - \frac{P_o(\vec{r})t}{w_f}\right]$$

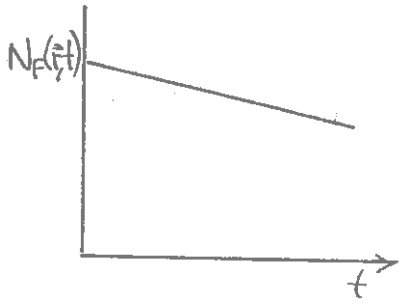

B. Calculational Methods

We have noted that the analysis of fuel depletion involves a variety of nuclear processes. These can be roughly classified into calculations involving:

(i) solution of the isotopic depletion equations: That is, solving for the nuclei densities as functions of time and position. But this requires a knowledge of the neutron flux.

(ii) solution of the multigroup diffusion equations for the neutrons flux. Of course, this task will usually also involve including thermal-hydraulic coupling. Furthermore, one must use as input the cross sections characterizing the depleting isotopes, and furthermore, must adjust the control representation to achieve core criticality.

It is customary to decouple these calculations such that the depletion equations are solved over time intervals in which the flux or power is

assumed to be constant. At the end of each time interval, the depleted densities are used to calculate new group constants, and the multigroup diffusion equations are solved to determine a new flux shape for the next time interval.

1. Isotopic Depletion Equations

The reaction rate equations describing the number of densities of nuclei in the core can be derived using simple balance ideas. If $N_A(\vec{r},t)$ is the number density characterizing a nuclide of type A, then the general rate equation characterizing a production-decay scheme as shown below

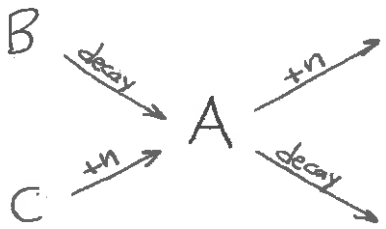

takes the form

$$\frac{dN_A}{dt} = -\lambda_A N_A - \left[\sum_g \sigma_{ag}^A \phi_g\right] N_A + \lambda_B N_B + \left[\sum_g \sigma_{cg}^C \phi_g\right] N_C \quad (13\text{-}33)$$

Here,

$\lambda_A N_A$ loss due to radioactive decay of A

$\left[\sum_g \sigma_{ag}^A \phi_g\right] N_A$ loss due to neutron capture by A

$\lambda_B N_B$ gain due to decay of B to A

$\left[\sum_g \sigma_{ag}^C \phi_g\right] N_C$ gain due to transmutation of C to A via neutron capture

The fluxes and microscopic cross sections appearing in these equations are multigroup averages and must be generated by suitable group constant generation codes and multigroup diffusion calculations.

These equations are nonlinear and inhomogeneous because the fluxes and microscopic cross sections not only vary in space in time, but depend as well upon the densities of the depleting isotopes as well. Such equations must be written for each species of interest. Typical chains of interest in uranium fueled reactors are shown in Figures 13-20 and 13-21. In a detailed study of fuel depletion in a modern power reactor, some 15 to 24 heavy nuclides and 25 to 50 fission products are required for analysis. When one adds to this the fact that the differential equations describing isotopic depletion contain both long and short time constants which complicate their numerical solution, it is apparent that fuel depletion calculations can become quite involved.

EXAMPLE: Let us derive a simplified set of isotopic depletion equations for a thermal reactor fueled with enriched uranium. The most significant reactions aside from capture and fission of U^{235} include

(i) $n + U^{238} \rightarrow U^{239} \rightarrow Np^{239} \rightarrow Pu^{239}$

(ii) $n + Pu^{239} \rightarrow$ fission or Pu^{240}

(iii) $n + Pu^{240} \rightarrow Pu^{241}$

(iv) $n + Pu^{241} \rightarrow$ fission or Pu^{242}

Now Pu^{239} is formed by both thermal and resonance capture, but disappears via thermal capture. If we note that the number of neutrons absorbed in U^{238} resonance can be expressed in terms of fissioning isotopes and the resonance capture probability, (1-p), we can write

FIGURE 13-20: ISOTOPE CHAINS

Uranium-Fueled Cores

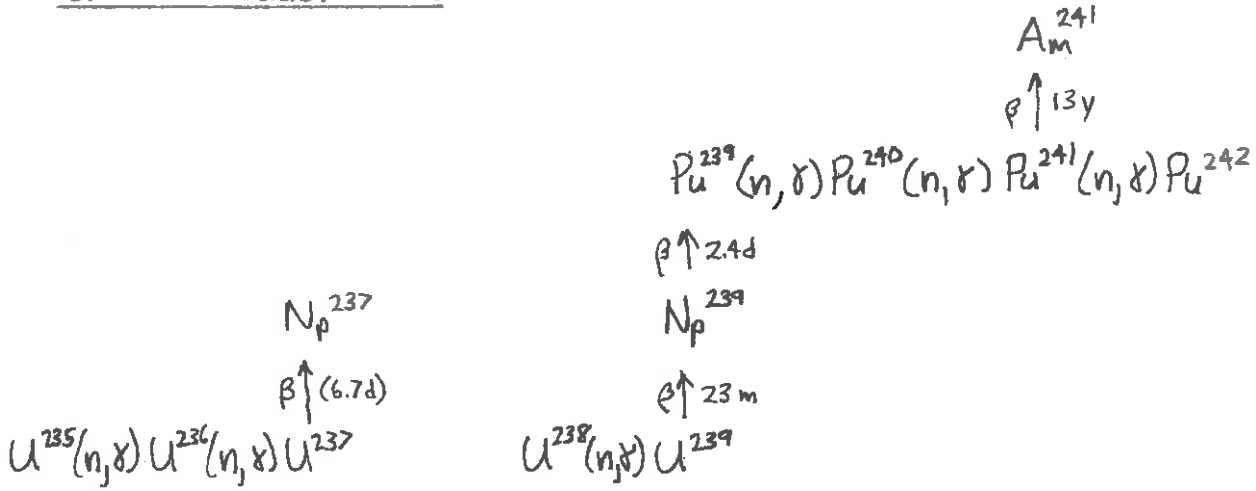

Thorium-Fueled Cores

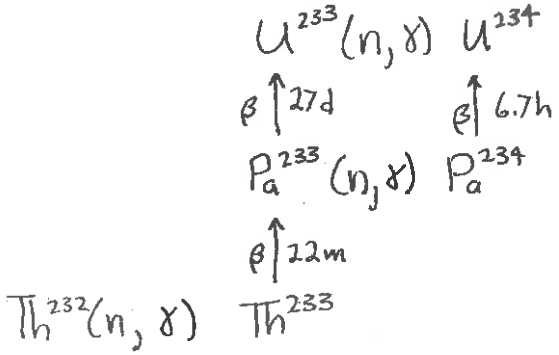

FIGURE 13-21

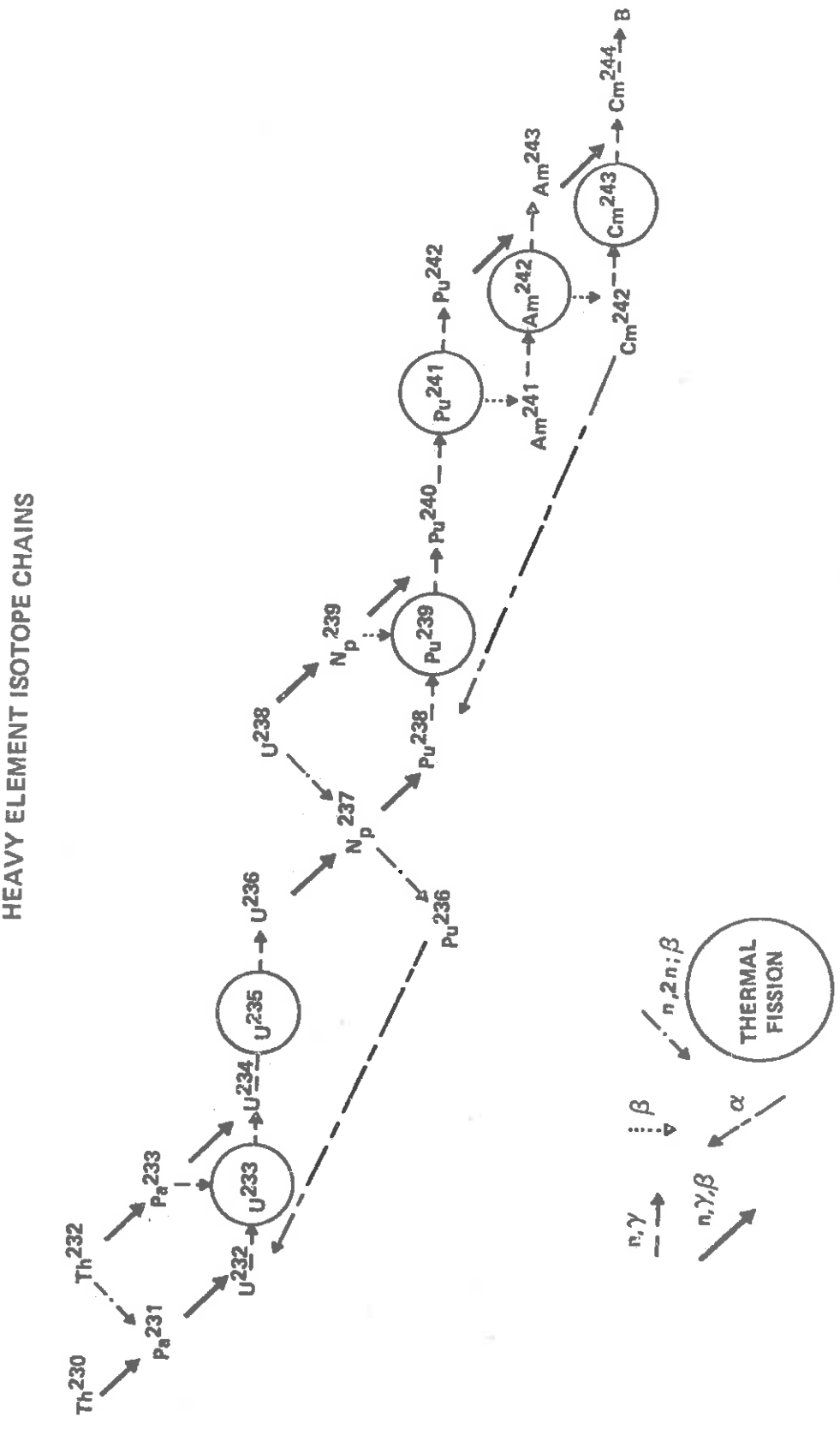
HEAVY ELEMENT ISOTOPE CHAINS
Th230
Th232
Pa231
Pa233
U232
U233
U234
U235
U236
U238
Np237
Np239
Pu236
Pu238
Pu239
Pu240
Pu241
Pu242
Am241
Am242
Am243
Cm242
Cm243
Cm244
B
n,γ
β
α
n,γ,β
n,2n;β
THERMAL FISSION

FIGURE 13-21'

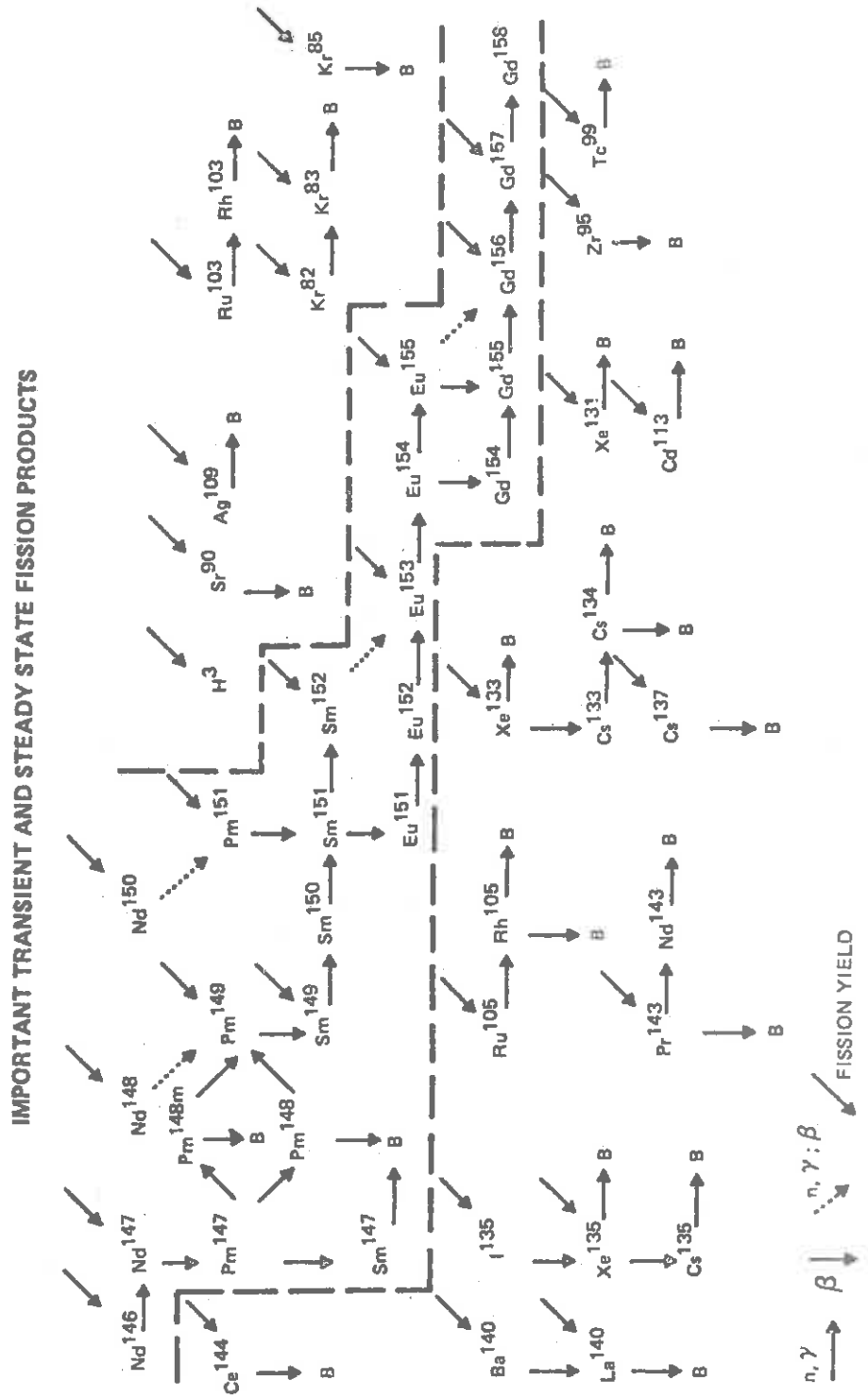
IMPORTANT TRANSIENT AND STEADY STATE FISSION PRODUCTS
FISSION YIELD

$$\frac{dN_{49}}{dt} = N_{28}\bar{\sigma}_a^{28}\phi + (1-p)\epsilon P_{NFL}\left(\nu_{25}N_{25}\bar{\sigma}_f^{25} + \nu_{49}N_{49}\bar{\sigma}_f^{49} + \nu_{41}\bar{\sigma}_f^{41}\right)\phi - N_{49}\bar{\sigma}_a^{49}\phi$$

Furthermore

$$\frac{dN_{40}}{dt} = \left(N_{49}\bar{\sigma}_a^{49} - N_{40}\bar{\sigma}_a^{40}\right)\phi$$

$$\frac{dN_{41}}{dt} = \left(N_{40}\bar{\sigma}_a^{40} - N_{41}\bar{\sigma}_a^{41}\right)\phi$$

2. Generation of Macroscopic Group Constants

A very important facet of any depletion analysis is the generation of the necessary few group constants. Our earlier discussion of a typical macroscopic cross section module in 13-22 illustrated several aspects of such calculations. We recall that these group constants consisted of two factors: the number densities supplied from the depletion module (or perhaps the thermal-hydraulic module or input), and the microscopic group constants generated either by fast and thermal spectrum codes or by parameterization

$$\Sigma_{x_g}(\vec{r},t) = \sum_j N_j(\vec{r},t)\,\bar{\sigma}_{x_g}^{\,j}(\vec{r},t)$$

The microscopic cross sections will change in time as the fuel depletes, since the neutron spectrum in the fuel cell will change, as will the effect of self-shielding. Many cross sections are sufficiently slowly varying with fuel depletion that they need only be recalculated at several time steps and can be linearly interpolated at intermediate times. More rapidly

varying cross sections which exhibit strong depletion dependence of self-shielding factors or spectrum will require adjustment at shorter time intervals.

3. Flux-Power Calculations

One must use these few group constants in the multigroup diffusion equations to determine the flux and power distribution in the core. Interaction with a control adjustment module is usually necessary in order to adjust core multiplication back to critical after a depletion time step. Such flux-power calculations may range from 0-D to 3-D descriptions.

4. Solution of the Depletion Equations

The direct solution of the coupled equations describing the number densities of core materials, and the multigroup diffusion equations describing the neutron flux is impractical. Instead, one must separate these calculations. The coupling between the depletion and neutronics calculations can be handled in one of several ways:

a) Spatial Treatment: The multigroup diffusion equations must be solved many times as depletion proceeds. Such solutions become very expensive if detailed spatial treatments are required. One can distinguish between two different approaches:

(i) Point-subdivision method: In such a scheme, the isotopic depletion equations are solved at every spatial mesh point required by the multigroup diffusion calculation. Such a brute force scheme is very expensive, but does provide a detailed analysis of spatial depletion effects.

(ii) Regionwise depletion: In this scheme, the depletion equations are solved for a region associated with several mesh points of the diffusion calculation by homogenizing the cross sections over this larger region.

One can also distinguish between methods that consider only the depletion of a particular cell in the reactor (typically 1 to 4 fuel assemblies) or those that use separable parametric multigroup lattice cell calculations to determine the few group constants to be used in a global reactor depletion evaluation. These two approaches are contrasted in the diagrams in Figures 31-23 and 13-24.

b) Time Treatment: The treatment of the time dependence of the material density depletion and the changes in the flux distributions are usually handled by separating the depletion calculation from the neutronic calculation. To illustrate this approach, suppose that one knows the initial nuclei densities in the clean, fresh core at time t = 0. Then the macroscopic group constants can be generated, and the multigroup fluxes can be calculated (although a control adjustment may be required to achieve core criticality).

Next, the depletion equations are solved for times $0 < t < \Delta t$ by assuming that over this time step either

(i) constant flux for $0 < t < \Delta t$: $\phi_g(\vec{r},t) = \phi_g(\vec{r},0)$

(ii) constant power density for $0 < t < \Delta t$:

$$\Sigma_{fg}(\vec{r},t)\phi_g(\vec{r},t) = \sum_j N_j(\vec{r},t)\sigma_{fg}^j\phi_g(\vec{r},t) = \Sigma_{fg}(\vec{r},0)\phi_g(\vec{r},0) \quad (13\text{-}34)$$

FIGURE 13-23

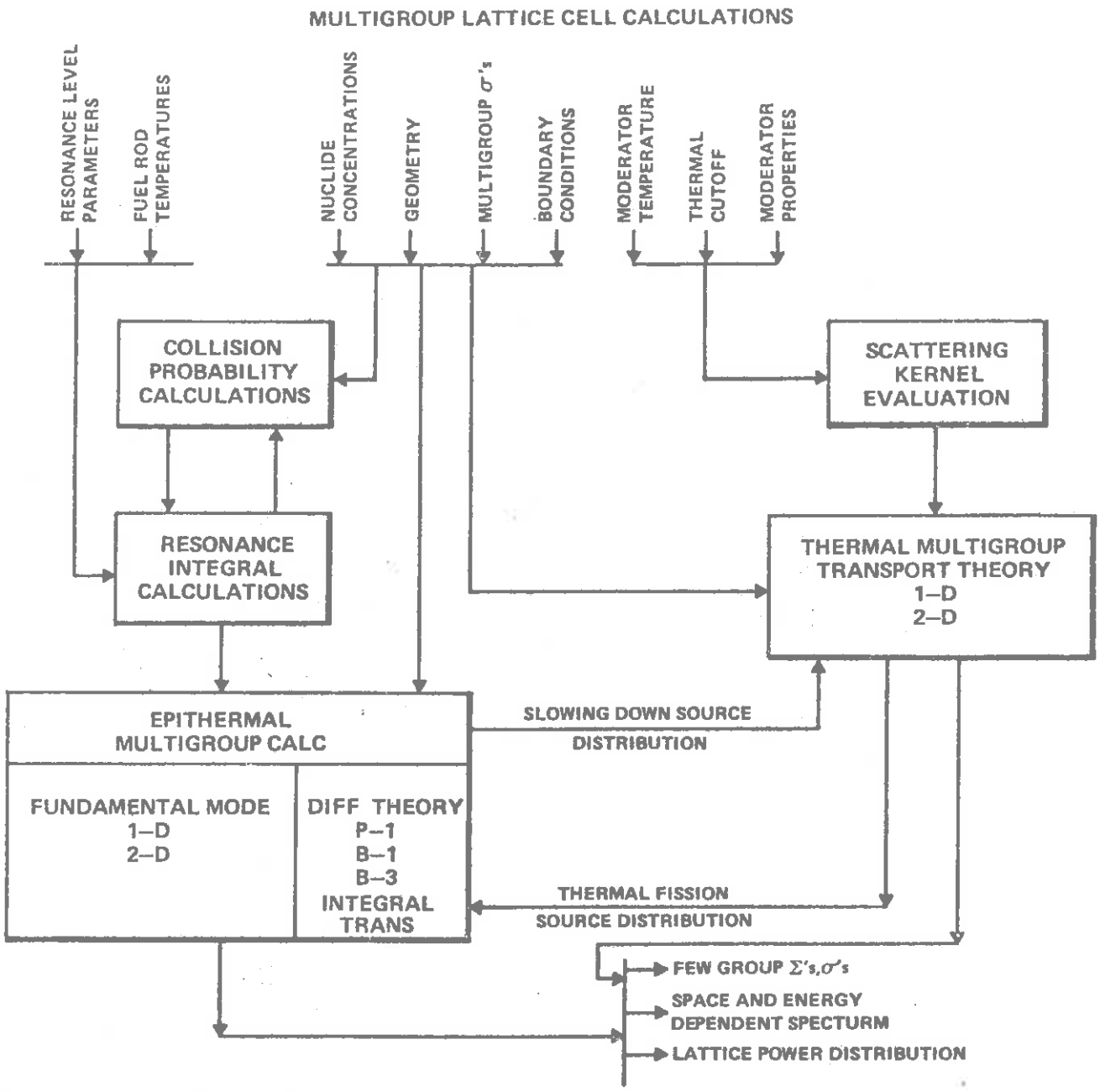
MULTIGROUP LATTICE CELL CALCULATIONS
RESONANCE LEVEL PARAMETERS
FUEL ROD TEMPERATURES
NUCLIDE CONCENTRATIONS
GEOMETRY
MULTIGROUP σ's
BOUNDARY CONDITIONS
MODERATOR TEMPERATURE
THERMAL CUTOFF
MODERATOR PROPERTIES
COLLISION PROBABILITY CALCULATIONS
SCATTERING KERNEL EVALUATION
RESONANCE INTEGRAL CALCULATIONS
THERMAL MULTIGROUP TRANSPORT THEORY 1–D 2–D
EPITHERMAL MULTIGROUP CALC
FUNDAMENTAL MODE 1–D 2–D
DIFF THEORY P–1 B–1 B–3 INTEGRAL TRANS
SLOWING DOWN SOURCE DISTRIBUTION
THERMAL FISSION SOURCE DISTRIBUTION
FEW GROUP Σ's,σ's
SPACE AND ENERGY DEPENDENT SPECTURM
LATTICE POWER DISTRIBUTION

FIGURE 13-24

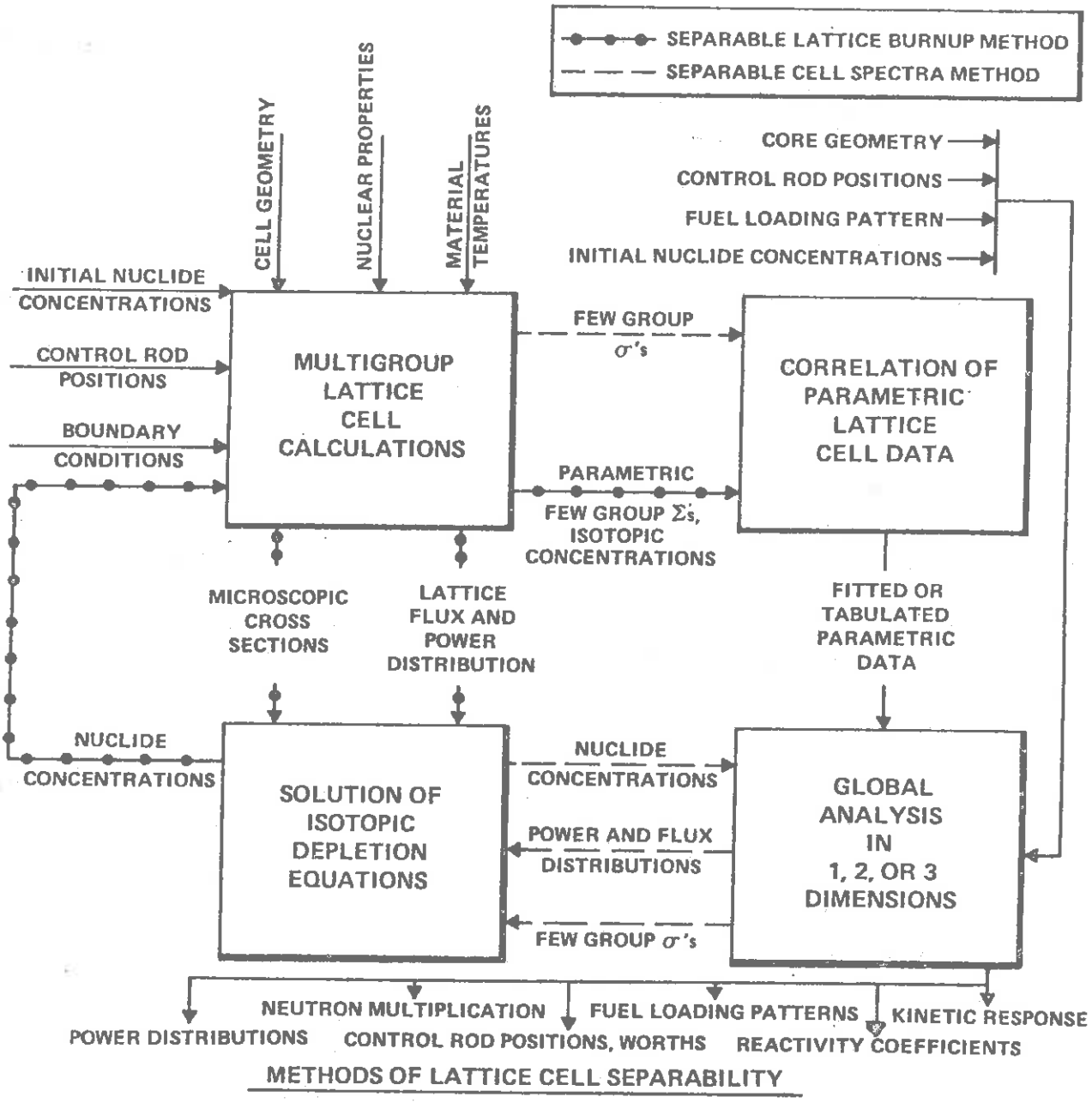

METHODS OF LATTICE CELL SEPARABILITY

(One usually applies the constant flux approximation, since the assumption of constant power density is difficult to apply for more than one fissile isotope.) Under these assumptions, the isotopic depletion equations (written here in matrix notation for convenience)

$$\frac{d\underline{N}}{dt} = \underline{\underline{A}}\,\underline{N}(t) + \underline{F}(t) \qquad (13\text{-}35)$$

can be solved (in the constant flux approximation for purposes of illustration) as

$$\underline{N}(t+\Delta t) = e^{\underline{\underline{A}}\,\Delta t}\,\underline{N}(t) + \underline{\underline{A}}^{-1}\left(e^{\underline{\underline{A}}\,\Delta t} - 1\right)\underline{F}(t) \qquad (13\text{-}36)$$

Of course one must choose the time step size Δt such that the variation of the flux over this time step is negligible.

Having determined the number densities N_j at the later time $t = \Delta t$, one can now generate new multigroup constants (either by using parameterized cross sections or repeating spectrum calculations), and then use these to calculate a new multigroup flux distribution. Once again, control adjustment will be required to achieve core criticality, as will flux normalization to maintain the required core thermal power output.

This scheme can then be continued for another time step, $t < t < 2\Delta t$ (which may have a variable size), and so on until the excess reactivity of the core drops sufficiently low that core life is terminated.

A variety of depletion codes have been used in the analysis of core burnup. These range from zero dimensional codes such as LEØPARD used for survey calculations (such as those to determine the approximate fuel

FIGURE 13-25

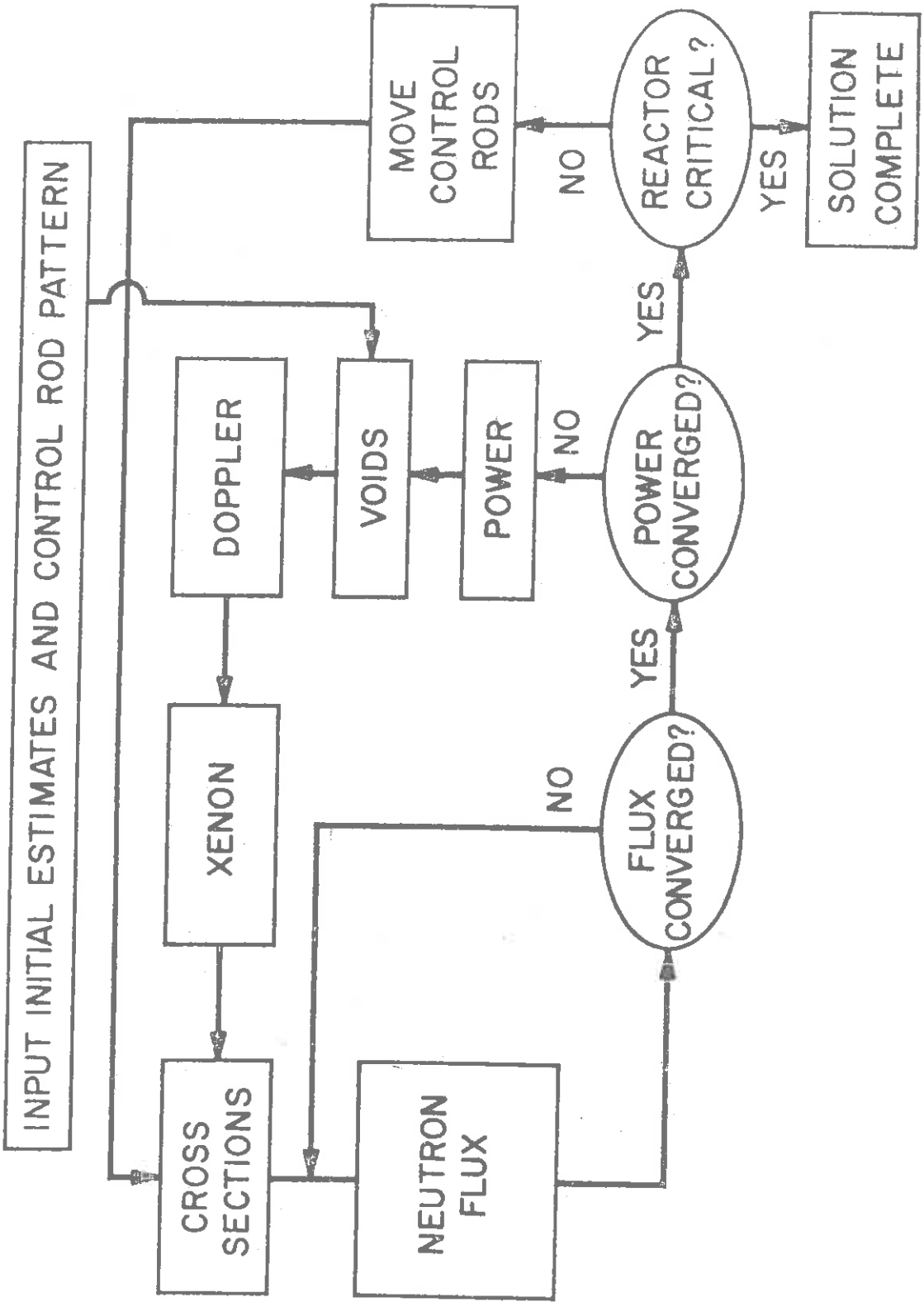
INPUT INITIAL ESTIMATES AND CONTROL ROD PATTERN
CROSS SECTIONS
NEUTRON FLUX
FLUX CONVERGED?
NO
YES
XENON
DOPPLER
VOIDS
POWER
POWER CONVERGED?
NO
YES
MOVE CONTROL RODS
REACTOR CRITICAL?
NO
YES
SOLUTION COMPLETE

enrichment required to yield a desired burnup) to 2-D and 3-D codes such as PDP-HARMØNY which are used in final design calculations to give detailed nuclei densities and power distributions useful for the study of control management.

5. A Simple Example

Although any realistic study of fuel depletion requires numerical methods, it is of interest to illustrate the ideas involved in the solution of the isotopic depletion equations and control adjustment by considering a simple model in which the neutronic analysis is bypassed by assuming an infinite one speed reactor characterized by a multiplication $k = \eta f$. That is, we assume a simple model of an infinite, homogeneous, thermal reactor with a single fissile isotope (e.g., U^{235}) and no fertile material. We will represent the control rods used to balance the excess reactivity of the initial coreloading by a uniformly distributed absorption cross section, $\Sigma_c(t)$. Notice that we must continually adjust $\Sigma_c(t)$ to keep the core critical. The criticality condition for this simple model is just

$$k_\infty = \eta f = \frac{\eta \Sigma_a^F(t)}{\Sigma_a^F(t) + \Sigma_a^M + \Sigma_a^P(t) + \Sigma_c(t)} = 1 \qquad (13\text{-}35)$$

fuel — moderator — fission product poison

We can solve this for the required control

$$\Sigma_c(t) = (\eta - 1)\Sigma_a^F(t) - \Sigma_a^M - \Sigma_a^P(t) \qquad (13\text{-}36)$$

Now as the core life proceeds, the fuel cross section $\Sigma_a^F(t)$ decreases, while the poison concentration increases. Hence $\Sigma_c(t)$ will drop to zero eventually at some time t_ℓ, corresponding to the end of core life. It is possible to calculate t_ℓ, provided the power history of the reactor is known.

For simplicity, we will suppose that the reactor is operated at constant power over the core life. This implies

$$\Sigma_a^F(t)\phi(t) = \Sigma_a^F(0)\phi(0) \tag{13-37}$$

where $\Sigma_a^F(0)\ \phi(0)$ characterizes the initial core loading. After a time t,

$$\begin{aligned} N_F(t) &= N_F(0) - \Sigma_a^F(0)\phi(0)t \\ &= N_F(0)\left[1 - \sigma_a^F\phi(0)t\right] \end{aligned} \tag{13-38}$$

or

$$\Sigma_a^F(t) = \Sigma_a^F(0)\left[1 - \sigma_a^F\phi(0)t\right] \tag{13-39}$$

If we plug this into (10-146), we can solve for the flux

$$\phi(t) = \frac{\phi(0)}{1 - \sigma_a^F\phi(0)t} \tag{13-40}$$

[Note how $\phi(t)$ must increase as the fuel is depleted in order to yield a constant power production.]

We can now use this flux history to compute the fission product poison concentrations. Recall from our earlier work that the equilibrium fission product concentrations are given by:

$$\Sigma_a^X(t) = \frac{(\gamma_I+\gamma_X)\Sigma_f\phi}{\phi_X+\phi} = \frac{(\gamma_I+\gamma_X)\Sigma_f(0)\phi(0)}{\phi_X+\phi(t)}, \quad \phi_X \equiv \frac{\lambda_X}{\sigma_a^X} \tag{13-41}$$

for xenon, and

$$\Sigma_a^S(t) = \gamma_p \Sigma_f(t) \tag{13-42}$$

for samarium. [Note here that $\Sigma_f(t) = \Sigma_a^F(t)/(1+\alpha)$.]

We must also worry about non-saturating or "permanent" poisons

$$\Sigma_{pp} = \sigma_{pp}\Sigma_f(t)\phi(t)t = \sigma_{pp}\Sigma_f(0)\phi(0)t \tag{13-43}$$

Plugging all of these into our expression for the control cross section, Eq. (10-145), we find

$$\Sigma_c(t) = (\eta-1)\Sigma_a^F(0)\left[1-\sigma_a^F\phi(0)t\right] - \Sigma_a^M - \frac{(\gamma_I+\gamma_X)\Sigma_f(0)\phi(0)}{\phi_X+\phi(t)}$$
$$- \gamma_p\Sigma_f(0)\left[1-\sigma_a^F\phi(0)t\right] - \sigma_{pp}\Sigma_f(0)\phi(0)t \tag{13-44}$$

If we now plug in Eq. (13-40) for $\phi(t)$, and then set $\Sigma_c(t_\ell) = 0$, we can solve for the core lifetime t_ℓ as

$$t_\ell \simeq \frac{\eta \rho_x (1+\alpha) - (\gamma_I + \gamma_x)\phi(0)/\phi_x - \gamma_\rho}{[(\eta-1)(1+\alpha)\sigma_a^F - \gamma_\rho \sigma_a^F + \sigma_{\rho\rho}]\phi(0)} \quad \text{for } \phi(t) << \phi_x \qquad (13\text{-}45)$$

or

$$t_\ell \simeq \frac{\eta \rho_x (1+\alpha) - (\gamma_I + \gamma_x + \gamma_\rho)}{[(\eta-1)(1+\alpha)\sigma_a^F - (\gamma_I + \gamma_x + \gamma_\rho)\sigma_a^F + \sigma_{\rho\rho}]\phi(0)} \quad \text{for } \phi(t) >> \phi_x \qquad (13\text{-}46)$$

where $\rho \equiv k_\infty(0) - 1 / k_\infty(0)$ is the initial excess reactivity.

For example, consider burnup calculations performed on the Yankee PWR. The figure below gives the concentrations of various fuel isotopes vs. the neutron fluence

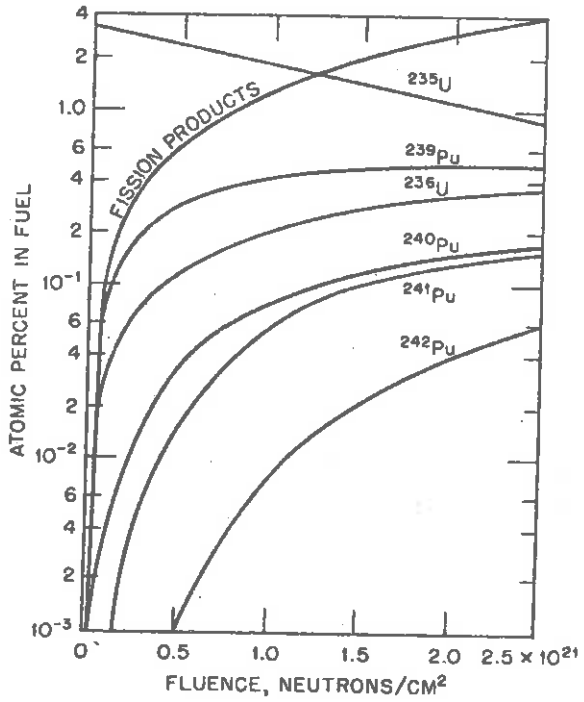

CHANGE IN FUEL COMPOSITION VS NEUTRON FLUENCE

The highest fluence corresponds to an average burnup of 23,000 MW-days/tonne. It is also of interest to compare the power density in the core initially with its shape late in the core life:

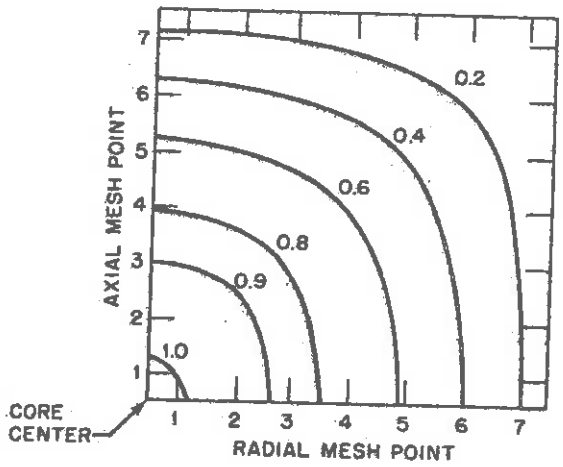

INITIAL CALCULATED SPATIAL POWER DENSITY DISTRIBUTION IN ONE QUADRANT OF REACTOR FOR UNIFORM FUEL LOADING (AFTER M. BENEDICT,

The peak of the maximum power density has shifted well away from the center of the core, corresponding to the higher fuel burnup at the core center. Note also the depression in the flux at the center of the core.

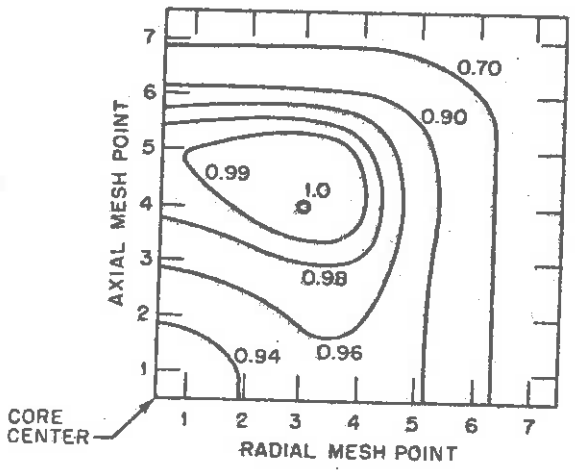

CALCULATED SPATIAL POWER DENSITY DISTRIBUTION AFTER AVERAGE BURNUP OF 23,000 MW-DAYS/TONNE (AFTER M. BENEDICT, *ET AL.*, REF. 48).

CHAPTER 14: REACTIVITY CONTROL

I. INTRODUCTION

Nuclear reactors must be initially loaded with a significantly larger amount of fuel than that required to merely achieve criticality, since the intrinsic multiplication of the core will change over core operation due to processes such as fuel burnup and fission product production. Sufficient excess reactivity must also be provided to compensate for effects such as temperature feedback. For example, in large light water power reactors, the initial enrichment of fissile material may be as much as 50 to 100% larger than that required for core criticality. In the same sense that the core volume is primarily determined by the required thermal power output and the power density consistent with thermal design limitations, the excess reactivity present in the core fuel is determined by the desired core operating lifetime.

To compensate for this excess reactivity, it is necessary to introduce an amount of negative reactivity into the core which one can adjust or control at will. This control reactivity not only allows one to compensate for the excess reactivity necessary for long term core operation, but it as well allows one to adjust the power level of the reactor, to bring the core to power, to follow load demands, and to shut the core down. The control reactivity is most often present in the form of a strong neutron absorber which can be inserted into or withdrawn from the core (although moveable reflectors have also been used for reactivity control). In this introductory section, we will classify the control

requirements of nuclear reactor cores, as well as the types of control elements commonly used in power reactors.

It is first useful to introduce several definitions characterizing reactivity control:

Excess reactivity $\rho_{ex} \equiv$ The core reactivity present with all control elements withdrawn from the core. ρ_{ex} will be a function of both time (due to fuel burnup and isotope production) and temperature (due to reactivity feedback). In general, larger values of ρ_{ex} imply longer core lifetimes, but at the expense of larger control requirements and poorer neutron economy.

Shutdown margin $\rho_{sm} \equiv$ The negative reactivity of the core present when all control elements have been fully inserted to achieve minimum core multiplication. Again, the shutdown margin, ρ_{sm}, is a function of time and temperature. The shutdown margin will affect the rate at which the reactor power level may be reduced in an emergency shutdown or "scram". In particular, the prompt jump approximation implies that the fractional power level decrease achievable immediately after control insertion is given by

$$\frac{\text{Power after control insertion}}{\text{Power before control insertion}} = \frac{1-\rho_{sm}}{1-(\rho_{sm}/\beta)} \qquad (14\text{-}1)$$

Typically, the shutdown multiplication is kept below 0.97, or consistent with the "stuck-rod" criterion, below 0.99 with the most reactive control rod stuck in the full "out" position.

Total control element worth $\Delta\rho \equiv$ The difference between the excess reactivity and the minimum reactivity when all control elements are fully inserted. That is,

$$\Delta\rho = \rho_{ex} + \rho_{sm} \tag{14-2}$$

[The precise definition of reactivity worth is occasionally given a slightly different characterization, depending upon whether the control element of interest is intended for power level changes or for fuel burnup compensation. (See Lamarsh, for example.) We will utilize the simple definition implied by Eq. (14-2) here.]

Of course, in determining the required control reactivity worth, one must be concerned with the speed with which the control can be inserted--such as in a scram situation in which the control must be capable of shutting the reactor down under any credible operating conditions.

One can distinguish several different types of control requirements:

(i) scram control elements: The function of these elements is to shut the reactor core down under all credible operating circumstances. Such elements must be capable of inserting negative reactivity very rapidly and must operate with extremely high reliability.

(ii) power regulation: Certain control elements are designed to compensate for small reactivity transients caused by changes in load demand, core temperature, and for power level maneuvering.

(iii) shim control elements: Shim control elements are designed to cover the excess reactivity necessary to compensate for long

term fuel depletion and fission product buildup. Shim elements are also used to shape the power profile in order to obtain a more uniform fuel burnup.

There are several schemes used for introducing control absorption into a nuclear reactor core. One common method is to insert moveable rods of absorbing material into the core. Such moveable control elements not only can be used to adjust the core power, but because of their rapid response can also be used for scramming the reactor, as well as for shim and power shaping. Fixed absorbing materials are sometimes fabricated into the core, with the intent that such absorption will gradually burn out along with the fuel. Such burnable poisons are useful for extending the initial core lifetime of reactors. A third very popular control mechanism in light water reactors involves dissolving a poison such as boric acid in the coolant itself. Such a soluble poison provides a very uniformly distributed shim which minimizes spatial power profile perturbations.

In the early days of nuclear reactor development, control elements were typically cylindrical in shape. However, in todays tightly packed fuel lattices, control elements are most typically cruciform shaped blades or clusters of narrow control rods. The control requirements and type of control vary considerably among reactor types. For example, the control requirements in light water reactors are compared in the table below:

Control Characteristics	Reactivity ρ BWR	PWR
Excess Multiplication of Clean Core (Uncontrolled): ρ_{ex}		
at 68°F	0.25	0.293
at Operating Condition, Clean	-	0.248
at Operating Condition, Xe & Sm equil.	-	0.181
Worth of Control Rods	-0.17	-0.07
Worth of Borated Control Curtains	-0.12	None
Total Worth of Soluble Poison	None	- .25
Total Worth of Control $\Delta\rho$	-0.29	- .32
cold & clean ρ_{sm}	.04	.03
hot & equil. Xe & Sm	-	.14

More specific control elements of these reactor types include:

PWR: (i) Shim: In a PWR, a major portion of shim control is provided boric acid dissolved in the coolant. The reactivity worth of this soluble poison is typically -0.25. Such soluble poisons not only provide a uniform shim, but also tend to reduce the costs required for moveable control elements. They have the disadvantage in that they have a very slow response and substantially perturb the moderator void coefficient of reactivity.

(ii) Shim and control: The moveable control elements are in the form of control rod clusters consisting of a stainless steel clad silver-cadmium alloy. Typically the reactivity worth

of these elements is about $\Delta\rho = -0.09$. These have a rapid response, and since they are distributed about the core, can be used for power shaping. They are expensive, however. Such rods are inserted from the top of the core with a gravity and a rack and pinion or magnetic drive. A schematic of such a control rod cluster is shown in Figure 14-1.

BWR: (i) Shim: Shim is provided by burnable poisons in the form of a gadolinium alloy, Gd_2O_3 which is mixed into the UO_2 pellets of certain fuel elements in each subassembly. [Earlier BWR designs utilized boron loaded control curtains.] The initial reactivity of the burnable poison is about $\Delta\rho \tilde{=} -0.12$. Such poisons extend core lifetime by compensating for enhanced excess reactivity. They are usually utilized only until the equilibrium fuel cycle is reached.

(ii) Shim and control: In BWR's, moveable cruciform control blades which contain stainless tubes of steel clad B_4C powder are used, with a reactivity worth of $\Delta\rho \tilde{=} -0.17$. [See Figure 14-2.] Such control elements must be inserted from the bottom of the core because of the presence of steam drying equipment in the top of the pressure vessel. However, bottom insertion does possess some advantages since it allows one to compensate for the rather marked flux peaking which would occur at the bottom of the core to moderator density variations.

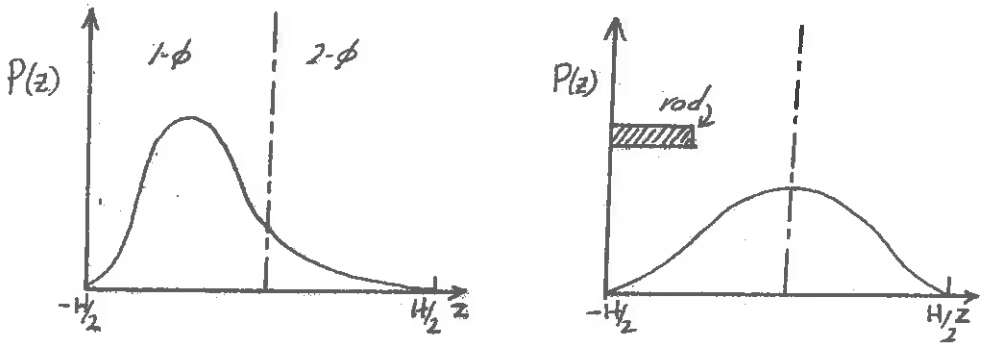

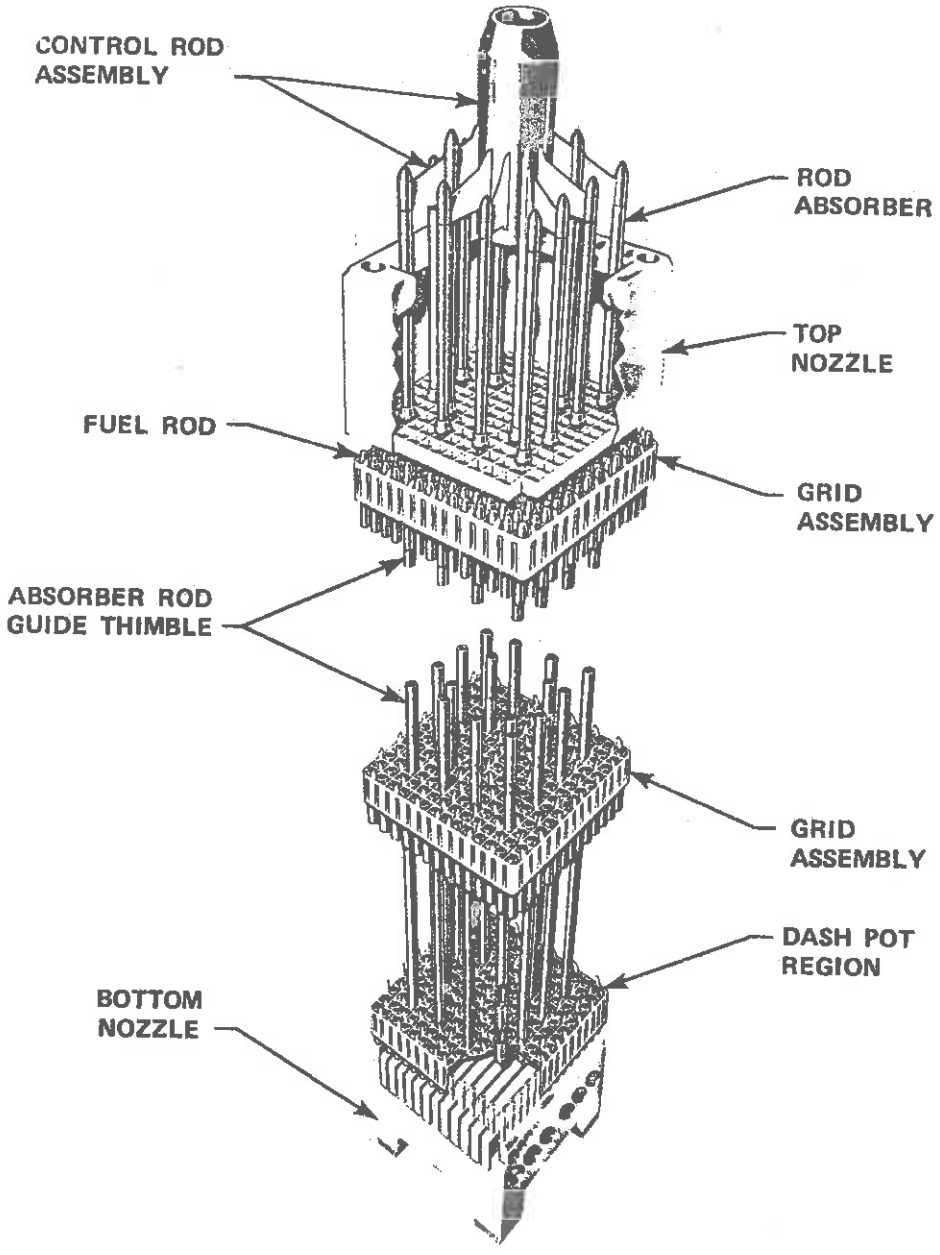

Figure 14-1. PWR Rod Cluster Control Assembly

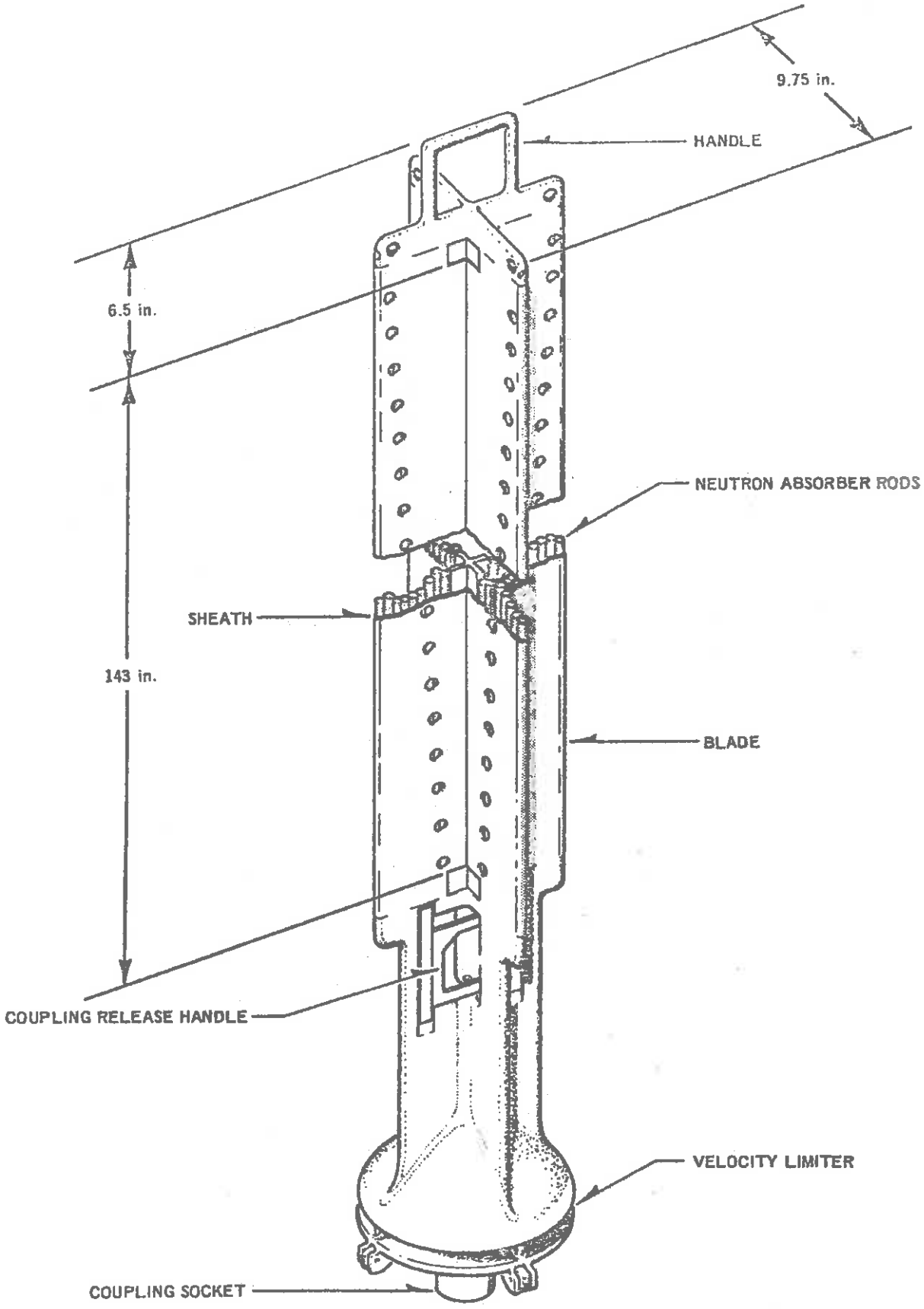

Figure 14-2. BWR Control Rod Assembly

Since gravity feed is not available for bottom inserted rods, one must rely on hydraulic drive mechanisms.

HTGR: Large high temperature gas cooled reactors customarily use burnable poisons composed of B_4C pins inserted into the graphite block fuel assemblies (see Figure 14-4) as shim control. Moveable control rods of B_4C are inserted at various positions in the core (typically 40-50 pairs of such rods). The control requirements of an HTGR are somewhat smaller because of the absence of a strong moderator void coefficient, as the table below indicates:

Type of Measurement	Reactivity Effect	
	Measured	Calculated
Temperature defect		
36°C to 315°C	-.024 ±.002 Δρ	-.022
36°C to operating temperature	-.070	-.063
Temperature coefficient		
36°C	-9.0×10^{-5}/°C	-8.6×10^{-5}/°C
315°C	-8.1	-7.0
Operating temperature	-3.6	-4.9

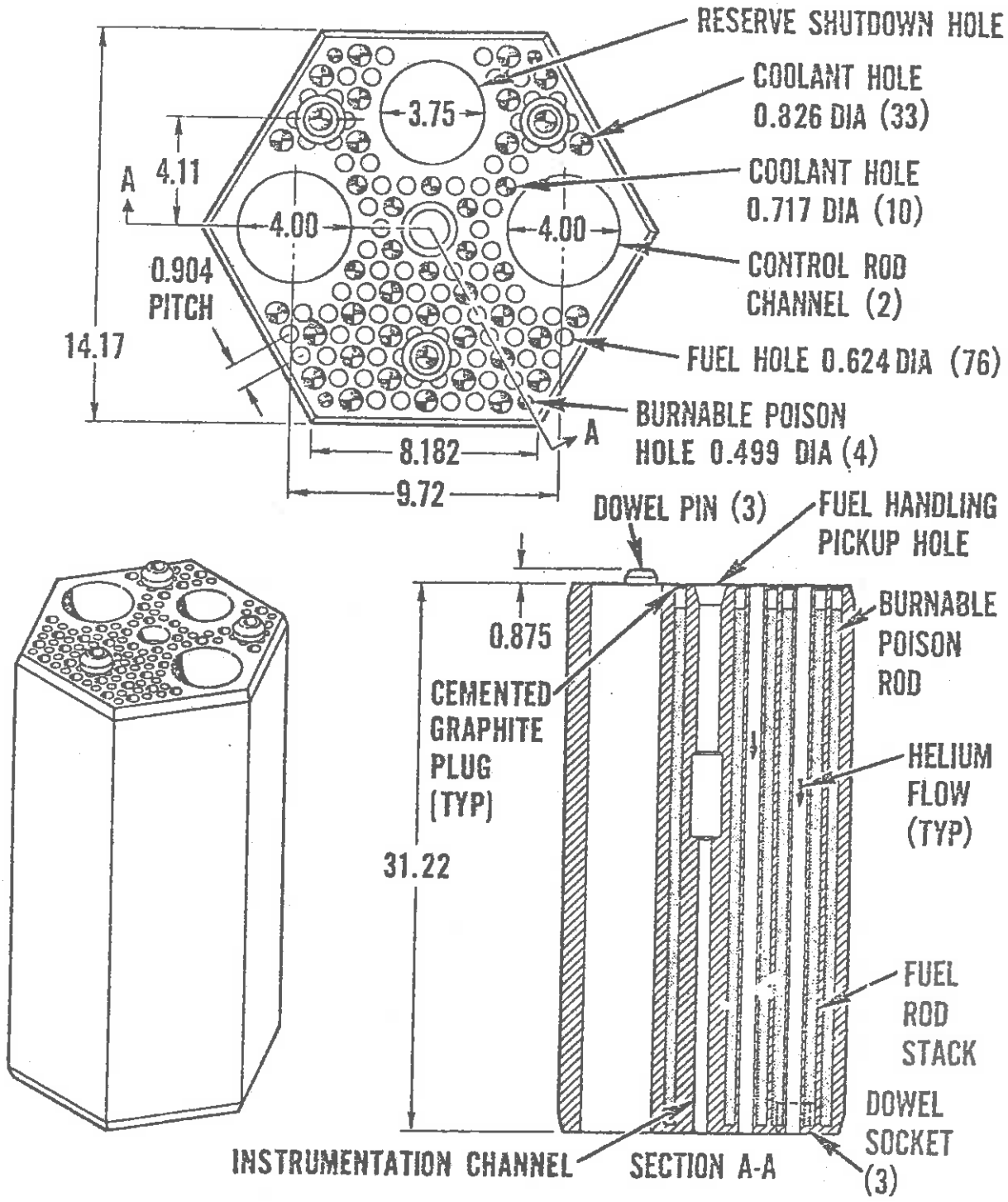

FIGURE 14-4: HTGR Control Fuel Assembly

LMFBR: The control requirements in fast breeder reactors are not nearly so large since the production of plutonium during core operation compensates for fuel burnup and decreases the required core excess reactivity. However, the delayed neutron fraction β is somewhat smaller, while the prompt neutron lifetime is much smaller than in thermal reactors. This places somewhat more stringent requirements on control response. The control requirements for a typical LMFBR design are shown in the table below:

Control Requirements for Typical Fast Reactor System

	Per cent $\Delta k/k$
Burnup (equilibrium cycle)	3.7
Cold to Hot, Zero Power	0.5
Zero to Full Power	0.8
Shutdown Margin	2.4
Total	7.4

II. MOVEABLE CONTROL RODS

A. General Considerations Involved in Control Rod Selection

Moveable control rods are used for a variety of purposes--to control reactivity for power maneuvering, shim control, or scram purposes. They have been designed in variety of shapes, including cylinders, slabs or blades, cruciform blades, or clusters of rods (as sketched below):

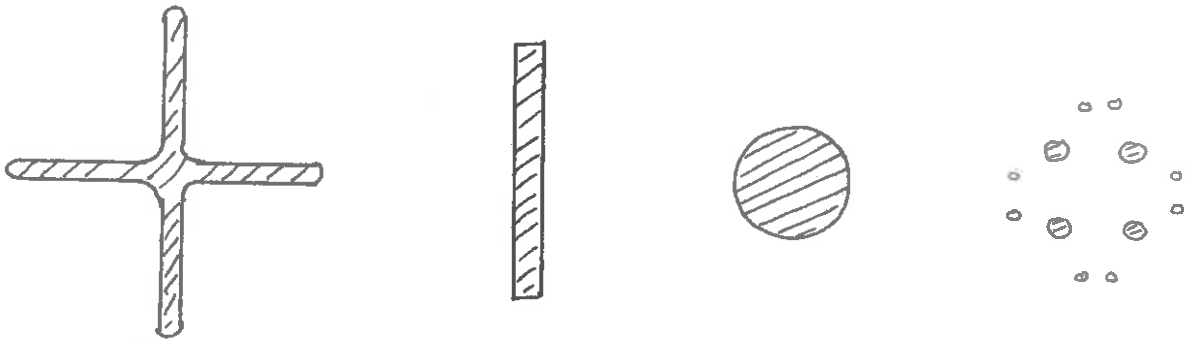

A number of factors are involved in the design of such control elements. For example, one would desire to achieve the required reactivity worth with a minimum perturbation on the flux distribution in the core. Obviously, if the control rod is too highly absorbing (too "black"), there will be a very pronounced flux depression in its vicinity. Hence one generally attempts to design rods such that their thickness is not much over two mean absorption lengths. Such considerations place a premium on high surface to volume ratios for control elements (such as those characterizing cruciform blades).

In thermal reactor control, most of the neutron absorption in control elements (some 60% to 80%) occurs in the thermal energy range. However, there will be an epithermal absorption effect due to resonance absorption. In an ideal design, a mixture of absorbing isotopes would be used to provide absorption over a range of neutron energies.

A tabulation of thermal absorption cross sections for typical control materials is given below:

Thickness for $\Sigma_a t = 2$ (2200 m/sec)

Material	$\sigma_a{}^{th}$	$\Sigma_a{}^{th}$	t(in)
Cd	2450	118	.007
Hf	105	4.8	.364
gd	46,000	1300	.0006
B	755	104	.0075
B_4C	-	83	.0085

There are a number of other considerations involved in designing a control element. For example, one desires a composition and design which will have a long lifetime against absorber depletion. This requires a large number of absorbing atoms per unit volume. The depletion of absorber material is a prime factor in determining control rod thickness, as the table of thicknesses required for one year of operating at a power density of 100 watts/cm^3 below indicates:

	ρ_A	a-absorber half thickness	
	moles/cm^3	cm	in
Cd	.0094	0.103	.042
Ef	.092	0.011	.0043
B	.043	0.024	.0095

The control element must also be designed with consideration given to mechanical performance. For example, the intense radiation environment in which the rod must function will cause high radiation damage. Furthermore, the control element must exhibit good resistance to corrosion,

as well as being able to tolerate the high operating temperatures in the core. Such temperatures are accentuated by the heat generated within the element due to neutron capture. Finally, the fabrication costs of the element will be an important factor in determining the design. That such fabrication costs will be appreciable is evident from the detailed configurations of the typical PWR and BWR control elements shown in Figures (14-1) and (14- 2).

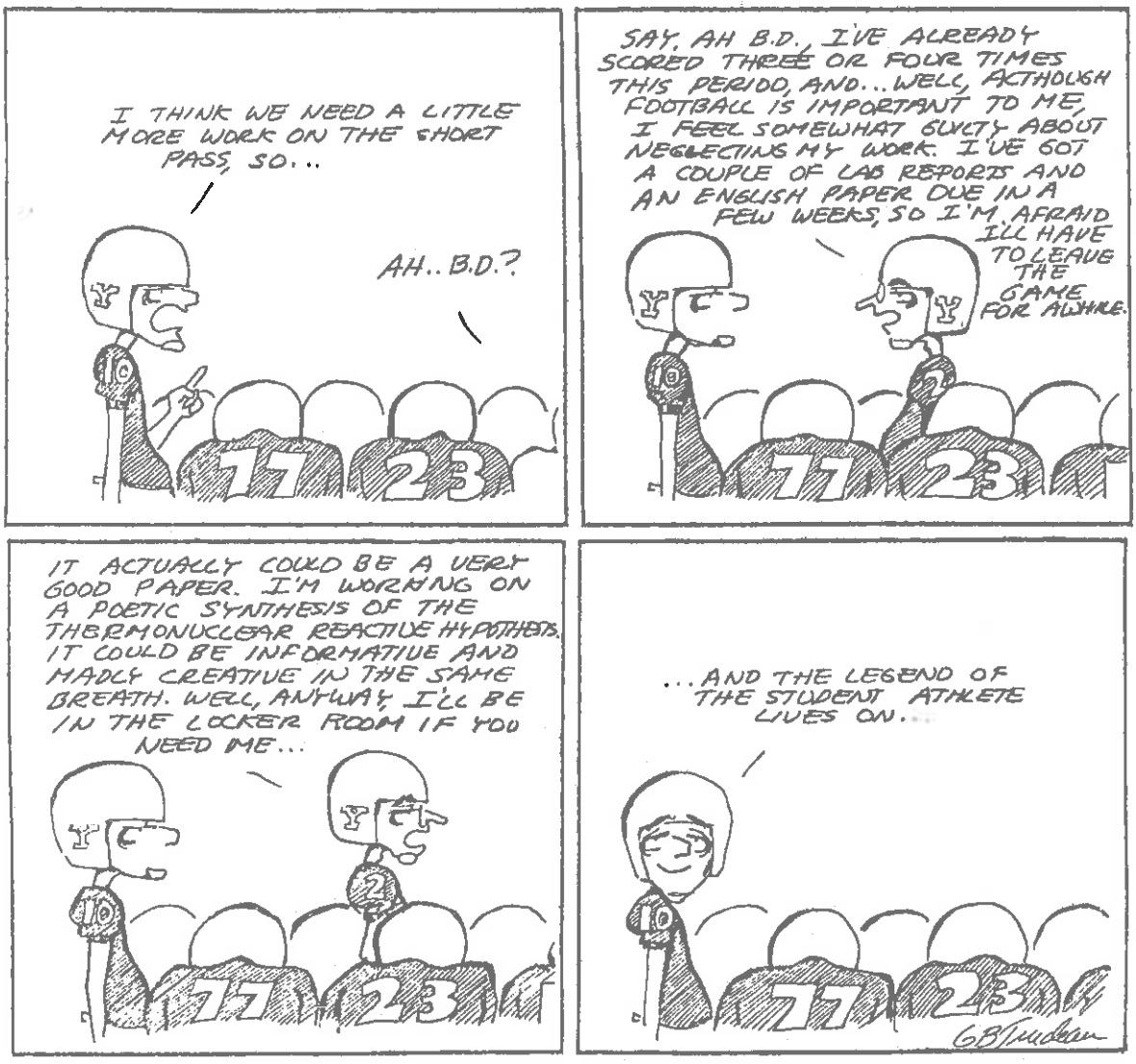

B. The Calculation of Control Rod Worth

The calculation of the reactivity worth of individual control elements and groups of such control elements and the effects that such elements have upon the power distribution in the core of a nuclear reactor constitute a very important facet of nuclear reactor design. A variety of methods have been developed to calculate control rod worth.

One might be tempted to utilize perturbation theory to estimate the effect of a localized control absorber on core multiplication. Unfortunately, however, the strong absorption characterizing a control element causes a severe local distortion of the flux, particularly in those fuel assemblies adjacent to the rod. The control element is characterized by strong self-shielding, much as fuel pins are. Hence perturbation theory is of limited usefulness in control studies, unless the control element is characterized by relatively weak absorption. [Although the control absorption is usually too strong to allow meaningful perturbation theory estimates in thermal reactors, the decrease of absorption cross sections and increase in mean free paths with increasing neutron energy allows some justification for perturbation methods in fast reactor control studies.] As we will see later, however, even though perturbation theory does usually not provide meaningful estimates of absolute control rod worths, it does in fact prove useful in studying the relative worth of various control element patterns and positions.

A more common approach involves the use of one-speed diffusion theory treatments which utilize transport corrected boundary conditions at the surface of the control rod. The literature abounds with

diffusion theory studies of cylindrical rods inserted into bare, homogeneous cylindrical reactor cores--either on or off core axis. However, such analyses are of little relevance to control studies of large power reactors with relatively tight fuel lattices in which large numbers of elements are distributed about the core in an effort to achieve a more uniform power distribution.

We will instead approach the calculation of control rod worths in a manner very similar to that which was utilized for the inclusion of fuel lattice heterogeneities in the generation of thermal group constants. We will use the fact that modern power reactors contain large numbers of control elements which tend to be reasonably uniformly distributed across the core to allow us to divide the core into cells, each of which contains one control element. We will then perform a detailed analysis of one such control cell, similar to the analysis we presented earlier for a fuel cell, in an effort to determine an effective absorption cross section for the control element which, when multiplied by the average flux in the control cell, yields the correct absorption rate in the element. Such effective cross sections can then be included in the multigroup diffusion theory analysis of the overall core. Obviously, such a scheme is very similar to the generation of "self-shielded" thermal group constants which was discussed in Chapter 10.

1. Control Cell Calculations

As in Chapter 10, our approach will be to isolate a local region in the vicinity of the control element from the remainder of the core and to analyze the neutron flux in the region in detail. Typical control cells for PWR's and BWR's are sketched below by way of illustration

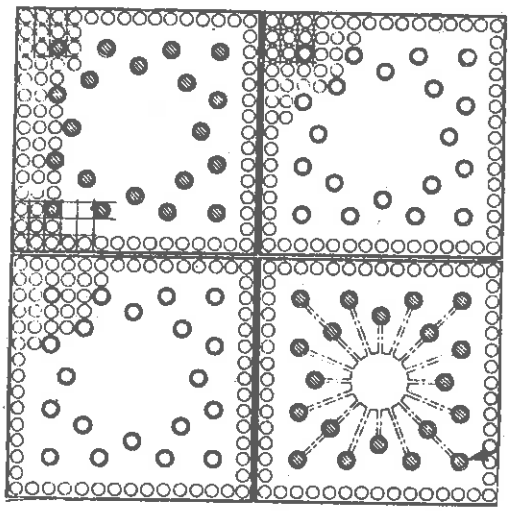

As in our earlier analysis, we will decouple the control cell from the rest of the core by demanding that the net neutron current across the cell boundary is zero. [The influence of adjacent cells can be represented by relaxing this boundary condition to allow nonzero flux gradients across the boundary, as discussed in NRH, Sec. 4-3.]

Our approach will be to use diffusion theory with transport corrected boundary conditions of the control element surface in order to determine the flux in the control cell. We can then use this flux to determine an effective cross section Σ_c^{eff} characterizing the control element by requiring that

$$V_f \bar{\phi} \Sigma_c^{eff} = S_c J_c \qquad (14\text{-}3)$$

where $\bar{\phi}$ is the volume average flux in the cell, V_f is the fuel volume, and S_c the control element of the surface area, respectively, while J_c is the average neutron current at the surface of the constant element. This usually reduces to a two-dimensional problem (such as those sketched above), in which case we can write

$$\Sigma_c^{eff} = \frac{P_c}{A_f} \frac{J_c}{\bar{\phi}} \qquad (14\text{-}4)$$

where P_c is the exposed perimeter and A_f is the cross sectional area of the fuel.

Hence our task is obviously to determine the ratio $J_c/\bar{\phi}$ since this will infer Σ_c^{eff}. The highly absorbing nature of the control element invalidates the direct application of diffusion theory. Instead one uses a diffusion theory calculation outside the element, collision probability methods within it, and then couples these at the control element boundary using "blackness theory" (much as was done in the ABH method).

The advantage of this approach is that it yields a cell parameter, $J_c/\bar{\phi}$, which is relatively insensitive to the material composition surrounding the control element. Hence the detailed calculation of $J_c/\bar{\phi}$ need be performed only once and can be reused even though the cell composition may change (due to fuel depletion, moderator density changes, or fission product buildup).

To indicate more clearly just what is involved in such a calculation, let us consider the explicit example of a cruciform shaped control blade inserted into a homogeneous cell. We will not attack this 2-D problem directly, but rather we will replace it by an equivalent one dimensional problem which preserves the same ratio of control rod surface to fuel volume. Such a scheme should give a reasonable estimate

if the span ℓ of the control blade is substantially greater than the diffusion length L characterizing the surrounding medium. The surface to volume ratio of the rod is

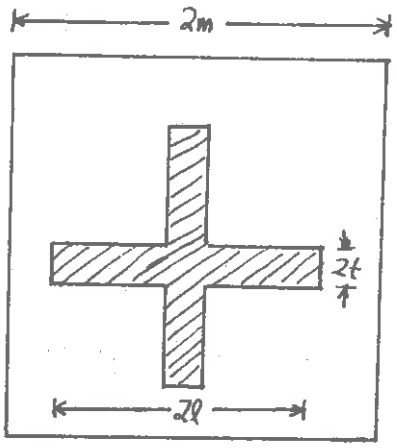

$$\frac{8\ell}{4m^2-8t\ell+4t^2} = \frac{2\ell}{m^2-2t\ell+t^2} \qquad (14\text{-}5)$$

Our equivalent one dimensional problem will be as shown with a surface to volume ratio of $1/a$; hence we will demand

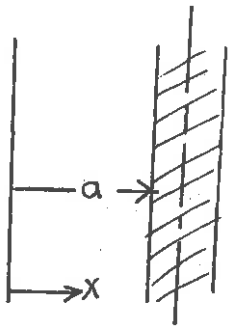

$$\frac{1}{a} = \frac{2\ell}{m^2-2t\ell+t^2} \qquad (14\text{-}6)$$

We will now use one speed diffusion theory to determine the flux in the fuel

$$-D\frac{d^2\phi}{dx^2} + \Sigma_a\phi(x) = S_o \qquad (14\text{-}7)$$

where we assume a uniformly distributed source of neutrons, S_o, slowing down in the fuel. The boundary conditions corresponding to the cell are

$$\text{(i)} \quad -D\frac{d\phi}{dx}\Big|_{x=0} = 0$$

$$\text{(ii)} \quad -\frac{D}{\phi}\frac{d\phi}{dx}\Big|_{x=a} = \frac{J(a)}{\phi(a)} = \alpha \qquad (14\text{-}8)$$

Notice that we have introduced a parameter, α , which characterizes the ratio of the current to the flux at the surface of the control rod. Since the control rod is a strong absorber, α must be determined from a separate transport calculation--much as one determines the extrapolation length characterizing a free plane surface, $z_o = .7104\,\lambda_{tr}$. The transport parameter α is closely related to another parameter--the so-called blackness coefficient of the rod

$$\beta = \frac{J_+(a) - J_-(a)}{J_+(a)} \tag{14-9}$$

where $J_\pm$ are the partial currents into and out of the surface. If we recall that in diffusion theory

$$J_\pm = \tfrac{1}{4}\phi \pm \tfrac{1}{2}J \tag{14-10}$$

then we can find

$$\beta = \frac{4\alpha}{1+2\alpha} \tag{14-11}$$

It is convenient to rewrite our expression for the effective control cross section as

$$\Sigma_c^{eff} = \frac{P_c}{A_f}\,\frac{J_c}{\phi_c}\,\frac{\phi_c}{\bar{\phi}} = \left(\frac{P_c}{A_f}\right)\alpha\left(\frac{\phi_c}{\bar{\phi}}\right) \tag{14-12}$$

We will solve the above diffusion equation in the fuel to determine the ratio of the surface flux ϕ_c to the average flux, $\bar{\phi}$. This

formulation is particularly enlightening because it stresses that the diffusion equation is only being used to describe the flux outside of the control element.

If we seek a general solution of the form

$$\phi(x) = A\cosh x/L + B\sinh x/L + S_o/\Sigma_a \qquad (14\text{-}13)$$

then we find that

$$\text{b.c.(i)} \Rightarrow J(0) = -\frac{D}{L}\left[A\sinh x/L + B\cosh x/L\right]_{x=0} \Rightarrow B = 0$$

while

$$\text{b.c.(ii)} \Rightarrow \frac{J(a)}{\phi(a)} = \alpha = \frac{-\frac{D}{L}A\sinh a/L}{A\cosh a/L + S_o/\Sigma_a}$$

or

$$A = \frac{-\alpha S_o/\Sigma_a}{\alpha\cosh a/L + \Sigma_a L\sinh a/L}$$

Hence we find

$$\phi(x) = \frac{S_o}{\Sigma_a}\left[1 - \frac{\alpha\cosh x/L}{\alpha\cosh a/L + \Sigma_a L\sinh a/L}\right] \qquad (14\text{-}14)$$

and can compute

$$\frac{\phi(a)}{\bar{\phi}} = \frac{\Sigma_a}{\left(\Sigma_a + \frac{\alpha}{L}\coth\frac{a}{L}\right) - \frac{\alpha}{a}} \qquad (14\text{-}15)$$

If we note that $P_c/A_f = \frac{1}{a}$ for our one dimensional problem, we can find

$$\Sigma_c^{eff} = \frac{\Sigma_a}{a\left(\frac{\Sigma_a}{\alpha} + \frac{1}{L}\coth\frac{a}{L}\right) - 1} \qquad (14\text{-}15)$$

In particular, notice that the control rod worth (which is proportional to Σ_c^{eff}) increases as the control rod surface to fuel volume increases (i.e., a decreases) or as fuel absorption decreases, as we might have expected. Rod worth also increases with increasing fuel diffusion length, since more of the fuel volume is then sensitive to flux perturbations introduced by the rod.

The calculation of the transport correction parameter α involves the use of transport theory or collision probability methods. If the control element were a perfectly black absorbing slab, then a transport calculation indicates that $\alpha = 0.47$. For grey elements, the result is more complicated and depends upon the geometry of the control element. For a slab element of width t, such an analysis yields

$$\alpha = \frac{1 - 2E_3(\Sigma_a t)}{2\left[1 + 3E_4(\Sigma_a t)\right]} \qquad (14\text{-}16)$$

where $E_n(z)$ is the exponential integral

$$E_n(z) = \int_1^\infty e^{-zu} u^{-n}\, du \qquad (14\text{-}17)$$

For more complicated element geometries, such as sandwich or pin structures

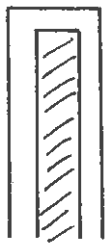

sandwich

or

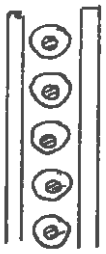

pin

more complex expressions for α must be used. In a similar sense, one can calculate $\phi_c/\bar{\phi}$ for more complicated cell geometries such as those shown below

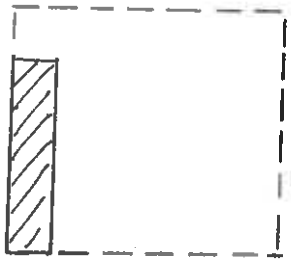

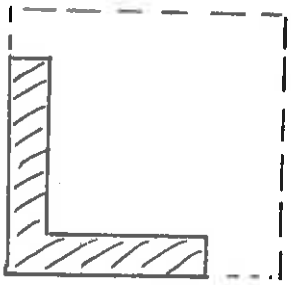

Such calculations are beyond the scope of this presentation, but can be found in ANL-5800 .

A number of other considerations must be included in a more accurate determination of control rod worth. For example, most control blades have structural materials in their tips which protrude into high flux regions. The effective cross section of these regions must usually be calculated separately. Furthermore, one finds a flux depression at

the corner of the rod, with a corresponding flux peaking at the opposite corner of the cell. The effective control cross section must be corrected for this effect.

C. Control Rod Effects on Core Power Distributions

The primary function of control elements in a reactor core is to control core reactivity. However, we have seen that the strongly absorbing nature of control elements will cause major perturbations in the neutron flux in the vicinity of the control element. Thus far we have confined our treatment to a consideration of such perturbations on a local scale such as in a control cell. But, of course, as the control elements are inserted or withdrawn, they will also strongly affect the overall flux distribution and hence the power distribution of the reactor core. It is extremely important to predict the interaction of control elements on core power distributions in order to assure that the power density limitations demanded by thermal considerations such as those discussed in Chapter 12 are not exceeded. Furthermore, control rod patterns can actually be used to shape the power distribution into a more favorable profile for core thermal performance and fuel burnup.

A large power reactor will contain many control elements which are distributed in a pattern about the core in an effort to achieve efficient reactivity control within flux peaking limitations, as well as to facilitate power shaping. For example, the control element pattern in a typical large PWR core is shown in Figure 14-5. The arrangement of such control rods into groups, the determination of the control rod withdrawal sequence and the coordination of moveable control elements

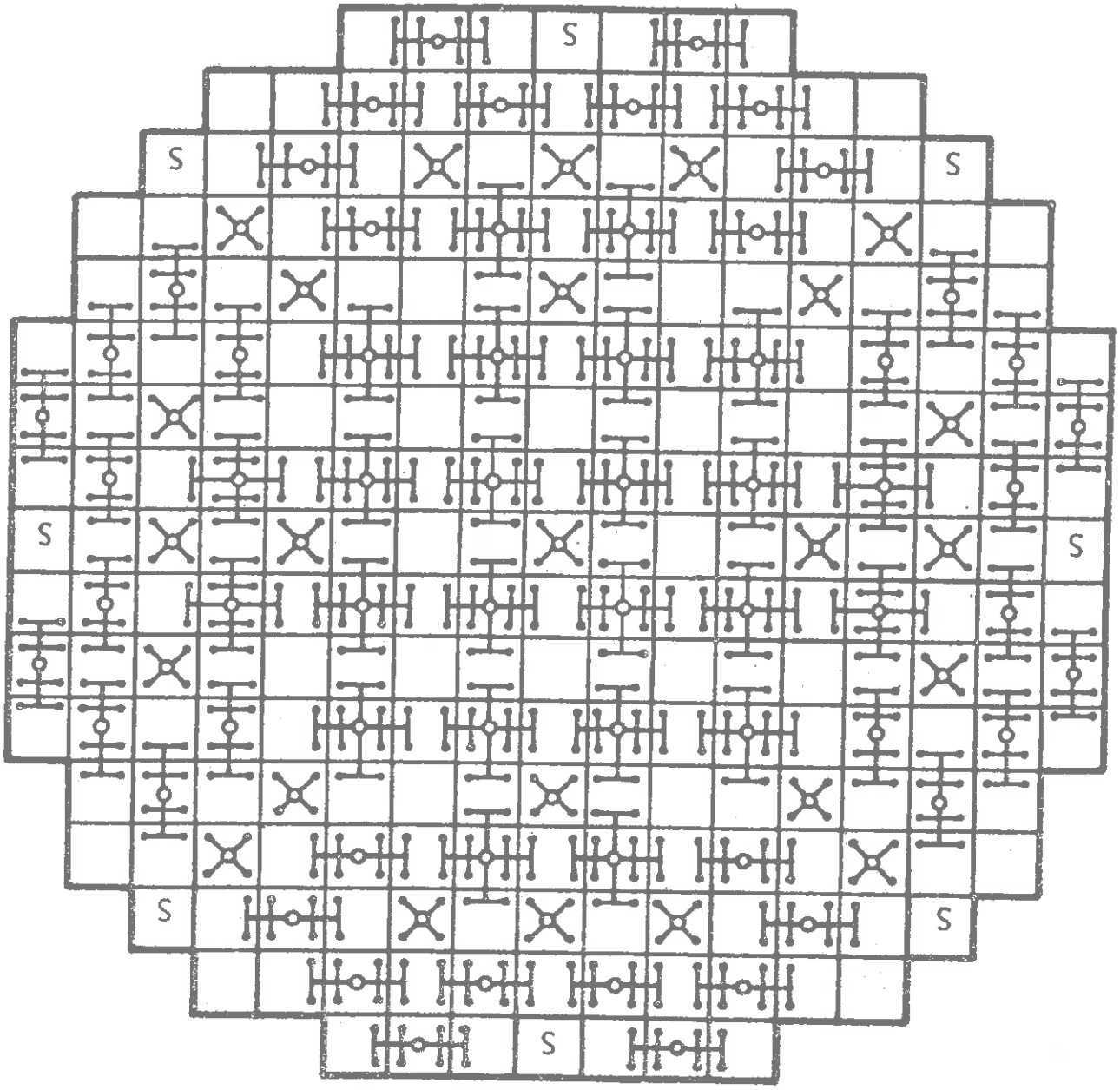

FIGURE 14-5: Location of Control Assemblies in a PWR Core

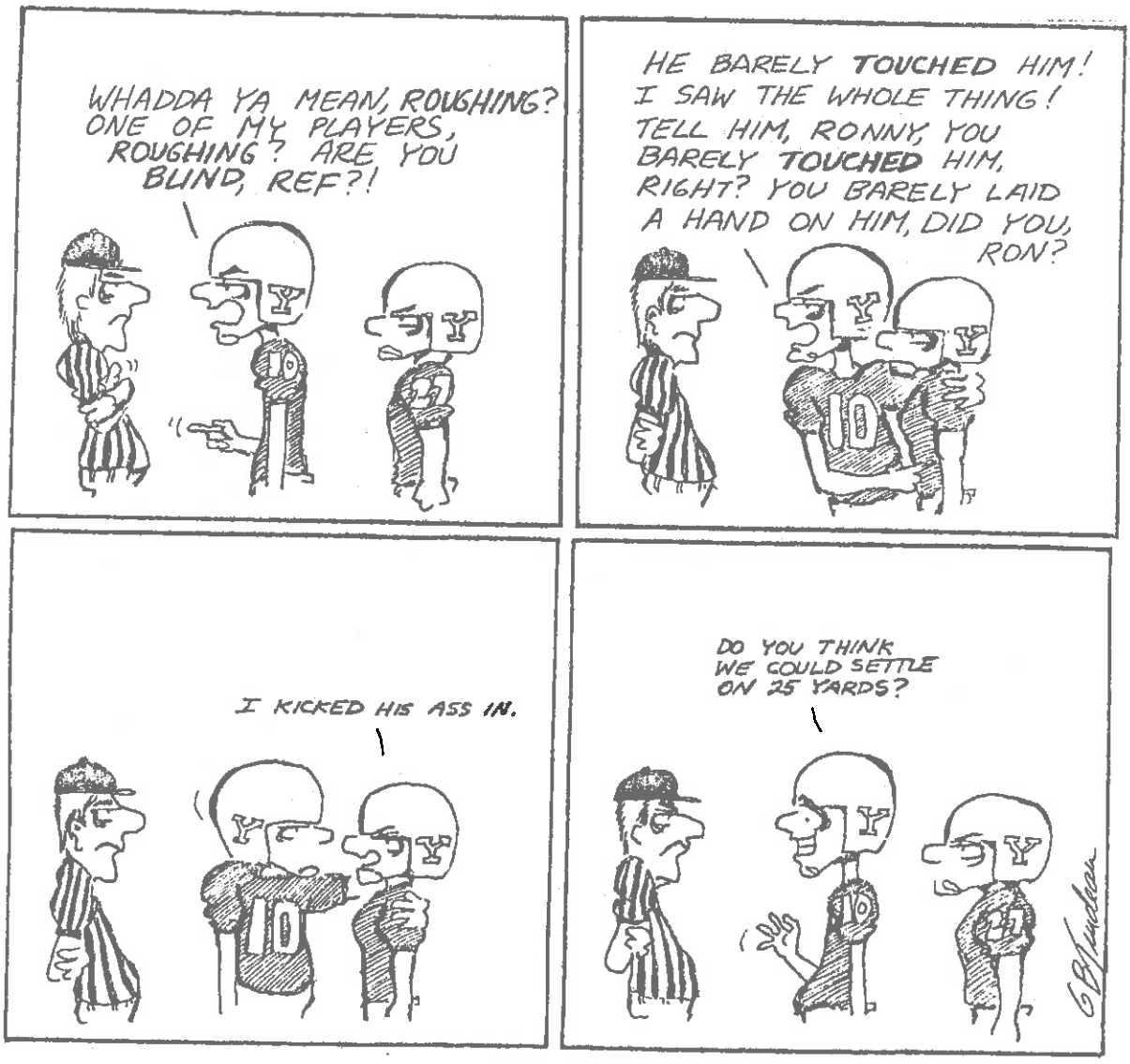
WHADDA YA MEAN, ROUGHING? ONE OF MY PLAYERS, ROUGHING? ARE YOU BLIND, REF?!
HE BARELY TOUCHED HIM! I SAW THE WHOLE THING! TELL HIM, RONNY, YOU BARELY TOUCHED HIM, RIGHT? YOU BARELY LAID A HAND ON HIM, DID YOU, RON?
I KICKED HIS ASS IN.
DO YOU THINK WE COULD SETTLE ON 25 YARDS?

with burnable and soluble control poisons all fall under the heading of "control management".

In determining the effects of control rod insertion patterns upon core power distributions, one must be careful to include the many interactions which will affect the power profile. For example, suppose we consider the variation in the axial power profile of a core which is controlled by rod insertion from the top. At the beginning of core life, the rods must be inserted to compensate for the large excess reactivity of the fresh core loading. The region of the

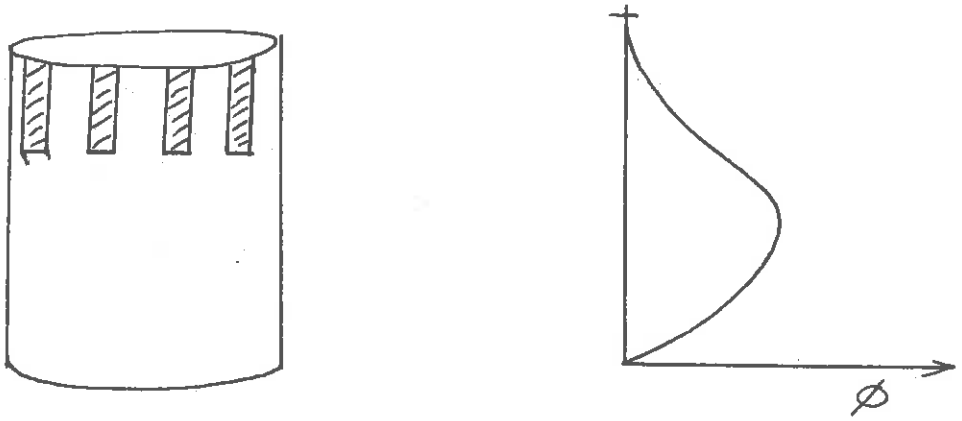

core in which the rods have been inserted will experience decreased multiplication and hence relatively lower fluxes. Hence, since the overall reactor power will be kept constant, there will be a flux peaking near the bottom of the core. As the fuel in the core is depleted, the control rods will be gradually withdrawn to compensate for the reduced reactivity of the fuel. During the early stages of core life, the fuel near the bottom of the core will have been exposed to relatively higher fluxes and hence experience larger burnup, whereas the fuel in the rodded core region will experience lower burnups. Thus as the control rods are withdrawn, the flux peak will shift towards

the top of the reactor core. Such interactions between rods and fuel burnup can be minimized by using more uniformly distributed control such as

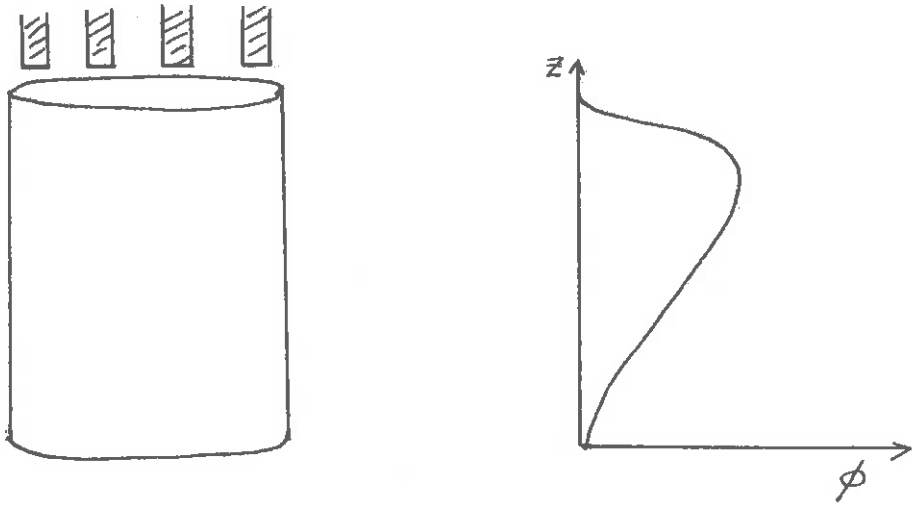

burnable poisons and chemical shim.

We have seen the interaction of control rods with spatial xenon oscillations in Chapter 6. This is an instance in which the incorrect management of control rod patterns can lead to instability of these spatial oscillations.

Yet a third type of interaction is found in BWR cores in which the large water density towards the bottom of the core leads to a bottom peaked flux profile. By inserting control rods from the core bottom, one can compensate for the enhanced reactivity introduced by the higher moderator density and hence achieve a somewhat more uniform axial flux profile.

Of course, there are some disadvantages to the use of control elements for power profile shaping. For example, the achievement of favorable radial power profiles is sometimes accomplished only at the expense of satisfactory axial profiles. Furthermore, the achievement of optimal

fuel burnup may be partially offset by the poor neutron economy of a core with high control insertion. These factors must be considered in devising an optimal control management scheme.

To more explicitly study the effects of rod insertion upon core power distributions, let us consider a simple model of the interaction of a bank of control rods with an axial flux profile. We will model the reactor as a cylinder, and treat the "rodded" and "unrodded" regions of the core as homogeneous. Hence the insertion or withdrawal of the control rod bank is represented by a shift of the boundary between the two regions.

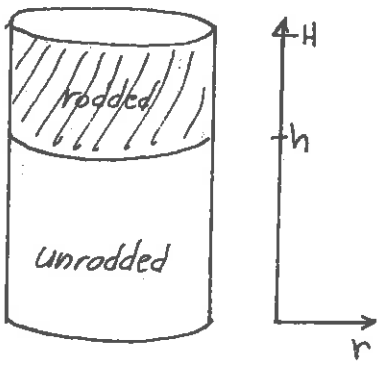

We will assume that the flux is separable in the r and z variables in a given region

$$\phi_i(r,z) = R(r)\,Z_i(z) \qquad i = ur,\ r \qquad (14\text{-}18)$$

(Note we have assumed the radial profile is the same in both the rodded and unrodded regions). If we substitute this form into

$$\nabla^2\phi + B_i^2\phi = 0 \qquad (14\text{-}19)$$

we can separate variables to find an equation for the axial profile

$$\frac{d^2Z_i}{dz^2} + B_{z_i}^2 Z_i(z) = 0 \qquad (14\text{-}20)$$

where the axial buckling is defined by

$$B_{z_i}^2 = B_i^2 - B_r^2 \tag{14-21}$$

where B_r^2 is the radial buckling which is given by

$$\frac{1}{r}\frac{d}{dr}\left(r\frac{dR}{dr}\right) + B_r^2 R(r) = 0 \tag{14-22}$$

For a uniform core composition, we recall

$$B_{z_i}^2 = \frac{k_{\infty_i} - 1}{L^2} - \left(\frac{2.405}{R}\right)^2 \tag{14-23}$$

We now solve the axial equation in both the rodded and unrodded regions

$$\begin{aligned} \mathcal{Z}_{ur}(z) &= A_{ur} \sin B_{zur} z, \quad 0 \le z \le h \\ \mathcal{Z}_r(z) &= A_r \sinh\left[B_{z_r}(H-z)\right], \quad h \le z \le H \end{aligned} \tag{14-24}$$

If we require

$$\phi_{ur}(r;h) = \phi_r(r;h)$$

and (14-25)

$$J_{ur}(r;h) = J_r(r;h)$$

then we find a criticality condition

$$\frac{\tan B_{zur}}{B_{z_{ur}}} = -\frac{\tanh B_r(H-h)}{B_{z_r}} \tag{14-26}$$

(assuming $D_{ur} = D_r$). We can sketch the axial flux profile for various rod insertions as shown below

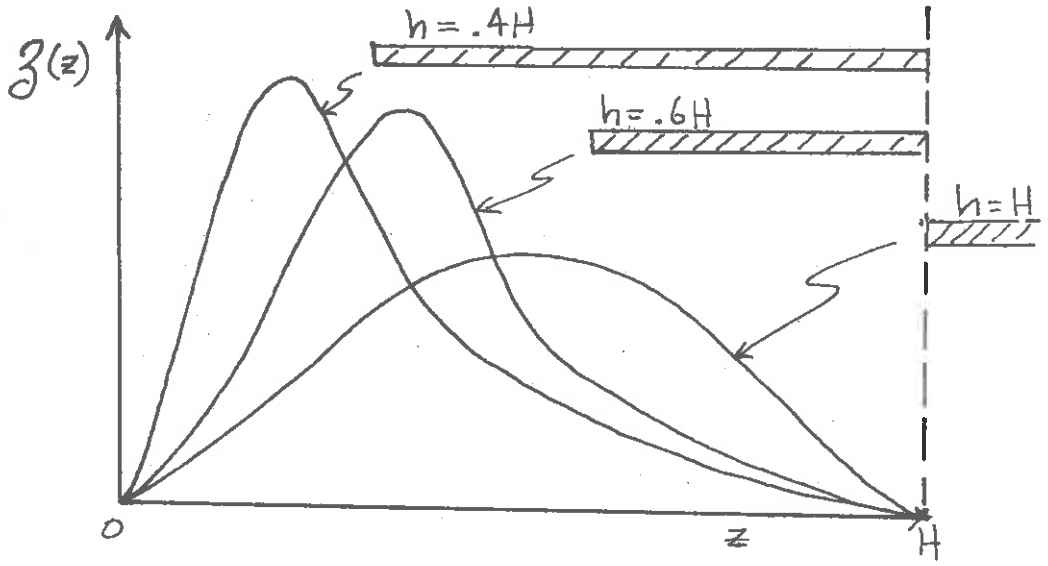

It is also of interest to compute the different control rod worth. From our perturbation theory example in Chapter 5, we recall

$$\frac{d\rho}{dh} = \Delta\rho(H) \frac{\mathcal{F}^2(h)}{\int_0^H \mathcal{F}^2(z)\,dz} \qquad (14\text{-}27)$$

This is sketched below for various total rod worths $\Delta\rho(H)$:

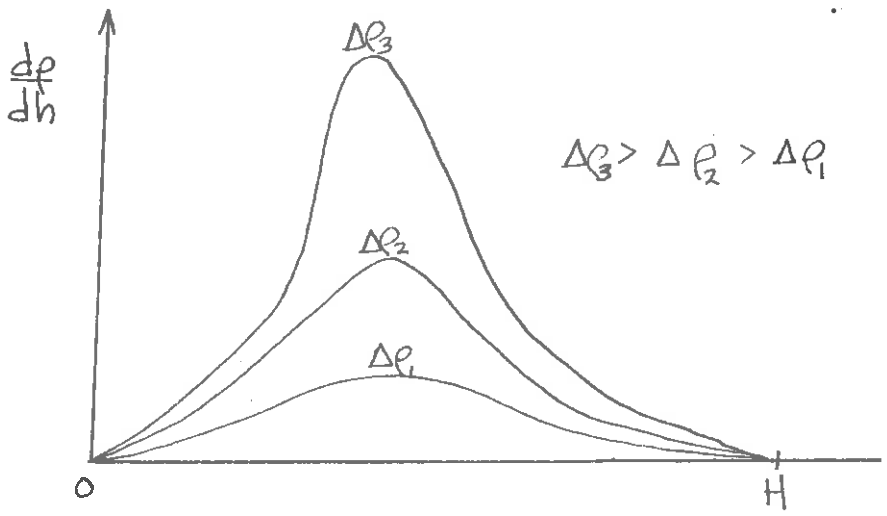

Note how the peak of $d\rho/dh$ shifts towards the bottom of the core as the total control rod $\Delta\rho$ increases.

III. BURNABLE POISONS

The lifetime of a given core loading, that is, the period during which the core has sufficient excess reactivity to permit startup, is generally determined by the amount of fuel initially loaded into the reactor core. [Although it should be mentioned that another very important factor in determining core lifetimes in today's modern power reactors is the amount of radiation damage a fuel element can withstand before suffering failure.] Of course, the amount of fuel loaded into the reactor, or equivalently, the excess reactivity, will depend upon the amount of excess reactivity which can be safely compensated by the reactor control elements.

In order to increase the allowable initial core fuel loading, it is common to load into the core materials characterized by high neutron absorption cross sections (poisons) which compensate for such excess reactivity during the early stages of core life. Such absorbers are chosen such they "burnout" (i.e., are transmuted by neutron capture into isotopes with low capture cross sections) somewhat faster than fuel burnup, so that later in core life they contribute negligible negative reactivity. Hence these burnable poisons can come close to matching the time behavior of the excess fuel reactivity as it decreases over core life, thereby allowing larger initial fuel inventories without a corresponding increase in control requirements.

Hence burnable poisons possess a number of advantages. They increase core lifetime without any decrease in control safety. They also reduce the amount of mechanical control required. If the burnable poisons are distributed in a proper fashion, they can also improve core power distributions, for example by suppressing reactivity in high flux regions.

Such burnable poisons are usually fabricated into the initial core loading as either fixed control blades or curtains or mixed into certain fuel pins. For example, in present BWR designs, gadolinium loaded fuel pins with an initial reactivity worth of 0.12 are loaded into the core until an equilibrium fuel cycle is achieved. (After the equilibrium cycle is reached, fuel depletion will provide sufficient shim control.) The location of such burnable poisons are shown in a typical BWR fuel assembly-control cell in Figure 14-7. In PWR's, boro-silicate glass tubes are placed in the core.

From this discussion, several desired characteristics of burnable poisons are apparent. Obviously they should be characterized by absorption cross sections somewhat higher than those of the fuel, since then they will burn out more rapidly than the fuel, leaving minimal poison residue at the end of the fuel cycle. Furthermore, the isotopes formed by neutron capture in the poison should have low absorption cross sections. Finally, the burnable poison, as well as its surrounding clad or structural material, should not compromise the mechanical integrity of the core (such as by swelling).

In this section, we will examine two approaches for loading burnable poisons into a reactor core. The first merely assumes a uniform distribution

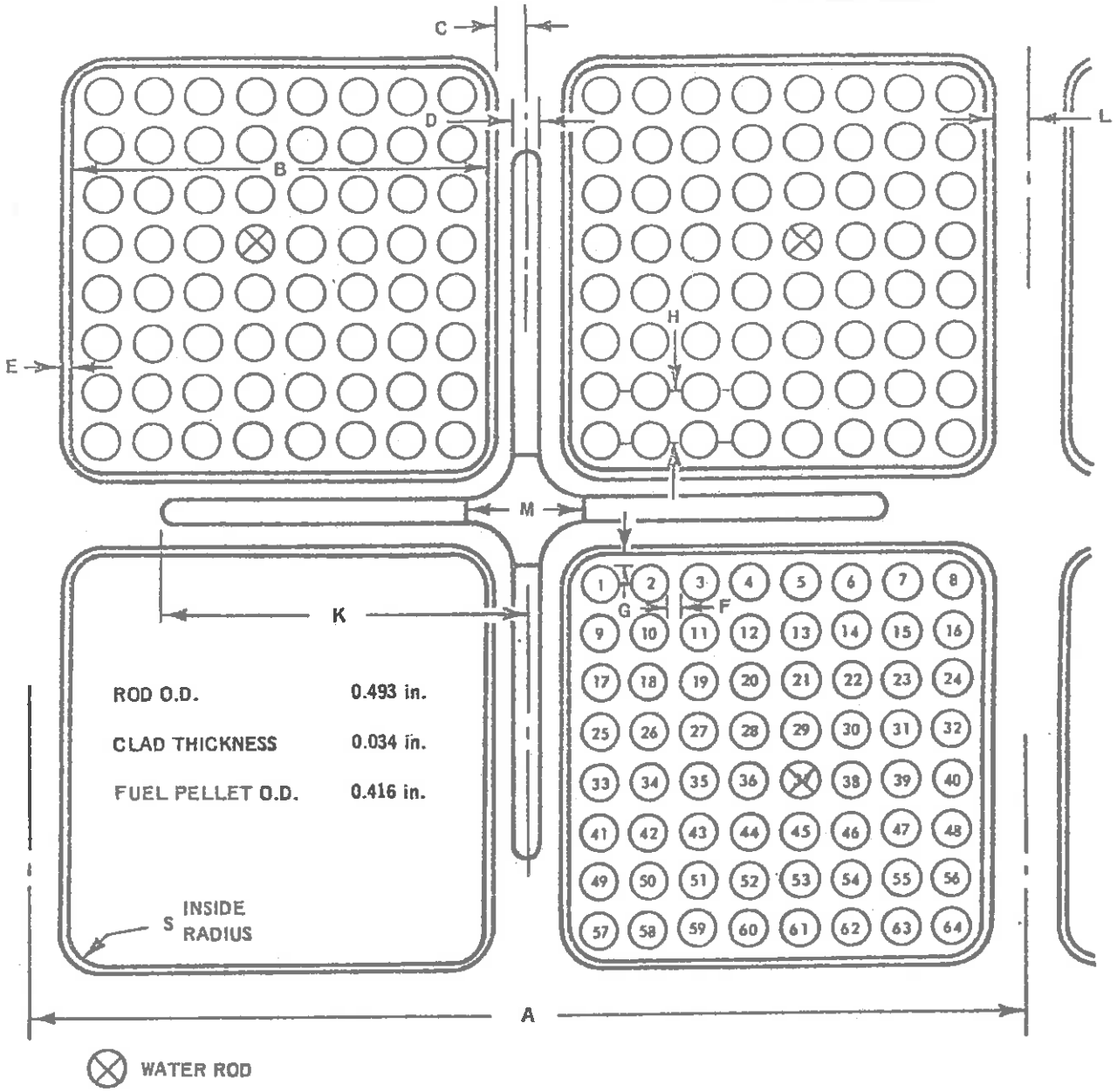

DIM. IDENTIFICATION	A	B	C	D	E	F	G	H	I	J
DIM. INCHES	12.0	5.278	0.241	0.260	0.120	0.147	0.1525	0.640		

DIM. IDENTIFICATION	K	L	M	N	O	P	Q	R	S	
DIM. INCHES	4.875	0.241	1.563						0.400	

FIGURE 14-7: BWR Control Cell

of the poison material among the fuel. As we will see by a simple analysis, such a homogeneous scheme encounters control problems. Hence a more desirable scheme is to load the poisons in a heterogeneous fashion to take advantage of self-shielding effects which can provide a closer match between poison burnout and fuel depletion.

2. Uniform Distribution of Burnable Poisons

For convenience, consider an infinite medium of homogeneously mixed fuel and poison. Then the rate equations describing the burnup of fuel and poison nuclei are just

$$\frac{dN_F}{dt} = -\sigma_a^F \phi(t) N_F(t)$$

$$\frac{dN_P}{dt} = -\sigma_a^P \phi(t) N_P(t) \qquad (14\text{-}28)$$

We can integrate each of these equations to find

$$N_F(t) = N_F(0)\, e^{-\sigma_a^F \varphi(t)}$$

$$N_P(t) = N_P(0)\, e^{-\sigma_a^P \varphi(t)} \qquad (14\text{-}29)$$

where $\varphi(t)$ is the integrated neutron flux or "neutron fluence"

$$\varphi(t) \equiv \int_0^t dt'\, \phi(t') \,. \qquad (14\text{-}30)$$

Now the core multiplication is given by

$$k = \frac{\nu \Sigma_f^F}{\Sigma_a^F + \Sigma_a^P} = \nu \sigma_a^F \frac{N_F(t)}{N_F(t)\sigma_a^F + N_p(t)\sigma_a^P}$$

$$= \eta \left[1 + \frac{N_p(0)}{N_F(0)} \frac{\sigma_a^P}{\sigma_a^F} e^{-(\sigma_a^P - \sigma_a^F)\varphi(t)} \right]^{-1} \qquad (14\text{-}31)$$

We can sketch the form of k(t) for various choices of poison cross section as shown:

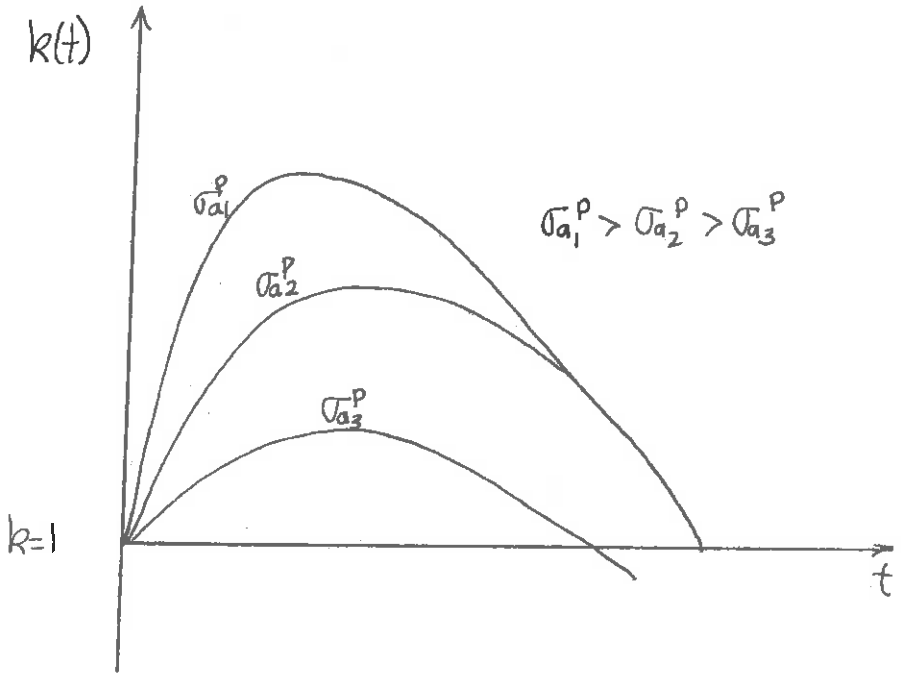

Initially, the change in reactivity will be high due to poison burnup. This results in a reactivity mismatch. The mismatch will be less severe for a poison with a small σ_a^P , but then there will be a poison residue which will shorten core life. Thus there is a certain fuel loading

and corresponding core life beyond which the reactivity rise due to the relatively rapid depletion of the posion will be greater than that which can be handled by the available mechanical control. Ideally, one would like to employ a poison of lower cross section early in core life (to reduce reactivity mismatch) and then switch to a poison of large cross section late in core life (to minimize poison residue). One can effectively achieve this by locating the poison in a region characterized by a different flux than that seen by the fuel.

3. Heterogeneous Distributions of Burnable Poisons

The general idea behind the use of heterogeneously lumped burnable poisons is to take advantage of the strong self-shielding which will occur in such poisons. Early in core life, the self-shielding will reduce the effective absorption cross section of the poison, thereby minimizing reactivity mismatch. As the poison depletes, however, the effective cross section of the poison relative to the fuel will increase, due to self shielding, which is the desired behavior in order to maintain reactivity as high as possible near the end of core life.

To be a bit more precise, reconsider our equation describing the time rate of change of the poison concentration

$$\frac{dN_p}{dt} = -f(t)\,\phi(t)\,\sigma_a^p\,N_p(t)$$

where f(t) is the self shielding factor which represents

$$f(t) = \frac{\text{ave. flux in poison}}{\text{ave. flux in fuel}}$$

Now f will vary as the poison burns out. This can be seen below

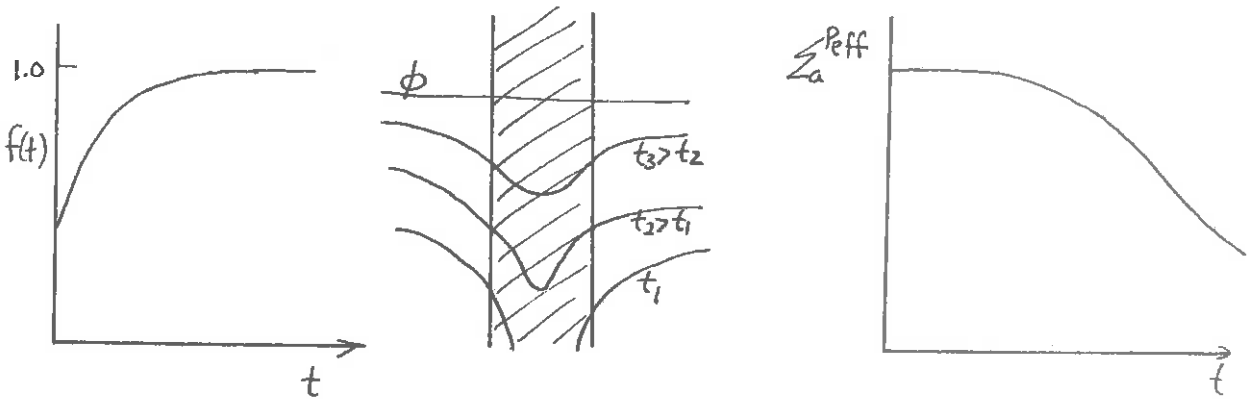

Hence, initially the poison burnout is relatively slow due to strong self shielding. However as poison depletion proceeds, self shielding becomes less significant until eventually $f(t) \rightarrow 1$. Hence by using combinations of differently self-shielded elements (e.g., boron or gadolinium), one can minimize the reactivity mismatch early in core life and still avoid a large residue of unburned poison which would shorten core lifetime.

Burnable poisons will also affect the reactivity coefficients of the reactor. Since most candidates for burnable poisons are $^1/_v$ absorbers, the microscopic absorption cross section of the poison will be larger in a cold core. Hence a lumped poison element will be more highly self-shielded and therefore less effective in a cold core than in a hot core. This enhances the negative behavior of the temperature coefficient of reactivity.

IV. CHEMICAL SHIM

In light water reactors, boric acid is frequently dissolved in the coolant (to concentrations of $\sim$ 1000 ppm) to act as shim control. Such soluble poisons or chemical shim have several advantages. Since the poison distribution is uniform and independent of the amount of reactivity being controlled, the fuel loading can be more easily distributed to yield a uniform power distribution, such as by zone loading patterns. Chemical shim reduces the mechanical control rod requirements quite considerably. Since such rods are expensive and occupy a sizeable fraction of the core volume, the elimination of mechanical control where possible is desirable.

In the table below, the relative mechanical and chemical control requirements of a typical PWR are listed. We have also sketched in Figure 14-8 the boron concentration required to compensate for excess reactivity over core life in this particular reactor design:

TABLE 1—Typical Reactivity Requirements*

	Reactivity (% Δρ)	
Reactivity effects	*Rods*	*Boron*
Safety shutdown	3.0	—
Cold-to-operating temperature change	—	2.0
Doppler effect	2.2	—
Samarium poisoning	—	0.8
Xenon poisoning	—	2.2
Operating control	0.8	—
Core lifetime (depletion)	—	9.0
	6.0	14.0

* For a closed-cycle water reactor with chem-shim (and rod) control

TABLE 2—Typical Boron Concentrations*

Refueling concentration	*3,300*
Hot-shutdown concentration (start of cycle)	*1,650*
Operating concentration (start of cycle)	*1,300*
Operating concentration (end of cycle)	*~10*

* Burnup is 11,000 Mwd/mtU; 825-Mwth reactor.

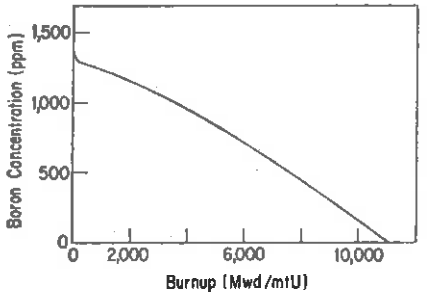

FIG. 2. CONTROL for the reactor of Table 2 requires concentrations shown

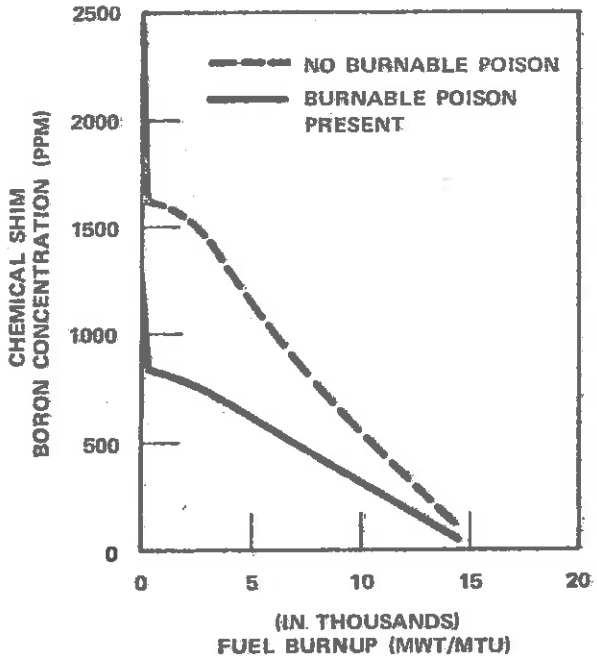

FIGURE 14-8: Boron Concentration versus First Cycle Burnup

A suitable soluble poison must be an isotope characterized by a large neutron absorption section which is soluble in the coolant. It should be of a non-corrosive nature and relatively stable so it will not adhere to core components. Boric acid possesses these requirements when used in light water reactors.

Chemical shim does have several disadvantages, however. Since the rate at which one can inject or withdraw appreciable amounts of poison from the coolant is quite small, the reactivity insertion rates are correspondingly small (typically on the order of $\sim 3 \times 10^{-5}$/sec). Hence chemical shim is only of use to compensate for relatively slow reactivity changes such as those due to fuel burnup or conversion,

fission product poisoning, and moderator temperature change (temperature defect).

Chemical shim can have a major effect upon the moderator void coefficient of reactivity. We have noted that in light water reactors, this void coefficient is usually quite negative, since a decrease in coolant density leads to a decrease in moderation and hence reactivity. But if a soluble poison is present, a decrease in coolant density will also lead to a decrease in poison concentration--a positive reactivity effect. The desire for a negative void coefficient will frequently limit the amount of chemical shim allowed (typically to some $\lesssim 14\%$).

There are other possible disadvantages, such as the possibility of sudden reactivity surges due to chemical shim which has been entrained in the core and suddenly breaks loose to escape. It can also interact in an unfavorable way with fission product transients (xenon and samarium) towards the end of core life.

Consider a reactor operating at some nominal power level towards the end of core life. Since the fuel will be relatively highly depleted, the amount of chemical shim present will be small. But since the rate at which reactivity can be changed is proportional to the soluble poison concentration, the reactivity response $d\rho/dt$ will also be small. Now suppose the reactor power level is suddenly reduced. Then, as we have seen in Chapter 6, the xenon concentration will begin to build up. One would then desire to decrease the poison

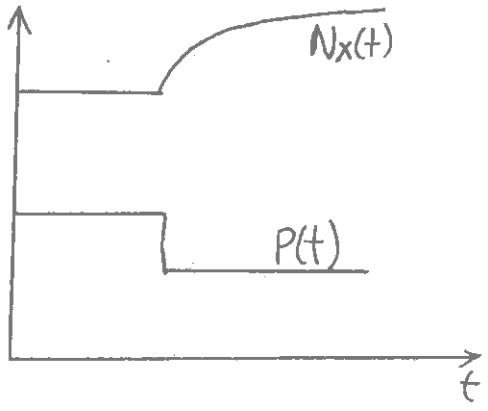

concentration to compensate for the negative reactivity introduced by the xenon transient. One encounters a similar situation following a power increase, since now chemical shim must be rapidly inserted into the coolant to compensate for xenon burnup. Such considerations place strong limitations on chemical shim requirements which must be anticipated in core analysis.

V. FEEDBACK EFFECTS AND REACTIVITY COEFFICIENTS

To complete our discussion of reactivity control, it is appropriate to turn to a more detailed consideration of the inherent reactivity requirements of large power reactors. We have already encountered a very brief discussion of temperature effects on reactivity in Chapter 6. We now will complete this development by considerating the principal reactivity effects in the primary classes of power reactors.

A. Types of Reactivity Effects

1. Temperature Effects

In our earlier discussion, we noted how temperature variations in the core affect multiplication, both because of the change in the thermal motion of the nuclei comprising the core and also because of thermal expansion. We characterized this effect by defining a temperature coefficient of reactivity

$$\alpha \equiv \frac{d\rho}{dT} \tag{14-32}$$

This should more properly be referred to as an isothermal temperature coefficient, since it assumes the core can be characterized by a uniform temperature T.

But, in fact, we know that there are enormous temperature variations across the core. For example, fuel centerline temperatures may range as high as 4000°F, while coolant temperatures are as low as 500°F. Furthermore, an increase in fuel temperature will propagate temperature changes to clad and coolant only after the time delay required for transport of heat.

For this reason, the temperature coefficient of reactivity is not really a very useful quantity. A more useful quantity is the change in reactivity caused by a change in reactor power. We will consider this in detail in the next section.

There is one useful quantity related to the temperature coefficient of reactivity, however. This is the so-called "temperature defect", $\Delta \rho_{TD}$, defined as the change in reactivity which occurs in taking the reactor core from the fuel loading temperature (i.e., the ambient temperature) to the zero power operating temperature

$$\Delta \rho_{TD} = \int_{T_{ambient}}^{T_{zero\ power}} \frac{\partial \rho}{\partial T}\, dT \qquad (14\text{-}32)$$

The magnitude of $\Delta \rho_{TD}$ is primarily determined by the coolant temperature coefficient of reactivity, and depends sensitively upon the moderator-to-fuel ratio, as well as the concentration of soluble poison in the coolant.

2. Power Coefficients of Reactivity

A far more useful parameter is the reactivity coefficient characterizing power level changes

$$\alpha_p \equiv \frac{d\rho}{dP} = \sum_i \left(\frac{\partial \rho}{\partial \bar{T}_i}\right)\left(\frac{\partial \bar{T}_i}{\partial P}\right) \qquad (14\text{-}33)$$

where the $\bar{T}_i$'s are the effective or average temperatures of each major component of the core--e.g., fuel, moderator, structure, etc. Obviously, if a reactor is to be inherently stable against power level fluctuations, it must be designed with $\alpha_p < 0$.

A closely related quantity is the "power defect" which is defined as the change in reactivity which takes place between zero power and full power

$$\Delta\rho_{PD} \equiv \int_0^P \frac{\partial \rho}{\partial P}\, dP \qquad (14\text{-}34)$$

The power defect can be quite sizeable, for example, $\Delta\rho_{PD} \sim 2\%$ in light water reactors.

The dependence of core multiplication upon power will obviously depend sensitively upon the heat transfer characteristics of the reactor. For slow power changes, one can use the steady-state analysis of Chapter 12 to determine the core temperatures for a given power level--e.g., q'--and hence the power coefficient of reactivity in terms of the temperature coefficients of the various components of the core. It should be noted that the heat transfer mechanisms are highly nonlinear. For example, in metal clad ceramic fuel elements, increasing power levels will increase

the gap thermal conductance h_g due to differential thermal expansion between fuel pellet and cladding.

The steady-state thermal analysis will no longer be valid for more rapid power transients. For example, the thermal time constant of the fuel is frequently as large as 10 seconds. For power transients on shorter time scales the fuel temperature coefficient of reactivity (principally determined by the Doppler effect) will be the dominant factor in determining the power coefficient of reactivity.

The accurate determination of power and temperature coefficinets of reactivity using involves performing a series of criticality calculations for various core temperatures and power levels.

3. Equilibrium Fission Product Poisons

A sizeable negative reactivity is contributed by fission product poisons such as xenon and samarium which build up to equilibrium levels in a reactor operating at a steady state flux level ϕ_o :

$$\Sigma_a^X = \frac{\Sigma_f (\gamma_I + \gamma_X)}{1 + \lambda_X / \sigma_a^X \phi_o}$$

$$\Sigma_a^S = \gamma_P \Sigma_f$$

Typical values of negative reactivity for various flux levels are shown below:

ϕ_o	10^{12}	10^{13}	10^{14}	∞
$\Delta\rho^{Xe}$	.3 %	1.8	3.5	3.9
$\Delta\rho^{Sm}$	.7	.7	.7	.7
$\Delta\rho^{tot}$	1.0	2.5	4.2	4.6

We have seen in Chapter 6 that following shutdown, the xenon and samarium concentrations will increase dramatically. It may be desirable to build in enough excess reactivity into the core loading to compensate for this negative reactivity to allow startup without waiting for xenon decay (such as in a propulsion reactor).

4. Fuel Depletion

Of course, the primary requirement on the excess reactivity in the core fuel loading is that of compensating fuel burnup to allow a satisfactory core life. Closely coupled are considerations of the conversion of fertile to fissile isotopes (e.g., U^{238} to Pu^{239}) and the buildup of non-saturating fission product poisons. The analysis of fuel burnup and depletion will be discussed in some detail in the next chapter.

5. Other Reactivity Effects

There are also reactivity requirements imposed by the desired operating performance of the reactor. For example, the control elements must be able to follow the time rate of change of reactivity, as well as to follow load level or power maneuvering. The rate of change of

reactivity can be calculated from a knowledge of the differential rod worth ($d\rho/dh$) and the rod insertion speed $\frac{dh}{dt}$

$$\frac{d\rho}{dt} = \left(\frac{d\rho}{dh}\right)\left(\frac{dh}{dt}\right) \tag{14-36}$$

For example, if we consider a nuclear reactor with a 2% power defect subject to a load change requirement of 5%/min (fairly typical for a large power plant) then such a reactor would require a reactivity insertion rate of

$$\frac{d\rho}{dt} = (.02)(.05) = 10^{-3}/\text{min} \tag{14-37}$$

If the control rod drive speed is 10 inches/min, then we require a differential rod worth of

$$\frac{d\rho}{dh} = \frac{d\rho}{dt}\Big/\frac{dh}{dt} = 10^{-4}/\text{in} \tag{14-38}$$

If the core height were 150 inches, then a control rod group worth of 1.5% would meet this requirement over the central 50% of its path of travel.

Of course, the perturbation in the axial flux increases as the core height and rod worth increase. For this reason it is desirable to subdivide the control into a large number of rods. But such rods require complex mechanisms to achieve the required insertion rates. One must compromise between control rod velocity and mechanism size and cost and perturbations in the power distribution.

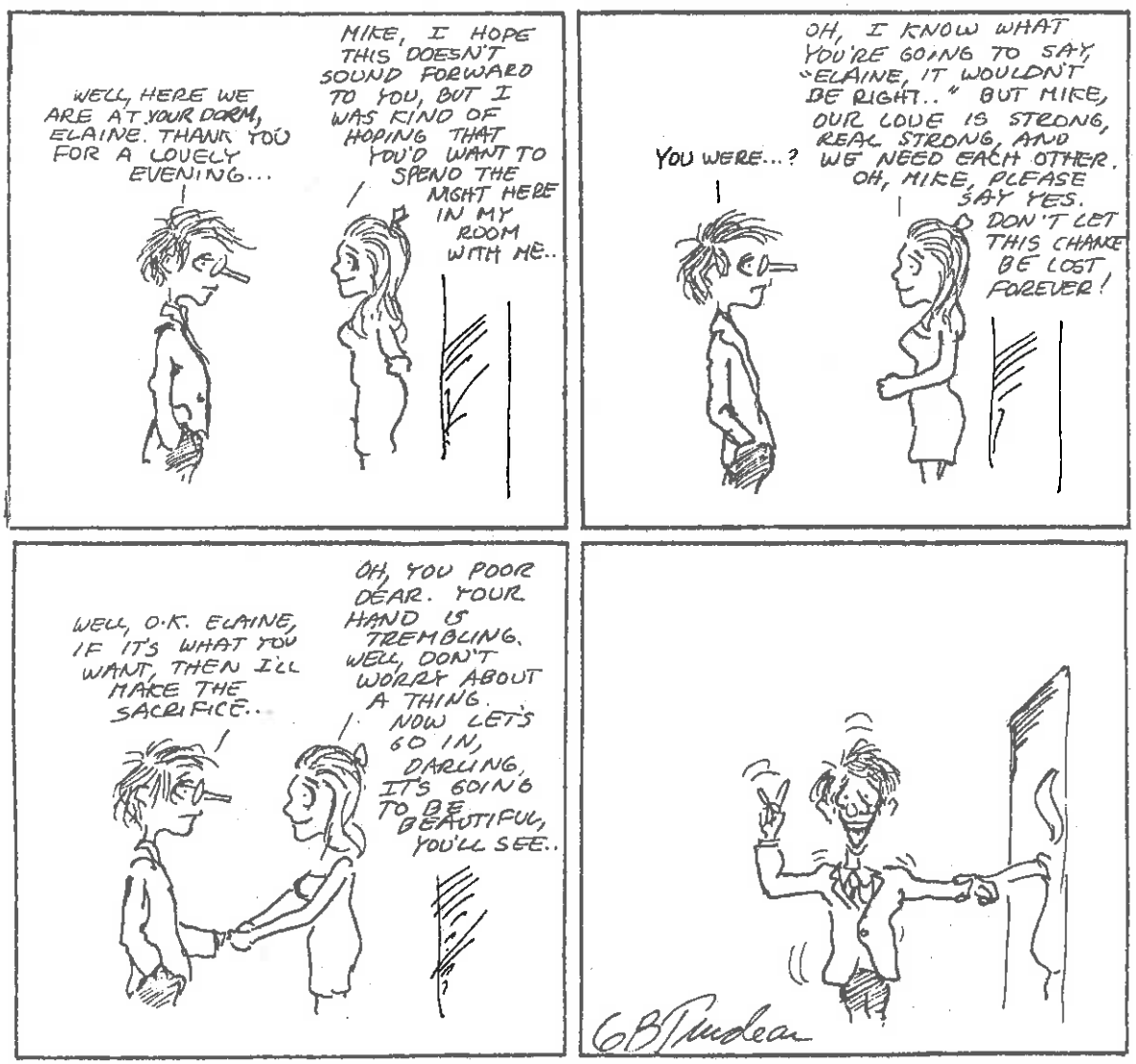
WELL, HERE WE ARE AT YOUR DORM, ELAINE. THANK YOU FOR A LOVELY EVENING...
MIKE, I HOPE THIS DOESN'T SOUND FORWARD TO YOU, BUT I WAS KIND OF HOPING THAT YOU'D WANT TO SPEND THE NIGHT HERE IN MY ROOM WITH ME..
YOU WERE...?
OH, I KNOW WHAT YOU'RE GOING TO SAY, "ELAINE, IT WOULDN'T BE RIGHT.." BUT MIKE, OUR LOVE IS STRONG, REAL STRONG, AND WE NEED EACH OTHER. OH, MIKE, PLEASE SAY YES. DON'T LET THIS CHANCE BE LOST FOREVER!
WELL, O.K. ELAINE, IF IT'S WHAT YOU WANT, THEN I'LL MAKE THE SACRIFICE..
OH, YOU POOR DEAR. YOUR HAND IS TREMBLING. WELL, DON'T WORRY ABOUT A THING. NOW LET'S GO IN, DARLING, IT'S GOING TO BE BEAUTIFUL, YOU'LL SEE..
GB Trudeau

B. Reactivity Effects in Specific Reactor Types

1. Light Water Reactors

Heating, evaporation, and motion of the coolant strongly affect the reactivity of water moderated reactors. Because of the large values of power, temperature, and burnup coefficients of reactivity typical of water reactors, reactivity control requirements are also large. The principal causes of reactivity effects in short term transients in water reactors include

Fuel Effects:

(i) Doppler effect: Recall that the resonance escape probability is given in terms of the resonance integral I as

$$p = \exp\left[-\frac{N}{\xi \Sigma_p} I\right] \tag{14-39}$$

We can get a qualitative idea of the effect of temperature upon p through Doppler broadening by using the Hellstrand correlation

$$I(T) = I(300°K)\left[1+\beta\left(\sqrt{T}-\sqrt{300°}\right)\right] \tag{14-40}$$

The Doppler coefficient of reactivity is then given by

$$\alpha_D = \frac{1}{P}\frac{dp}{dT} = \left[\ln p(300°K)\right]\frac{\beta}{2\sqrt{T}} \tag{14-41}$$

The dominant contribution to the Doppler effect in thermal reactors comes from U^{238}, although other strong resonance absorbers such as Pu^{240} may also have a strong influence.

(ii) Fuel motion: Fuel rod motions such as rod bowing can significantly affect core multiplication. But these can be controlled using proper mechanical design (rod spacers, etc.).

(iii) Core expansion: The temperature increase associated with power level increase will induce thermal expansion in the core. We have already noted that the differential fuel clad expansion can increase the gap thermal conductance. But the dominant expansion affect will be that of the coolant (some 20 to 50 times greater than most other core materials).

Moderator Effects:

(i) Moderator temperature: Moderator temperature changes will affect neutron temperature and hence affect quantities such as η, the number of neutrons produced per neutron absorbed in the fuel.

(ii) Moderator density: Perhaps the major reactivity effect is due to changes in moderator density, due to either thermal expansion or void formation (steam production). The various components of the reactivity effect due to decreasing moderator density are listed below:

Quantity	Explanation	Sign of the Contribution to reactivity
Fast effect ϵ	Less scattering of fission spectrum neutrons to below fast fission threshold	+
Age τ	Less slowing down to thermal and scattering within the reactor boundaries, and thus more fast leakage	-
Resonance Escape p	Increased resonance capture because of less slowing down	-
Thermal Utilization f	Less thermal neutron capture in the moderator due to less moderator	+
Thermal migration area	" "	-
$\frac{f_2}{M^2}$	Additional thermal capture outside of fuel due to a flattening of the intracell fine structure flux shape	- +
M^2	Less thermal scattering within the reactor boundaries, and thus more thermal leakage	-
Buckling B_g^2	Enhanced reflector effectiveness on a core which is leaking more neutrons	+

The dominant effect in light water reactors is the effect of water density change on resonance absorption. If we return to

$$p = \exp\left[-\frac{N}{\xi \Sigma_p} I\right] \tag{14-42}$$

then the moderator density change will appear through changes in Σ_p. If we write $\Sigma_p = N_M \sigma_p$, then

$$\frac{d\rho}{dT} = -\ln p \; \frac{1}{N_M} \frac{dN_M}{dT} \tag{14-43}$$

(iii) Moderator isotopic composition

(iv) Radiolytic gas formation

(v) Gas microbubbles

Other Effects:

(i) Chemical shim effects: Soluble poisons will make a positive contribution to the power coefficient of reactivity, since a power increase resulting in a decrease in coolant density will also decrease poison density.

(ii) Burnable poison effects: Solid absorbers will usually contribute a negative reactivity coefficient because of their strong self-shielding.

A summary of temperature coefficients for a light water reactor is given below. Spectrum changes are dominated by the Doppler effect, although the presence of Pu^{239} tends to counter this effect to a degree. Coolant expansion effects, such as upon the resonance escape probability p, dominate the composition effects.

Typical Water Reactor Temperature Coefficients

Component	Spectrum Effect	Composition (Expansion) Effect
η	$-U^{235}$ neg Pu^{239}	-
ϵ	-	pos
p	neg	neg
f	small neg $-U^{235}$ pos $-Pu^{239}$	pos
P_{NL}	-	neg

Total	-1 to -3×10^{-5}	-1 to -3×10^{-4}

2. High Temperature Gas Cooled Reactors

The relatively lower moderating power of carbon (compared to water) demands a larger moderator bulk in an HTGR. Hence the power densities of HTGR's are much smaller than those characteristic of light water reactors (typically 7 kw/liter as compared to 40 kw/liter in LWR's). An HTGR core is typically some 1.5 to 1.7 times larger in height than an LWR. However, the migration length in an HTGR is about 65 cm, compared to 15 cm for an LWR. Hence the HTGR core is actually some 3 times smaller than the LWR core when measured in migration lengths. This is extremely important from a reactivity point of view, because it implies that even though the HTGR power density is much lower, the neutronic behavior of the core is much more closely (and hence less susceptible to spatially dependent effects) than an LWR core.

There is relatively little neutronic-coolant interaction in an HTGR, since there is no phase change occurring as in an LWR. This removes the strong negative void coefficient which was present in LWR's.

Instead, one must rely upon the Doppler effect as the primary temperature feedback mechanism. For this reason, the assurance of an adequate negative temperature coefficient throughout core life will depend much more sensitively upon the nuclear analysis of the core than in an LWR design.

3. Liquid Metal Fast Breeder Reactors

The two dominant effects are the Doppler effect on resonance absorption, and the reactivity effect due to void formation in the liquid metal coolant:

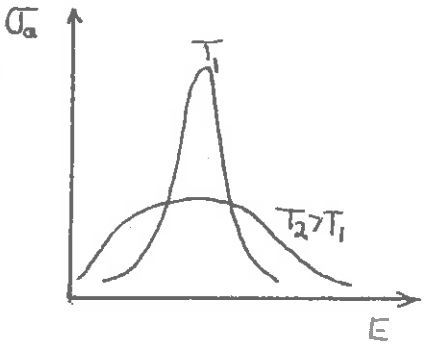

Doppler Effect: Recall that in thermal reactors, an increasing temperature implied a Doppler broadening of the absorption resonance (in U-238) which led to a decrease in the resonance escape probability, p_{re}, and hence a negative reactivity effect.

In a fast reactor, however, the neutron energy spectrum spans the resonance regions of both fertile and fissile materials. Hence increasing temperature will increase both $\Sigma_a \phi$ and $\Sigma_f \phi$. There may be a net increase in reactivity. Since the Doppler effect is a fast feedback mechanism, and since the prompt neutron lifetime of a fast core is so short, this is rather worrysome.

A positive Doppler coefficient is more pronounced in a core with a hard spectrum (such as in a metal fueled core). To soften the spectrum, one uses oxide fuels. Here, the oxygen will degrade the spectrum to yield a negative Doppler coefficient. The SEFOR reactor was constructed to verify this (and has done so).

Sodium Void Coefficient: In thermal reactors, the coolant void coefficient was negative. But in a large fast core, the sodium void coefficient may in fact be positive. That is, an increasing temperature will increase the void fraction, hence increasing reactivity and thereby temperature. There are two competing effects which determine the sign of $d\rho/d\alpha$:

(i) Spectrum effects: the coolant degrades the spectrum, hence lowering the effective $\bar{\eta}$. Hence any loss of sodium hardens the spectrum, implying $d\bar{\eta}/d\alpha > 0$.

(ii) Leakage effects: A loss of sodium near the edge of the core will increase leakage, hence implying $dP_{NL}/d\alpha < 0$.

These effects compete in such a way that the void coefficient is positive in the center of the core, and negative near the edge:

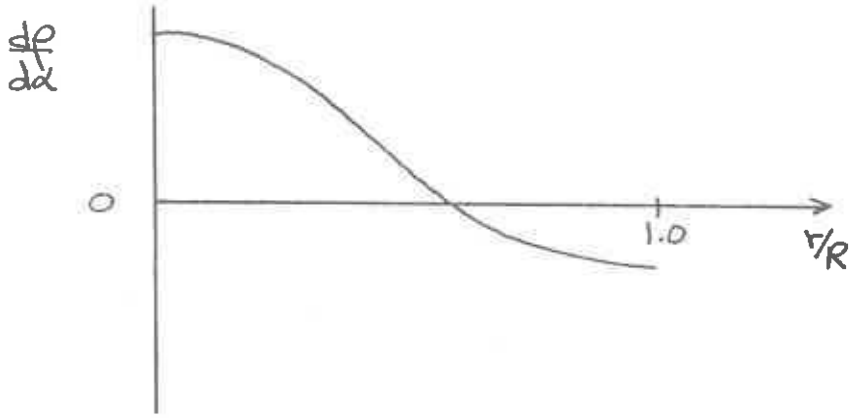

One finds this effect becomes more pronounced with larger cores

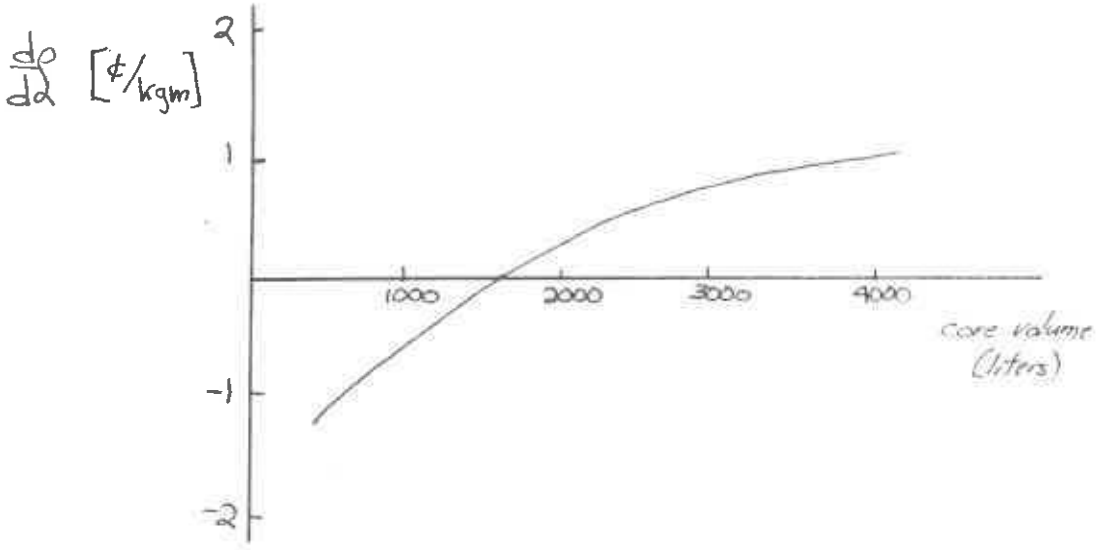

One can design around this effect by increasing leakage (see the "spoiled geometry" designs on the next page), but this will cost large penalties on fuel inventory and core breeding ratios.

C. Experimental Determination of Reactor Kinetic Parameters and Reactivity

The three most important parameters characterizing the kinetic behavior of a nuclear reactor are the

(i) reactivity ρ

(ii) prompt neutron lifetime ℓ

(iii) effective delayed neutron fraction β

A variety of experimental techniques can be used to measure these quantities. These can be grouped into static and dynamic measurement techniques.

1. Static Techniques for Reactivity Determination

(a) Neutron Multiplication Measurements (Reciprocal Multiplication Method)

We have already discussed critical loading experiments in which the steady state neutron flux resulting from a source in a subcritical assembly of multiplication $M = (1-k)^{-1}$ is measured. The usual procedure for safe approach to delayed critical consists of plotting 1/M (or the reciprocal neutron counting rate) as a function of some parameter that controls reactivity (e.g., fuel loading) and then extrapolating this 1/M plot to zero. During a stepwise approach to delayed critical by the reciprocal multiplication method, the neutron level following each addition of reactivity must be allowed to stabilize in order to obtain an accurate indication of the asymptotic multiplication before proceeding with the next reactivity addition. As one approaches delayed critical, the buildup of the precursor concentration is the principal headache.

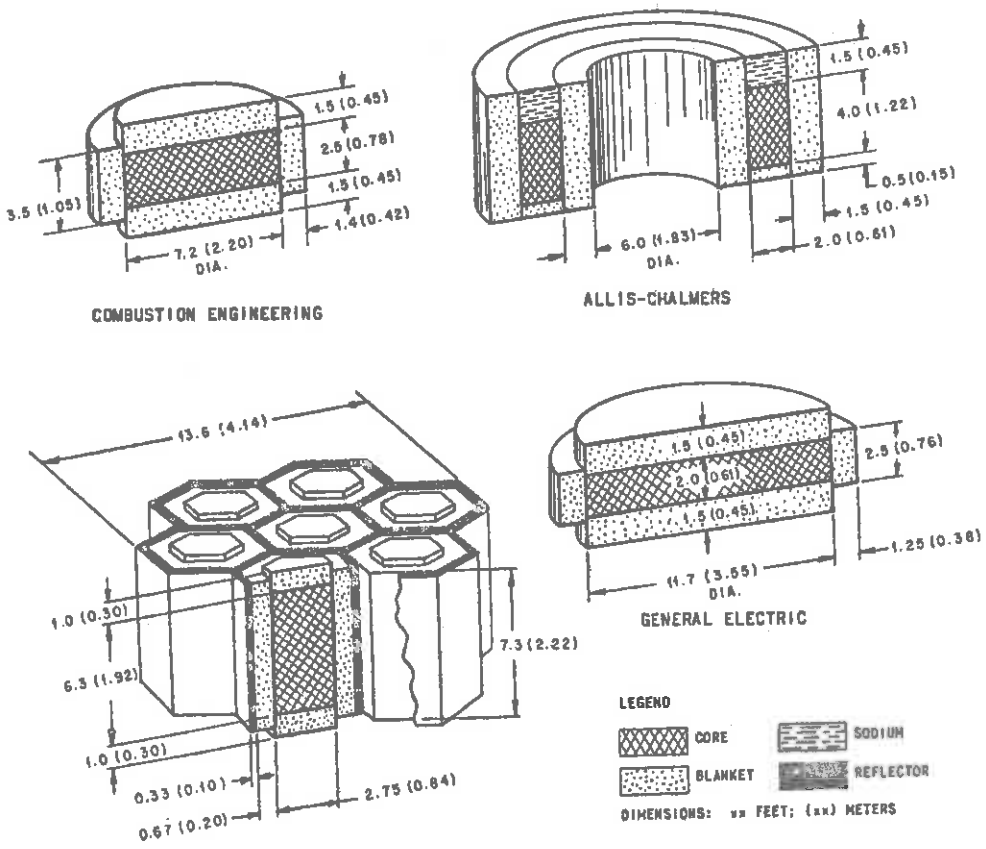

FUGURE 14-10: Reactor core arrangements in four 1000-MWe design studies.

Table 14-4: LMFBR Temperature Coefficients

TEMPERATURE COEFFICIENTS[39]

	Case					
	1	2	3	4	5	6
Isothermal Temperature Coefficients, 10^{-5} $\Delta k/k/°C$						
Sodium expansion	+1.00	+1.00	+1.00	−0.60	−0.60	−0.60
Canning						
Radial expansion	+0.10	+0.10	+0.10	−0.06	−0.06	−0.06
Axial expansion	+0.12	+0.12	+0.12	+0.12	+0.12	+0.12
Fuel axial expansion						
Fuel in contact with the canning	−0.38	−0.38	−0.38	−0.38	−0.38	−0.38
Fuel free in the canning	−0.21	−0.21	−0.21	−0.21	−0.21	−0.21
Core radial expansion	−0.92	−0.92	−0.92	−0.92	−0.92	−0.92
Doppler effect	−0.35	−0.70	−1.40	−0.35	−0.70	−1.40
Total isothermal with zero core radial expansion and fuel in contact with the canning	+0.49	+0.14	−0.56	−1.39	−1.74	−2.44
Power Coefficients, 10^{-7}/MW						
Sodium expansion	+3.00	+3.00	+3.00	−1.80	−1.80	−1.80
Canning						
Radial expansion	+0.54	+0.54	+0.54	−0.32	−0.32	−0.32
Axial expansion	+0.59	+0.59	+0.59	+0.59	+0.59	+0.59
Fuel axial expansion						
Fuel in contact with the canning	−1.88	−1.88	−1.88	−1.88	−1.88	−1.88
Fuel free in the canning	−8.05	−8.05	−8.05	−8.05	−8.05	−8.05
Core radial expansion	−2.76	−2.76	−2.76	−2.76	−2.76	−2.76
Doppler effect	−14.20	−28.40	−56.80	−14.20	−28.40	−56.80
Total power coefficient with zero core radial expansion and fuel in contact with the canning	−12.0	−26.2	−54.6	−17.6	−31.8	−60.2

(b) Fuel Poison Substitution Techniques

One can determine reactivity by uniformly substituting a poison for a small fraction of the fuel. The poison is usually chosen such that it has the same scattering and absorption properties of the fuel. Hence first order perturbation theory yields a reactivity change due to the substituted poison of

$$\Delta\rho = - \frac{\int_{poison} d^3r \; \phi^\dagger \delta\Sigma_a \phi}{\nu \int_{core} d^3r \; \phi^\dagger \Sigma_f \phi} \qquad (14\text{-}44)$$

This substitution method can be used for control rod calibration by balancing the effect of a given rod movement by adding a proper amount of distributed poison.

2. Dynamic Techniques for Reactivity Measurements

(a) Asymptotic Period Measurements

The basic idea here is to make a small perturbation in the core composition of a critical reactor, and then to measure the stable or asymptotic period of the resultant reactor transient. Using the inhour equation, one can then infer the reactivity from a measurement of the asymptotic period. It should be noted that the period method for all practical purposes applies only to positive periods, since negative periods are dominated by the longest delayed neutron precursor decay and hence provide very low sensitivity to negative reactivity.

(b) Rod Drop Method

Consider a reactor operating at some equilibrium level, n_0, when it is suddenly shut down by the introduction of a negative reactivity $-\delta k$ (the "rod drop"). Prior to the rod drop we know

$$0 = \frac{dn}{dt} = \frac{k_{p_0} - 1}{\ell} n_0 + \sum_i \lambda_i C_{i0}$$

$$0 = \frac{dC_i}{dt} = \frac{\beta n_0}{\ell} - \lambda_i C_{i0}$$

Hence we can solve for

$$n_0 = \frac{\ell \sum_i \lambda_i C_{i0}}{1 - k_{p_0}} = \frac{\ell \sum_i \lambda_i C_{i0}}{\beta} \qquad (14\text{-}45)$$

Now we also know from our studies of the inhour equation, that after a few prompt neutron lifetimes, the neutron population drops to a lower level determined by the new multiplication, k_{p_1}, and remains at this "quasistatic" level until it is ultimately decreased by delayed-neutron precursor decay. After this "prompt jump", the precursor concentrations C_i remain unchanged, while $\frac{dn}{dt} \sim 0$. This implies that the new neutron population level n_1 is given approximately by

$$n_1 \cong \frac{\ell \sum_i \lambda_i C_{i0}}{1 - k_{p_1}} \qquad (14\text{-}46)$$

If we combine this with (14-45), we find

$$\frac{n_1}{n_0} \sim \frac{1 - k_{p_0}}{1 - k_{p_1}} \cong \frac{\beta}{1 - k_{p_1}(1 - \beta)} \cong \frac{1}{1 + \frac{\delta k}{k}\beta} \qquad (14\text{-}47)$$

Hence

$$\text{rod worth in dollars} = \frac{\delta k}{k\beta} = \frac{n_0}{n_1} - 1$$

To determine n_1, one can simply extrapolate back the asymptotic behavior to t = 0.

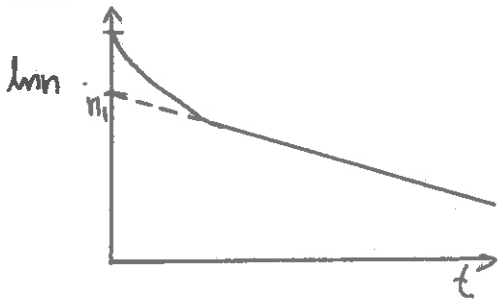

(c) Rod Oscillator Method

If one oscillates a control rod in a sinusoidal fashion in a critical reactor, there will be a corresponding oscillation in the neutron flux. Let n by the steady state neutron population, while δ n is the magnitude of the oscillating component of the neutron population. If the magnitude of the oscillating reactivity δ k induced by the rod is sufficiently small, then one can write

$$\frac{\delta n}{n} = W(i\omega)\,\frac{\delta k}{\beta} \tag{14-48}$$

where $W(i\omega)$ is the reactor transfer function

$$W(i\omega) = \frac{\beta}{i\omega\left[\ell + \sum_i \frac{\beta_i}{i\omega+\lambda_i}\right]} \tag{14-49}$$

For large ω such that $\omega >> \beta/\ell$,

$$W(i\omega) \sim \frac{\delta n}{n}\,\frac{\beta}{\delta k} = \frac{\beta}{\omega\ell} \tag{14-50}$$

or

$$\delta k = \omega\ell\,\frac{\delta n}{n} \tag{14-51}$$

Hence it is apparent that measuring δn at large $\omega >> \beta/\ell$ will yield the reactivity worth $\delta k/\ell$ of the rod.

(d) Source Jerk Method

Consider a subcritical system with a neutron source maintaining a level n_0. In equilibrium we know

$$0 = \frac{dn_0}{dt} = \frac{k_0 - 1}{\ell} n_0 + \sum_i \lambda_i C_{i_0} + S$$

$$0 = \frac{dC_i}{dt} = \beta_i \frac{k_0 n_0}{\ell} - \lambda_i C_{i_0}$$

Hence we can solve for

$$n_0 = \frac{\ell \sum_i \lambda_i C_{i_0} + \ell S}{1 - k_0} \tag{14-52}$$

Now suppose that the source is jerked out of the core. Then within a few prompt neutron lifetimes, the system will adjust to a lower "quasistatic" neutron level, n_1, determined by the multiplied delayed-neutron source strength alone

$$n_1 = \frac{\ell \sum_i \lambda_i C_{i_0}}{1 - k_0} \tag{14-53}$$

Hence we can solve for

$$\frac{n_2}{n_1} = 1 + \frac{\bar{\beta}}{\sum_i \lambda_i C_{i_0}} \tag{14-54}$$

But from the equilibrium equations above

$$\frac{\beta}{1-k_0} = \frac{n_0}{\ell} \quad , \quad \frac{n k_0 \beta}{\ell} = \sum_i \lambda_i C_{i0}$$

Thus we find

$$\frac{n_0}{n_1} = 1 + \frac{1-k_0}{k_0 \beta} \tag{14-55}$$

or

$$\text{Dollars subcritical} = \frac{n_0 - n_1}{n_1} \tag{14-56}$$

This method is similar to the rod drop method, but it requires only the removal of a small mass of material in contrast to the rapid release of one or more control rods.

(e) Pulsed Neutron Methods

Here the basic idea is to observe the transient behavior of the neutron flux in an assembly following a burst of neutrons injected into the assembly. Consider first the injection of a burst of neutrons at t = 0 into a non-multiplying assembly. Then, according to one-speed diffusion theory

$$\frac{1}{v}\frac{\partial \phi}{\partial t} = D\nabla^2\phi - \Sigma_a \phi$$

But using the spatial eigenfunctions satisfying

$$\nabla^2 \varphi_n + B_n^2 \varphi_n(\vec{r}) = 0$$

$$\phi(\vec{r},t) = \sum_n a_n \varphi_n(\vec{r}) e^{-(v\Sigma_a + DB_n^2)t} \sim a_0 \varphi_0(\vec{r}) e^{-(v\Sigma_a + DB_g^2)t}$$

Hence the asymptotic behavior of the flux is governed by the decay constant

$$\alpha_0 = \nu\Sigma_a + DB_g^2 \tag{14-57}$$

If we measure α_0 for various assembly sizes, we can determine $\nu\Sigma_a$ and D. Actually, there are higher order terms in B^2, such as

$$\alpha_0 = \nu\Sigma_a + DB^2 + CB^4 + \cdots$$

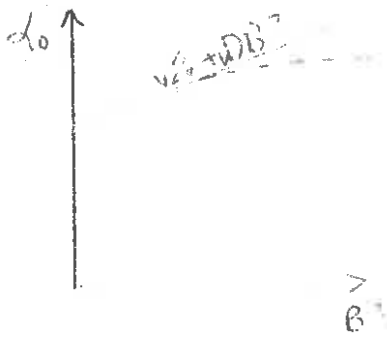

which add a curvature to the $\alpha_0(B^2)$ plot.

In multiplying assemblies, one uses

$$\frac{1}{v}\frac{\partial\phi}{\partial t} = D\nabla^2\phi - (\Sigma_a - \nu\Sigma_f)\phi$$

to find decay constants of the form

$$\alpha_0 = v(\Sigma_a - \nu\Sigma_f) + vDB^2 \tag{14-58}$$

In this case, the $\alpha_0(B^2)$ curves look as below:

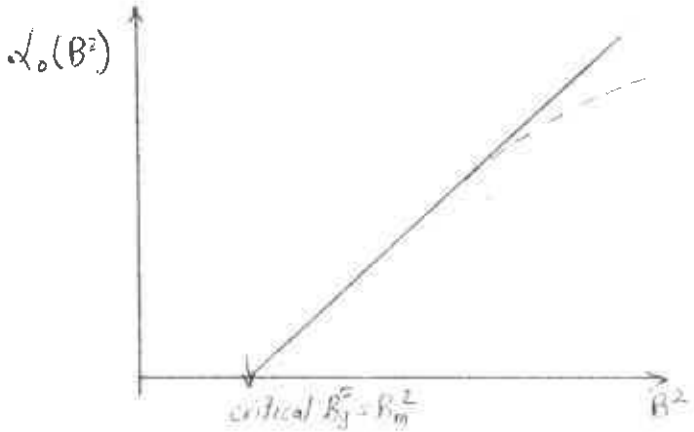

One can also use this technique to measure reactivity. The prompt neutron decay constant is given by

$$\alpha_o = \frac{1}{n}\frac{dn}{dt} = \frac{\left(\frac{k-1}{k}\right)-\beta}{\Lambda} = \frac{\beta}{\Lambda}(\$-1) \qquad (14\text{-}59)$$

Hence α_o is directly proportional to \$. One can use this technique to measure \$ directly. If the core is maintained at delayed critical, then \$ = 0, and the pulsed neutron measurement yields

$$\alpha_o = -\frac{\beta}{\Lambda} \qquad (14\text{-}60)$$

VI. IN CORE INSTRUMENTATION

- will be added later -

V. PERTURBATION THEORY

It is frequently of interest to compute the change in core multiplication caused by a small change in the core geometry or composition. Fortunately, if this change or "perturbation" is sufficiently small, one does not have to repeat the original criticality calculation, but instead can use well-known techniques of perturbation theory to express the corresponding change in multiplication in terms of the fluxes characterizing the unperturbed core.

For example, consider a very simple one speed diffusion model of a bare, homogeneous reactor in which the criticality relation is

$$k = \frac{\nu \Sigma_f / \Sigma_a}{1 + L^2 B^2} = 1 .$$

Now suppose we were to uniformly modify or perturb the absorption cross section to a new value

$$\Sigma_a' = \Sigma_a + \delta\Sigma_a ,$$

where we will assume that the perturbation $\delta\Sigma_a$ is small--i.e.,

$$\delta\Sigma_a << \Sigma_a .$$

Then the value of k' corresponding to the perturbed core can be written as

$$k' = \frac{\nu \Sigma_f / \Sigma_a'}{1 + L'^2 B^2} = \frac{\nu \frac{\Sigma_f}{\Sigma_a}\left(1 + \frac{\delta\Sigma_a}{\Sigma_a} + \cdots\right)}{1 + \frac{DB^2}{\Sigma_a}\left(1 + \frac{\delta\Sigma_a}{\Sigma_a} + \cdots\right)}$$

$$k' = k\left(1 + \frac{\delta\Sigma_a}{\Sigma_a} + \cdots\right)\left(1 - \frac{\delta\Sigma_a}{\Sigma_a(1+L^2B^2)}\right)$$

$$\simeq k\left(1 - \frac{\delta\Sigma_a}{\Sigma_a}\,\frac{L^2B^2}{1+L^2B^2}\right) .$$

Notice two things about this result: First, we have neglected all terms of higher than first order in the perturbation ($\delta\Sigma_a$). Second, we have managed to express the perturbed multiplication factor k' in terms of the unperturbed multiplication, k.

These general features appear in applications of perturbation theory to more general problems in nuclear reactor analysis in which the perturbations may be localized or in which the multigroup diffusion equations are used as the basic model of the core nuclear behavior. Although the general ideas are essentially as simple as those in the example above, it is helpful to introduce a few mathematical preliminaries to simplify notation. [For more details, the reader is referred to Appendix E.] Consider, by way of example, the one group diffusion equation characterizing a critical core.

$$\underbrace{-\nabla\cdot D(\vec{r})\nabla\phi(\vec{r}) + \Sigma_a(\vec{r})\phi(\vec{r})}_{M\phi} = \nu\,\underbrace{\Sigma_f(\vec{r})\phi(\vec{r})}_{F\phi} ,$$

where we will leave it as understood that the solution of this equation, $\phi(\vec{r})$, must satisfy appropriate boundary conditions such as $\phi(\tilde{R}) = 0$ on the surface of the core.

Now suppose we define the inner product (f,g) between any two functions $f(\vec{r})$ and $g(\vec{r})$ as

$$(f,g) \equiv \int_V d^3r\, f^*(\vec{r})\, g(\vec{r}) \quad ,$$

where $f^*(\vec{r})$ denotes the complex conjugate of $f(\vec{r})$, and V is the core volume.

We can now use this inner product to define the operator $M^\dagger$ adjoint to the operator M as that operator $M^\dagger$ for which

$$(M^\dagger f, g) = (f, Mg)$$

for every $f(\vec{r})$ and $g(\vec{r})$ which satisfy the boundary conditions $f(\tilde{R}) = 0 = g(\tilde{R})$.

We can use this definition to explicitly construct the adjoint of an operator. Consider for example, the operator

$$F\circ \equiv \xi_f(\vec{r})\circ$$

which simply corresponds to multiplying a function by $\xi_f(\vec{r})$. If we write

$$(f, Fg) = \int_V d^3r\, f^* \xi_f g = \int_V d^3r\, (\xi_f f)^* g$$

$$= (\xi_f f, g) = (F^\dagger f, g)$$

then we can merely shuffle $\Sigma_f(\vec{r})$ around in the integral (noting that Σ_f is real) to identify

$$F^\dagger \circ = \Sigma_f(\vec{r}) \circ$$

Notice that in this case, $F^\dagger$ and F are in fact identical. We refer to such operators as being self-adjoint.

For a more complicated example, consider the spatial derivatives in the diffusion operator M:

$$(f, \nabla \cdot D \nabla g) = \int_V d^3r \; f^* \nabla \cdot D \nabla g \quad .$$

Now if we use the vector identity

$$\nabla \cdot a\vec{b} = a \nabla \cdot \vec{b} + \vec{b} \cdot \nabla a \quad ,$$

we can rewrite this as

$$(f, \nabla \cdot D \nabla g) = \int_V d^3r \; \nabla \cdot [f^* D \nabla g] - \int_V d^3r \; [\nabla f^* \cdot D \nabla g] \quad .$$

But using Gauss's law, we can convert the first term into an integral over the surface:

$$\int_V d^3r \; \nabla \cdot [f^* D \nabla g] = \int_S d^2r \; f^* D \nabla g$$

But since we require that f and g vanish on the surface, this term vanishes. If we repeat this procedure we find we can rewrite

$$(f, \nabla\cdot D\nabla g) = \int_V d^3r\, [\nabla\cdot D\nabla f]^* g = (\nabla\cdot D\nabla f, g)$$

Hence we find that

$$\nabla\cdot D\nabla^\dagger \circ = \nabla\cdot D\nabla \circ$$

--again we have encountered a self-adjoint operator.

From these examples, it is apparent that the operator

$$M\circ \equiv -\nabla\cdot D\nabla\circ + \Sigma_a\circ$$

is also self adjoint:

$$M^\dagger\circ = M\circ$$

We will continue to distinguish between the adjoint and direct operators, $M^\dagger$ and M, however, since for more general multigroup diffusion calculations, M will not be self adjoint (see Chapter 7). We now define the adjoint flux $\phi^\dagger$ as that solution of

$$M^\dagger\phi^\dagger = \nu F^\dagger\phi^\dagger$$

[Although, again we keep in mind that $M^\dagger = M$ and $F^\dagger = F$ implies that $\phi^\dagger = \phi$ for the one-speed diffusion model of a reactor.]

To see how to use these concepts, let's go back to the criticality equation

$$-\nabla \cdot D\nabla\phi + \Sigma_a\phi = \nu\Sigma_f\phi$$

Now for a system which is not critical, we know that (↑) has no solution. But we can remedy this situation by modifying Eq. (↑) by inserting the multiplication factor k as

$$-\nabla \cdot D\nabla\phi + \Sigma_a\phi = \frac{1}{k}\nu\Sigma_f\phi$$

As we noted earlier, an alternative way to accomplish the same thing is to let ν vary from its true value ν_c . That is, we write our criticality equation as

$$-\nabla \cdot D\nabla\phi + \Sigma_a\phi = \nu\Sigma_f\phi$$

allowing ν to be a variable parameter. Criticality is then achieved when core geometry and composition are adjusted such that $\nu \rightarrow \nu_c$.

Now we will be interested in calculating the effects of small changes in core properties on core multiplication. To this end, it is useful to define the concept of core reactivity

$$\rho \equiv \frac{k-1}{k}$$

Hence, the reactivity of a critical core is just $\rho = 0$, while $\rho > 0$ and $\rho < 0$ imply core subcriticality and supercriticality, respectively.

We will be interested in computing the change in reactivity, say from ρ to ρ', due to a slight perturbation in core properties. In particular, note

$$\Delta\rho = \left(\frac{k-1}{k}\right) - \left(\frac{k'-1}{k'}\right) = -\frac{(\nu'-\nu)}{\nu_c} = -\frac{\Delta\nu}{\nu_c} \quad .$$

From these relationships, it is apparent that if we can compute the change in ν due to a perturbation in the core, we can immediately obtain the corresponding reactivity change $\Delta\rho$.

To be more specific, suppose we consider a core characterized by a criticality equation

$$(M - \nu F)\phi = -\nabla \cdot D\nabla\phi + (\Sigma_a - \nu\Sigma_f)\phi = 0 \quad .$$

Now suppose we perturb the macroscopic absorption cross section (say, by adding a localized absorber) to a new value

$$\Sigma_a'(\vec{r}) = \Sigma_a(\vec{r}) + \delta\Sigma_a(\vec{r}) \quad .$$

We will assume that this perturbation, $\delta\Sigma_a(\vec{r})$, is small and attempt to calculate the corresponding change in ν to ν' as governed by the perturbed criticality equation

$$(M' - \nu' F')\phi' = -\nabla \cdot D \nabla \phi' + (\Sigma_a' - \nu' \Sigma_f')\phi' = 0 \quad .$$

Now suppose we explicitly write $\nu' = \nu + \delta\nu$ and $\Sigma_a' = \Sigma_a + \delta\Sigma_a$ to find

$$(M' - \nu' F')\phi' = (M - \nu F)\phi' + \delta\nu \Sigma_f \phi' - \delta\Sigma_a \phi' = 0$$

Next, we take the inner product of this equation with $\phi^\dagger$ as defined by Eq. ( )

$$(\phi^\dagger, (M - \nu F)\phi') + (\phi^\dagger, \delta\nu \Sigma_f \phi') - (\phi^\dagger, \delta\Sigma_a \phi') = 0 .$$

But using our earlier definition of $M^\dagger$ and $F^\dagger$

$$(\phi^\dagger, (M - \nu F)\phi') = ((M^\dagger - \nu F^\dagger)\phi^\dagger, \phi') = 0 .$$

Hence we can immediately solve for

$$\Delta\nu = \frac{(\phi^\dagger, \delta\Sigma_a \phi')}{(\phi^\dagger, \Sigma_f \phi')} .$$

But, unfortunately, this expression for $\Delta\nu$ involves the perturbed flux ϕ' . Suppose we write

$$\phi' = \phi + \delta\phi$$

Then

$$\Delta\nu = \frac{(\phi^\dagger, \delta\Sigma_a \phi)}{(\phi^\dagger, \Sigma_f \phi)} + \frac{(\phi^\dagger, \delta\Sigma_a \delta\phi)}{(\phi^\dagger, \Sigma_f \phi)} - \frac{(\phi^\dagger, \delta\Sigma_a \phi)(\phi^\dagger, \Sigma_f \delta\phi)}{(\phi^\dagger, \Sigma_f \phi)^2} + \cdots$$

But if the perturbation $\delta\Sigma_a$ is small, then we can neglect second and higher order quantities to find

$$\Delta\nu \cong \frac{(\phi^\dagger, \delta\Sigma_a \phi)}{(\phi^\dagger, \phi)}$$

Since the one-speed diffusion operator is self-adjoint, we know $\phi^\dagger = \phi$, and hence we find

$$\Delta\rho = -\frac{\Delta\nu}{\nu_c} \cong -\frac{\int_V d^3r\, \phi(\vec{r})\, \delta\Sigma_a(\vec{r})\, \phi(\vec{r})}{\nu_c \int_V d^3r\, \phi(\vec{r})\, \Sigma_f(\vec{r})\, \phi(\vec{r})}$$

It should be noted that all of this analysis was exact until we neglected second order terms in Eq. ( ). Thus, we have calculated a first order estimate of the reactivity change $\Delta\rho$ due to introducing a localized absorber $\delta\Sigma_a(\vec{r})$ in terms of the unperturbed flux distribution.

EXAMPLE: Consider a bare slab reactor characterized by one group constants D, Σ_a, and $\nu\Sigma_f$.

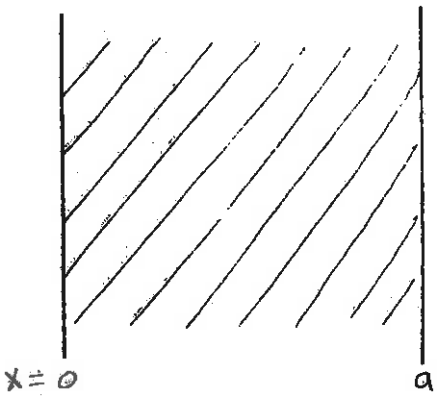

We will perturb this reactor by imagining that an additional absorber is uniformly inserted in the region $0 < x < h$. One might consider this to be a model of a bank of control rods inserted to a depth h in the core. Of course, to allow the application of perturbation theory, we must assume this absorption is relatively small.

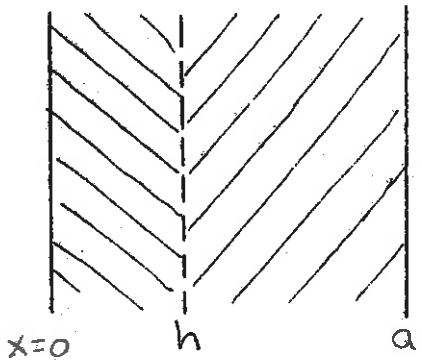

Hence our perturbation is

$$\delta\Sigma_a(x) = \begin{cases} \delta\Sigma_a & 0<x<h \\ 0 & h<x<a \end{cases} .$$

If we note that the unperturbed flux in this reactor is

$$\phi(x) = \phi_0 \sin\frac{\pi x}{a} ,$$

then we can compute the reactivity change due to an insertion of the absorber to a depth h as:

$$\Delta\rho(h) = -\frac{\int_0^a \delta\Sigma_a \phi^2 dx}{\nu\Sigma_f \int_0^a \phi^2 dx} ,$$

$$= - \frac{\phi_0^2 \delta\Sigma_a \int_0^h \sin^2 \frac{\pi x}{a} dx}{\phi_0^2 \nu\Sigma_f \int_0^a \sin^2 \frac{\pi x}{a} dx} = -\frac{2}{\pi} \frac{\delta\Sigma_a}{\nu\Sigma_f} \left[\frac{\pi h}{2a} - \frac{1}{4} \sin \frac{2\pi h}{a} \right]$$

It is customary to refer to the reactivity change due to such an absorber as the "worth" of the absorber. (This concept will be defined more precisely in Chapter 14.) Hence the reactivity worth can be sketched for various insertion depths h as shown below

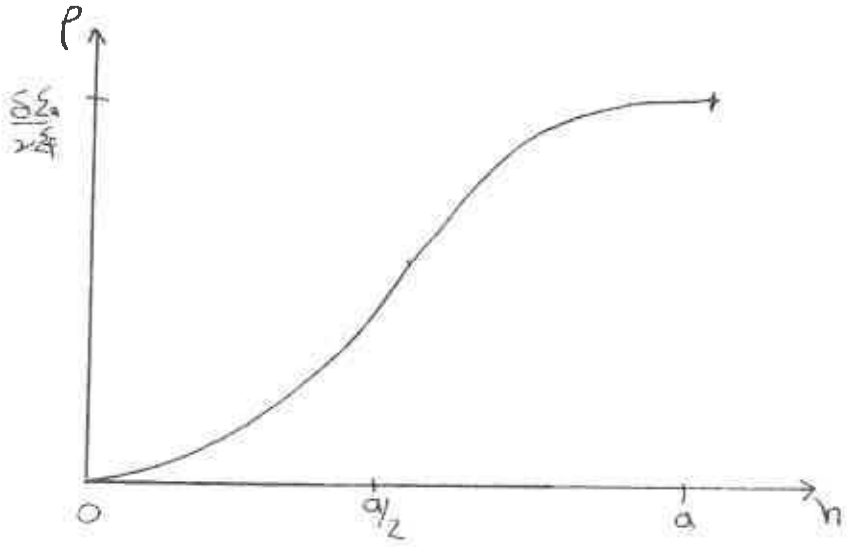

It is also of interest to compute the "differential worth" defined as

$$\frac{d\rho}{dh} = - \frac{\delta\Sigma_a}{a\nu\Sigma_f} \left[1 - \cos \frac{2\pi h}{a} \right]$$

Note that the differential worth is at a maximum when the edge of the absorbing region (e.g., the tip of the control rods) are in the region of largest flux in the center of the core:

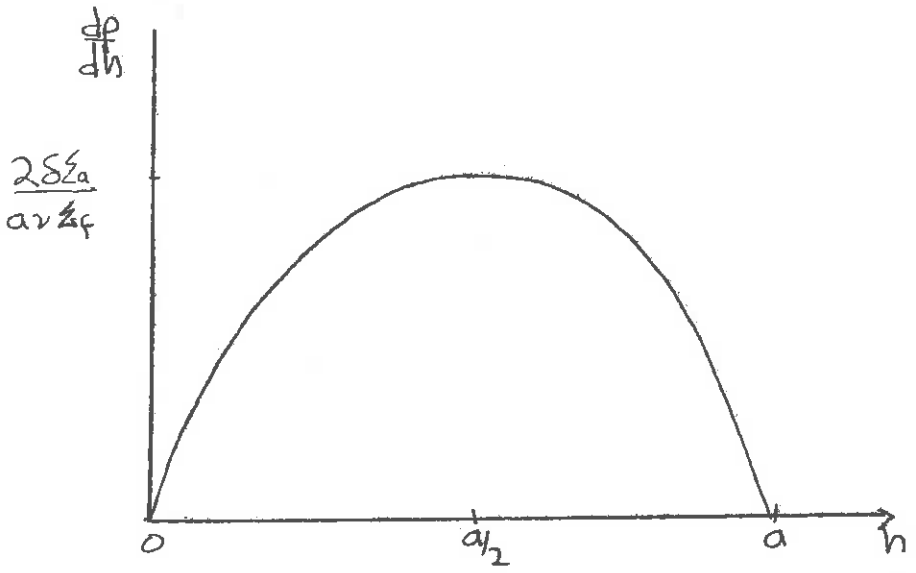

Such an analysis, while certainly of interest in illustrating general trends, is of limited usefulness in detailed control studies because of the highly absorbing nature of most control elements. Such elements very strongly perturb the flux in their vicinity, hence invalidating the use of perturbation theory. We will consider alternative methods which must be used for computing control rod worth in Chapter 14.

One can obtain more general expressions for the reactivity change induced by perturbations in the core parameters. For example, if we were to perturb

$$\Sigma_a' = \Sigma_a + \delta\Sigma_a$$

$$\Sigma_f' = \Sigma_f + \delta\Sigma_f$$

$$D' = D + \delta D$$

then the corresponding reactivity change would be

$$\Delta\rho = \frac{\int_V d^3r \left[(\nu\delta\Sigma_f - \delta\Sigma_a)\phi^2 - \delta D (\nabla\phi)^2 \right]}{\nu_c \int_V d^3r \, \Sigma_f \phi^2}$$

We will return later to discuss several more aspects of perturbation theory when we encounter the multigroup diffusion model.

The adjoint flux $\phi^\dagger(\vec{r})$ has a rather interesting physical interpretation. Suppose we imagine an absorber inserted into the reactor core at a point $\vec{r}_0$ such that

$$\delta\Sigma_a(\vec{r}) = \alpha\,\delta(\vec{r} - \vec{r}_0)$$

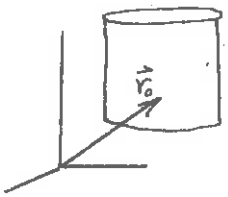

Here, α is the effective strength of the absorber. [If we were to imagine that the δ-function was, in fact, a mathematical idealization of an absorber of volume V_A, then $\alpha = \Sigma_a^A V_A$.] Now, strictly speaking, perturbation theory should not be valid for such a singular perturbation--but we will dismiss such concerns with a wave of the hand, and

use our earlier result to find the corresponding reactivity change as

$$\Delta\rho = - \frac{\int_V d^3r\, \phi^\dagger(\vec{r})\, \delta\Sigma_a(\vec{r})\, \phi(\vec{r})}{\nu_c \int_V d^3r\, \phi^\dagger(\vec{r})\, \Sigma_f(\vec{r})\, \phi(\vec{r})}$$

$$= - \frac{\alpha}{D}\, \phi^\dagger(\vec{r}_o)\, \phi(\vec{r}_o)$$

where we have denoted the denominator by a constant D (since it is independent of the perturbation). If we recognize that $\alpha\phi(\vec{r}_0)$ is just the absorption rate at $\vec{r}_0$, then we find

$$\phi^\dagger(\vec{r}_o) \sim \frac{-\Delta\rho}{\alpha\phi(\vec{r}_o)}$$

is simply proportional to the change in reactivity per neutron absorbed at $\vec{r}_0$ per second. In this sense, then, the adjoint flux $\phi^\dagger(\vec{r})$ is a measure of how effectively an absorber inserted at a position $\vec{r}$ is in changing the reactivity of the core. Evidently, if $\phi^\dagger(\vec{r})$ is large at $\vec{r}$, then the core multiplication will be quite sensitive to the absorption of neutrons at that point. For this reason, $\phi^\dagger(\vec{r})$ is sometimes referred to as the neutron "importance" of the "importance function".

One can see this from a somewhat different perspective if we consider the flux induced in a subcritical reactor by an arbitrary source $S(\vec{r})$ as governed by

$$(M-\nu F)\phi = -\nabla\cdot D\nabla\phi + (\Sigma_a - \nu\Sigma_f)\phi = S \quad .$$

Consider the adjoint problem

$$(M^\dagger - \nu F^\dagger)\phi^\dagger = -\nabla\cdot D\nabla\phi^\dagger + (\Sigma_a - \nu\Sigma_f)\phi^\dagger = S^\dagger \quad .$$

(Of course, for one-speed diffusion theory, $M = M^\dagger$ is self-adjoint, but we will retain the generality for a bit.) Notice that we have allowed the source $S^\dagger(\mathbf{r})$ appearing in the adjoint equation to be different.

Now suppose we multiply Eq. ( ) by $\phi^\dagger$ and integrate over $\vec{r}$, next multiply Eq. ( ) by ϕ and integrate, and then subtract these two results to find

$$(\phi^\dagger, (M-\nu F)\phi) - ((M^\dagger - \nu F^\dagger)\phi^\dagger, \phi) = (\phi^\dagger, S) - (S^\dagger, \phi)$$

But by the definition of the adjoint $M^\dagger - \nu F^\dagger$, the LHS is zero. Hence we find:

$$\int_V d^3r\, \phi^\dagger(\vec{r})\, S(\vec{r}) = \int_V d^3r\, S^\dagger(\vec{r})\, \phi(\vec{r}) \quad .$$

Since this must hold for any choice of $S(\vec{r})$ and $S^\dagger(\vec{r})$, we will use it to our advantage by specifying $S(\vec{r})$ as a unit point source at $\vec{r}_0$:

$$S(\vec{r}) = \delta(\vec{r}-\vec{r}_o)$$

and $S^\dagger(\vec{r})$ as the cross section $\Sigma_d(\vec{r})$ characterizing an imagined detector placed in the core. Then we find

$$\phi^\dagger(\vec{r}_o) = \int_V d^3r\ \Sigma_d(\vec{r})\,\phi(\vec{r})$$

Hence, in this instance, the adjoint flux is simply the response of a detector in the core to a unit point source inserted at a position $\vec{r}_o$. Once again we find that $\phi^\dagger(\vec{r}_o)$ is a measure of the <u>importance</u> of a neutron event (in this case, the production of a neutron rather than the absorption of a neutron) at a point $\vec{r}_o$ in contributing to the response of a detector with cross section $\Sigma_d(\vec{r})$ (as opposed to reactivity).

For the simple one-speed diffusion model we have been studying, the adjoint flux $\phi^\dagger(\vec{r})$ is identical to the flux itself. Hence perturbations which affect the creation or destruction of neutrons will have the most pronounced affect in those regions in which the flux is largest. This is not true, however, for the more general multigroup diffusion model, as we will see in Chapter 6.

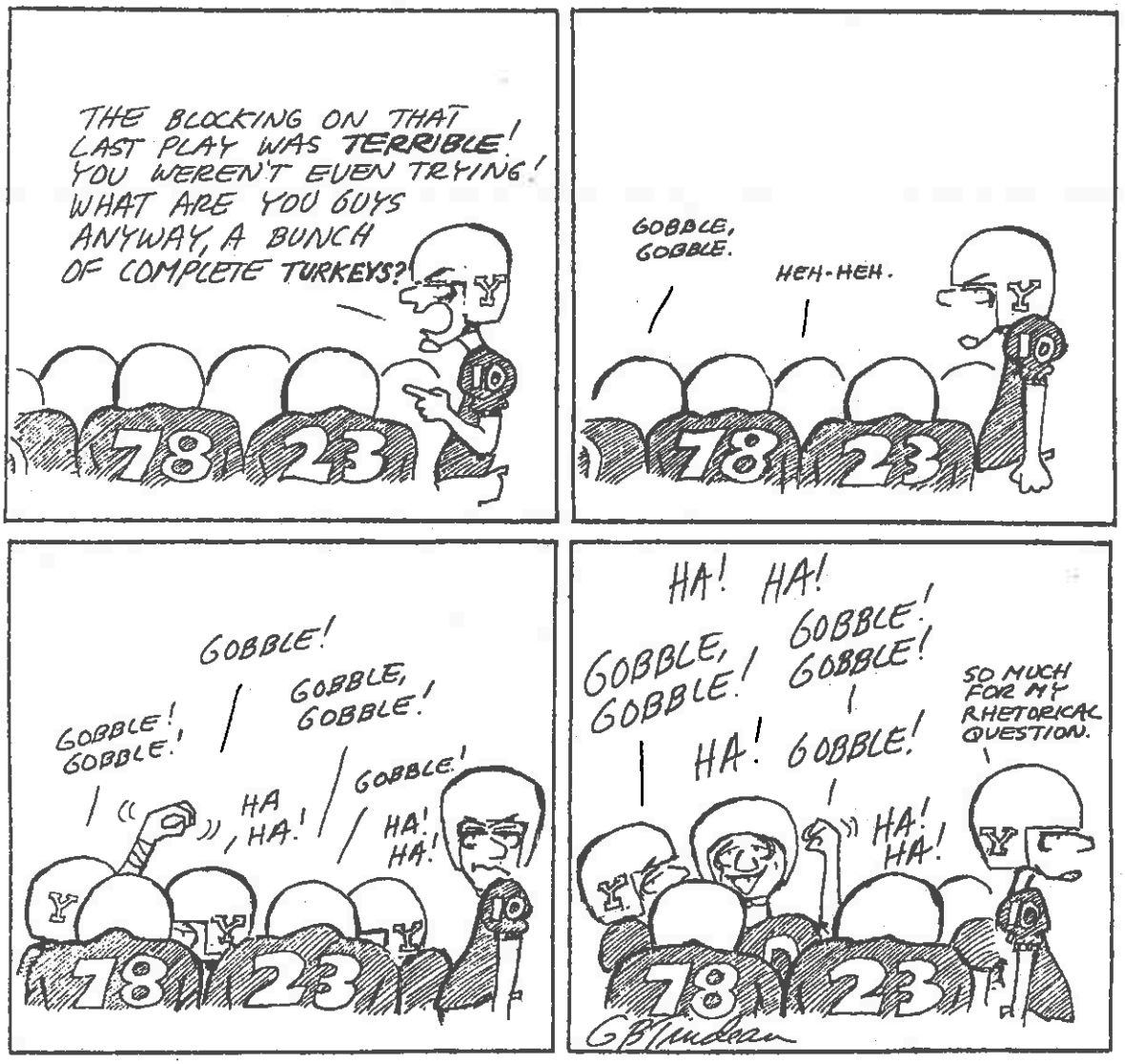
THE BLOCKING ON THAT LAST PLAY WAS TERRIBLE! YOU WEREN'T EVEN TRYING! WHAT ARE YOU GUYS ANYWAY, A BUNCH OF COMPLETE TURKEYS?
GOBBLE, GOBBLE.
HEH-HEH.
GOBBLE!
GOBBLE! GOBBLE!
GOBBLE, GOBBLE!
GOBBLE!
HA, HA!
HA! HA!
HA! HA!
GOBBLE, GOBBLE!
GOBBLE! GOBBLE!
HA! GOBBLE!
SO MUCH FOR MY RHETORICAL QUESTION.
HA! HA!
78 23

V. MULTIGROUP PERTURBATION THEORY

Let's once again rewrite our multigroup diffusion equations in matrix form

$$\begin{pmatrix} -\nabla\cdot D_1\nabla+\Sigma_{R_1} & 0 & \\ \Sigma_{s_{12}} & -\nabla\cdot D_2\nabla+\Sigma_{R_2} & \\ \Sigma_{s_{13}} & \Sigma_{s_{23}} & \cdots \\ & & \end{pmatrix}\begin{pmatrix}\phi_1\\ \phi_2\\ \phi_3\\ \vdots\end{pmatrix} = \frac{\nu}{k}\begin{pmatrix}\chi_1\Sigma_{f_1} & \chi_1\Sigma_{f_2} & \cdots\\ \chi_2\Sigma_{f_1} & \chi_2\Sigma_{f_2} & \cdots\\ \vdots & & \end{pmatrix}\begin{pmatrix}\phi_1\\ \phi_2\\ \phi_3\\ \vdots\end{pmatrix}$$

or

$$\underline{\underline{M}}\,\underline{\phi} = \frac{\nu}{k}\,\underline{\underline{F}}\,\underline{\phi}$$

In order to determine the change in reactivity induced in the core by a small perturbation, we must generalize somewhat our concept of inner products and adjointness to account for the vector nature of this equation. To this end, define the inner product between two G-dimensional vectors $\underline{f}(r)$ and $\underline{g}(r)$ as

$$(\underline{f},\underline{g}) \equiv \int_V d^3r \left[f_1^*(\vec{r})g_1(\vec{r}) + f_2^*(\vec{r})g_2(\vec{r}) + \cdots \right]$$

We can now use this inner product to construct the adjoint of the operators $\underline{\underline{M}}$ and $\underline{\underline{F}}$:

$$(\underline{\underline{M}}^\dagger \underline{f}, \underline{g}) = (\underline{f}, \underline{\underline{M}}\,\underline{g})$$

Since the adjoint of a matrix if obtained by first taking the transpose of the matrix and then complex-conjugating each of its elements, it is evident that

$$\underline{\underline{M}}^{\dagger} = \begin{pmatrix} -\nabla\cdot D_1\nabla + \Sigma_{R_1} & \Sigma_{s_{12}} & \cdots \\ 0 & -\nabla\cdot D_2\nabla + \Sigma_{R_2} & \cdots \\ \vdots & \vdots & \end{pmatrix},$$

and similarly

$$\underline{\underline{F}}^{\dagger} = \begin{pmatrix} \chi_1\nu\Sigma_{f_1} & \chi_2\nu\Sigma_{f_1} & \cdots \\ \chi_1\nu\Sigma_{f_2} & \chi_2\nu\Sigma_{f_2} & \\ \vdots & & \end{pmatrix}.$$

Note in particular that $\underline{\underline{M}}^{\dagger} \neq \underline{\underline{M}}$ and $\underline{\underline{F}}^{\dagger} \neq \underline{\underline{F}}$--that is, the multigroup criticality problem is not self-adjoint. Hence we find $\underline{\phi}^{\dagger} \neq \underline{\phi}$.

We can use our earlier expressions for the reactivity change corresponding to perturbations in the core composition, if we recognize that such perturbations will now have a matrix character--e.g.,

$$\underline{\underline{M}}' = \underline{\underline{M}} + \delta\underline{\underline{M}},$$

and

$$\underline{\underline{F}}' = \underline{\underline{F}} + \delta\underline{\underline{F}}.$$

For example, one could imagine a perturbation in the absorption cross section characterizing the second group as being represented by

$$\delta\underline{\underline{M}} = \begin{pmatrix} 0 & 0 & 0 & \cdots \\ 0 & \delta\Sigma_{a_2} & 0 & \\ 0 & 0 & 0 & \\ \vdots & & & \end{pmatrix}.$$

The corresponding reactivity change is then given by

$$\Delta\rho = \frac{(\underline{\phi}^\dagger, [\nu_c \underline{\underline{\delta F}} - \underline{\underline{\delta M}}]\,\phi)}{\nu_c\,(\underline{\phi}^\dagger, \underline{\underline{F}}\,\underline{\phi})} \quad .$$

To make these ideas more precise, let us consider the particularly simple example of two group diffusion theory:

$$-\nabla\cdot D_1\nabla\phi_1 + \Sigma_{R_1}\phi_1 = \nu\Sigma_{f_2}\phi_2$$

$$-\nabla\cdot D_2\nabla\phi_2 + \Sigma_{a_2}\phi_2 = \Sigma_{s_{12}}\phi_1$$

(we will regard ν as variable here for convenience)

where we have assumed all fissions occur in the thermal group for simplicitly. In matrix form this becomes

$$\begin{pmatrix} -\nabla\cdot D_1\nabla + \Sigma_{R_1} & 0 \\ \Sigma_{s_{12}} & -\nabla\cdot D_2\nabla + \Sigma_{a_2} \end{pmatrix} \begin{pmatrix} \phi_1 \\ \phi_2 \end{pmatrix} = \nu \begin{pmatrix} 0 & \Sigma_{f_2} \\ 0 & 0 \end{pmatrix} \begin{pmatrix} \phi_1 \\ \phi_2 \end{pmatrix}$$

$$\underline{\underline{M}} \qquad \underline{\phi} \qquad\qquad \underline{\underline{F}} \quad \underline{\phi}$$

The adjoint equations are

$$\begin{pmatrix} -\nabla\cdot D_1\nabla + \Sigma_{R_1} & \Sigma_{s_{12}} \\ 0 & -\nabla\cdot D_2\nabla + \Sigma_{a_2} \end{pmatrix} \begin{pmatrix} \phi_1^\dagger \\ \phi_2^\dagger \end{pmatrix} = \nu \begin{pmatrix} 0 & 0 \\ \Sigma_{f_2} & 0 \end{pmatrix} \begin{pmatrix} \phi_1^\dagger \\ \phi_2^\dagger \end{pmatrix}$$

$$\underline{\underline{M}}^\dagger \qquad \underline{\phi}^\dagger \qquad\qquad \underline{\underline{F}}^\dagger \quad \underline{\phi}^\dagger$$

Note that $\underline{\underline{M}}^{\dagger} \neq \underline{\underline{M}}$ and $\underline{\underline{F}}^{\dagger} \neq \underline{\underline{F}}$, hence $\underline{\phi}^{\dagger} \neq \underline{\phi}$.

Suppose we consider the reactivity change induced by perturbing the thermal absorption cross section by an amount $\delta\Sigma_{a_2}$. Then

$$\delta\underline{\underline{F}} = 0$$

$$\delta\underline{\underline{M}} = \begin{pmatrix} 0 & 0 \\ 0 & \delta\Sigma_{a_2} \end{pmatrix}$$

Hence we can compute

$$(\underline{\phi}^{\dagger}, \delta\underline{\underline{M}}\,\underline{\phi}) = \int_V d^3r \; \phi_1^{\dagger}\phi_2^{\dagger} \begin{pmatrix} 0 & 0 \\ 0 & \delta\Sigma_{a_2} \end{pmatrix} \begin{pmatrix} \phi_1 \\ \phi_2 \end{pmatrix} = \int_V d^3r \; \phi_2^{\dagger}\,\delta\Sigma_{a_2}\,\phi_2$$

to find

$$\Delta\rho = -\frac{\int_V d^3r \; \phi_2^{\dagger}\,\delta\Sigma_{a_2}\,\phi_2}{\nu(\underline{\phi}^{\dagger}, \underline{\underline{F}}\,\underline{\phi})} = -\frac{1}{c}\int_V d^3r \; \phi_2^{\dagger}\,\delta\Sigma_{a_2}\,\phi_2$$

In analogy with our earlier one-speed calculation, suppose we set

$$\delta\Sigma_{a_2} = \alpha\,\delta(\vec{r} - \vec{r}_0)$$

Then

$$\Delta\rho = -\frac{\alpha}{c}\,\phi_2^{\dagger}(\vec{r}_0)\,\phi_2(\vec{r}_0)$$

Thus we find

$$\phi_2^\dagger(\vec{r}_0) = -\frac{c\Delta\rho}{\alpha\phi_2(\vec{r}_0)} = \begin{array}{l}\text{fractional change in}\\ \text{reactivity per neutron}\\ \text{absorbed per unit time.}\end{array}$$

In particular, if $\phi_2^\dagger$ is large at $\vec{r}_0$, then the change in ρ introduced by a thermal absorber at $\vec{r}_0$ will be large. That is, $\phi_2^\dagger(\vec{r})$ measures the "importance" of the point $\vec{r}$ with respect to reactivity changes induced by perturbing the thermal absorption at that point.

For the more general multigroup problem, $\phi_g^\dagger(\vec{r})$ can be identified as the neutron importance function for group g, since $\phi_g^\dagger(\vec{r})$ is proportional to the gain or loss in reactivity of a reactor due to the insertion or removal of one neutron per second in the group at point $\vec{r}$.

In general, one finds that the multigroup neutron importance (or adjoint fluxes) differ substantially from the multigroup fluxes as shown. This is shown for a two-group calculation for a reflected spherical core below:

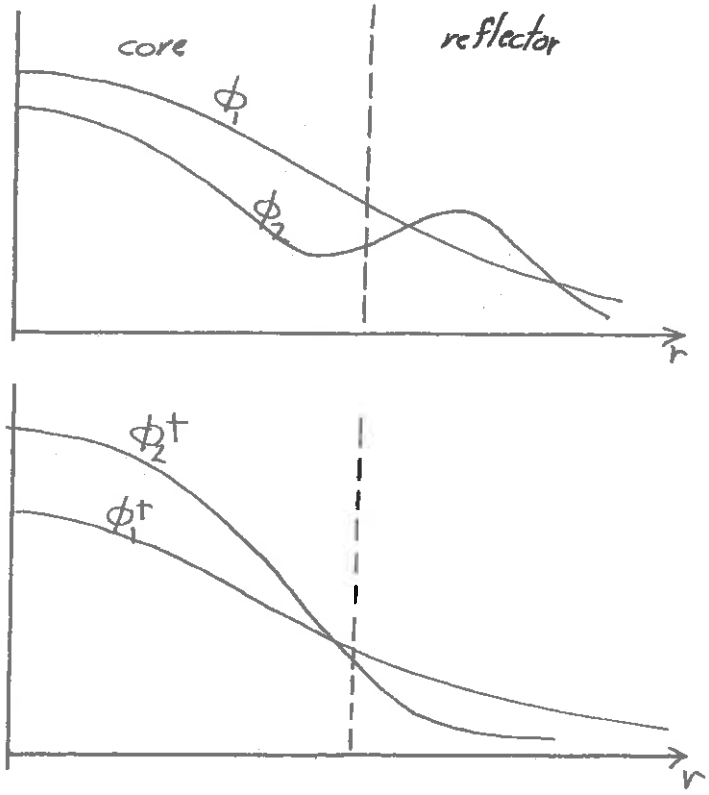

PART V

NUCLEAR POWER SYSTEMS ANALYSIS

CHAPTER 15: THE NUCLEAR STEAM SUPPLY SYSTEM

I. INTRODUCTION

A. Preliminary Remarks

Our principal concern in this text has been with the nuclear analysis of the core of a nuclear fission reactor. We have developed those concepts and methods which are utilized in nuclear core analysis, and furthermore, we have illustrated these topics by giving a brief introduction to the design of a nuclear power reactor core. Throughout this development, we have tried to indicate how the nuclear analysis of a reactor core interacts with other facets of core design such as its thermal-hydraulic performance.

It is also very important to understand how reactor core design and analysis interacts with the other aspects of designing a nuclear power system. Hence in this last part of the text we will broaden our perspective by considering the nuclear reactor core as just one component of the overall nuclear power plant.

In Chapter 15 we will consider the nuclear steam supply system (NSSS), that is, the nuclear reactor, primary coolant loops and pumps, and steam generators (if present) in an effort to illustrate how overall systems considerations influence the nuclear design of the core. In particular, we will give a brief discussion of the thermodynamic analysis of the NSSS. We will also discuss those aspects of nuclear reactor operation which influence reactor design, such as reactor startup, maneuvering, shutdown, and so on. We will consider as well one of the

most important aspects of nuclear reactor analysis which involves the ability of the reactor system to perform safely under any conceivable operating conditions. Throughout, we will draw upon specific examples taken from various power reactor systems to illustrate the considerations arising in this discussion.

B. A General Discussion of the Nuclear Steam Supply System

The fission heat energy produced in the nuclear reactor core is converted first into mechanical energy by a thermal cycle in which a fluid is vaporized by the fission heat energy, then expands against the blades of a turbine to produce mechanical energy, and is finally recondensed into liquid again before being pumped back through the cycle. The turbine then is used to power an electrical generator to convert this mechanical energy into electrical energy. In essentially all large nuclear power plants, the "working fluid" used to drive the turbine is high temperature steam. [Although we will later briefly discuss an alternative nuclear power system which utilizes a gas turbine.] Hence, the primary function of the nuclear reactor is to provide a source of heat which can be used to turn feedwater into steam. In this sense then, the nuclear steam supply system merely replaces the boiler in the more familiar fossil-fueled power plant. We can see this more clearly by comparing the crude diagrams of a nuclear power plant (in this case, a PWR) and a fossil-fueled plant in Figures 15-1 and 15-2.

The NSSS is isolated within the reactor containment structure, and is composed of the reactor core itself, one or more coolant loops and associated coolant pumps, and a heat exchanger (or "steam generator") used to transform the heat of the primary coolant which flows through

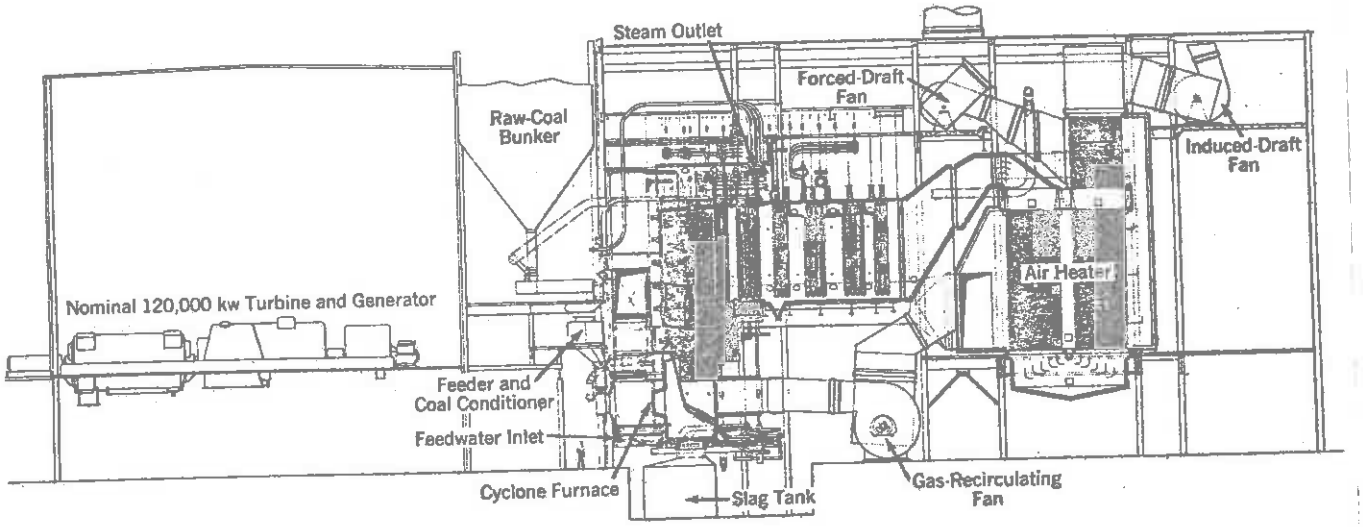

: Elevation view of a 120-Mw generating unit served by a B&W Universal-Pressure (UP) boiler operating at 5500-4500 ps
1150F, with reheats to 1050F and 1000F.

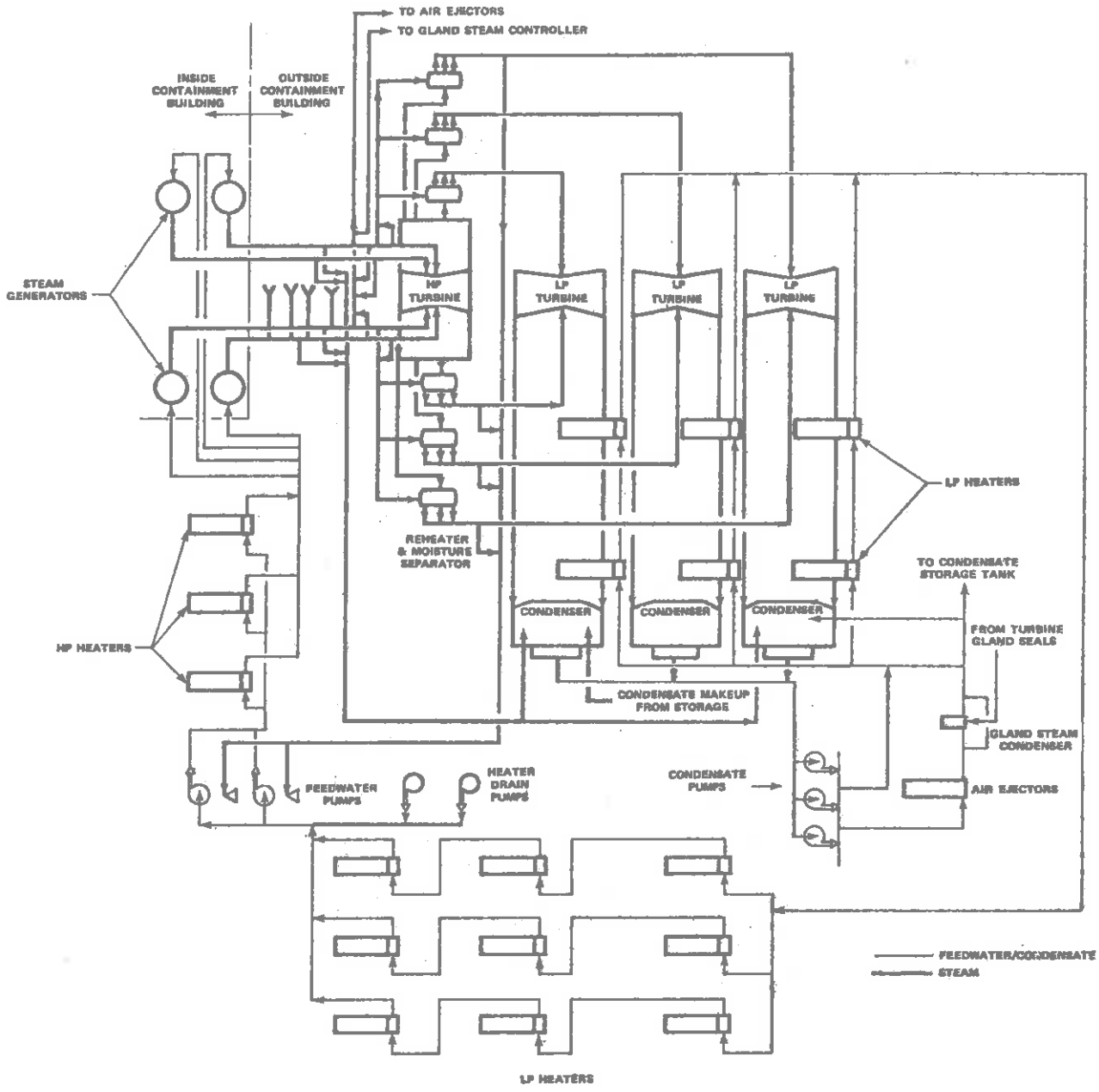

Main Steam and Feedwater System, One-Line Diagram

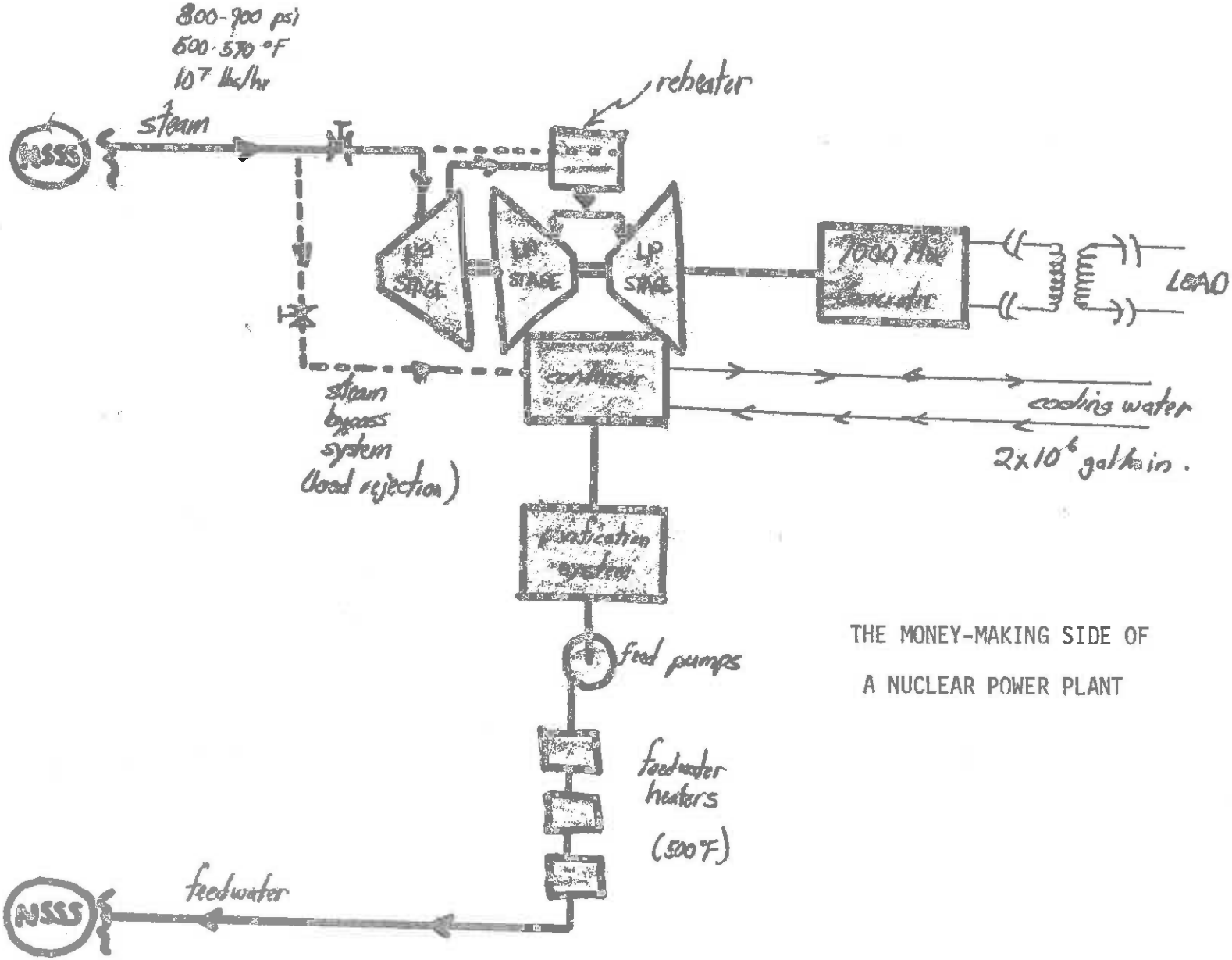

THE MONEY-MAKING SIDE OF

A NUCLEAR POWER PLANT

the reactor core into the latent energy associated with boiling the inlet feedwater into steam.

Of course, there is considerable variation among NSSS's characterizing different reactor types. For example, one may actually produce the steam in the reactor core itself, as in the BWR. Or one may use a single phase primary coolant (e.g., in a PWR or LMFBR) to transfer the fission heat energy to a heat exchanger outside the reactor pressure vessel where it is used to produce steam. We will discuss the actual components comprising the NSSS and their functions by considering several specific examples.

1. PWR-NSSS

In a pressurized water reactor, water serves as both coolant and moderator. But its functions as a primary coolant and a working fluid are separated by using a multiple loop cooling system as shown below:

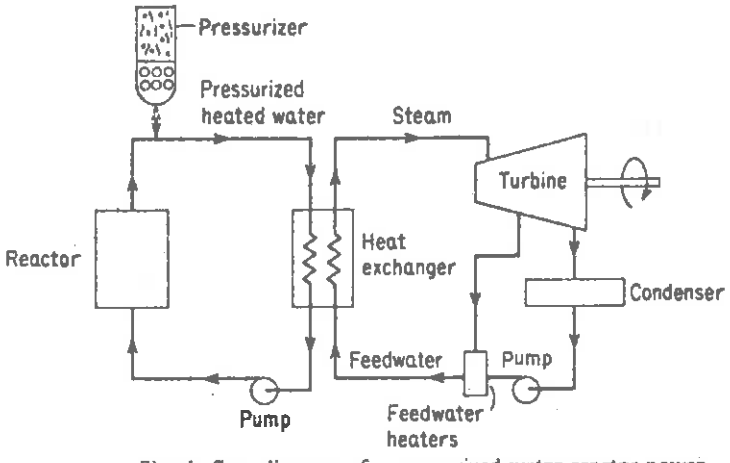

Simple flow diagram of a pressurized-water reactor power plant.

In the primary coolant loop, water is kept under very high pressure ($\sim$2200 psia) to allow high coolant temperatures without steam formation (aside from a small amount of subcooled boiling to facilitate heat transfer). The heat transported out of the reactor core by the primary coolant is then transferred to a secondary loop containing the working fluid by a heat exchanger known as a "steam generator" since it is within this component that the inlet feedwater is converted into steam.

In addition, a surge chamber or "pressurizer" is added into the primary coolant loop to maintain the very high system pressure as well as to accommodate coolant volume changes in the primary loop. The primary coolant loop also contains primary coolant pumps, as well as auxiliary systems to control coolant purity, soluble poison concentrations, makeup, and so on. We will give a more detailed description of each of these components of the NSSS below.

a) Reactor pressure vessel

The nuclear reactor pressure vessel contains the reactor core itself, the core support structures, control assemblies, coolant circulation channels, and thermal shields. The pressure vessel is designed with inlet and outlet nozzles for each primary coolant loop. The upper head of the vessel is designed such that it can be removed for refueling and maintainence.

The vessel is fabricated out of low alloy carbon steel designed to accomodate the high coolant pressures and temperatures, as well as to withstand radiation damage from fast neutrons and gammas which escape the core. A thermal shield is inserted between the core and the pressure vessel to protect the vessel from excessive radiation flux and to reduce

the thermal stresses in the vessel resulting from gamma heat deposition. It also serves to form an annual flow channel which routes coolant to the core. A tabulation of the design parameters characterizing a modern PWR pressure vessel is given below in Table 15-1.

Table 15-1

TYPICAL FOUR-LOOP REACTOR VESSEL PARAMETERS

Overall length of assembled vessel, closure head, and nozzles	43 ft, 10 in.
Inside diameter of shell	173 in.
Radius from center of vessel to nozzle face	
Inlet	10 ft, 11 in.
Outlet	10 ft, 3 in.
Nominal cladding thickness	7/32 in.
Minimum cladding thickness	1/8 in.
Coolant volume with core and internals in place	4740 cu ft
Operating pressure	2250 psia
Design pressure	2500 psia
Design temperature	650°F
Vessel material	Carbon steel
Cladding material	Stainless steel
Number of vessel material surveillance capsules, total	8

The internal structure of the reactor vessel includes lower and upper core support structures as well as an in-core instrumentation support structure. The lower core structure supports the core barrel, the lower core plate and support column (and thereby the core fuel assemblies) and the thermal shield. It also provides passageways for coolant flow and facilitates coolant flow distribution. The core support structure is shown in Figures 15-3 and 15-4.

b) Steam generators

Since the primary coolant in a PWR does not serve as a working fluid, remaining in its liquid phase, large heat exchangers are required to generate steam in the secondary loop. Such steam generators use the heat drawn off the core by the primary coolant (pressurized water) to convert lower pressure feedwater in the secondary loop into steam for use in the turbogenerator. Such steam generators assume mammoth proportions, as the illustrations in Figure 15-5 indicate. These can be of either U-tube or counter flow design. They are customarily divided into evaporator sections in which the boiling occurs, and moisture separator sections in which the boiling occurs, and moisture separator regions in which dry saturated steam ($\sim$99.75% quality) is separated out and flows on to the turbine, while saturated water leaves the separators, flows back down the sides of the steam generator, and is mixed with entering feedwater.

c) Pressurizer

Since liquids are practically incompressible, small changes in volume due to changes in coolant temperature (such as from load changes) can cause severe pressure changes in the primary coolant loop. For

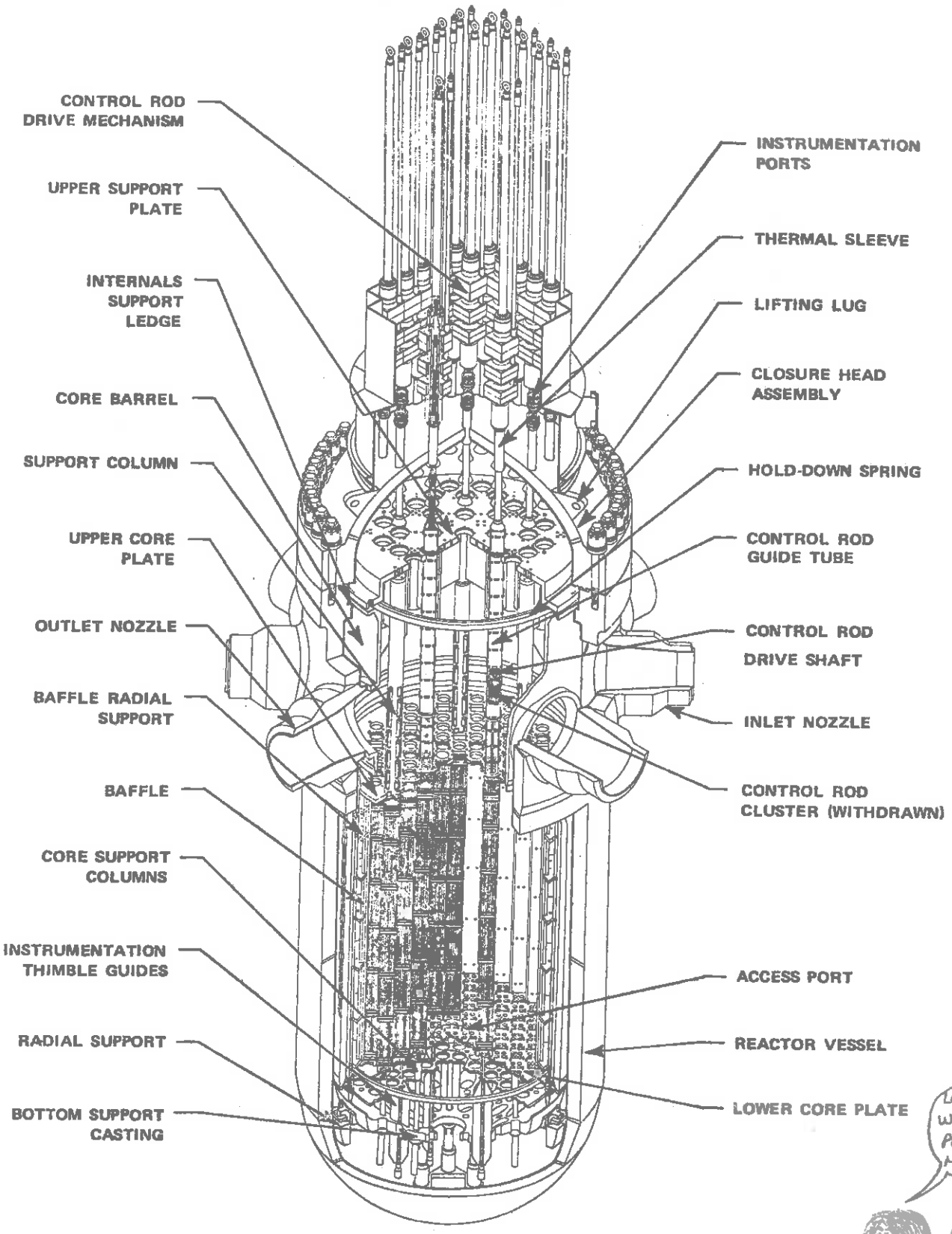
CONTROL ROD DRIVE MECHANISM
UPPER SUPPORT PLATE
INTERNALS SUPPORT LEDGE
CORE BARREL
SUPPORT COLUMN
UPPER CORE PLATE
OUTLET NOZZLE
BAFFLE RADIAL SUPPORT
BAFFLE
CORE SUPPORT COLUMNS
INSTRUMENTATION THIMBLE GUIDES
RADIAL SUPPORT
BOTTOM SUPPORT CASTING
INSTRUMENTATION PORTS
THERMAL SLEEVE
LIFTING LUG
CLOSURE HEAD ASSEMBLY
HOLD-DOWN SPRING
CONTROL ROD GUIDE TUBE
CONTROL ROD DRIVE SHAFT
INLET NOZZLE
CONTROL ROD CLUSTER (WITHDRAWN)
ACCESS PORT
REACTOR VESSEL
LOWER CORE PLATE


LOOKS LIKE A WESTINGHOUSE PUR TO ME, MAN.

Figure 15-3

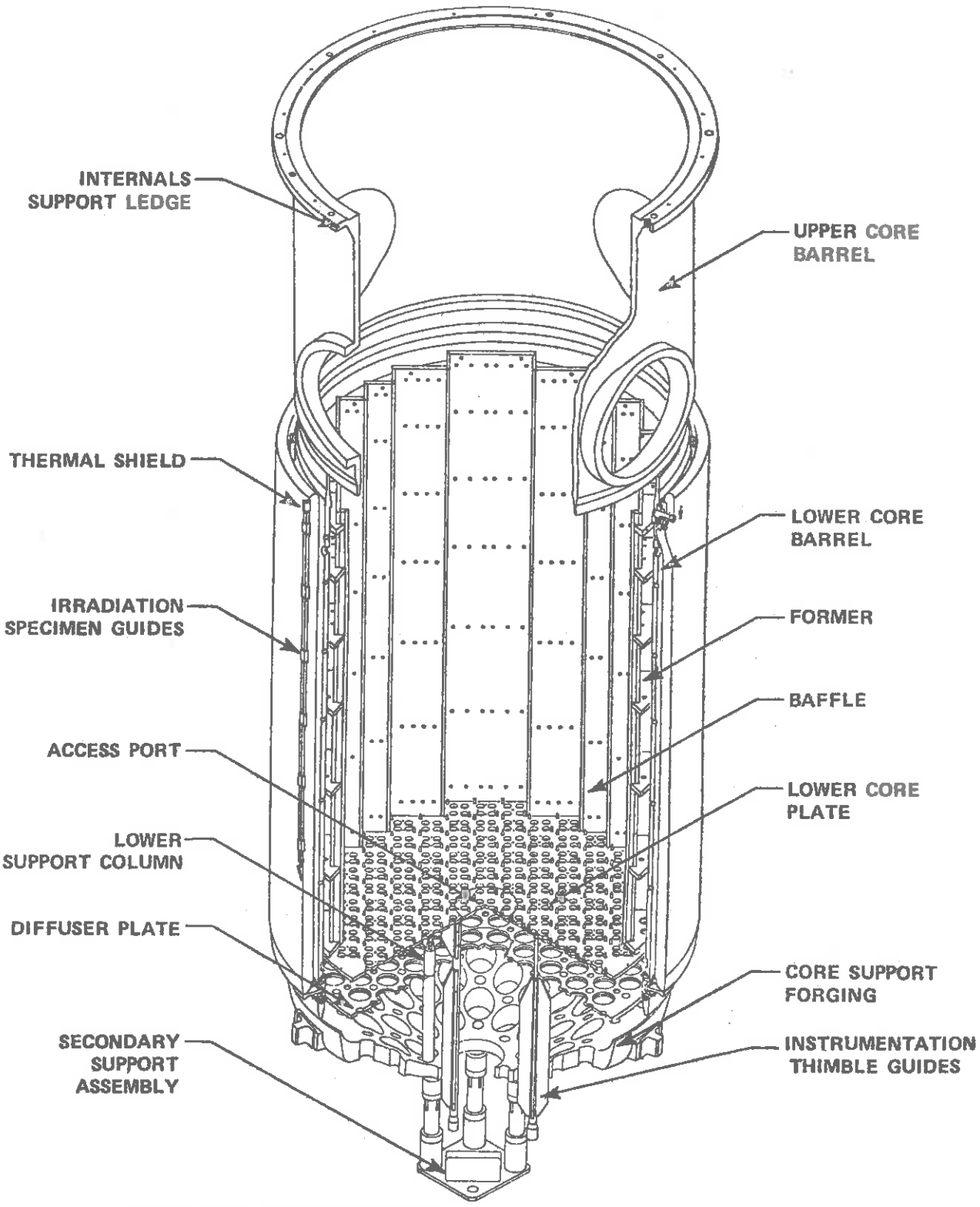

Lower Core Support Structure

Figure 15-4

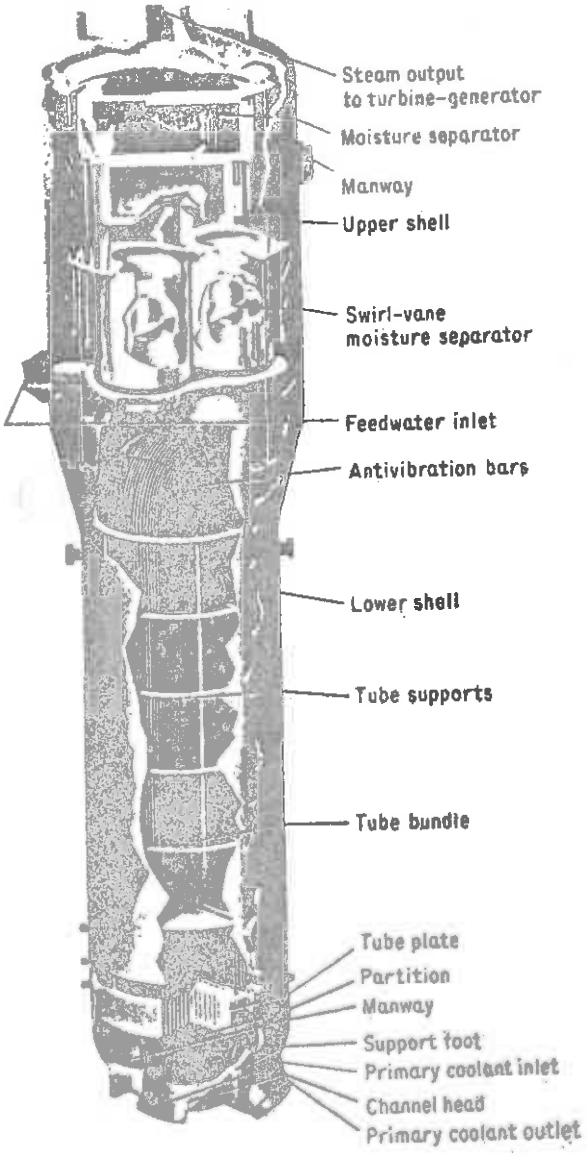

PWR steam generator. (Courtesy Westinghouse Electric Corporation.)

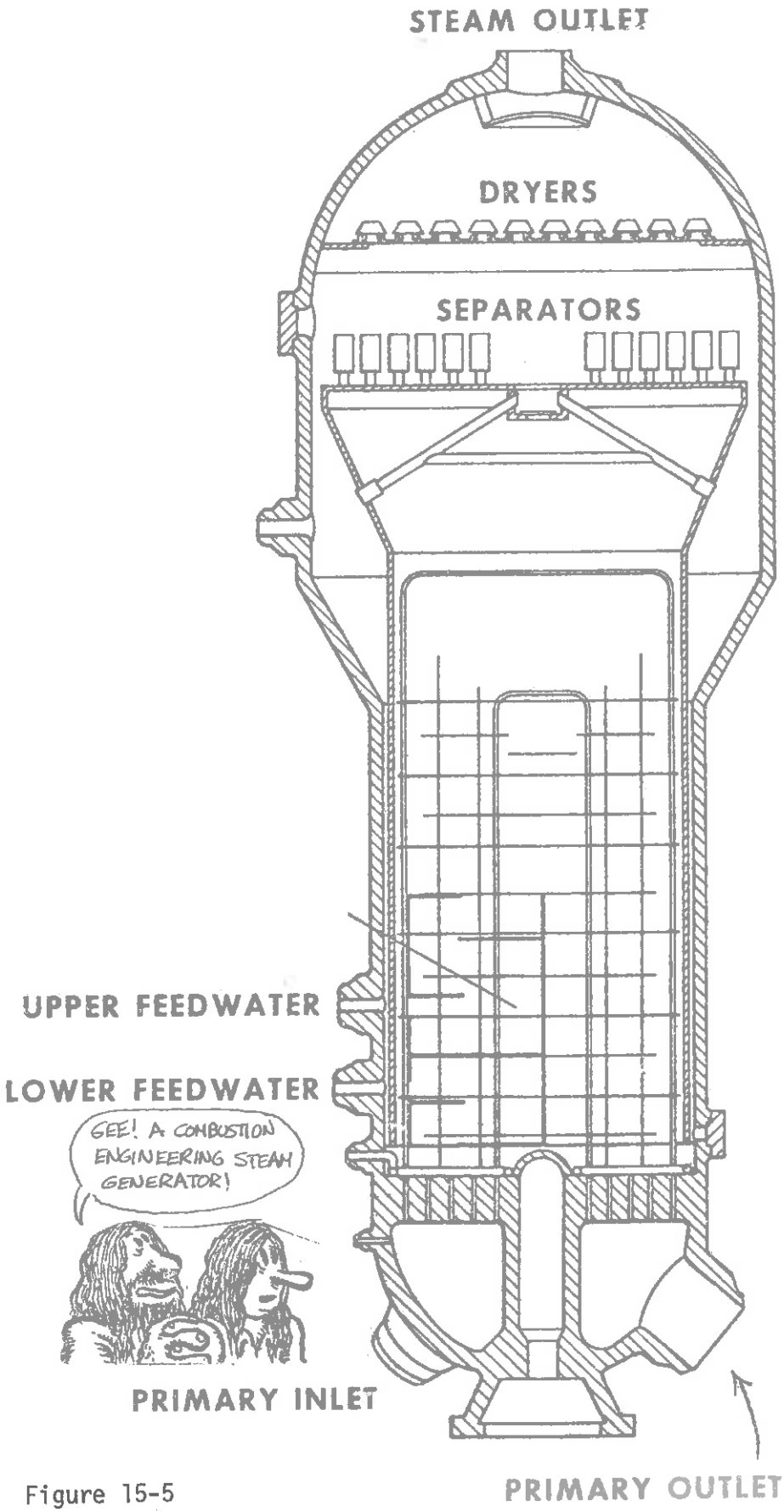

Figure 15-5

Table 15-2

TYPICAL DESIGN DATA FOR STEAM GENERATORS

Number and type	4 vertical, U-tube steam generators with integral steam-drum
Height overall	67 ft, 8 in.
Upper shell OD	14 ft, 8-3/8 in.
Lower shell OD	11 ft, 3½ in.
Operating pressure, tube side	2250 psia
Design pressure, tube side	2500 psia
Design temperature, tube side	650°F
Full load pressure, shell side	1000 psia
Maximum moisture at outlet (full load)	0.25%
Design pressure, shell side	1200 psia
Reactor coolant flow rate	34,600,000 lb/hr
Reactor coolant inlet temperature	618.5°F
Reactor coolant outlet temperature	557.2°F
Shell material	Mn-Mo steel
Channel head material	Carbon steel clad internally with stainless steel
Tube sheet material	Mo-Cr-Ni steel clad with Inconel on primary face
Tube material	Inconel
Tube OD	7/8 in.
Average tube wall thickness	0.050 in.
Steam generator weights	
Dry weight, in place	688,300 lb
Normal operating weight, in place	829,000 lb
Flooded weight (cold)	1,123,000 lb

example, if pressure increases occur, component damage may result. A decrease in local pressure could cause local flashing of water into steam, or burnout at the fuel clad surface. Hence it is necessary to provide a surge chamber to ride out such volume changes.

Such pressurizers not only act to limit pressure changes in the primary coolant loop, but as well to maintain the required system pressure, both in startup and under normal operating conditions. The pressurizer (shown in Figure 15-6) consists of a tank inserted into the hot leg of the primary coolant loop in which, under normal conditions, a 60% water, 40% vapor volume composition is maintained. A combination of automatically controlled sprays and electric heaters are used to regulate system pressure. During a positive surge in coolant volume, the vapor component is compressed, thereby preventing pressure surges. The spray valves are also automatically activated to limit any attendant pressure rise. A negative surge in coolant volume decreases the liquid volume in the pressurizer, expanding the vapor region and causing a momentary reduction in the pressure within the pressurizer which causes some flashing of the liquid into steam. Electric heaters are used to maintain the overall system pressure.

The pressurizer can also be used to adjust the level of boron concentration in the primary coolant loop. Indeed, the size of the pressurizer is usually dictated by requiring adequate steam void to allow for boron injection sufficient to achieve cold shutdown margins.

d) Primary pumps

A typical primary pump is shown in Figure 15-8. The principal components of the pump include the electrical driving motor, a seals

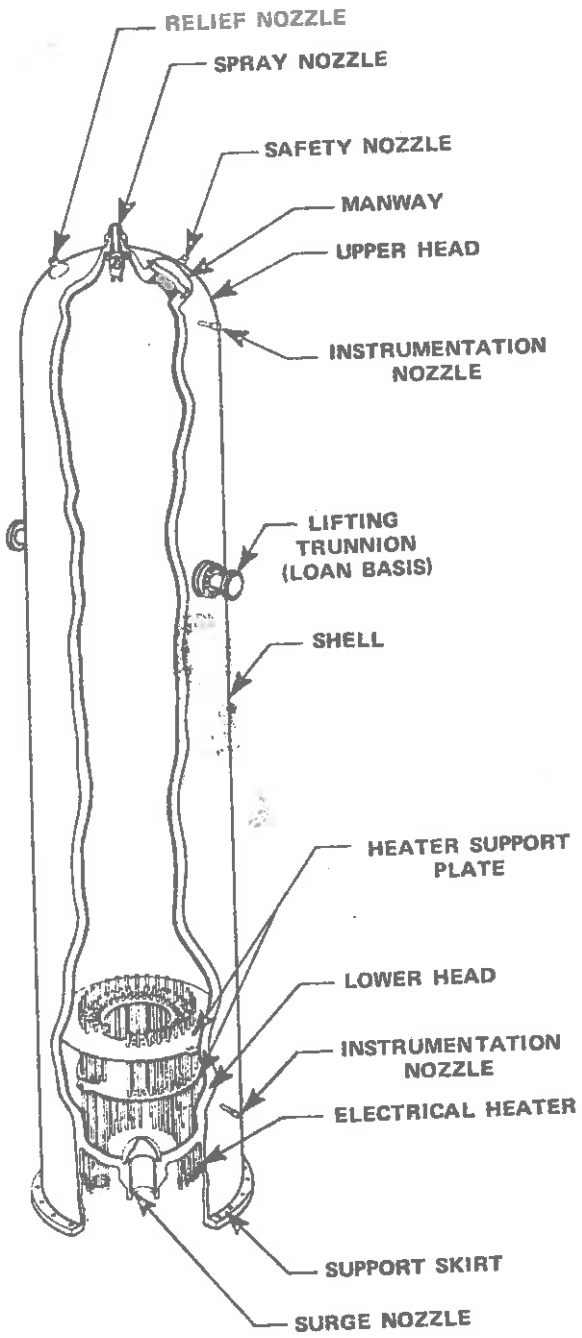

Cutaway of a Typical Pressurizer

Figure 15-6

PRESSURIZER TYPICAL DESIGN DATA

Number and type	1 two-phase water and steam pressurizer
Overall height	52 ft, 9 in.
Overall diameter	7 ft, 8-3/8 in.
Water volume	1080 cu ft
Steam volume	720 cu ft
Design pressure	2500 psia
Design temperature	680°F
Type of heaters	Electric immersion
Number of heaters	78
Installed heater power	1800 kw
Number of relief valves	2 power-operated
Number of safety valves	3 self-actuating
Spray rate	
Pressure transient	800 gpm
Continuous	1 gpm
Shell material	Mn-Mo steel, clad internally with stainless steel
Dry weight	235,000 lb
Normal operating weight	276,000 lb
Flooded weight (70°F)	347,320 lb

Figure 15-8

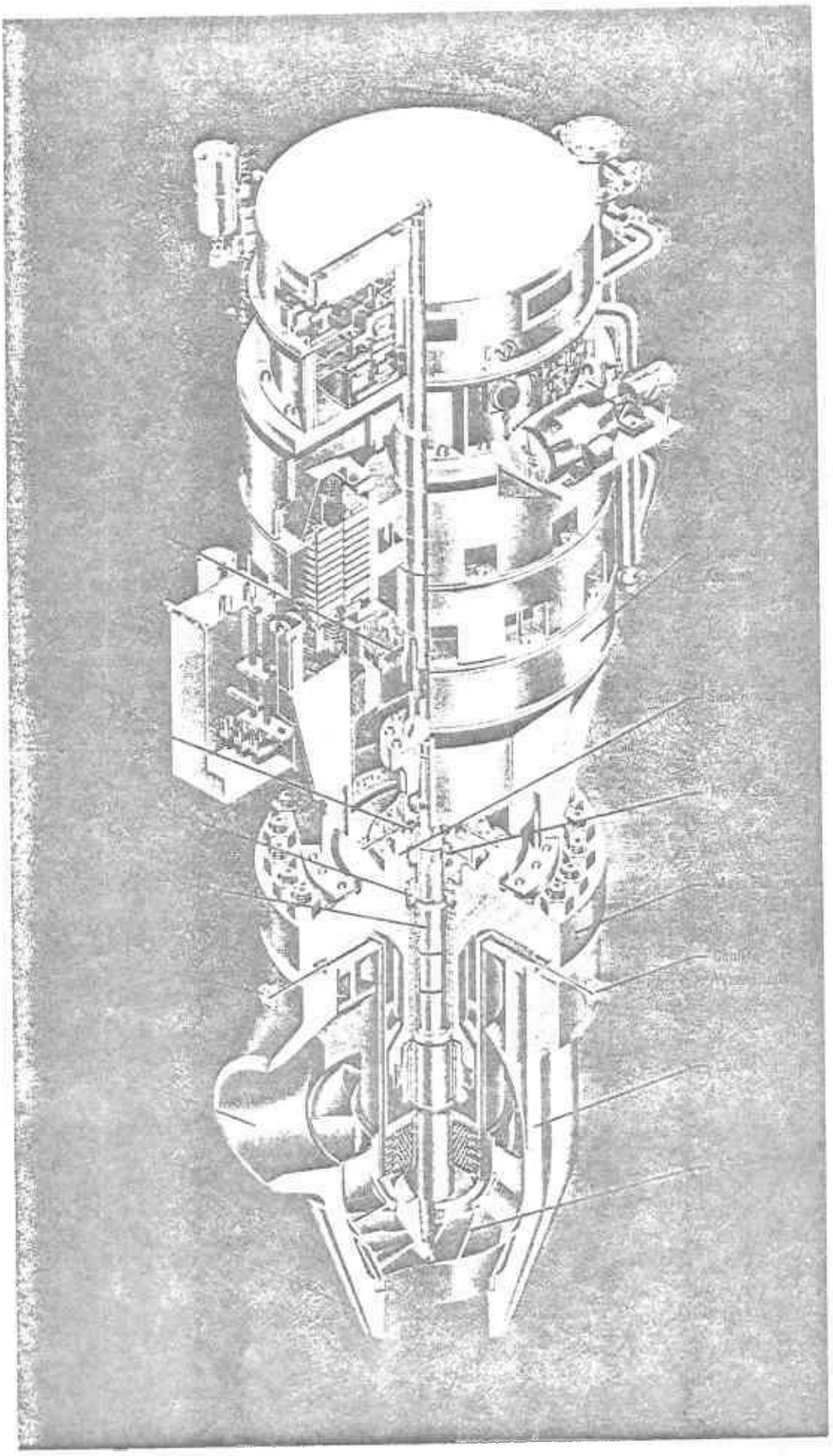

Cutaway of a Typical Reactor Coolant Pump

TYPICAL DESIGN PARAMETERS FOR REACTOR COOLANT PUMPS

Number and type	4 vertical, single-stage, shaft-seal circulating water pumps
Design capacity	93,000 gpm
Design head	305 ft
Design pressure	2500 psia
Design temperature	650°F
Suction temperature at full power	557.2°F
Motor type	ac induction
Motor voltage	4000 volts
Casing diameter	6 ft, 4 in.
Overall height	26 ft.
Operating speed	1189 rpm
Ambient temperature	120°F

assembly, and the hydraulic pumping unit. The coolant is pumped by an impeller attached to the bottom of the rotor shaft.

e) Auxiliary systems

A variety of auxiliary systems are interconnected with the primary loop of the NSSS. These include

(i) a water purification system

(ii) a system to inject chemical shim into the primary loop

(iii) a system to add makeup water into the loop

(iv) an emergency backup system to supply core cooling capability in the event of a rupture of the primary loop

We will return later to discuss these systems in Chapter 17.

f) Variations

The various NSSS which involve pressurized water reactors differ in the number and manner in which the primary loops are laid out. Diagrams of the particular NSSS configurations presently marketed by each of the major suppliers of PWR's are illustrated in Figure 15-9.

2. Boiling Water Reactor NSSS

In a boiling water reactor, the primary coolant water not only serves as moderator but also as the working fluid, since boiling is allowed to occur within the reactor core. Hence only a single coolant loop is required:

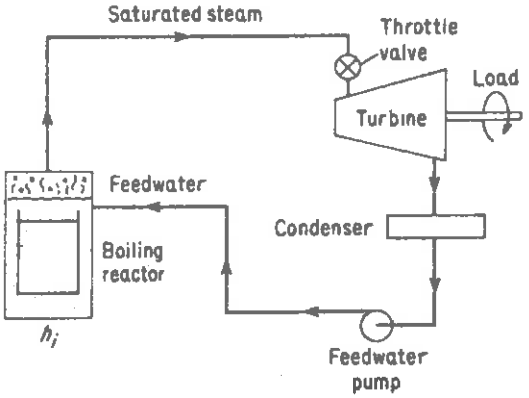

Direct-cycle boiling-reactor plant.

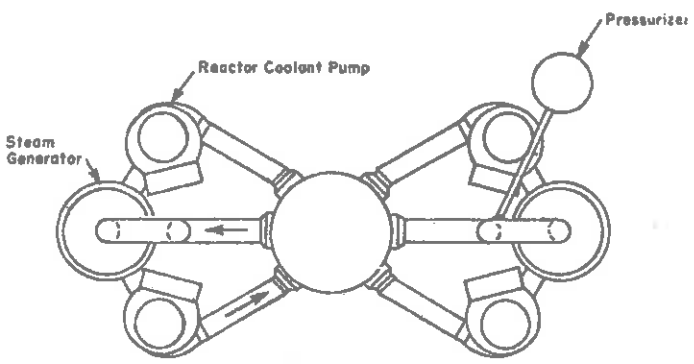

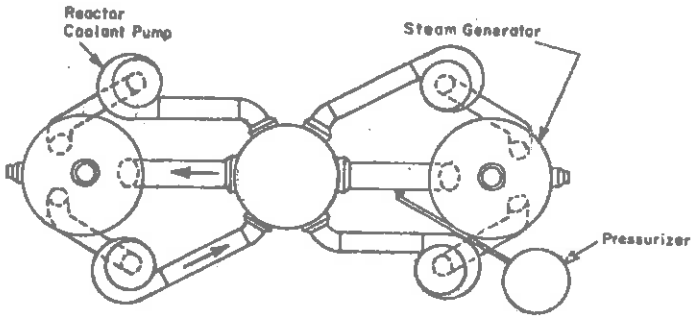

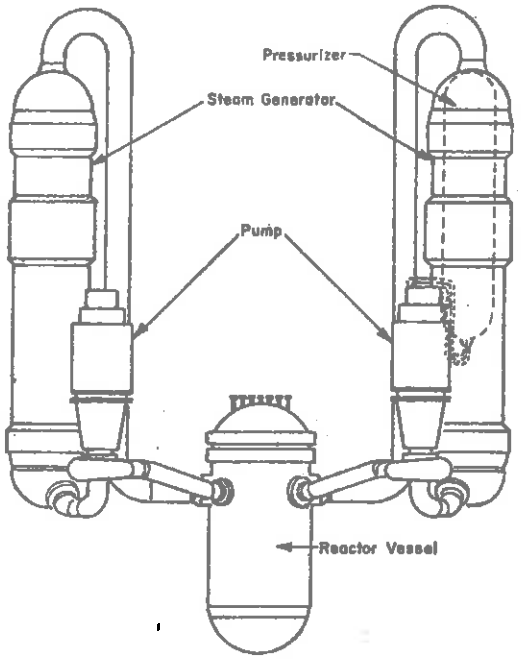

Babcock & Wilcox

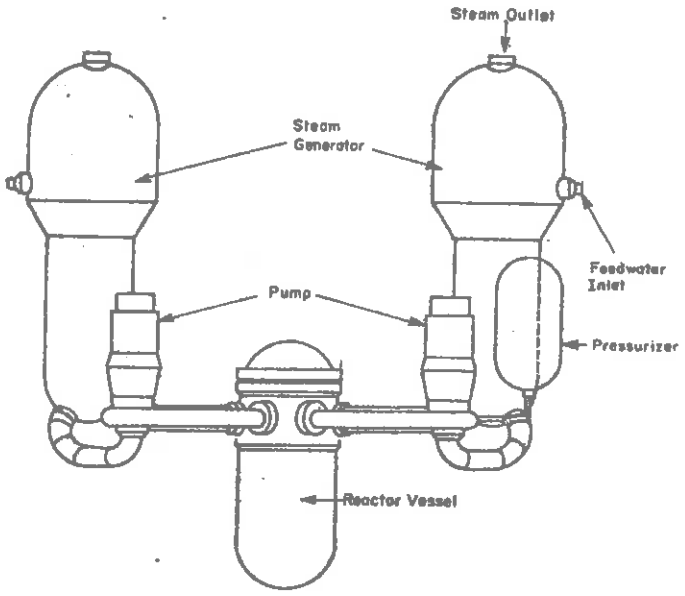

Combustion Engineering

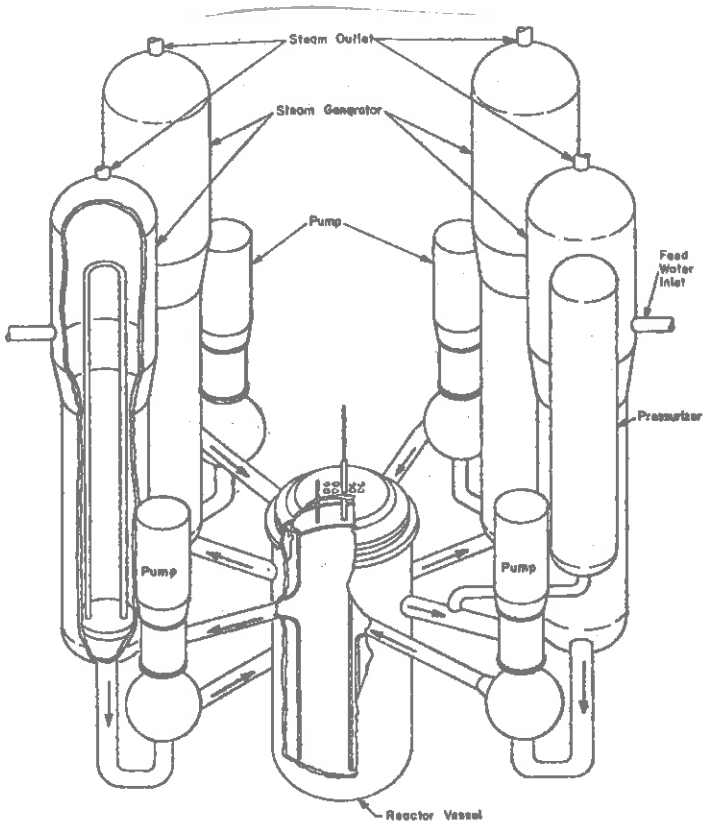

Westinghouse

Figure 15-9

The need for a separate steam generator is eliminated. Also since there is appreciable steam volume in the primary loop, a pressurizer tank is not required to accomodate pressure surges.

The coolant water rising to the top of the core is a very wet mixture of liquid and vapor. Hence moisture or steam separators must be used to separate off the steam which is then piped outside the reactor pressure vessel to the turbine, then through the condensor, before it is pumped back into the core as liquid condensate. The saturated liquid that is separated off by the moisture separators flows downward around the core via downcomers and mixes with the return condensate. This natural recirculation is assisted by recirculation pumps which are added to yield favorable load following behavior of a BWR-NSSS.

The ratio of the recirculating liquid to saturated vapor is known as the recirculation ratio. More specifically

$$\text{recirculation ratio} = \frac{\text{reactor inlet flow rate}}{\text{plant steam flow rate}}$$

Since the exit quality of the coolant in a BWR must be kept at only a few percent to avoid large void fractions (and hence low moderation and enhanced tendency towards DNB), the recirculation ratios are quite large, ranging from 10 to 25.

Since boiling in the BWR core is desired, one can operate at much lower system pressures ($\sim$1000 psia) with an attendant reduction in pressure vessel requirements. However, the necessity of steam separating equipment at the top of the core results in somewhat larger BWR pressure vessel sizes than those characterizing PWR's. It also prevents one from using top inserted control elements (although bottom inserted

elements are advantageous in a BWR to compensate for flux peaking due to void formation near the top of the core). Furthermore, the apprecable void formation in a BWR core leads to lower power densities than those characteristic of PWR's.

There are other disadvantages to the direct cycle of the BWR. Since the working fluid actually passes through the reactor core before passing out of the containment structure and through the turbine, one must be particularly careful to avoid radiation hazards. For example, the primary coolant water must be very highly purified to avoid impurities which might be subject to radioactive activation when exposed to the high neutron fluxes in the core. Furthermore, the turbines must be shielded which complicates maintainance activities.

Yet another problem involves a procedure for handling rapid decreases in bad demand. Suppose, for example, the electrical load on the turbogenerators suddenly dissappeared. Obviously one cannot instantaneously lower the core and primary coolant temperatures. Hence, for a short period of time, one is faced with the headache of disposing of some 4,000 MW of live steam. In a PWR in which the steam is generated in a secondary loop, a bypass valve can be opened which shunts this steam past the turbines, dumping it directly into the condensor.

In a direct cycle BWR NSSS, however, the radioactive nature of the steam produced in the primary loop necessitates that it be disposed of within radioactive containment in the event of loss of load. Hence BWR's must be equipped with elaborate steam dump suppression systems such as the torus shaped tank shown in Figure 15-11.

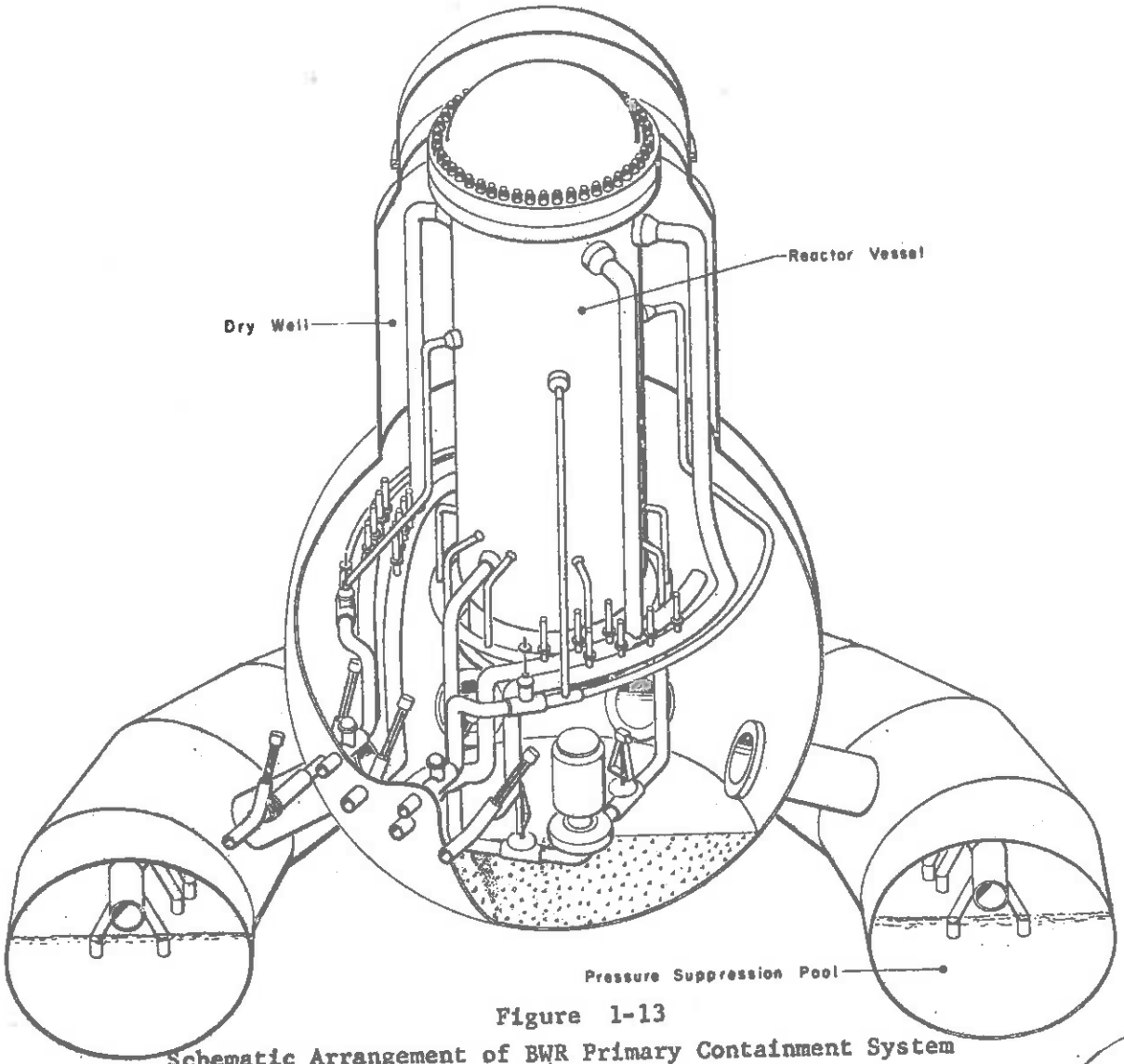

Figure 1-13
Schematic Arrangement of BWR Primary Containment System

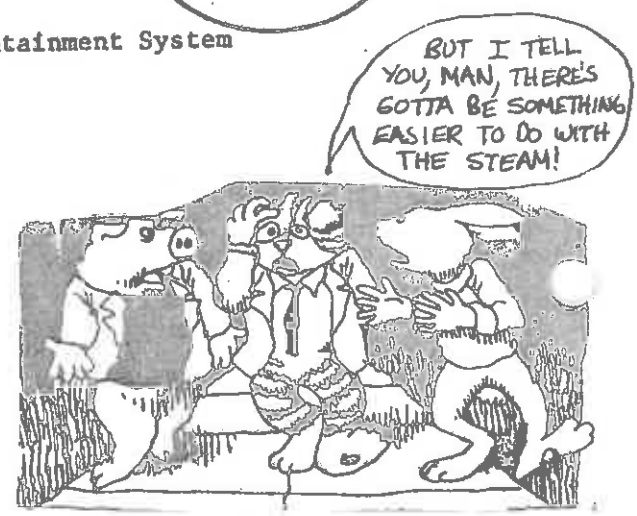

Figure 15-11

Yet another disadvantage of the BWR is the low quality (wet) steam it produces. This necessitates rather carefully designed turbines which are capable of withstanding the appreciable moisture content which arises in the lower pressure turbine stages.

A more detailed comparison of the respective advantages and disadvantages of BWR vs. PWR steam supply systems is given in Table 15-8. This comparison will be supplemented by a comparison with HTGR and LMFBR systems in Table 15-9 and 15-10.

Steam Separators: As we have mentioned, steam separating equipment must be inserted in the BWR pressure vessel to separate out the appreciable moisture content of the coolant emerging from the coolant channels in the core. Even with the equipment, the steam produced by a BWR is quite wet (low quality) and requires special turbine considerations.

Recirculation Pumps: The moisture separated out by the steam dryers is recirculated in the BWR by pumps. Such forced recirculation is necessary to yield suitable load following capability.

To see this more clearly, first consider how the PWR steam supply system responds to a load level change, such as an increased load on the turbine, for example. The throttle valve on the turbine steam supply line will open, hence allowing more steam flow with a resultant increase in secondary coolant flow through the steam generator. This, in turn, will cause more heat to be withdrawn from the primary coolant, and hence a decrease in the core inlet primary coolant temperature will occur. Since the coolant temperature coefficient in a PWR is negative (i.e., a decrease in coolant temperature corresponds to an increase in moderator

Table 15-8

ADVANTAGES AND DISADVANTAGES OF BWR VS. PWR

	BWR	PWR
1. THERMODYNAMIC CYCLE	SINGLE LOOP - * turbine steam directly from reactor increases lower capital cost	TWO LOOPS decreases higher capital cost
	Lower pressure (1000 psia - 550 F) decreases	Higher pressure * (2000 psia - 630 F) increases
2. POWER DENSITY & DISTRIBUTION	Low PWR Density due to boiling core is under moderated	High PWR Density * all liquid in core gives good moderation
	Better PWR Distribution * boiling tends to flatten power distribution radially	Poorer PWR Distribution must depend more on zone enrichment to flatten PWR.
3. MAJOR EQUIPMENT	Larger Pressure Vessel due to lower PWR density	Smaller Press. Vessel * due to higher PWR density
	Thinner Vessel Wall * lower pressure	Thicker Vessel Wall higher pressure
	Steam Separator *	Steam Generator Pressurizer
4. CONTROL	All Control by Rods	Chem. Shim & Control Rods *
	Requires simultaneous change in coolant flow rate and/or control rod positions to follow load changes	Natural ability to follow load changes *

	BWR	PWR
5. BURNUP, FUEL RODS AND ASS'YS	Larger Rods due to control difficulties, BWR is limited to smaller burnup	Smaller Rods * (near optimum for maximum k) larger burnup
	to compensate for * lower burnup, BWR uses larger diameter fuel rods, thus reducing fabrication cost	more, smaller rods thus higher fabrication cost
	Use of larger rods * reduces pressure drop, lowers pumping power (aided by natural convection)	Smaller rods, thus more pumping power
6. MATERIAL PROBLEMS CHEMISTRY	Operates at lower * temperatures, simplifying material problems (e.g., thermal stresses)	Higher temperatures, more difficult material problems
	Little control over impurities, oxygen hydrogen content of coolant - corrosion a problem	Very good control * over coolant purity corrosion far less a problem

* Indicates Favored System

density and hence an increase in core multiplication), there will be an increase in core power output sufficient to meet the increase in load demand. In this sense, the PWR-NSSS is said to be naturally load following.

By way of contrast, the BWR is not load following, without the addition of forced recirculation. Consider once again an increase in turbine load. Again the turbine throttle will open calling for more steam. But in this case, the immediate result is a decrease in primary system pressure. Since the BWR has a negative void coefficient of reactivity, a decrease in pressure will yield a decrease in reactivity and hence a decrease in core power output--which is opposite to the desired effect.

To correct this behavior, a BWR is equipped with recirculation pumps which are automatically activated to pump increased amounts of coolant water into the core in the event of an increase in load demand, thereby decreasing the core volume fraction and increasing reactivity and hence power. Both centrifical recirculation pumps and variable flow injection (jet) pumps are used to perform this function. A schematic of the recirculation system for a typical BWR is shown in Figures 15-13 and 15-14.

3. High Temperature Gas Cooled Reactors NSSS

Gas cooled nuclear reactors have been used for central station power generation for many years. The earliest such power plants were the Magnox reactors in the United Kingdom which used CO_2 as the coolant for a natural uranium fueled, graphite-moderated core. More recently interest has been directed towards the HTGR which uses high pressure

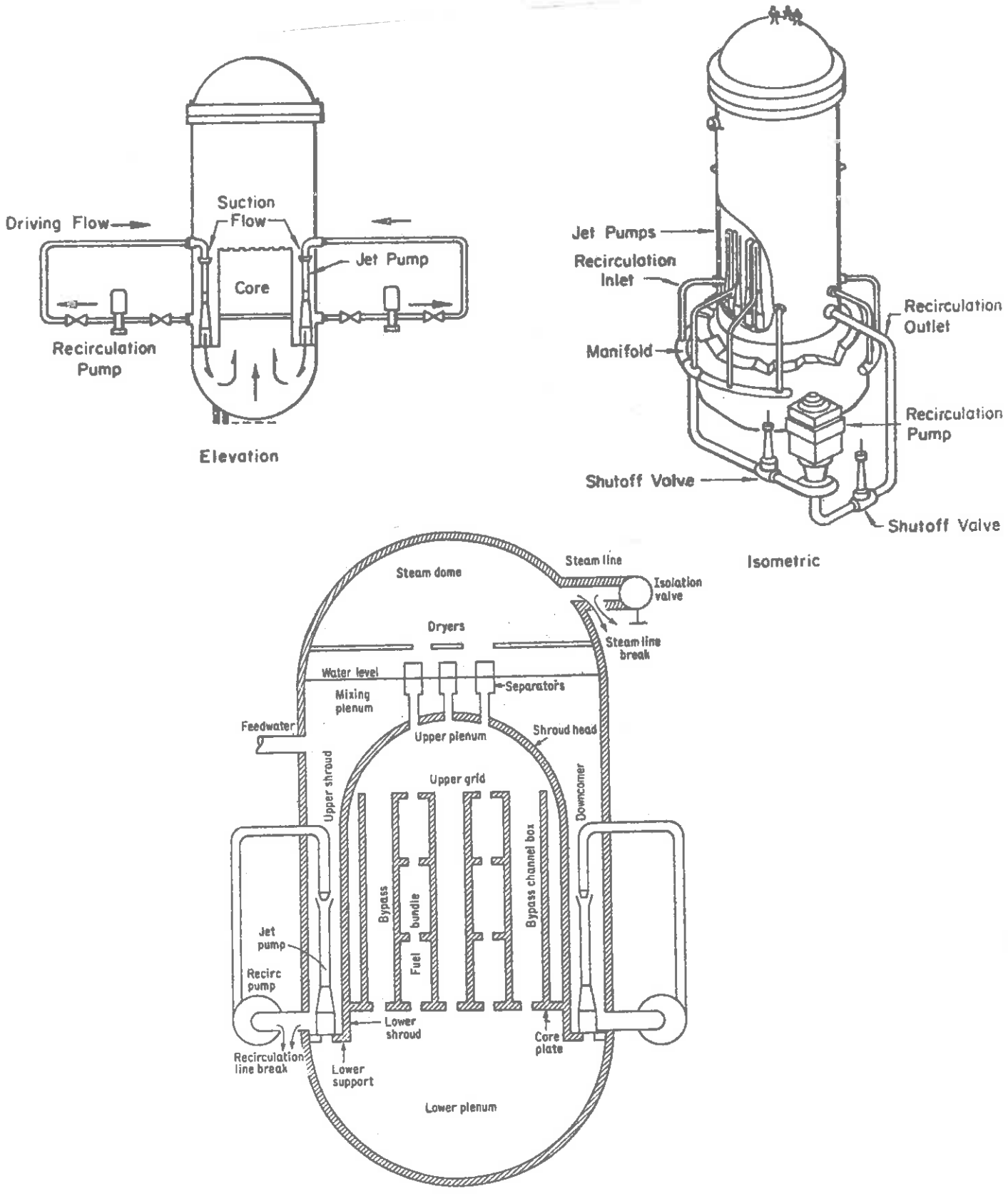

Figure 15-13: BWR Recirculation System

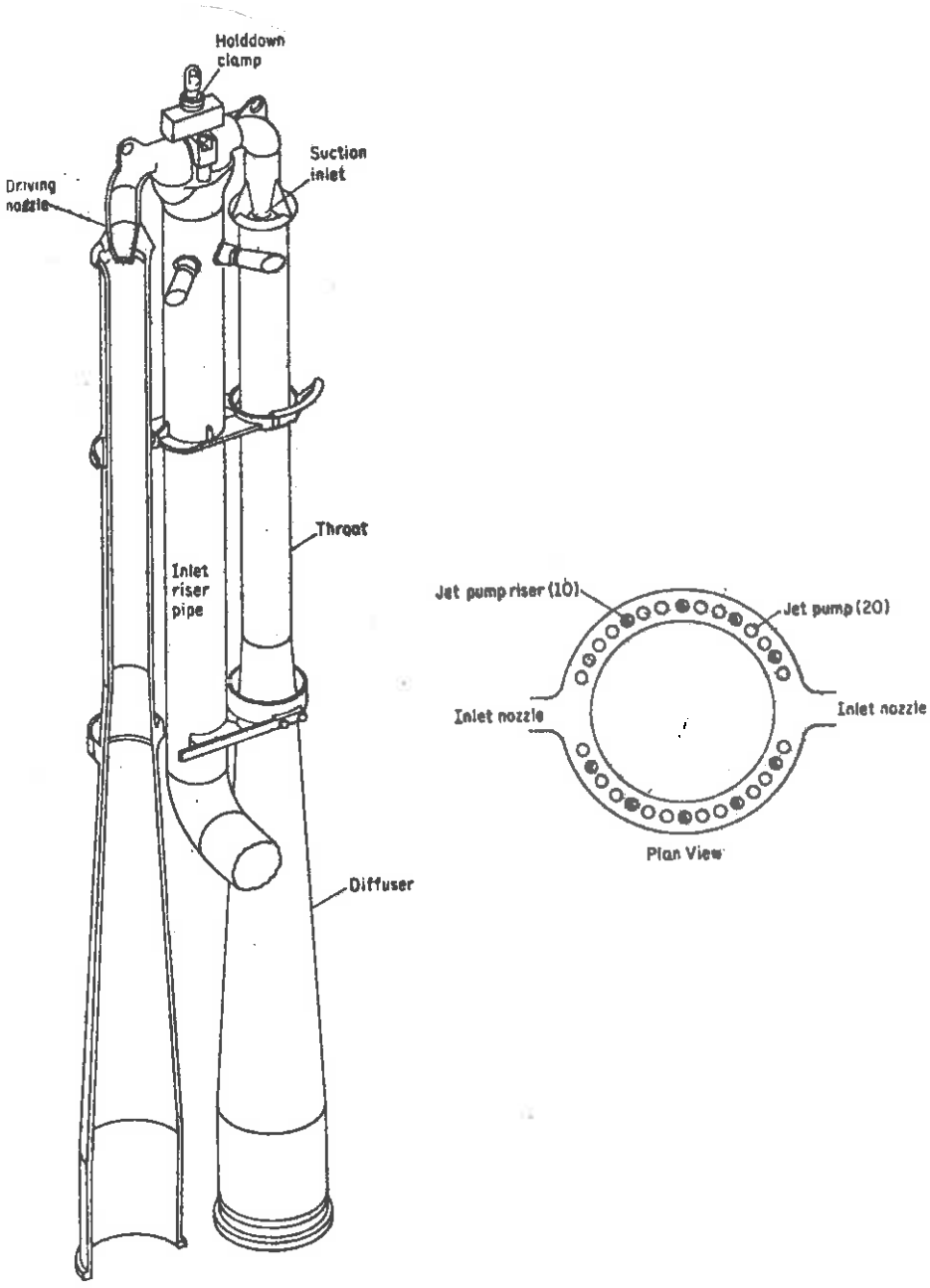

Jet pump arrangement.

Figure 15-14: Jet Pumps

helium to cool an enriched uranium-graphite core. To date all such reactors have been operated using a two loop thermal cycle similar to that of a PWR in which the primary helium coolant loop transfers thermal energy via steam generators to a secondary loop containing water as the working fluid. The high pressure steam produced in this loop is then used to power a turbogenerator. Such a NSSS is diagramed in Figure 15-16.

Such HTGR's are capable of operating at relatively high temperatures, thereby producing high temperature (1000°F) high pressure (2400 psia) steam with the attendant increase in thermodynamic efficiency and easing of turbine requirements. Moreover, HTGR's have the potential of being run in a direct cycle configuration in which high temperature helium is used directly to drive a gas turbine. This would result in even higher thermal efficiencies, as we shall show in the next section.

The HTGR exhibits numerous other advantages. For example, we have seen that it allows the use of a thorium-U^{233} fuel cycle which implies much lower fuel requirements because of larger conversion ratios. The use of helium as a coolant not only allows higher operating temperatures at moderate pressures, but as well provides flexibility in the selection of the optimum coolant temperature, pressure, and flow rate conditions (because of the weak thermal-hydraulic-neutronic coupling). It also eliminates that scourge of all reactor designers, the loss of coolant accident. Since the coolant always remains in the same phase, the worst that can happen in the event of a rupture of the primary coolant loop is a loss of pressure, that is, a depressurization of the primary

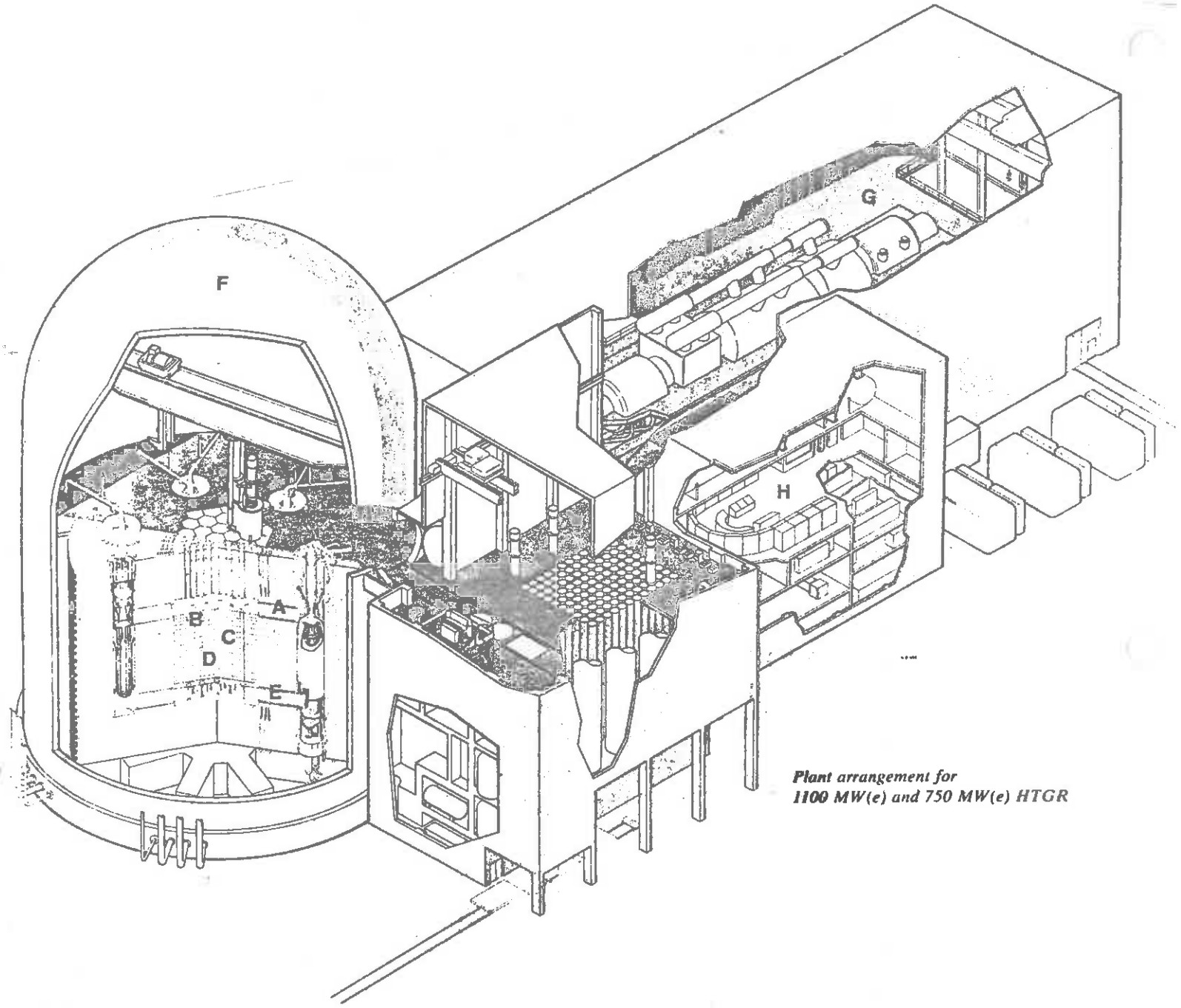

Plant arrangement for
1100 MW(e) and 750 MW(e) HTGR

Figure 15-16

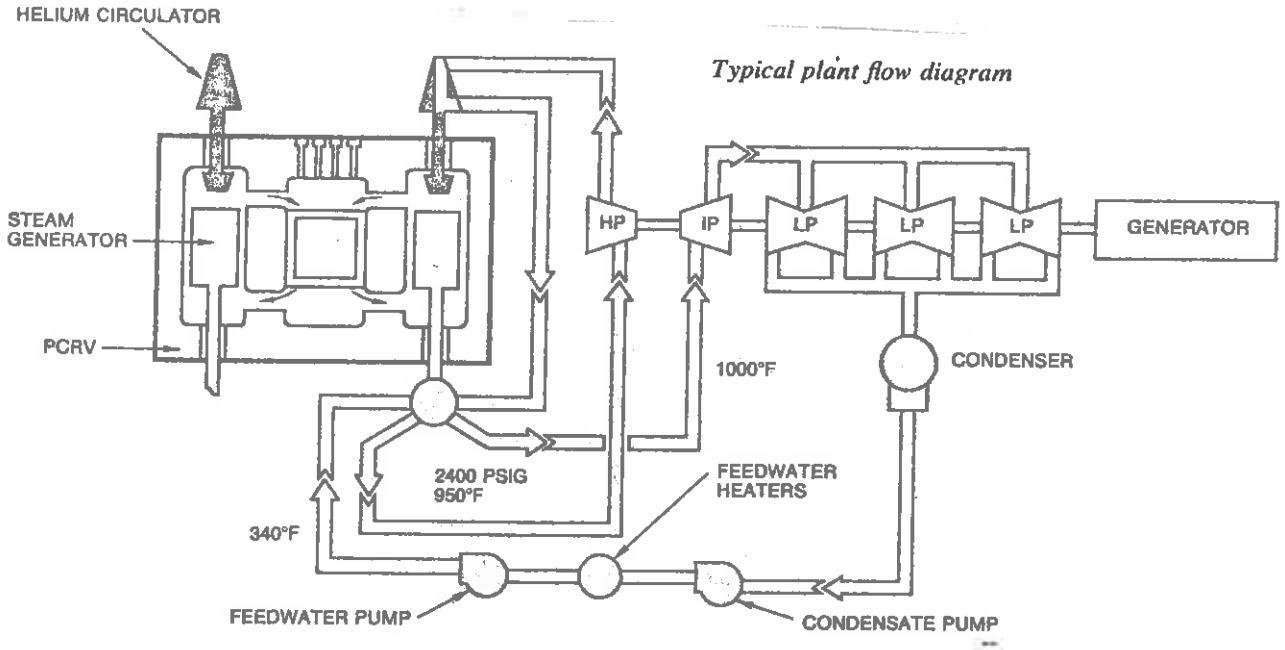

Typical plant flow diagram

reactor system to one atmosphere. And in an HTGR, even natural circulation of helium at atmospheric pressure is sufficient to remove the radioactive decay heat given off by the core following shutdown.

But the gas coolant also implies low power densities and hence large core sizes. Indeed, core sizes are sufficiently large that steel pressure vessels would be highly impractical. Hence a very significant breakthrough in the successful development of the HTGR was the design of large prestressed concrete reactor vessels (PCRV).

Prestressed Concrete Reactor Vessels: In an HTGR, a steel lined PCRV is used to contain all of the major components of the primary system, including the reactor core, steam generators, and helium circulators. It also provides the necessary biological shielding. Such PCRV produce compact installations. They can be field erected, thereby reducing transport problems. But their major advantage lies in the safety they inherently provide by eliminating major external primary coolant piping. This obviates the possibility of coolant accidentally escaping from large, interconnecting piping such as that found in light water reactor NSSS.

Such PCRV incorporate a multiplicity of steel tendons within and around their concrete walls which are tensioned before pressurizing the vessel. The compressive stresses in the concrete exceed the tensile stresses generated by the internal system pressure. Thus the concrete vessel is held in compression under all operating conditions. At operating system pressures, the net stresses in the concrete are small in magnitude.

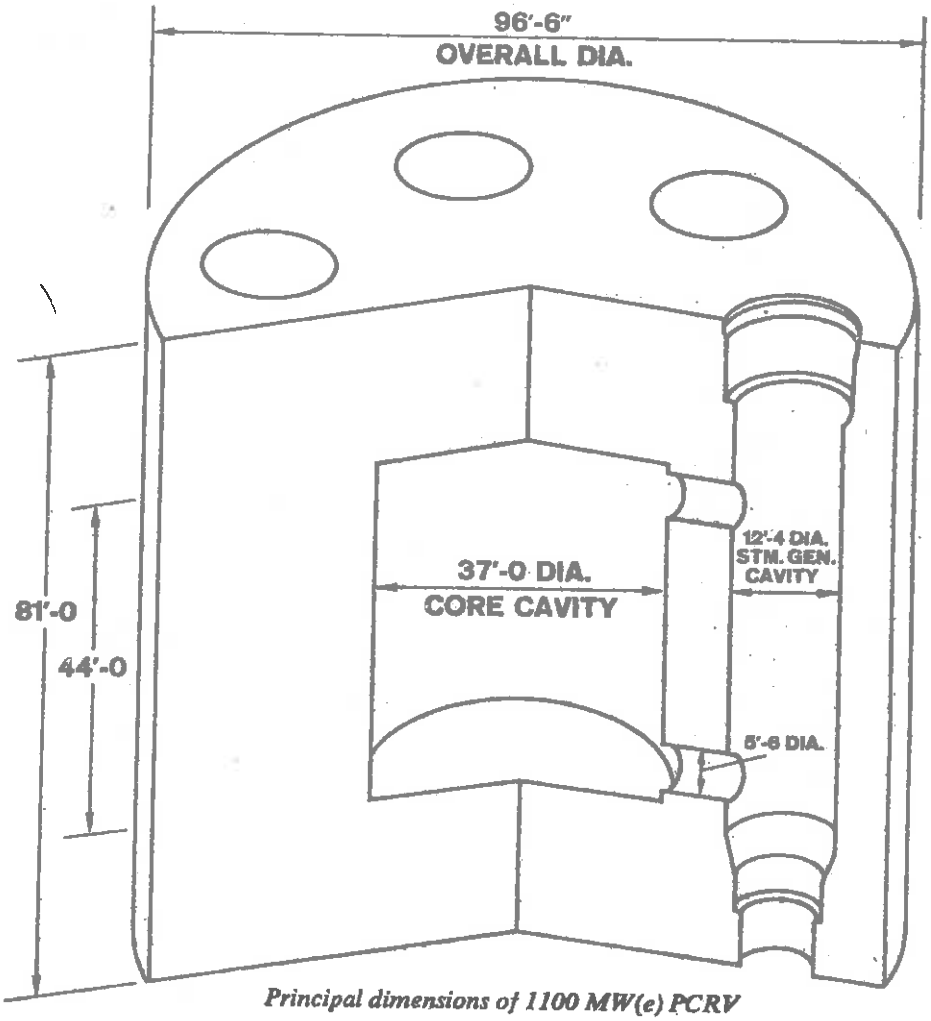

Principal dimensions of 1100 MW(e) PCRV

GENERAL ARRANGEMENT LARGE HTGR

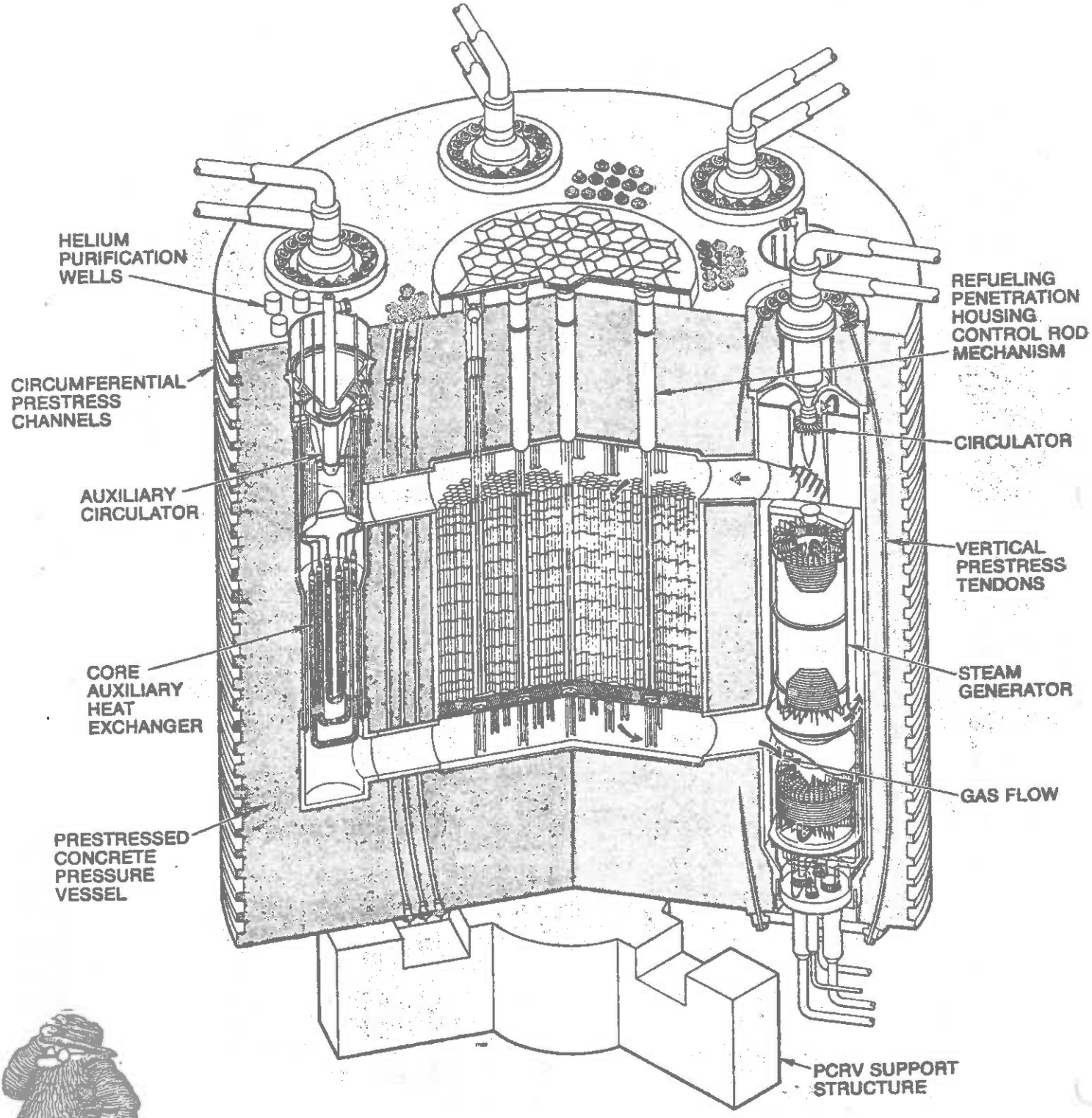

The PCRV contains a central cavity for the core, which is surrounded by a series of smaller cavities, each of which houses a steam generator and circulator.

Coolant System: The HTGR primary system operates at moderate pressures (700 psia). The helium coolant is circulated by axial flow compressors which force it down through the core where it reaches an exit temperature of 1400°F. It then passes through steam generators where it transfers its heat to water in the secondary system before being recirculated through the core.

The helium circulators are powered by steam mass flow produced by the steam generators themselves. The total power requirements for such circulators are quite large in comparison with other types of NSSS, as shown in the table below:

Type	Pumping Power Requirements
PWR	20 - 25 MWe
BWR	14
HTGR	60
LMFBR	45

The system steam produced by the HTGR is almost comparable to that of a fossil fueled plant, being some 950° - 1000 °F at 2400 psia. This yields a thermodynamic efficiency of 40% and allows the use of fairly conventional turbine equipment.

DESIGN FEATURES

Helium Coolant—A

1. Noncorrosive
2. Absorbs essentially no neutrons
3. Essentially zero reactivity
4. Optically transparent
5. Single phase (gas)

Graphite Moderator—B

6. Very low neutron capture cross-section
7. Excellent thermal conductivity
8. Excellent high-temperature strength
9. High specific heat

Uranium-Thorium Carbide Fuel—C

10. High conversion ratio due to high *eta* value of bred U^{233}
11. Discrete fuel particles individually clad with ceramic coatings
12. Particle coatings have excellent fission-product retention properties at high temperature and high burnup.
13. Semi-automated particle production process permits close quality control.

Core Design—D

14. Neutronically desirable quasi-homogeneous arrangement of fuel and moderator
15. Graded fuel loading
16. Flexibility in choice of fuel cycle and recycling mode
17. All ceramic construction, eliminating parasitic neutron capture and neutron activation effects associated with metallic structural materials
18. Negative temperature coefficient of reactivity at all temperatures of interest
19. Large heat capacity
20. High specific power
21. High burnup
22. Low annual fuel make-up requirement

Coolant System—E

23. Moderate primary system pressure
24. Circulation of coolant at atmospheric pressure sufficient to remove decay heat from core during shutdown periods
25. Secondary system employs modular-type steam generators

Reactor Plant—F

26. All major components of primary system compactly installed in a steel-lined Prestressed Concrete Reactor Vessel (PCRV)
27. No major primary coolant piping carried outside reactor vessel
28. Multiplicity and redundancy of pre-stressing tendons makes PCRV immune to catastrophic failure
29. Prestressing tendons shielded from neutron embrittlement
30. PCRV field erected
31. Reactor installation housed in a reinforced concrete independent secondary containment building
32. Ready access to reactor containment building during operation

Turbine Plant—G

33. Highly superheated steam produced by reactor system permits the use of standard 3600-rpm turbine generator
34. High thermal conversion efficiency
35. Dual coolant cycle ensures no entrainment of radioactivity into turbine system

Plant Control System—H

36. NSS-follow-turbine control principle

4. The Liquid Metal Fast Breeder Reactor NSSS

We have already seen the motivation behind the nuclear design of the fast breeder reactor and the arguments advanced for the use of liquid sodium as a coolant (such as high core power densities, the desire for a coolant with low moderating properties). We will concentrate instead on the NSSS for such reactors.

There are two basic approaches one can take to designing such a NSSS. One could follow a design similar to that of the PWR in which the primary sodium loop is brought outside the pressure vessel to a heat exchanger. Such a loop design has been chosen for the LMFBR demonstration plant.

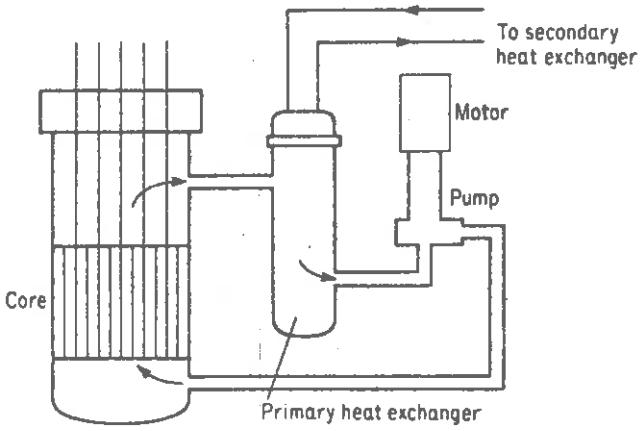

Schematic of a loop-type arrangement.

The alternative approach submerges all of the primary system in a pot within the pressure vessel as shown below:

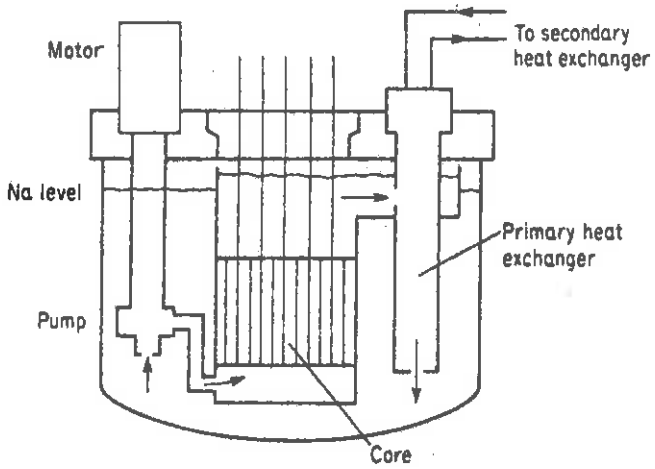

Schematic of a pool-type arrangement.

The high induced radioactivity of the sodium in the primary loop requires an intermediate loop. The particular system diagramed in Figure 15-18 corresponds to the U.S. demonstration plant. A key component in this system is the steam generator in which hot sodium is used to produce steam. Because of the explosive interaction between water and sodium, this element requires a very careful design, and, indeed, may be the most critical design problem in future commercial LMFBR's.

The high primary coolant temperatures (900°F) which are achievable using sodium, even under moderate pressures, allow some degree of superheating, as shown by the multiple steam generator loops in Figure 15-18.

5. The Gas Cooled Fast Breeder Reactor

-to be added later-

Figure 15-18

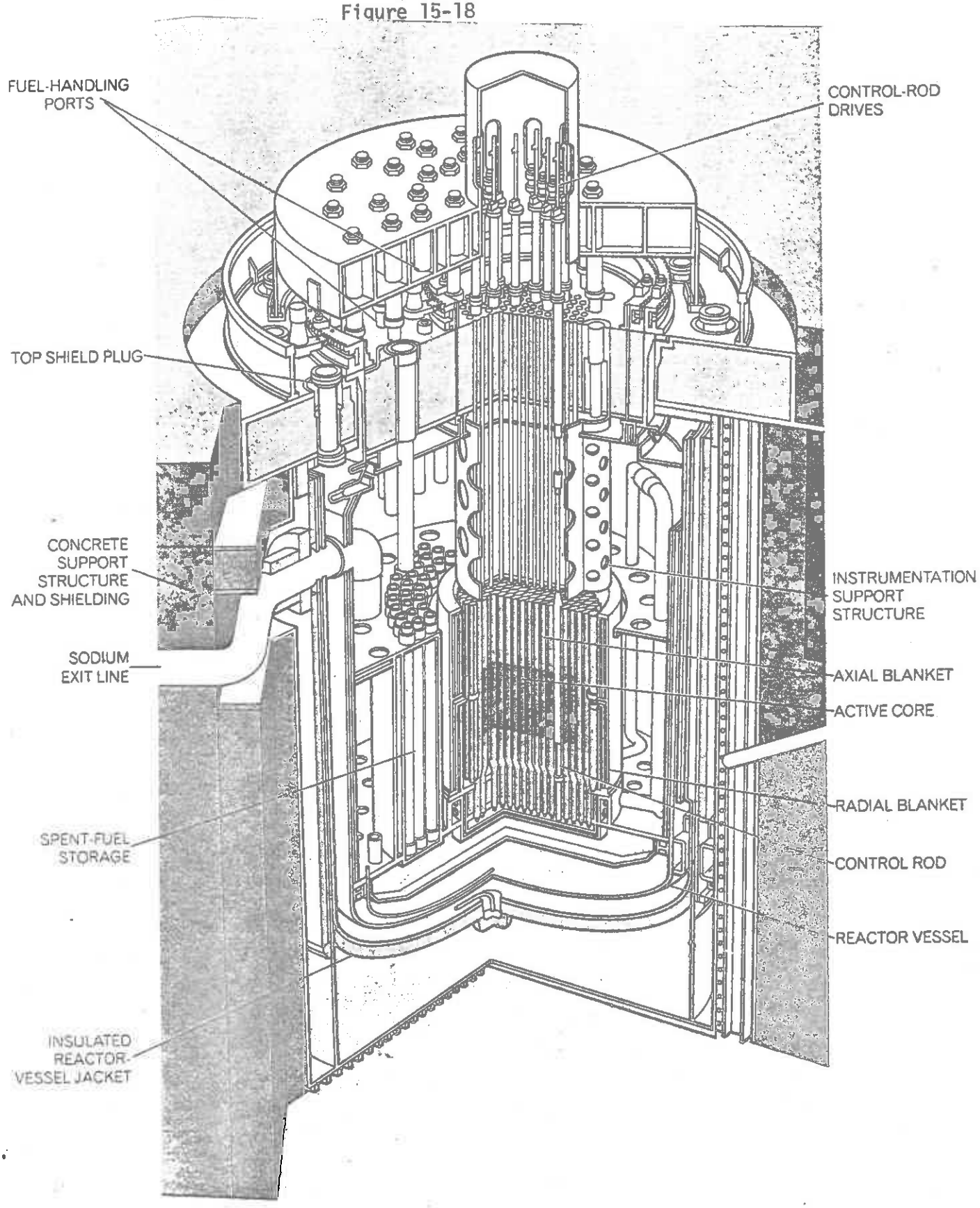

LIQUID-METAL REACTOR of the fast-breeder type is depicted on the basis of a design for a demonstration plant that would produce some 500 megawatts of electricity. A full-scale commercial plant, scheduled for operation by 1984, would be of 1,000-megawatt capacity. This design is of the loop type, meaning that the reactor proper, which is contained in a large tank of liquid sodium, is separated from the primary heat exchangers and the associated pumps by loops of piping through which sodium coolant flows.

Figure 15-19: LMFBR NSSS

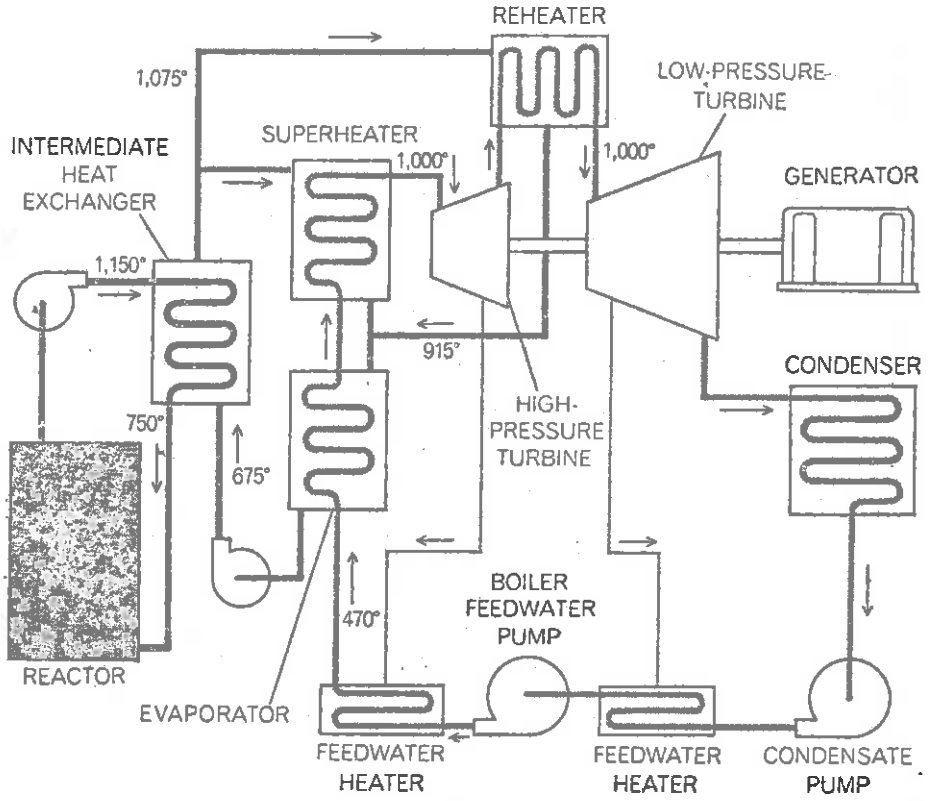

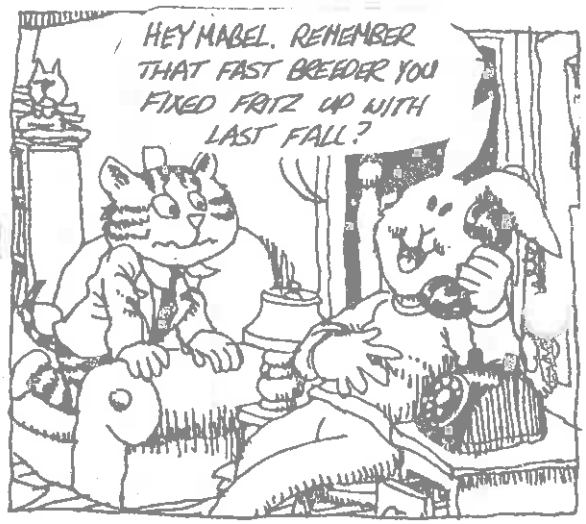

Figure 15-20

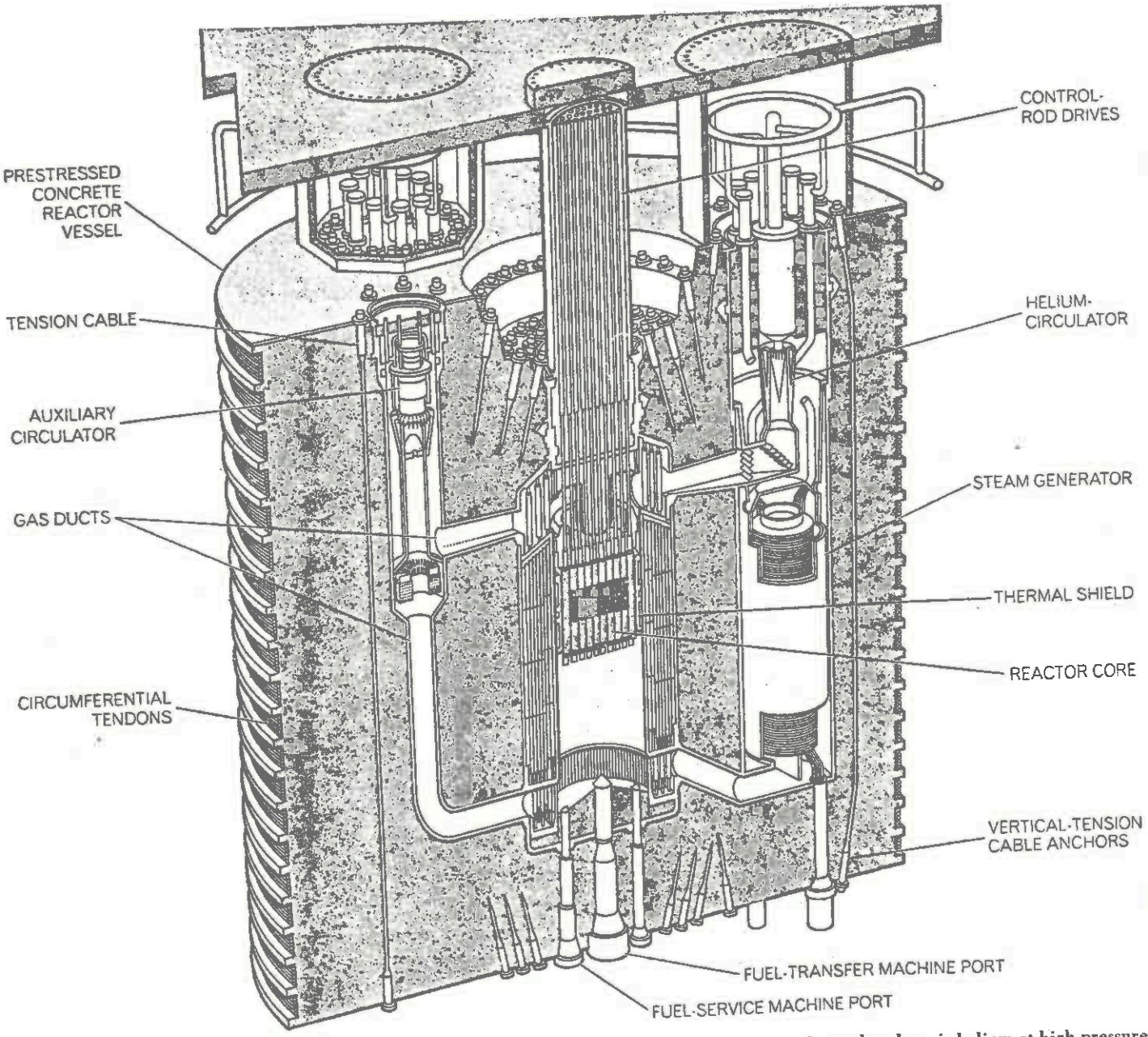

GAS-COOLED REACTOR is depicted in the form it might take for a demonstration breeder plant with a capacity of 300 megawatts of electric power. The chief difference between such a reactor and a liquid-metal one is that the coolant here is helium at high pressure instead of liquid sodium at low pressure. Because of the pressure the reactor is contained within a prestressed-concrete vessel.

Figure 15-21: GCFBR NSSS

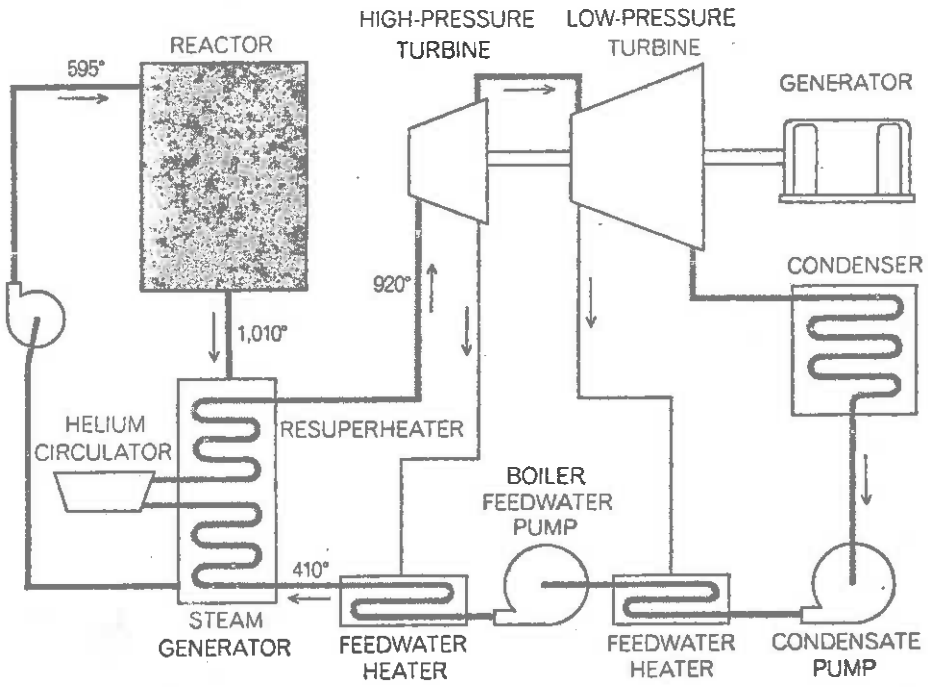

C. Nuclear Vs. Fossil-Fueled Steam Supply Systems

Nuclear steam supply systems exhibit more simularities to fossil-fueled systems than differences, particularly insofar as they influence the design of the remainder of the power plant. For example, the actual operation of a nuclear power station is no more complicated than that of a modern fossil fueled plant.

There are some important differences in steam properties, however. For example, a typical PWR-NSSS produces steam at temperatures of 600°F and pressures of 1075 psia. By way of contrast, a modern fossil fueled plant produces steam at 1010°F and 3845 psig. Hence the relatively wet steam produced by NSSS places more stringent requirements on steam turbine design and results in somewhat lower system efficiencies (33% as compared to 40%). However, even this disadvantage will be obviated by the introduction of HTGR and LMFBR plants with their higher operating temperatures.

The more dramatic differences between nuclear plants and fossil plants lie in their analysis, design, and particularly in their licensing. The extensive testing of designs and equipment prior to licensing of a nuclear plant unprecedented in the construction of conventional fossil fueled plants.

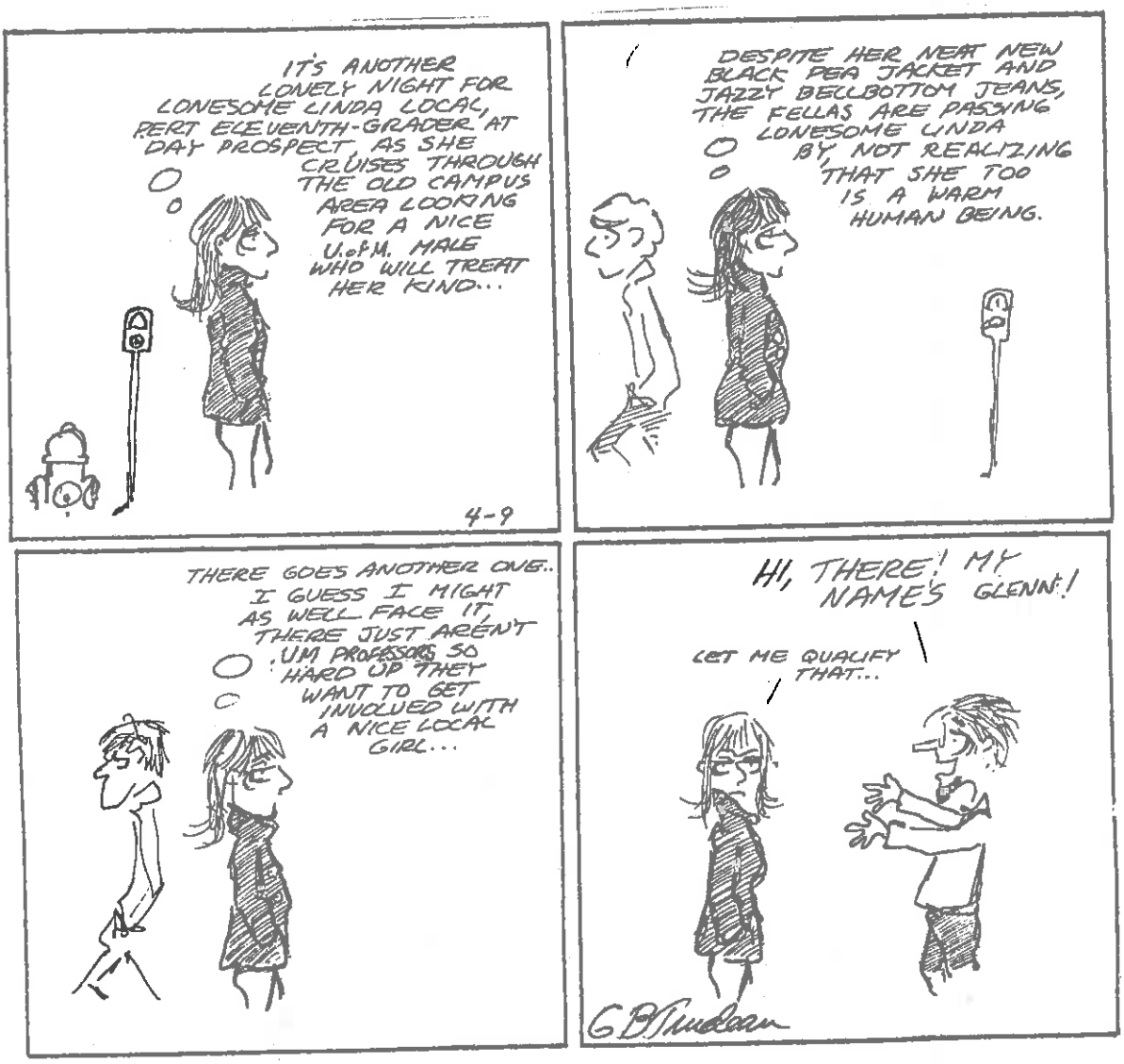
IT'S ANOTHER LONELY NIGHT FOR LONESOME LINDA LOCAL, PERT ELEVENTH-GRADER AT DAY PROSPECT, AS SHE CRUISES THROUGH THE OLD CAMPUS AREA LOOKING FOR A NICE U. of M. MALE WHO WILL TREAT HER KIND...
4-9
DESPITE HER NEAT NEW BLACK PEA JACKET AND JAZZY BELLBOTTOM JEANS, THE FELLAS ARE PASSING LONESOME LINDA BY, NOT REALIZING THAT SHE TOO IS A WARM HUMAN BEING.
THERE GOES ANOTHER ONE.. I GUESS I MIGHT AS WELL FACE IT, THERE JUST AREN'T UM PROFESSORS SO HARD UP THEY WANT TO GET INVOLVED WITH A NICE LOCAL GIRL...
HI, THERE! MY NAME'S GLENN!
LET ME QUALIFY THAT...
G B Trudeau

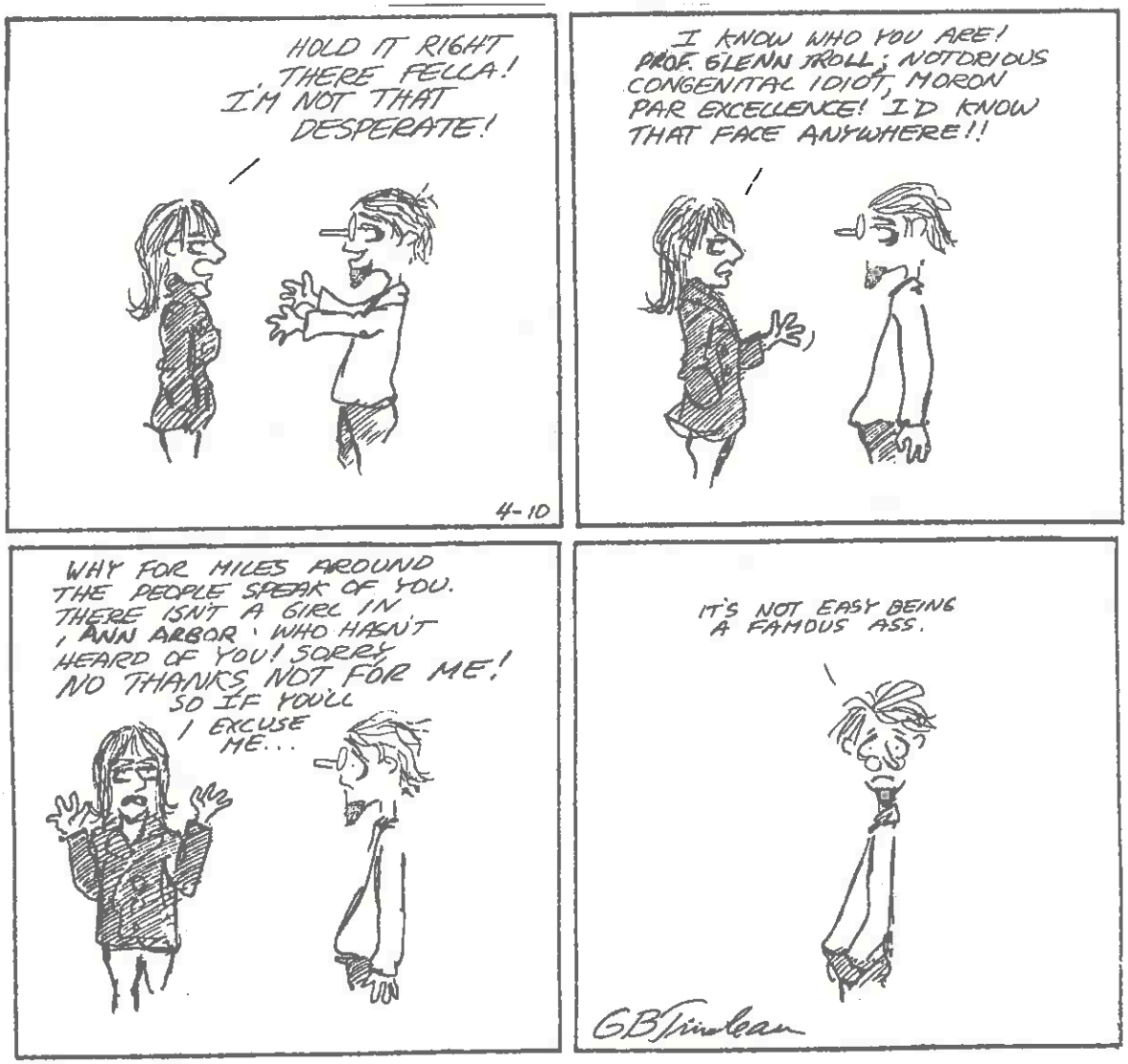
HOLD IT RIGHT THERE FELLA! I'M NOT THAT DESPERATE!
4-10
I KNOW WHO YOU ARE! PROF. GLENN TROLL; NOTORIOUS CONGENITAL IDIOT, MORON PAR EXCELLENCE! I'D KNOW THAT FACE ANYWHERE!!
WHY FOR MILES AROUND THE PEOPLE SPEAK OF YOU. THERE ISN'T A GIRL IN ANN ARBOR WHO HASN'T HEARD OF YOU! SORRY, NO THANKS, NOT FOR ME! SO IF YOU'LL EXCUSE ME...
IT'S NOT EASY BEING A FAMOUS ASS.
GB Trudeau

II. THERMODYNAMIC ANALYSIS OF NUCLEAR POWER SYSTEMS

A. A Review of Thermodynamics

1. The Laws of Thermodynamics

Essentially all nuclear power systems use a thermal cycle to convert fission heat into mechanical energy. Such cycles involve the utilization of a "working fluid" which absorbs this heat and then expands, doing work against the blades of a turbine. The thermodynamic laws governing the conversion of such heat energy into work are well known. However, since such knowledge is usually retained in the dimmer, less readily accessible areas of most students' memory, it is perhaps useful to first review some of the basic thermodynamic principles involved in the study of thermal cycles. We begin with a discussion of the first and second laws of thermodynamics:

The First Law of Thermodynamics: Energy must be conserved in any thermodynamic process.

Hence in any system or device, an exact balance must be obeyed by the various forms of energy added to or withdrawn from the system. Energy may be converted from one form to another, such as from heat to work, but there must always be a conservation of the total energy involved. If we characterize the system by a speed v, a pressure p, an internal energy u, then the first law of thermodynamics can be given in mathematical form as:

$$\frac{V_b^2}{2g} + P_b V_b + U_b + \Delta Q = \frac{V_a^2}{2g} + P_a V_a + U_a + \Delta W \qquad (15\text{-}1)$$

where the subscripts b and a describe the state of the system before and after the process of interest, while ΔQ represents the heat added to the system, and ΔW the mechanical work performed by the system during this process. We have written all of these quantities per unit mass of working fluid for convenience.

The Second Law of Thermodynamics: The change in entropy within an isolated system is always greater than or equal to the ratio of the heat added to the temperature at which the heat is added:

$$\Delta s \geq \frac{\Delta Q}{T} \tag{15-2}$$

If the process being described is reversible, then the equality holds

$$\Delta s = \frac{\Delta Q}{T} \tag{15-3}$$

[There is a third law of thermodynamics which states that the entropy vanishes as the temperature of the system approaches absolute zero, i.e.,

$$\lim_{T \to 0} S = 0$$

However, in engineering work, only changes in entropy are important, hence entropies are usually specified relative to a reference state not at absolute zero temperature.]

Two useful relationships which relate the thermodynamic variables characterizing a simple fluid at rest are

$$Tds = du + pdv$$

$$Tds = dh - vdp \qquad (15\text{-}4)$$

2. Thermodynamic Properties

The thermodynamic state of a system is usually specified in terms of a variety of thermodynamic variables:

p = pressure

T = temperature

v = specific volume

ρ = density = 1/v

u = internal energy

h = enthalpy

s = entropy = $\int dQ/T$

The state of a fluid composed of a uniform, single phase can be specified using only two independent thermodynamic variables. For example, when the pressure and temperature are specified for a fluid, its density, internal energy, enthalpy, entropy, and so on can be uniquely determined. Such relationships among thermodynamic variables are occasionally referred to as equations of state.

3. Thermodynamic Data

Thermodynamic properties are represented in many different forms, depending on the type of system under study. For a perfect gas, the equation of state is sufficient:

$$p\,v = R\,T \qquad (15\text{-}5)$$

For incompressible substances (e.g., solids or water near room temperature)

$$h = c_p T \tag{15-6}$$

More complex substances frequently are described by empirical equations of state, such as the Van derWaal equation

$$p = \frac{RT}{v-b} - \frac{a}{v^2} \tag{15-7}$$

However, most frequently, thermodynamic properties of substances are tabulated. For example, extensive tables exist for steam, air, the common gases, liquid metals, and so on. References for several of the more useful of such tabulations are given below:

J. H. Keenan, F. G. Keyes, P. G. Hill, and J. G. Moore, "Steam Tables", Wiley, New York, 1969.

W. J. Lick, and H. W. Emmons, "Thermodynamic Properties of Helium", Harvard University Press, Cambridge, 1962.

F. Din, "Thermodynamic Functions of Gases", Vol. 3, Butterworth's, London, 1956.

N. Sittig, "Sodium, Its Manufacture, Properties, and Uses", Reinhold, New York, 1956.

In practical calculations, such tables are frequently stored in a form suitable for computer data, and interpolation routines are provided.

Charts of thermodynamic properties are not only useful as sources of data, but are also frequently used to represent thermodynamic cycles. The thermodynamic state of the working fluid as it passes through the cycle is conveniently represented as a path on a chart of the properties of the fluid. For example, one useful type of chart is a p-v diagram in which lines of constant temperatures (isotherms) are shown:

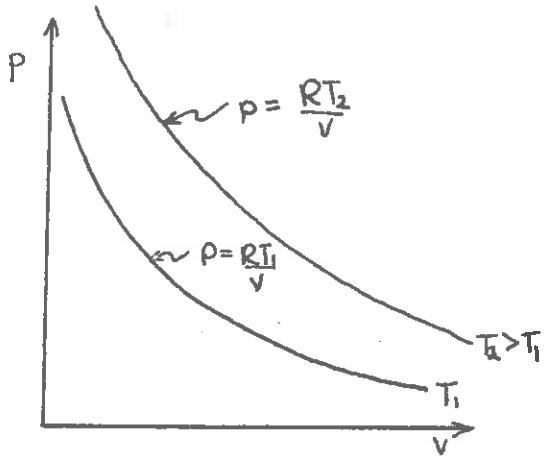

ideal gas

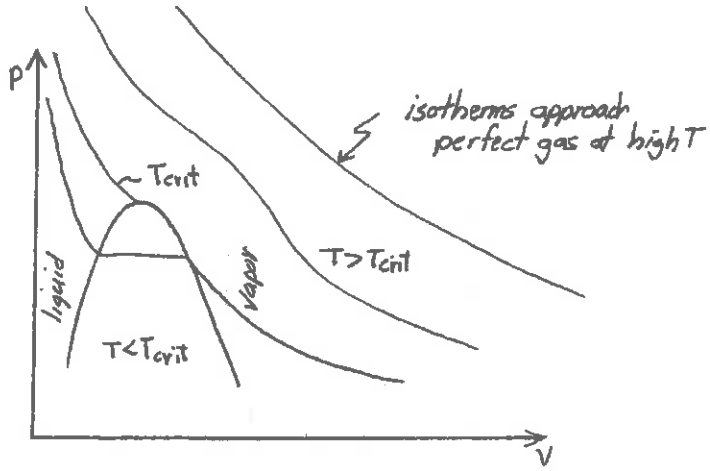

real gas

Other diagrams of interest are those of enthalpy vs. entropy (Mollier diagrams)

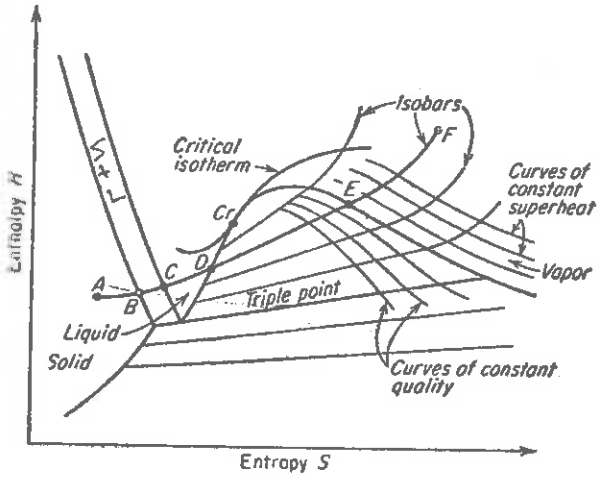

Mollier diagram for water.

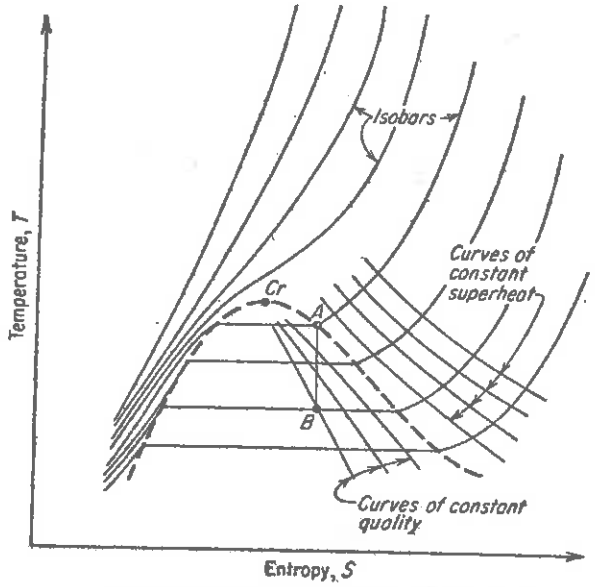

T-S diagram for wet and for superheated steam.

or of temperature vs. entropy. On each of these diagrams, one usually indicates lines of constant p or v.

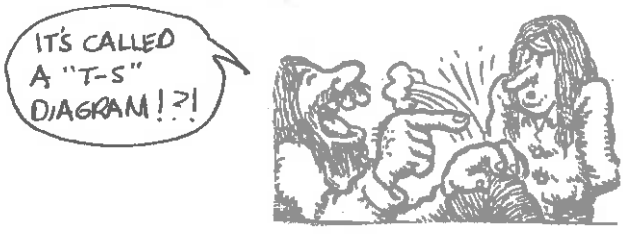

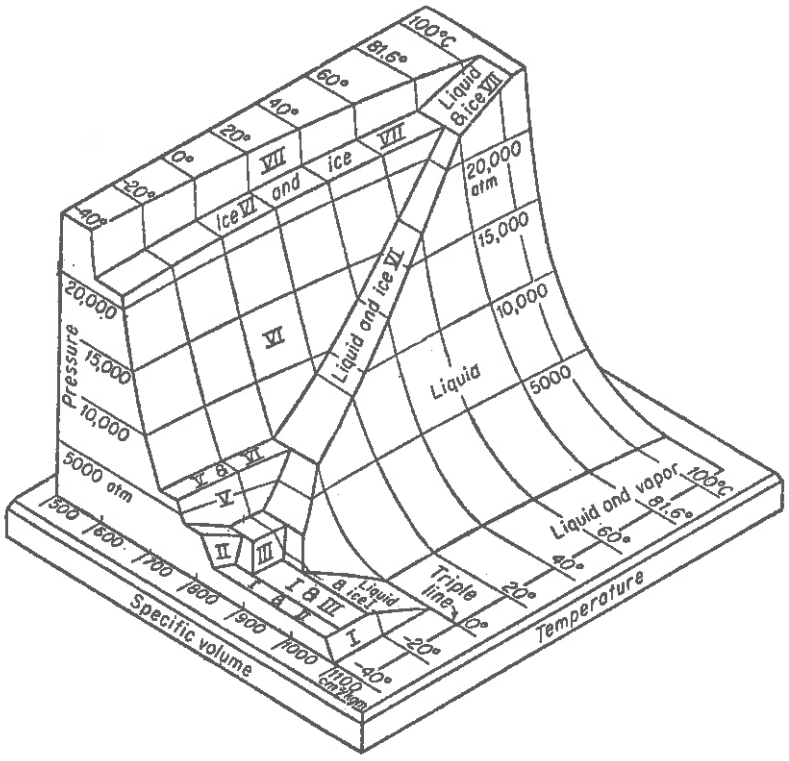

P-V-T surface for water, showing all the triple points. Constructed by Verwiebe on the basis of measurements by Bridgman.

B. The Carnot Cycle

Thermodynamic cycles correspond to closed paths on a chart of thermodynamic properties of the working fluid, and each segment of the path represents a certain process performed on or by the fluid. Such thermal cycles can be characterized by a thermodynamic efficiency representing the ratio between the work performed by the fluid to the amount of heat added to the system. The goal of every red-blooded thermal cycle is to achieve the efficiency characterizing the reversible Carnot cycle, which yields the highest efficiency which can be obtained for any heat engine operating between two reservoirs at given temperatures. On a T-s diagram, a Carnot cycle can be represented as shown:

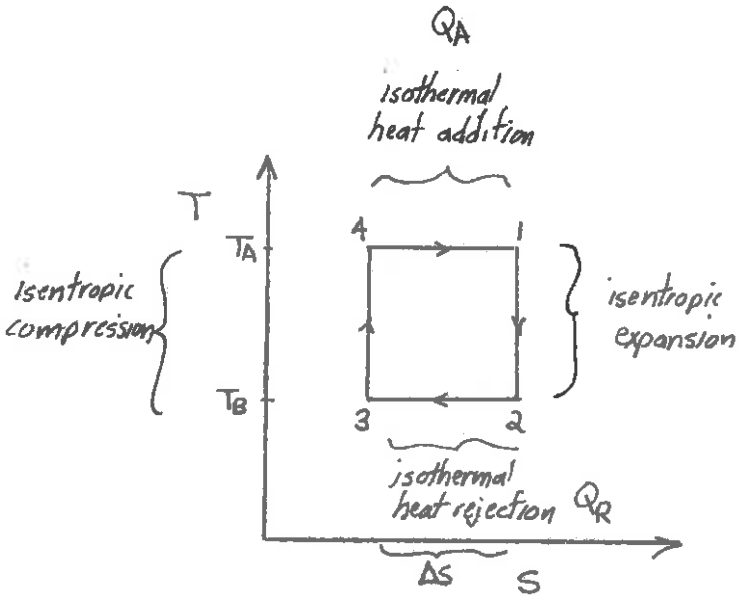

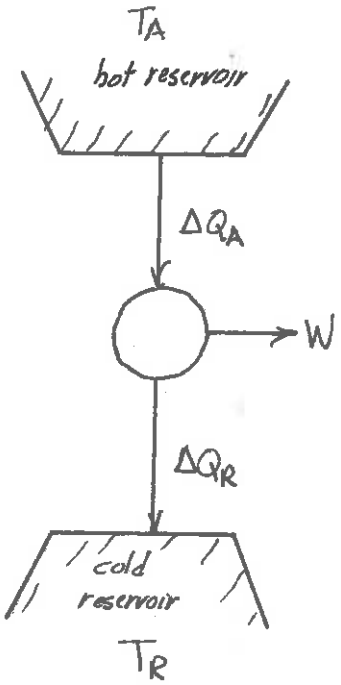

If we recall that for a reversible process, the entropy change is given by Eq. (15-3), then we can write the heat added or rejected in a process as

$$\Delta Q = T \Delta S \tag{15-8}$$

Hence the heat added and rejected during the isothermal phases of the Carnot cycle can be written as

$$\Delta Q_A = T_A \Delta S$$
$$\Delta Q_R = T_R \Delta S \tag{15-9}$$

Now the thermal efficiency of the cycle can be written as

$$\eta = \frac{\Delta W}{\Delta Q_A} = \frac{\Delta Q_A - \Delta Q_R}{\Delta Q_A}$$
$$= \frac{T_A - T_R}{T_A} = 1 - \frac{T_R}{T_A} \tag{15-10}$$

This is the ultimate efficiency which can be achieved by any heat engine (i.e., working fluid) operating between the temperature limits T_A and T_R, where these temperatures are in absolute units (°R or °K).

In a nuclear power system, the maximum temperature at which heat can be added to the working fluid is usually limited by the melting point of the fuel or the clad. The minimum temperature T_R at which the waste heat can be rejected is dictated by whatever condensor coolant is available (usually the ambient temperature of the reactor environment). For example, in a PWR producing steam at 600°F and rejecting waste heat at 100°F, the maximum achievable efficiency is

$$\eta = 1 - \frac{(493 + 100)}{(493 + 600)} = 46\%$$

Of course, no power plant can approach this theoretical maximum because of the impossibility of ever achieving a Carnot cycle, and because of irreversible processes which enter into any actual thermal cycle. To be more specific, a Carnot cycle involves heat transfer to the working fluid with zero temperature difference. But we know that heat can only be transferred as the result of a temperature difference, so isothermal heat addition or rejection is clearly impossible. Furthermore, the Carnot cycle assumes that no fluid friction occurs in the working fluid as it expands and contract during the cycle. This is once again clearly an idealization.

C. Thermodynamic Analysis of Steam Thermal Cycles

1. Component Behavior

In any actual thermal cycle, each portion of the cycle corresponds to a particular component of the system, such as a pump or turbine or condensor. We can describe the functioning of each of these devices in an idealized fashion as follows:

Pump: reversible adiabatic compression for which $dS = 0$:

Hence we can calculate the work performed by the pump using one of our T-S equations (15-4)

$$Tds = dh - vdp = 0 \Rightarrow dh = vdp \qquad (15\text{-}11)$$

to find

$$\Delta w_{a\to b} = \int_a^b v\,dp = \int_a^b dh$$

$$= h_b - h_a \qquad (15\text{-}12)$$

The corresponding p-v and T-s diagrams for a pump are shown below:

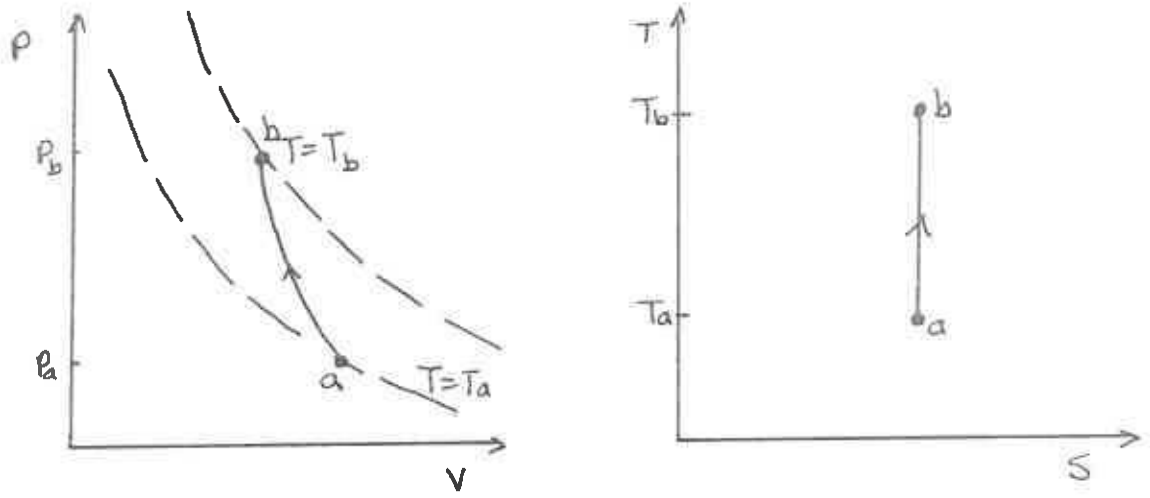

Turbine: reversible adiabatic expansion: dS = 0

We can merely adapt the results obtained for the pump, except now the path of the working fluid is in the opposite direction

$$\Delta w_{b\to a} = \int_b^a v\,dp = \int_b^a dh = h_a - h_b \qquad (15\text{-}13)$$

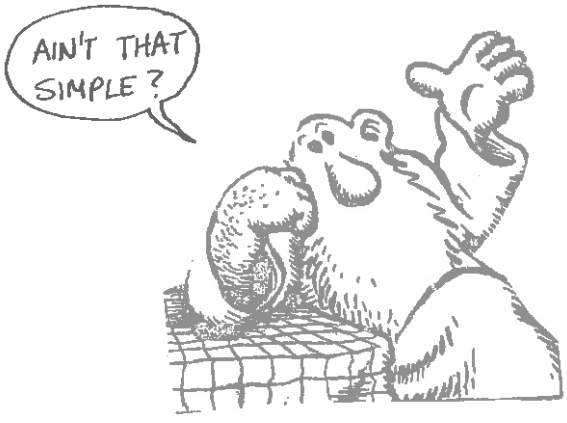

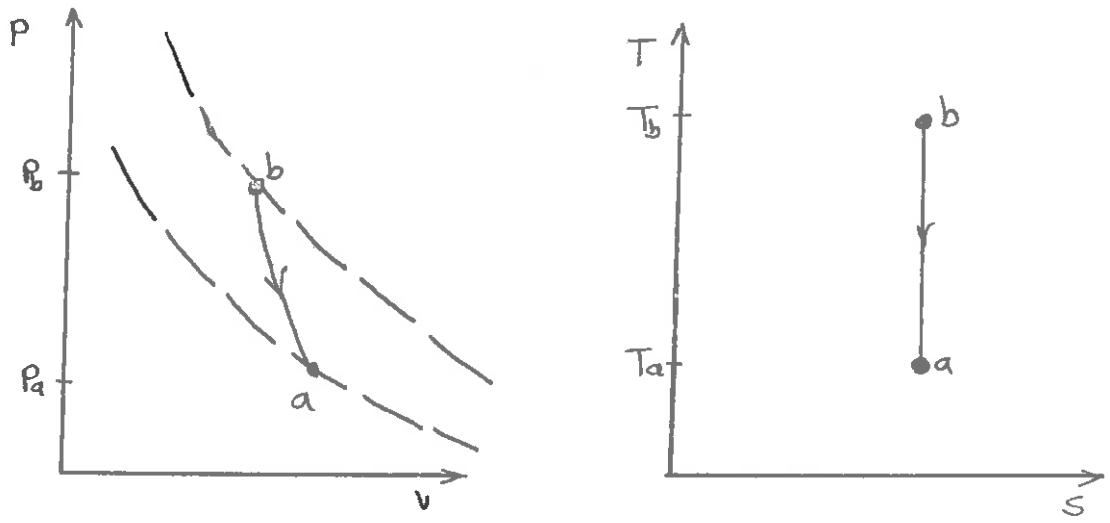

Heater or Boiler: constant pressure heat addition: dp = 0

(if no phase change, then a heater; if a phase change, then a boiler). Again using the T-s equations

$$Tds = dh - vdp = dh$$

$$dQ = Tds = dh \qquad (15\text{-}14)$$

$$\therefore \Delta Q = \int_a^b dQ = \int_a^b dh = h_b - h_a$$

and the corresponding thermodynamic diagrams are

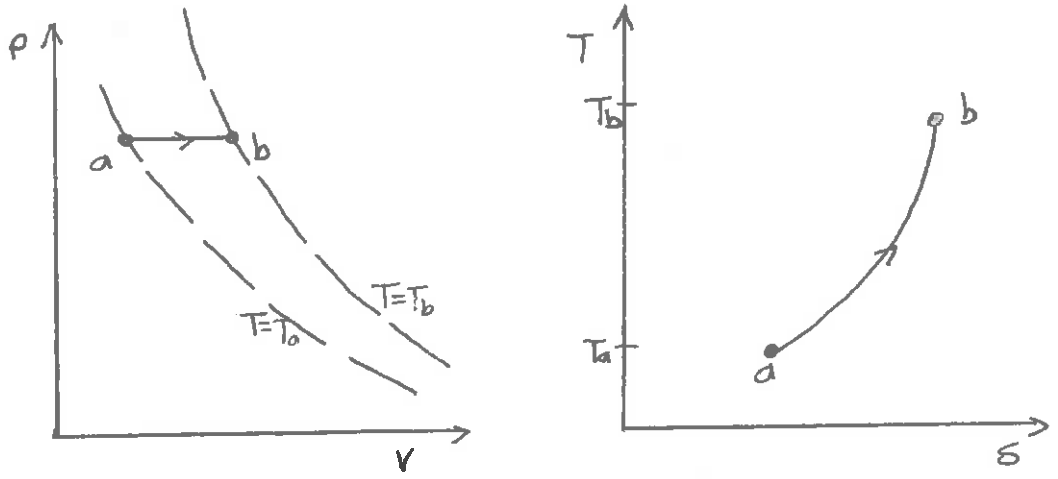

Cooler (radiator) or condenser: constant pressure heat removal

Again, it is simply the reverse process to constant pressure heat addition:

$$\Delta Q = h_b - h_a \qquad (15\text{-}15)$$

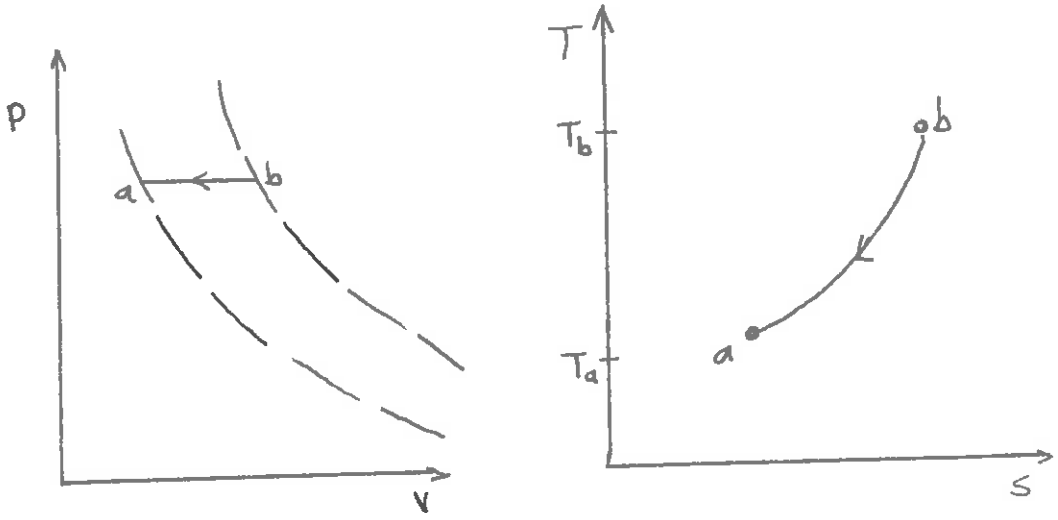

Heat exchanger: Depending on which side one is interested in, this is simply the same as a cooler or a heater.

Pipe with Frictional Loss: This is an irreversible process which involves an adiabatic pressure drop. Hence dh = 0 (a "throttling process") and the corresponding thermodynamic diagrams are shown below:

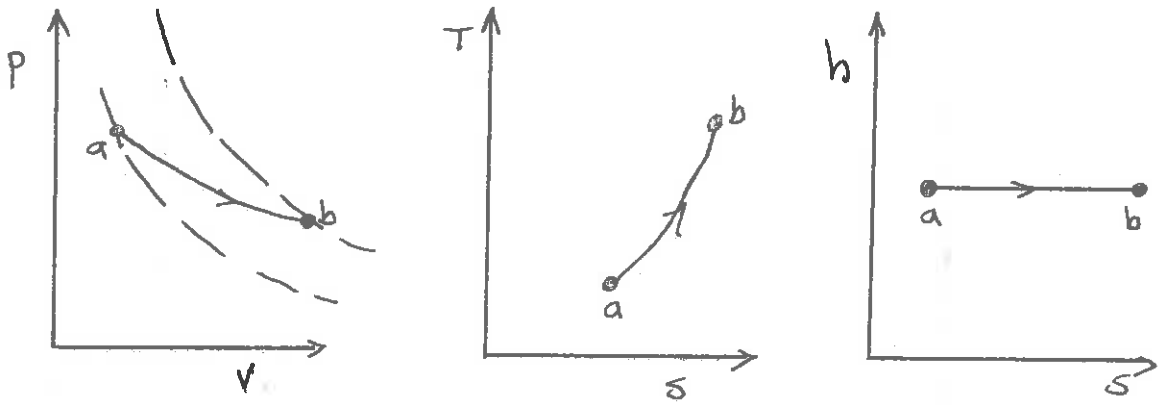

2. The Rankine Cycle

The thermal cycle which most closely resembles that of an actual steam power plant is the Rankine cycle which utilizes a condensable working fluid such as steam, characterized by the T-s diagram as shown below:

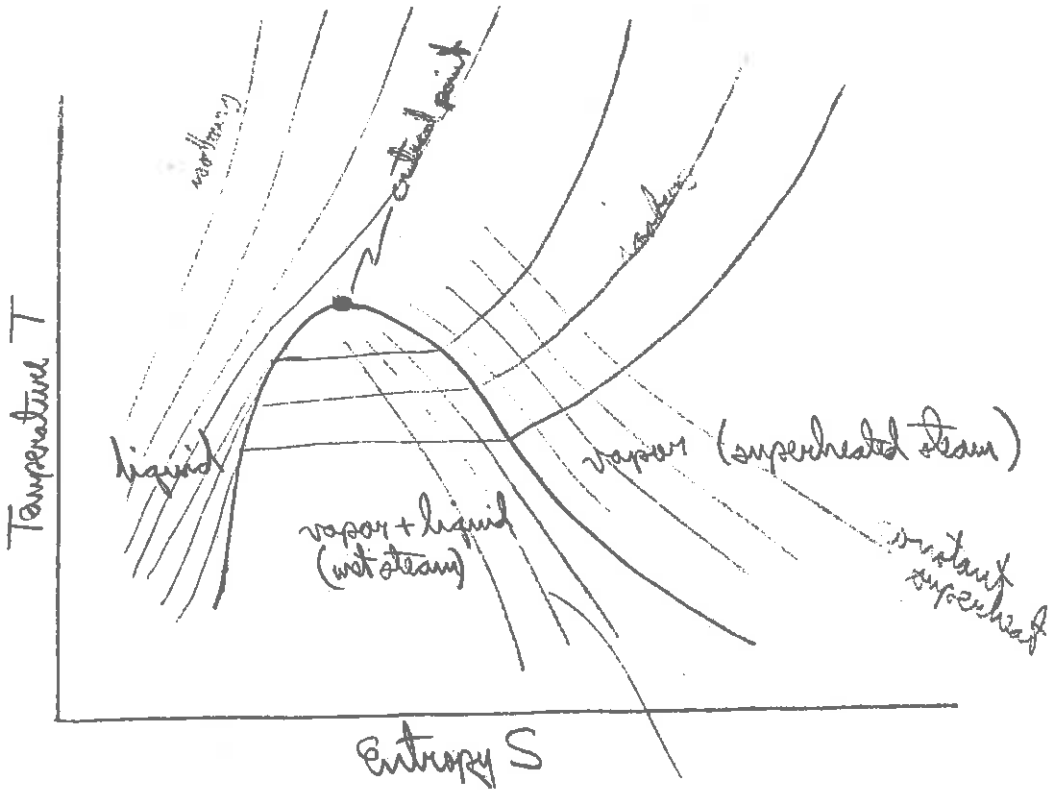

T-s diagram for H_2O

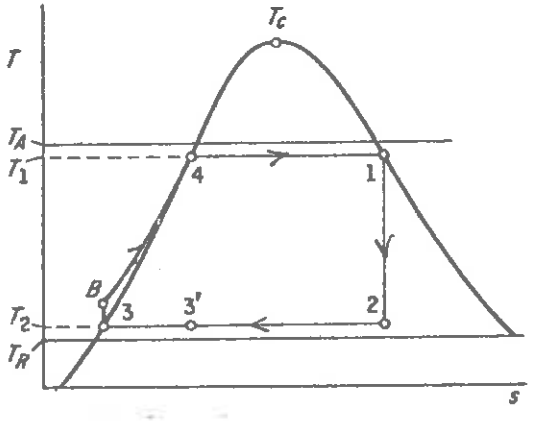

Rankine Cycle

The Rankine cycle consists of the following processes:

1→2: Saturated vapor at T_1 expands adiabatically in a turbine

2→3: The vapor is condensed at T_2 at constant pressure

3→B: It is then pumped to higher pressure (the same pressure as at point 1 before entering the turbine).

B→4→1: It is then heated in a heat exchanger at constant pressure, receiving "sensible heat" from B→4 and "latent heat" from 4→1.

For a PWR steam supply system, the corresponding points on a system diagram are shown below:

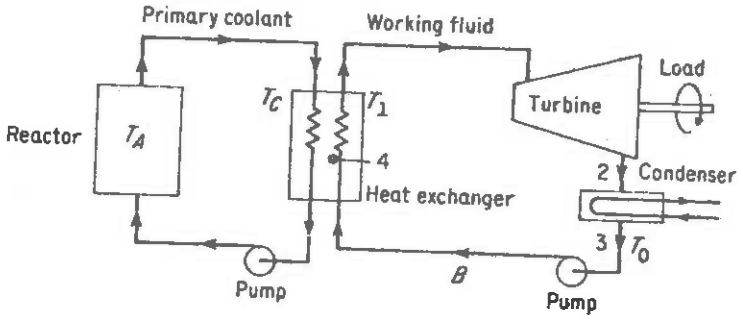

[Obviously, such a thermal cycle would also characterize HTGR and LMFBR steam supply systems. For a BWR, we would simply apply the Rankine cycle to the primary loop, replacing the steam generator by the reactor core itself.]

It is useful to analyze this cycle to determine the thermodynamic efficiency for a system characterized by parameters typical of those of a modern NSSS:

Boiler pressure p_B=2000 psia

Max. steam temperature T_{max}=1500°R=1040°F

Condenser temperature T_c=590°R=40°F

Condenser pressure (follows from T_c since a is on liquid saturation line) = .1217 psia

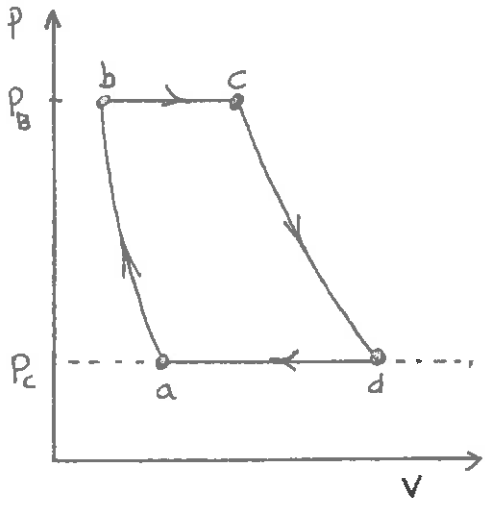

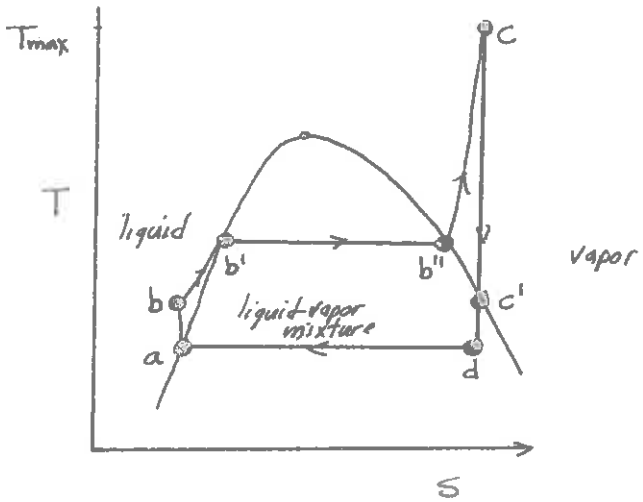

a → b: pumping from condenser pressure to boiler pressure. Since condenser temperature is 40°F,

$$h_a = 8.05 \text{ Btu/lbm}$$
$$s_a = .0162 \text{ Btu/lbm-F}$$
(From Table 1 of ref. 3)

$s_b = s_a$ (since the compression is assumed reversible)
$= .0162$ Btu/lbm-°F

h_b must be found for liquid at s=.0162 Btu/lbm-°F and p=2000 psia. Using Table 4 of ref. 3, for properties of the compressed liquid, $h=h_f=5.9$ Btu/lbm starting from initial .1217 psia.

So, $h_b = h_a + 5.9 - 8.05 + 5.9 = 13.95$ Btu/lbm

The Pump work is

$W_{pump} = W_{ab} = h_b - h_a = 5.9$ Btu/lbm

b → c: Heat addition in boiler, at p=2000 psia. Heat to 1040°F=T_{max}.

Find h_c and s_c from Table 2 of ref. 3 by interpolation

$$h_c = 1474.5 + \frac{1505.7 - 1474.5}{1050 - 1000}(1040 - 1000)$$
$$= 1499.5 \text{ Btu/lbm}$$

$$s_c = 1.5603 + \frac{1.5813 - 1.5603}{1050 - 1000}(1040 - 1000)$$
$$= 1.5771 \text{ Btu/lbm-°F}$$

The heat input to the cycle is

$$Q_{in} = h_c - h_b = 1499.5 - 13.95$$
$$= 1435.5 \text{ Btu/lbm}$$

c → d: Expansion through turbine. Assume reversible expansion, $s_d=s_c=1.5771$ Btu/lbm-F, to the pressure in the consenser, .1217 psia

(or to the temperature of the condenser, 40°F). Since the entropy of the pure vapor at 40°F saturation, is greater than 1.5771, the result of expansion must be only partially vapor. We determine the fraction of vapor (quality) from the requirement

$$s = \chi s_g + (1 - \chi) s_f$$

$$1.5771 = \chi\,(2.1597) + (1 - \chi)\,(.0162)$$

$$= .0162 + 2.1435\,\chi$$

$$\therefore\ \chi = .728$$

The enthalpy follows since the quality is known:

$$h_d = \chi h_g + (1 - \chi) h_f$$

$$= h_f + \chi h_{fg}$$

$$= 8.05 + 1071.3\chi$$

$$= 791 \text{ Btu/lbm}$$

The work output through the turbine shaft is

$$W_{out} = h_c - h_d$$

$$= 1499.5 - 791$$

$$= 708.5 \text{ Btu/lbm}$$

The net work output is the shaft work less the pumping power

$$W_{net} = W_{out} - W_{pump} = 768.5 - 5.9$$

$$= 702.6 \text{ Btu/lbm}$$

d → a: constant pressure cooling in the condenser, at .1217 psia, 40°F. h_a is known from the start of the cycle.

The heat rejected is

$$Q_{out} = h_a - h_d$$

$$= 791 - 8.05$$

$$= 783 \text{ Btu/lbm}$$

Summary:

Q_{in} = 1485.5 Btu/lbm

W_{net} = 702.6 Btu/lbm

Q_{out} = 783 Btu/lbm

while W_{pump} = 5.9 Btu/lbm

The thermal efficiency is

$$\eta = \frac{W_{net}}{Q_{in}} = \frac{702.6}{1485.5} = 47.2\%$$

3. Reheating and Regeneration

There are a couple of modifications that are usually made to the Rankine cycle in an actual steam power plant. In the idealized cycle we have studied, the expansion of the working fluid gave rise to a mixture of vapor and considerable liquid in the lower pressure end of the turbine. This would result in turbine inefficiency and blade erosion. To prevent this, one removes steam from the turbine before it expands to the saturation temperature, and reheats it by passage through another heating device, a reheater, before reinserting in into the turbine for further expansion. A simple diagram of such a reheating cycle is shown below

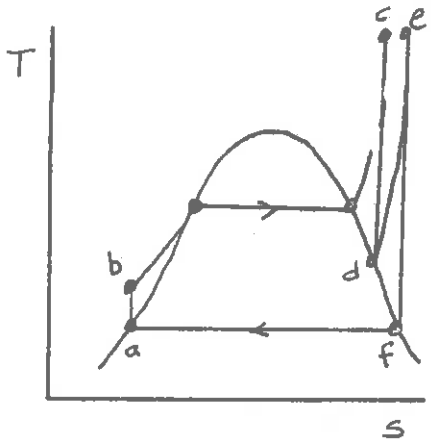

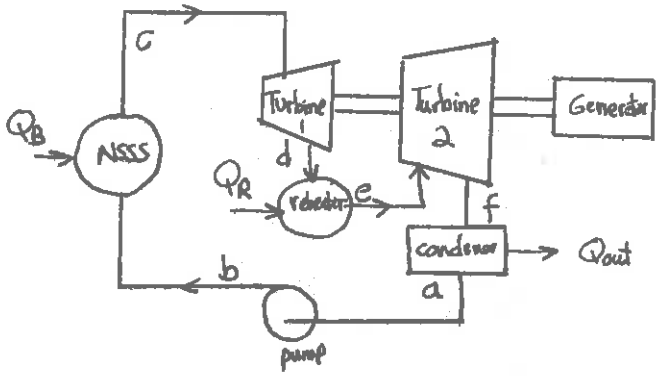

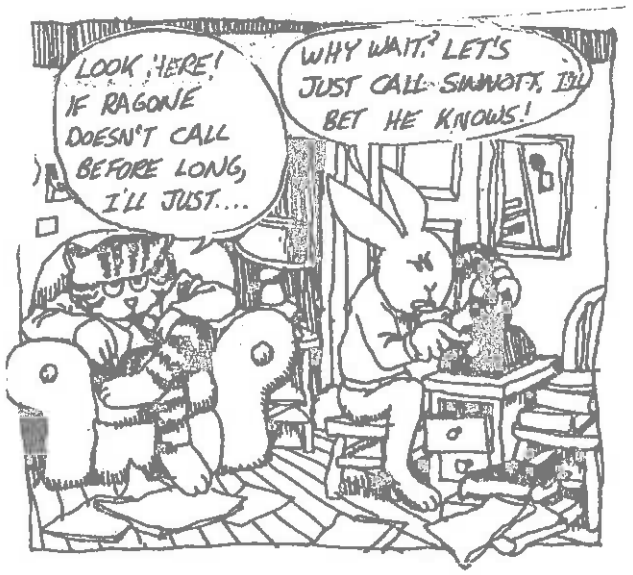

Yet another modification made to the Rankine cycle is introduced to avoid as much heat addition to the feedwater at low temperatures as possible, since this would give rise to a considerable loss in efficiency (recall our formula for the efficiency of the ideal Carnot cycle). One instead uses a regenerative cycle in which heat is transferred reversible from the working fluid in the turbine to the passing feedwater. This is possible in principal because as expansion proceeds in the turbine, the fluid temperature decreases. Hence at any point during expansion and feedwater heating, the local steam temperature is made equal to (infinitestimally greater than) the local temperature of the water which receives the heat. The total of heat added from external sources (in the boiler) is added at constant temperatures, thereby producing steam.

A diagram of a regenerative feed-heating cycle is shown below:

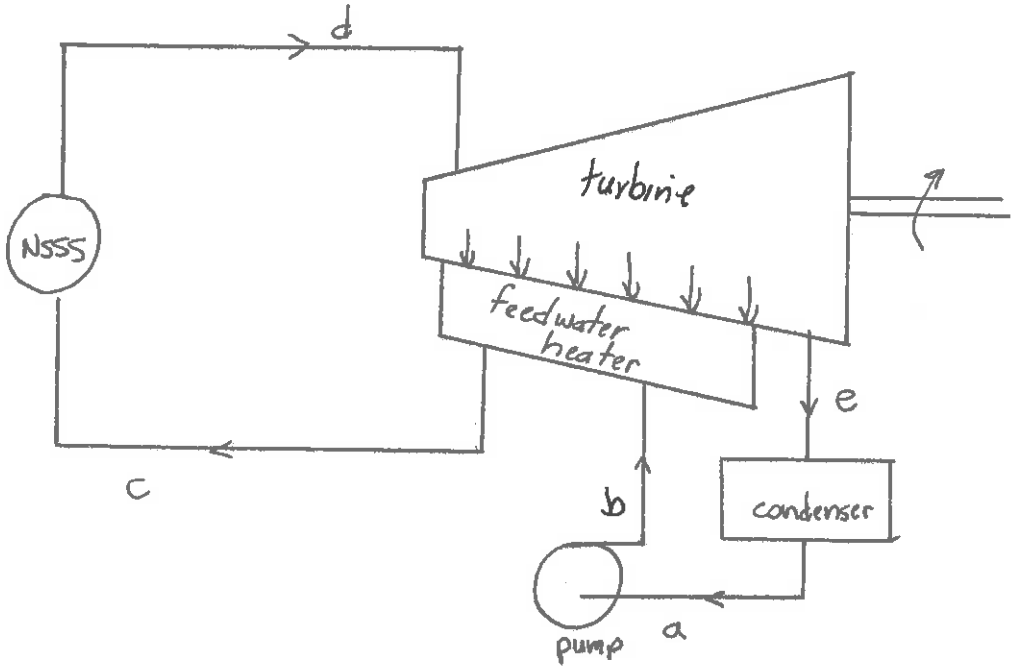

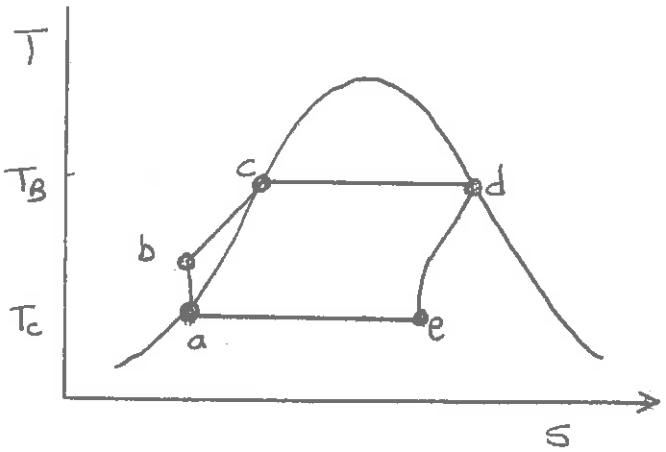

D. The Brayton Cycle

Thus far we have directed our attention towards nuclear power systems in which the fission heat energy is used to produce steam, which then expands in a steam turbine, thereby producing mechanical work and hence electrical energy. However the use of a gas coolant allows the possibility of an alternative to the Rankine cycle for the HTGR. In this cycle, the gas heated within the HTGR core would be used directly to drive a gas turbine in a simple closed cycle as shown below:

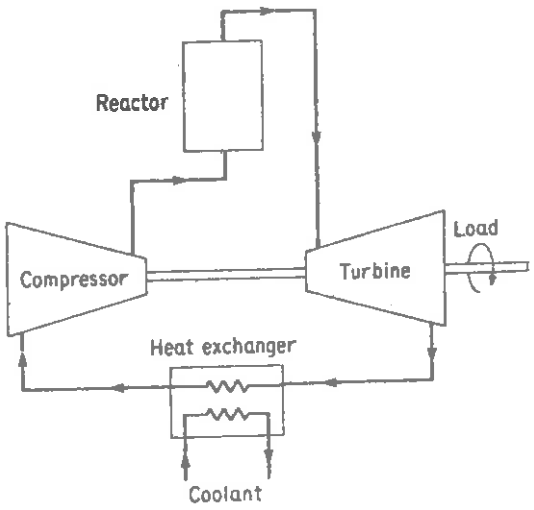

Such a thermal cycle is known as a Brayton cycle and is characterized by a thermodynamic diagram as shown below:

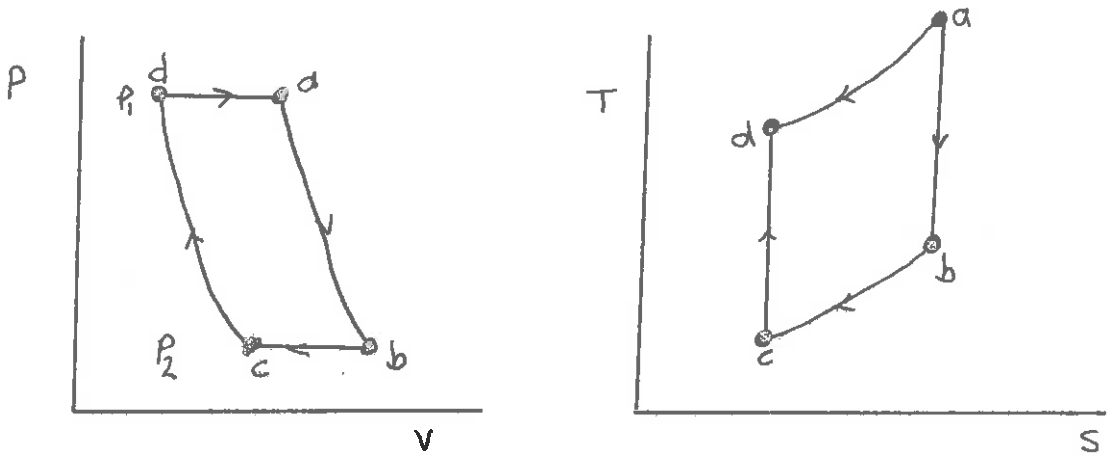

One can easily determine the efficiency of this cycle, if the working fluid is assumed to behave as a perfect gas. Consider each step of the cycle:

a → b: isentropic expansion in the turbine

$$pv^{\gamma} = \text{const.}$$

$$\Rightarrow p_a V_a^{\gamma} = p_b V_b^{\gamma} \Rightarrow T_a p_a^{-\frac{\gamma-1}{\gamma}} = T_b p_b^{-\frac{\gamma-1}{\gamma}} \qquad (15\text{-}16)$$

also, $W_{a\to b} = h_a - h_b = c_p (T_a - T_b)$

b → c: isobaric cooling in the cooler

$$Q_{b\to c} = c_p (T_c - T_b) \tag{15-17}$$

c → d: isentropic compression in the compressor

$$T_d p_a^{-\frac{\gamma-1}{\gamma}} = T_c p_2^{-\frac{\gamma-1}{\gamma}}$$
$$W_{c\to d} = c_p (T_c - T_d) \tag{15-18}$$

d → a: isobaric heating in the reactor core

$$Q_{d\to a} = c_p (T_a - T_d) \tag{15-19}$$

The net work out is

$$W_{net} = W_{a\to b} + W_{c\to d} = c_p \left[(T_a - T_b) + (T_c - T_d) \right] \tag{15-20}$$

The heat in is

$$Q_{in} = Q_{d\to a} = c_p (T_a - T_d) \tag{15-21}$$

Hence the efficiency is conveniently expressed in terms of the high and low pressures of the cycle, p_1 and p_2:

$$W_{net} = c_p \left[T_a \left(1 - \frac{T_b}{T_a}\right) - T_d \left(1 - \frac{T_c}{T_a}\right) \right]$$

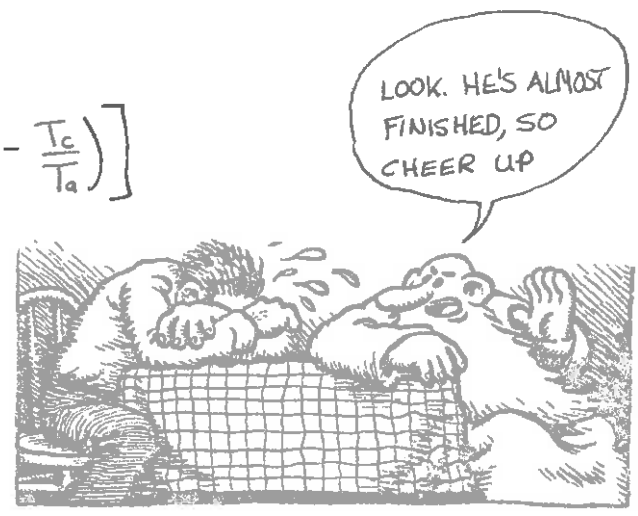

$$T_b/T_a = \left(P_b/P_a\right)^{\frac{\gamma-1}{\gamma}} = \left(P_2/P_1\right)^{\frac{\gamma-1}{\gamma}}$$

$$T_c/T_d = \left(P_c/P_d\right)^{\frac{\gamma-1}{\gamma}} = \left(P_2/P_1\right)^{\gamma-1/\gamma} \qquad (15\text{-}22)$$

$$W_{net} = C_p(T_a - T_d)\left[1 - \left(\frac{P_2}{P_1}\right)^{\frac{\gamma-1}{\gamma}}\right]$$

$$= Q_{in}\left[1 - \left(\frac{P_2}{P_1}\right)^{\frac{\gamma-1}{\gamma}}\right] \qquad (15\text{-}23)$$

or finally

$$\eta = \frac{W_{net}}{Q_{in}} = 1 - \left(\frac{P_2}{P_1}\right)^{\frac{\gamma-1}{\gamma}} \qquad (15\text{-}24)$$

For helium, $\gamma = 1.659$. Hence for pressures $p_1 = 1000$ psia, $p_2 = 100$, one finds an ideal Brayton cycle effiency of

$$\eta =$$

Hence there is strong incentive to eventually develop gas turbines of sufficient capacity to match an HTGR power plant.

III. POWER REACTOR OPERATION

A. Nuclear Power Reactor Startup and Testing

Nuclear power plants are subjected to a degree of testing prior to operation which is quite different from that required for conventional power plants. Prior to the issuing of an operating license, a formal field test program must be conducted to verify the satisfactory operation of each component of the nuclear plant. Such field test programs will vary from one reactor type to another, as will the detailed procedures followed in reactor operation. Our intent in this section is not to attempt an exhaustive study of power reactor testing and operation, but merely to illustrate several of the considerations involved. Hence we will confine ourselves to a detailed consideration of only one reactor type, the pressurized water reactor.

Several phases of a field test program which are characteristic of those conducted on a modern PWR plant include:

Precritical testing: Prior to fuel loading, the nuclear steam supply system is subjected to a number of tests of nonnuclear components. The general sequence of such a testing program includes

(i) inspection of system components

(ii) tests of electrical equipment and circuitry

(iii) instrumentation tests

(iv) hydrostatic tests (all fluid components and systems)

(v) functional tests (in which components are operated)

(vi) operational tests (in which systems are operated under conditions as close to the normal operating condition as possible)

Following the functional tests of each system component, the reactor coolant system is brought to a hot standby condition in which system temperature and pressure are raised to zero power levels using the primary coolant pumps as a heat source. (It should be stressed that there is still no fuel in the core.) There then follows a period of stimulated operational testing with the reactor coolant system in a hot standby condition.

Fuel loading and zero-power testing: Prior to fuel loading, neutron detectors and sources are loaded into the core. Fuel loading then takes place with the reactor vessel and fuel handling pool filled with water at ambient temperature containing 2000 ppm boron to assure a nuclear multiplication factor of less than 0.90. (Even if all of the control rods were removed, the boron content is chosen such that the core multiplication during fuel loading would never exceed 0.99.)

At this point, fuel loading begins. Throughout the fuel loading, frequent measurements are made of core multiplication, and frequent pauses are taken to relocate sources and neutron monitors with frequent checks on results until all of the core fuel assemblies are in place.

After fuel loading, one begins low power critical testing. The initial heating and pressurization of the primary coolant system is accomplished as in the precritical tests using the heat generated by the primary coolant pumps. After the NSSS has reached operating temperatures, the reactor is brought to criticality at low power. One then measures control rod reactivity worths, reactivity coefficients, soluble poison worth, core excess reactivity, and core power distributions.

Power testing: The reactor is then brought to somewhat higher power levels (e.g., 15% of rated power) at normal operating temperatures and pressures, with the steam generated dumped to the condensor through the turbine bypass system. Several measurements are performed at this time:

(i) Calibration of the power range nuclear instrumentation, with particular emphasis on verifying the overlap between intermediate and full power range instrumentation.

(ii) Initial operation of in-core nuclear instrumentation is checked.

(iii) The plant computer programming necessary to handle core power distributions, fuel assembly power distributions, xenon concentration, and hot channel conditions is checked.

Finally, the plant is brought to 100% of rated power, and a new series of tests is performed:

(i) The plant performance characteristics are evaluated at steady state.

(ii) The power coefficient of reactivity is measured.

(iii) Several reactor physics tests are performed at full power, including the measurement of boron worth and differential and integral control rod worths.

(iv) In-core and external nuclear instrumentation are correlated.

(v) The plant transient response is evaluated by initiating various step and ramp load changes and measuring the plant load following characteristics.

(vi) Xenon reactivity worth measurements are made by varying the reactor power level.

(vii) The reactor response to a turbine trip is investigated.

The above list contains only a representative sample of the many tests which must be performed on a nuclear reactor system prior to on-line power production.

B. Reactor Startup Under Normal Operating Conditions

A modern nuclear power plant is an incredibly complicated system. One cannot start up such a plant by simply throwing a switch which withdraws a bank of control rods. Instead, a complicated, but well-prescribed, sequence of operations must be followed in the startup procedure. The actual startup procedures that are followed will depend on whether the reactor coolant is in a hot, standby condition at operating temperature and pressure, or in a cold condition in which the coolant systems must first be pressurized and heated to operating conditions before reactor criticality can be initiated. Hence a hot startup actually comprises a subset of the cold startup procedure. The initial parameters characterizing the coolant system prior to cold and hot startup are given below:

Parameter	Cold	Hot
Reactor coolant temperature, °F	140	557
Reactor coolant pressure, psia	400	2250
Pressurizer level, % full	100	25
Pressurizer temperature, °F	140	652

We will furthermore assume that all pre-startup testing has been completed of system components.

A table giving the steps and the approximate time required for each step in both hot and cold startup procedures are given on the right. In Figures 15-18 and 15-19 we have sketched the primary coolant temperature and pressure and the reactor power level as functions of time during the startup operation. A more detailed description of the individual steps involved in the startup procedure follows:

ESTIMATED STARTUP TIME IN HOURS REQUIRED BY NSSS

Operation	Hot*	Cold**
1. Raise primary system pressure to 400 psig and raise pressurizer temperature to saturation at 400 psig	—	6.5
2. Drain pressurizer to no-load operating level, maintaining system pressure at 400 psig	—	2
3. Withdraw rods to criticality and raise output to power range level	0.5	0.5
4. Raise RCS to no-load conditions (T_{avg} = 557°F, system pressure 2250 psia)	—	3.5
Secondary plant operations, such as drawing a vacuum in the main condenser and rolling the turbine, can be done before the RCS reaches no-load conditions.		
5. Raise the NSSS output to full power (5 percent per minute)	0.5	0.5
The loading rate is restricted by turbine considerations. The cold startup time given above represents the NSSS capability.		
Total	1.0	13.0

* Hot—557°F RCS temperature, 2250 psia, no-load pressurizer level.

**Cold—Less than 140°F RCS temperature, 140°F in "solid" pressurizer.

Step 1: The pressurizer heaters are energized to start the heatup of the pressurizer necessary in drawing the steam bubble.

Step 2: The reactor coolant pumps are started sequentially and the pump heat is used to raise the temperature and pressure of the primary coolant loop.

Step 3: Boron dilution is then started to bring the boron concentration from its shutdown level to that required for the cold shutdown criticality condition.

Step 4: When the pressurizer temperature reaches saturation, steam formation in the pressurizer begins. The primary coolant system is maintained at 400 psig by adjusting the pressurizer heater and/or pressurizer sprays.

Step 5: At this point the shutdown bank of control rods is withdrawn and criticality is achieved. A startup rate of about 0.5 decade per minute is established, and power is increased to the level at which a heatup rate of 50°F per hour is maintained in the primary system.

Step 6: When the primary coolant temperature exceeds 400°F, steam is drawn from the steam generators to warm up the secondary plant. A vacuum is drawn in the main condensers, and some steam is put on to begin to slowly roll the turbines.

Step 7: The primary system heatup and pressurization continues until a zero load coolant temperature of about 550°F and a pressure of 2250 psia are reached. At this point the plant is in the hot standby condition, and the hot startup procedure is followed.

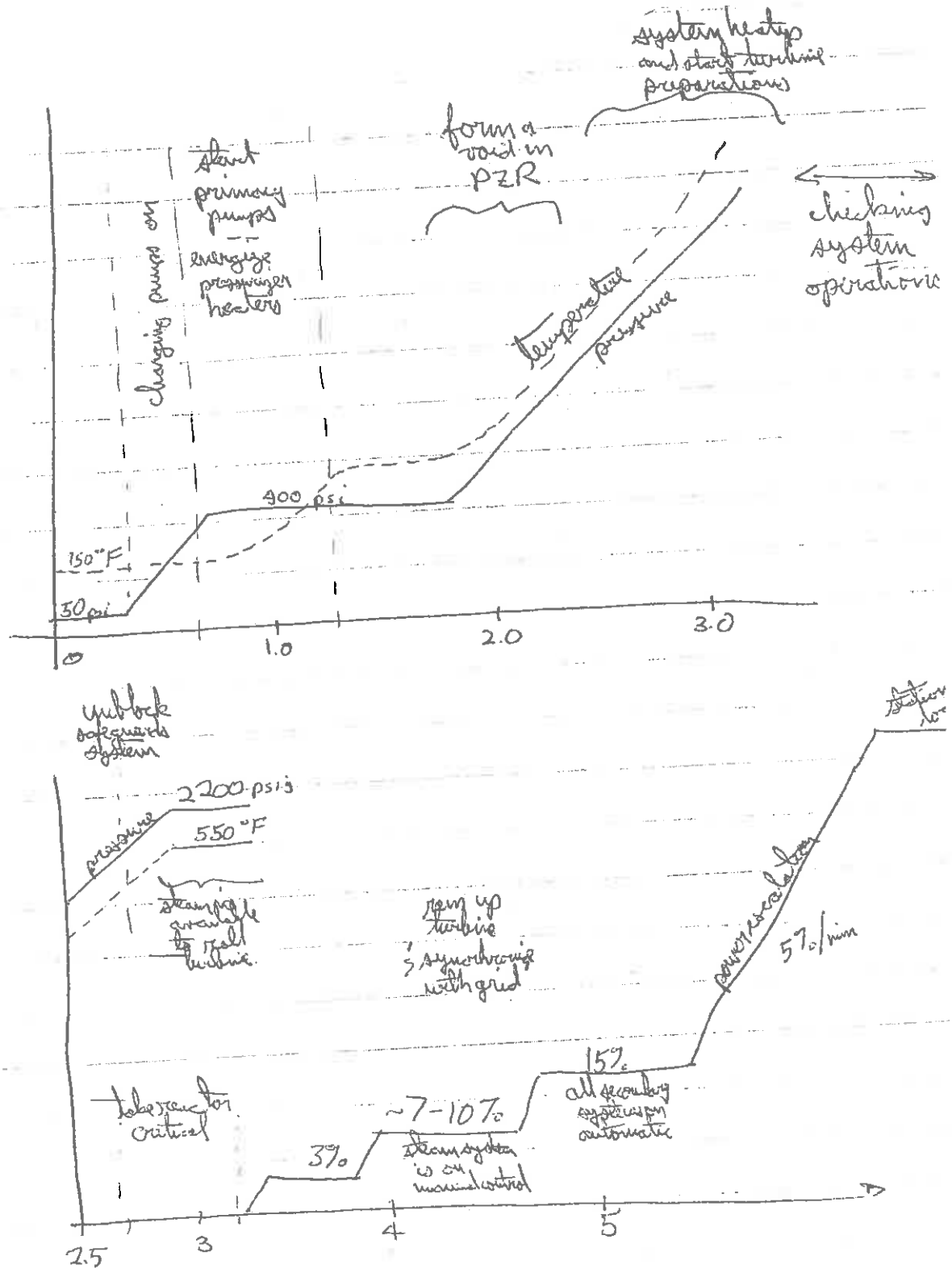
system heatup and start turbine preparations
form a void in PZR
start primary pumps
energize pressurizer heaters
charging pumps on
temperature
pressure
checking system operations
400 psi
150°F
30 psi
0
1.0
2.0
3.0
Yubbok safeguards system
2200 psig
pressure
550°F
steam available to roll turbine
ramp up turbine & synchronize with grid
power escalation
5%/min
1%
3%
~7-10%
steam system is on manual control
15%
all secondary systems on automatic
2.5
3
4
5


NOW THAT'S WHAT I CALL SLOPPY, MAN!

Step 8: The turbine-generator is brought up to synchronization speed and paralleled to the main electrical grid. The reactor is then brought manually to about 15% of full power, at which point the system is switched to automatic control and plant loading is continued to full power at a rate not exceeding 5% of full power per minute.

C. Normal Operation of Nuclear Power Reactors

By normal operation we are referring to power generation at normal system operating temperatures and pressures. In a PWR system, the operating pressure is maintained by the pressurizer control system, while the system temperatures is controlled by an automatic control system. Load changes on a nuclear power station initially appear as load demand on the turbine-generator. Small load changes can be accomodated by the natural load following capability of the NSSS. However any electrical power plant will be subjected to more dramatic variations in load. For example, a reference daily load cycle usually involves plant operation at full power for 12 hours, followed by a load reduction to approximately 50% of full power in 3 hours, remaining at 50% for 6 hours, and then returning to full power in 3 hours. Such load level changes require a corresponding change in reactivity control involving both control rod motions and chemical shim control.

For example, following a change in load demand, the reactor power level may be changed using control rod adjustment. However boron concentration adjustments will usually be made as well to compensate for slowly varying xenon concentration changes (resulting from the flux level change) and to prevent the control rods from approaching the limits of their

maneuvering band. During the last 15% of the fuel cycle, the chemical shim reserve is sufficiently low that the control rods are usually allowed to drift out of their maneuvering band to compensate for xenon reactivity changes, with some accompanying decrease in load following capability.

A very important aspect of power reactor operation is to provide the system with a capability to withstand a loss of the turbine load reactor scram. This is accomplished by controlled dumping of the turbine throttle steam either directly to the main condenser or to the main condenser and the atmosphere.

The steam dump serves as a short-term artificial load which allows the reactor to automatically cut back power without scramming. The steam dump can be controlled to reduce NSSS load as rapidly as the reactor control can reduce core power level without allowing system variables to exceed allowable operating limits.

D. Reactor Shutdown

If the plant is operating at some power level in excess of 15%, the initial shutdown step is to unload the turbogenerator. As the power output decreases to 15%, the reactor control and steam generator water level control are transferred to manual operation. The station auxiliary electrical loads are transferred from the turbogenerator to the outside source, and the turbogenerator is then completely unloaded, disconnected from the grid, and taken out of service.

The control rods are then inserted to reduce power level and place the coolant system in a hot standby condition. Steam dump may be required initially to remove residual heat.

If it is desired to take the plant to a cold shutdown state, boration of the primary coolant water is initiated to bring the boron concentration to the cold shutdown value. Steam dump is adjusted to start a cooldown rate of 50°F per hour. When the reactor coolant reaches 200°F, the secondary side of the steam generators are filled. After assuring that the boron concentration is at the proper cold shutdown value, the remainder of the control rods are inserted and unlatched. Reactor coolant pumps are run only as needed to assure uniform loop cooldown and to provide spray for pressurizer cooldown. Eventually the system is completely depressurized by letdown. The time required for complete plant cooldown is approximately 20 hours.

E. Core Refueling

Nuclear power systems differ dramatically from conventional fossile fueled plants since they must be shutdown and dismantled before refueling can commence. At the designated time of refueling, the reactor is shutdown, cooled down, and depressurized, much as described above. When the reactor coolant system pressure has been reduced sufficiently low, the system is vented, and the coolant level is lowered to a point just below the flange separating the pressure vessel and the vessel head. The control rod drive service lines and other attachments to the heat are disconnected, the control rod drives are decoupled, and the mechanisms holding the head in place are de-tensioned and removed. The pressure vessel head is then lifted from the vessel. At this time the area above the open vessel is flooded with water to provide a radiation shield. As the upper core support structure is removed, the core is exposed and refueling commences. The spent fuel assemblies of the

core are removed first and transferred to the underwater storage pool, where they will be stored for several months before they are shipped off for reprocessing. The partially spent fuel assemblies are then transferred to new locations, and the new fuel assemblies are loaded into the core.

In a similar manner, spent control rods will be replaced and necessary core maintainance will be carried out. Following refueling and maintainance, the reactor is reassembled by the reverse of the disassembly procedure.

Before the system is repressurized and brought to operating temperature, a battery of precritical tests is again performed, as well as a subsequent series of critical zero-power and low power tests. The total down time requirements for refueling presently range from one to two weeks (although the actual fuel handling time is usually much shorter--on the order of two days).

IV. SAFETY ANALYSIS OF NUCLEAR STEAM SUPPLY SYSTEMS

A. Abnormal Reactor Operations

We now turn our attention to situations in which the NSSS may be subjected to abnormal operating conditions, caused, for example, by component malfunction, operator error, or a host of other possible events which could lead to a nuclear reactor accident. Hence we enter into that mystifying, yet vitally important world of reactor safety analysis.

The principal safety problems inherent in nuclear reactor operation are not caused by the possibility of a nuclear explosion. (Such an

event is quite impossible in thermal reactors, and it requires an agile mind to concoct a sufficiently fantastic scenario to initiate such an explosion even in a fast reactor.) Rather it is the large inventory of radioactive fission products which accumulate in the reactor fuel which causes the problem. As long as these fission products remain in the fuel, they represent no hazard to people outside the plants. But should they be released and transported to populated areas, then substantial damage could occur.

Hence nuclear reactors must be designed such that under no credible--or even incredible--operating situation could such radioactive material be released from the core. To achieve this guarantee, not only must the reactor core and coolant system be carefully designed against every imagined accident situation, but as well auxiliary systems must be incorporated into the core--so-called "engineered safeguards"--to insure core integrity.

The subject of nuclear reactor safety is exceedingly complex, emmeshed in a labyrinth of complex technical, regulatory, political, philosophical, and, yes, even emotional issues. We will avoid all but the first of these topics in this chapter, since we are only concerned with illustrating those aspects of nuclear reactor analysis which arise in questions of reactor safety. In fact, we will only look at two problems--an analysis of the so-called design basis accidents for light water reactors and fast breeder reactors.

B. The Loss of Coolant Accident (LOCA) for LWR's

The design basis accident for LWR's (that is, the worst thing that could conceivably happen to a LWR) involves a rupture of the primary

coolant system in which all coolant is voided from the core. The loss of moderation immediately shuts the core down, but the residual decay heat would tend to raise the fuel and clad temperatures to their melting point, leading to clad failure and the release of fission products from the primary coolant system unless auxiliary core cooling is provided.

To be a bit more precise, let's describe the LOCA as postulated by those devious minds who dream up such scenarios to challange the sanity of reactor designers. One assumes that the reactor has been operating at full design power for some time when a double-ended fracture of the cold leg of the primary piping system occurs

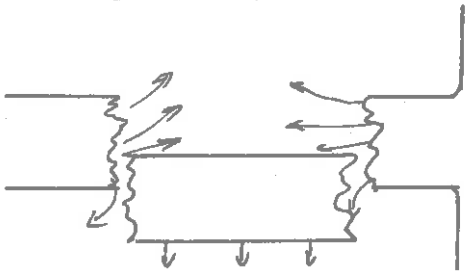

[A double-ended break is assumed to yield the most rapid voiding of coolant.] The coolant in the pressure vessel rapidly depressurizes and blows out of the rupture as a two-phase mixture. The voiding of coolant from the core is referred to as the blowdown phase. The reactor core goes subcritical as soon as significant boiling occurs, since the reduction in the mass of water corresponds to a decrease in moderation.

However, the decay heat generated in the core continues to be substantial ($\sim$5% of the operating power) and will lead to rapid fuel cladding temperature rise unless auxiliary cooling is put into effect. To this end, the NSSS is equipped with an emergency core cooling system (ECCS) to avoid fuel element failure. Both active and passive systems are used. Large tanks of borated coolant water called accummulators

are maintained at pressures lower than system pressure. In the event of a blowdown accident, the water from the accumulator discharges to the reactor system whenever the system pressure falls below the pressure of the accumulator. The operation of the accumulator is completely passive in that no separate control device is required to enable it to function.

The ECCS system also contains active systems involving low and high pressure coolant injection pumps. The high pressure injection pumps are intended to provide a source of coolant during LOCA resulting from smaller area breaks. The low pressure injection pumps are high capacity and are intended for large LOCA and to provide for long term core cooling.

A very important task of the reactor analyst is to show that following the LOCA, the fuel clad temperature is maintained below a critical limit (for Zirconium, this limit is 2300°F) by the ECCS. Since it is impractical to blowdown a full scale power reactor, such an investigation relies very heavily upon mathematical models of the thermal-hydraulic behavior of the core and ECCS.

The results of such calculations for a typical PWR LOCA are shown in a series of plots of system parameters given below:

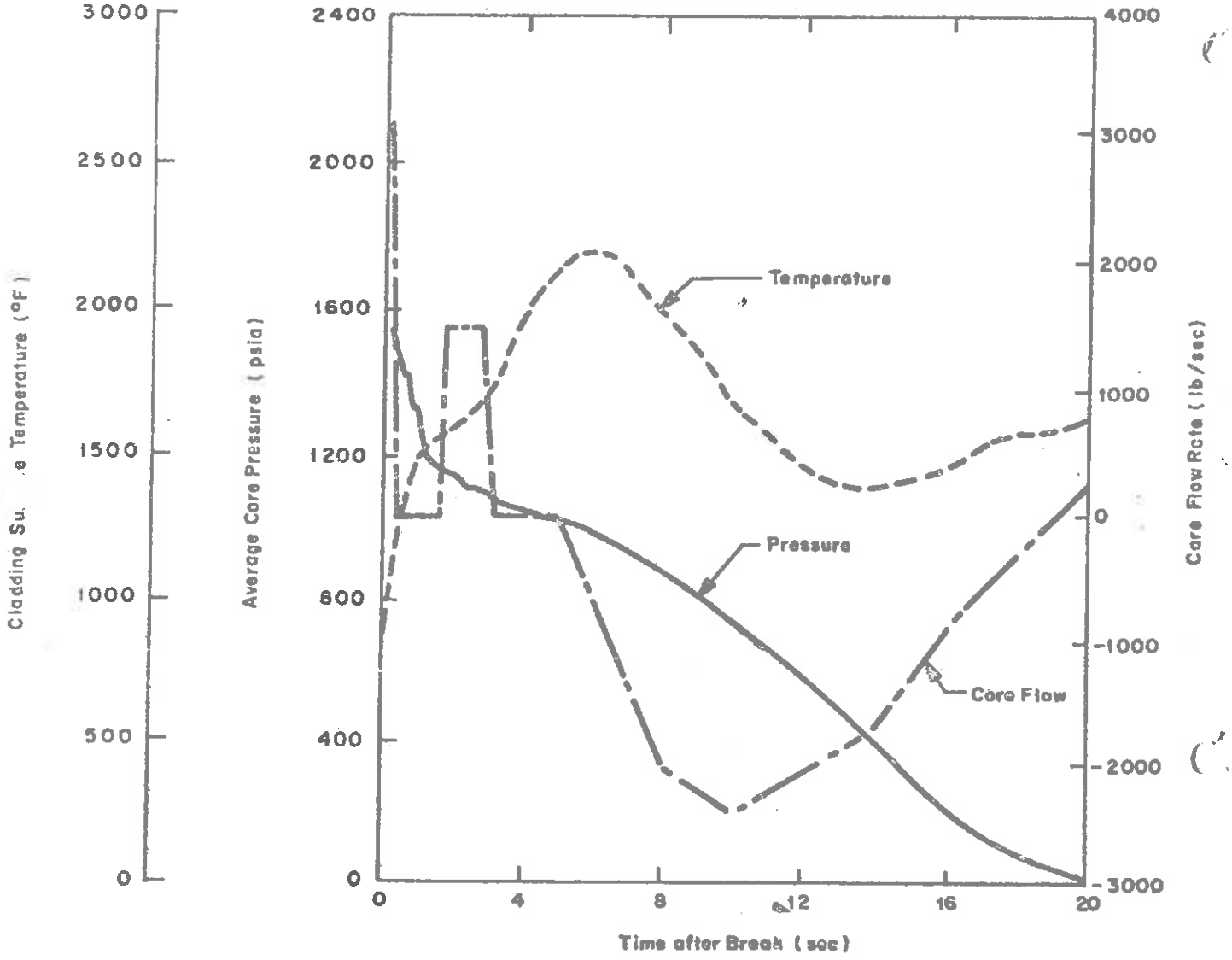

Typical Responses to LOCA for a PWR.

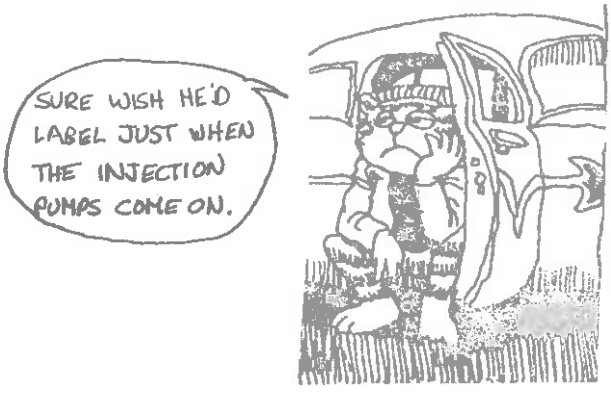

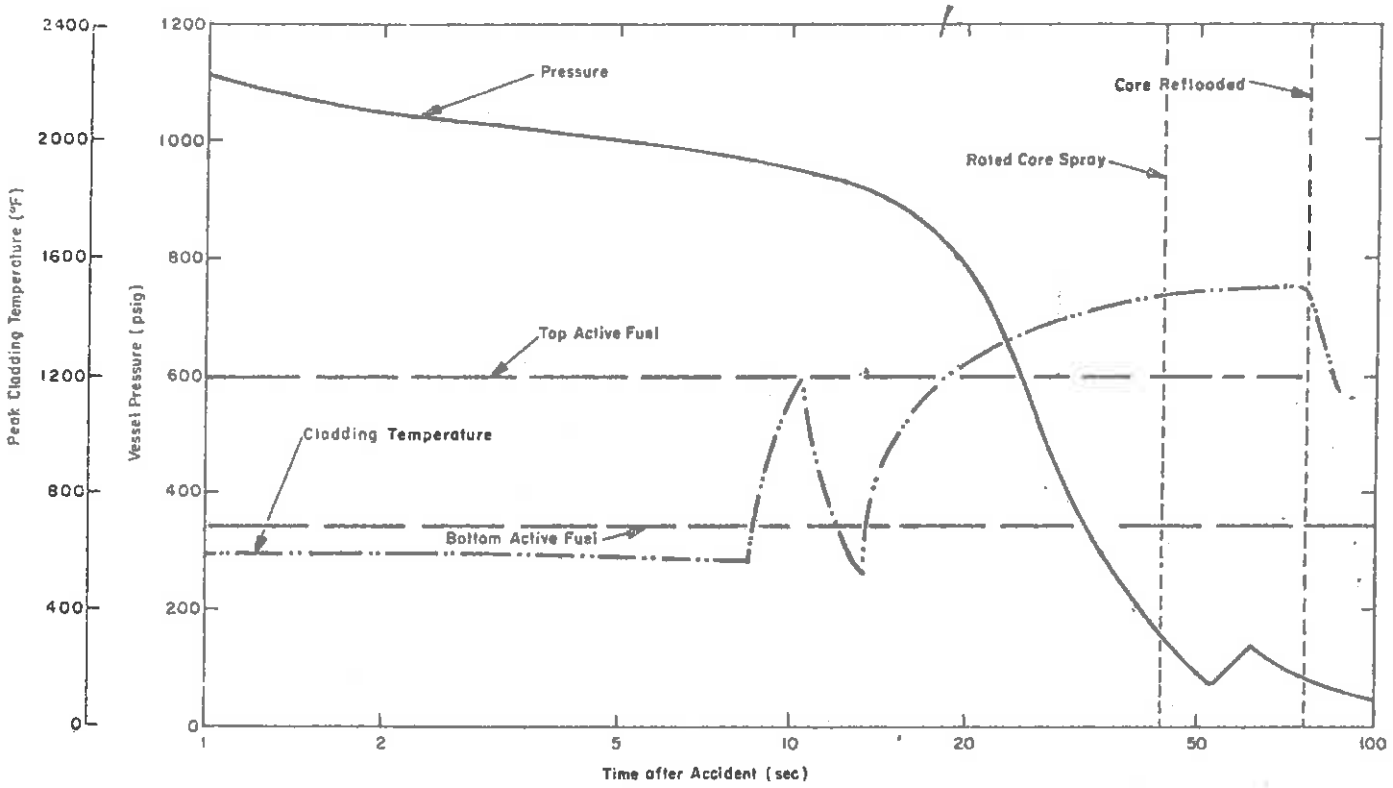

Typical Responses to LOCA Phenomena for a BWR.

C. Fast Breeder Reactor Power Excursions

We now turn our attention to a study of large power transients in fast breeder reactors such as might be experienced in a reactor accident. In these situations one usually imagines that a large reactivity in excess of prompt critical has been inserted, and then studies how the excursion is terminated by temperature shutdown mechanisms. [In this regard, one must be very careful since the point reactor model is of questionable validity for such transients.]

1. The Fuchs-Hansen Model of Reactor Excursions*

We will consider a step insertion of reactivity $\rho_0 > \beta$. Since the reactor is super-prompt-critical, we can then neglect delayed neutrons to write

$$\frac{dP}{dt} = \left[\frac{\rho(t)-\beta}{\Lambda}\right] P(t) \qquad (15\text{-}20)$$

[Here we have switched our dependent variable in the point reactor kinetics equation from the total neutron population n(t) to the reactor power P(t).] We will assume that the temperature feedback reactivity is proportional to the total <u>energy</u> (not power) generated such that

$$\rho(t) = \rho_0 - \gamma E(t) = \rho_0 - \gamma \int_0^t dt' P(t') \qquad (15\text{-}21)$$

*Bell and Glasstone, Pg. 517-522

Hence (15-21) becomes

$$\frac{dP}{dt} = P(t)\left[\alpha_0 - b\int_0^t dt' P(t')\right] \tag{15-22}$$

where $\alpha_0 \equiv \frac{\rho_0 - \beta}{\Lambda}$, $b \equiv \gamma/\Lambda$

Amazingly enough, we can solve this equation exactly to find

$$P(t) = \frac{2c^2 A e^{-ct}}{b\left[Ae^{-ct}+1\right]^2} \tag{15-23}$$

and

$$E(t) = \frac{\alpha_0 + c}{b}\left[\frac{1-e^{-ct}}{Ae^{-ct}+1}\right] \tag{15-24}$$

where $c \equiv \sqrt{\alpha_0^2 + 2b P_0}$, $A \equiv \frac{c+\alpha_0}{c-\alpha_0}$

To interpret this more easily, assume the initial power level is low such that

$$c \sim \alpha_0, \quad A \sim \frac{2\alpha_0^2}{bP_0} >> 1 \tag{15-25}$$

Then at early times, both the energy and power generated increase exponentially

$$E(t) \sim P(t) \sim e^{\alpha_0 t} \tag{15-26}$$

The power eventually reaches a maximum when

$$\frac{dP}{dt} = \frac{2\alpha^3 A}{b} \frac{e^{-\alpha t}\left[Ae^{-\alpha t} - 1\right]}{\left[Ae^{-\alpha t} + 1\right]^3} = 0$$

$$\Rightarrow Ae^{-\alpha t} = 1$$

Hence

$$t_{P_{max}} = \frac{\ln A}{\alpha} \sim \frac{\ln A}{\alpha_0} \qquad (15\text{-}27)$$

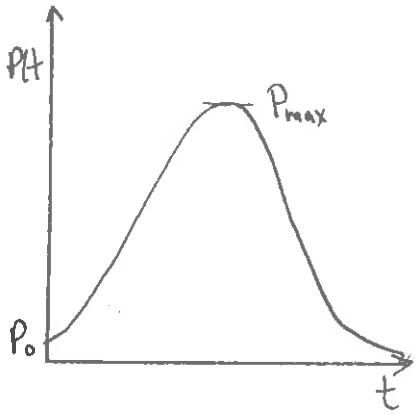

The maximum power achieved in the excursion is

$$P_{max} \sim \frac{\alpha_0^2}{2b} = \frac{(\rho_0 - \beta)^2}{2\Lambda\gamma} \qquad (15\text{-}28)$$

For long times, $P(t) \sim e^{-\alpha_0 t}$, which suggests a symmetric pulse shape. Actually the power tails off more slowly because of delayed neutrons (which have not been included in our simple model).

The total energy generated in the excursion is

$$E(t) \xrightarrow[t\to\infty]{} \frac{2\alpha_0}{b} = \frac{2(\rho_0 - \beta)}{\gamma} \qquad (15\text{-}29)$$

Note that the essential parameters are the excess reactivity $\rho_0 - \beta$ and the feedback coefficient γ. But the peak power also depends on the prompt generation time Λ. This is important, since the peak pressures, etc. in the core will depend on P_{max}. Since $\Lambda \sim 10^{-4}$ sec in thermal reactors, while $\Lambda \sim 10^{-8}$ in fast systems, we can see that the potential for a damaging power excursion is far more serious in the latter. This

analysis suggests that the reactor should have a large negative feedback coefficient to counteract this effect.

2. Analysis of Fast Reactor Accidents

As we have seen, peak powers and pressures accompanying a reactivity excursion in a fast reactor will be very much greater than in a thermal reactor. Further there is much more fissile material in a fast reactor core. Once again, the maximum credible accident for such a system involves a complete loss of coolant. The reactor will be shut down immediately, but subsequent fission product decay leads to core meltdown and reassembly in a prompt critical mass in the bottom of the pressure vessel. The parameters necessary for the analysis of such an accident include the gross core geometry, initial power level, and the rate of reactivity increase during the supercritical phase.

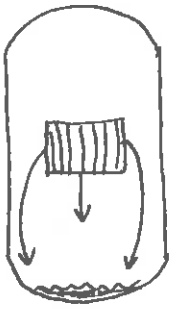

We will essentially outline the Bethe-Tait* analysis of such an accident. Assume that the collapsing core achieves prompt criticality at t = 0. Since the delayed neutrons are insignificant, we write

$$\frac{dP}{dt} = \frac{\rho - \beta}{\Lambda} P(t) \qquad (15\text{-}30)$$

*H. A. Bethe and J. H. Tait, NDA-14-170 (1957)
W. J. McCarthy and D. Okrent, in "Technology of Nuclear Reactor Safety", ed. by T. J. Thompson and J. G. Beckerly, MIT Press, 1964, Vol. I, Chapt. 10

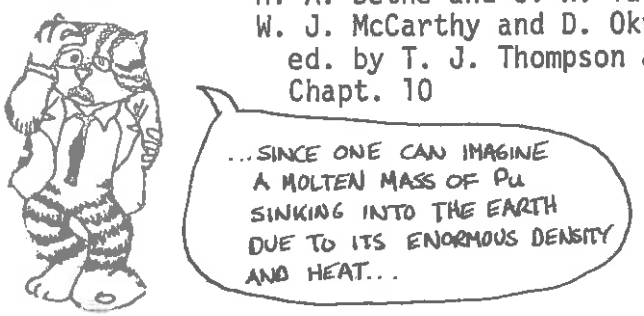

Now suppose the reactivity is increasing in a linear manner with time

$$\rho(t) = \beta + \dot{\rho}_o t \tag{15-31}$$

where $\dot{\rho}_o$ must be estimated from the model of core collapse. Then we can solve (15-30) for

$$P(t) = P(0)\, e^{\dot{\rho}_o t^2/2\Lambda} \tag{15-32}$$

Now suppose that the feedback is negligible until the total energy generated is E_1. If this energy is generated at a time t_1, then

$$\rho(t_1) = \beta + \dot{\rho}_o t_1 \Rightarrow \rho(t_1) - \beta = \dot{\rho}_o t_1 \tag{15-33}$$

where t_1 is defined by

$$E_1 = \int_0^{t_1} P(t)\,dt = P(0) \int_0^{t_1} dt\, e^{\dot{\rho}_o t^2/2\Lambda} \tag{15-34}$$

If we approximate

$$E_1 \sim \frac{P(0)\Lambda}{\dot{\rho}_o t_1} e^{\dot{\rho}_o t_1^2/2\Lambda} \tag{15-35}$$

we can solve for

$$t_1^2 \sim \frac{\Lambda}{\dot{\rho}_o}\left[\ln\left(\frac{E_1^2 \dot{\rho}_o}{P^2(0)\Lambda}\right)\right] \tag{15-36}$$

which yields

$$\rho(t_1) - \beta = \sqrt{\Lambda \dot{\rho}_o \ln\left(\frac{E_1^2 \dot{\rho}_o}{P^2(0)\Lambda}\right)} \qquad (15\text{-}37)$$

This then is the excess reactivity over prompt critical which is reached when feedback becomes significant. In some cases, $\rho(t_1) - \beta$ may range up to β .

We now must introduce the feedback. The Doppler coefficient is the only mechanism which can be relied on (one major reason for its significance in fast reactor design).

In the Bethe-Tait analysis, it is postulated that there is no feedback mechanism until an energy E = E* at which point the core material vaporizes. The vaporizing core builds up a pressure which causes the core to expand--hence decreasing reactivity and terminating the excursion (the reactor blows up). To analyze this, one must really use a coupled neutronics-hydrodynamics calculation. Typical results are

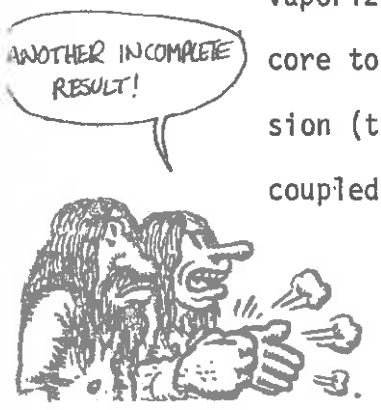

$$\left(\frac{E}{E^*} - 1\right) \sim \left[\frac{(\Delta\rho)^3 R^2}{\Lambda^2}\right]^{2/9} \qquad (15\text{-}38)$$

But

$$\frac{(\Delta\rho)^3}{\Lambda^2} \sim \frac{\dot{\rho}_o^{3/2}}{\Lambda} \qquad (15\text{-}39)$$

Thus $\dot{\rho}_o$, the reassembly reactivity rate, is the single most important factor in determining how serious a fast reactor accident might be.

When applied to the Enrico Fermi LMFBR, the Bethe-Tait analysis indicated that a uniform collapse of the core could yield an energy release of 600 Kgm of TNT (for an initial operating power level of 100 MW)--a rather sizeable amount of energy.

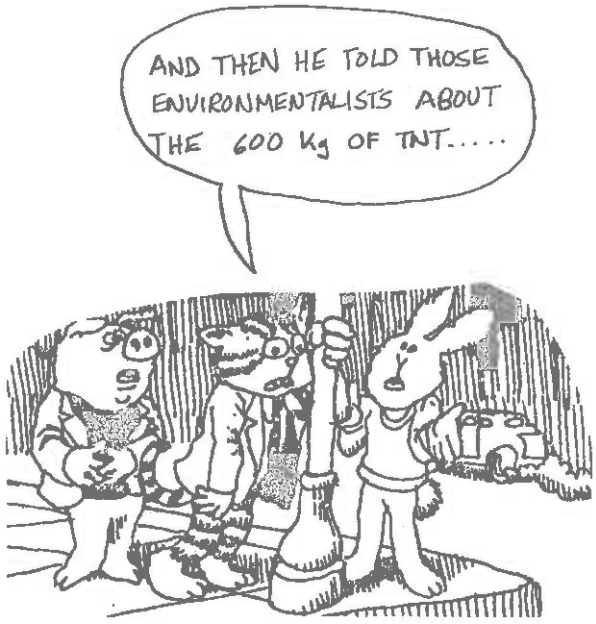

CHAPTER 16: THE NUCLEAR FUEL CYCLE AND NUCLEAR FUEL MANAGEMENT

I. THE NUCLEAR FUEL CYCLE

A. Introduction

The bulk of the nuclear power plant construction current underway in the United States is directed towards the generation of electrical power. The justification for such nuclear plants must reside in their economic advantages over more conventional sources of electrical power--e.g., fossil fuel or hydroelectric power. The cost of electrical power can be broken down into a number of factors: (i) the initial cost of constructing the power station (capital costs), (ii) the annual cost of operating and maintaining the plant, and (iii) the annual costs for the fuel. The capital investment required for the construction of nuclear power plants is presently greater than that required for conventional fossil fueled power plants. Furthermore, operating and mainte nance costs account for only a small fraction of the total cost of generating electricity. Hence any economic advantages realized by nuclear power must reside in the lower cost of its fuel.

It is important to recognize that nuclear fuels are totally different from fossil fuels, both in their processing and utilization, as well as in their costs. There are a large number of sophisticated and expensive processing operations required by the fuel before it is inserted into the reactor core. It is then "burned" in the reactor for several years before being removed. Even after several years of use in a reactor, the fuel still possesses a sizeable concentration of fissile material.

Hence it must be removed from the core, reprocessed, and refabricated into new fuel elements. The byproduct waste from the reprocessed fuel is highly radioactive and must be disposed of with considerable care.

Those operations involved in the extraction, preparation, utilization, reprocessing, and disposing of nuclear fuels are referred to as the nuclear fuel cycle. Such a cycle extends over a period of several years, and the costs associated with the nuclear fuel cycle must be monitored over this period of time. In this sense, nuclear fuel costs are much different than fossil fuel costs, since a number of charges other than direct materials costs are involved which may lead, or lag utilization of the fuel material by several years. The primary costs associated with the nuclear fuel cycle include:

1.) Costs of net isotope consumption which result from the conversion of uranium and plutonium into fission products and from the reduction in the U^{235} enrichment of the uranium remaining in the spent fuel. These costs are associated with the exploration, mining, and enrichment of the uranium.

2.) Processing costs, such as those incurred in uranium purification, conversion, fuel fabrication, and reprocessing.

3.) Financing costs associated with the large working capital requirements of the nuclear fuel cycle.

The magnitudes of each of these components can be best illustrated by considering the fuel cycle cost projection for a typical PWR (1,150 Mwe, 1975 start-up, 80% capacity factor):

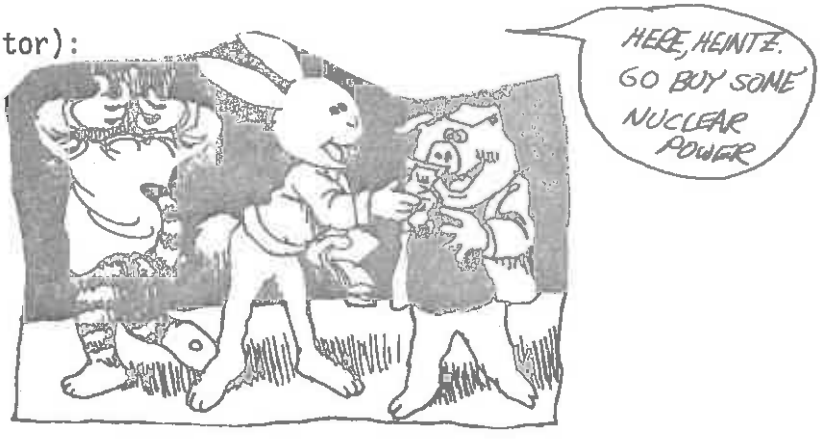

	Fuel Cost (mills/kwhr)			
	Consumption costs	Financing costs	Total	% of cost
Uranium ore (@ \$8/lb U_3O_8)	0.56	0.18	0.74	36
Conversion & enrichment	0.62	0.16	0.78	37
Fabrication (@ \$70/kg U)	0.34	0.08	0.42	20
Spent fuel shipping & rep.	0.19	-0.04	0.15	7
Pu and U credits	-0.35	0.08	-0.27	--
	1.36	0.46	1.82	100

Ref: E. A. Mason, in The Nuclear Fuel Cycle, ed. by E. M. Elliot and L. E. Weaver (U. of Oklahoma Press, 1972)

M. M. El-Wakil, Nuclear Energy Conversion (Intext, 1971), Chpt. 17
H. W. Graves, N. E. 561 notes, 1971

Such a 1,150 MWe plant would require 100 metric tons of fuel with an initial in core value of \$31 million. The annual fuel cycle bill for such a reactor is \$14.7 million. Of this, the cost of the materials consumption and processing amounts to \$11 million, and the financing costs to \$3.7 million.

Recent studies have indicated a very decided economic advantage for nuclear power generation over fossil fuel plants when fuel supply, plant performance, environmental impact, and safety are taken into account. For example, an economic projection for the period 1981-84 indicates power generation costs as tabulated below:

	Oil	Coal	Nuclear
Capital costs ($/kw)	389	588	702
Fuel costs (mills/kwhr)	15.0	9.2	3.1
Power generation costs (mills/kwhr)	27.3	25.5	21.3 (single unit) 20.3 (dual unit)

(These costs are given in 1973 dollars.) The fossil fuel plants were rated at dual 800 MWe units (selected as the optimum size for present fossil-fueled plants), while a single 1150 MWe unit was considered for the nuclear plant.

These figures indicate the sharp contrast in fuel costs between fossil fuel and nuclear power generation. For example, in a coal fired plant, fuel costs represent 36% of power generation costs, while capital costs account for some 56% of these costs. For a nuclear plant, fuel costs account for only 14% of power generation costs, while capital costs account for 79%. Such figures certainly bear out our contention that the primary economic advantage enjoyed by nuclear power generation is in its very low fuel costs.

It should be remarked that there will be a tendency for even nuclear and fossil-fuel plant capital costs to become more comparable, not because nuclear plant costs will decrease, but rather because of the rising costs of plant construction of all types. Furthermore, operating experience has indicated that nuclear plants perform with a higher degree of reliability than comparable sized fossil plants.

The principal disadvantage of nuclear plants rests with the complicated licensing procedure necessary for plant construction and operation which tends to increase the construction period of such plants over those of fossil plants (presently, some 8 years from order to on-line power production, as opposed to 4-5 years for a coal fired plant). However, as the licensing procedure is streamlined, even this disadvantage is expected to disappear.

B. An Overview of the Nuclear Fuel Cycle

The various steps in obtaining, processing, using, and disposing of nuclear fuel are shown schematically below.[1] These steps include:

1. Mining: Both underground and open pit techniques are used to mine uranium ore in a manner similar to that used in other low grade ore mining. The ore obtained from mines in this country average about 0.25% uranium oxide (U_3O_8).

2. Concentration: Milling is necessary to extract uranium from the raw ore. The ore is pulverized and leached with sulfuric acid to dissolve the U_3O_8. One then uses solvent extraction or ion exchange to recover the dissolved U_3O_8. Calcination (roasting) is then performed to produce yellow cake, a crude oxide containing some 70-90% U_3O_8. Yellow cake is the form of uranium most commonly traded in commodity markets. Further calcination and solvent extraction is used to refine the yellow cake to essentially pure UO_3.

3. Conversion: Hydrogenation is first used to convert UO_3 to UO_2. Then reacting UO_2 with hydrogen fluoride produces UF_4 which can

---

[1] E. A. Mason, ibid

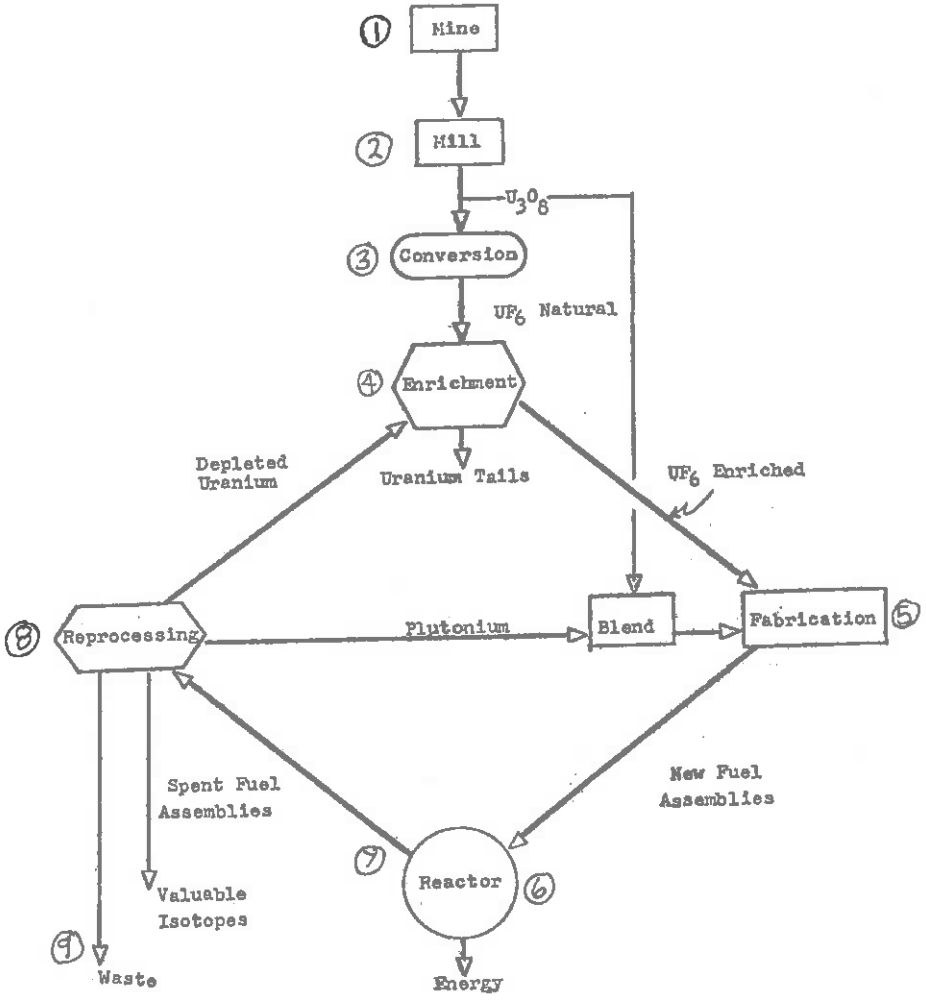

Fuel Cycle Flow Diagram

URANIUM REQUIREMENTS FOR A 1000 MWe PWR

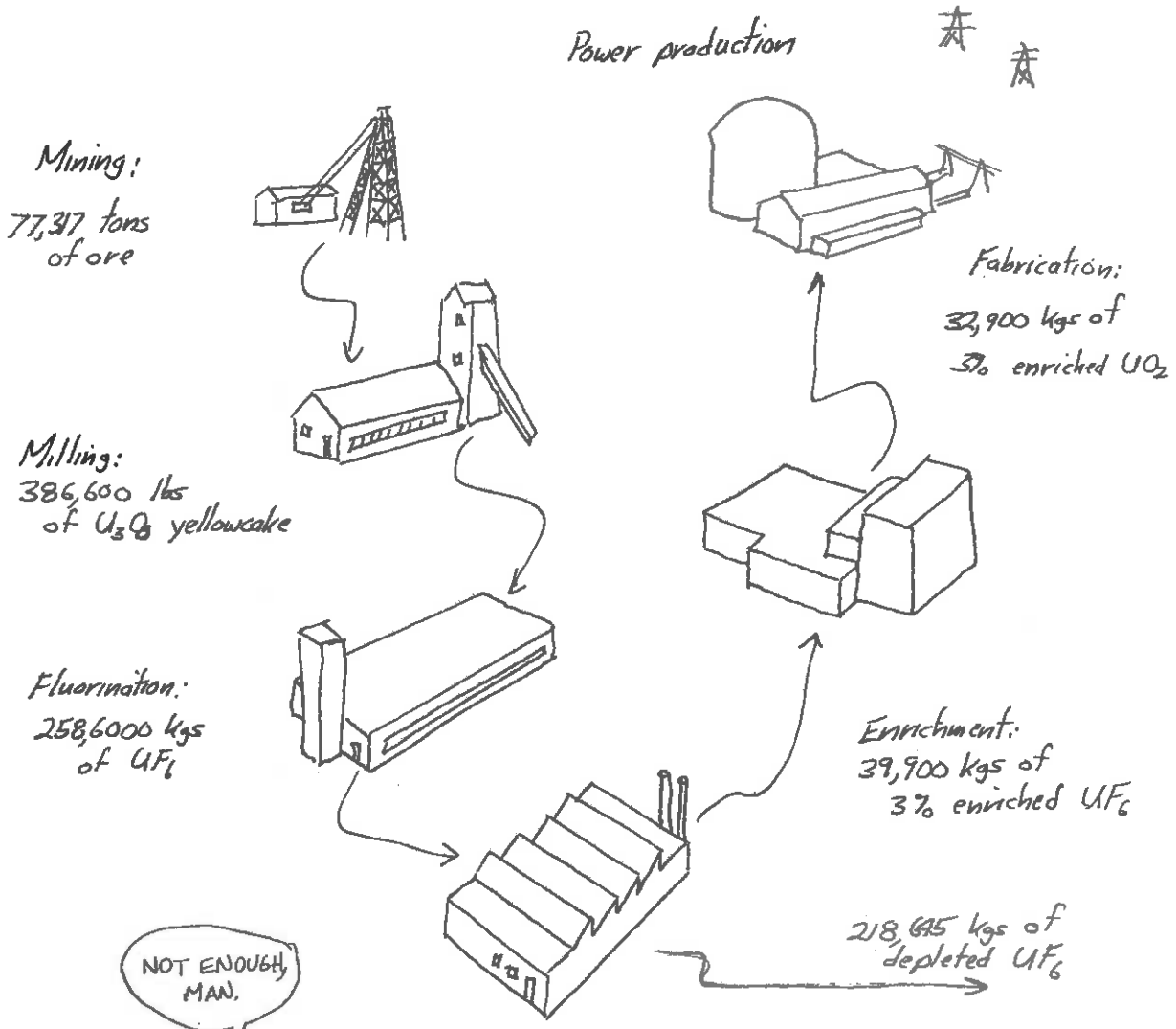

then be converted into uranium hexafluoride, UF_6, by adding fluorine salt.

4. Enrichment: Essentially all power reactors (with the exception of heavy-water reactors or the early gas-cooled, graphite moderated reactors) utilize enrichment uranium, that is, uranium with higher than the natural 0.7% concentration of U^{235} (at least in their initial core loading). The enrichment of uranium is a very difficult and expensive process since it involves separating two isotopes, U^{235} and U^{238}, with very little mass difference and essentially no chemical difference. A variety of separation techniques have been used or proposed:

   (i) electromagnetic separation: essentially using huge mass spectrometers

   (ii) gaseous diffusion: since the diffusion coefficient for a gas to pass through a porous membrane is inversely proportional to the square-root of its mass, one can pass the UF_6 gas through hundreds of porous barriers to separate the UF_6 (U^{235}) from the UF_6 (U^{238}).

   (iii) ultracentrifuges: simply very high speed centrifuges used to separate the two isotopic forms of UF_6.

   (iv) laser excitation: Of more recent consideration are schemes which use high powered lasers to selectively excite UF_6 (U^{235}) by tuning the laser wavelength to select out the isotopic mass shift in the electronic energy levels of the compounds. Then standard chemical separation techniques can be used to skim off the excited compound.

The gaseous diffusion method has been the primary technique used for uranium enrichment for the past 20 years. Recently, however, developments in ultracentrifuge design have suggested that these latter methods may, in fact, be superior to gaseous diffusion techniques. Most recently, advances in the development of high-powered tunable lasers has given rise to a large scale research effort in laser separation techniques.

(5.) Fabrication: Following enrichment, the UF_6 is then chemically converted into the form to be used in the fuel element. This is usually a ceramic such as UO_2 or UC. The resulting ceramic powder is then compacted (and sintered) into small pellets, which are then loaded into metallic tubes (the clad) or into the fuel matrix (as in the HTGR).

(6.) Fuel Burnup in the Reactor Core: The fuel assemblies are loaded into the reactor core for power production. These assemblies are typically irradiated in the core for a period of several years. The fuel burnup or lifetime can be limited by either reactivity considerations (i.e., the multiplication of the core drops too low for further power production) or by limitations of materials' stability under high radiation fluences. It is usually the latter limitation which determines the lifetime of fuel in today's high-burnup designed cores.

(7.) Spent Fuel Storage and Decay: After being irradiated in the core, the fuel is intensely radioactive due to fission product buildup. The used or spent fuel is removed from the core and stored in water pools for several months to allow the short-lived fission products to decay out.

8. Reprocessing: The spent fuel is then shipped to reprocessing facilities to reclaim unused uranium (which can then be recycled back as UF_6 for conversion or re-enrichment) and plutonium.

9. Waste Disposal: The radioactive waste products remaining after reprocessing are then converted into either liquid or solid forms for storage and are shipped to various depositories for burial (and survelliance).

The above outline is a description of only the uranium-plutonium fuel cycle used in most modern power reactors. However, other possible fuel cycles have been considered for future reactors, such as the thorium-U^{233} cycle proposed for HTGR operation. We will discuss these cycles in more detail in the next section.

The management of the various activities involved in obtaining, irradiating, and disposing of fuel materials is referred to as nuclear fuel management and is a principal concern of nuclear engineering. Such activities must be performed subject to several very important constraints. Of course, one desires to minimize electrical generation costs. But one must also insure that the safety of the reactor is not compromised--e.g., the fuel temperature must always be kept below melting, the control margin must be maintained within safe limits, and so on.

The management of the processes involved in the nuclear fuel cycle can be decomposed into three types of activities:

(i) head-end fuel management: mining, conversion, enrichment, fuel fabrication

(ii) in-core fuel management: evaluation of reactivity and control requirements, power distribution analysis, core capability evaluation

(iii) tail-end fuel management: fuel storage, shipping, reprocessing, waste disposal

We will consider each of these activities in some detail in later sections of this chapter. However, it is first useful to consider in more detail the various fuel cycles of interest in power reactor operation.

C. Power Reactor Fuel Cycles

1. Light Water Reactors

The fuel cycle for a typical light water reactor of the 1,000 MWe class is diagrammed below. We recall that such reactors are fueled with enriched uranium (from 2-3%) in oxide form (UO_2). The spent fuel is

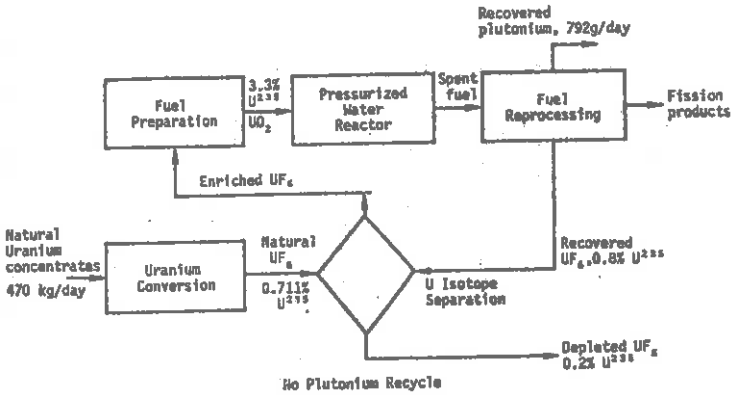

discharged from the core with a U^{235} concentration of roughly .8%. The conversion of U^{238} has resulted in a plutonium concentration of about the same magnitude. This plutonium is recovered by fuel reprocessing.

At the present time, the plutonium recovered from spent fuel elements is simply stockpiled. However, there is strong incentive to recycle the plutonium back into the light water fuel cycle, as shown in the diagram below. This would reduce the requirement for uranium by approximately one third. There are several technical problems involved in plutonium recycling, including the complications of fabricating plutonium (a very toxic and radioactive material) and matching the nuclear performance of a mixed oxide fuel (PuO_2 and UO_2) with enriched uranium fuel in a core. Such problems do not seem formidable, however, and the large inventory of plutonium which is beginning to accumulate from the existing generation of large power reactors (coupled with the lagging commercial development of the fast breeder reactor, which would provide an alternative market for this plutonium) provide strong incentives for implementing plutonium recycle.

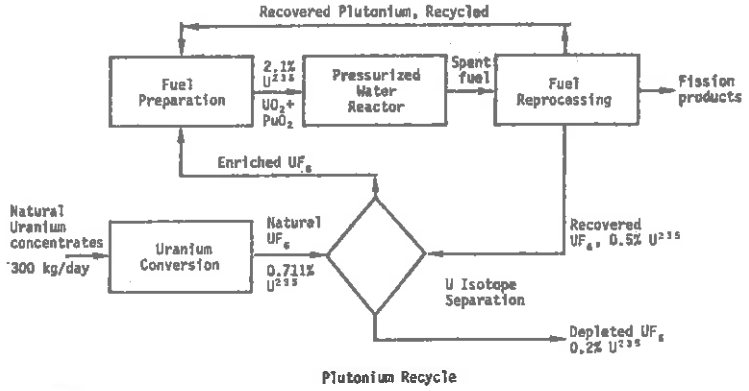

Plutonium Recycle

2. HTGR Fuel Cycles

The fuel cycle of the HTGR is quite different than that of light water reactors since it is based upon a thorium-U^{233} conversion cycle. As the fuel cycle diagram below indicates, the initial loading of the HTGR core is with highly enriched uranium ($\sim$ 93% U^{235}) in the form of uranium carbide mixed with thorium oxide or carbide as the fertile material. The thorium is then converted to U^{233}, which is recovered and cycled back (eventually) to be mixed into reload fuel.

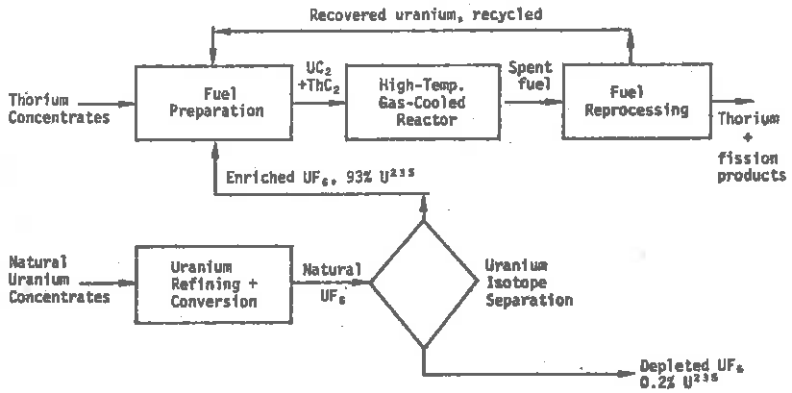

High-Temperature Gas-Cooled Reactor

The motivation behind using such a fuel cycle is primarily due to nuclear considerations. The number of neutrons per neutron absorbed in U^{233} is some 10% larger than that characterizing U^{235}. Hence it is possible to achieve much higher conversion ratios using U^{233} (indeed, such "advanced converter" reactors are capable of operating with a conversion ratio very close to unity). The higher core temperature of the HTGR favors the use of U^{233} over Pu^{239} as a reload fuel, since η^{49} tends to decrease with increasing core temperature.

As we have seen, the fuel design of the HTGR is much different than that of either the LWR or the LMFBR in order to facilitate high temperature operation. The fuel composition is of small pellets of UC or ThO_2 coated with graphite and loaded into graphite blocks. Such a fuel design leads to much higher fabrication costs however, and hence the fuel elements of an HTGR must be run to much higher burnups (some 80,000 MWD/MTU as compared to 30,000 MWD/MTU for a LWR or 100,000 MWD/MTU for the LMFBR).

The higher conversion ratio of the HTGR leads to a more efficient utilization of uranium. In fact, an HTGR requires only about half the fuel feed U_3O_8 of an LWR of similar rating.

3. LMFBR Fuel Cycles

The fuel cycle of the fast breeder reactor differs from that of the LWR and HTGR in that the larger conversion ratio allows a net gain in the amount of fissile material produced during core operation. It is estimated that the LMFBR can utilize some 60 to 70% of the energy available in natural uranium (taking account of the transmutation of U^{238} to Pu^{239}). The more efficient utilization of available fuel resources is the primary justification for the LMFBR, although there are side

benefits such as higher coolant temperatures (and hence lower waste heat release).

A typical fuel cycle for the LMFBR is sketched below, in which it is recognized that most of the transmutation of U^{238} into Pu^{239} will occur in the blanket, while the fuel burnup and power production will occur in the core. The LMFBR can be fueled either with natural uranium or depleted uranium from the tails of the isotope separation plants.

4. Interaction Among Fuel Cycles

It should be recognized that there will be a very substantial interaction among these various fuel cycles in a mature nuclear power industry. For example, the substantial amounts of plutonium produced by LWR's can either be directly recycled or can be used to fuel the first generation of fast breeder reactors. Similarly, the excess plutonium produced by the LMFBR can be used to fuel either future LMFBR's, or it can be fed back into the LWR fuel stream.

There will also be strong interaction with the fuel cycle of "advanced converter reactors" such as the HTGR, which can be used to greatly stretch out the usefulness of available fuel, without, however, having to carry the high fissile fuel inventory of true fast breeders (since the relatively dilute fuel of the HTGR's can be run at around twice the fissile rating typical of fast breeder reactors).

Such interactions will determine to a very large degree the cost of the nuclear fuel cycle, since they not only influence the cost of the fresh fuel loading, but as well determine the value of the spent fuel (i.e., the value of the plutonium produced in the core). Such

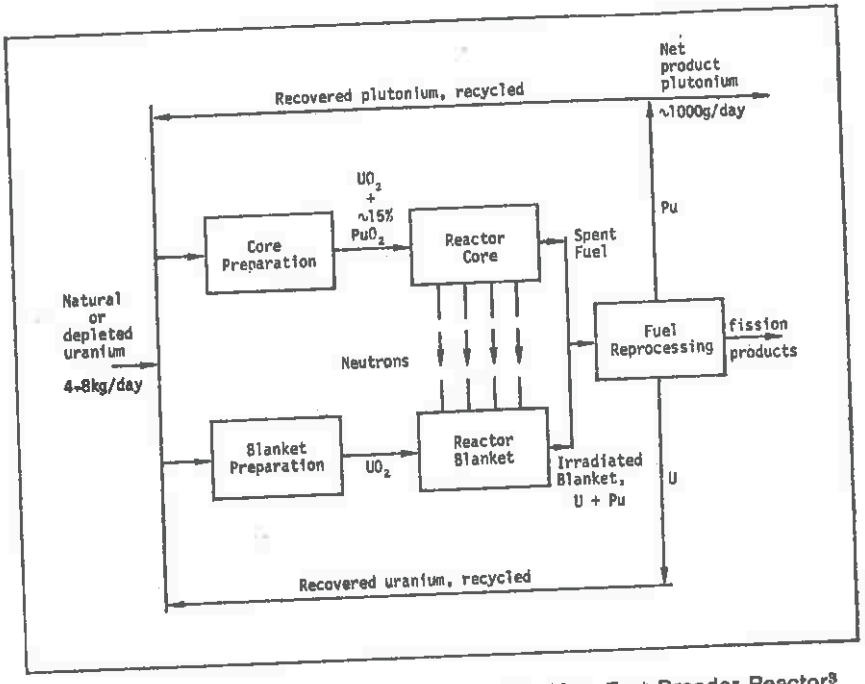

Fuel Processing Flow Sheet for 1,000 Mwe Fast Breeder Reactor[3]

interactions are quite complicated and no doubt will lead to even more uncertainty in the future fuel costs of nuclear power reactors.

Nevertheless, some idea of the comparison between the fuel costs of the various reactor types can be gained by the rough figures indicated in the Table below:

Costs (mills/kwhr)	1975	Potential (1980-2000)		
	LWR	LWR	HTGR	LMFBR
Investment	4.0-4.8	3.0-3.6	2.7-3.3	3.2-3.8
Fuel	1.7-1.9	1.4-1.6	1.0-1.2	0.6-0.8
Operating & maintenance	0.3	0.3	0.3	0.3
	6.0-7.0	4.7-5.5	4.0-4.8	4.1-4.5

It is apparent from these figures that the real incentive for developing new types of reactors such as the LMFBR is based almost entirely upon expected improvements in the economics of their fuel cycles, rather than changes in their capital costs of operating costs.

II. HEAD END FUEL MANAGEMENT

A. Mining and Milling

Most of the uranium ore mined in the United States comes from the Colorado Plateau area and yields about 0.1% to 1% U_3O_8 (in contrast to the pitchblende deposits found in Canada, Czechoslovakia, and the Congo which can yield up to 20% U_3O_8). The exploration for and development of new uranium reserves has been closely geared to demand. The uranium mining industry grew very rapidly during the 1950's in response

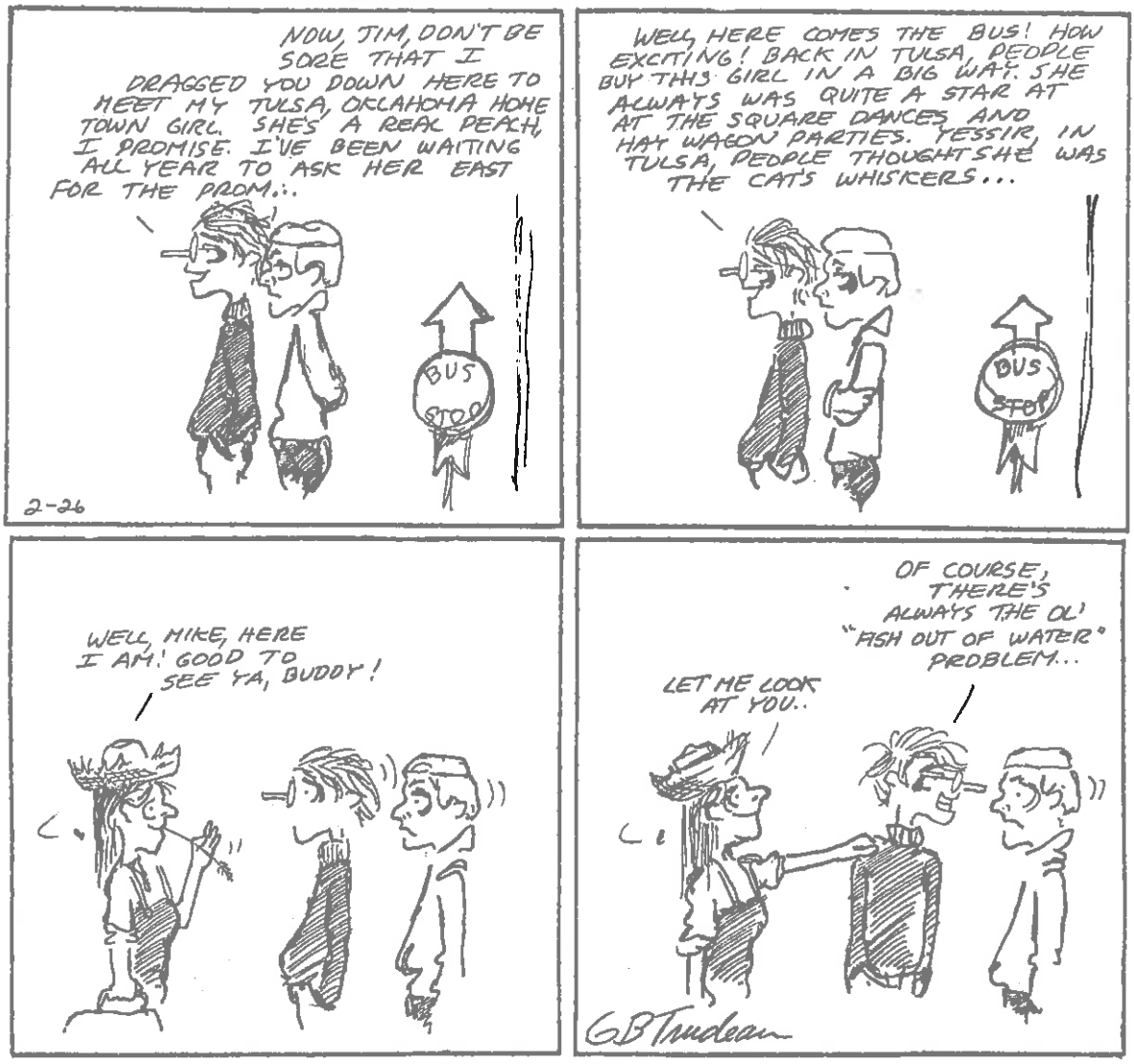
NOW, JIM, DON'T BE SORE THAT I DRAGGED YOU DOWN HERE TO MEET MY TULSA, OKLAHOMA HOME TOWN GIRL. SHE'S A REAL PEACH, I PROMISE. I'VE BEEN WAITING ALL YEAR TO ASK HER EAST FOR THE PROM...
BUS STOP
2-26
WELL, HERE COMES THE BUS! HOW EXCITING! BACK IN TULSA, PEOPLE BUY THIS GIRL IN A BIG WAY. SHE ALWAYS WAS QUITE A STAR AT THE SQUARE DANCES AND HAY WAGON PARTIES. YESSIR, IN TULSA, PEOPLE THOUGHT SHE WAS THE CAT'S WHISKERS...
BUS STOP
WELL, MIKE, HERE I AM! GOOD TO SEE YA, BUDDY!
LET ME LOOK AT YOU..
OF COURSE, THERE'S ALWAYS THE OL' "FISH OUT OF WATER" PROBLEM..
GBTrudeau

to the military requirements for fissionable material. But the cutback in government requirements for uranium in the mid-1960's, accompanied by the lagging development of commercial power reactors, caused a corresponding leveling off in uranium production which is only now beginning to pick up again as the demands of the nuclear power industry become more apparent. Present estimates are that some 600,000 tons of U_3O_8 are available at a cost of under $10/lb. Domestic resources are being discovered at such a rate that low cost uranium ($8-$12/lb) should be available to meet nuclear power requirements at least into the mid-1980's. Although present production levels are roughly 16,000 tons of U_3O_8 per year, future industry requirements are expected to reach the level of 35,000 tons per year by 1980, hence requiring a buildup in uranium mining and processing capability. It should be emphasized, however, that the exploration for and development of uranium resources, like most other metals, will never be more than a few years in advance of production because such advanced development is costly, risky, and uneconomical for the producer. To compound this uncertainty is the artificial price structure of uranium ore set by the earlier government demand for and control over fissionable material. For the first time in history, a metal has become a source of energy, and this in itself has led to added uncertainty in the metals commodity market. It is becoming increasingly apparent that utilities must plan very carefully to insure adequate uranium supplies over the 30 year operating lifetime of a nuclear power plant.

Much of the technology involved in the exploration and production of uranium has been adopted from other mineral industries. Uranium, however, has one characteristic not common to other metals--radioactivity. This

characteristic has created the possibility of novel approaches for the exploration for uranium--but has also created new problems for mining, milling, and waste disposal (a la Grand Junction).

The mining techniques used include both underground and open pit mining, the choice depending on the depth, size of the ore body, assay, and type of rock formation in which the ore is found. One usually exploits surface or shallow deposits first, using underground techniques only for deeper deposits.

Mills are located near the mines for concentrating the uranium ore (and thereby reducing transportation costs associated with shipping the ore to facilities where further processing is performed). The mined ore is first milled or crushed to a sugar-like consistency. Water is added in the last crushing step to create a slurry. The uranium in this slurry is then extracted by a process known as solvent extraction. First the slurry is pumped to large tanks where sulfuric or nitric acid is added until all the uranium present in the ore is dissolved. The sand or tailings is physically separated by either centrifugal means or rake-type classifiers. The U_3O_8 is then extracted from the solvent by adding ammonia and air and heating the mixture to precipitate out the U_3O_8. The slurry from the settling tanks is then dried to calcinated to produce "yellowcake", a crude oxide or salad concentrate assaying some 70-90% U_3O_8. As we mentioned earlier, it is this yellowcake which is regarded as the commodity which is traded as uranium ore. A diagram of the various mining and milling processes is sketched below:

MINING AND MILLING

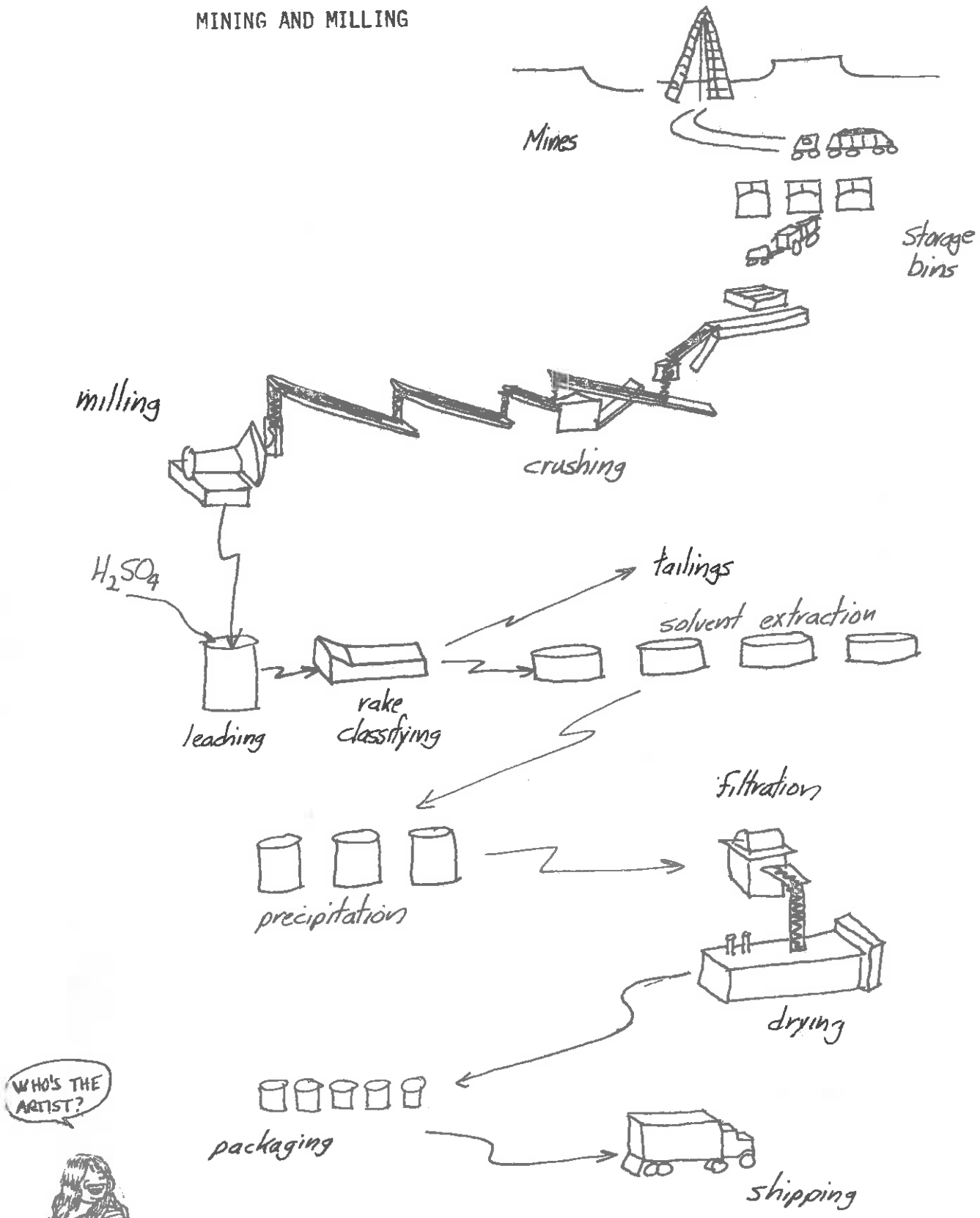

B. Conversion

Most modern power reactors (with the exception of heavy water reactors) utilize uranium in which the concentration of U^{235} has been enriched above its natural value of 0.7%. In order to achieve the enrichment of natural uranium, one must first convert the uranium compound to a gaseous form. A diagram of this process, known as conversion, is shown below

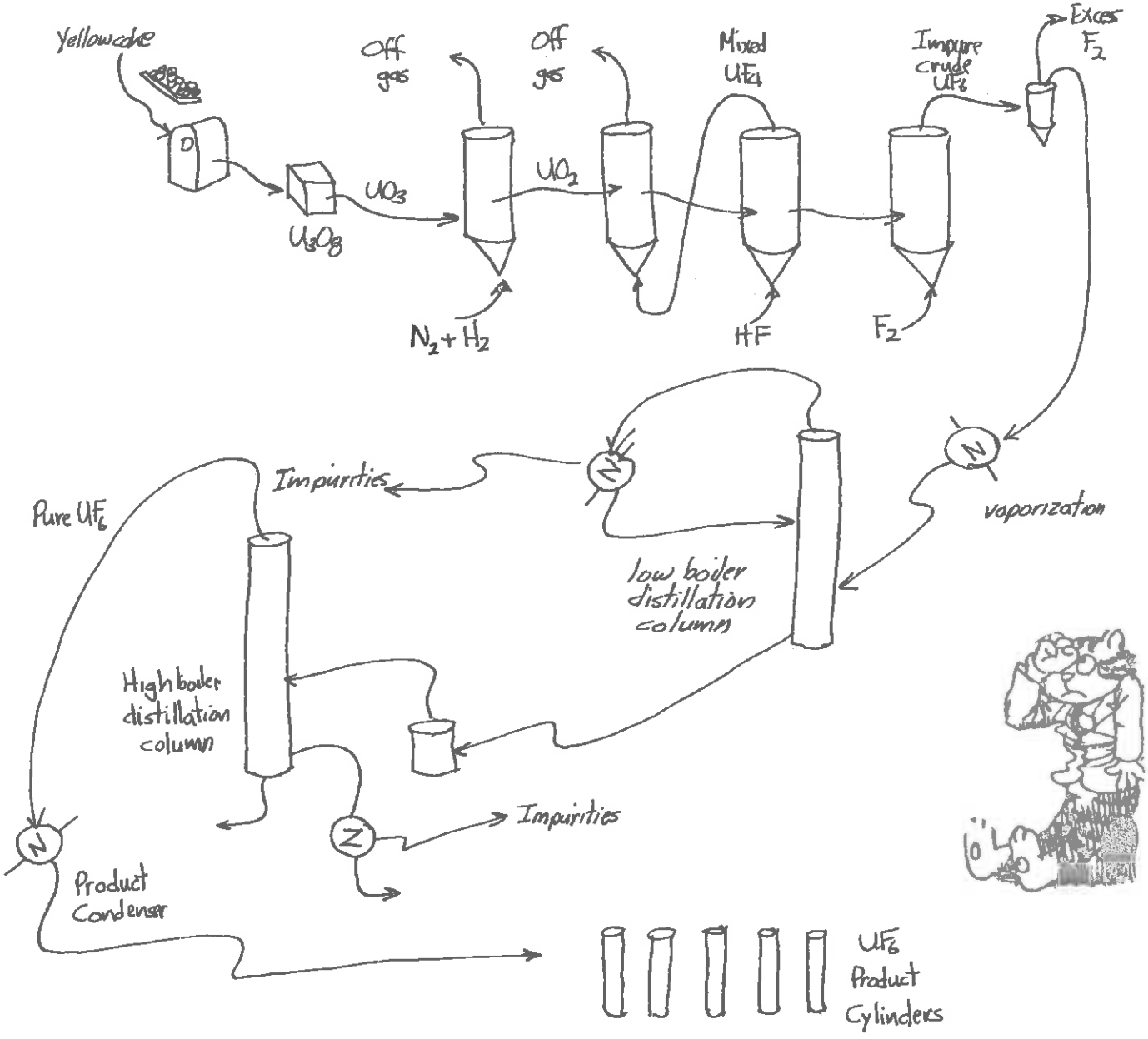

In it, yellow cake (U_3O_8) is converted to uranium hexafluoride (UF_6) using either the dry fluoride volatility process or the refining fluorination process. Although UF_6 is a solid under STP conditions, at somewhat higher temperatures or lower pressures it becomes a gas. The purity of the UF_6 produced in the conversion process is exceptional--about 99.97%.

C. Enrichment

An essential step of the nuclear fuel cycle is the enrichment of uranium from its natural concentration of 0.7% U^{235} to the higher concentrations required in modern power reactor fuels (e.g., 2-3% for LWR, 90% for HTGR). In the two principal processes in use today, gaseous diffusion and ultracentrifuge techniques, this separation is achieved by utilizing the small mass difference between the two isotopic forms of UF_6 to separate the uranium isotopes. Since this mass difference is very small, the amount of separation which can be achieved in a given device is similarly quite small. Hence to achieve appreciable separation, a large number of separation devices must be arranged in series or "cascades". Such a separation operation is extremely expensive, accounting for some 30% of the total fuel cycle costs. The facilities necessary for the separation process require an enormous capital investment and have been the responsibility of the federal government until very recently. (Although private enterprise is being strongly encouraged to move into the nuclear fuel enrichment area.) In this section, we will examine three alternative methods for uranium enrichment: gaseous diffusion, ultracentrifuges, and laser separation. The fourth technique, electromagnetic separation, has not been utilized since the

days of the Manhattan Project. The dominant technique utilized today is gaseous diffusion, although there is substantial activity and hope for the ultracentrifuge techniques. We have also included a brief discussion of a rather novel new approach, laser isotope separation, because of its potential for future applications.

1. Gaseous Diffusion

The gaseous diffusion separation rate utilizes the difference in the rates at which gases of different molecular weights diffuse through a porous membrane. Consider a mixture of two gases of molecular weights m_1 and m_2 confined in a container with a porous wall. If both gases are maintained at the same temperature and pressure, then the lighter gas molecules in the mixture move more rapidly (since $\langle v \rangle \sim \sqrt{3kT/m}$) and hence strike the porous wall more frequently, thereby escaping the container at a more rapid rate.

Since the rate of diffusion is universely proportional to the square root of the molecular weight, it is apparent that the best separation that can be achieved by diffusion through a single membrane is

$$\alpha = \sqrt{\frac{m_2}{m_1}} = \sqrt{\frac{\text{mass}(U^{238}F_6)}{\text{mass}(U^{235}F_6)}} = \sqrt{\frac{352}{349}} = 1.0043$$

[Here, α is termed the "separation factor" for the process.] It is evident that since the enrichment per stage is very small, a large number of stages in series or cascade is required to produce significant enrichment. For example, the production of 4% enrichment from natural uranium requires about 1,500 stages in cascade.

The effort involved in separating isotopes is referred to as separative work and is measured in "separative work units" (SWU) such as those tabulated below:

ENRICHED URANIUM DATA

Enrichment	Kg Natural U Feed Material to Diffusion Plant	Lbs. U_3O_8 to be Purchased*	Equivalent Units of Separative Work†
% Weight U-235	Per Kg of Enriched Uranium Product		
Nat. 0.711	1.000	2.613	0.000
0.8	1.174	3.068	0.104
0.9	1.370	3.580	0.236
1.0	1.566	4.092	0.380
1.2	1.957	5.114	0.698
1.4	2.348	6.136	1.045
1.6	2.740	7.160	1.413
1.8	3.131	8.182	1.797
2.0	3.523	9.206	2.194
2.1	3.718	9.716	2.397
2.2	3.914	10.228	2.602
2.3	4.110	10.740	2.809
2.4	4.305	11.250	3.018
2.5	4.501	11.762	3.229
2.6	4.697	12.274	3.441
2.7	4.892	12.784	3.656
2.8	5.088	13.296	3.871
2.9	5.284	13.808	4.088
3.0	5.479	14.318	4.306
3.1	5.675	14.830	4.526
3.2	5.871	15.342	4.746
3.3	6.067	15.854	4.968
3.4	6.262	16.364	5.191
3.5	6.458	16.876	5.414
3.6	6.654	17.388	5.638
3.7	6.849	17.898	5.864
3.8	7.045	18.410	6.090
3.9	7.241	18.922	6.316
4.0	7.436	19.432	6.544

*0.5% U_3O_8 to UF_6 conversion losses included
†Tails assay at 0.2% weight U-235

The separative work required for enrichment is proportional to both the flow rate through the separative device, and to $(\alpha - 1)^2$. Evidently, if the separation factor α is close to unity (e.g., $\alpha = 1.0043$), then the flow rate must be large to achieve appreciable enrichment.

The basic separation stage in a gaseous diffusion plant is shown schematically below:

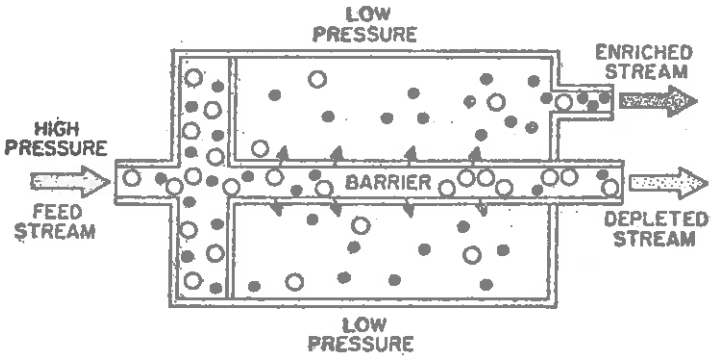

High pressure UF_6 is fed into tubes made of the porous barrier material. The UF_6 diffusing through these barriers is slightly enriched (< 1.00429) due to the difference in isotopic diffusion rates. This slightly enriched UF_6 is drawn off at lower pressure, while the remaining material (which is now slightly depleted of the U^{235} isotope) is drawn off from the end.

It is apparent that the separation stage must contain three components:

(i) the barriers themselves (the converter)

(ii) a compressor to maintain the pressure differential across the barriers

(iii) a heat exchanger to remove the heat of compression

Such a separation stage is shown below:

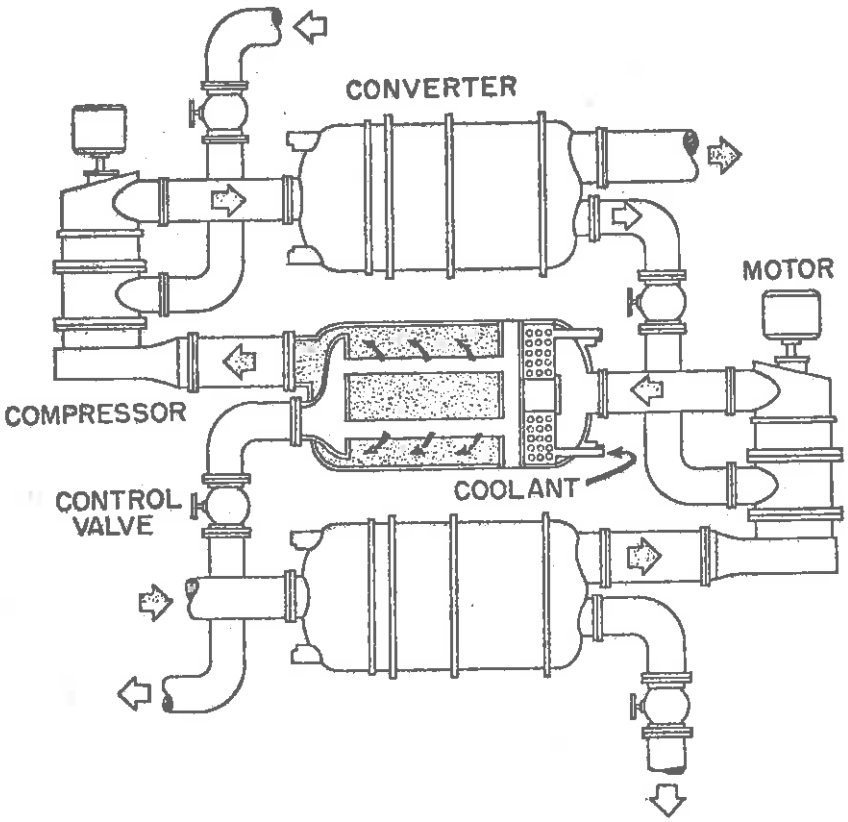

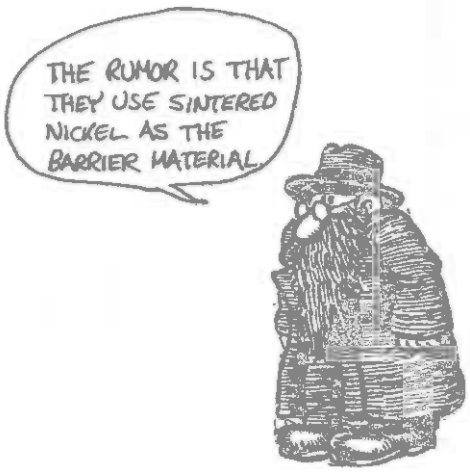

These stages are coupled together into a cascade as shown below:

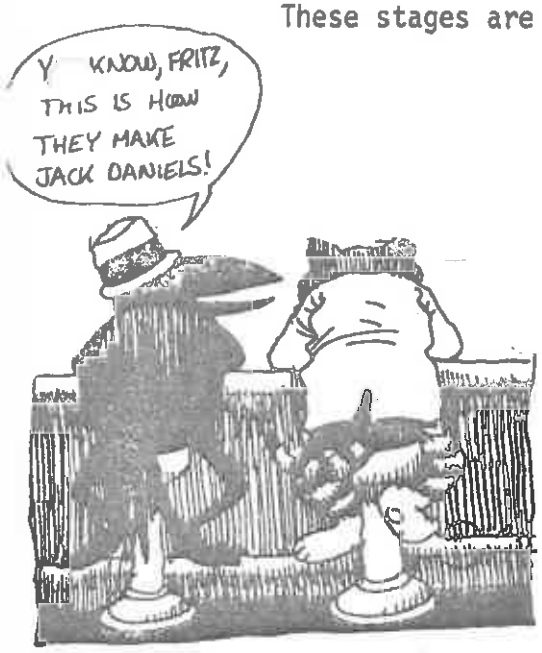

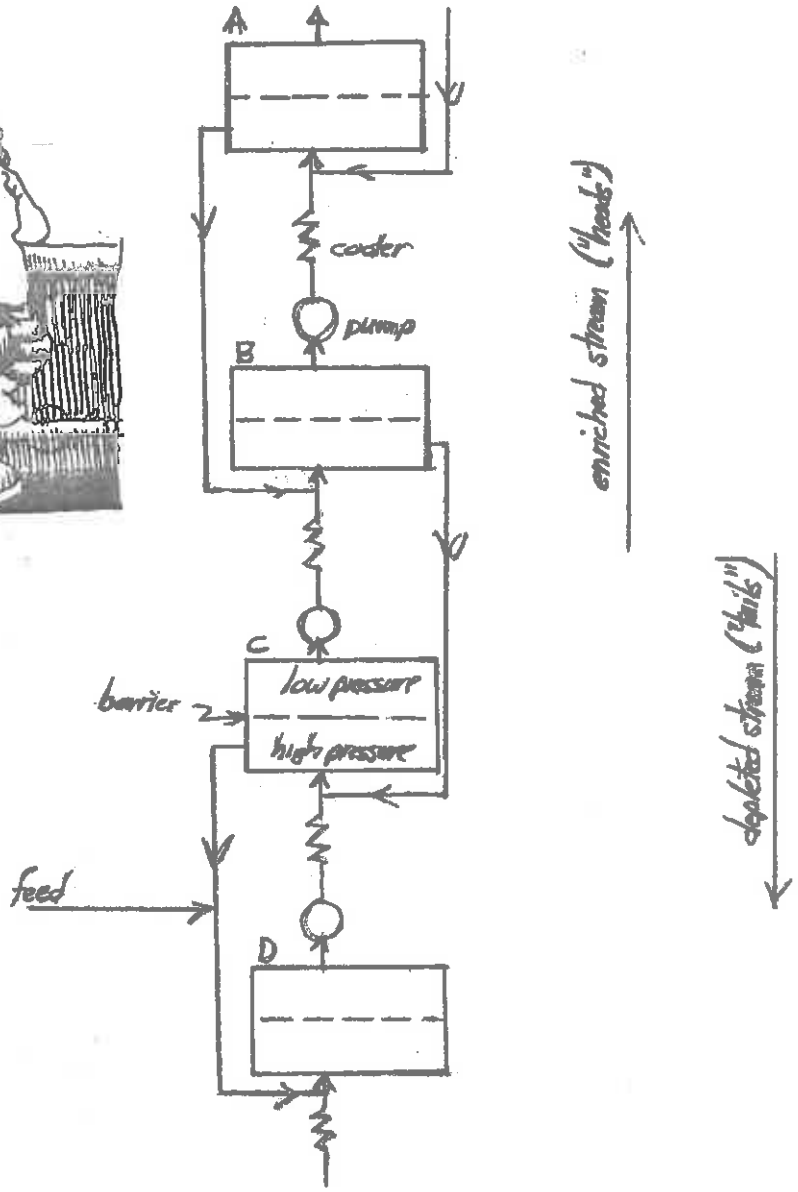

To understand the flow in such a cascade, consider UF_6 gas entering stage B. About one-half of the UF_6 passes through the barrier and is enriched, flowing on to the next stage A. The remaining (and now depleted) gas is pumped back to stage C to be recycled--the enriched component ("heads") going on to B while the depleted component ("tails") is pumped back still

further to D. Hence the gas moving upward through the cascade becomes increasingly enriched--and that moving downwards becomes decreasingly depleted. Such a scheme is analogous to a fractional distillation process--and hence the analysis of the gaseous diffusion cascade is a well understood facet of chemical engineering.*

The gaseous diffusion stages require large amounts of power to maintain the pressure differential across the thousands of membranes. Indeed, the three gaseous diffusion plants operated by the USAEC (at Oak Ridge, Tennessee; Paducah, Kentucky; and Portsmouth, Ohio), if run at their potential capacity, would require almost 6,000 MWe of electrical power. [Although at present, these plants operate at 2,980 MWe.] Of the current cost of separative work, about 49% corresponds to power costs, 35% to capital costs, and 16% to operational costs. The capital investment in these three plants alone is over $2 billion.

Nevertheless, the enrichment capacity of these plants will soon be exceeded by the fuel demands of the burgeoning nuclear power industry, and it has become imperative to rapidly develop additional capacity. Unfortunately, the enormous capital investment required for such facilities combined with the uncertainty surrounding future technological developments (such as in ultracentrifuge or laser separation techniques) have inhibited the entrance of private industry into uranium enrichment, and may result in a shortage in enrichment capacity in several years.

---

*For example, see M. Benedict and T. Pigford, Nuclear Chemical Engineering (McGraw-Hill, 1957), Chapter 10

Table 1. Diffusion Plant Capacities

Plant Location	Country	Capacity (10^6 SWU/yr)
Oak Ridge, Tennessee	US	4.7
Portsmouth, Ohio	US	5.2
Paducah, Kentucky	US	7.3
Capenhurst	UK	0.4
Pierrelatte	France	0.2*

** Estimated, actual capacity classified*[3]

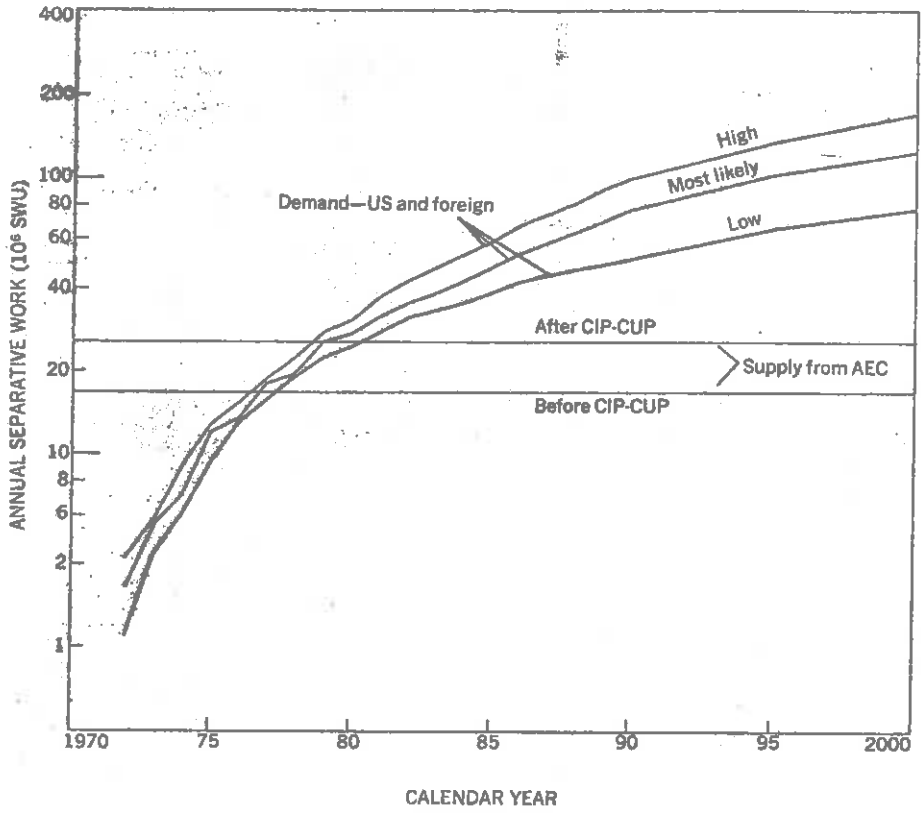

Uranium enrichment capacity. Demand versus supply in terms of total annual separative work as a function of year. Based on information in WASH-1139 (72). CIP-CUP refers to AEC program to upgrade existing diffusion plants. Tails at 0.3%.

2. Ultracentrifuge Techniques

The idea of separating the two isotopic forms of UF_6 gas using very high speed centrifuges was considered in the early days of the Manhattan project, but discarded because of the difficulty in achieving the high speeds necessary for separation without destroying the centrifuges. However developments in centrifuge design during the early 1960's has led to a renewed interest in this method.

The basic phenomenon involved in centrifuge separation is the tendency for centrifugal force to compress the gas towards the outer radius which is countered by the thermal motion of the gas molecules which attempts to even out such density variation. Since the latter effect is larger for lighter molecules (they move faster), there is a tendency for the heavier molecules to concentrate towards the outer surface of the centrifuge. Unlike the gaseous diffusion process, the separation factor characterizing the centrifuge is proportional to the difference of the masses of the isotopes (rather than the ratio). Hence centrifuge stages are characterized by much larger separation factors, e.g., α = 1.1-1.4. Only a relatively few centrifuges need be connected in series to achieve substantial enrichment. However, since the flow rates possible in centrifuges are much lower than in gaseous diffusion stages, large number of centrifuges in parallel are required for appreciable enrichment capability.

A schematic of a ultracentrifuge stage is shown below.

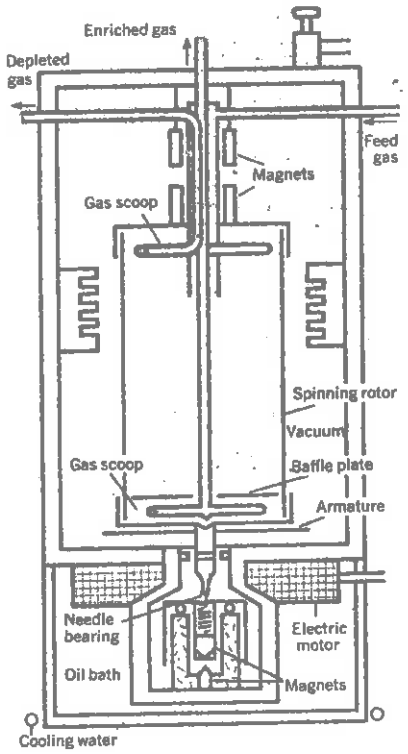

Gaseous centrifuge stage

There is very considerable activity in the development of centrifuge separation facilities, particularly in Europe. This scheme utilizes only some 10-15% of the power required by gaseous diffusion techniques, and appears to be capable of comparing quite favorably to the latter method in the overall cost of separative work.

3. Laser Isotope Separation

It has long been known that monochromatic light of the right wavelength can selectively excite the energy levels of gas molecules. With the recent development of powerful tunable lasers, it has now become possible to tune the wavelength of the light incident on a gas such that it can selectively excite the gas molecules of one isotopic species in preference to another (taking account of the isotopic shift in molecular energy levels). Once excited, the molecules can be easily separated from the unexcited molecules by conventional chemical methods.

The use of lasers to separate isotopes is a very recent application, having first been achieved for C^{12}-C^{14} separating in 1972. Nevertheless, there is a very substantial research and development program directed at large scale laser separation of uranium isotopes. The first appreciable separation of U^{235} from U^{238} using lasers was achieved in 1974 by Exxon Corporation.

D. Fuel Element Fabrication

The next step in the fuel cycle is the conversion of the enriched UF_6 to a solid ceramic or metallic form, and then the fabrication of this material into a fuel element. As we have seen, the fuel assemblies in a modern power reactor are extremely complex. Each assembly is, in fact, not only a source of fission energy, but as well a heat exchanger which must operate in a severe radiation and thermal environment without failure for a period of several years. These assemblies must be manufactured to very fine tolerances in order to optimize core nuclear and thermal performance. Hence it is understandable why fuel fabrication costs account for almost 20% of the total fuel costs.

The first step in the fuel fabrication process is the conversion of gaseous UF_6 to solid form. The enriched UF_6 from the isotope separation plant is received as a frozen solid at ambient temperatures in high pressure cylinders. It must be converted into the form to be utilized in the reactor fuel. For modern power reactors, this form is a ceramic: usually UO_2 or UC (although nitrides have been proposed for advanced fast breeder reactor fuels). For example, for light water reactor fuels, the UF_6 gas is reacted with water to form a UO_2F_2 solution which is then mixed with ammonia water to precipitate the uranium out as yellow ammonium diurinate. The precipitate is dried, calcinated to U_3O_8, and reduced to UO_2 with hydrogen. (This is known as the ammonium diuranate or Adu process.) The product of this process is a fine oxide powder containing 88.15% uranium with a theoretical density of 10.97 g/cm^3.

The UO_2 powder is milled, blended to a uniform powder batch, and dry pressed to the shape of right cylinders. These are then sintered in hydrogen at 1,650 °C, and finally ground to the required final diameter.

The fuel pellets are then loaded into cladding tubes (either zircaloy or stainless steel), which are evacuated to high vacuum, and backfilled with helium or a helium-argon mixture and sealed with end plugs. These individual fuel elements are then assembled together using grid plates and spacer grides to create a fuel assembly. At each stage of the fabrication, the fuel is inspected by a variety of techniques to insure quality control. A sketch of the various steps in the fabrication of the fuel assemblies is given below:

PROCESS FLOW – FUEL FABRICATION

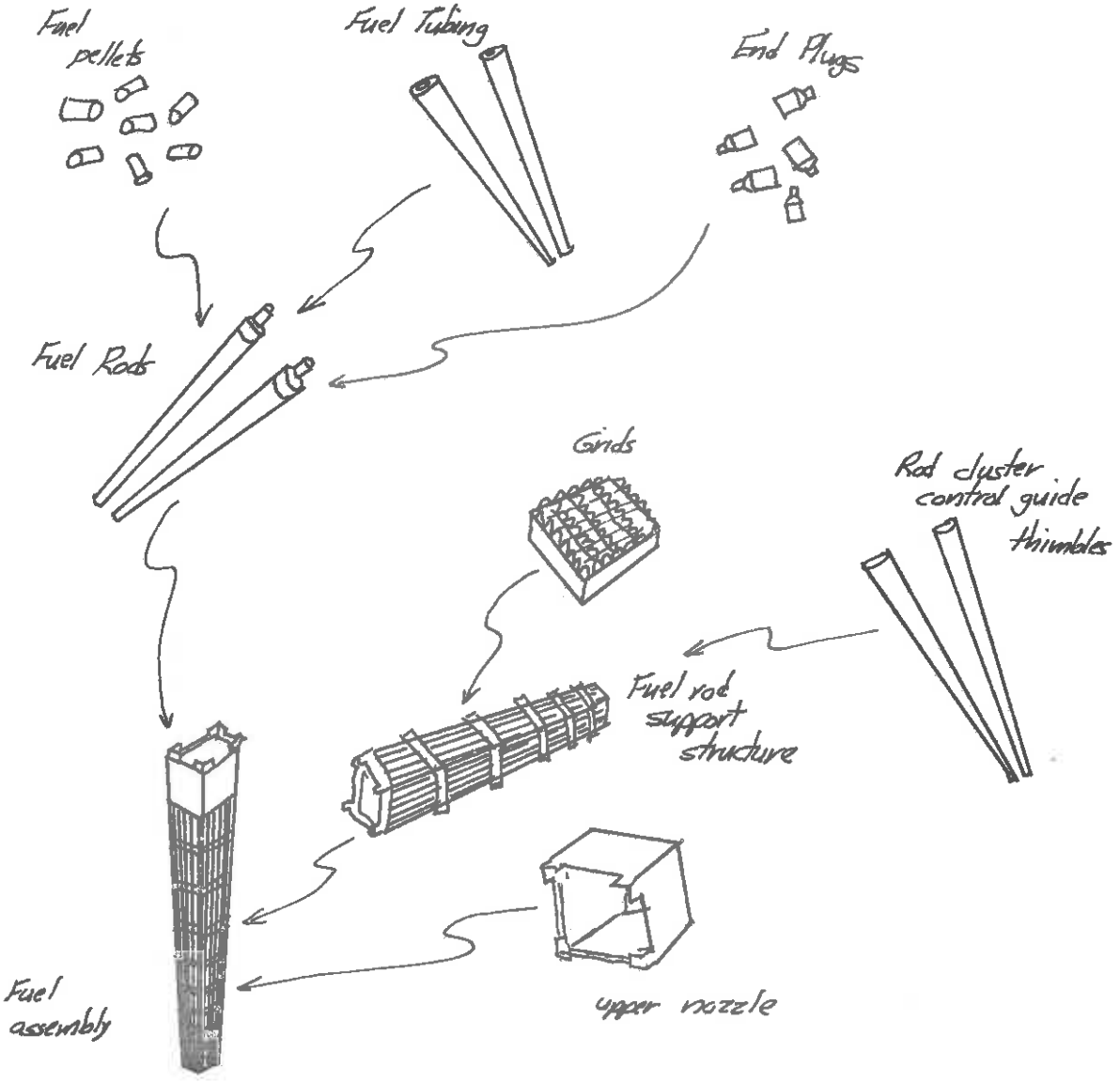

Very similar steps are followed for the mixed oxide fuel which results from plutonium recycle. The pelletized UO_2-PuO_2 recycle is produced and encapsulated into fuel rods by very similar processes, and then fabricated into fuel assemblies. The major variations occur in the method of producing the mixed oxide feed and in handling the plutonium, since these require the use of gloveboxes.

III. IN-CORE FUEL MANAGEMENT

A. Introduction

1. General Fuel Management Considerations

Perhaps the most important responsibility of the nuclear engineer concerned with the nuclear fuel cycle is the management of the fuel in the core--including the selection of refueling schedules, fuel loading patterns, the prediction (and measurement) of fuel burnup and isotope buildup, etc., in an effort to satisfy both nuclear and economic constraints. In this section we will consider only a few of the many facets of in-core fuel management.

It is during fuel irradiation that many of the debit aspects of fuel economics occur (e.g., in the depletion of fissile material such as U^{235}). But the in-core portion of the fuel cycle is also where all of the credit aspects such as plutonium production occur. The variation of U^{235} and Pu^{239} concentrations for a typical PWR are sketched below

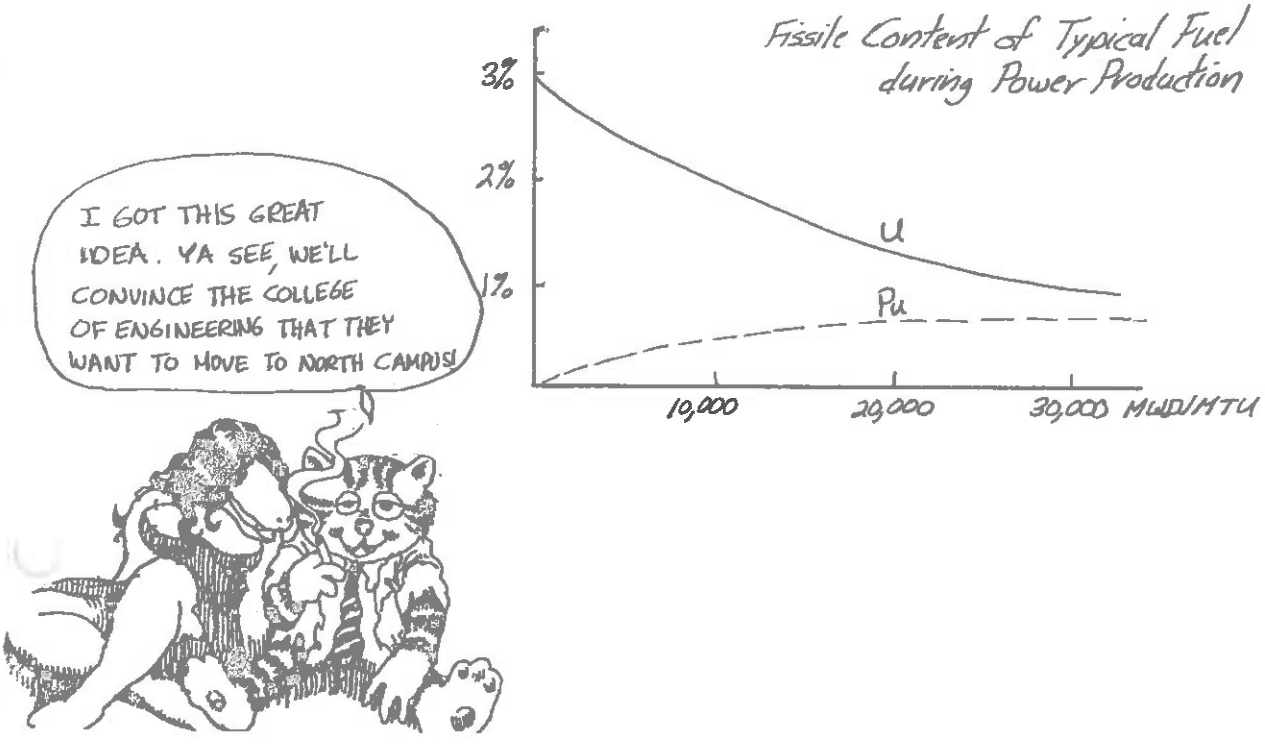

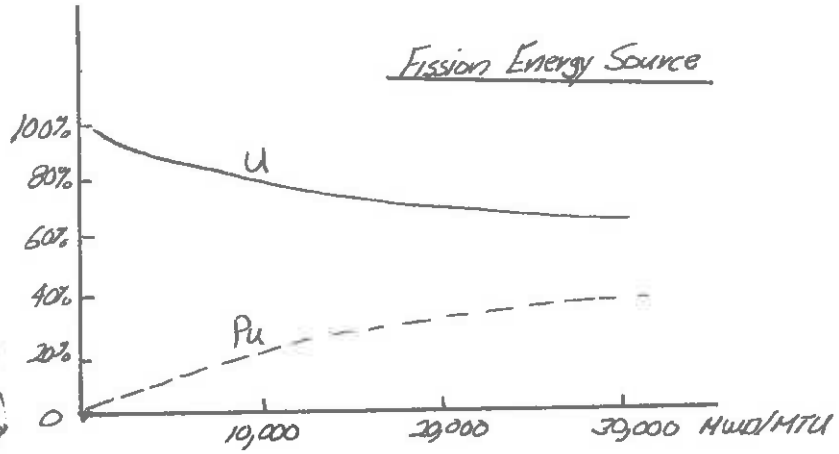

The nuclear engineer would like to achieve minimum fuel costs consistent with nuclear and thermal constraints on the core performance. To this end, he must determine the optimum distribution of fuel enrichment for both the initial as well as reload cores. The refueling period and reload strategy must be specified, along with the control management of both moveable rods and shim (soluble and burnable poisons). Hence the nuclear engineer has considerable flexibility (and considerable responsibility) in managing the in-core utilization of the fuel.

2. Constraints

The task of determining the optimum arrangement of fuel assemblies and loading is extremely complex, involving as it does the core geometry and composition, neutronic-thermal-hydraulic coupling, reactivity control, and operational requirements. In a typical core design, the core size, fuel assembly design, control devices, and coolant

conditions will be fixed before the detailed in-core fuel management scheme is determined. The variables at the nuclear engineer's disposal are then the enrichment of fresh fuel assemblies, the frequency of fuel reloading, the reloading pattern, and the associated control management program. A number of constraints on in-core fuel management must be considered:

a) Power density and coolant enthalpy limitations

We noted earlier that the two principal thermal limitations on core performance involved the requirements that the fuel centerline temperatures remained below melting point, and that the heat flux did not exceed its DNB limit. Such requirements place limits both on the local power density (in the case of the fuel centerline temperatures) as well as upon the integral of the power density up each coolant channel (in the case of the critical heat flux limit). Such limitations must be kept in mind when determining a fuel arrangement, since the core must be capable of operating at its rated power level throughout the reactor cycle without exceeding these thermal limitations. Since the core power distribution will change over core life as fuel depletion occurs, one must be able to predict the local power density throughout the cycle. This is an extremely expensive and time consuming aspect of fuel management.

b) Excess reactivity limitations

The reactivity control system must always be capable of controlling the excess reactivity loaded into the core to compensate for fuel depletion. Although this excess reactivity is usually larger in the initial core loading (since all of the fuel is fresh), one can use

burnable poisons and/or chemical shim to adequately control it. In later reload cores, there are fewer alternatives available, since, for example, burnable poisons cannot be easily inserted into irradiated fuel assemblies. Such considerations impose serious upper limits on the allowable fuel burnup of a core.

c) Fuel burnup limitations

Fuel burnup is limited to some degree by the amount of radiation damage the fuel can withstand without experiencing appreciable probability of failure. For example, fuel irradiation can induce swelling of the fuel which places a strain on the cladding. Furthermore, the buildup of gaseous fission products within the element can cause a stress on the clad which leads to a plastic deformation of the fuel rod at high temperature (high temperature creep). The enormous thermal gradients across the fuel pin and cladding, combined with the variations in temperature which occur during reactor startup and shutdown (thermal cycling) can also lead to clad fracture in the intense radiation environment of the core. Such fuel failure limitations on fuel burnup are particularly significant when very high burnups are required, such as in the LMFBR. We will return later in this chapter to discuss fuel performance in more detail.

d) Reactivity response requirements

The reactor should always be capable of responding to load demand changes. Since the control rod worth is dependent upon the flux profile, and since this flux profile will change over core life, one must insure that adequate reactivity response is available for such power maneuvering.

e) Refueling interval limitations

There are frequently external requirements placed upon the scheduling of core refueling. For example, one wishes to avoid a reactor shutdown for refueling during periods of peak power demand (e.g., in the middle of the summer or winter months). We will return later to discuss some of the considerations involved in scheduling refueling, but suffice it to note here that in general, more frequent refueling leads to lower fuel inventory requirements (less excess reactivity is required for shorter core lifetimes), but at the expense of more reactor down time and enhanced thermal cycling.

3. Some Terminology

Before proceeding further with a discussion of in core fuel management, it is useful to first introduce some terminology frequently used in fuel management analysis:

fuel cycle: This usually refers to the complete sequence of events including mining, refining, enrichment, fabrication, burnup, and reprocessing) of one batch of fuel for the reactor core

reactor cycle: The time period between core refuelings. (Note there may be several reactor cycles in one fuel cycle.)

fuel loading: the total weight of fissile and fissionable material in the core

fuel inventory: the total fuel weight in the fuel cycle

specific power: thermal power produced per unit of loading

specific burnup: total energy release per unit mass of fuel material (MWD/MTU)

fuel residence time: calendar time between insertion of a given batch of fuel and its removal from the reactor

plant capacity factor: the ratio of the average power level of the plant to its rated power level (this is frequently taken as .80)

plant load factor: ratio of the average load carried by the plant to its peak load

B. Refueling Schedules

Rarely does one replace the entire core of a reactor in a refueling operation. Rather only a fraction of the core is replaced with fresh fuel at any one time. The time period between such refuelings will be referred to as a "reactor cycle", and in any partial refueling scheme, the complete fuel cycle consists of a number of such reactor cycles.

It is possible to give a very simple illustration* of the advantages of partial refueling by using a model very similar to that used to illustrate fuel depletion in Chapter 13. Any such model of fuel burnup involves two types of processes

(i) neutron criticality condition (reactivity balance)

(ii) nuclide burnup

Usually these processes must be described by the multigroup diffusion equations and the isotopic depletion equations, respectively. To simplify this analysis, we will reconsider our model of an infinite, homogeneous, one-speed reactor fueled with a single fissile isotope (e.g., U^{235}). The criticality condition for this model was given in Chapter 13 as

$$k = \eta f = \frac{\eta \Sigma_a^F(t)}{\Sigma_a^F(t) + \Sigma_a^M + \Sigma_a^P(t) + \Sigma_c(t)} = 1 \qquad (16\text{-}1)$$

*This model was first developed by Dr. Harvey Graves, Jr.

or

$$(\eta-1)\Sigma_a^F(t) = \Sigma_c(t) + \Sigma_a^M + \Sigma_a^P(t) \qquad (16\text{-}2)$$

where $\Sigma_c(t)$ is the required control, and $\Sigma_a^P(t)$ corresponds to fission product poisons.

In contrast to our earlier analysis, we will now decompose $\Sigma_a^P(t)$ into two components:

(i) saturating fission products Xe and Sm: We will furthermore assume the concentration of these isotopes to be constant in time at their saturation level.

(ii) nonsaturating fission products: If we assume each fission products a non-saturating fission product pair with an effective absorption cross section of σ_a^{FP}, then we can calculate the number density of fission products by balancing against the loss of fissile nuclides as:

$$N_F(0) - N_F(t) = \alpha N_{FP}(t) + N_{FP}(t) \qquad (16\text{-}3)$$

where α is the capture to fission ratio. Hence the corresponding macroscopic absorption cross section is

$$\Sigma_a^P(t) = \Sigma_a^{Xe+Sm} + \left[\frac{N_F(0)-N_F(t)}{1+\alpha}\right]\sigma_a^{FP} \qquad (16\text{-}4)$$

Now recall that the end of core life (i.e., the end of the reactor cycle) occurs when the reactivity balance Eq. (16-2) can only be satisfied with zero control-- $\Sigma_c \equiv 0$ --which corresponds to

$$(\eta-1)\,\sigma_a^F N_F = \Sigma_a^M + \Sigma_a^{Xe+Sm} + \sigma_a^{FP} N_{FP} \qquad (16\text{-}5)$$

Now we can use our earlier expression (16-3) to solve for N_F in terms of N_{FP} as

$$N_F = N_F(0) - (1+\alpha)\, N_{FP} \qquad (16\text{-}6)$$

If we plug this into our reactivity balance at the end of the reactor cycle we find

$$(\eta-1)\,\sigma_a^F \left[N_F(0) - (1+\alpha)\, N_{FP}\right] = \Sigma_a^M + \Sigma_a^{Xe+Sm} + \sigma_a^{FP} N_{FP} \qquad (16\text{-}7)$$

Hence we can solve for the initial fuel loading required to yield a given fission product concentration N_{FP} at the end of core life as

$$N_F(0) = \underbrace{\frac{\Sigma_a^M + \Sigma_a^{Xe+Sm}}{(\eta-1)\sigma_a^F}}_{C_1} + \underbrace{\frac{\sigma_a^{FP} + (1+\alpha)\sigma_a^F(\eta-1)}{(\eta-1)\sigma_a^F}}_{C_2} N_{FP} \qquad (16\text{-}8)$$

Now we really don't give a damn about the concentration of unsaturated fission products at the end of core life in itself. It is only a useful quantity since it happens to be proportional to the energy production

$$(\text{energy production/cm}^3) = E = \left(\frac{\text{energy}}{\text{fission}}\right) \times \left(\frac{\text{fission product pairs}}{\text{cm}^3}\right) = \gamma N_{FP} \tag{16-9}$$

Hence we can solve for the energy produced by a given fuel batch in terms of the initial fuel loading $N_F(0)$ as

$$E = \frac{\gamma}{C_2}\left[N_F(0) - C_1\right] \tag{16-10}$$

This very simple linear behavior is easily understood if we recognize that C_1 is just the minimum concentration required for reactor criticality with no fission products present. It should also be stressed that this behavior holds only if we assume that the entire core was initially loaded with fresh fuel of uniform enrichment.

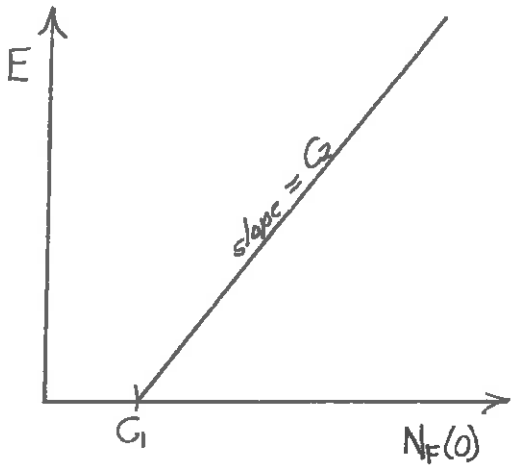

To see how this conclusion is modified for partial refueling schemes, suppose only <u>one-half</u> of the fuel in the core is replaced at the end of each reactor cycle. For convenience we will define

$$\begin{aligned} N_{F_1} &= \text{fuel concentration after one reactor cycle} \\ N_{F_2} &= \text{fuel concentration after two reactor cycles} \end{aligned} \tag{16-11}$$

Now after the end of the first reactor cycle, we can use the reactivity balance Eq. (16-5) to write

$$(\eta-1)\sigma_a^F N_{F_1} = \Sigma_a^M + \Sigma_a^{Xe+Sm} + \sigma_a^{FP} N_{FP_1} \qquad (16\text{-}12)$$

If we now replace one-half of the fuel in the core, then after the second cycle this balance relation becomes

$$(\eta-1)\sigma_a^F\left(\frac{N_{F_1}}{2}+\frac{N_{F_2}}{2}\right) = \Sigma_a^M + \Sigma_a^{Xe+Sm} + \sigma_a^{FP}\left(\frac{N_{FP_1}}{2}+\frac{N_{FP_2}}{2}\right) \qquad (16\text{-}13)$$

Now if the power density is maintained at a constant value during the irradiation of each fuel batch, the number of fission product pairs is constant, as is the U^{235} lost per batch. Define ΔN_{FP} as the number of fission product pairs produced each reactor cycle. Then

$$\begin{aligned} N_{F_1} &= N_F(0) - (1+\alpha)\Delta N_{FP} \\ N_{F_2} &= N_F(0) - 2(1+\alpha)\Delta N_{FP} \end{aligned} \qquad (16\text{-}14)$$

Hence we find

$$\frac{1}{2}\left[2N_F(0) - 3(1+\alpha)\Delta N_{FP}\right] = \frac{\Sigma_a^M + \Sigma_a^{Xe+Ys}}{(\eta-1)\sigma_a^F} + \frac{\sigma_a^{FP}}{(\eta-1)\sigma_a^F}\frac{3\Delta N_{FP}}{2} \qquad (16\text{-}15)$$

or solving

$$\begin{aligned} N_F(0) &= C_1 + \tfrac{3}{2} C_2 \Delta N_{FP} \\ &= C_1 + \tfrac{3}{2}\frac{C_2}{\gamma}\Delta E \end{aligned} \qquad (16\text{-}16)$$

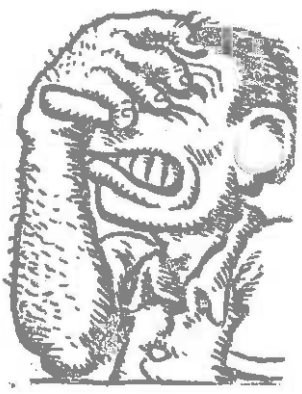

If the initial fuel loading $N_F(0)$ is the same as in the single cycle case, it is apparent that

$$\Delta E\Big|_{cycle} = \tfrac{2}{3} E_1 \tag{16-17}$$

where E_1 is the energy produced in the single cycle batch. Hence since each batch stays in two cycles, we can get an increase in the energy supplied per batch of 33%

$$E_2 = 2\Delta E\Big|_{cycle} = \tfrac{4}{3} E_1 \tag{16-18}$$

This is due to the fact that the average fission product concentration at the end of a cycle in the two-cycle core is less than that in the one cycle core (i.e., we "clean up" the fission products in one-half of the core one-half of the way through the batch burnup).

In general, the neutron balance at the end of a cycle for an n-cycle scheme is

$$(\eta-1)\sigma_a^F\left(\frac{N_{F_1}+N_{F_2}+\cdots N_{Fn}}{n}\right) = \Sigma_a^M+\Sigma_a^{Xe+Sm}+\sigma_a^{FP}\left(\frac{N_{FP_1}+\cdots+N_{FP_n}}{n}\right) \tag{16-19}$$

Furthermore, in analogy with Eq. (16-14)

$$N_{Fi} = N_F(0) - i\,(1+\alpha)\,\Delta N_{FP} \tag{16-20}$$

If we substitute these into (16-19)

and note that

$$\sum_{i=1}^{n} = \frac{n(n+1)}{2}$$

then we find

$$N_F(0) - (1+\alpha)\left(\frac{n+1}{2}\right)\Delta N_{FP} = \frac{\Sigma_a^M + \Sigma_a^{X_e+S_m}}{(\eta-1)\sigma_a^F} + \frac{\sigma_a^{FP}\left(\frac{n+1}{2}\right)}{(\eta-1)\sigma_a^F}\Delta N_{FP} \qquad (16\text{-}21)$$

or

$$N_F(0) = C_1 + C_2\left(\frac{n+1}{2}\right)\Delta N_{FP} \qquad (16\text{-}22)$$

If we note that the energy produced by a batch of fuel is

$$E_n = n\,\gamma\,\Delta N_{FP} \qquad (16\text{-}23)$$

then we can solve for

$$N_F(0) = C_1 + \left(\frac{n+1}{2n}\right)\frac{C_2}{\gamma}\Delta E \qquad (16\text{-}24)$$

This formula tells us that in the case of continuous refueling ($n \longrightarrow \infty$), we can double the energy available from single cycle core replacement:

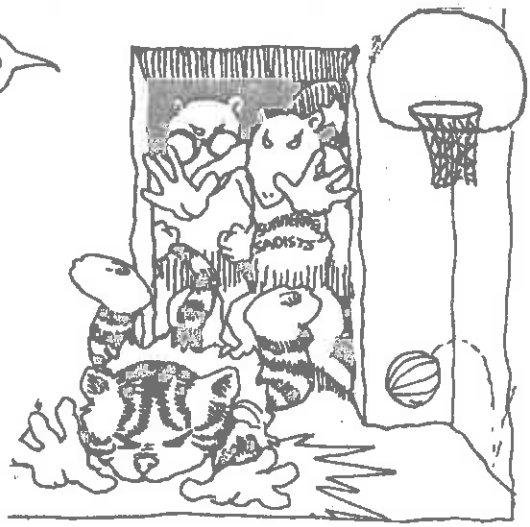

*SUMMERFIELD TRANSLATION: "NO BLOOD, NO BONUS!"

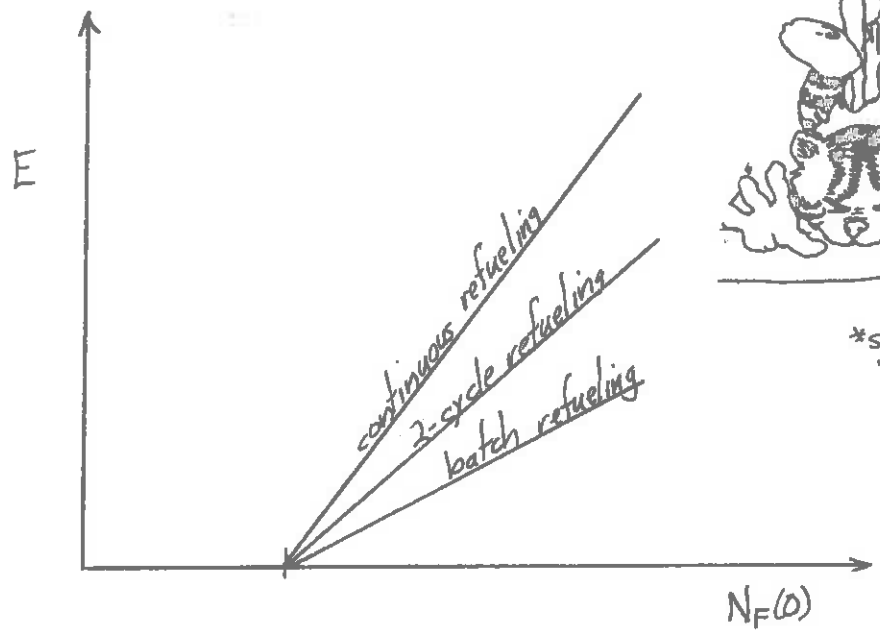

It is useful to compare also the final fuel concentration, N_f^{25}, for batch vs. continuous refueling

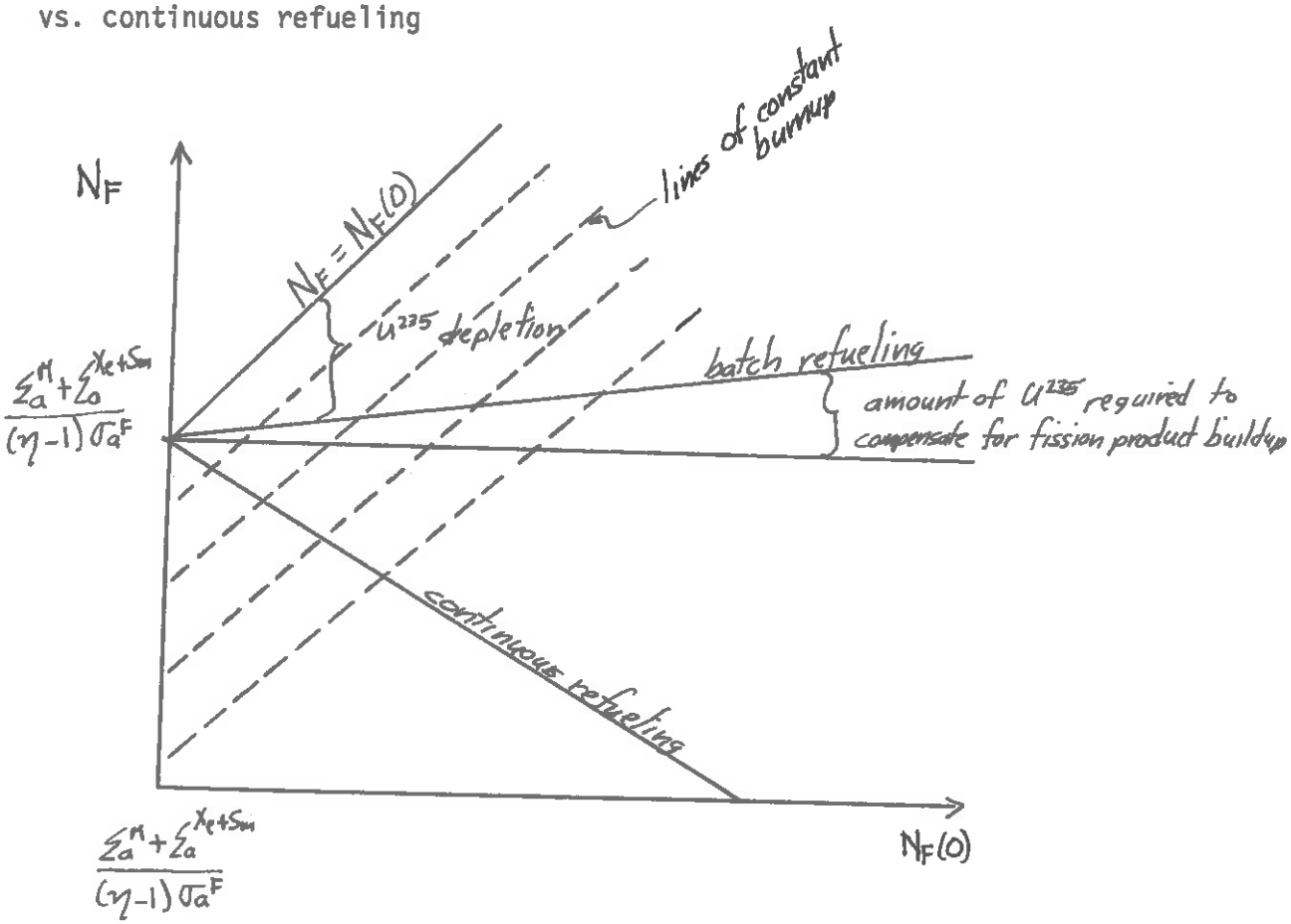

The dashed lines represent lines of constant burnup (i.e., such that $N_o^{25} - N_f^{25}$ is constant). It is of interest to note also that the U^{235} concentration at the end of core life and the fission product concentration are the same--regardless of the cycling procedure. [This is a consequency of the constant power density approximation.]

This simple calculation indicates that the fuel inventory required for a given energy production decreases as the frequency of partial refueling increases. However, there is a tradeoff here, since more frequent core refueling can lead to increased shutdown time and hence increased costs due to power outage. For some time now, most reactors have been refueled on a yearly basis. However, recently alternative refueling cycles have been proposed.

For example, the development of rapid refueling systems for PWR's have made possible refueling times of 3 to 4 days. Such rapid refueling allows semiannual refueling at 6 month intervals, with considerable savings in fuel inventory (estimated at some 10% of the annual fuel cycle costs). The tendency for BWR's has been to move in the direction towards longer reactor cycles, with refueling now proposed on an 18 month basis. This refueling frequency appears economically attractive to the BWR because of the ease with which its fuel lifetime can be stretched by adjusting coolant void fractions.

Annual refueling schedules of LWR's tend to replace 1/3 to 1/4 of the core during each refueling operation. However, shifting to a semiannual schedule will allow the replacement of only 1/6 of the core at a time. The present refueling schedule for the HTGR involves yearly replacement for 1/6 of the core. In this latter case, the long fuel cycle is permitted by the high burnup and conversion ratio of the HTGR fuel.

C. Refueling Patterns

We now turn our attention to a consideration of how the fresh fuel is distributed in the reactor core during refueling, and just which spent fuel elements are withdrawn (assuming that partial refueling schemes will be used). Suppose we attempted to load the core with a uniform enrichment. Then, the flux peaking at the center of the core would lead to higher burnup of these fuel elements with a considerable flattening of the core power distribution towards the end of core life:

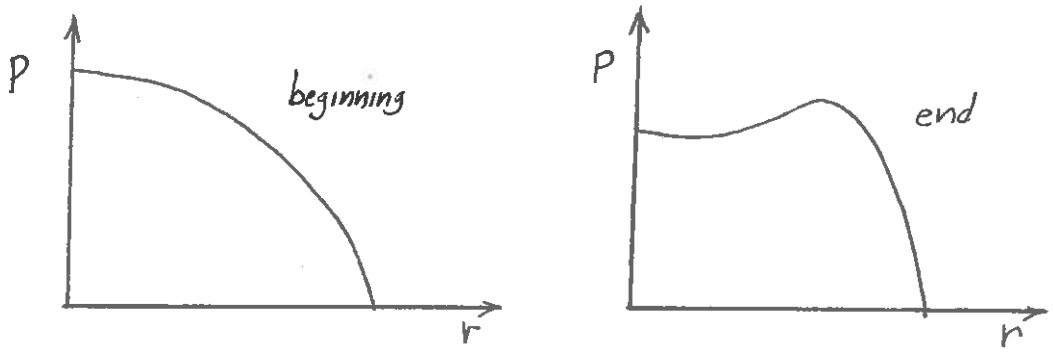

But unfortunately, such a uniform arrangement leads to a larger power peaking factor, F_q^N, over core life. It also results in a very low burnup of fuel elements inserted towards the edge of the core.

Hence a non-uniform core loading is clearly desireable--both in the initial core and in subsequent replacement cores. We will investigate two different refueling schemes:

1. Zonal Loading (in-out cycling):

In this scheme, one loads unirradiated fuel in a zone on the periphery of the core. The irradiated fuel is shuffled in towards the inner zone, while the fuel in the central zone is withdrawn from the core. The motivation in this scheme is to make use of the inherent reduction in reactivity which accompanies fuel depletion as a power flattening

mechanism. By way of example, a three-cycle zonal pattern is shown below:

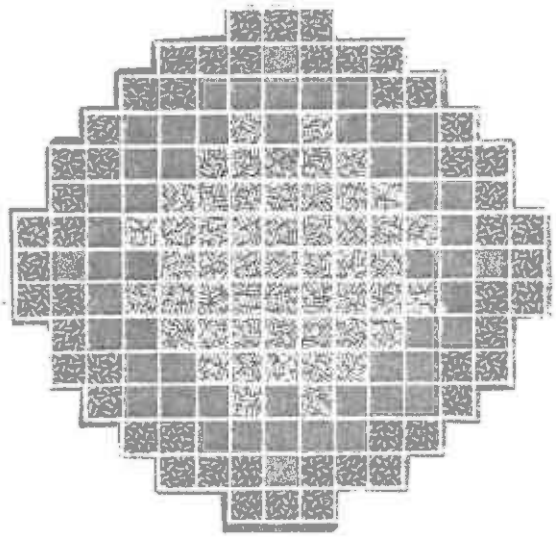

initial loading pattern

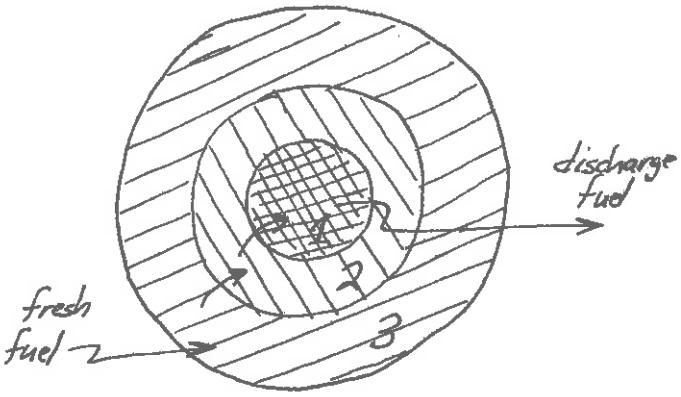

fuel shuffling

Such a pattern can even be implemented on the initial core loading by using fuel assemblies with varying enrichments.

Zonal loading does have disadvantages, however. In large cores subjected to high burnups, appreciable distortions in the flux distribution can arise which could lead to large power peaking factors.

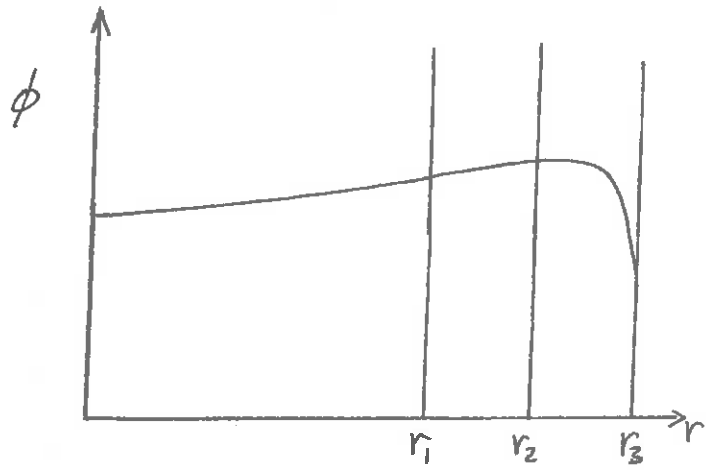

intermediate burnup
(~15,000 MWD/MTU)

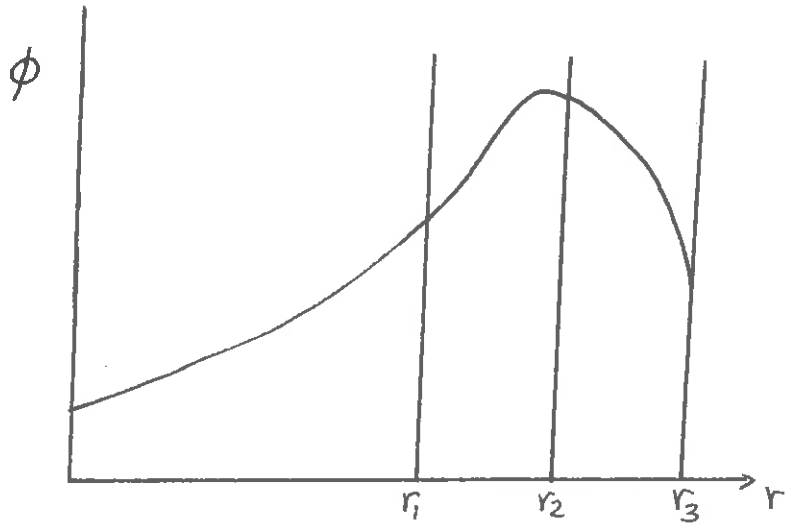

2. Scatter (Roundelay) Loading

An alternative scheme loads fuel in a scatter or random pattern to achieve a more uniform fuel distribution. One still will get some power flattening since the average burnup in the central zones of the core is more pronounced than near the core periphery:

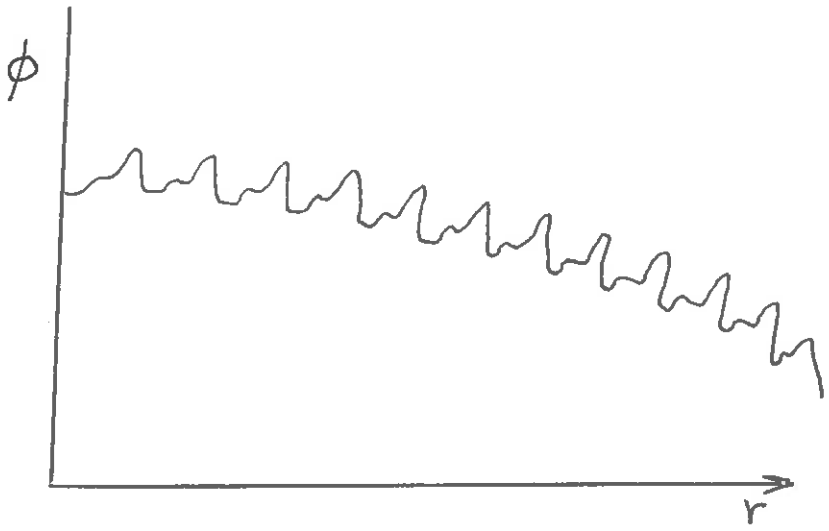

The power distribution characterizing a scatter loaded core has a somewhat flattened form of the distribution characterizing a uniformly loaded core. There is a fine scale ripple in the local power density, however.

Scatter loading has the additional advantage that no reshuffling of irradiated fuel is required.

3. Combination Schemes

In practice, most refueling schemes involve some combination of zonal and scatter loading techniques. For example, many PWR's are loaded in such a fashion that fresh fuel is loaded into the outer zone, while the fuel irradiated in the outer zone is scatter loaded into the center zones.

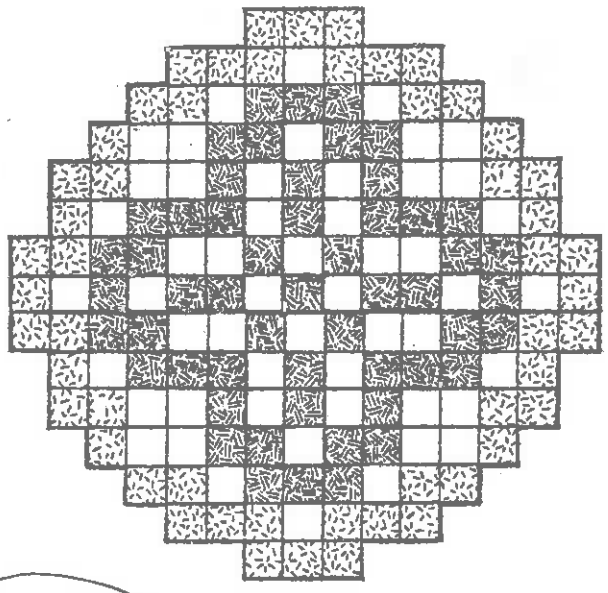

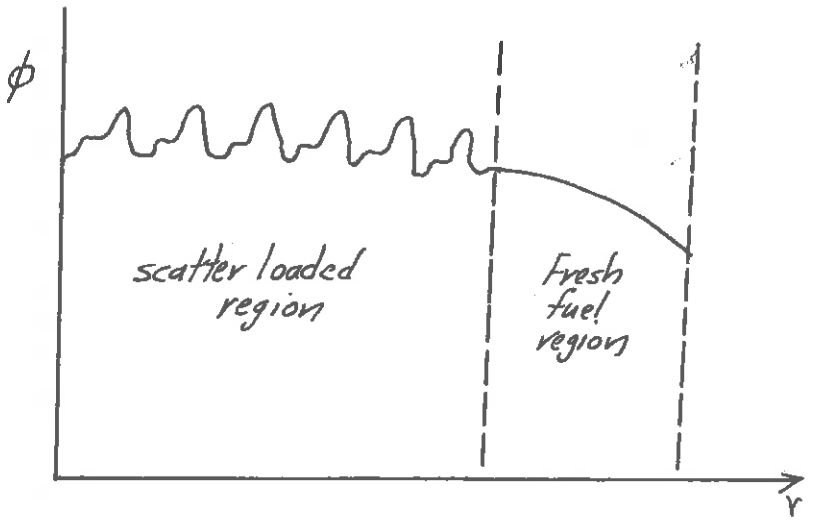

The detailed analysis and optimization of in-core fuel arrangement is a very complicated process. One must take into account core geometry, control management schemes, the coupling between core neutronics and thermal-hydraulic performance, and the constraints placed upon core performance, by operational requirements. Although this aspect of fuel management is still frequently performed by trial and error, using liberal dashes of physical intuition, there is now more of a tendency to attempt to implement more direct optimization methods (e.g., linear programming) for in-core fuel management.

However, a very big headache with any elaborate fuel management scheme is the fluxibility which is frequently required of a refueling program. For example, an unexpected alteration of a refueling pattern may be required to remove a fuel assembly leaking fission products. Hence a capability is required to allow the rapid evaluation of new loading pattern to insure that various thermal-hydraulic-mechanical-nuclear limitations are not exceeded during the subsequent core operation.

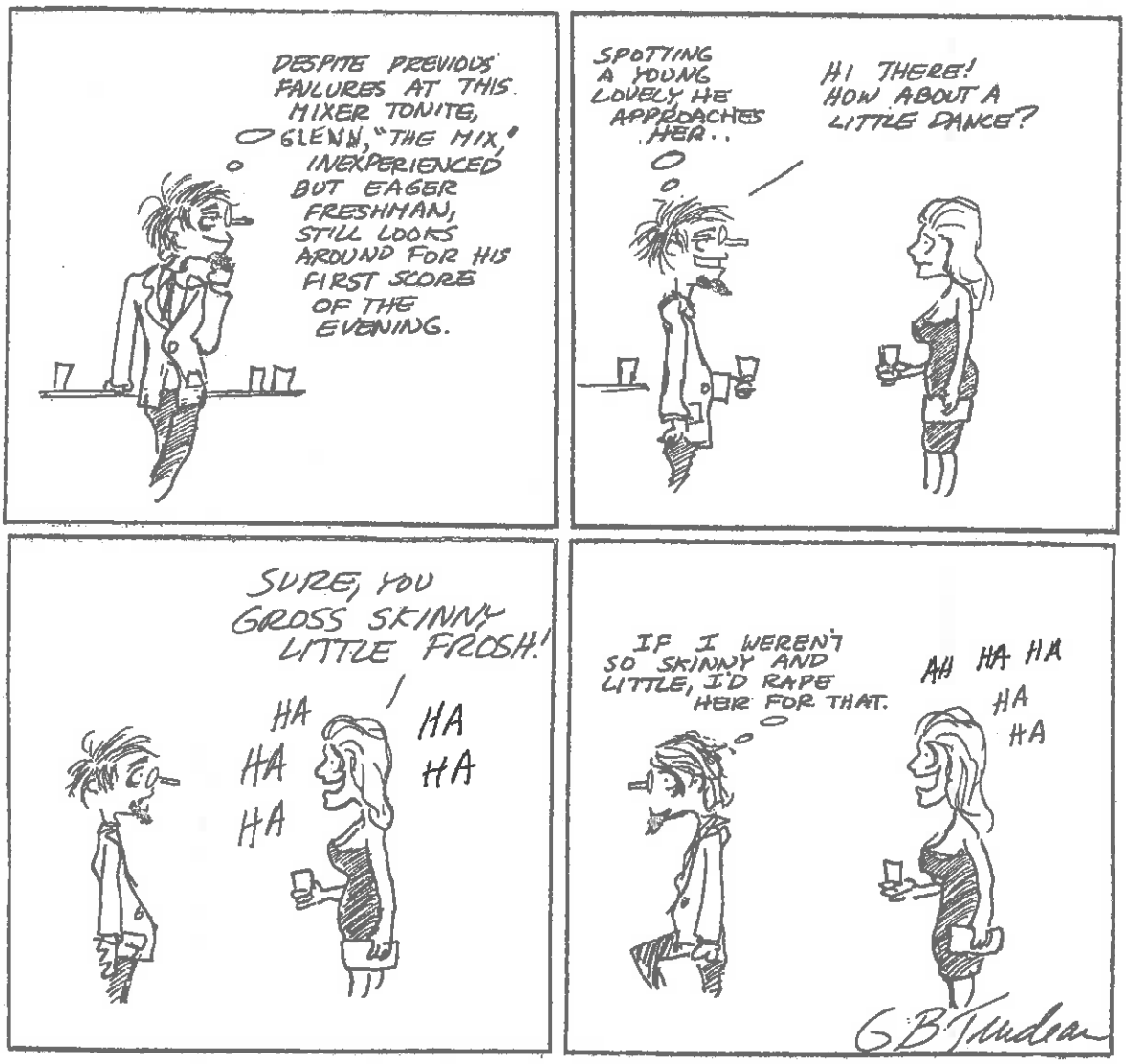
DESPITE PREVIOUS FAILURES AT THIS MIXER TONITE, GLENN, "THE MIX," INEXPERIENCED BUT EAGER FRESHMAN, STILL LOOKS AROUND FOR HIS FIRST SCORE OF THE EVENING.
SPOTTING A YOUNG LOVELY HE APPROACHES HER..
HI THERE! HOW ABOUT A LITTLE DANCE?
SURE, YOU GROSS SKINNY LITTLE FROSH!
HA HA HA HA HA HA
IF I WEREN'T SO SKINNY AND LITTLE, I'D RAPE HER FOR THAT.
AH HA HA HA HA
G.B. Trudeau

D. Fuel Element Performance

- to be added later -

IV. TAIL END FUEL MANAGEMENT

A. Removal and Storage of Spent Fuel Elements

At the end of each reactor cycle, a certain fraction of the irradiated fuel in the core will be removed. Since this fuel still contains an appreciable concentration of fissile material (for a typical LWR, the spent fuel contains approximately 1% U^{235} and 1% Pu^{239}), it is still of considerable value if properly reprocessed. However, the spent fuel is also very highly radioactive due to the large concentration of radioactive fission products contained in it. Such radioactivity represents a formidable problem in both shielding and removal of the associated decay heat of the spent fuel.

The spent fuel elements are removed from the core and transferred to water filled storage pools where they are kept for a period of roughly three months to let the shorter lived fission products decay out. A rough sketch of fission product activity vs. time after discharge is given below:

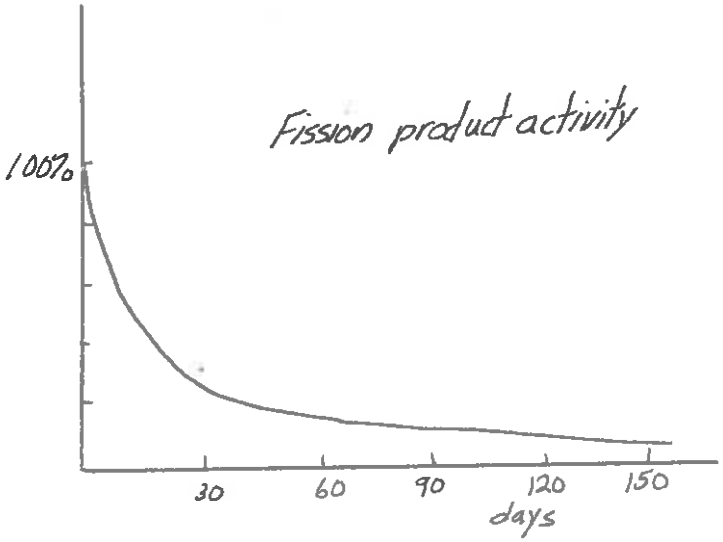

The underwater storage not only serves as a shield against the spent fuel radioactivity, but also as a means to remove the considerable amount of decay heat produced in such assemblies. A very useful estimate of the magnitude of the decay heat generated by spent fuel assemblies is given by the Way-Wigner formula

$$P(t) = 0.012\, P_o\, t^{-1.2}$$

where P_0 is the operating power generated by the fuel element, while the time t is measured in seconds. For longer times, the decay heat load of the spent fuel levels out at about 0.1% of the fuel operating power. It is this residual decay heat which must be contended with when shipping the spent fuel assemblies to reprocessing facilities.

B. Transportation of Spent Fuel Elements

The spent fuel is allowed to cool in the onsite storage pools for about three months. It is then loaded into heavily shielded and cooled casks for shipping to reprocessing facilities by either truck or rail. Throughout the handling, storage, and shipping the fuel must always be kept in configurations such that inadvertant criticality can be avoided. In fact, the number of fuel assemblies in a shipping container is usually limited by criticality considerations.

The shipping containers must be carefully designed to insure their integrity in the event of any shipping accident. The shielding, cooling, and safety demands placed upon shipping containers leads to enormous weights (150,000 pounds) and sizes (see Figure 16- 16).

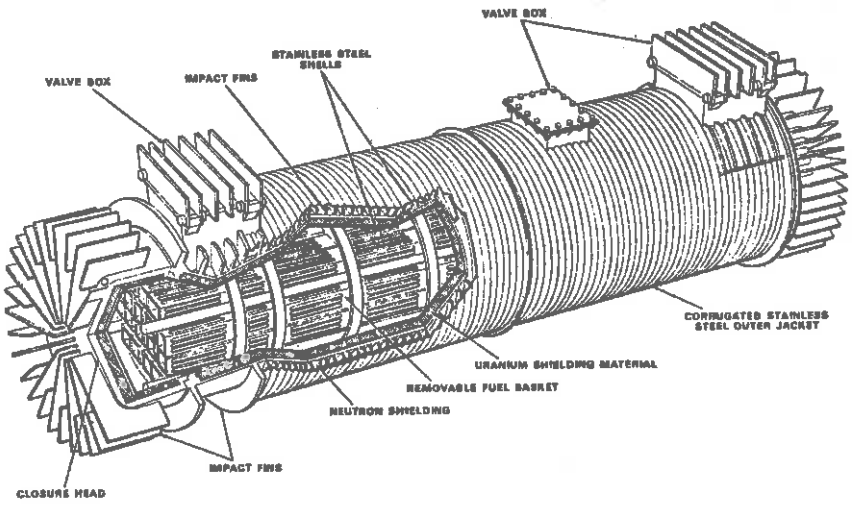

General Electric IF 300 Spent Fuel Shipping Cask

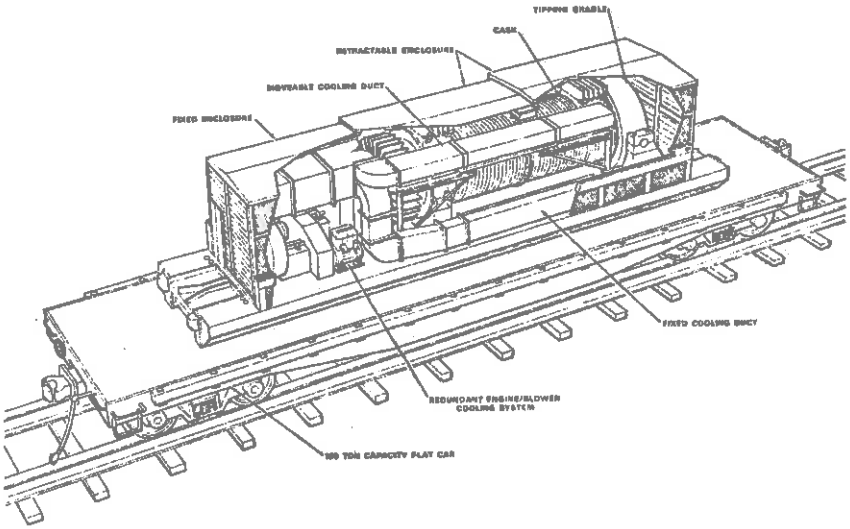

General Electric IF 300 Spent Fuel Shipping Cask
(Shown in Normal Rail Transport Configuration)

C. Spent Fuel Reprocessing

The spent fuel is shipped to reprocessing plants where the fissile material and valuable isotopes in the fuel can be separated out, and the remaining fission product waste can be concentrated for final deposition. The principal scheme used for commercial recovery of uranium, plutonium, and neptunium from low enrichment, UO_2 type, LWR fuels is the hybrid aqueous-fluorination process. The spent fuel is received at the reprocessing plant, unloaded from its shipping cask, and stored under water until processing. It is then mechanically disassemblied, sheared into short segments, and the UO_2 fuel is leached from the cladding. The leached cladding hulls are then rinsed and removed as waste.

The dissolver solution is then treated and sent to a solvent extraction step which results in the separation of more than 99.9% of the fission product wastes activity from the uranium, plutonium, and neptunium products. The aqueous stream from this extraction step is then concentrated. Chemical adjustments are made, and the stream is then passed through a semi-continuous anion exchange unit where the plutonium is extracted from the uranium-neptinium solution and purified. Subsequent chemical adjustments are then made to the valence of the neptunium, and the solution passed through a second anion exchange unit.

The acqueous uranium nitrate is concentrated and calcined to UO_3 in a fluid bed calciner. It then passes to the fluid bed fluorinator where it is fluorinated using elemental fluorine. The UF_6 is then passed through a series of purification steps and loaded directly into UF_6 cylinders for storage until shipment.

The spent fuel shipping and reprocessing industry is in a period of transition from a developmental basis to full commercial operation to meet the expected demand of the growing nuclear power industry. Only within the past few years have the large (1,000 MWe) commercial reactors begun to discharge fuel. The anticipated spent fuel recovery load is shown below:

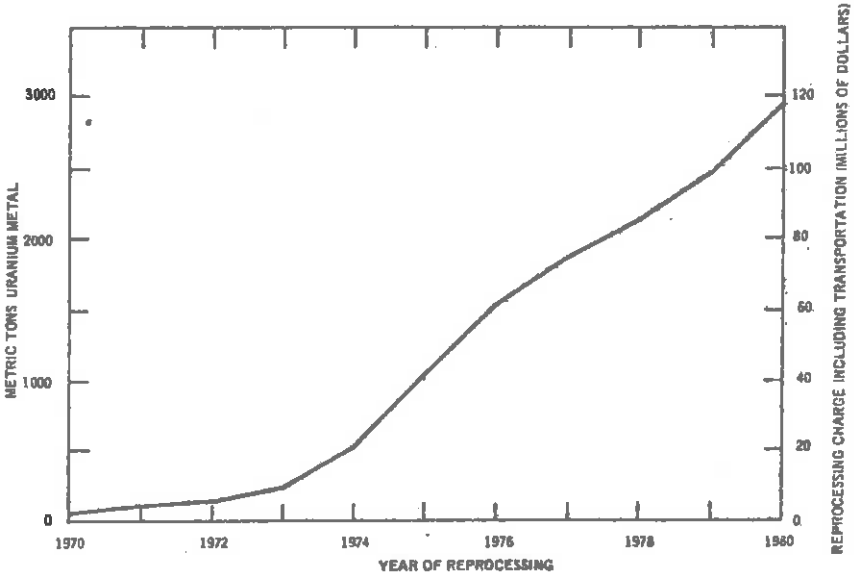

Annual Spent Fuel Recovery Volume

D. Burnup Evaluation

It is very important to the economics of the nuclear fuel cycle to accurately evaluate the burnup and composition of the spent fuel. A small error in this evaluation can lead to a sizeable error in depletion charges. The composition of the fuel will consist of a number of valuable heavy isotopes--notably U-235, U-236, U-238, Pu-239, Pu-240, Pu-241, and Np-237. (There will be other radioactive isotopes of some value, and we will return to discuss these later.)

All procedures used in determining the fuel composition involved mass spectrometry and usually consist of comparing the spectrometric analysis of the fuel sample of interest with a similar sample which has been spiked with a known amount of the isotope to be evaluated. Once these compositions have been determined, one can then evaluate the fuel burnup.

Of course, if the entire core of the reactor had been removed during refueling, one could merely divide the core thermal output by the fuel mass. But the complexities of variable enrichment and partial refueling require more elaborate methods for burnup evaluation. The composition data can be used to estimate the fission ratio of each of the fissionable isotopes, i.e.,

$$F_i = \frac{\text{fissions in isotope } i}{\text{initial heavy atoms}}$$

Then the burnup is given by

$$B = K \sum_i \gamma_i F_i$$

where γ_i is the MeV/fission in isotope i, while K is a conversion factor from MeV/initial heavy atom to MWD/MTU.

One can also evaluate burnup by measuring the decay of radioactive fission products such as Cs^{137} or Sr^{90}. Another alternative is to measure the production of a stable fission product such as Nd^{148}.

E. Radioisotope Production in Nuclear Power Reactors

During core operation, a large number of exotic isotopes, both radioactive and stable, are produced either directly as fission products or by subsequent decay or neutron capture. A number of these isotopes have value in other applications, such as energy sources (e.g., for space power supplies, nuclear pacemakers, etc.), radiopharmaceutical applications, and so on. Hence there is strong motivation to separate out such isotopes for commerical sale,

Unfortunately, virtually all of the design features of modern power reactors that contribute to efficient production of power are in direct contradiction to the practical requirements of commercial production and marketing of all but a few radioisotopes. For example, most power reactors are designed to operate with a relatively low neutron flux--which immediately rules out the production of a number of isotopes used in medical and biological applications, since these usually require activities achievable only in flux levels well above $10^{14}/cm^2 sec$. The annual refueling cycle is also very inefficient for the production of short-lived isotopes.

Hence any potential isotope production must involve isotopes that are relatively long-lived, which can be efficiently produced by long irradiations at low neutron flux, and whose production capacity in power reactors

is not grossly disproportionate to reasonably anticipated future market demand.

The primary isotopes which fit these requirements are Pu-238, tritium, carbon-14, and cobalt-60. Fission products of interest include desium-137, strontium-90, and promethium-147. All of these materials have current or developing applications that could result in significant future market demands.

V. NUCLEAR FUEL ECONOMICS

The economic analysis of nuclear fuel costs is quite different from that of conventional fossil fuels. Whereas the economics of conventional fuels hinge almost exclusively upon their purchase price, nuclear fuel costs are spread out over a considerable period before, during, and after irradiation. For example, the value of a typical PWR fuel batch is sketched below as a function of time

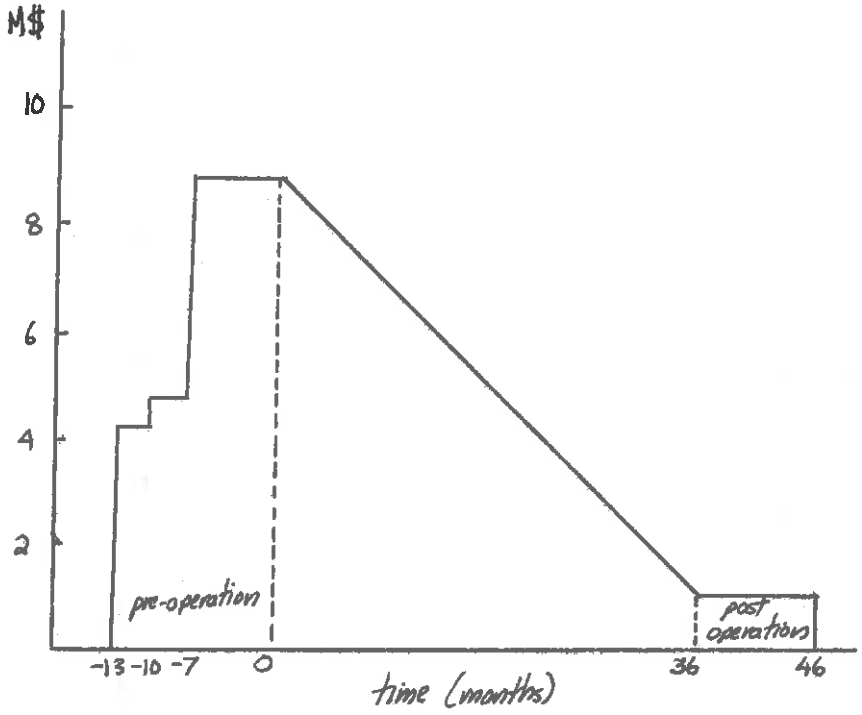

The nuclear engineer can have a considerable impact on nuclear fuel costs both in the manner in which he manages the nuclear fuel cycle, and in the choice of the core design itself. To better understand the considerations involved in determining nuclear fuel economics, we will study in detail the fuel costs associated with a batch of fuel irradiated in a typical PWR.

In such a PWR, roughly 1/3 of the fuel is replaced each year.* The fuel in the PWR core is divided into five regions, and we will concentrate on one such region in our economic analysis which is characterized by the parameters below:

Region power	1,000 Mw thermal
Region loading	29,500 kg-U
Enrichment	33% (weight) U^{235}
Burnup	31,500 MWD/MTU
Discharge loading	28,000 kg-U
Discharge plutonium	180 kg
Capacity factor	85%
Region lifetime	36 months
Total energy produced	7.6×10^{13} BTU

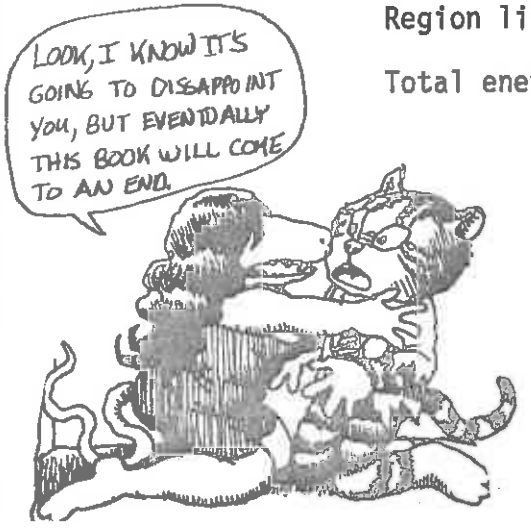

*Nuclear Fuel Economics", Westinghouse Electric Corporation, 1970

Our cost assumptions will be:

Yellowcake	\$7.50/lb of U_3O_8
Conversion	\$2.52/kg of U
Enrichment	\$26/unit of work
Design & Fabrication	\$80/kg of U loaded
Ship spent fuel	\$5/kg of U discharged
Reprocessing	\$37/kg of U discharged
Plutonium value	\$8,000/kg of fissile Pu

These cost assumptions result in an "investment timetable" showing the investments and credits at each step of the nuclear fuel cycle:

Investment Timetable (typical of 1000 MWe Plant)

Fuel Cycle Step	Month	\$
Buy yellowcake	-13	\$3,508,000
Purify & convert to UF_6	-10	451,000
Enrich U^{235}	-7	3,810,000
Design & fabricate fuel assemblies	-11 through -2	2,360,000
		\$10,129,000*
Start operation	0	0
End operation	36	0
Net residual value after discharge		1,284,000
Ship spent fuel	43	140,000
Reprocess spent fuel	45	1,036,000

*Total pre-operation investment

Uranium credit	46	(1,020,000)
Plutonium credit	46	(1,440,000)

Hence the nuclear fuel cycle is characterized by large investments before operation, the long duration of preparation and operation, and the high residual value of the fuel after operation.

One can use this data to construct an "investment time diagram" for the enriched uranium in the region as shown

Step	Month	$
U_3O_8	-13	3,508,000
conv	-10	451,000
enri	-7	3,810,000
		7,769,000
U credit	46	(1,020,000)

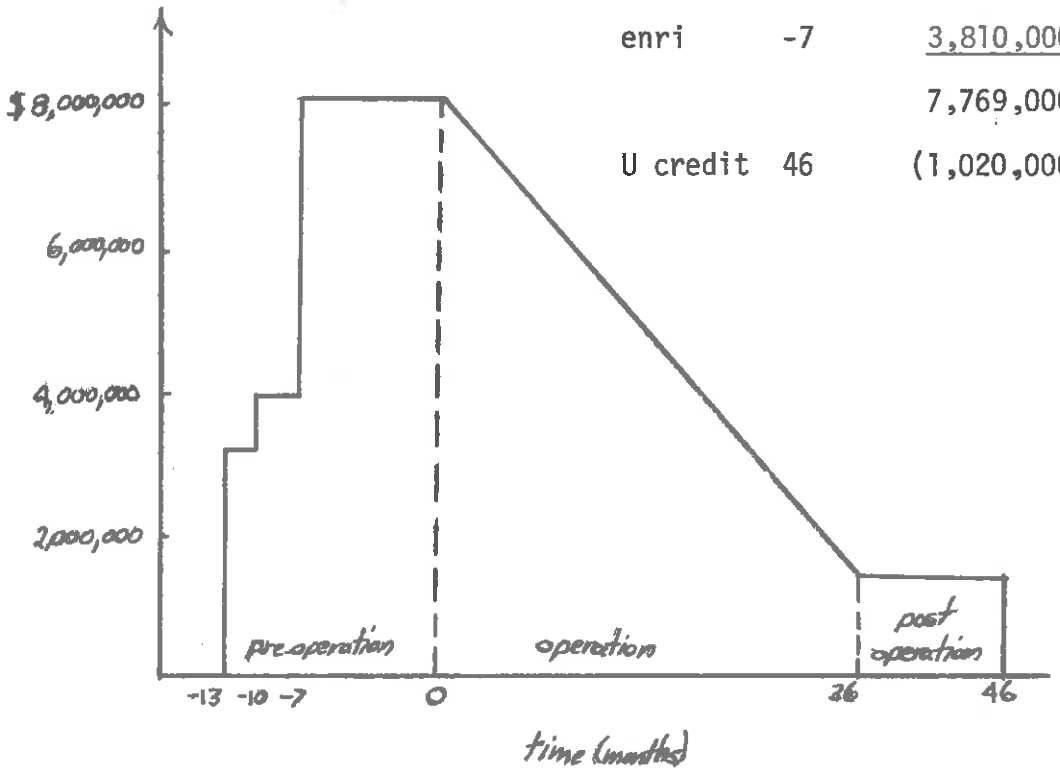

There are two components to the cost of each of the investment items:

(i) depreciation: the difference between the initial and final investment or the capital consumed during operation

(ii) carrying charge: the fuel carrying charge rate applies to the remaining investment in the fuel

A table of typical rates is shown on the next page.

	Nuclear Fuel Carrying Charge Rate	Nuclear Plant Fixed Charge Rate
Return to Investors	6.50%	6.50%
Depreciation	--	2.58%
Federal Income Taxes	4.10%	2.57%
Local & State Taxes	1.40%	1.40%
	12.00%	13.05%

These two fuel cost components can be isolated in the investment-time diagram. Depreciation can be calculated as just the difference between initial and final investment (in this case, $6,740,000). At 12% interest, the carrying charges amount to $9,201,000.

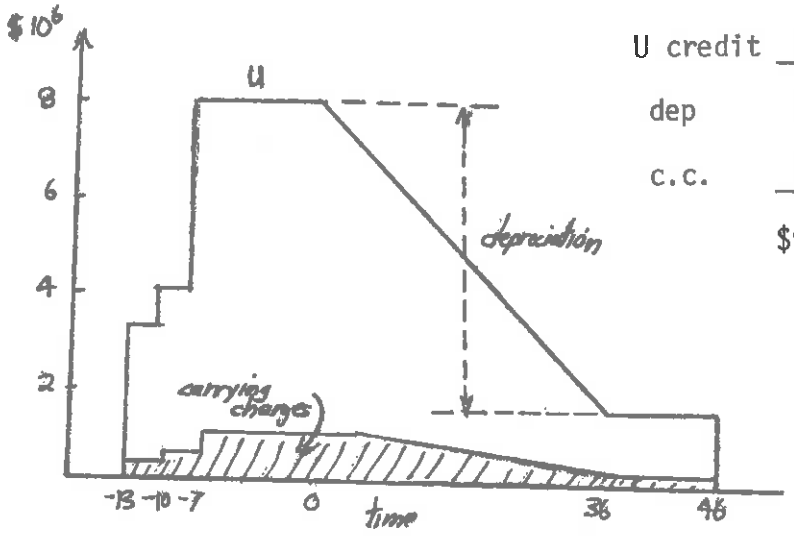

U	$7,679,000
U credit	1,020,000
dep	6,749,000
c.c.	2,452,000
	$9,201,000

A similar investment time diagram can be developed for the plutonium content of the fuel:

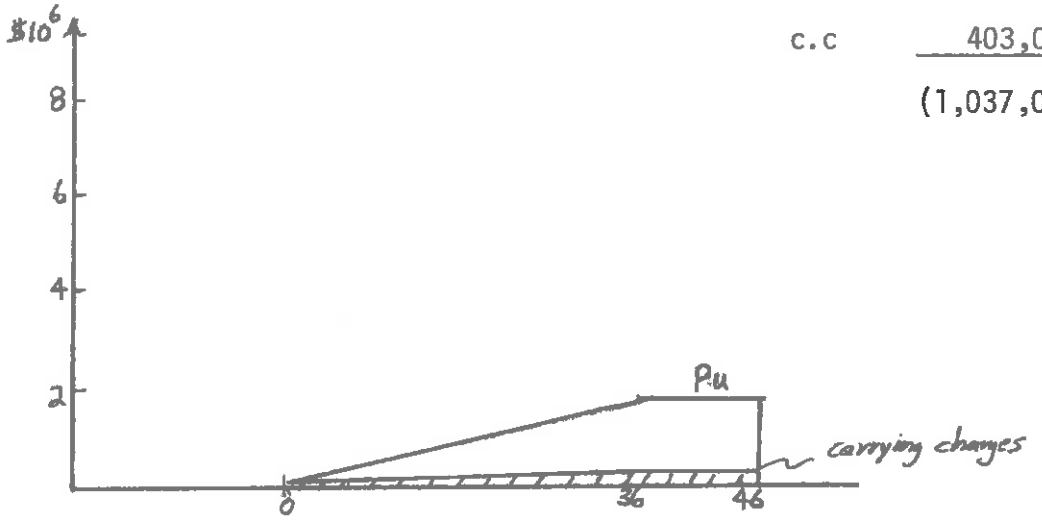

Pu credit	(1,440,000)
c.c	403,000
	(1,037,000)

One can develop similar investment-time diagrams for other components of nuclear fuel costs, such as fuel design and fabrication, spent fuel shipping, and reprocessing. Typical diagrams for these components are shown below

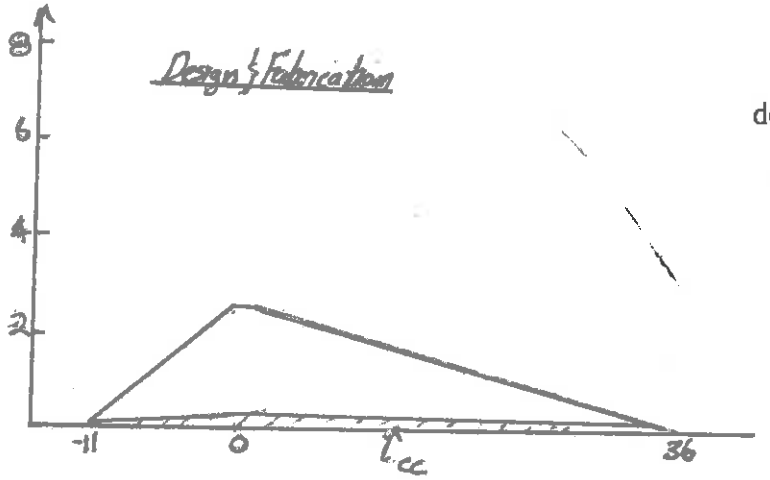

dep	$2,360,000
cc	578,000
	2,938,000

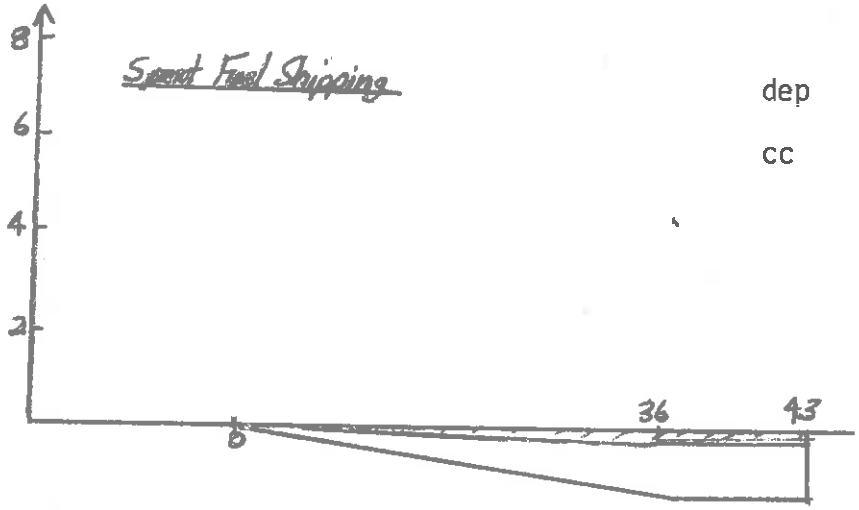

dep	$140,000
cc	(35,000)
	105,000

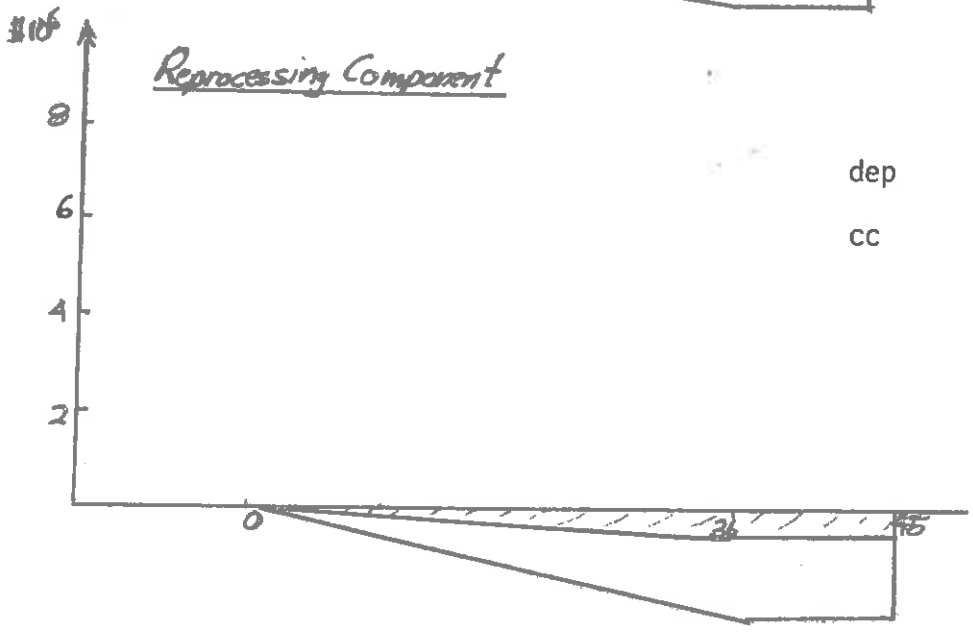

dep	$1,036,000
cc	(280,000)
	756,000

The total fuel costs are arrived at by combining these diagrams:

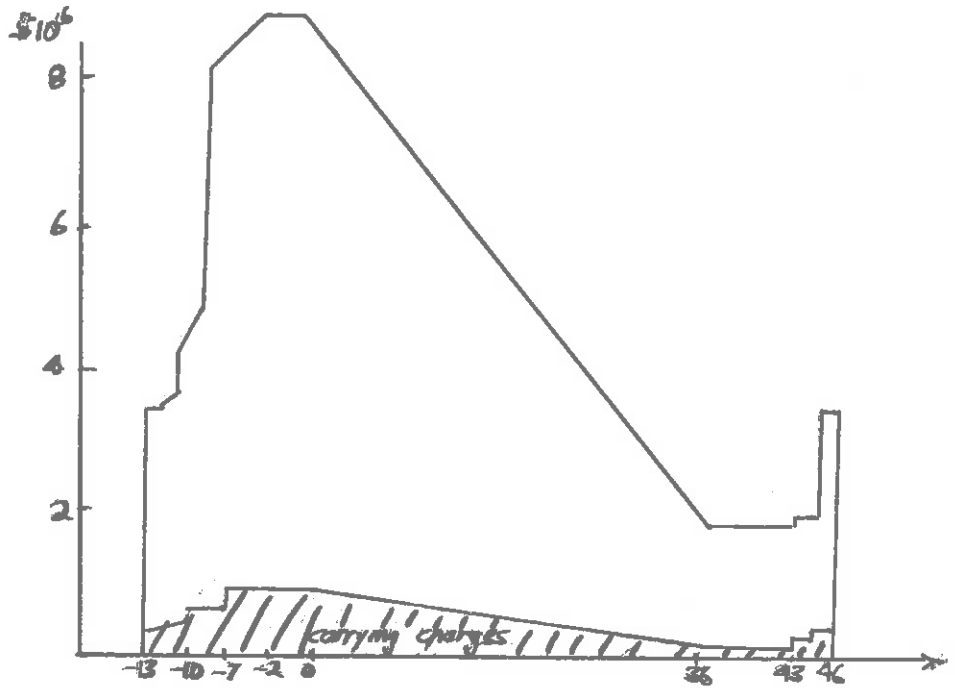

Fuel Cost Summary (¢/Million BTU)

Component	Depreciation	Carrying Charges	Total
Uranium & Plutonium	6.98	3.75	10.73
Design & Fabrication	3.10	0.76	3.86
Spent Fuel Shipping	0.19	(0.05)	0.14
Reprocessing	1.36	(0.37)	0.99
	11.63	4.09	15.72

We must remember again that these costs apply only to one of the five regions of the core. We can combine similar investment-time diagrams for each of these five regions, noting the period of irradiation overlap

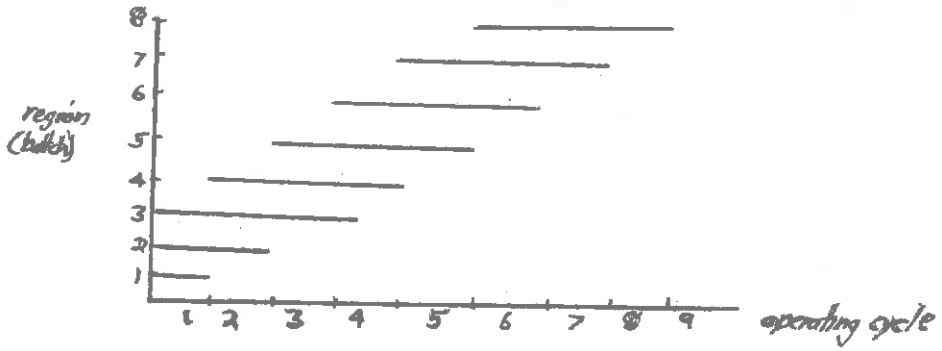

as shown below

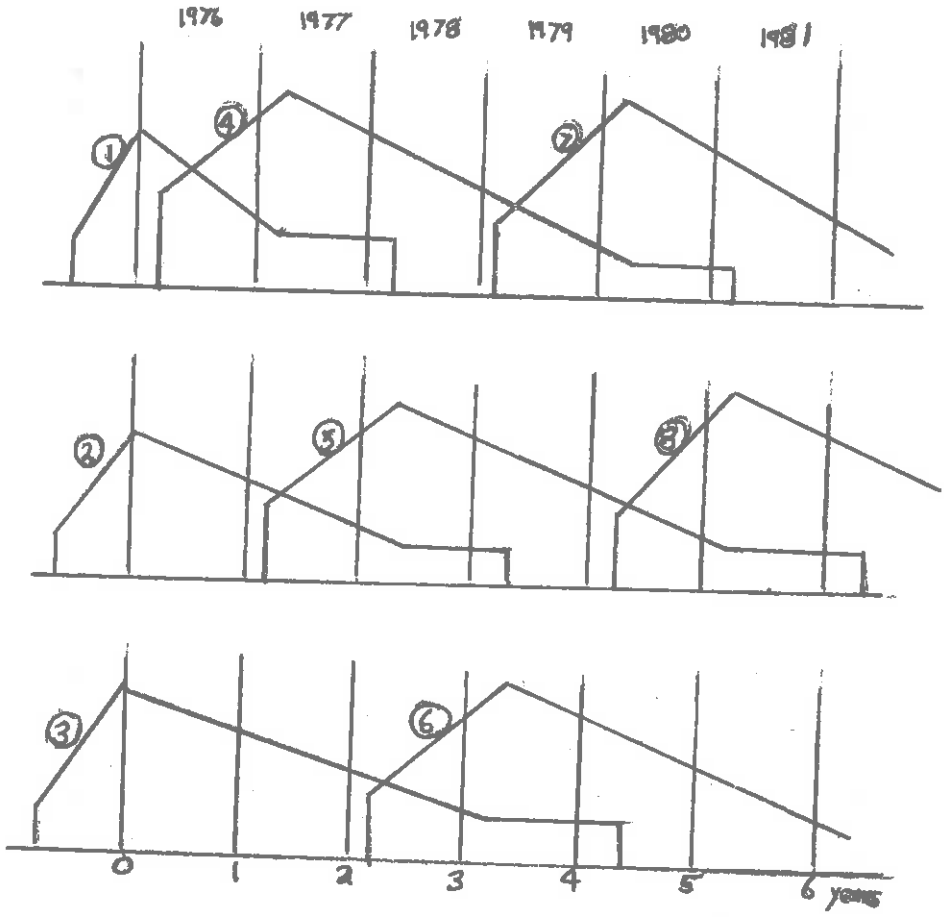

It should be noted that as the core approaches an equilibrium core cycle, the annual fuel costs will decrease

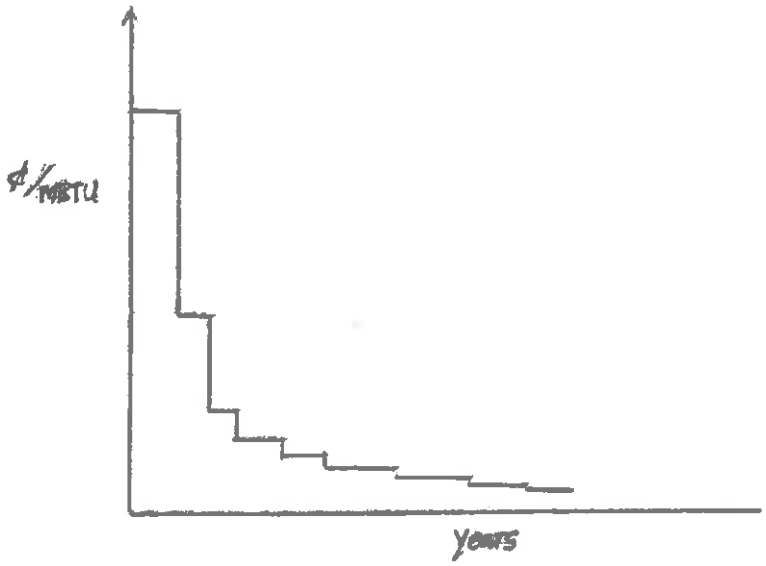

It is important to "levelize" these costs in order to arrive at a true measure of fuel costs for the reactor.

CHAPTER 17: NUCLEAR POWER PLANTS

I. AN OVERVIEW OF CENTRAL STATION NUCLEAR POWER PLANTS

A. System Layout

The trend in our development of topics in nuclear reactor analysis has been more from the study of individual components, such as the nuclear reactor fuel element design, to more complex systems, such as the nuclear reactor core or the nuclear steam supply system. We will now turn our attention to a consideration of the totality of systems which comprise a modern, central station nuclear power plant. Although many of the components contained in such plants are nonnuclear in nature, their design is frequently affected by the fact that a nuclear reactor rather than a fossil-fueled boiler is being used to generate the steam driving the turbine-generator. Furthermore, such nonnuclear systems frequently will affect the reactor design itself. Hence the nuclear engineer should be familiar with the various systems comprising a modern nuclear plant.

The overall arrangement of a typical plant--in this case, a PWR system--is shown in Figure 17-1. The nuclear steam supply system is located within a steel-lined concrete containment structure designed to withstand and contain the contents of the primary reactor coolant system in the unlikely event of a loss-of-coolant accident. The containment building houses the reactor itself, the primary coolant system including the primary pumps, steam generators, pressurizer, piping, and the safety injection equipment.

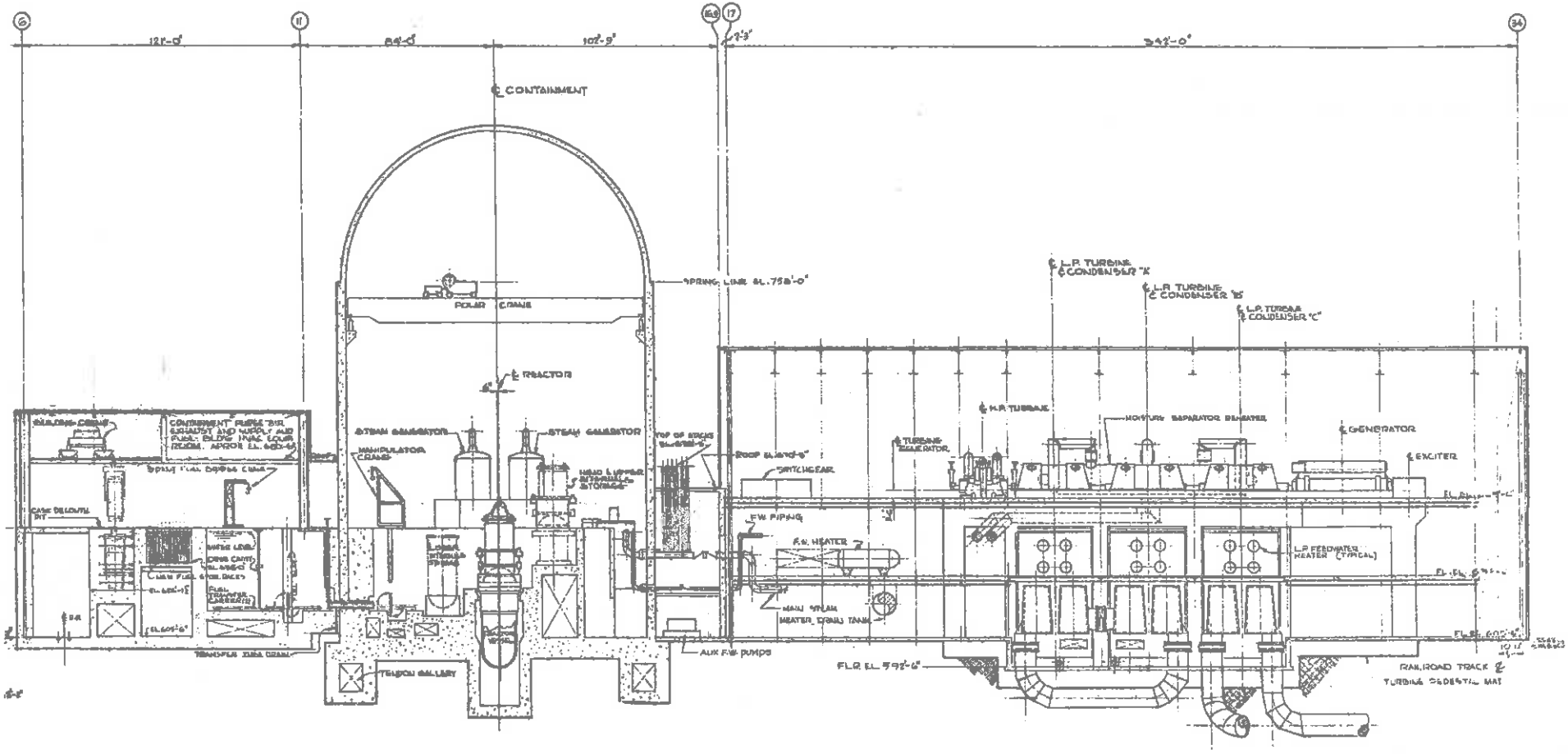

FUEL HANDLING BUILDING

CONTAINMENT BUILDING

TURBINE BUILDING

The reactor vessel is adjacent to and below a fuel transfer canal to permit the underwater transfer of spent fuel to the underwater storage pool, the latter being external to reactor containment.

The main steam system is primarily contained in the turbine hall which houses the entire turbine-generator unit, the moisture separator-reheaters, the condensers, and piping.

We will give a brief discussion of each of the systems which comprise a nuclear power plant. These can be conveniently grouped into three classes: (i) major systems, such as the nuclear reactor or reactor coolant system, (ii) auxiliary systems such as the chemical shim control system, and (iii) engineered safeguards systems such as the high and low pressure injection systems.

B. Major Systems

1. Nuclear Reactor

Obviously the key major system is the nuclear reactor itself, with associated control and instrumentation systems. Since our emphasis for the past 1000 pages has been concerned with this system, we will not give a rehash of the description of a nuclear power reactor here.

2. Reactor Coolant System (RCS)

a.) Pressure vessel

The pressure vessel itself is a major component in the reactor coolant system since it contains the nuclear reactor core, control mechanisms, instrumentation, (recirculation pumps and steam separators in a BWR, helium circulators and steam generators in an HTGR).

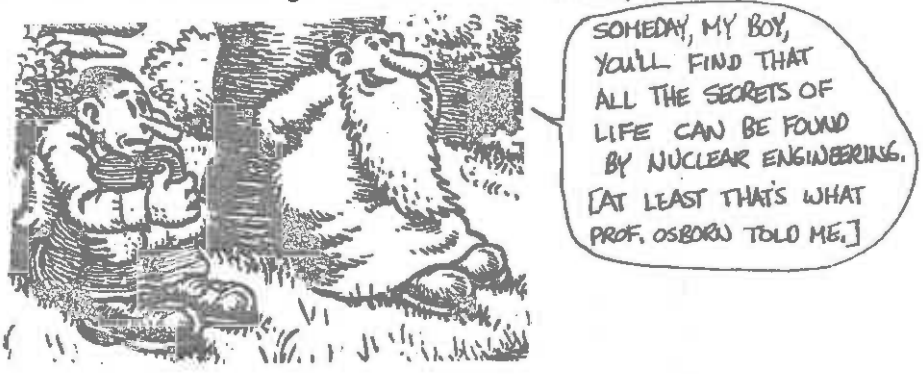

b.) Primary loop piping and pumps

We have already given a brief discussion of the primary pumps characteristic of a PWR in Chapter 15, and hence we will not repeat this discussion here. It should be remembered, however, that in general the NSSS will have more than one primary loop and set of pumps, arranged in parallel to provide steam generation and cool the reactor core.

c.) Steam generators

With the exception of the BWR, most reactor systems utilize large heat exchangers to transfer the heat drawn off of the reactor core by the primary coolant to the working fluid, water/steam, in the secondary loop containing the turbine.

d.) Pressurizers

In a PWR NSSS, a pressurizer tank is used to maintain system pressure and to compensate for coolant volume changes. In the BWR, the pressure vessel itself performs this function since there is appreciable void formation within the vessel. In an HTGR, coolant volume changes are accomodated by the circulators and the helium charging system. In the LMFBR, this function is assumed by the primary sodium pumps and the cover gas atmosphere above the coolant.

2. Reactor Containment Structure

The containment building completely encloses the entire reactor and reactor coolant system and ensures that an acceptable upper limit for leakage of radioactive materials to the environment would not occur even if gross failure of the reactor coolant system were to occur. The containment encloses the reactor, steam generators, reactor coolant loops, and portions of the auxiliary and engineered safeguards systems.

It is designed for all credible conditions of loading, including normal loads, loads during loss-of-coolant accident, test loads, and loads due to adverse environmental conditions (e.g., earthquakes or tornados). Typical containment structures have concrete walls up to 3 1/2 feet thick with a steel liner.

Of primary concern in the design of the containment structure is that it will able to safely withstand the overpressure and temperature resulting from any rupture of the RCS up to and including the severance of a reactor coolant pipe. Transients resulting from the design basis accident analysis and other, lesser accidents serve as the basis for a containment design pressure of 60 psig. Such an overpressure can be reduced by a factor of four by using an ice condensor system in which the steam released in a rupture of the primary coolant system is condensed on an ice bed (the ice condenser) located within the containment structure. Such a passive engineered safeguard system has very high reliability.

Yet another engineered safeguard system within containment is a spray system designed to limit the pressure of the containment atmosphere to below containment design pressure and to remove iodine from the containment atmosphere to limit the off-site and site boundary doses.

3. Power Extraction System (The "Secondary" Loop or "Steam System"

The main steam system carries the steam produced by the steam generators out of the containment building and to the various system components in the turbine building. Although the principal utilization of the steam produced by the NSSS is to drive the turbine-generator, it is also used for a variety of other purposes, including turbine

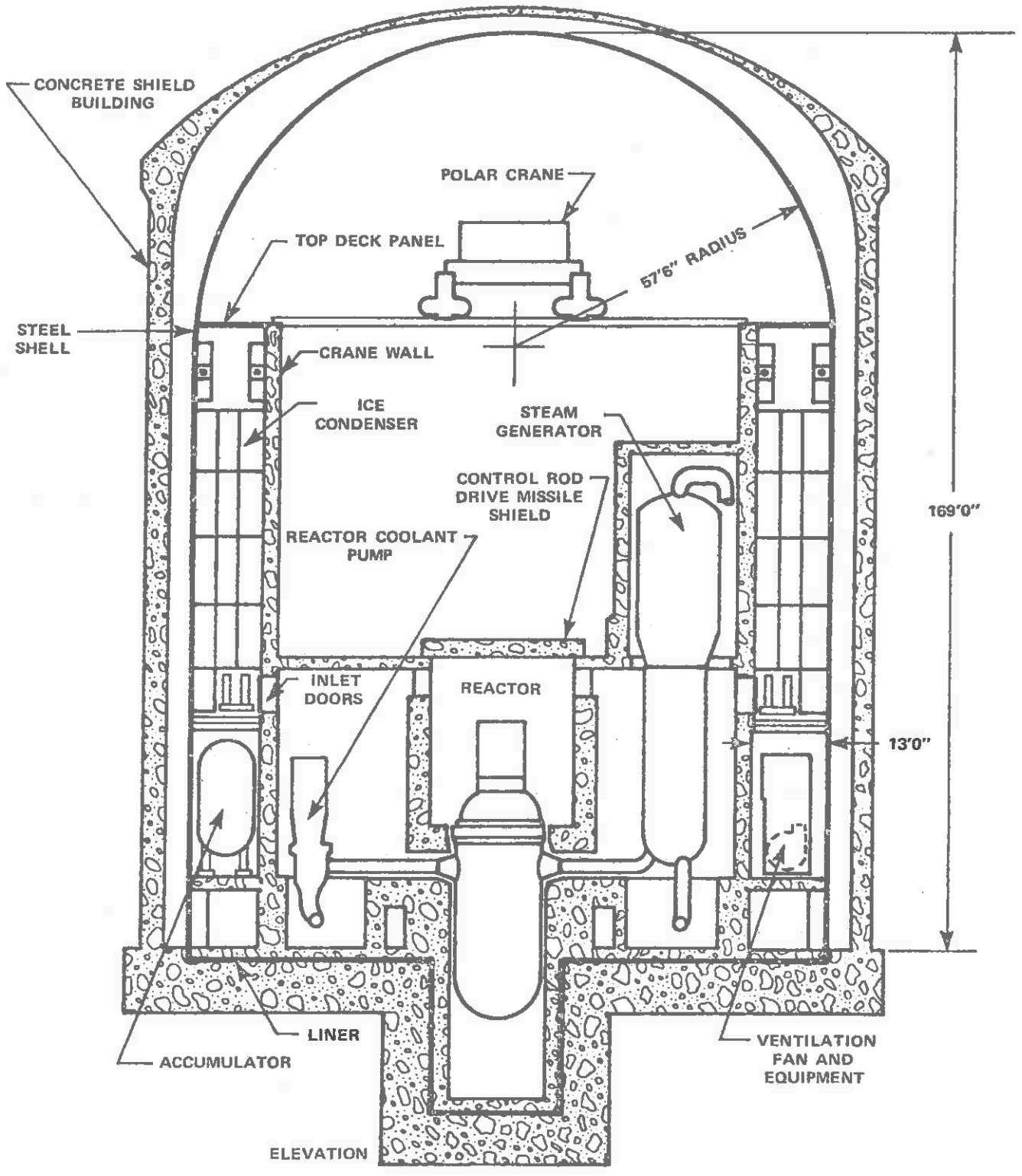
CONCRETE SHIELD BUILDING
POLAR CRANE
TOP DECK PANEL
57'6" RADIUS
STEEL SHELL
CRANE WALL
ICE CONDENSER
STEAM GENERATOR
CONTROL ROD DRIVE MISSILE SHIELD
REACTOR COOLANT PUMP
INLET DOORS
REACTOR
169'0"
13'0"
LINER
ACCUMULATOR
VENTILATION FAN AND EQUIPMENT
ELEVATION

drives for the main and auxiliary feedwater pumps, and steam jet air ejectors, shaft steam seals, and systems associated with steam generator pressure relief such as the steam dump values. The principal components of the power extraction system include:

a.) Steam generators

Of course, the source of the steam in the secondary loop is the steam generators of the NSSS. Since we have already given a brief description of these components in Chapter 15, we will avoid a further discussion here.

b.) Main steam turbine

A typical multistage steam turbine is shown in Figure 17-4. This particular turbine consists of one double-flow high pressure stage in tandem with three double-flow low-pressure stages. Between the high and low pressure stages, combination moisture-separator steam reheater systems are used to dry and superheat the steam.

Steam inlet to the high pressure stage is controlled by governor valves with quick acting stop valves ahead of them for rapid isolation in an emergency. The pressure after the first expansion stage is monitored as a load index for the reactor control system.

c.) Moisture separators and reheaters

Upon leaving the high pressure, the steam has an appreciable moisture content of approximately 10%. Not only is such a high moisture content undesirable from the point of view of turbine efficiency, but it as well could lead to appreciable cavitation damage on the blades of the low pressure turbines. Hence upon leaving the high pressure stage, the steam is passed through a moisture separator and reheater to remove

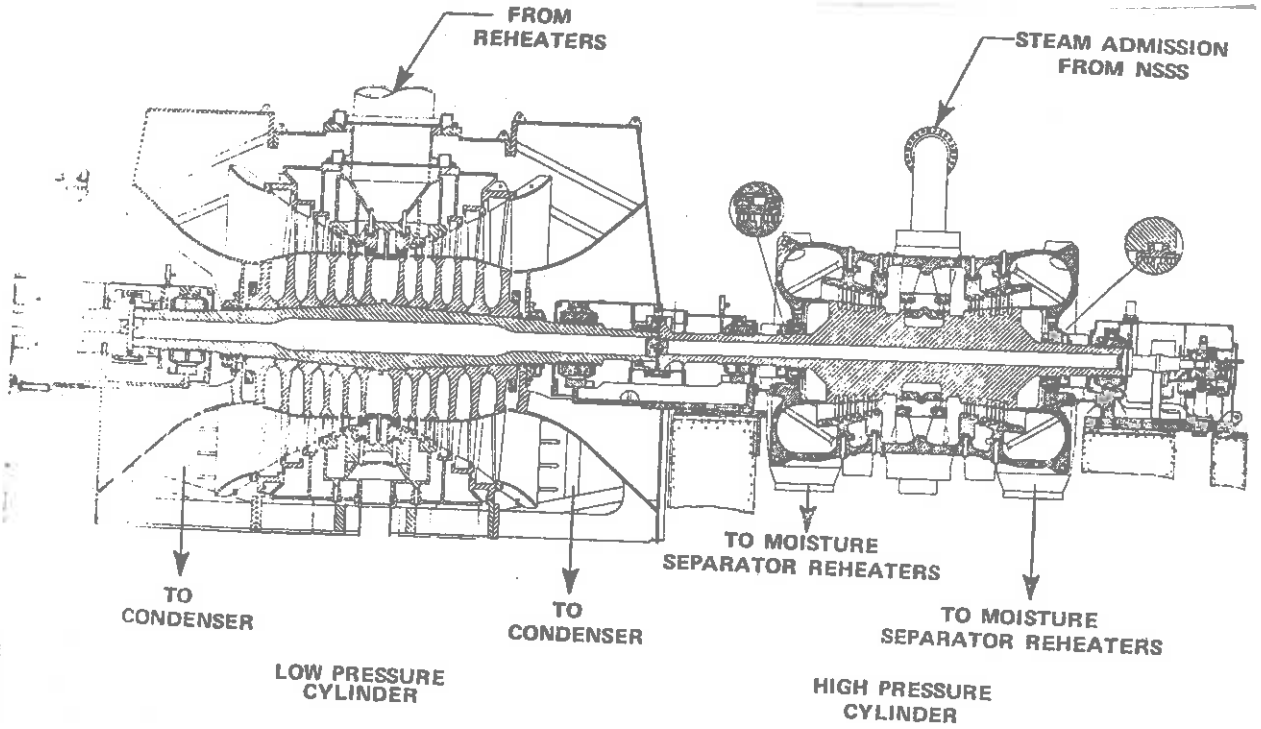
FROM
REHEATERS
STEAM ADMISSION
FROM NSSS
TO MOISTURE
SEPARATOR REHEATERS
TO
CONDENSER
TO
CONDENSER
TO MOISTURE
SEPARATOR REHEATERS
LOW PRESSURE
CYLINDER
HIGH PRESSURE
CYLINDER

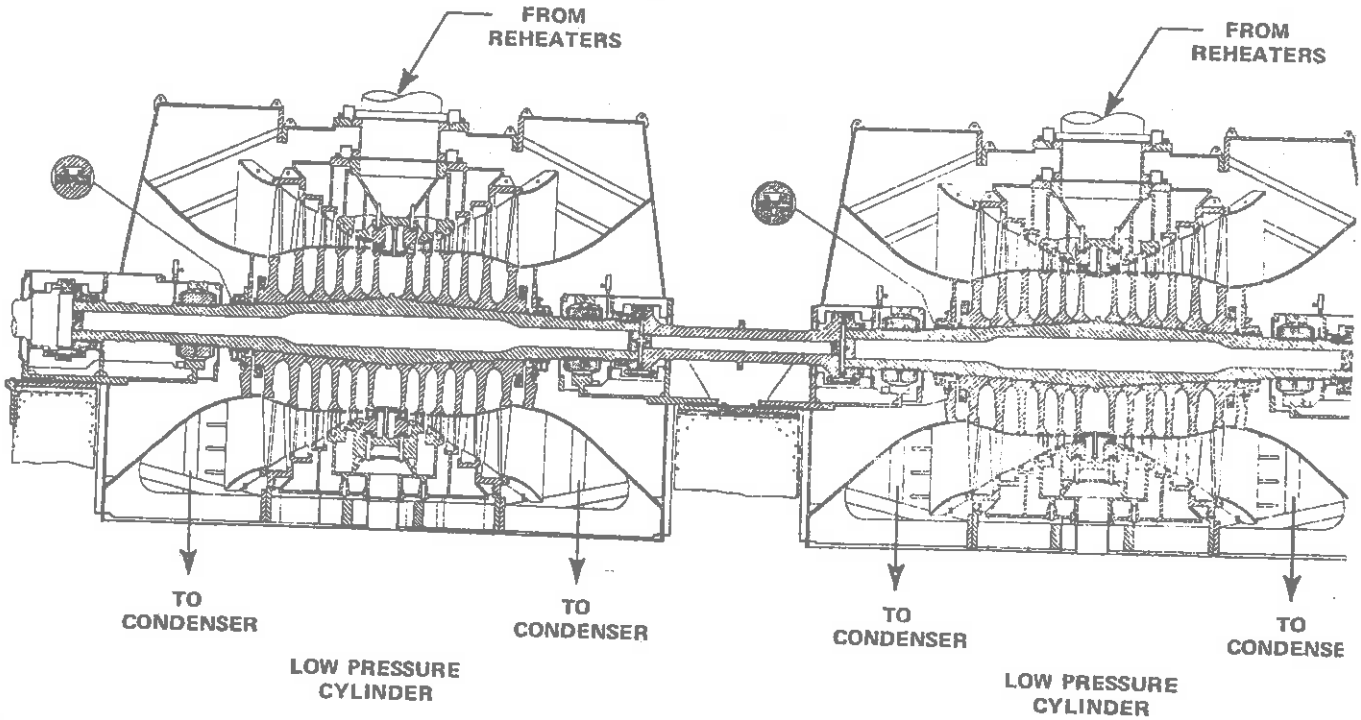
FROM
REHEATERS
FROM
REHEATERS
TO
CONDENSER
TO
CONDENSER
TO
CONDENSER
TO
CONDENSE
LOW PRESSURE
CYLINDER
LOW PRESSURE
CYLINDER

about 10% of the exhaust steam as moisture. The remaining 90% of the steam flow receives about 100°F as super heat from the reheaters.

A typical moisture-separator reheater system is shown in Figure 17-5. In such a system, the wet steam from the high pressure turbine enters the moisture removal section and rises through chevron-type moisture-separators where the water is removed and drained to the feedwater heater system. The dried steam then passes through the reheater section where it is reheated by a portion of the main steam which is withdrawn before the turbine throttle values and passed through the tube bundles where it condenses in the tubes and is drained to the feedwater heater. The reheated steam goes to the low-pressure turbines and to the main feedwater pump turbines.

d.) Condensing equipment

The main condenser is actually just a large heat exchanger connected to the low pressure turbine exhaust. Cooling water passes through tubes in the condenser unit with the condensing steam flowing over the outside of the tubing. Condensate is then collected in a chamber called a hotwell. The main condenser also handles the exhaust from the feedwater pump turbines.

e.) Feedwater heaters and pumps

We have seen in Chapter 15 that steam is bled off of the turbines and used to heat the condensate feedwater in feedwater heaters in order to achieve a more nearly isothermal steam generation process. The steam condensate is pumped through several stages of low pressure feedwater heaters, before passing through the main feedwater pumps. The water discharge from the feedwater pumps is then passed through one stage of high-pressure heaters and then into the steam generators.

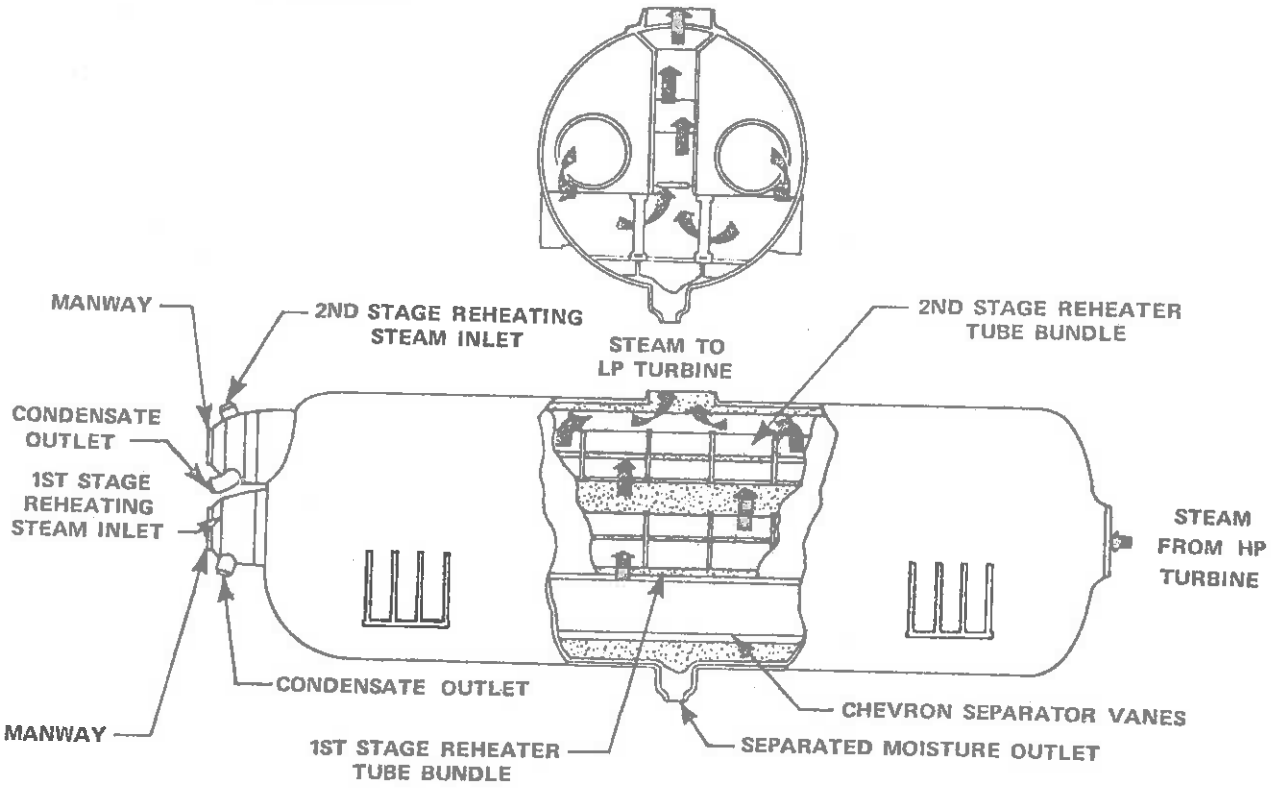

Moisture Separator Reheater, Two Stage

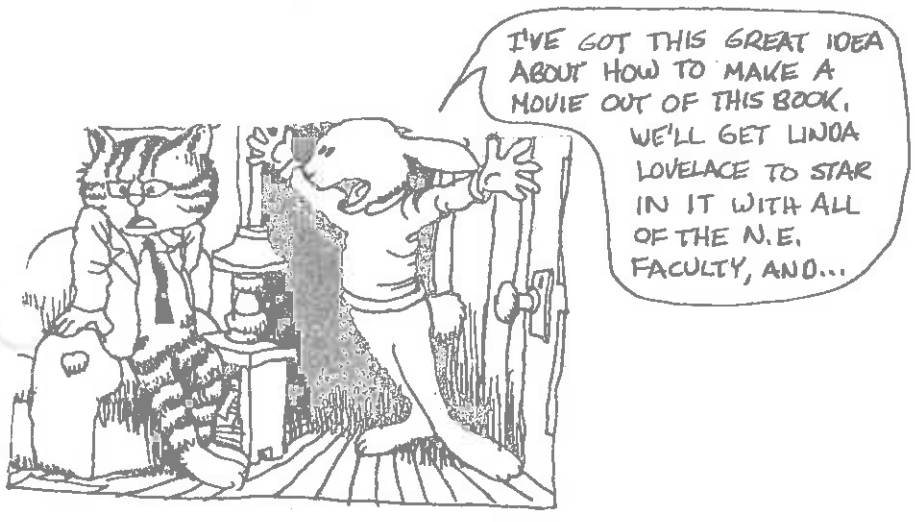

The main feedwater pumps are turbine driven with hot reheat steam, although usually one feedwater pump is motor driven to be used in startup or for reserve pumping capability.

f.) Electrical generator

The electrical generator for a modern nuclear power plant is a mammoth device. The ratings on a typical generator are tabulated below:

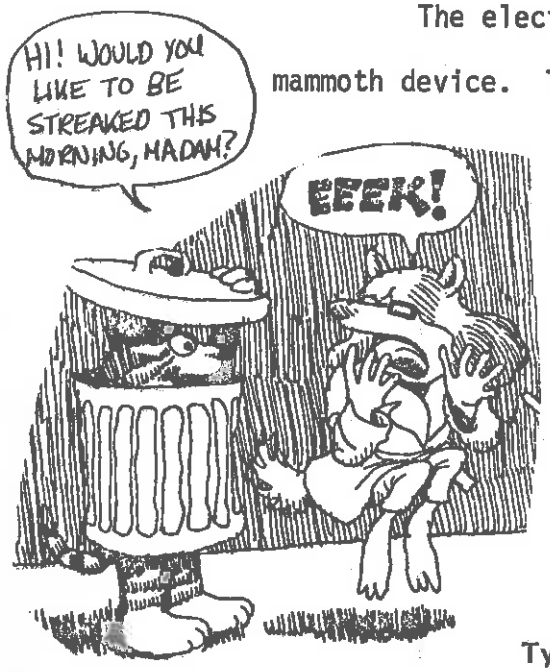

Type - Hydrogen inner-cooled synchronous generator with a water-cooled stator

Rating - 1220 mva

Power Factor - 0.9

Hydrogen Pressure - 75 psig

Output Voltage - 22,000 to 25,000 volts, three-phase, 60 Hz.

Excitation - Shaft-driven, air-cooled brushless exciter

A sketch of such a generator is given in Figure 17-6.

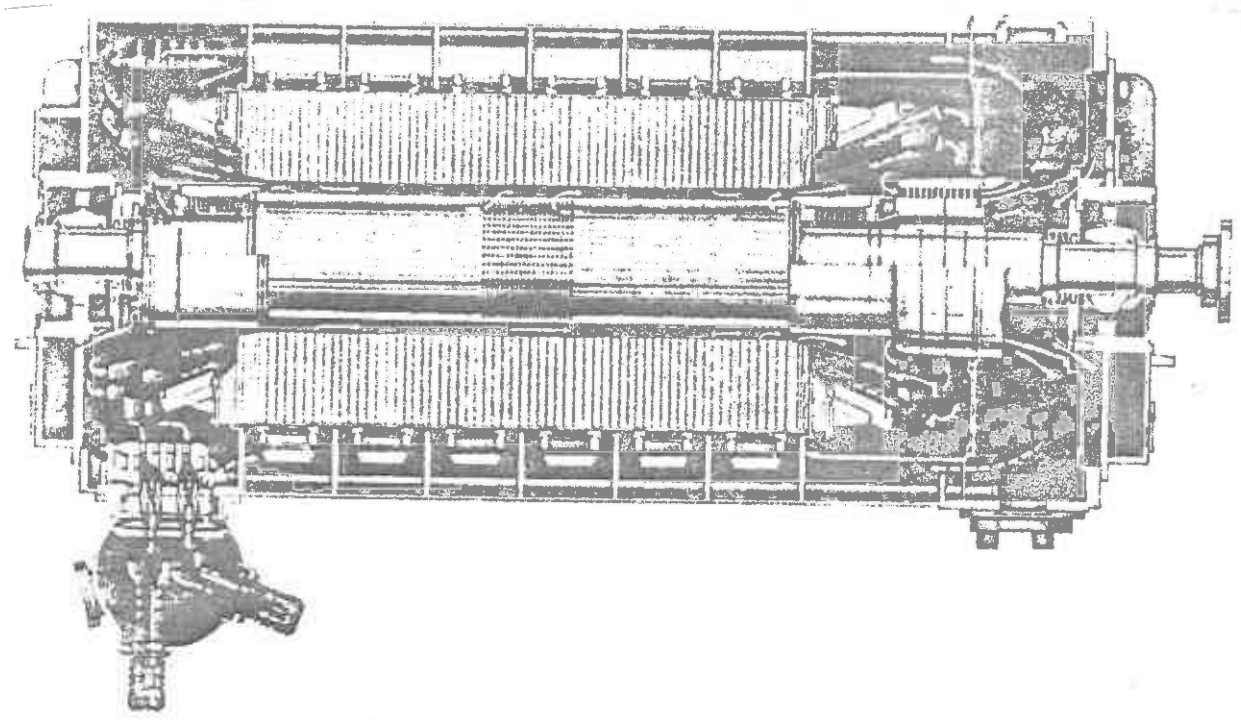

1800 Rpm Inner-Cooled Generator

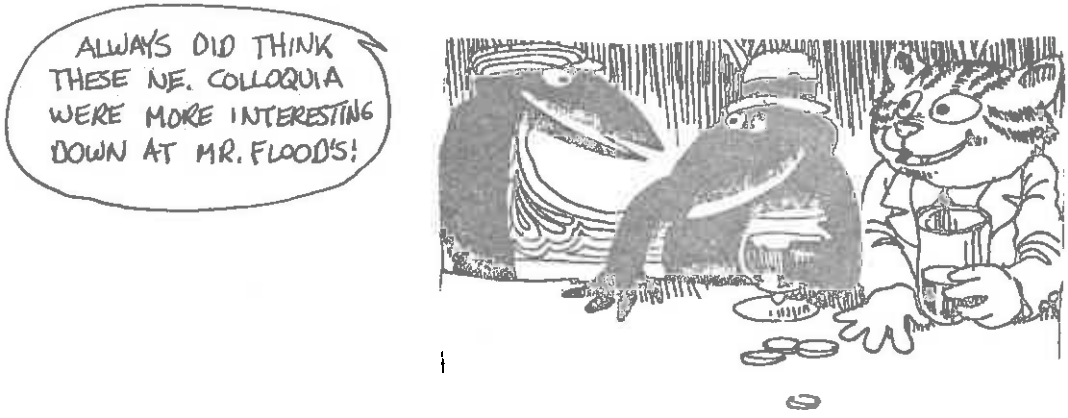

4. Auxiliary Systems

a.) Chemical and volume control systems (CVCS)

It is necessary to provide a system for injecting chemical shim (boric acid), as well as for purifying the coolant water, and providing new makeup water. These functions are performed by the chemical and volume control system which maintains a continuous feed-and-bleed stream of coolant water to the reactor coolant system (at flow rates of roughly 100 gpm).

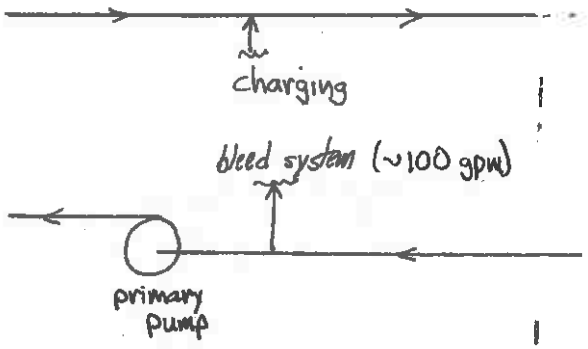

The more specific functions of the CVCS include

(i) Filling the reactor coolant system.

(ii) Providing a source of high pressure water for pressurizing the primary system when cold.

(iii) Maintains the water level in the pressurizer when the primary system is hot.

(iv) Reduces the concentration of corrosion and fission products in the coolant by purification.

(v) Adjusts the boric acid concentration of the reactor coolant for chemical shim control.

(vi) Provides high pressure seal water for the reactor coolant pump seals.

A rough diagram of the CVCS is shown in Figure 15-8. In this system, the letdown water bled off of the primary coolant loop is passed through the shell side of the regenerative heat exchanger where it gives up its heat to makeup water being returned to the primary loop. It then flows

INSIDE CONTAINMENT

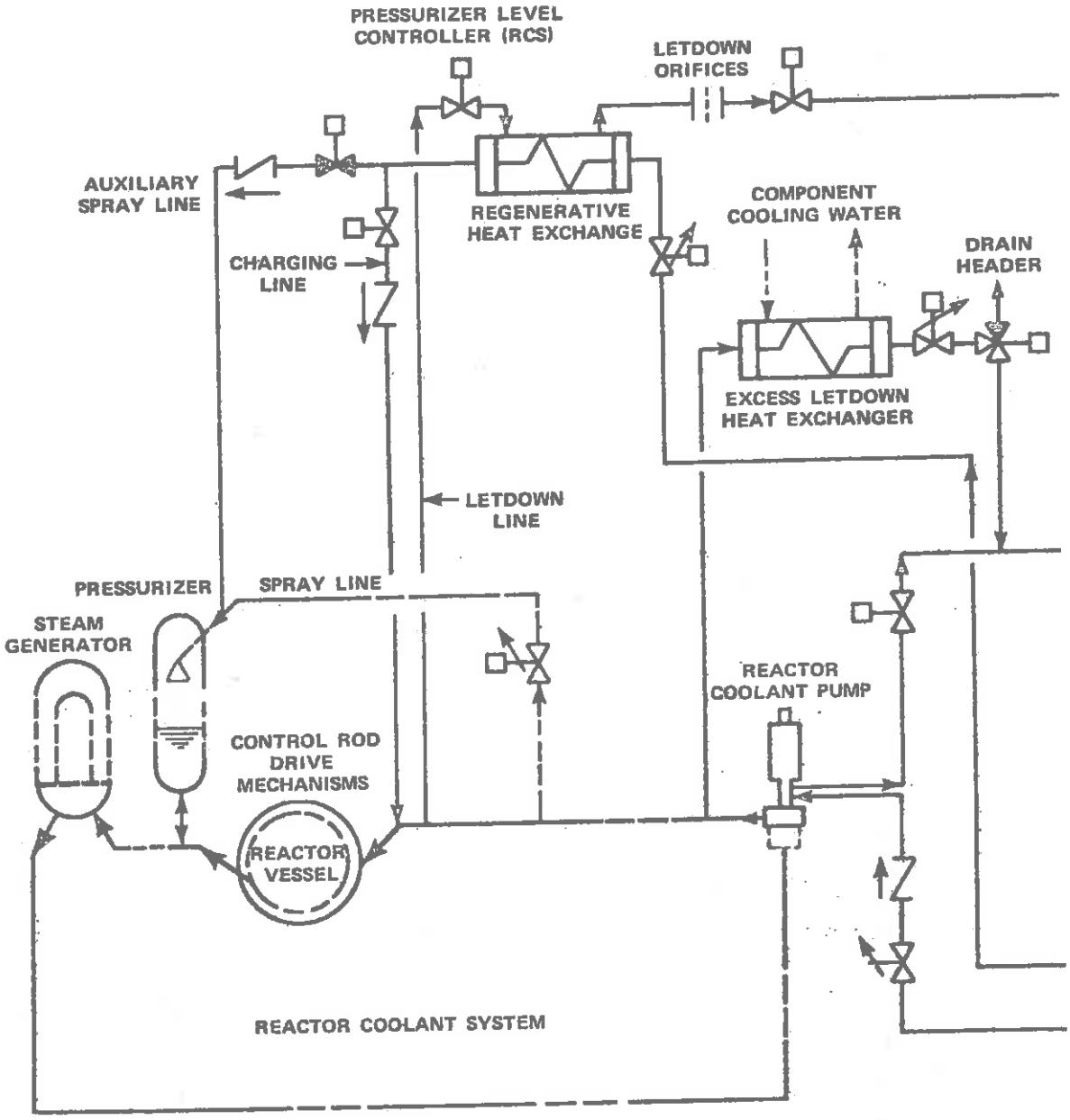

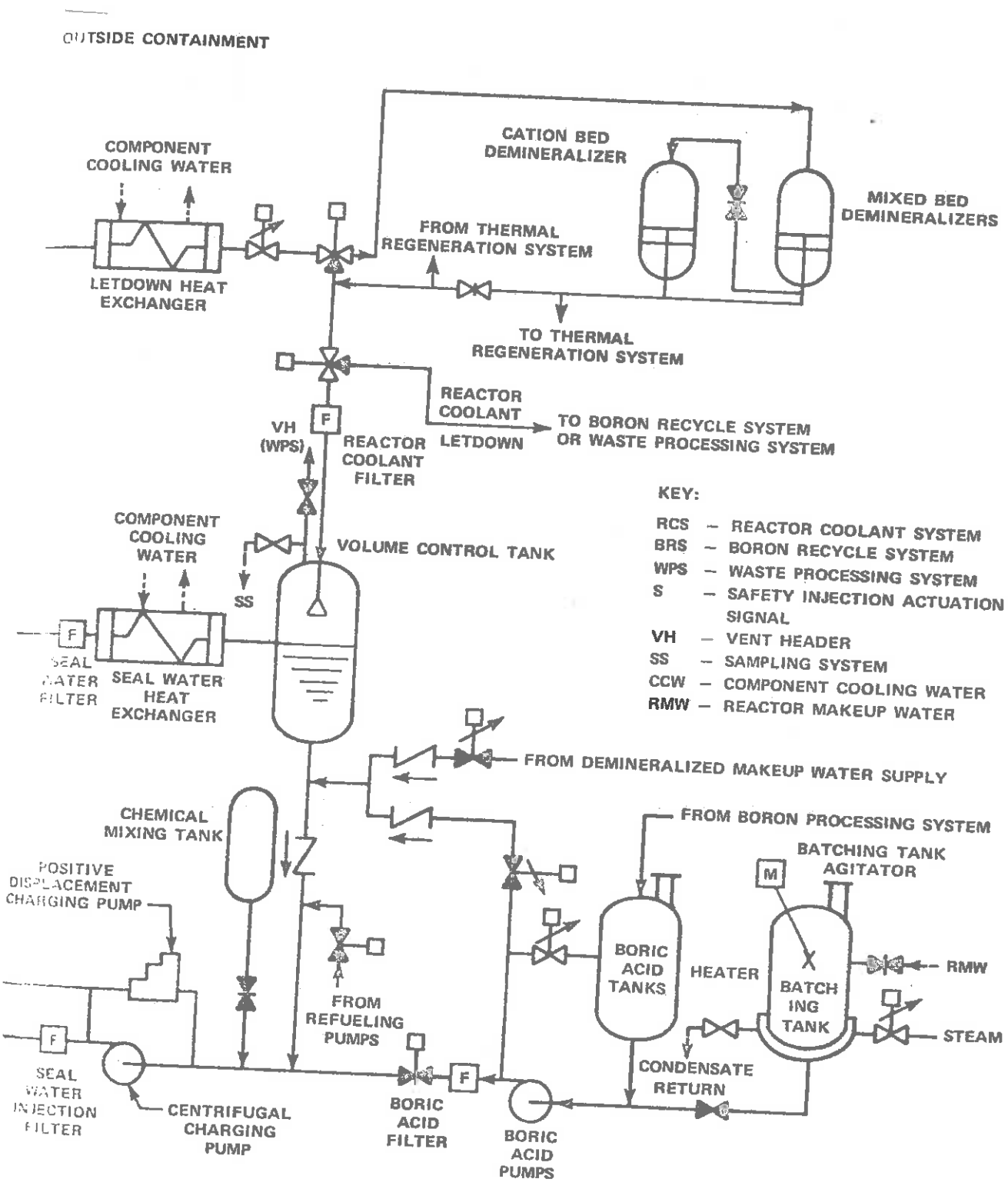

Chemical and Volume Control System, Flow Diagram

through orifices to reduce its pressure, followed by a letdown heat exchanger, and a purification system, and finally a volume control tank (VCT). This tank serves as an additional reservoir of water to use to back up the pressurizer. Connected onto this system are also the boric acid tank (BAT) and the refueling water storage tank (RWST).

Makeup to the CVCS comes from several sources including a demineralized and deaerated water supply, the boric acid tank, a blend of demineralized and deaerated water and concentrated boric acid to match the reactor coolant boron concentration for normal plant makeup.

b.) Residual heat removal system (RHRS)

The primary function of a residual heat removal system is to transfer heat energy from the core and primary coolant system during plant shutdown and refueling operations. However, the RHRS also is utilized in conjunction with the safety injection system for emergency core cooling during LOCA. The RHRS consists of dual heat exchangers and circulating pumps plus associated piping.

c.) Component cooling water systems

A variety of auxiliary cooling water systems are used to supply cooling functions to the many types of equipment in the plant. For example, the service water system supplies all the equipment cooling water for the plant. The component cooling system removes heat from the heat exchangers, pumps, and waste disposal systems. The spent fuel pit cooling systems provides cooling to remove the decay heat generated by spent fuel elements during on-site storage.

d.) Circulating water system

The condenser and component cooling water is supplied by the circulating water system which serves as the major heat sink for the plant by providing large amounts of cooling water. This system encompasses the various cooling devices (cooling towers, ponds, spray ponds) utilized as heat dumps for the plant.

e.) Radioactive waste processing system

A modern nuclear power plant is designed such that under normal operating conditions, no radioactive effluents are released from the plant. Hence provision has to be made for processing liquid and gaseous radioactive wastes generated within the plant. The liquid waste handling system processes both potentially tritiated and non-tritiated effluents. The gas handling protion of the rad waste system is capable of retaining radioactive gases within the gas decay tanks or slightly above atmosphere pressure for the life of the plant. The tritium produced in the primary coolant is retained within the plant for extended periods without undue operational restrictions.

5. Engineered Safeguards Systems

a.) Safety injection system

The safety injection system is designed to provide emergency core cooling in the event of a rupture of the primary coolant system. It consists of several independent subsystems characterized by equipment and flow redundancy.

(i) Accumulator tanks: In Chapter 15, we saw that PWR systems contained large tanks of borated water which could be used to flood the core in the event of a LOCA. These tanks are typically maintained at

pressures of 650 psig (using a nitrogen cover atmosphere), and when the NSSS pressure drops below this level, check values automatically open, providing rapid cooling of the core. Such accumulator tanks are an example of a passive ECCS.

(ii) Active safety injection: Both low pressure and high pressure pumps are also utilized to compensate for loss of coolant by injecting borated water into the primary system in the event of a rupture.

b.) Auxiliary feedwater system

The function of the auxiliary feedwater system is to provide adequate cooling water to the steam generators in the event of turbine trip coupled with a loss of offsite power. Auxiliary feedwater pumps are used to provide enough feedwater to safely cool the unit down to the temperature at which the residual heat removal system can be utilized.

II. NUCLEAR POWER PLANT CONSTRUCTION AND SITING

A. Plant Siting and Environmental Considerations

A great deal of evaluation and study goes into the choice of a suitable power plant site. Not only must one be concerned with the technical requirements of the plant, such as adequate cooling water, suitability as an electrical transmission point, etc., but one must also consider very carefully the environmental impact of the plant, as well as evaluate the site characteristics with a mind towards plant safety. We will give only a brief discussion of each of these types of site criteria: